Editor-in-Chief: Murugan Ramalingam

Faculty of Medicine, U977, University of Strasbourg, 11 Rue Humann, 67085 Strasbourg, France
Tel: +33-(0)3 68 85 32 58   Fax: +33-(0)3 68 85 33 79   E-mail: editorjbt@gmail.com

SUBMISSION OF MANUSCRIPT

Authors should submit manuscript electronically either as a PDF or Microsoft Word file to the Editor-in-Chief, or one of the Regional Editors, or one of the Associate Editors listed above. Authors are highly encouraged to submit manuscript electronically to save time for the reviewing process.

ON THE COVER:

RESEARCH ARTICLES

Aims and Scope:

Journal of Biomaterials and Tissue Engineering (JBT) is being created as an international peer-reviewed journal that covers all aspects of biomaterials, tissue engineering and regenerative medicine. The journal has been developed to create a new forum of scientific publications at the interface of biomaterials, tissue engineering and drug delivery research. JBT publishes original rapid communications, full research papers and timely state-of-the-art reviews (with author's photo and biography) encompassing the fundamental and applied research in the fields of biomaterials, tissue engineering and regenerative medicine. Rapid communications on new findings with breakthrough results will be considered for accelerated publication. The journal also publishes thematic special issues featuring selected peer-reviewed research papers from major conferences in the related disciplines. To speed up the reviewing process, we will provide on-line refereeing of all articles submitted in electronic form. Authors will receive the following benefits:

- Electronic submission of articles
- Fast reviews
- Rapid times to publication
- No page charges
- Free color where justified
- Distinguished editorial board
- Availability in print and online editions

Research Topics Covered (but not limited to):

The journal focuses on the broad spectrum of research topics regarding theoretical and experimental aspects of biomaterials and tissue engineering including polymeric biomaterials, metallic biomaterials, ceramic biomaterials, composites, biomimetics, biomolecular assembly, nano-/biomaterials, synthesis, characterization, chemical, physical, mechanical, biological and toxicological properties, byproducts, bioimplants and medical devices, biofilms, bioimaging, BioMEMS/NEMS, biosensors, performance of biomaterials, physiology and pathology, biomechanics, biological microarrays, surface functionalization, fibers, tissue scaffolds, porous biomaterials, combinatorial gradients, micro-/nanofabrication systems, cell patterning, cellular microenvironments, stem cell engineering, tissue engineering and modeling, artificial organs, hard and soft tissue applications, tissue interfaces, interactions between biomaterials, blood, cells, tissues, and organs, DNA technology, protein and drug delivery, gene delivery, molecular therapy, molecular biopharmaceutics, drug screening and delivery systems, polymeric drugs and polymeric drug conjugates, prodrugs, and medical nanotechnology related to the molecular design concepts, synthesis, production, characterization, nanomedecine as diagnostics and therapeutics tools, treatment of all types of diseases, regenerative medicine and nanomedicine, clinical performance, medical and clinical evaluation of drugs and delivery systems *in vitro* and *in vivo*

Readership:

The journal is of particular interest to the scientists, engineers and clinicians from academia and industry who are involved in research and development of biomaterials, regenerative tissues and drug discovery, everyone working in biomaterials, tissue engineering, materials science and engineering, bioengineering, pharmaceutical sciences, medicine, clinical pharmacology, biotechnology, microbiology, chemical biology, biochemistry, biochemical engineering, biomedical sciences, and other related areas of health care science and technology.

Submit Your Manuscript Electronically as a PDF or MS Word file to the Editor-in-Chief.

Editor-in-Chief

Dr. Murugan Ramalingam, Ph.D.
Professeur Associé des Universités
Faculty of Medicine, University of Strasbourg
67085 Strasbourg Cedex, France
E-mail: editorjbt@gmail.com

Website: www.aspbs.com/jbt

Journal Policy:

It is journal policy to publish only original and unpublished research work and, therefore, the *Journal of Biomaterials and Tissue Engineering* does not wish to receive any papers on research work that has already been reported in parts or contains already published text, data, figures, tables or other illustrations or any copyright materials whatsoever that has been submitted or accepted for publication either in a journal or conference proceedings elsewhere in any form, in print or in electronic media.

Honorable Claim Period:

Claims for issues not received will be honored only if submitted within 90 days of the issue date for subscribers in North America or 180 days for all other subscribers. Send your written request to American Scientific Publishers.

Digital Object Identifier (DOI):

The DOI identification system for digital media has been designed to provide persistent and reliable identification of digital objects. Information on the DOI and its governing body, the International DOI Foundation, can be found at http://www.doi.org. The DOI appears in the lower right of the first page of each article.

Copyright and Reprint Permissions:

Authorization to photocopy is granted by the ASP, provided that the appropriate fee is paid. Prior to photocopying, please contact the Copyright Clearance Center, Customer Service, 222 Rosewood Dr., Danvers, MA 01923, USA; +1 (508) 750-8400. For all other copying such as distribution, promotional, advertising, sale, collective work permission, write to: American Scientific Publishers, 26650 The Old Road, Suite 208, Valencia, California 91381-0751, USA

A Special Issue on
Nanomedicine in Latin America

This special issue of *Journal of Biomaterials and Tissue Engineering* includes articles from Latin American researchers that work in an emerging discipline at the interface of biomaterials science, nanotechnology and therapeutics called Nanomedicine and that comprises the use of different mono, bi and three-dimensional nano-objects (e.g., nanoplates, nanoparticles, nanotubes, etc.) to address different medical problems. A peculiarity of Nanomedicine is its pivotal role in the articulation of different complementary research disciplines such as pharmaceutical technology (aimed to develop drug dosage forms) and bioengineering (aimed to engineer medical devices without pharmacological, immunological or metabolic activity). In the first case, drug-loaded *ad-hoc* designed nano-objects enable to control pharmacokinetics and intracellular traffic of drugs without modifying their chemical structure. Silver and zinc oxide nanoparticles are examples of nano-objects displaying physical or redox activity and used as antimicrobials in advanced medical devices. In the second case, nano-objects can be used to modify the function of the cellular machinery by delivering genetic material; for instance switching to new metabolic pathways is a competence of cell engineering. Besides, biocompatible and potentially extremely bioactive nano-objects can be used to build artificial extracellular matrices. By tailoring cell-matrix interactions at the molecular level, a fine control of signal transduction pathways can be triggered to modify cell spreading, migration, proliferation and differentiation. This fine control improves the development of *in vitro* and *in vivo* tissue and it is the competence of biomaterials, tissue engineering and bioartificial organs areas. Undoubtedly, the use of nano-objects to execute controlled functions in the health field is blurring frontiers among disciplines that were well defined until very recent times.

In this very dynamic scenario, the social and economic impact of Nanomedicine has to be undertaken by a scientific community that envisages and fully understands the profound consequences of its intervention in living beings. Unfortunately, a misinterpretation of the scope encompassed by Nanomedicine made at first glance in Latin America gave access almost exclusively to chemistry and physics experts. This vision restricted the involvement of biomedical researchers in the nanotechnology arena and, as a result of this phenomenon, most of the Latin American countries and particularly Argentina, delayed the local development of the nanomedicine education programs and scientific platforms.

The foundation of any emerging applied research field demands the strategic investment of extensive governmental funds and the consequent generation of a critical mass of young, motivated and highly-qualified scientists that will later develop powerful and versatile technological platforms and educate a next generation of scientists. Hence, to push the field forward, in 2010, we founded the Argentine Society for Nanomedicines (NANOMED-ar). One of the urgent issues to be addressed in Latin America is the absence of a public health agenda focused on Nanomedicine; priority research lines and disease-oriented research projects have not been identified yet. In Argentina, the critical mass of nanomedical scientists remains relatively small and most of the activities are concentrated by a few highly qualified research groups in public institutions distributed across the country. These research groups own solid expertise, know-how and nanotechnology platforms in areas such as (i) synthesis, modification and characterization of polymeric and non-polymeric carriers; (ii) design and development of drug delivery implants; (iii) encapsulation, release and targeting of drugs, genes and vaccines and (iv) development of standard and innovative pharmaceutical formulations and *in vitro* and preclinical studies, among others. However, in the absence of a general consensus and long-term development plans, efforts fade away in a number of research lines that are in the best of the cases self-sustained, but that owing to complex economic, political and social contexts are not likely to be translated into products.

A serious debate remains to be opened. In the framework of neglected diseases, the development of innovative medicines represents a less profitable niche for the pharmaceutical industry and a fine equilibrium between innovation and affordability needs to be achieved. In other words, in these specific cases, nanotechnologies need to be more scalable and cost-viable. An approach to make these technologies more cost-viable is to develop robust and versatile platforms that can be implemented in different drug families displaying similar physicochemical and pharmacokinetic drawbacks. Challenges related to scale-up, toxicity, stability and regulatory issues, as well as environmental impact and management of waste products derived from the production of nano-objects will not be solved

1

in the absence of new academic knowledge and an intimate industry-academia interaction. Improved and deeper knowledge could guide—at least partially—industrial stakeholders to start their own way with fewer risks. In this sense, our vision fits very well that of the European initiatives (see the documents "Nanomedicine. A European Science Foundation—European Medical Research Councils (EMRC) Forward Look report, 2005," and the "European Technology Platform, Strategic Research Agenda for Nanomedicine, 2006).

Summarizing, Argentina and other countries in the region undergo a transition and expansion period characterized by the availability of a small number of highly-qualified research groups that are very eager to take Nanomedicine from an explorative to a more applied level. This goal can be achieved mainly by improving the interaction with industry. Conversely, global pharmaceutical companies are increasingly interested in extending the utility of their expired patents and enrich their intellectual portfolio. In this context, the current circumstances represent a unique and advantageous milieu for future fruitful academia-industry collaborations in our countries. Cooperative research between Brazil and Argentina was absent in the last years. This situation began to change and it is expected that the intervention of initiatives such as Nanomed-ar and other scientific and professional forums will contribute to improve the interaction and exchange. The next challenge will be to make this incipient interaction extensive to other countries of our region for the common benefit of our patients.

Guest Editors

Gustavo A. Abraham
Research Institute for Materials Science and Technology, INTEMA (UNMdP-CONICET). Av. Juan B. Justo 4302. B7608FDQ Mar del Plata, Argentina

Eder L. Romero
Programa de Nanomedicinas, Universidad Nacional de Quilmes, R. Saenz Pena 352, Bernal, B1876BXD, Buenos Aires, Argentina

Alejandro Sosnik
The Group of Biomaterials and Nanotechnology for Improved Medicines (BIONIMED), Department of Pharmaceutical Technology, Faculty of Pharmacy and Biochemistry, University of Buenos Aires. 956 Junín St. 6th Floor, Buenos Aires, 1113, Argentina

ABOUT THE GUEST EDITORS

Gustavo A. Abraham obtained his Ph.D. in Materials Science from the School of Engineering, National University of Mar del Plata, Argentina, and is working at the Research Institute for Materials Science and Technology (INTEMA) as independent researcher for the National Research Council (CONICET). He is Associate Professor of Chemistry and Biomaterials at the School of Engineering of the National University of Mar del Plata, Argentina. His research interests include polymeric biomaterials, scaffolding, tissue engineering, and biomimetic nanomaterials. He has authored more than 45 peer-reviewed research papers, 13 book chapters, and over 110 conference proceedings. His research supports are from the Argentinean National Agency of Scientific and Technological Promotion, the National Research Council, the Ibero-American Programme For Science, Technology And Development (CYTED), and the National University of Mar del Plata. He is an active member of the European Society for Biomaterials, Latin American Society for Biomaterials, Artificial Organs and Tissue Engineering, Argentinean Nanomedicine Association, and Argentinean Materials Association. He serves on the editorial board of the Journal of Biomaterials and Tissue Engineering as Regional Editor for South America. Dr. Abraham has been recognized with the Bernardo Houssay Award from the Ministry of Science, Technology and Productive Innovation of Argentina, in 2012.

2

J. Biomater. Tissue Eng. 3, 1–3, **2013**

Eder L. Romero is Biochemist from University of La Plata, Argentina and received a Ph.D. in Exact Sciences (1996). Following a post-doctoral research in Groningen University, The Netherlands (1997–1998), she returned to Argentina being currently an Independent Researcher at the National Council of Scientific and Technological Research (CONICET) (2010) and Associate Professor of Chemistry (tenure position 2008), at the Department of Science and Technology, National University of Quilmes, Buenos Aires, Argentina. From 2007 she is leading the Nanomedicine Research Program (NRP). The NRP is aimed to develop and follow the intracellular traffic of nanomedicines to be applied for topical/mucosal routes against infectious and inflammatory diseases and also in developing vaccination strategies employing biodegradable nano vesicles, to be applied by parenteral/topical/mucosal routes.

Alejandro Sosnik is Adjunct Professor (tenure) of Pharmaceutical Technology (Faculty of Pharmacy and Biochemistry, University of Buenos Aires) and Investigator of the National Science Research Council (CONICET). He received a Pharmacy degree of the University of Buenos Aires (1994) and a and Ph.D. in Applied Chemistry (Biomaterials Science) at the Casali Institute of Applied Chemistry (The Hebrew University of Jerusalem, Israel, 2003), under the supervision of Prof. Daniel Cohn. Between 2003 and 2006, Dr. Sosnik spent a postdoctoral stay in the laboratory of Prof. Michael Sefton (Institute of Chemical Engineering and Applied Chemistry, University of Toronto, Canada). Upon his return to Argentina in 2006, he founded "The Group of Biomaterials and Nanotechnology for Improved Medicines" (BIONIMED), a research group that works at the interface of biomaterials science, nanotechnology and pharmaceutical sciences. His main research interests are focused on the exploration of novel micro/nanotechnologies for the encapsulation, delivery and targeting of drugs involved in the pharmacotherapy of poverty-related diseases. He is a founding member of the Argentine Society for Nanomedicines (NANOMED-ar), where he serves as Secretary. He is also visiting professor and scientist at the National University of Colombia (Colombia), the University of Santiago de Compostela (Spain) and the Coucil for Scientific and Industrial Research (South Africa). He currently coordinates the "Iberoamerican Network of New Materials for the Design of Advanced Drug Delivery Systems in Diseases of High Socioeconomic Impact" (RIMADEL) of the CYTED Program.

Gold Nanoparticle-Membrane Interactions: Implications in Biomedicine

Ana Riveros[1, 2, †], Komal Dadlani[1, 2, †], Edison Salas[1, 2, 3], Leonardo Caballero[2, 3], Francisco Melo[2, 3, *], and Marcelo J. Kogan[1, 3, *]

[1]*Facultad de Ciencias Químicas y Farmacéuticas, Departamento de Química Farmacológica y Toxicológica, Universidad de Chile, Sergio Livingstone 1007, Independencia, Santiago, Chile*
[2]*Avenida Ecuador 3493, Estación Central, Santiago, Chile*
[3]*Departamento de Física, Universidad de Santiago de Chile, Avenida Ecuador 3493, Estación Central, Casilla 307, Correo 2, Santiago, Chile*

There has been an increase in the research towards the use of nanoparticles as a promising tool for nanomedicine, from imagenology, drug and gene delivery, to phototherapy. Little is known regarding the interaction between nanoparticles and cell membranes despite its importance to achieve an efficient therapy avoiding adverse effects, such as cytotoxicity and accumulation in undesired targets. Gold nanoparticles have demonstrated to be a perfect candidate to use in biological systems because of their dimension, ease of characterization, biocompatibility, and ability to conjugate to different compounds, such as active peptides. There are different biophysical properties such as: shape, size, conjugation, surface charge and ligand arrangement that affect gold nanoparticle-membrane interactions. In this review we will analyze how these properties are involved in the mechanisms of interaction with membranes and the internalization pathways of gold nanoparticle systems into cells. A new approach towards gold nanoparticles systems and model lipid membranes is rising to better understand this interaction at an atomic level in order to extrapolate it to a cellular level. We will discuss how gold nanoparticles interact with lipid membrane models and cell membranes analyzing its relationship to cell penetration, which is relevant for drug delivery.

Keywords: Gold Nanoparticles, Lipid Membrane Model, Drug Delivery, Cell Membrane, Nanotoxicology.

CONTENTS

*Authors to whom correspondence should be addressed.
†These authors contributed equally to this work.

1. INTRODUCTION

Nanotechnology offers tremendous potential for medical diagnosis and therapy. A variety of nanomaterials such as gold nanoparticles (GNPs) of different shapes and composition (Fig. 1) have been tested for biomedical purposes,[1–3] resulting in their widespread application in biological systems.[4–6] GNPs have been employed for imaging,[7–13] screening,[14] and biosensing[15–17] due to both their optical and electrical properties.[18–23] Furthermore, GNPs are currently used in gene and drug delivery,[24–26] cancer diagnostics and therapeutic applications,[27, 28] taking advantage of their high payloads of drugs compared to other known vehicles. In the field of neurodegenerative diseases we recently proposed to destroy toxic aggregates of β-amyloid (Aβ) after microwave irradiation in the presence of metal nanoparticles. Gold Nanospheres (GNSs) were conjugated

Ana Riveros was born in Chile, in 1977. She is a Biochemistrygraduate from Universidad de Chile, she received her Ph.D. in Biochemistryin the same university. She is currently a post-doctoral fellow at the Department of Chemical Pharmacology and Toxicology at Facultad de Ciencias Químicas y Farmaceúticas, Universidad de Chile. During her post-doc she has been a visiting researcher at the Department of Chemical Technology of Surfactants at Instituto de Química Advanzada de Cataluña (IQAC) at Consejo Superior de Investigación Científica (CSIC), Universidad de Barcelona in Barcelona, Spain where she studied the interaction of Nanoparticles and Liposomes. Her research interests are focused on nanobiotecnology, including cellular biology, microscopy and proteomics for biomedical applications.

Komal Dadlani was born in Chile, 1988. She recently received her B.Sc. in Biochemistry from Universidad de Chile and she is currently undergoing her Master's in Biochemistry in the same institution, for which she received a Scholarship from the National Commission for Scientific and Technological Research (CONICYT). She has been working at the Soft Matter Research and Technology Center (SMAT-C), studying the interaction between conjugated nanoparticles and Supported Lipid Bilayers through Atomic Force Microscopy. She has been President of the National Association of Biochemistry Students in Chile, participating in several scientific outreach programs.

Edison Salas was born in 1985 in Chile. He recently received his B.Sc. in Biochemistry from Universidad de Santiago de Chile. He is affiliated to the Soft Matter Research and Technology Center (SMAT-C) Santiago, Chile and to the Department of Chemical Pharmacology and Toxicology at Facultad de Ciencias Químicas y Farmacéuticas de la Universidad de Chile, where he is working to date. He has focused his research activities on Nanobiotechnology for drug delivery and biomedical applications, and the interactions of gold nanoparticles with membrane bilayers through Atomic Force Microscopy.

Leonardo Caballero is a Research Engineer at Universidad de Santiago de Chile. He graduated in Physical Engineering from the same institution. During his carrier he has been involved in several research projects related to heterogeneous media, electronic and instrumentation as well as Atomic Force Spectroscopy.

Francisco Melo is a Physics Professor at Universidad de Santiago de Chile. He graduated in Physics at the same institution and received a Ph.D. degree from Ecole Normale Supérieure de Lyon, France. His main research areas are Nonlinear Physics and Soft Materials. Today he is involved in the study of the mechanical properties of biomolecules and membranes as well as biomaterials growth by means of atomic force techniques.

REVIEW

Marcelo J. Kogan is Associated Professor at the Department of Pharmacology and Toxicology of the School of Pharmacy at the University of Chile. He is the Director of the Laboratory of Nanobiotecnology at the University of Chile. In 2006 he was a Visitant Professor at the University of Texas Medical Branch and in 2002 Visitant professor at University of Barcelona. Biochemist and Pharmacist from the University of Buenos Aires and Ph.D. in Organic Chemistry from the same University. His interest is centered in the applications of nanobiomaterials in biomedicine for diagnosis and treatment of conformational diseases including drug delivery, Alzheimer, Diabetes, Cancer and Chagas. He is a pioneer in the field for use of metal nanoparticles for the disaggregation of amyloids. He has published 55 articles in international ISI Journals, four reviews, and two chapter books. He was invited to present around 14 conferences in international meetings. He belonged to different organizing committees of international meetings.

to the amphipatic peptide CLPFFD that recognizes $A\beta$, increasing the stability of nanoparticles by steric effect and favoring the crossing of the blood brain barrier.[6, 29–32] In general terms, GNPs show a low degree of toxicity, which depend on their size, shape, charge and capping.[33–35] GNPs can be functionalized with different molecules of biological interest offering a high selectivity for drug delivery[36] and due to their size they have the ability to spread and cross biological barriers reaching specific targets with difficult access, such as the brain.[31] The optical and electrical properties of GNPs are some of the basis of their biomedical applications.[18–23] GNPs are characterized by a localized surface plasmon resonance, and depending on their size and shape, they are capable of absorbing electromagnetic radiation in the visible region for GNSs and infrared region for Gold Nanorods (GNRs) and Gold Nanoshells (GNShs),[37, 38] dissipating the absorbed energy in the form of local heat which gives rise to the so-called photothermal therapy and may thus destroy tumor cells or disaggregate toxic protein aggregates.[6]

A relevant biomedical issue is the penetration of nanoparticles (NPs) through the cell and biological barriers. Important biological barriers are the cell membranes, which are dynamic, fluid structures essential to de life of a cell,[39, 40] they are formed by amphipathic lipids, which consist of hydrophobic and hydrophilic portions. These properties are the physical basis of the spontaneous formation of membranes in aqueous environments.[40, 41] The lipid molecules are arranged as a continuous double layer of about 4 to 5 nm thick.[39, 40] The basic constituents of the cell membrane are the phospholipids, which could be saturated or unsaturated. The rate of saturation within lipid membranes determines the fluidity of the membrane.[42, 43]

Nanoparticles can interact and enter to a cell by two possible means; endocytosis and membrane penetration. In endocytosis nanoparticles could be internalized by endosomes without reaching the cytosol (accumulated in vesicular bodies) or not.[44, 45] On the other hand, nanoparticles (by preference cationic) pass through the cell membrane generating holes or pores in it contributing to the cytotoxicity on the cell.[46, 47]

The first interaction between NPs and membrane constituents could dictate the fate of a nanoparticle (NP) into the cell. In order to retrieve information about the physical rules governing the interaction between biological membranes and nanoparticles, model lipid bilayers are being used as a promising approach.[46–50] Such model systems are mainly employed to characterize the interactions between protein and lipid membranes, but they are also well adapted to understand membrane-nanoparticles interactions. These models are: Giant Unilamellar Vesicles (GUVs), Black Lipid membranes (BLMs), and Supported Lipid Bilayers (SLBs).[51, 52] The supported lipid bilayer (SLB) is typically formed by vesicle fusion or Langmuir transfer to a suitable surface.[53, 54] The latter model is a promising tool to understand the interaction between nanomaterials and membranes.[46–48] SLBs have the advantage of being studied at a nanometric scale as a planar system observed through Atomic Force Microscopy (AFM).[54–57] However the natural curvature presented in a cell is underestimated by this model.[51] A typical example of SLB is the use of a mixture of dioleoylphosphatidylcholine/dipalmitoylphosphatidyl choline (DOPC/DPPC), which is composed by unsaturated and saturated lipids respectively, mimicking the fluidity of a cell membrane.[39, 54, 58]

In this review we will discuss the different factors that influence in the interaction between GNPs and membranes. We will focus on how the surface charge density affects in the interaction and subsequent internalization of the GNPs into the cell. Then, we shall emphasize the importance of the ligand arrangement in GNPs and its impact on cellular uptake. Finally, we will examine on how the different size and shape of GNPs affect on their uptake in a cell discussing the possible mechanisms of interaction with lipid membranes.

2. HOW GNPS COATED WITH DIFFERENT SURFACE CHARGED DENSITIES INTERACT WITH MEMBRANES

In this section we shall summarize an important aspect while studying the interaction between GNPs and
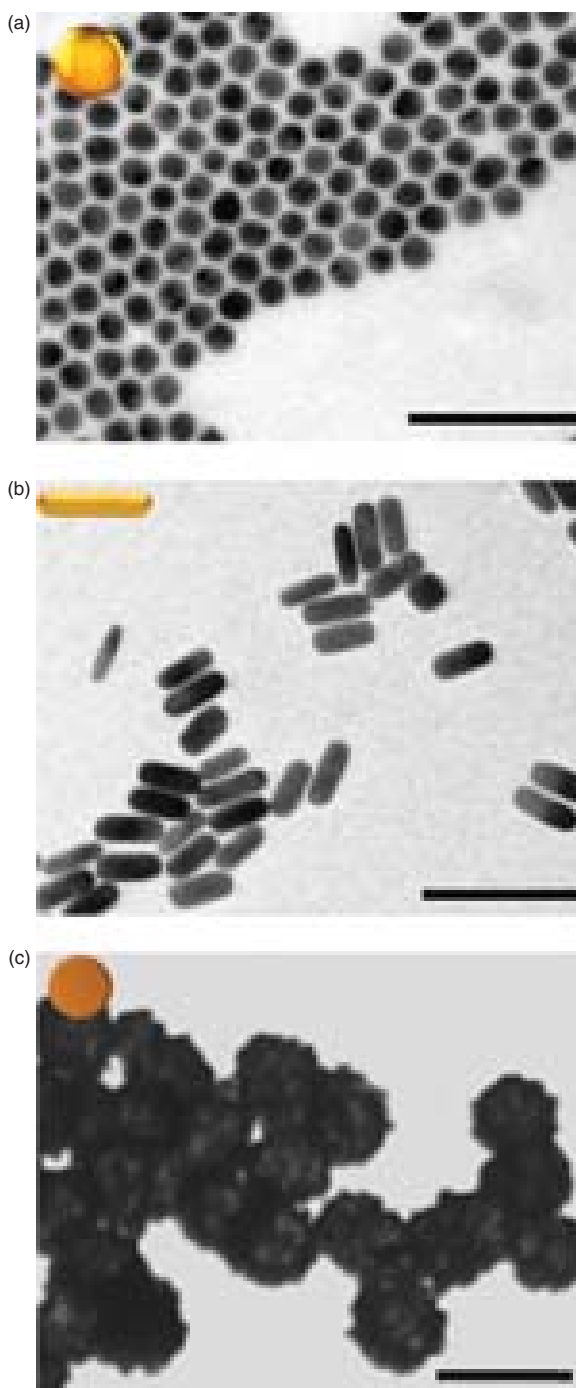
Fig. 1. Gold nanoparticles of different morphologies and components represented by TEM: (a) gold nanosphere, (b) gold nanorods, (c) gold nanoshells. Scale bars are 100 nm. (a) and (b) adapted with permission from [61], D. Bartczak et al., Interactions of human endothelial cells with gold nanoparticles of different morphologies. *Small* 8, 122 (**2012**). © 2012, Wiley-VCH Verlag GmbH & Co. KGaA, Weinheim. (c) adapted with permission from [113], D. Bartczak et al., Laser-induced damage and recovery of plasmonically targeted human endothelial cells. *Nano Lett.* 11, 1358 (**2011**). © 2011, American Chemical Society.

membranes: the surface charge density. There are explanations on how charged functional groups on GNPs affect in the interaction with membranes.[33, 34, 46, 47, 59–66] First, we shall analyze this interaction with model lipid membranes and secondly with cell membranes.

2.1. Interaction of GNPs with Model Lipid Membranes

To the date, only a few works have addressed the interaction of nanoparticles with model lipid membranes.[67–71] An important tool for such studies is AFM that allows the research of early biophysical interactions between nanomaterials and model membranes, which is relevant to understand the subsequent cell penetration of nanoparticles. In Atomic Force Microscopy, force curves provide us with a quantitative tool to investigate the biophysical features of nanoparticle-membrane interactions. When pressing on a SLB for instance, the approaching force curve presents a repulsive component until the bilayer is ruptured and the tip makes contact with the substrate. Such jumps are observed in a variety of bilayers.[57] An interesting example can be described by Schneider et al.[72] where they investigate the influence of the chemical properties of the tip on the tip-lipid bilayer contact using gold-thiol coated tips.[72] Studies conducted by Leroueil et al.[46, 47] using AFM and SLB to understand membrane-nanoparticles interactions, showed that various types of cationic nanoparticles induce defects in SLBs.[46, 47] Positively charged nanoparticles destabilized and disrupted the membrane, forming holes or expanding the existing holes. An increasing disruptive effect was observed at higher positive charge densities. The latter experiments were mainly conducted with different generations of polyaminodoamine dendrimers on SLBs, where the dendrimers with higher charged density presented a major disruption on the SLB. These authors also found that GNPs conjugated with an amine group disrupted the SLB through the expansion of pre-existing defects on the surface and appeared to aggregate on the mica surface (Fig. 2). In this experiment, it is necessary to take into account that the substrate (mica) offers a negatively charged surface which could contribute in the formation of the membrane holes, attracting the GNP-NH$_2$ to the mica, therefore disrupting the membrane. These defects, holes or pores in a membrane can be referred as a wide range of structural changes that could lead to an enhanced permeability ranging from the formation of an actual hole in the membrane to more subtle changes in the content of the membrane leading to an increased diffusion rate. These authors demonstrated that all the cationic nanoparticles studied (regardless of shape and chemical composition) showed a disruption on SLBs.[46, 47] This is an important result that could correlate the interaction of NPs and SLBs with NPs and cell membranes, providing valuable information on how nanoparticles could influence in the nanotoxicity.

Fig. 2. The GNP-NH$_2$ nanoparticles depicted in (a) were injected onto a DMPC-supported lipid bilayer represented in an AFM imagine in (b). After the injection the GNPs expanded the pre-existing defects within the supported lipid bilayer and appeared to aggregate on the mica surface as it is shown in the image (c). Scale bar is 500 nm. Adapted with permission from [47], P. R. Leroueil, et al., Wide varieties of cationic nanoparticles induce defects in supported lipid bilayers. *Nano Lett.* 8, 420 (**2008**). © 2008, American Chemical Society.

Besides this model, GUVs have also been used to study the interaction of nanoparticles and phospholipids because of their similarity of size and morphology to native cells. There are not many studies that detail the interaction between GUVs and gold nanoparticles, nevertheless Zhang et al.[70] have studied the interaction between GUVs as model membranes and SiO$_2$ NPs, the authors demonstrated that a competition between adhesion and elastic energy at the membrane interface takes place leading to membrane crumpling and micropore-formation.[70] The morphological changes of GUVs, observed under confocal microscopy, after interacting with SiO$_2$ NPs were strongly dependent on the size of these NPs. Small SiO$_2$ NPs create permanent holes in GUVs, transforming the previously smooth and spherical GUVs into crumpled objects with micropores, whereas, the interaction between GUVs and bigger SiO$_2$ NPs of 182 nm lead to wrapping events which are clearly observed on the surfaces of GUVs. The authors suggest that the wrapping events deplete the lipids and eventually lead to a GUV breakdown.[70] In this study, fluorescence recovery after photobleaching (FRAP) is employed to investigate the modifications in lateral lipid mobility. It is found that small SiO$_2$ NPs (less than 18 nm) cause a "freeze" effect on fluid membranes decreasing phospholipids lateral mobility, while large NPs (> 78 nm) promote membrane wrapping along with significant increase in lateral lipid mobility and in a complete vesicle disruption. The energy balance leads the authors to conclude that the energy required for membrane bending is the dominant barrier when particles are small, suppressing membrane wrapping,[70] whereas, Van der Waals forces and electrostatic interaction, between the negative charges on the SiO$_2$ surface and the positively charged region of the DOPC ($P^- - N^+$ dipole) are identified as the main contributions to the adhesion in this system. A change in the tilt angle of the head groups would be responsible of increasing the lipid packing density leading to a rigid membrane with a high lateral tension and small mobility. This tension is eventually released creating a single microsized hole in the membrane.[70] This interaction example is studied between GUVs and SiO$_2$NPs, and we believe further studies with GNPs should be conducted.

Recently, GUVs have been employed to investigate the thermal effect induced by the laser heating of GNPs.[73] offering valuable data for GNPs biomedical applications. While studying the interaction between GNPs and GUVs, these model membranes are well suited to study the variations in membrane permeability due to the local heating produced by GNPs while absorbing laser radiation near their surface plasmon resonance. The temperature field surrounding a GNP optically trapped can be characterized by simply measuring the distance between the particle and a leaking GUV. The method is based on the fact that a lipid vesicle becomes leaky at the phase transition and it is intimately connected while triggering the release of encapsulated molecules.[73] GUVs in combination with GNPs absorbing radiation have been used in a new method to deliver hydrophilic substances through the membrane. The method basically combines optical tweezers with local heating: an optical tweezers traps individual GNPs and pushes it to through the gel-phase membrane, while the optical heating of the GNPs causes the formation of a nanopore in the gel-phase membrane. This finding is relevant, since membranes are impermeable to most hydrophilic substances and numerous methodologies have been developed to surpass this natural barrier imposed by living cells in biomedical applications.[73] This novel method offers important opportunities for future studies in single cells and provides the community a new method to design and deliver GNPs.

Another interesting model to study are Black Lipid Membranes (BLMs), which constitute of thin lipid films placed across small apertures separating two chambers containing ionic solutions. This model allows the study of channels and pore formation in a lipid membrane,[71] technique that would be useful to study the interaction of

nanoparticles with this model membrane. To the authors knowledge there are no published studies regarding the interaction between GNPs and BLMs.[71, 74]

Given the complexity of nanobiosystems, computer simulations have emerged as effective alternatives to describe relevant aspects of NP-Membrane interactions.[61, 62]

Molecular dynamics studies propose that the interaction between GNPs and lipid bilayers depend on the surface charge density of the GNPs. GNPs with lower charge densities penetrate a negatively charged bilayer, whereas a highly charged cationic GNPs disrupts the membrane (Fig. 3).[49, 62, 63] In addition, recent simulations in the "coarse grain" approximation carried out by Lin et al.[62] provide valuable information and insight regarding the interaction mechanisms of GNPs with model membranes. It is found that GNPs with different sign and density charge either adhere or penetrate the membrane. The maximum energy gain, upon adhesion and penetration, is a key aspect to be considered for GNP-membrane penetration. Lin et al.[62, 63] modeled several interesting situations and in this review only two of the effects observed by the authors are discussed. First, to explore a range of interactions and charge densities, GNPs were functionalized with different fractions of ammonium (positively charged), carboxylate (negatively charged) and hydrophobic groups. Second, to feature a neutral membrane a pure DPPC was considered, whereas the negatively charged membrane was modeled by a mixture of DPPC and dipalmitoylphosphatidylglycerol (DPPG). The potential mean force (PMF) showed

deep minima inside the negatively charged membrane for cationic GNPs, whereas minima were observed near the surface of neutral membrane for both, cationic and anionic GNPs. In contrast, these simulations predict that GNPs do not penetrate neither neutral nor negative membrane, probably due to the reduced local minimum of PMF which locates at a few nanometers from the membrane (Fig. 3). This latter result contrasts the observations made by other authors[45, 60] in which the inclusion of such GNPs inside the membrane with experiments performed in a serum free conditions was demonstrated. This point will be discussed in the forthcoming sections. It is worth nothing that, for charged GNPs, PMF wells are about 100 KJ/mol deep and 1 nm or 2 nm wide which implies an energy barrier per molecule of $\Delta E = 2 \times 10^{-19}$ J, leading to forces of about 200 pN/molecule. This range of forces being accessible by means of AFM, it would be instructive to characterize PMF wells using AFM gold-tips functionalized following the same strategy described above.

2.2. Interaction of GNPs with Cell Membranes

In contrast to the model membranes studies, there are several works related to cell membranes. In this section we will present some illustrating works. Studies with cell membranes conducted by Cho et al.[75] have shown that the uptake of GNSs by SK-BR-3 cells was dependent on the surface charge, where positively charged GNSs present a higher uptake rate compared to the neutral or negatively charged GNSs.[75] Negatively charged GNSs were taken
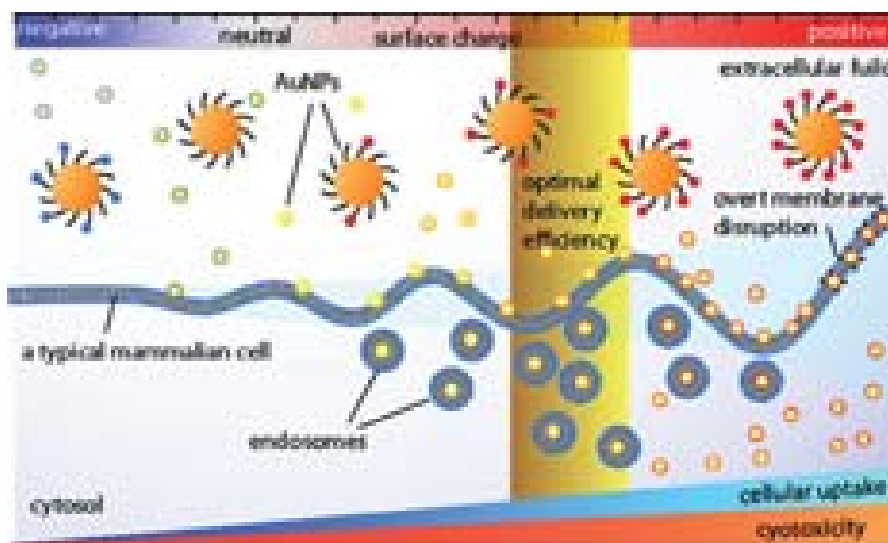
Fig. 3. A schematic illustration indicating the effect of GNPs surface charge on their cellular uptake and cytotoxicity of a typical mammalian cell. Cationic GNPs are favored by the cell membrane while anionic and hydrophobic GNPs cannot reach the membrane easily. Increasing GNPs surface charge density will promote uptake but also raise cytotoxicity. Exceeding a threshold of surface charge density may have the GNPs escape an endocytotic route and diffuse directly into the cytosol. Further increase of charge density may result in overt disruption of the membrane and thus cause acute toxic effect to cells. A certain amount of surface charge density may allow the GNPs to strike a balance between cellular uptake and cytotoxicity to achieve optimal delivery efficiency. Adapted with permission from [62], J. Lin, et al., Penetration of lipid membranes by gold nanoparticles: Insights into cellular uptake, cytotoxicity, and their relationship. *ACS Nano* 4, 5421 (**2010**). © 2010, American Chemical Society.

up by the cells at a slightly higher level than the neutral GNSs.[75] The authors suggest that this could be due to some of the positively charged domains in the membrane that would be interacting with the negatively charged GNSs,[75] nevertheless, it has been discussed by others authors[76, 77] that certain serum proteins bind to charged ligands promoting the entry of these GNPs into the cell through endocytosis. An effective cellular internalization of oligonucleotide-modified GNSs was observed despite of its negative surface coating.[76, 77] Knowing that a negative GNSs interacts little or nothing with a generally negative membrane[75] the oligonucleotide coated GNSs were internalized,[77] therefore the authors showed that serum proteins were adsorbed on the surface, becoming the latter a contributing factor in the interaction of GNPs with cell membranes.

2.2.1. The Charge Influences the Interaction of GNPs with Serum Proteins and Consequently Its Cell Penetration

While studying the internalization or biophysical interaction between GNPs and membranes it is fundamental to know the interaction between the GNPs and the culture medium in order to correctly interpret the results obtained in these studies, because the medium presents electrolytes and serum proteins which can be adsorbed by the surface of these nanoparticles forming the called "Protein Corona"[78, 79] modifying its dimensions and surface charge, being this an important aspect to consider in future biomedical applications.[33, 59, 76, 77] It is also important to know which are those proteins, because according to the GNP's coating different proteins shall interact with the system affecting its interaction with the membrane and subsequent entry to the cell. For instance, Alkilany et al. studied the cellular internalization of GNRs coated with cetultrimethylammonium bromide (CTAB) and polyacrylic acid (PAA) as positive ligands and poly (alkylamine) hydrochloride (PHA) as negative ligands, thus modifying the surface charge of the GNR.[33] Remarkably, the physicochemical surface properties of these GNRs substantially changed after being in contact with the biological environment by adopting the surface charge of adsorbed macromolecules (ζ potential = -20 mV) increasing their size by 22 to 36%. Interestingly these GNRs, despite having the same charge and similar size, they enter into the cells in different proportions, being internalized in the following order: GNR-PHA > GNR-PAA > GNR-CTAB.[33]

These results suggest that the net charge of the nanoparticle under study does not directly influence in the internalization of the GNRs, but it influences in the type and degree of adsorbed serum protein, and consequently the type of receptor-mediated endocytosis pathways. In this context, there is an interesting study.[59] in which different shaped GNPs were functionalized with Poly(ethylene glycol) (PEG), a widely used synthetic ligand, as it is biocompatible it improves the stability of the colloid and it prevents non-specific interactions with proteins.[80, 81] All the studied models, showed that GNPs functionalized with PEG penetrate much less, compared to those uncoated GNPs, this is because PEG reduces the protein adsorption around the GNPs reducing the interaction with the cell membrane and subsequently its endocytic process.[59]

In order to conduct complete studies on how GNPs are internalized into a cell, it is essential to take into consideration the biological media components that could possibly interact with GNPs.

Not only the surface charge or the serum proteins play an important role in the internalization process, but the hydrophilic/hydrophobic balance and the structure of the GNP ligand are relevant factors to take into account while studying this complex interaction between NPs and cell membranes. An illustrative example has been shown by Lund et al.[60] where they conjugated spherical-GNPs with hydrophilic ligands, such as the negatively charged peptide glutathione (at physiological pH) and the positive PEG-NH_2 and hydrophobic-neutral ligand such as glucose.[60] These authors observed that GNSs coated with glutathione (GNP-GSH) were internalized more efficiently compared to the spherical-GNPs coated with PEG-NH_2 or glucose.[60] These authors demonstrated that while inhibiting all the endocytic pathways the entry mechanisms are independent to it. Moreover their experiments were conducted in serum free conditions ruling out any secondary interaction. The authors suggest that the remarkable higher uptake of a negatively charged ligand could be due to the glutathione structure, which is composed by a multitude of hydrogen bond donors and acceptors, two carboxyl groups and one free amine forming a compact structure on the surface of the GNPs, a structure that could have cell penetrating properties.[60] The latter consideration brings up another important feature that influence in the interaction between GNPs and membranes, ligand arrangement.

3. THE LIGAND ARRANGEMENT ON A GOLD NANOPARTICLE IS IMPORTANT FOR ITS INTERACTION WITH CELL MEMBRANES AND SUBSEQUENT PENETRATION

Taking into consideration the natural mechanisms of Cell Penetrating Peptides (CPPs), the group of Stellacci examined the cell-penetrating ability of organically coated amphiphilic GNPs, which they called "striped" nanoparticles, a self-assembled monolayer coated GNPs with an alternating composition.[45] While studying the uptake of coated GNPs presenting the same size, ζ-potential, ligand packing density and hydrophobic content, being the only difference in the studied models the ligand arrangement, Verma et al.[45] reported that while GNPs were coated in

an alternating composition (striped or structured) their cellular uptake was higher than those coated with a randomly arranged ligand (unstructured) where the latter were inefficient in breaching the cell membrane barriers and were instead trapped in endosomes (Fig. 4). Interestingly, the striped GNPs displayed no disruption or pore formation in a manner similar to some of the cell penetrating peptides.[45, 82]

Moreover, Lund and colleagues[60] found that GNPs functionalized with a proportional mixture of glucose (hydrophobic ligand) and PEG-NH$_2$ (hydrophilic ligand) had a 18-fold higher penetration compared to the GNPs functionalized with these ligands individually (GNP-glucose and GNP-PEG-NH$_2$ only).[60] Based on the work of Verma and colleagues[45] the authors postulate that glucose and PEG-NH$_2$ would be organized in an orderly manner in the form of hydrophilic and hydrophobic discs on the surface of the nanoparticle facilitating their internalization. On the contrary a very low cell penetration of GNPs functionalized with a mixture of glutathione and glucose was observed, this might be because the structure of glutathione becomes unstable in the presence of glucose, generating a less ordered ligand arrangement in the GNPs.[60]

Based on the studies of Verma et al.[45] and Lund et al.[60] we know that striped nanoparticles enter to the cell with a higher rate than those unstructured nanoparticles.[45, 60] Nevertheless, there is not a clear understanding on the mechanisms governing the interactions between striped nanoparticles and membranes. In the following paragraphs we hypothesize a possible mechanism on how these striped nanoparticles interact with the phospholipids forming the cell membrane.

3.1. Which Could be the Possible Interaction Mechanism Between Striped Nanoparticles and Cell Membranes?

Striped nanoparticles offer hydrophobic–hydrophilic domains whose dimensions are of the order of the phospholipids molecule's length. We believe such domains act as templates over which ordered phospholipids molecules could spontaneously organize themselves to diminish the global energy of the Nanoparticle-bilayer system. It is intuitive that ordered structures optimize energy more suitably than unstructured systems, since in the former the energy associated to the domain boundaries is less (Fig. 5).

For example in a negatively amphyphilic charged NP, one possible phospholipids-structured nanoparticle-coverage, induced during nanoparticle membrane penetration, corresponds to hydrophobic tails, which lay on the hydrophobic nanoparticle domains, locating their negative heads close to the negatively charged domains of the NP. Although there might be an energy loss, a global energetic gain would be obtained if the interactions, between the polar heads and the charged nanoparticle domains, were

mediated by the layers of water molecules. For such a process to take place, an energy barrier due to the flip of some phospholipids would be required. Such a flip mechanism has already been conjectured to mimic hydrophobic nanoparticle interactions with lipid membranes.[83]

Further understanding onto NPs penetration into the cell has been achieved by using "Dissipative Particles Dynamics Simulations." This method basically consists in searching the solution of Newton's equations for suitable designed beads, which are specially designed to feature ligands and phospholipids.[49] When NPs are decorated with hydrophobic ligands by means of dynamic bonds (reversible non-covalent dynamic bond) they can spontaneously penetrate the membrane. The degree of penetration depends on several factors including, ligand type and density as well as NPs size and shape. For instance, for increasing NPs diameter at constant ligand number, it is found that the penetration efficiency decreases and is only 5% when the NPs size is 4.8 nm, which is attributed to a decrease of ligands density. It is to be noted, that while increasing the ligand's density, in this case, the nanoparticles-ligands complex is more hydrophobic making it easier for the NP to enter the bilayer. It is important to emphasize that the hydrophilic NPs can adhere to the membrane due to the lipid headgroup-NP interaction and when this interaction is strong enough the NPs are totally engulfed by the membrane. In turn, hydrophobic NPs can move into the bilayer, where they remain due to their preference for lipids tails. Ding et al.[49] designed a new type of NPs, which combine subtle effects in a way that NPs can effectively pass across the membrane taking advantage of its reversible dynamic bonds.[49]

The hydrophobic/hydrophilic interplay illustrated by Hong-mim Ding et al.[49] may also be related to understand the greater efficiency of striped NPs for cell penetration in contrast to the homogeneous or unstructured NPs, as described by Stellacci's group.[45] We conjecture that when a relatively small NP approaches the membrane due to the hydrophobic interaction, its hydrophobic component might favor the entry of the NP. Once the NP reaches the membrane interior, its hydrophilic component might, in turn, promote its further translocation into the cell. Thus, striped NPs seem to be adapted to smooth the energy barrier out, due to the domains of hydrophobic tails of the phospholipids: NPs with sufficiently large domains are expected to rotate and align with the hydrophobic/hydrophilic portions of the membrane which should facilitate translocation. Numerical simulations as the ones described above should prove useful while corroborating this hypothesis (refer to Fig. 5 for a description).

3.2. GNPs Ligand Arrangement and Possible Biomedical Applications

Given all the abovementioned discussion, an important aspect while studying the interaction between
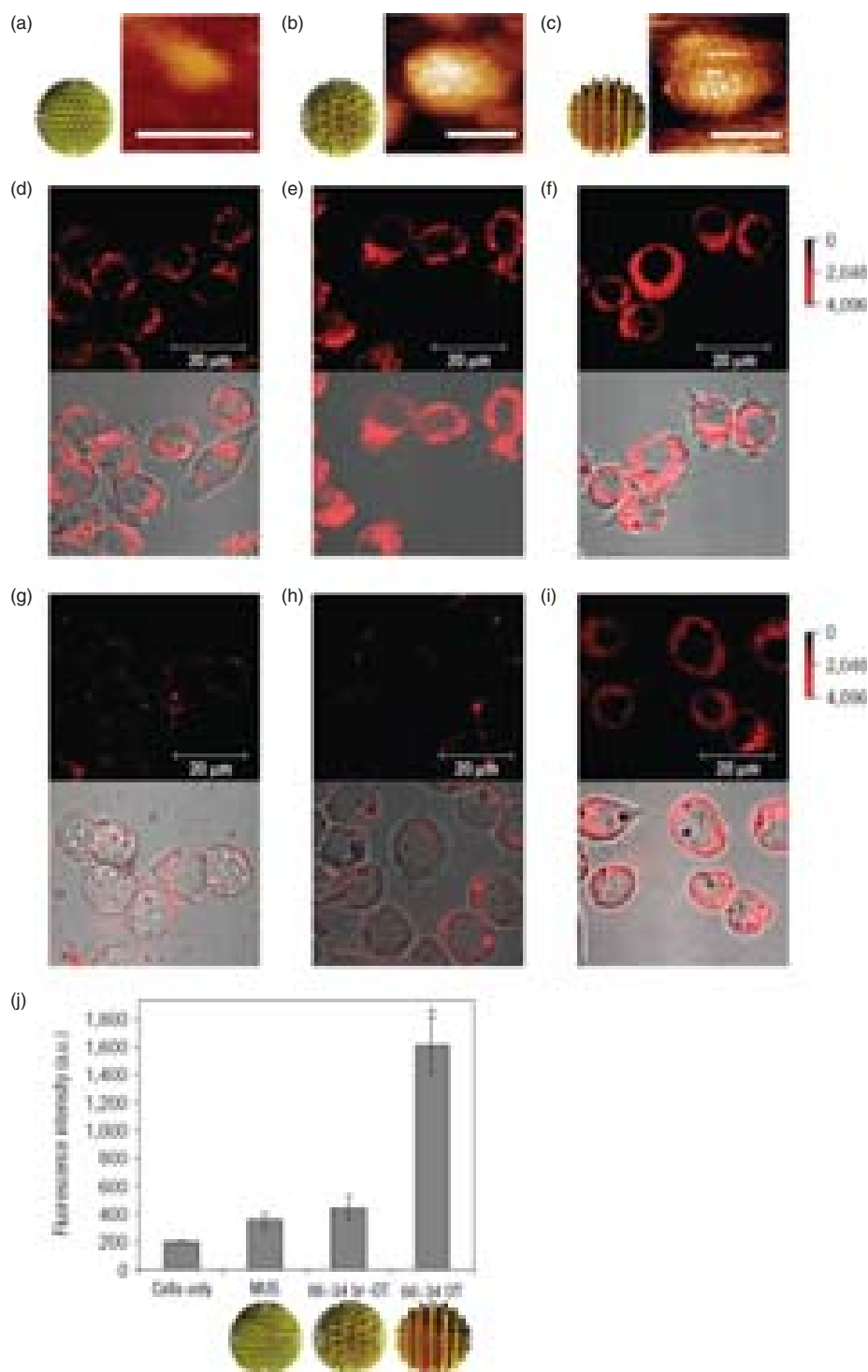
Fig. 4. Nanoparticles with ordered arrangements of hydrophilic and hydrophobic surface functional groups play a key role in cell membrane penetration. Schematic diagrams of the nanoparticle's ligand shell structure; (a) homogenous; (b) unstructured and (c) structured ligand shell, and their representative Scanning Tunneling Microscopy (STM) (scale bars 5 nm). Confocal microscopy experiments were performed with mouse dendritic cells incubated with nanoparticles at 37 °C (d)–(f) and 4 °C (g)–(i) in serum free conditions. Adapted with permission from [45], A. Verma, et al., Surface-structure-regulated cell-membrane penetration by monolayer-protected nanoparticles. *Nat. Mater.* 7, 588 (**2008**). © 2008, Macmillan Publishers Ltd.
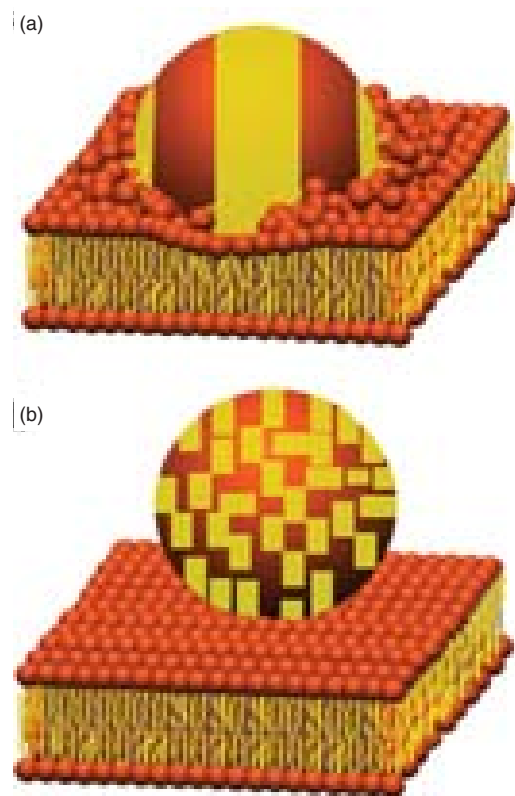
Fig. 5. Schematic diagram: (a) Striped GNP functionalized with amphipathic molecules, ordered and structured on the surface. Represented in orange are the hydrophilic domains and in yellow the hydrophobic domains. The ordered arrangement of the hydrophobic and hydrophilic domains, energetically favors the interaction with the self-assembled phospholipid bilayer. This diagram represents the interaction between the hydrophobic domains of the nanoparticle (represented in yellow) and the hydrophobic domains of the phospholipid's tails, which favor the internalization of the nanoparticles. (b) A GNP functionalized with unstructured amphipathic molecules, which are disordered on the surface, do no interact with the lipid bilayer in an energetically favored manner as it happens in the structured case.

nanoparticles and membranes is the ligand arrangement.[76] Not all the published works emphasize on the ligand arrangement in a nanoparticle or in the used culture medium and we believe it is of utmost importance to have the knowledge of it in order to compare and analyze its effects on a cell or model membrane. Our group has studied the ligand arrangement of amphipathic peptides conjugated on spherical GNPs.[30, 84] The conformation and charge exposure of peptides attached to colloidal GNSs are critical for both the colloidal stability and for the recognition of biological targets in biomedical applications such as diagnostics and therapy. We have shown that the peptide sequence affects the conjugation and stability of GNSs, and therefore in their interaction with target molecules. We have prepared GNSs conjugated with different isomers peptides capable of recognizing toxic aggregates of the

amyloid beta protein ($A\beta$) involved in Alzheimer's disease, namely, CLPFFD-CONH$_2$ and CLPDFF-CONH$_2$ as shown in the Figure 6. In the case of GNS-CLPFFD-NH$_2$, the peptide is oriented orthogonally to the gold surface adopting a β secondary structure, while in GNS-CLPDFF-NH$_2$, the peptide is in a disordered structure. In this work we demonstrated that GNPs conjugated to the peptide that adopts a β secondary structure (CLPFFD-NH$_2$) is more stable and presents a higher affinity for $A\beta$ fibrils in contrast to the GNSs coated with the peptide that forms a disordered structure (CLPDFF-CONH$_2$).[30, 84] We have demonstrated that the peptide sequence, the steric effects, the charge and disposition of hydrophilic and hydrophobic residues are determining parameters when considering the design of GNP-peptide conjugates for biomedical applications, such as binding of GNSs to $A\beta$ fibrils.[30, 84]

The use of GNPs in cancer therapeutics and diagnostics has widely been studied.[85–88] The group of Chan[88, 89] has studied the efficiency of tumor targeting through different GNPs design.[89] They examined the effect of nanoparticle size (10–100 nm) and surface chemistry on passive targeting of tumors *in vivo*. Their GNPs were conjugated with different sets of methoxy-polyethylene glicol (*m*PEG) and in their findings they describe how the physical and
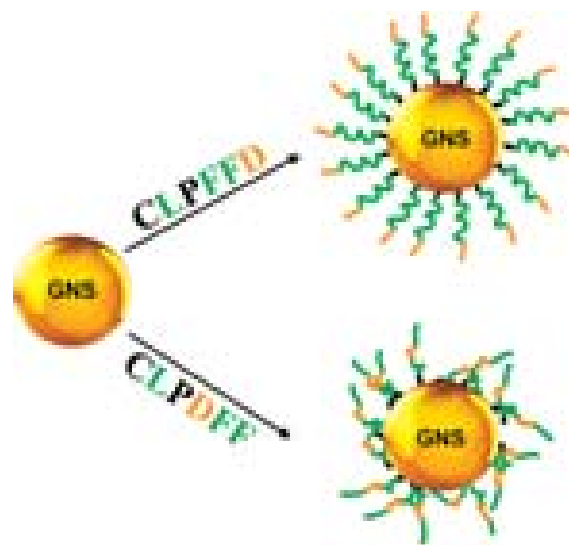
Fig. 6. Schematic diagram of GNS conjugated to isomers CLPFFD-NH$_2$ and CLPDFF-NH$_2$. The hydrophobic groups are represented in green and the hydrophilic groups in orange. In the case of GNS-CLPFFD-NH$_2$, the peptide anchored to the GNS adopts a β secondary structure increasing the ability to interact with $A\beta$ fibrils, while in GNS-CLPDFF-NH$_2$, the isomer CLPDFF-NH$_2$ adopts a more disordered structure avoiding the accommodation of molecules, reducing the degree of functionalization, the stability, and the affinity for $A\beta$ fibrils. The scale of the molecules is not in proportion with the nanoparticles. Figure adapted with permission from [30], I. Olmedo, et al., How changes in the sequence of the peptide CLPFFD-NH$_2$ can modify the conjugation and stability of gold nanoparticles and their affinity for β-amyloid fibrils. *Bioconjugate Chem.* 19, 1154 (**2008**). © 2008, American Chemical Society.

chemical properties of their mPEG-GNPs influence the pharmacokinetic behavior of the GNP in the blood, which ultimately determines the tumor accumulation capacity and the permeation of the GNP within the tumor. Their study describes how larger nanoparticles appear to stay near the vasculature while smaller nanoparticles rapidly diffuse throughout the tumor matrix. These are important features to be considered for drug delivery and imagining in cancer.[89] When the aim is to maximize the amount of GNPs delivered into the tumor compartment but localization within the tumor mass is unimportant, moderate particle cores protected with large mPEG could be used to improve diagnostic sensitivity.[89] The future perspective of this work towards tumor targeting is promising but we believe it could be boosted and improved if its basic nanoparticle design considers the ligand arrangement.

For a therapeutic approach, nanoparticles need to reach the lumen of the cancer and tumor matrix and in order to accomplish this the nanoparticle ligand design is important to reach target tumor cells. The work of Li et al.[90] used dual-ligand gold nanoparticles to explore the therapeutic benefits of multivalent interactions between GNPs and cancer cells.[90] This system was tested on human epidermal cancer cells, which had high expression of folate receptors. These researchers demonstrate that dual-ligand GNPs of folic acids and glucose show enhanced binding to the folate receptor on cancer cells with a higher internalization than particles with folic acid alone, allowing dual-ligand GNPs to enter selectively to the cancer cells.[90] However the interaction mechanism between the cancer cells and the dual-ligand GNP is yet to be established, a consideration in the ligand arrangement might improve this understanding.

Taking into consideration the aforementioned, the group of Lund et al.[60] explored the uptake of single and dual-ligand GNPs in colorectal cancer cells, where they analyzed the ligand arrangement of a dual ligand formed by glucose (hydrophobic ligand) and PEG-NH$_2$ (hydrophilic ligand). Changing the hydrophilic and hydrophobic ratios, they show that the uptake of GNPs in these cancer cells is not determined by the charge of the ligands but rather by the way how the ligands are organized on the surface of the particles as discussed earlier.[60]

Moreover, Yang et al.[91] studied dual-ligands GNPs by including multiple surface ligands on GNPs surface. This was done, by using two types of lipids and two surface chemical procedures, in which patchy phospholipids layers were obtained on GNPs surface depending on the ligand. Mixed-lipid-coated GNPs are biocompatible as they allow the mimicry of cellular surfaces in terms of solvent-facing functional groups and charge density.[91] In this work the researchers successfully incorporated a biotinylated lipid in their hybrid lipid GNP system, thus, as inspired by this study,[91] for multifunctional targeting, imaging and therapeutic applications purposes, one can imagine GNPs functionalized with several specific ligands, each one devoted to a specific target. For instance, optimized ligands would be used for membrane penetration or disruption, whereas other ligands would collect or deliver specific drugs in the cell. This knowledge could be efficiently used in tumor imagining, for example, researchers have demonstrated a promising strategy to target cancer imaging through the use of GNPs stabilized with biotinylated PEG.[88] In this work the accumulation of a fluorescent contrast in an *in vivo* tumor model is studied, as represented in Figure 7. In the experiment the researchers passively inject
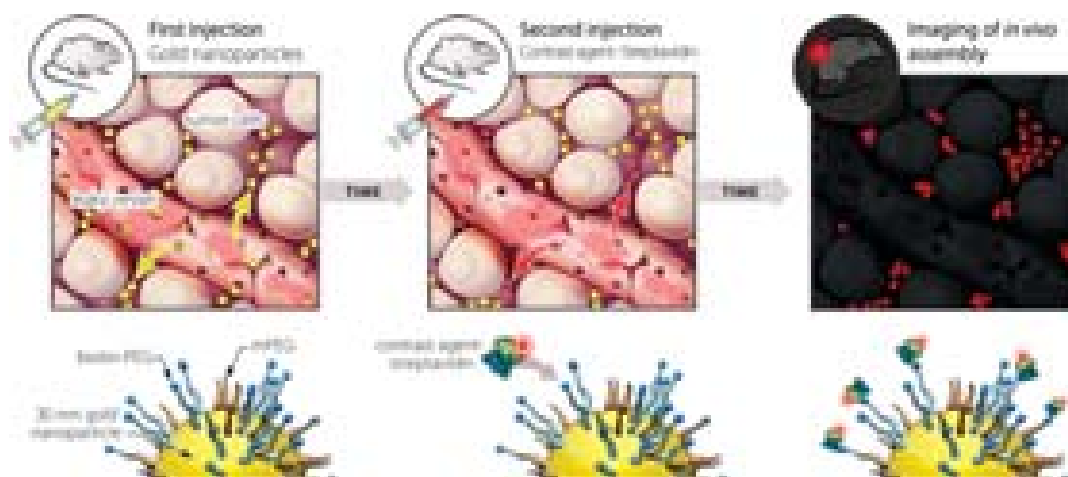
Fig. 7. Schematic of nanoparticles assembling with contrast agent *in vivo*. Gold nanoparticles stabilized with biotinylated PEG are injected as a first step. These enter tumors through leaky vasculature and passively accumulate in the extracellular matrix over 24 h. Fluorescently labeled streptavidin is injected, leaks into tumors, and interacts with biotin on the gold nanoparticles in the interstitium. This favorably alters the contrast agent's tumor accumulation kinetics. Adapted with permission from [88], S. D. Perrault and W. C. W. Chan, *In vivo* assembly of nanoparticle components to improve targeted cancer imaging. *Proceedings of the National Academy of Sciences* 107, 11194 (**2010**). © 2010, National Academy Sciences.

REVIEW

biotinylated-PEG-GNPs into a tumor xenograft model, followed by a second injection of streptavidin labeled with a fluorescent contrast agent. The streptavidin interacts with biotin on the GNPs allowing the imagining on an *in vivo* assembly.[88] This targeted cancer imagining seems to be a promising tool in nanomedicine, nevertheless, we believe that further investigations towards the arrangement of the ligands could improve the targeting to specific cells.

To the date, three generations of nanoparticles have been designed for biomedical applications.[87] The first generation of nanoparticles considered the material design, water solubility and biocompatibility, but their biological challenges were instability, removal by phagocytic cells and poor tumor targeting. Therefore, a second generation of nanoparticles was developed using PEG and specific antibodies that maximized delivery and specified targeting. Unfortunately for the later, the addition of excess targeting ligands increased the clearance by phagocytes and promoted a higher interaction with culture medium, moreover there was no universal antigen to be considered.[87] Taking into consideration the ongoing concerns, a third generation of nanoparticles is being developed considering the dynamic properties of the nanoparticles such as size, shape and surface chemistry, because these are features that influence the environment-responsiveness and membrane penetration. However, we believe that a fourth generation of nanoparticles that consider ligand arrangement would definitely enhance membrane penetration allowing the use of nanoparticles for different biomedical applications.

4. HOW THE SIZE AND SHAPE OF GNPS INFLUENCE IN THE INTERACTION WITH MEMBRANES AND CELL PENETRATION

4.1. Spherical GNPs

Studies to the date show that the different means of entry to a cell highly depend upon the GNP's size. In this section we will discuss, firstly, the effect of the NP size on the interaction with model membranes and secondly on the interaction with cell membranes and its subsequent uptake.

4.1.1. Effect of the Size on the Interaction with Model Membranes

Despite the fact that the size effect is well recognized in nanoparticle's uptake and adhesion to a cell, only few studies address this issue in simple model systems, which are not experimented with GNPs. Evidence of NP size effects has been obtained by Roiter et al.[48] in the case of silica NPs interacting with lipids membranes. Nanoparticles whose diameter ranged from 1 to 140 nm were first deposited onto silicon wafers and subsequently a lipid membrane was grown onto such "decorated nanoparticles" substrate. Combining phase images provided by AFM, Confocal Microscopy and TEM, these authors showed

that membranes can sustain stable pores around silica nanoparticles when their size ranges from 1.2 to 22 nm, while larger nanoparticles are mostly covered with lipids bilayer without piercing the membrane.[48] Moreover, Hou et al.[92] investigated the size distribution and surface functionalities of functionalized GNPs breaching SLBs, and they observed that equally functionalized small GNPs distributed into the lipid bilayers more rapidly than large GNPs. These experiments were performed through Scanning electron microscopy (SEM) and TEM.[92]

Roiter's model indicates that a lipid membrane spread over larger nanoparticles with little cost on bending energy associated to membrane curvature. In contrast, a membrane pore would be caused by the inability of the membrane to produce highly curved zones imposed when wrapping small nanoparticles. Thus, a pore is formed to the unfavorable bending energy compared to the attractive force pulling the membrane to the substrate, and this is despite the energetic cost of introducing membrane distortion at the pore. Thus, size effects can be explained by the optimization between an energy cost due to bending and an energy gain provided by the surface energy. This conclusion is confirmed experimentally since the critical nanoparticle size, for the wrapping-unwrapping transition, was about 22 nm, which is close to that predicted by a balance of adhesion and bending membrane energy.[48]

4.1.2. The Effect of GNP's Size on Cellular Uptake

It has been described that small spherical GNPs of sizes between 1, 4 nm to 5 nm enter the cell.[45, 93–97] and it has been shown that GNS of 5 nm are internalized passively not involving an endocytic,[45, 60] lipid raft-mediated or other energy-demanding pathways.[60] Verma et al. and Lund et al. hypothesize that the entry of these small spherical GNPs occurs through transient holes without membrane disruption. It is known that GNPs of bigger size, from 20 nm to 50 nm, are internalized through endocytosis,[35, 98, 99] whereas GNP of size greater than 70 nm do not enter, and if they do, they enter in a very low proportion,[35, 99, 100] therefore, we could say that there is a tendency in which the cellular uptake is inversely proportional to the GNPs size.[59] On the other hand, the group of Warren Chan showed that GNPs of 50 nm enter with a higher rate compared to those of 14 nm and 100 nm, this difference could be due to the fact that the entry mechanism studied in their work is with GNPs coated with transferrin, a plasma protein carrier of iron, which enters the cell via receptor-mediated endocytosis.[98] Refer to Figure 8 for an illustrative diagram.

These authors demonstrated through Transmission Electron Microscopy (TEM) the entry of a single GNPs of 50 nm, whereas GNPs of smaller size require at least 6 GNPs to cluster and enter a cell.[98] and DPD simulations studies have also shown that the internalization of multiple small NPs is a cooperative process.[101] This can be
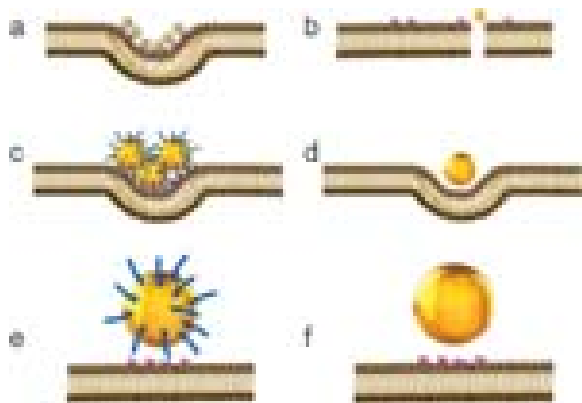
Fig. 8. Schematic representation on how different GNPs sizes affect in the interaction with cell membranes and therefore its possible internalization. Diagrams (a), (c) and (e), exemplify how GNPs coated with transferrin ligands are internalized through receptor mediated endocytosis. Adapted and modified from [98], B. D. Chithrani, et al., Determining the size and shape dependence of gold nanoparticle uptake into mammalian cells. *Nano Lett.* 6, 662 (**2006**). © 2006; From [102], B. D. Chithrani and W. C. W. Chan, Elucidating the mechanism of cellular uptake and removal of protein-coated gold nanoparticles of different sizes and shapes. *Nano Lett.* 7, 1542 (**2007**). © 2007. Whereas diagrams (b), (d) and (f) represent uncoated GNPs and their possible interaction with cell membranes. (a) and (b) represent GNP from 4 to 14 nm; (c) and (d) represent GNP from 30 to 50 nm; (e) and (f) represent GNP > 70 nm.

explained due to the binding capacity of the GNPs to the receptors. Experimental results showed a smaller dissociation constant value for 40 nm GNPs compared to smaller GNPs, therefore the authors suggest these GNPs could anchor to the cell surface with a higher binding avidity in contrast to 2 nm GNPs that lack multivalent binding and dissociate from the receptors before being wrapped.[100] GNPs larger than 70 nm lack membrane wrapping due to their high contact area and multivalent binding which reduces the receptor diffusion, restraining the cellular internalization given the depletion of receptor within the area of binding limiting the process of membrane wrapping that is necessary for nanoparticle internalization.[100] Chithrani et al.[102] showed that bigger NPs require a reduced wrapping time because of the slower receptor diffusion kinetics leading to the uptake of fewer NPs. As stated by Chithrani et al.[102] "The cellular uptake can be considered only as a result of competition between thermodynamic driving force for wrapping and the receptor diffusion kinetics. The thermodynamic driving force refers to the amount of free energy required to drive the NPs into the cell while the receptor diffusion kinetics refer to the kinetics of recruitment of receptors to the binding site." [102] Refer to Figure 8 for an illustrative diagram.

An interesting study has shown that 75 nm GNPs tend to immobilize in the cell membrane, although GNPs of 45 nm enter the cell through endocytosis and are accumulated in endosomal vesicles. The authors of this work suggest the different uses that these nanoparticles could have in nanomedicine, like imagenology for a 75 nm GNPs and drug delivery for a 45 nm (Fig. 9).[99]

It is fundamental to consider how the experiment was performed and which were the techniques used to define the amount of GNPs entering a cell. Not all the experiments that measure the uptake of GNPs through Inductively coupled plasma mass spectrometry (ICP-MS) or Inductively coupled plasma atomic emission spectroscopy (ICP-AES).[33, 35, 61, 103–105] consider the actual entry of GNPs. The analysis of ICP could also include those GNPs that are on the membrane surface, in such case an etching solution with low toxicity should be used in order to selectively remove the GNPs from the surface of a cell[59, 75] maintaining those GNPs inside a cell. Experiments that use Transmission Electron Microscopy[102] and/or Optical Sectioning Microscopy with Dark-field Illumination[99] provide a better picture on what happens in a cell regarding the GNPs uptake (Fig. 9).

4.2. GNRs

While studying the interaction of nanoparticles with membranes, the case of GNRs is different to spherical-GNPs mainly because of the aspect ratio between the length and width, which is an important factor regarding the interaction with the plasma membrane and subsequent cellular uptake. Qiu and co-workers.[103] conducted studies with GNRs capped with CTAB analyzing four aspect ratios (30×33, 21×40, 17×50 and 14×55 nm) demonstrating that as the aspect ratio increases, fewer GNRs were taken-up. Therefore, this authors postulate that the aspect ratio mediates the cellular uptake.[103]

In turn, Chithrani et al.[102] studied the internalization of GNRs coated with transferrin, presenting an aspect of 20×30, 14×50 and 7×42 nm. In this work, the authors conclude that the internalization of these GNRs decrease while their aspect ratio increases. They state that the width of a gold nanorod (GNR) would be more important than its length. The latter is because it is at the ends of the GNR where the ligand resides.[102, 106] Therefore, while GNR present a greater width, there is a higher coating degree that makes it more likely for the ligand molecule to contact its receptors.

On the other hand, Ghandehari's group[35] showed that GNRs coated with PEG, presenting an aspect ratio of 10×45 nm, were taken-up in greater proportion than the 10×35 nm GNRs. Therefore these authors say that GNRs with higher aspect ratio are internalized more than those with lower aspect ratio.[35]

The different conclusions presented by these works rely in several factors, for instance, in the different coatings used. Qiu et al.[103] worked with GNR coated with CTAB, which is a cationic surfactant used for the synthesis of GNR, this molecule is able to be placed on
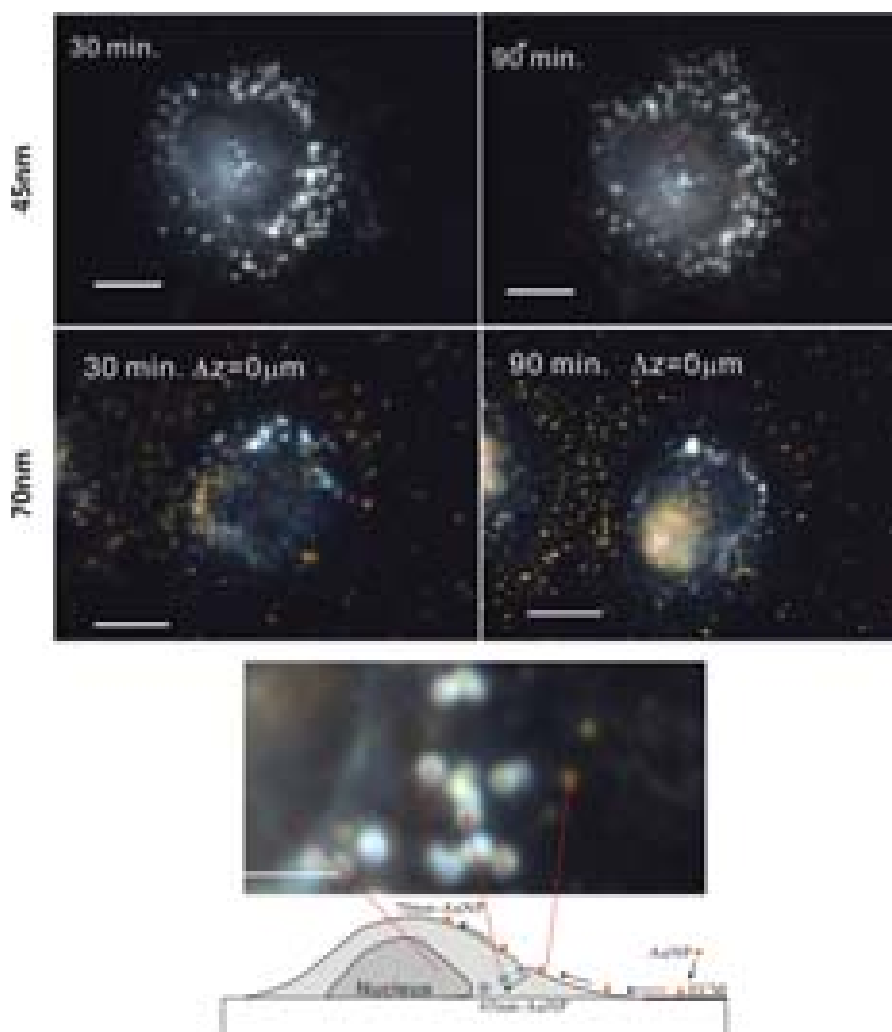
Fig. 9. Dark-field CCD images for 70-nm, 45-nm-GNPs and cells at different interaction time. The focus plane was fixed near the glass substrate, i.e., $\Delta z = 0$. The scale bar is 10 μm. An enlarged image with a representative diagram depicting the fact that many 45 nm GNPs are moved and then uptaken by cell, while many 75 nm-GNPs only moved to the apical surface of the cells. Adapted with permission from [99], S. H. Wang, et al., Size-dependent endocytosis of gold nanoparticles studied by three-dimensional mapping of plasmonic scattering images. *J. Nanobiotechnology* 8, 33 (**2010**). © 2010, Biomed. Central.

a GNR surface and thereby provides a positive coating in the entire GNR surface, which could contribute to its adsorption to the cell membrane[106] facilitating its internalization. Additionally, Ghandehari's group[35] used GNRs functionalized with PEG, preventing the interaction with certain proteins and molecules, thus decreasing it cellular internalization.[59, 107, 108] Considering the fact that GNR's functionalization occurs mainly at its ends,[109] the remaining CTAB molecules would stay throughout the length of the GNR, providing a positive surface charge density. Thus, GNRs with higher aspect ratio would have a greater positive surface charge density that would contribute to its internalization as it discussed in the case of cationic gold nanoparticles.[62, 63] Another factor that could affect in the internalization of GNRs is the exposure time, which is

different in the works herein discussed, and this could be a contributing factor in the internalization process.

Although the work of Qiu et al.[103] and Chithrani et al.[102] strongly demonstrate that the GNR internalization is greater when the aspect ratio is lower. These authors do not study GNRs with the same width; therefore this does not illustrate what are the effects in the uptake considering the same width. We believe that future investigations should analyze the uptake of GNRs with different aspect ratios, maintaining the width or length constant.

4.3. GNShs

To the best of our knowledge, there are very few published works regarding the use of GNShs in biomedicine, and

most of these works are based on the synthesis, characterization and functionalization of GNShs for its potential applications.[38, 110, 111] To the date, there are very few published studies regarding the toxicity and internalization of GNSh in cell cultures. This is mainly because the synthesis is more complex than other types of nanoparticles.

Liang and colleagues[65] studied the cellular internalization of 231 nm GNShs functionalized with meso-2,3-dimercaptosuccinic-acid (DMSA), which promotes intracellular destination.[112] It was shown that GNSh and GNSh-DMSA were able to enter in all the cell lines studied, observing a higher internalization for GNSh-DMSA. The authors suggest that this could be due to the different physicochemical properties affecting the interaction between the GNShs and serum proteins, which would affect in their interaction with cell membranes.[65] Moreover, a comparative study between GNS, GNR and GNShs functionalized with a negative ligand, demonstrated that 51 nm GNSh enter at a much lower rate than a 25 nm GNSs and a 17×47 nm GNRs.[61] The possible difference in the cellular uptake of the compared GNPs is due to the different surface charge densities and size, not due to its shape,[61] though GNSs and GNShs present similar shape, in this study they were not strictly compared. Therefore we believe that in order to understand how the shape of a GNShs affects in the cellular uptake and interaction with cell membrane, it is compulsory to maintain constant parameters between the nanoparticles of similar shape.

5. CONCLUSIONS AND FUTURE PROSPECTS

In this review we have summarized the different aspects that are important for the interaction between nanoparticles and membranes as surface charge, shape, size, order in the surface and capping of the nanomaterials. Most of the studies are focused in the interaction with cells and internalization processes; however it is necessary to extend the investigation to biophysical studies to determine the influence of the abovementioned parameters in the interaction with membrane cells. To obtain information of these interactions, it is fundamental to take advantage of the different existing techniques such as; AFM, cryo-TEM, SEM, Confocal Microscopy, Fluorescence Recovery After Photobleaching (FRAP), Fourier Transform Infrared Spectroscopy (FTIR). STM and Small Angle X-rays Scattering (SAXS) which will help us reveal structural details of the effects of nanomaterials on the membranes, for example by using SLB or liposomes. This investigation is in progress in our laboratories.

On the other hand, it is relevant to analyze the interaction of the nanomaterials with proteins that are present in the culture cell or *in vivo* which form the so-called Protein Corona. The true entity that is interacting with the biological system is the capped nanoparticle. Thus, it is important to carry out biophysical studies with the complete entity i.e., nanomaterial capped with the protein corona with model membranes. In this regard, the identification of the proteins that are forming the Protein Corona, by the use of proteomic tools, is currently in progress in our laboratory.

Several studies regarding the penetration of nanomaterials into cells have been carried out, but before this mechanism starts, the early biophysical interaction between the nanomaterial and membrane is crucial. In this regard, there is an open avenue to address this relevant issue. The phospholipids arrangement on nanoparticles surfaces is an important piece of information in the understanding of membrane-nanoparticle interactions and this aspect has received little attention. Indeed, most of the literature findings hypothesize about the final arrangement of phospholipids on the nanoparticle surface claiming that some energy gain would drive either their inclusion or penetration. In general, the energy cost is associated to various effects including, membrane bending and disruption, membrane distortion or defects generation and also unfavorable phospholipids surface interactions, whereas energy gain relies mainly on favorable phospholipids surface interaction. Experimental methods are now available to study phospholipids arrangement in a wide variety of substrates and templates, and this should prove valuable to the basic understanding of membrane-nanoparticle interactions, which is a crucial aspect when it comes to the biomedical applications of nanoparticles.

Current investigations address towards a new area of research; the surface charge density, size, shape, ligand feature and arrangement could govern the earlier interactions with cell membranes indicating the fate of the nanoparticle in the cell. In this sense, we believe it is necessary to emphasize biophysical studies for a thorough understanding of the NP-biological behavior in order to create better nanomaterials for drug-delivery.

References and Notes

1. P. Alivisatos, The use of nanocrystals in biological detection. *Nat. Biotech.* 22, 47 (**2004**).
2. J. Kim, S. Park, J. E. Lee, S. M. Jin, J. H. Lee, I. S. Lee, I. Yang, J.-S. Kim, S. K. Kim, M.-H. Cho, and T. Hyeon, Designed fabrication of multifunctional magnetic gold nanoshells and their application to magnetic resonance imaging and photothermal therapy. *Angew. Chem. Int. Ed.* 45, 7754 (**2006**).
3. E. Katz and I. Willner, Integrated nanoparticle—biomolecule hybrid systems: Synthesis, properties, and applications. *Angew. Chem. Int. Ed.* 43, 6042 (**2004**).
4. Z. Krpetic, F. Porta, and G. Scarì, Selective entrance of gold nanoparticles into cancer cells. *Gold Bulletin* 39, 66 (**2006**).

5. J. Panyam, W.-Z. Zhou, S. Prabha, S. K. Sahoo, and V. Labhesetwar, Rapid endo-lysosomal escape of poly(DL-lactide-co-glycolide) nanoparticles: Implications for drug and gene delivery. *The FASEB Journal* 16, 1217 (**2002**).

6. M. J. Kogan, N. G. Bastus, R. Amigo, D. Grillo-Bosch, E. Araya, A. Turiel, A. Labarta, E. Giralt, and V. F. Puntes, Nanoparticle-mediated local and remote manipulation of protein aggregation. *Nano Lett.* 6, 110 (**2006**).

7. O. Veiseh, C. Sun, J. Gunn, N. Kohler, P. Gabikian, D. Lee, N. Bhattarai, R. Ellenbogen, R. Sze, A. Hallahan, J. Olson, and M. Zhang, Optical and MRI multifunctional nanoprobe for targeting gliomas. *Nano Lett.* 5, 1003 (**2005**).

8. I. H. El-Sayed, X. Huang, and M. A. El-Sayed, Surface plasmon resonance scattering and absorption of anti-egfr antibody conjugated gold nanoparticles in cancer diagnostics: Applications in oral cancer. *Nano Lett.* 5, 829 (**2005**).

9. W. Jiang, E. Papa, H. Fischer, S. Mardyani, and W. C. W. Chan, Semiconductor quantum dots as contrast agents for whole animal imaging. *Trends in Biotechnology* 22, 607 (**2004**).

10. D. Boyer, P. Tamarat, A. Maali, B. Lounis, and M. Orrit, Photothermal imaging of nanometer-sized metal particles among scatterers. *Science* 297, 1160 (**2002**).

11. S. Berciaud, L. Cognet, G. A. Blab, and B. Lounis, Photothermal heterodyne imaging of individual nonfluorescent nanoclusters and nanocrystals. *Phys. Rev. Lett.* 93, 257402 (**2004**).

12. C. Sönnichsen, T. Franzl, T. Wilk, G. von Plessen, J. Feldmann, O. Wilson, and P. Mulvaney, Drastic reduction of plasmon damping in gold nanorods. *Phys. Rev. Lett.* 88, 077402 (**2002**).

13. J. Yguerabide and E. E. Yguerabide, Resonance light scattering particles as ultrasensitive labels for detection of analytes in a wide range of applications. *J. Cell. Biochem.* 84, 71 (**2001**).

14. P. Englebienne, A. Van Hoonacker, and M. Verhas, High-throughput screening using the surface plasmon resonance effect of colloidal gold nanoparticles. *Analyst* 126, 1645 (**2001**).

15. M. Karhanek, J. T. Kemp, N. Pourmand, R. W. Davis, and C. D. Webb, Single DNA molecule detection using nanopipettes and nanoparticles. *Nano Lett.* 5, 403 (**2005**).

16. I. L. Medintz, A. R. Clapp, J. S. Melinger, J. R. Deschamps, and H. A. Mattoussi, Reagentless biosensing assembly based on quantum dot–donor förster resonance energy transfer. *Advanced Materials* 17, 2450 (**2005**).

17. T. A. Taton, G. Lu, and C. A. Mirkin, Two-color labeling of oligonucleotide arrays via size-selective scattering of nanoparticle probes. *JACS* 123, 5164 (**2001**).

18. V. Haguet, D. Martin, L. Marcon, T. Heim, D. Stievenard, C. Olivier, O. El-Mahdi, and O. Melnyk, Combined nanogap nanoparticles nanosensor for electrical detection of biomolecular interactions between polypeptides. *Appl. Phys. Lett.* 84, 1213 (**2004**).

19. L. Marcon, D. Stiévenard, and O. Melnyk, Characterization of nanogap chemical reactivity using peptide-capped gold nanoparticles and electrical detection. *Bioconjugate Chem.* 19, 802 (**2008**).

20. R. Möller, A. Csáki, J. M. Köhler, and W. Fritzsche, Electrical classification of the concentration of bioconjugated metal colloids after surface adsorption and silver enhancement. *Langmuir* 17, 5426 (**2001**).

21. S.-J. Park, A. A. Lazarides, C. A. Mirkin, P. W. Brazis, C. R. Kannewurf, and R. L. Letsinger, The electrical properties of gold nanoparticle assemblies linked by DNA. *Angew. Chem. Int. Ed.* 39, 3845 (**2000**).

22. S.-J. Park, T. A. Taton, and C. A. Mirkin, Array-based electrical detection of dna with nanoparticle probes. *Science* 295, 1503 (**2002**).

23. O. D. Velev and E. W. Kaler, *In situ* assembly of colloidal particles into miniaturized biosensors. *Langmuir* 15, 3693 (**1999**).

24. N. Kohler, C. Sun, J. Wang, and M. Zhang, Methotrexate-modified superparamagnetic nanoparticles and their intracellular uptake into human cancer cells. *Langmuir* 21, 8858 (**2005**).

25. J. Panyam and V. Labhasetwar, Biodegradable nanoparticles for drug and gene delivery to cells and tissue. *Advanced Drug Delivery Reviews* 55, 329 (**2003**).

26. P.-H. Yang, X. Sun, J.-F. Chiu, H. Sun, and Q.-Y. He, Transferrin-mediated gold nanoparticle cellular uptake. *Bioconjugate Chem.* 16, 494 (**2005**).

27. J. Chen, B. Wiley, Li, Z.-Y., D. Campbell, F. Saeki, H. Cang, L. Au, J. Lee, X. Li, and Y. Xia, Gold nanocages: Engineering their structure for biomedical applications. *Adv. Mater.* 17, 2255 (**2005**).

28. L. R. Hirsch, R. J. Stafford, J. A. Bankson, S. R. Sershen, B. Rivera, R. E. Price, J. D. Hazle, N. J. Halas, and J. L. West, Nanoshell-mediated near-infrared thermal therapy of tumors under magnetic resonance guidance. *Proceedings of the National Academy of Sciences* 100, 13549 (**2003**).

29. E. Araya, I. Olmedo, N. G. Bastus, S. Guerrero, V. F. Puntes, E. Giralt, and M. J. Kogan, Gold nanoparticles and microwave irradiation inhibit beta-amyloid amyloidogenesis. *Nanoscale Research Letters* 3, 435 (**2008**).

30. I. Olmedo, E. Araya, F. Sanz, E. Medina, J. Arbiol, P. Toledo, A. Álvarez-Lueje, E. Giralt, and M. J. Kogan, How changes in the sequence of the peptide CLPFFD-NH$_2$ can modify the conjugation and stability of gold nanoparticles and their affinity for β-amyloid fibrils. *Bioconjugate Chem.* 19, 1154 (**2008**).

31. S. Guerrero, E. Araya, J. L. Fiedler, J. I. Arias, C. Adura, F. Albericio, E. Giralt, J. L. Arias, M. S. Fernández, and M. J. Kogan, Improving the brain delivery of gold nanoparticles by conjugation with an amphipatic peptide. *Nanomedicine* 5, 897 (**2010**).

32. S. Guerrero, J. R. Herance, S. Rojas, J. F. Mena, J. D. Gispert, G. A. Acosta, F. Albericio, and M. J. Kogan, Synthesis and *in vivo* evaluation of the biodistribution of a 18f-labeled conjugate gold-nanoparticle-peptide with potential biomedical application. *Bioconjugate Chem.* 23, 399 (**2012**).

33. A. M. Alkilany, P. K. Nagaria, C. R. Hexel, T. J. Shaw, C. J. Murphy, and M. D. Wyatt, Cellular uptake and cytotoxicity of gold nanorods: Molecular origin of cytotoxicity and surface effects. *Small* 5, 701 (**2009**).

34. H. J. Parab, H. M. Chen, T.-C. Lai, J. H. Huang, P. H. Chen, R.-S. Liu, M. Hsiao, C.-H. Chen, D.-P. Tsai, and Y.-K. Hwu, Biosensing, cytotoxicity, and cellular uptake studies of surface-modified gold nanorods. *J. Phys. Chem. C Nanomater. Interfaces* 113, 7574 (**2009**).

35. A. Malugin and H. Ghandehari, Cellular uptake and toxicity of gold nanoparticles in prostate cancer cells: A comparative study of rods and spheres. *J. Appl. Toxicol.* 30, 212 (**2010**).

36. M. J. Kogan, I. Olmedo, L. Hosta, R. A. Guerrero, L. J. Cruz, and F. Albericio, Peptides and metallic nanoparticles for biomedical applications. *Nanomedicine* 2, 287 (**2007**).

37. A. M. Alkilany and C. J. Murphy, Toxicity and cellular uptake of gold nanoparticles: What we have learned so far? *J. Nanopart Res.* 12, 2313 (**2010**).

38. T. Pham, J. B. Jackson, N. J. Halas, and T. R. Lee, Preparation and characterization of gold nanoshells coated with self-assembled monolayers. *Langmuir* 18, 4915 (**2002**).

39. B. Alberts, A. Johnson, J. Lewis, M. Raff, K. Roberts, and P. Walter, Molecular Cell Biology, 5th edn., Garland Science, New York (**2007**).

40. G. van Meer, D. R. Voelker, and G. W. Feigenson, Membrane lipids: Where they are and how they behave. *Nat. Rev. Mol. Cell Biol.* 9, 112 (**2008**).

41. K. Simons and W. L. Vaz, Model systems, lipid rafts, and cell membranes. *Annu. Rev. Biophys. Biomol. Struct.* 33, 269 (**2004**).

42. W. Dowhan, Molecular basis for membrane phospholipid diversity: Why are there so many lipids? *Annual Review of Biochemistry* 66, 199 (**1997**).

REVIEW

43. M. Edidin, The state of lipid rafts: From model membranes to cells. *Annu. Rev. Biophys. Biomol. Struct.* 32, 257 (**2003**).

44. S. D. Conner and S. L. Schmid, Regulated portals of entry into the cell. *Nature* 422, 37 (**2003**).

45. A. Verma, O. Uzun, Y. Hu, H. S. Han, N. Watson, S. Chen, D. J. Irvine, and F. Stellacci, Surface-structure-regulated cell-membrane penetration by monolayer-protected nanoparticles. *Nat. Mater.* 7, 588 (**2008**).

46. P. R. Leroueil, S. Hong, A. Mecke, J. R. Baker, B. G. Orr, and M. M. B. Holl, Nanoparticle interaction with biological membranes: Does nanotechnology present a janus face? *Accounts of Chemical Research* 40, 335 (**2007**).

47. P. R. Leroueil, S. A. Berry, K. Duthie, G. Han, V. M. Rotello, D. Q. McNerny, J. R. Baker, B. G. Orr, and M. M. B. Holl, Wide varieties of cationic nanoparticles induce defects in supported lipid bilayers. *Nano Lett.* 8, 420 (**2008**).

48. Y. Roiter, M. Ornatska, A. R. Rammohan, J. Balakrishnan, D. R. Heine, and S. Minko, Interaction of nanoparticles with lipid membrane. *Nano Lett.* 8, 941 (**2008**).

49. H.-M. Ding, W.-D. Tian, and Y.-Q. Ma, Designing nanoparticle translocation through membranes by computer simulations. *ACS Nano* 6, 1230 (**2012**).

50. A. Mecke, I. J. Majoros, A. K. Patri, J. R. Baker, M. M. B. Holl, and B. G. Orr, Lipid bilayer disruption by polycationic polymers: The roles of size and chemical functional group. *Langmuir* 21, 10348 (**2005**).

51. A. Alessandrini and P. Facci, Unraveling lipid/protein interaction in model lipid bilayers by atomic force microscopy. *J. Mol. Recognit.* 24, 387 (**2011**).

52. Y. H. Chan and S. G. Boxer, Model membrane systems and their applications. *Curr. Opin. Chem. Biol.* 11, 581 (**2007**).

53. A. Berquand, M. P. Mingeot-Leclercq, and Y. F. Dufrene, Real-time imaging of drug-membrane interactions by atomic force microscopy. *Biochim. Biophys. Acta* 1664, 198 (**2004**).

54. M. P. Mingeot-Leclercq, M. Deleu, R. Brasseur, and Y. F. Dufrene, Atomic force microscopy of supported lipid bilayers. *Nat. Protoc.* 3, 1654 (**2008**).

55. G. Kada, F. Kienberger, and P. Hinterdorfer, Atomic force microscopy in bionanotechnology. *Nano Today* 3, 12 (**2008**).

56. J. K. Vasir and V. Labhasetwar, Quantification of the force of nanoparticle-cell membrane interactions and its influence on intracellular trafficking of nanoparticles. *Biomaterials* 29, 4244 (**2008**).

57. S. Garcia-Manyes, P. Gorostiza, and F. Sanz, titration force microscopy on supported lipid bilayers. *Anal. Chem.* 78, 61 (**2005**).

58. S. H. Park, S. G. Oh, J. Y. Mun, and S. S. Han, Loading of gold nanoparticles inside the DPPC bilayers of liposome and their effects on membrane fluidities. *Colloids Surf. B Biointerfaces* 48, 112 (**2006**).

59. E. C. Cho, Q. Zhang, and Y. Xia, The effect of sedimentation and diffusion on cellular uptake of gold nanoparticles. *Nat. Nano* 6, 385 (**2011**).

60. T. Lund, M. F. Callaghan, P. Williams, M. Turmaine, C. Bachmann, T. Rademacher, I. M. Roitt, and R. Bayford, The influence of ligand organization on the rate of uptake of gold nanoparticles by colorectal cancer cells. *Biomaterials* 32, 9776 (**2011**).

61. D. Bartczak, O. L. Muskens, S. Nitti, T. Sanchez-Elsner, T. M. Millar, and A. G. Kanaras, Interactions of human endothelial cells with gold nanoparticles of different morphologies. *Small* 8, 122 (**2012**).

62. J. Lin, H. Zhang, Z. Chen, and Y. Zheng, Penetration of lipid membranes by gold nanoparticles: Insights into cellular uptake, cytotoxicity, and their relationship. *ACS Nano* 4, 5421 (**2010**).

63. J. Q. Lin, Y. G. Zheng, H. W. Zhang, and Z. Chen, A simulation study on nanoscale holes generated by gold nanoparticles on negative lipid bilayers. *Langmuir* 27, 8323 (**2011**).

64. R. R. Arvizo, O. R. Miranda, M. A. Thompson, C. M. Pabelick, R. Bhattacharya, J. D. Robertson, V. M. Rotello, Y. S. Prakash, and P. Mukherjee, Effect of nanoparticle surface charge at the plasma membrane and beyond. *Nano Lett.* 10, 2543 (**2010**).

65. Z. Liang, Y. Liu, X. Li, Q. Wu, J. Yu, S. Luo, L. Lai, and S. Liu, Surface-modified gold nanoshells for enhanced cellular uptake. *Journal of Biomedical Materials Research Part A* 98A, 479 (**2011**).

66. C. M. Goodman, C. D. McCusker, T. Yilmaz, and V. M. Rotello, Toxicity of gold nanoparticles functionalized with cationic and anionic side chains. *Bioconjugate Chem.* 15, 897 (**2004**).

67. C. L. Ting and Z.-G. Wang, Interactions of a charged nanoparticle with a lipid membrane: Implications for gene delivery. *Biophysical Journal* 100, 1288 (**2011**).

68. Y. Li, X. Chen, and N. Gu, Computational investigation of interaction between nanoparticles and membranes: Hydrophobic/hydrophilic effect. *J. Phys. Chem. B* 112, 16647 (**2008**).

69. V. V. Ginzburg and S. Balijepalli, Modeling the thermodynamics of the interaction of nanoparticles with cell membranes. *Nano Lett.* 7, 3716 (**2007**).

70. S. Zhang, A. Nelson, and P. A. Beales, Freezing or wrapping: The role of particle size in the mechanism of nanoparticle—biomembrane interaction. *Langmuir* 28, 12831 (**2012**).

71. K. Weiß and J. Enderlein, Lipid diffusion within black lipid membranes measured with dual-focus fluorescence correlation spectroscopy. *Chem. Phys. Chem.* 13, 990 (**2012**).

72. J. Schneider, W. Barger, and G. U. Lee, Nanometer scale surface properties of supported lipid bilayers measured with hydrophobic and hydrophilic atomic force microscope probes. *Langmuir* 19, 1899 (**2003**).

73. A. S. Urban, T. Pfeiffer, M. Fedoruk, A. A. Lutich, and J. Feldmann, Single-step injection of gold nanoparticles through phospholipid membranes. *ACS Nano* 5, 3585 (**2011**).

74. J. Raz and K. Sofiya, Membrane interactions of host-defense peptides studied in model systems. *Current Protein and Peptide Science* 6, 103 (**2005**).

75. E. C. Cho, J. Xie, P. A. Wurm, and Y. Xia, Understanding the role of surface charges in cellular adsorption versus internalization by selectively removing gold nanoparticles on the cell surface with a I2/KI etchant. *Nano Lett.* 9, 1080 (**2009**).

76. A. Verma and F. Stellacci, Effect of surface properties on nanoparticle-cell interactions. *Small* 6, 12 (**2010**).

77. D. A. Giljohann, D. S. Seferos, P. C. Patel, J. E. Millstone, N. L. Rosi, and C. A. Mirkin, Oligonucleotide loading determines cellular uptake of DNA-modified gold nanoparticles. *Nano Lett.* 7, 3818 (**2007**).

78. S. H. D. P. Lacerda, J. J. Park, C. Meuse, D. Pristinski, M. L. Becker, A. Karim, and J. F. Douglas, Interaction of gold nanoparticles with common human blood proteins. *ACS Nano* 4, 365 (**2009**).

79. M. A. Dobrovolskaia, A. K. Patri, J. Zheng, J. D. Clogston, N. Ayub, P. Aggarwal, B. W. Neun, J. B. Hall, and S. E. McNeil, Interaction of colloidal gold nanoparticles with human blood: Effects on particle size and analysis of plasma protein binding profiles. *Nanomedicine: Nanotechnology, Biology and Medicine* 5, 106 (**2009**).

80. M. Zheng, F. Davidson, and X. Huang, Ethylene glycol monolayer protected nanoparticles for eliminating nonspecific binding with biological molecules. *J. Am. Chem. Soc.* 125, 7790 (**2003**).

81. M. Zheng, Z. Li, and X. Huang, Ethylene glycol monolayer protected nanoparticles: Synthesis, characterization, and interactions with biological molecules. *Langmuir* 20, 4226 (**2004**).

82. L. N. Patel, J. L. Zaro, and W. C. Shen, Cell penetrating peptides: Intracellular pathways and pharmaceutical perspectives. *Pharm. Res.* 24, 1977 (**2007**).

83. B. Jing and Y. Zhu, Disruption of supported lipid bilayers by semi-hydrophobic nanoparticles. *J. Am. Chem. Soc.* 133, 10983 (**2011**).

84. A. R. Guerrero, L. Caballero, A. Adeva, F. Melo, and M. J. Kogan, Exploring the surface charge on peptide-gold nanoparticle conjugates by force spectroscopy. *Langmuir* 26, 12026 (**2010**).

20

*J. Biomater. Tissue Eng. 3, 4–21, **2013***

85. A. S. Thakor, J. Jokerst, C. Zavaleta, T. F. Massoud, and S. S. Gambhir, Gold nanoparticles: A revival in precious metal administration to patients. *Nano Lett.* 11, 4029 (**2011**).

86. L. Hosta-Rigau, I. Olmedo, J. Arbiol, L. J. Cruz, M. J. Kogan, and F. Albericio, Multifunctionalized gold nanoparticles with peptides targeted to gastrin-releasing peptide receptor of a tumor cell line. *Bioconjugate Chem.* 21, 1070 (**2010**).

87. A. Albanese, P. S. Tang, and W. C. Chan, The effect of nanoparticle size, shape, and surface chemistry on biological systems. *Annu. Rev. Biomed. Eng.* 14, 1 (**2012**).

88. S. D. Perrault and W. C. W. Chan, *In vivo* assembly of nanoparticle components to improve targeted cancer imaging. *Proceedings of the National Academy of Sciences* 107, 11194 (**2010**).

89. S. D. Perrault, C. Walkey, T. Jennings, H. C. Fischer, and W. C. W. Chan, Mediating tumor targeting efficiency of nanoparticles through design. *Nano Lett.* 9, 1909 (**2009**).

90. X. Li, H. Zhou, L. Yang, G. Du, A. S. Pai-Panandiker, X. Huang, and B. Yan, Enhancement of cell recognition *in vitro* by dual-ligand cancer targeting gold nanoparticles. *Biomaterials* 32, 2540 (**2011**).

91. J. A. Yang and C. J. Murphy, Evidence for patchy lipid layers on gold nanoparticle surfaces. *Langmuir* 28, 5404 (**2012**).

92. W. C. Hou, B. Y. Moghadam, C. Corredor, P. Westerhoff, and J. D. Posner, Distribution of functionalized gold nanoparticles between water and lipid bilayers as model cell membranes. *Environ Sci. Technol.* 46, 1869 (**2012**).

93. C. C. Leduc, J.-M. Jung, R. R. Carney, F. Stellacci, and B. Lounis, Direct investigation of intracellular presence of gold nanoparticles via photothermal heterodyne imaging. *ACS Nano* 5, 2587 (**2011**).

94. J. A. Ryan, K. W. Overton, M. E. Speight, C. N. Oldenburg, L. Loo, W. Robarge, S. Franzen, and D. L. Feldheim, Cellular uptake of gold nanoparticles passivated with BSA-SV40 large T antigen conjugates. *Anal. Chem.* 79, 9150 (**2007**).

95. M. Tsoli, H. Kuhn, W. Brandau, H. Esche, and G. Schmid, Cellular uptake and toxicity of Au55 clusters. *Small* 1, 841 (**2005**).

96. E. E. Connor, J. Mwamuka, A. Gole, C. J. Murphy, and M. D. Wyatt, Gold nanoparticles are taken up by human cells but do not cause acute cytotoxicity. *Small* 1, 325 (**2005**).

97. Y. Pan, A. Leifert, D. Ruau, S. Neuss, J. Bornemann, G. Schmid, W. Brandau, U. Simon, and W. Jahnen-Dechent, Gold nanoparticles of diameter 1.4 nm trigger necrosis by oxidative stress and mitochondrial damage. *Small* 5, 2067 (**2009**).

98. B. D. Chithrani, A. A. Ghazani, and W. C. W. Chan, Determining the size and shape dependence of gold nanoparticle uptake into mammalian cells. *Nano Lett.* 6, 662 (**2006**).

99. S. H. Wang, C. W. Lee, A. Chiou, and P. K. Wei, Size-dependent endocytosis of gold nanoparticles studied by three-dimensional mapping of plasmonic scattering images. *J. Nanobiotechnology* 8, 33 (**2010**).

100. W. Jiang, B. Y. Kim, J. T. Rutka, and W. C. Chan, Nanoparticle-mediated cellular response is size-dependent. *Nat. Nanotechnol.* 3, 145 (**2008**).

101. T. Yue and X. Zhang, Cooperative effect in receptor-mediated endocytosis of multiple nanoparticles. *ACS Nano* 6, 3196 (**2012**).

102. B. D. Chithrani and W. C. W. Chan, Elucidating the mechanism of cellular uptake and removal of protein-coated gold nanoparticles of different sizes and shapes. *Nano Lett.* 7, 1542 (**2007**).

103. Y. Qiu, Y. Liu, L. Wang, L. Xu, R. Bai, Y. Ji, X. Wu, Y. Zhao, Y. Li, and C. Chen, Surface chemistry and aspect ratio mediated cellular uptake of Au nanorods. *Biomaterials* 31, 7606 (**2010**).

104. De W. H. Jong, W. I. Hagens, P. Krystek, M. C. Burger, A. J. Sips, and R. E. Geertsma, Particle size-dependent organ distribution of gold nanoparticles after intravenous administration. *Biomaterials* 29, 1912 (**2008**).

105. Y. Liu, M. K. Shipton, J. Ryan, E. D. Kaufman, S. Franzen, and D. L. Feldheim, Synthesis, stability, and cellular internalization of gold nanoparticles containing mixed peptide-poly(ethylene glycol) monolayers. *Anal. Chem.* 79, 2221 (**2007**).

106. J. Y. Chang, H. Wu, H. Chen, Y. C. Ling, and W. Tan, Oriented assembly of Au nanorods using biorecognition system. *Chem. Commun.* (*Camb.*) 1092 (**2005**).

107. M. R. Hamblin, J. L. Miller, I. Rizvi, H. G. Loew, and T. Hasan, Pegylation of charged polymer-photosensitiser conjugates: Effects on photodynamic efficacy. *Br. J. Cancer* 89, 937 (**2003**).

108. D. P. K. Lankveld, R. G. Rayavarapu, P. Krystek, and A. G. Oomen, H. W. Verharen, T. G. van Leeuwen, W. H. De Jong, and S. Manohar, Blood clearance and tissue distribution of PEGylated and non-PEGylated gold nanorods after intravenous administration in rats. *Nanomedicine* 6, 339 (**2011**).

109. K. K. Caswell, J. N. Wilson, U. H. F. Bunz, and C. J. Murphy, Preferential end-to-end assembly of gold nanorods by biotin-streptavidin connectors. *Journal of the American Chemical Society* 125, 13914 (**2003**).

110. G. Wu, A. Mikhailovsky, H. A. Khant, and J. A. Zasadzinski, Synthesis, characterization, and optical response of gold nanoshells used to trigger release from liposomes, Methods Enzymol (**2009**), Chap. 14, Vol. 464, p. 279.

111. N. Garrett, M. Whiteman, and J. Moger, Imaging the uptake of gold nanoshells in live cells using plasmon resonance enhanced four wave mixing microscopy. *Opt. Express* 19, 17563 (**2011**).

112. C. Wilhelm, C. Billotey, J. Roger, J. N. Pons, J. C. Bacri, and F. Gazeau, Intracellular uptake of anionic superparamagnetic nanoparticles as a function of their surface coating. *Biomaterials* 24, 1001 (**2003**).

113. D. Bartczak, O. L. Muskens, T. M. Millar, T. Sanchez-Elsner, and A. G. Kanaras, Laser-induced damage and recovery of plasmonically targeted human endothelial cells. *Nano Lett.* 11, 1358 (**2011**).

REVIEW

REVIEW

Nanoparticle-in-Microparticle Delivery Systems (NiMDS): Production, Administration Routes and Clinical Potential

Julieta C. Imperiale[1] and Alejandro Sosnik[1, 2, *]

[1]*Faculty of Pharmacy and Biochemistry, The Group of Biomaterials and Nanotechnology for Improved Medicines (BIONIMED), Department of Pharmaceutical Technology, University of Buenos Aires, Buenos Aires CP1113, Argentina*
[2]*National Science Research Council (CONICET), Buenos Aires, Argentina*

Microparticles (MPs) and nanoparticles (NPs) have received considerable attention for the design of drug delivery systems (DDS) with unique properties owing to the increased surface area and the ability to fine tune the release process. More recently, a new type of DDS that capitalize on the advantages of both NPs and MPs has been introduced. Nanoparticle-in-Microparticle Delivery Systems (NiMDS) comprise the encapsulation of NPs within MPs and lead to features that are unique and different from those of the individual components. These technology platforms can be produced employing from conventional to more sophisticated methodologies and equipment and they are administered by different routes such as oral, pulmonary or even parenteral. Moreover, if designed appropriately, "they can (i) protect drug payloads and prevent physical and chemical instability phenomena in the biological environment, (ii) improve the release profile of the encapsulated agent, (iii) reduce or eliminate the burst effect and (iv) target specific cells, tissues and organs." Should be changed to "they can protect drug payloads and prevent physical and chemical instability phenomena in the biological environment, improve the release profile of the encapsulated agent, reduce or eliminate the burst effect and target specific cells, tissues and organs."

Keywords: Nanoparticle-in-Microparticle Delivery Systems, Burst Effect Control, Release Kinetics Fine Tuning, Drug Targeting.

CONTENTS

1. INTRODUCTION

Over the last decades, the development of drug-loaded microparticles (MPs) and nanoparticles (NPs) have revolutionized the field of pharmaceutical technology. The ability to control the particle size and the unique properties conferred by the increased surface area allowed these particles to become key players in the drug delivery market. However, some drawbacks such as initial burst effect, difficulty in controlling the release profile, inability of targeting the drug to specific body sites still persist and they jeopardize the chances of bench-to-bedside translation.[1, 2] In light of this, researchers have devoted great efforts to modify these systems in order to exploit the advantages derived from their small dimension, while overcoming the main limitations. In this context, a novel technological platform called Nanoparticle-in-Microparticle Delivery System (NiMDS) has emerged. These carriers are comprised of three main components: (i) the core material or nano-platform, (ii) the payload to be released and (iii) the shell material or micro-platform (Fig. 1).
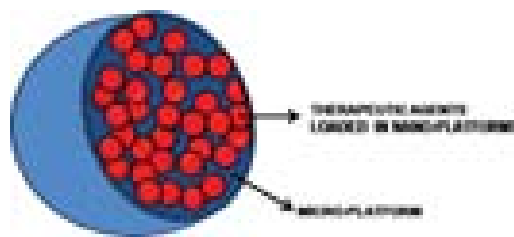
Fig. 1. Schematic illustration showing the components of Nanoparticle-in-Microparticle Delivery Systems (NiMDS).

The NPs can be dispersed through the entire MP matrix (Fig. 2(A)), they can encapsulated within the MP core (Fig. 2(B)) or adsorbed onto the surface of the MP (Fig. 2(C)). This unique disposition permits to control the pattern and rate of the drug release process.

A thorough review of the literature shows that there are numerous types of organic and inorganic nano-platforms that could be encapsulated within the micro-platform. Organic nano-platforms include polymeric[3–5] and solid lipid NPs,[6,7] polymeric micelles[8] and liposomes.[9–12] Meanwhile, inorganic nano-platforms usually comprise metallic[13,14] and silica NPs.[15–17] Due to their more extensive application in drug delivery, this work will be dedicated exclusively to organic nano-platforms. It is worth mentioning that employment of pure drug NPs (nano-crystals) as the nano-platform to be microencapsulated is a simplified useful strategy;[18–20] nanocrystals are drug NPs composed of 100% drug. In this case, there is not nanocarrier and the NiMDS is limited to two components. The main use of pure drug NPs is in dissolution enhancement because according to the Noyes and Whitney law, the greater the surface area of the powder, the greater and the faster the dissolution rate. For this reason, nanocrystals represent an effective tool to increase the dissolution rate of poorly water soluble drugs classified in the Class II and IV of the Biopharmaceutic Classification System (BCS) show poor aqueous solubility and do not dissolve adequately during their transit through the gastrointestinal tract (GIT). This nanoplatform is meaningless for most of the Class I and III compounds because their entire dose would dissolve rapidly in the biological environment. Several groups have developed drug nanocrystals that were further microencapsulated to achieve not only a better dissolution, but also a better control of the release kinetics.[18–20]

The selection of the core material is widely dependent on the properties of the encapsulated payload such

REVIEW

Julieta C. Imperiale received a Pharmacy degree at the Faculty of Pharmacy and Biochemistry of the University of Buenos Aires (FFyB-UBA) in 2010. Currently, she is a Ph.D. candidate in The Group of Biomaterials and Nanotechnology for Improved Medicines (BIONIMED), Department of Pharmaceutical Technology (FFyB-UBA) under the direction of Professor Dr. Alejandro Sosnik. Her research is focused on the application of micro/nanotechnology strategies for the improvement of the pharmacotherapy of Human Immunodeficiency Virus/Acquired Immunodeficiency Syndrome.

Alejandro Sosnik is Adjunct Professor (tenure) of Pharmaceutical Technology (Faculty of Pharmacy and Biochemistry, University of Buenos Aires) and Investigator of the National Science Research Council (CONICET). He received a Pharmacy degree of the University of Buenos Aires (1994) and a and Ph.D. in Applied Chemistry (Biomaterials Science) at the Casali Institute of Applied Chemistry (The Hebrew University of Jerusalem, Israel, 2003), under the supervision of Professor Daniel Cohn. Between 2003 and 2006, Dr. Sosnik spent a postdoctoral stay in the laboratory of Professor Michael Sefton (Institute of Chemical Engineering and Applied Chemistry, University of Toronto, Canada). Upon his return to Argentina in 2006, he founded "The Group of Biomaterials and Nanotechnology for Improved Medicines" (BIONIMED), a research group that works at the interface of bio-materials science, nanotechnology and pharmaceutical sciences. His main research interests are focused on the exploration of novel micro/nanotechnologies for the encapsulation, delivery and targeting of drugs involved in the pharmacotherapy of poverty-related diseases. He is a founding member of the Argentine Society for Nanomedicines (NANOMED-ar), where he serves as Secretary. He is also visiting professor and scientist at the National University of Colombia, the University of Santiago de Compostela, the Council for Scientific and Industrial Research of South Africa and the National Autonomous University of Mexico. He currently coordinates the "Iberoamerican Network of New Materials for the Design of Advanced Drug Delivery Systems in Diseases of High Socioeconomic Impact" (RIMADEL) of the CYTED Program.
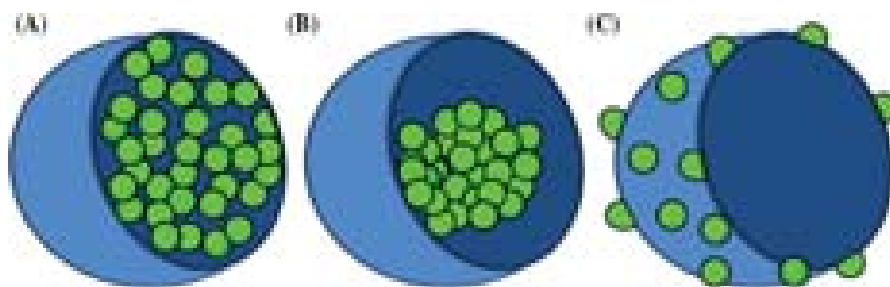
Fig. 2. Schematic representation of the three possible dispositions of NPs within MPs. (A) NPs dispersed through the entire MP matrix, (B) NPs encapsulated within the MP core and (C) NPs adsorbed onto the surface of the MP.

as size, lipophilicity, surface charge and therapeutic index. A main technological advantage of the nano-platform is its high encapsulation capacity. Based on this, NiMDS have become an appealing strategy to combine both nano-structure for maximum drug loading and microstructure to improve the delivery of the payload.[21, 22]

This review describes the most popular methods for NiMDS preparation and the administration routes explored and it highlights the potential advantages of NiMDS over simple NPs and MPs. A thorough overview of the poly-mers feasible for this application and the variety of drugs that have been explored is presented. This integrated glance about NiMDS permits to understand how this novel hybrid technology provides a valuable platform for the enhancement of drug delivery.

2. APPLICATIONS OF NiMDS

2.1. Protection of the Payload

MPs and NPs are useful means to protect the payload against enzymatic and hydrolytic degradation in the GIT by preventing the direct contact between the drug and the biological fluids.[23, 24] However, sometimes the protec-tion provided by these particles is not efficient enough to prevent the release of the drug at an inappropriate time point/rate and body site. For example, gelatin is one of the most promising materials for the delivery of nucleic acids, peptides and proteins owing to its hydrophilic nature, non-toxicity, good biocompatibility and biodegradability properties.[25] It is reported that gelatin undergoes fast degra-dation by proteases, abundantly present in the stomach. Since nucleic acids, peptides and proteins are also sensi-tive to low pH values and gastric enzymes, gelatin becomes an ineffective carrier for the oral administration of these cargos because it would allow their early release in the stomach. In this context, the microencapsulation of gelatin NPs using a polymer that withstands the gastric pH and degrades or dissolves in the bowel would ensure the release of the drug-loaded NPs and the encapsulated agent in the appropriate site. For example, Bhavsar and Amiji devel-oped plasmid DNA encoding ß-galactosidase or enhanced green fluorescent protein (EGFP), respectively, loaded

within gelatin NPs that were further encapsulated in PCL microspheres.[26] Optimization of this system was achieved using a 3^3 randomized full factorial design through which it was possible to assess the influence of variables such as polymer concentration in the organic phase, amount of NPs added as internal phase and the homogenization speed on the particle size of NiMDS.[27] To evaluate the biodis-tribution, ^{111}In-radiolabeled gelatin NPs alone or encapsu-lated within PCL microspheres were administered by the oral route to fasted Wistar rats. Organs were harvested at different time points to measure the ^{111}In concentration. Gelatin NPs went through the GIT rather quickly and a high accumulation was found in the large intestine after 1 h. Conversely, NiMDS resided first in the stomach (1 h) and then they were transferred predominantly to the large intestine (after 2 h).[26] To assess the effect of this biodis-tribution profile on transfection, DNA-loaded gelatin NPs and NiMDS were administered orally to fasted rats and after five days, they were sacrificed and the GIT was har-vested for analysis. Results did not show any transfection with DNA-loaded gelatin NPs, while apparent transgene expression in the small and large intestines was observed with DNA-loaded NiMDS (Fig. 3).

Based on these results, Bhavsar et al. suggested that free gelatin NPs were degraded by proteolytic enzymes present in stomach and the gut and that the high radioac-tivity levels found in the large intestine derived proba-bly from protein fragments rather than intact NPs. In the case of NiMDS, a certain fraction remained intact until it reached the large intestine and it could potentially trans-fect the encapsulated plasmid DNA. Similar results were obtained in studies conducted with Balb/c mice.[28] Other groups have reproduced the same platform, namely, gelatin NPs in PCL microspheres to load diverse pharmacologi-cally active agents like TNF-α-specific small interfering RNA (siRNA),[29] TNF-α and cyclin D1-specific siRNA[5] and plasmid DNA encoding IL-10,[30] obtaining in the all cases encouraging results.

Similar to gelatin, liposomes display an extremely low stability in the gastrointestinal environment where they are rapidly degraded[2] and in the blood stream[31] where they are phagocytozed by cells of the reticuloendothelial sys-tem (RES). Thus, the microencapsulation of liposomes
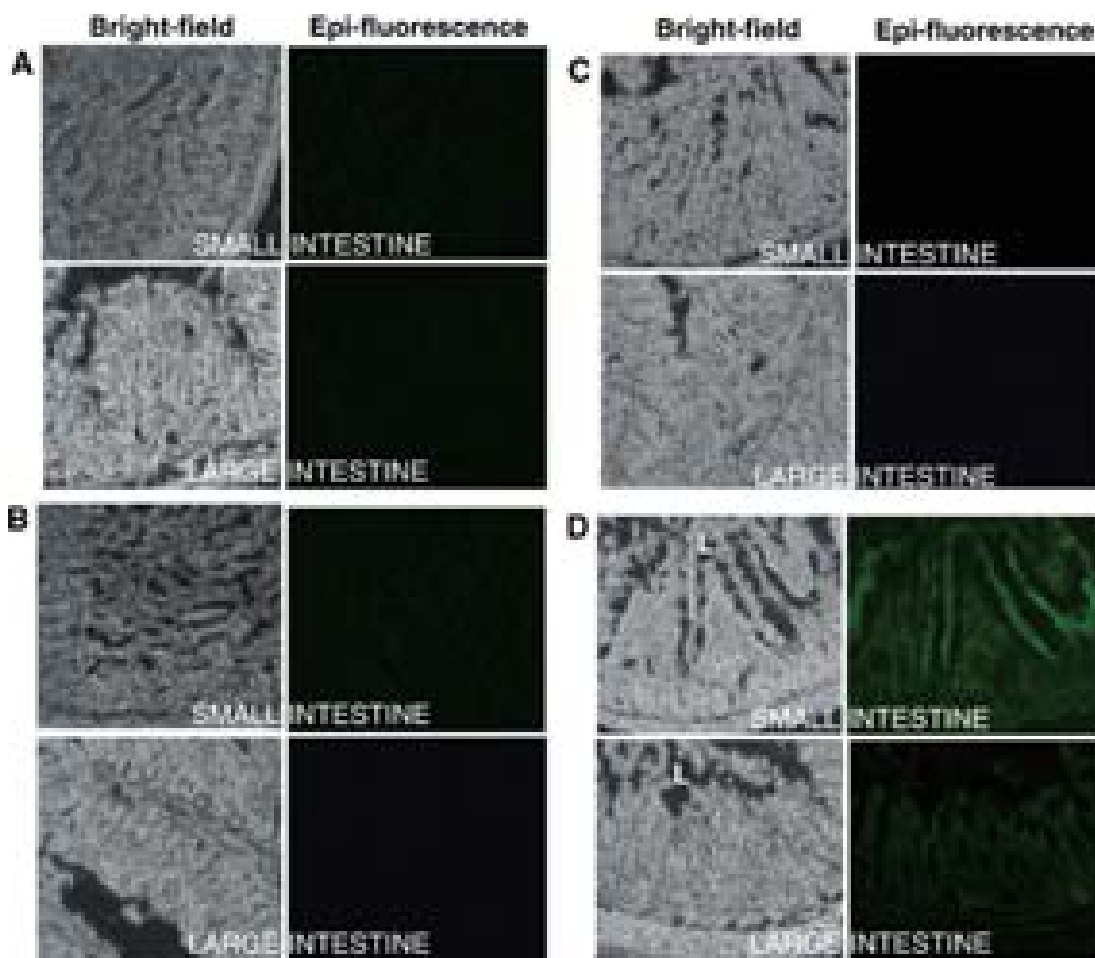
Fig. 3. Qualitative enhanced green fluorescent protein (EGFP) expression in the small and large intestines of Wistar rats after oral administration of saline (A), naked pEGFP-N1 plasmid DNA (B), EGFP-N1 plasmid DNA encapsulated in gelatin NPs (C), and EGFP-N1 plasmid DNA encapsulated in NiMDS (D). Reproduced with permission from [26], M. D. Bhavsar and M. M. Amiji, *J. Control Release* 119, 339 (**2007**). © 2007, Elsevier.

stabilized them in the hydrolytic environment of the GIT[2] and prolonged the circulation time upon parenteral administration.[11, 32]

2.2. Reduction or Elimination of the Burst Effect

Burst effect is a phenomenon taking place during the first minutes of contact between the DDS and the biological environment. It is characterized by the fast release of a substantial fraction of the cargo before a stable release profile is attained and it may lead to adverse effects, especially in case of low therapeutic index drugs.[33, 34] MPs and NPs are not an exception and they often exhibit a burst effect *in vivo* which is unpredictable and difficult to control[1, 35, 36] There are several reasons for which this early release occurs:

 (i) Heterogeneous drug distribution owing to the presence of drug crystals having ready access to the particle surface either by direct contact with the medium or through pores and channels that connect the interior with the microsphere

surface; in this case the release of these drug is not controlled by the polymeric matrix.[37–44]

 (ii) Temperature, that affects not only drug distribution but also the morphology of the particles, is another parameter of consideration.[45]

 (iii) The physicochemical nature of the polymer and the drug also play fundamental roles;[46, 47] it is well known that the diffusion coefficient of a dispersed drug is much higher in an amorphous polymer than in a crystalline one.[48, 49] Thus, the degree of crystallinity will have a tremendous impact on the release rate and the appearance of burst effect.

 (iv) The lipophilicity of both the polymer and the drug. The lipophilic nature of the polymer slows down the permeation of water molecules into the polymeric matrix, whereas a more hydrophilic drug will tend to diffuse more quickly towards the surrounding aqueous phase.

 (v) The size of the loaded drug is an additional noteworthy parameter; larger particles have a greater chance of an

incomplete encapsulation than smaller ones, bursting the release.[50–55]

(vi) The porosity of the particles due to the use of the emulsion-solvent evaporation/extraction technique; the elimination of the organic solvent leads to the formation of pores distributed across the structure.[33, 56]

Aiming to prevent the burst effect and to control the release kinetics, several strategies have been pursued.[10, 36, 57–59] Among them, NiMDS have shown very promising results.[54, 60, 61] As abovementioned, smaller particles are more likely to be completely encapsulated than larger ones. Thus, two approaches could be followed to reduce the size of the drug payload to the nano-scale and to ensure the efficient microencapsulation in a later stage: (i) production of pure drug NPs by nanonization[52, 62, 63] or (ii) drug encapsulation within a nanocarrier.[32, 50, 64] Besides, when the drug is not nanonized but it is previously encapsulated within a polymeric or lipidic nanocarrier, drug molecules have to overcome two barriers to be released. First, the NP matrix and second the outer matrix of the microparticle, the latter contributing more crucially to decrease the burst effect.[34] Comparing the release profile of NPs, MPs and NiMDS, it could be concluded that the burst release is much more notorious in NPs than in MPs due to their smaller size. The lowest burst effect being achieved with NiMDS[36, 65] (Table I). Moreover, the fine tuning of the carrier lipophilic-hydrophilic balance (HLB) plays an important role in achieving a decrease of the burst effect. NiMDS made with hydrophobic polymers such as poly(lactic acid) (PLA), poly(lactic-co-glycolic) acid (PLGA) acid (PLGA), PCL, Eudragit® RS 100 (a copolymer of ethylacrylate, methylmethacrylate and methacrylic acid esterified with quaternary ammonium groups), ethylcellulose (EC) for both the NP and the MP diminish or eliminate the burst effect more effectively than hydrophilic polymers such as gelatin, alginate, and chitosan.[36]

Furthermore, there are differences among the hydrophobic polymers; the greater the hydrophobicity of the polymer, the smaller the burst effect. For example, Eudragit® RS 100 is more hydrophilic than EC due to the presence of quaternary ammonium moieties that increase the permeability to water and thus the burst effect and the drug release (Table I).

Summarizing, it was demonstrated by different research groups that NiMDS can reduce or eliminate burst effect efficiently, which is of special interest in formulations intended to release over several weeks or months[36] and to diminish and control the toxic side effects of highly potent drugs.[34]

2.3. Fine Tuning of the Release Profile

In recent years, a lot of research was dedicated to develop drug-loaded NPs and MPs that ensure greater bioavailability, constant drug levels in plasma, reduced side effects, minimized dosing frequency and increased patient compliance.[66] For this purpose, hydrophobic polymers such as PCL, PLA, PLGA and EC were extensively used.[67, 68] Furthermore, by varying the composition of the polymeric matrix or the molecular weight, it was possible to attain the desired release rate.[69, 70] However, hydrophilic drugs are often difficult to encapsulate within hydrophobic polymers due to the low affinity that exists between them, resulting in low encapsulation efficiency. On this basis, researchers have initially loaded hydrophilic drugs into hydrophilic NPs and further microencapsulated them in a hydrophobic polymer.[26, 71] Moreover, to achieve sustained release of a hydrophobic protease inhibitor (e.g., indinavir free base), it was possible to microencapsulate pure drug NPs within MPs of the mucoadhesive polymer chitosan. This NiMDS would prolong the residence time of drug at the absorption site (e.g., intestine).[72]

Independently of the hydrophilicity of the encapsulated drug, NiMDS provide an additional diffusion layer that serves as an extra barrier and that prolongs the release time with respect to single NPs or MPs.[31]

A different strategy to produce NiMDS that provide controlled release is the introduction of NPs that adsorb the drug incorporated into the MPs and that serve as a diffusion barrier for the drug release.[14] Li et al. evaluated a formulation consisting of ZnS NPs encapsulated along with aspirin in alginate/chitosan microcapsules.[73] The incorporation of ZnS resulted in a dramatic decrease of the burst effect and the release rate owing to its ability to adsorb aspirin (Fig. 4). Moreover, the greater the amount of ZnS NPs, the slower the release rate of the microencapsulated drug, probably because ZnS NPs occupied pores in the hydrogel microcapsules and hindered the release of the drug[73] (Fig. 5).

Table I. Mean cumulative drug release (expressed in %) from polymeric NPs, MPs and NiMDS after 15 min.

Formulation	Drug	Polymer	Drug release (%)	Ref.
NP	Ibuprofen	PCL	86.00 ± 6.90	[34]
MP		PLGA	21.50 ± 6.10	
NiMDS		PCL/PLGA	8.70 ± 4.10	
NP	Diclofenac sodium	PCL + EC	88.31 ± 1.15	[65]
MP		EC	61.12 ± 8.20	
NiMDS		PCL + EC/EC	23.46 ± 0.77	
NP	Ibuprofen	PCL	71.70 ± 12.10	[36]
MP		RS	45.80 ± 1.20	
		EC	19.90 ± 5.30	
NiMDS		RS	32.90 ± 6.50	
		EC	27.70 ± 9.70	
NP	Triptorelin acetate	PCL	71.00 ± 11.20	
MP		RS	56.90 ± 3.20	
		EC	7.10 ± 4.30	
NiMDS		RS	26.70 ± 2.20	
		EC	5.40 ± 7.80	

Notes: PCL: poly(epsilon-caprolactone); PLGA: poly(lactic-co-glycolic) acid; EC: Ethylcellulose; RS: Eudragit RS 100, a copolymer of ethylacrylate, methyl-methacrylate and methacrylic acid esterified with quaternary ammonium groups.

Fig. 4. *In vitro* release profile of aspirin from dry powders (pure aspirin) and microspheres without and with ZnS NPs. Reproduced with permission from [73], Z. Li, et al., *Mat. Sci. Eng. C* 29, 2250 (**2009**). © 2009, Elsevier.

Similar results were obtained with gold NPs encapsulated within thioridazine-containing EC microcapsules.[14]

2.4. Drug Targeting

To achieve specificity in the release and thus greater effectiveness, while constraining the systemic exposure and reducing side effects, numerous DDS have been designed.

Active targeting is based on the decoration of the particle surface with ligands that are selectively recognized by specific receptors. For example, lectins are a type of transmembrane glycoprotein that bind to specific carbohydrates such as glucose, mannose and galactose.[74, 75] Since not only the normal but also the diseased intestine presents a heterogeneous sugar distribution pattern, lectins became useful for targeting specific areas of the GIT.[76] For this reason, these proteins have been coined as "second generation mucoadhesives" and they were anchored to the surface of NPs and MPs to improve their accumulation in specific zones of the GIT.[21, 77] More recently, the modification of NiMDS was also reported.[21] In addition, these hybrid systems displayed their own typical advantages:

(i) high drug entrapment efficiency,
(ii) controlled drug release,
(iii) potential enhanced absorption.[21]

On the other hand, although it was possible to attain selective targeting using the aforementioned strategies, this
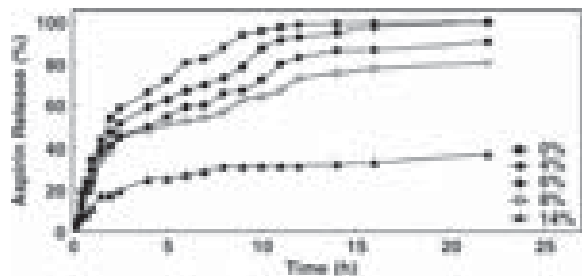
Fig. 5. Release profile of aspirin from microcapsules containing different amounts of ZnS NPs in PBS. Reproduced with permission from [73], Z. Li, et al., *Mat. Sci. Eng. C* 29, 2250 (**2009**). © 2009, Elsevier.

could led to the accumulation of the polymeric carrier in non-diseased cells owing to the often basal expression of antigens, carbohydrates and receptors. Moreover, the chemical modification of particles with specific ligands might demand complex synthetic pathways that substantially increases the cost of the medication. Thus, its implementation in diseases that mainly hit developing nations could eventually reduce patient affordability.[78–82]

In this context, the use of stimuli-responsive formulations that release the payload in response to specific environmental changes would be another promising alternative with better chances of translation into clinics. For example, the selective delivery to a specific region of the GIT was possible employing either pH-[58, 83] or enzymatic-sensitive polymers[31, 50, 64] to produce the micro-platform of NiMDS. In the first case, the MP matrix withstands the acid pH of the stomach, allowing the fast release of the encapsulated NPs exclusively in the intestine. On the other hand, some polymers are sensitive to the enzymatic degradation. For instance, gelatin and PCL are degraded by proteases and lipases abundant in the stomach and the intestine, respectively. In this way, NiMDS made of gelatin NPs in PCL MPs would be able to protect the payload during its transit through the stomach and to release the NPs specifically in the intestine as it was previously discussed.

Independently of the strategy, it is noticeable that the control of the particle size is critical to obtain an efficient targeted drug delivery.[84, 85] For example, particles with an aerodynamic size between 1 to 5 μm could be targeted to the deep lung when they are administered by the pulmonary route[17, 57] (see Section 3.3). Conversely, NiMDS in the same size range could be used to increase the uptake by the M-cells of the Peyer's patches in the small intestine when they are administered orally.[86]

3. ADMINISTRATION ROUTES FOR NiMDS

3.1. Oral Route

Oral administration represents the most popular and patient compliant route.[4, 26] Furthermore, the GIT displays a large surface area for drug absorption, becoming very useful for the treatment local and systemic diseases.[26, 29, 76]

For the design of an effective oral delivery system, it is necessary to take into account that these platforms have to overcome anatomical (e.g., mucus and epithelial layer) and physiological barriers (e.g., varying pH, degradation enzymes).[87] For these purpose, many NPs and MPs have been developed. Notwithstanding, the protection provided by simple particles is not always sufficient in all the cases, as it was discussed in Section 2.1. In light of this, NiMDS would represent attractive devices to protect payloads from the aggressive environment of the GIT. Thus, the micro-platform provides stability and selective delivery of the payload, while the nano-platform enables not only a greater loading of the drug but rather a more efficient

*J. Biomater. Tissue Eng. 3, 22–38, **2013***

27
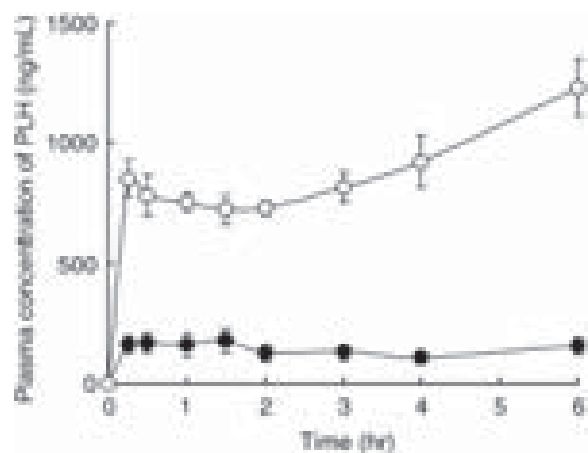
Fig. 6. Plasma concentrations of pranlukast hemihydrate (PLH) in rats, after oral administration of (●) PLH powder and (○) PLH/mannitol NiMDS. Reproduced with permission from [88], T. Mizoe, et al., *J. Control Release* 122, 10 (**2007**). © 2007, Elsevier.

retention in the mucosal layer of the intestinal tract owing to their small size. The high retention permits a more prolonged absorption of the drug increasing the area-under-the curve (AUC)[88] (Fig. 6).

3.2. Parenteral Route

Administration of therapeutic agents by the parenteral route is a common practice due to the high bioavailability achieved. In fact, most of the proteins on the market are destined for this route. However, injections do not supply sustained plasma concentrations and proteins have relatively short half lives, leading to the necessity of a repeated administration. This, together with the fact that injections are painful, compromises patient compliance.[54] In this context, NPs and MPs are attractive carriers to provide controlled release and to diminish the number of administrations over a certain period. Besides, they are useful to administer poorly water soluble drugs that cannot be formulated as aqueous solution and drugs that are more stable in suspension than in solution form.[54, 89, 90] Particles can be injected directly through a needle as a suspension or they can be dried to form a free-flowing powder that is re-suspended in an injectable liquid vehicle immediately before the administration.[42, 91, 92] Despite the abovementioned benefits, micron and sub-micron particles show a clear disadvantage: the appearance of an initial burst release which is a significant problem especially when the encapsulated agent has a very narrow therapeutic window. Thus, burst control is one of the main challenges of parenteral administration.[34] For this reason, a large amount of work has been devoted to formulate NiMDS (see Section 2.2). In addition, NiMDS can be manipulated to develop injectable drug delivering scaffolds containing cells. These sophisticated systems play a

dual function. First, they support cell adhesion, proliferation and function to promote tissue regeneration, and at the same time they allow the delivery of an encapsulated agent (e.g., growth factor, antibiotics) that improves the therapeutic outcome.[93] To obtain an effective scaffold, the polymeric matrix needs to be highly porous and interconnected to allow cell adhesion and proliferation.[94, 95] This tissue engineering approach is exemplified in Figure 7.[93]

3.3. Pulmonary Route

The pulmonary route is receiving great attention for the delivery of therapeutic agents due to unique features such as large alveolar surface area (~ 140 m^2) available for drug absorption, reduced thickness of the alveolar epithelium in the deep lung (0.1–0.2 μm), profuse vascularization, low proteolytic activity relative to other administration routes and less remarkable first-pass metabolism with respect to liver.[22, 57, 96–100] These attributes enable the use of the deep lung not only for local but also for systemic drug administration, a route known as transpulmonary.[22, 91, 101] Independently of the anatomical and physiological advantages previous depicted, inhalatory delivery also constitutes a minimally invasive administration route.[102] In this framework, there is a considerable interest in developing drug carriers suitable for inhalatory administration to the deep lung. However, achieving this goal is not trivial because the airways present numerous mechanisms such as their own tortuous structure, mucociliary clearance, phagocytosis by alveolar macrophages and enzymatic activity (protease inhibitors, isozymes of the cytochrome P-450 family and lysozyme) put together to eliminate foreign and potentially harmful substances.[96, 98, 103, 104] In light of this, researchers have investigated the development of different inhalatory NPs[105–107] and MPs.[108] Both types of carriers display advantages and drawbacks. NPs have a significantly increased surface area (per total particle mass) with respect to MPs.[22, 109] Furthermore, NPs can evade mucociliary clearance and phagocytic mechanisms.[110, 111] On the other hand, NPs have to face at least two limitations. First, the too small size does not allow the efficient deposition in the deep lung thereby most of them are exhaled after the administration.[112–118] Second, due to their small dimensions, they tend to undergo agglomeration.[119, 120] For that reason, managing of NPs is very difficult not only in liquid but also in solid form.[19, 57, 121] Conversely, MPs can be adjusted to fit the size range for deposition in the deep lung; authors agree that particles with an aerodynamic diameter between 1–5 μm deposit efficiently in the deep lung (bronchiole and alveolar region),[57, 122] although this range is restricted to 2–3 μm in some systems.[98, 101, 112–114, 123–126] Particles with a greater aerodynamic diameter will mostly deposit in the upper regions (bronchial region and oropharyngeal cavity),[112–114, 125, 126] while those with a smaller aerodynamic diameter will be predominantly exhaled. To capitalize on the features of both types of particles,

28

J. Biomater. Tissue Eng. 3, 22–38, **2013**
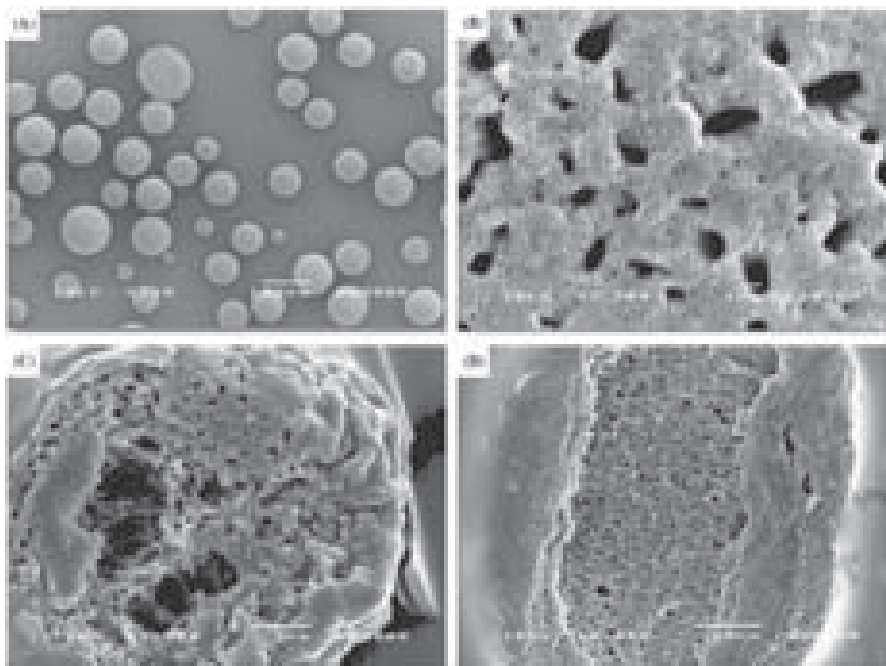
Fig. 7. SEM micrographs of thrombin receptor activator peptide-6 (TRAP-6)-loaded PLA NPs encapsulated within monomethoxypoly(ethylene glycol)-PLGA MPs (A), surface porosity of NiMDS (B), interior structure of simple MPs (C) and interior surface of NiMDS (D). Reproduced with permission from [93], Y. Wen, et al., *J. Control Release* 156, 11 (**2011**). © 2011, Elsevier.

different types of NiMDS have been produced for pulmonary delivery.[8, 19, 22, 127–130] These platforms present the maximum drug loading capacity characteristic of NPs and the suitable aerodynamic diameter of MPs, so that they can reach the deep lung where the NPs are later delivered.[19, 131] Pharmaceutical excipients such as mannitol or lactose that are highly soluble in water have been used to produce the micro-platform, so it may dissolve immediately in the aqueous environment of the lung ephitelium allowing the delivery of the encapsulated NPs.[57, 127–130, 132, 133] By virtue of their high aqueous solubility, these excipients did not affect the release profile of the payload,[57, 129, 132] as exemplified in Figure 8 for insulin.[57] However, if the nano-platform of NiMDS is formed by hydrophobic drug nanocrystals, they could be retained in the pulmonary mucous, resulting in more prolonged absorption.[88]

Another interesting strategy was the production of a respirable hybrid system that exhibited a geometric diameter of 10–15 μm. Due to the highly porous nature of the matrix, they showed the appropriate aerodynamic size for targeting to the lung (1–5 μm). This size pattern avoided uptake by alveolar macrophages because the maximum phagocytic activity in the lung is for particles having a geometric diameter of 1–2 μm, this activity decreasing substantially for smaller and larger particles.[111, 134, 135] Furthermore, their great flowability and aerosolization efficiency achieved by virtue of the large geometric size made their use extensive as dry powders.[17, 136]

Different options have been proposed to develop systems with the preceding features including:

(i) large porous particles with web-like or hollow interior that host drug-loaded NPs (Fig. 9),[18]

(ii) micron-sized agglomerates of NPs that are hollow or not and that are designed to disassociate into primary NPs in the aqueous environment of the lung,[16, 17, 131, 137]

(iii) semi-interpenetrating polymer network (IPN) hydrogel microspheres loaded with NPs which have appropriate aerodynamic size in dry state and larger geometric diameter when swollen after deposition in the moist lung.[3, 48]

Fig. 8. Release profile of insulin from chitosan NPs (●) and NiMDS consisting of chitosan NPs within mannitol MPs (□) in PBS, at 37 °C. Reproduced with permission from [57], A. Grenha, et al., *Eur. J. Pharm. Sci.* 25, 427 (**2005**). © 2005, Elsevier.
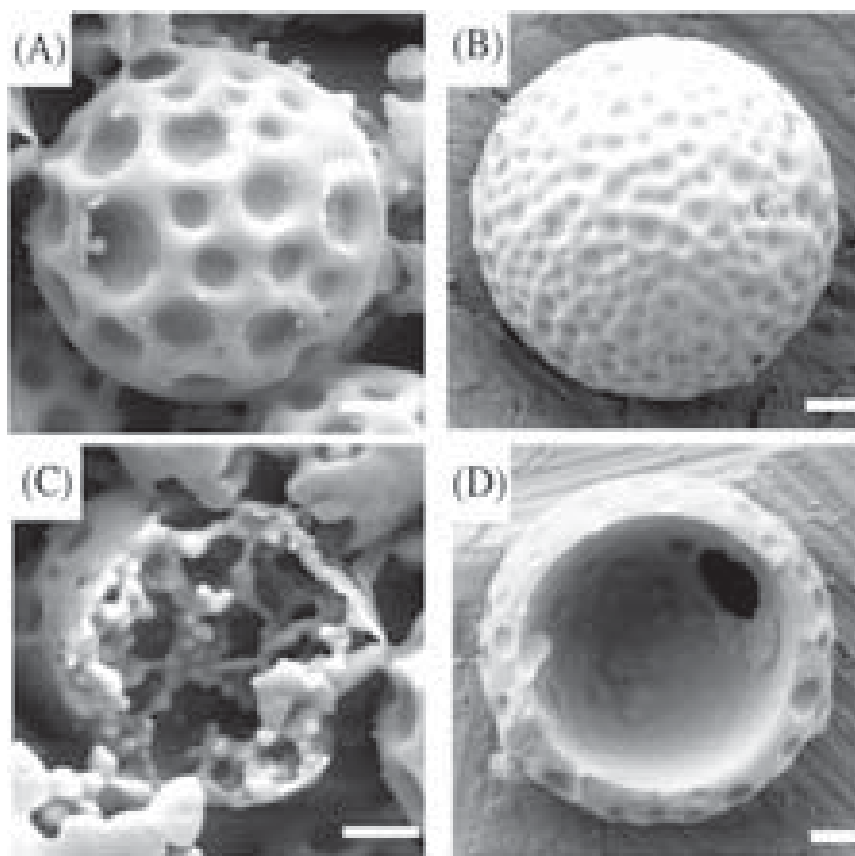
Fig. 9. SEM micrographs of the surface (A), (B) and the interior (C), (D) of large porous particles with web-like (A), (C) or hollow interior (B), (D). Reproduced with permission from [18], M. M. Arnold, et al., *J. Control Release* 121, 100 (**2007**). © 2007, Elsevier.

In addition to the optimal properties to target the deep lung which have been challenging in recent years, these platforms could be designed to achieve controlled or sustained release.[3, 6, 7, 18, 132] Grenha et al. reported on
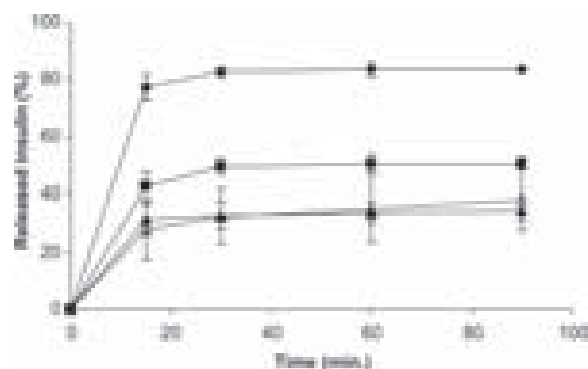
Fig. 10. Release profile of insulin from (♦) chitosan nanoparticles, (■) complexes (DPPC)/chitosan NPs, (▲) complexes DPPC-DMPG/chitosan NPs and (△) NiMDS containing DPPC-DMPG/chitosan NPs in mannitol microspheres. Reproduced with permission from [132], A. Grenha, et al., *Eur. J. Pharm. Biopharm.* 69, 83 (**2008**). © 2008, Elsevier.

the production of microspheres containing insulin-loaded lipid/chitosan NPs complexes.[132] The two phospholipids used were dipalmitoyl phosphatidylcholine (DPPC) and dimiristoyl phosphatidylglycerol (DMPG) because they are endogenous and principal constituents of the pulmonary surfactant.[138] These phospholipids represent an extra barrier that the encapsulated protein had to overcome before its release, so the presence of the lipid layer is a determining factor in controlling the delivery, especially when both lipids were present in the system (Fig. 10).

Biodegradable PLGA NPs loaded with rifampicin (RIF), a first-line anti-tuberculosis drug, were microencapsulated in mannitol microspheres employing a four-fluid nozzle spray-dryer.[128] The *in vivo* uptake of the drug included NiMDS by alveolar macrophages in rat lungs was improved significantly with respect to RIF-containing PLGA or mannitol microparticles. This work represents a hallmark in the one-step production of NiMDS.

4. DEVELOPMENT OF NiMDS

As previously described, NiMDS generally consist of three main components. The selection of the different materials

and the production methodology depend on the active agent that will be encapsulated and the administration route.[139] In this section, we will discuss the key variables to design and develop NiMDS suitable for different applications.

4.1. Biomaterials for the Production of NiMDS

NiMDS can be produced with different types of natural and synthetic biomaterials such as polymers, lipids and sugars. Nevertheless, there is a tendency to use polymers of proven biocompatibility, biodegradability and non- or low toxicity like chitosan, alginate, gelatin, PCL and PLGA. In the present section we will overview the most popular polymers used for the production of NiMDS, according the administration route.

4.1.1. Oral Route

Various polymers have been used to produce NiMDS for oral administration. Among them, PCL has been widely used due to its ability to extend the release over more prolonged periods than PLA and its copolymers.[140] Jelvehgari et al. reported a microstructured hybrid matrix consisting of PCL and EC.[65] EC is non-toxic, non-irritant, safe and stable polymer[141, 142] that is water permeable but not water soluble.[167] The mixture of EC with PCL conferred a slower and more progressive drug release. On the other hand, the muco-adhesiveness and the ability to transiently open epithelial tight junctions have granted chitosan a central role in the development of oral NiMDS.[4, 21, 61] Besides, it can be blended with alginate in order to achieve a more stable matrix and more controlled release profile. Other polymers extensively used for the production of the nano- and/or the micro-platform are Eudragit,[83] gelatin[5, 29] and PLGA.[83]

4.1.2. Parenteral Route

For parenteral delivery, NiMDS must be produced with biodegradable polymers like dextran,[9] PLGA,[34, 52, 63, 93] PLA[54] or blends of them.[54, 62] Furthermore, if NiMDS is administered as a depot implant, the use of biodegradable polymers prevents the surgical retrieval of the matrix from the site of administration after the drug release was completed. The result would be the improvement of the patient compliance and the lowering of the therapeutic cost. On the other hand, the aforementioned polymers have a great potential for controlled drug release which is widely important in this administration route.[67, 68, 144, 145]

4.1.3. Pulmonary Route

The most commonly used biomaterials for pulmonary route are polymers such as chitosan and alginate, and carbohydrates specially mannitol and lactose. Carbohydrates mentioned above are approved by the US Food and Drug Administration (FDA) and other regulatory agencies for pulmonary delivery[123] by virtue of their non-toxicity and biodegradability and they are extensively implemented in the production of dry powder inhalers (DPI). In general, these carriers are employed as the micro-platform that contains nanocrystals or drug-loaded NPs, homogeneously dispersed owing to their ability to prevent NPs agglomeration.[146, 147] At the same time, the high water solubility allows an immediate release of the NPs after the deposition in the moist epithelium of the deep lung. Thereby, it only serves as an inert carrier of the NPs to the alveolar region[148] A difference between mannitol and lactose is that the former is non-hygroscopic as opposed to the latter.[123, 141] In this context, handling lactose powders during and after production is often difficult because they become sticky upon the absorption of environmental humidity.[57]

As abovementioned, chitosan is a natural polysaccharide obtained by deacetylation of chitin which presents special properties of biocompatibility, biodegradability and low or non-toxicity.[149–154] In addition, chitosan is muco-adhesive[155, 156] and opens the intercellular tight junction of the lung epithelium enabling the permeation of macromolecules through well-organized epithelia.[157–162] Moreover, chitosan can be degraded by the pulmonary lysozyme.[163] That is why chitosan can be used to produce the micro-platform where the NPs will be embedded[3] and the nano-platform itself.[6, 57, 130, 133]

Phospholipids like DDPC and DMPG are main constituents of the lung surfactant.[138, 164, 165] Thereby, their inclusion at the surface of NiMDS decreases the phagocytic mechanisms.[166, 167] Furthermore, they are necessary additives to facilitate the formation of large porous particles.[168, 169]

Finally, PLA, PLGA and other aliphatic polyesters are extensively used to attain controlled drug release.[67, 170] That is why some groups have proposed their use in the production of the microstructure of NiMDS.[18] However, the toxicological evaluation of these biomaterials upon pulmonary administration still needs to be assessed.[171, 172]

4.2. Therapeutic Agents Encapsulated in NiMDS

NiMDS are able to load different substances such as
(i) hydrophilic and hydrophobic drugs,
(ii) peptides and proteins and
(iii) nucleic acids. For that reason, NiMDS has turned into a versatile platform especially useful in the field of nanomedicine.

4.2.1. Hydrophilic and Hydrophobic Drugs

With a careful selection of the nanocarrier, the polymers and the methodology of production, NiMDS can be exploited to incorporate both hydrophilic[4, 50] and

REVIEW

hydrophobic[20, 88] drugs. For example, one of the main drawbacks exhibited by most of the hydrophilic drugs is the burst effect which occurs even in sustained drug delivery devices. This problem might be approached by developing this new platform. In fact, several groups have demonstrated the advantage of encapsulating NPs in MPs to reduce the burst effect of hydrophilic drugs.[50, 58, 63, 173]

4.2.2. Peptides and Proteins

The short half-life and instability of peptides and proteins reveal the need to develop sustained delivery systems with very controlled burst effects to reduce the dosing frequency, therefore increasing patient compliance.[38, 174, 175] As it was discussed before, NiMDS are promising platforms to achieve these requirements. However, a challenge in protein drug delivery is to preserve its tertiary/quaternary structure, vital for the bioactivity. Exposure of proteins to unfavorable conditions during the manufacturing process tended to decrease their bioactivity.[176] Two general approaches have been used to avoid protein denaturation during the production of NiMDS. One strategy relied on the incorporation of solid protein NPs into hydrophobic polymeric MPs that would release the protein slowly.[19, 52, 54, 62] It was reported that the protein in solid state is kinetically trapped in the original (and bioactive) thus hampering conformational changes.[54, 89] The second strategy aimed to use a combination of polymers of different HLB to form the nano- and the microstructure; hydrophilic polymers are biocompatible with peptide and protein drugs, while hydrophobic polymers are not. It is worth mentioning that achieving controlled release with hydrophilic polymers is difficult. On the other hand, hydrophobic polymers might provide sustained release though their hydrophobicity might induce unfolding of peptide or protein drugs.[21, 177, 178] Thus, peptides/proteins could be primarily encapsulated

in NPs made of hydrophilic polymers such as dextran[64] or gelatin[71] and then microencapsulated in a hydrophobic polymer like PLGA[64, 71] to attain sustained release.

4.2.3. Nucleic Acids

Many therapeutic nucleic acid-based macromolecules such as siRNA or DNA-plasmids were discovered in the past years.[28] Thereby, the design of an effective carrier able to protect these substances from degradation is an emerging challenge. The most common vehicles for the delivery of nucleic acids are viral and non-viral vectors.[179, 180] Viral vectors are questioned due to their limited transfection capacity and unknown toxicity, issues that are especially crucial upon chronic administration.[145, 181, 182] In this framework, non-viral vectors have received meaningful attention[87, 183–185] because they showed better chances of translating an experimental strategy into a clinical reality.[186, 187] Following this conceptual trend, NiMDS could become another valuable non-viral vector. One of the most important advantages of using NiMDS is the ability to extensively increase nucleic acid loading, thus overcoming the shortcomings exhibited by viral vectors. Moreover, NiMDS might permit the delivery of the nucleic acid in a specific area of GIT such as the intestine using a pair of polymers: (i) an acid pH-resistant polymer for the shell to protect the loaded NPs from the degradation and (ii) a compatible polymer with the structure of nucleic acid to produce the core (see Section 2.1.).[5, 28, 30] On the other hand, taking advantage of the negative charge of the DNA, it is possible to complex anionic nucleic acids with cationic gold NPs, obtaining nanoplexes with overall negative charge, which are further complexed with cationic gold MPs.[13] These NiMDS formed only by electrostatic attraction between nanoplexes onto the surface of the MPs

Table II. Description of the techniques most commonly used to prepare NiMDS.

Conventional methodology	Modified methodology	Ref.
Spray drying	(i) The nanosuspension can be spray dried either immediately after its preparation to obtain nanoparticles aglommerates or mixed with an adequate polymer obtaining NPs embedded in MPs	[4, 7, 16, 17, 19, 21, 48, 131, 133]
	(ii) The sediments of NPs ontained following centrifugation of the fresh nanosuspensions which are mixed with an appropriate polymer solution and then spray dried	[57, 127, 129]
Emulsion/solvent evaporation	(i) The nanosuspension may act as the inner phase of the emulsion	[14, 34]
	(ii) The lyophilized NPs may be redispersed in the internal phase of the emulsion	[5, 26–30, 36, 50, 65, 71, 83]
S/O/O* or S/O/O/O** emulsion	(i) The lyophilized NPs are suspended in a polymer solution (inner oil phase) which is then emulsified into the outer phase	[52, 54, 60, 63]
Emulsification/chemical cross- linking	(i) The nanosuspensions might be mixed with CHT which is dispersed in an oil emulsion to be gelated in NiMDS	[61]
	(ii) The nanoparticulate powder might be mixed with a CHT solution which is dispersed in an oil emulsion to be gelated in NiMDS	[6]

Notes: *S/O/O: Solid-in-oil-in-oil emulsion; **S/O/O/O: Solid-in-oil-in-oil-in-oil emulsion.

32

J. Biomater. Tissue Eng. 3, 22–38, 2013

provide a great protection capacity against degradation,[188] leading to a sharp increase of the transfection efficiency.

4.3. Manufacturing Technologies

Several methodologies have been developed to prepare NiMDS. Generally, this process involves two steps. First, the production of the nano-platform by any of the available methods and second, the further microencapsulation of such NPs. To fulfill this goal, NPs must be incorporated in some of the different production stages of conventional MPs.

There are two pathways that can be followed to accomplish this purpose. The nanosuspension is directly used or, conversely, this formulation is primarily dried (e.g., lyophilization) and, only then, the solid NPs are incorporated into the micro-platform. The most common methods for the preparation of NiMDS are summarized in Table II.

5. CONCLUSIONS

After the great revolution caused by micro and nanotechnology in the field of pharmaceutical technology, a new era has arrived. The combination of these platforms in more complex and advantageous systems such as NiMDS constitutes a useful tool to develop systems capable of carrying and protecting high drug amounts that can be released in a more controlled manner without burst effect and with selective targeting. The foregoing shows that NiMDS can be made with different materials, prepared in a variety of diverse conditions, applied by many routes of administration and designed to deliver a wide variety of therapeutic substances resulting in versatile platforms able to address a broad range of health concern. Taking into account the state-of-the-art, we believe that NiMDS show unique features to play a key role in the emergence of a new generation of DDS.

References and Notes

1. K. Fu, R. Harrell, K. Zinski, C. Um, A. Jaklenec, J. Frazier, N. Lotan, P. Burke, A. M. Klibanov, and R. Langer, A potential approach for decreasing the burst effect of protein from PLGA microspheres. *J. Pharm. Sci.* 92, 1582 (**2003**).

2. C. Dong and J. A. Rogers, Acacia-gelatin microencapsulated liposomes: preparation, stability, and release of acetylsalicylic acid. *Pharm. Res.* 10, 141 (**1993**).

3. I. M. El-Sherbiny and H. D. Smyth, Biodegradable nano-micro carrier systems for sustained pulmonary drug delivery: (I) self-assembled nanoparticles encapsulated in respirable/swellable semi-IPN microspheres. *Int. J. Pharm.* 395, 132 (**2010**).

4. F. Q. Li, R. R. Ji, X. Chen, B. M. You, Y. H. Pan, and J. C. Su, Cetirizine dihydrochloride loaded microparticles design using ionotropic cross-linked chitosan nanoparticles by spray-drying method. *Arch. Pharm. Res.* 33, 1967 (**2010**).

5. C. Kriegel and M. M. Amiji, Dual TNF-α/Cyclin D1 Gene Silencing With an Oral Polymeric Microparticle System as a Novel Strategy for the Treatment of Inflammatory Bowel Disease. *Clin. Transl. Gastroenterol.* 2, e2 (**2011**).

6. K. Dharmala, J. W. Yoo, and C. H. Lee, Development of chitosan-SLN microparticles for chemotherapy: in vitro approach through efflux-transporter modulation. *J. Control Release* 131, 190 (**2008**).

7. Y. Z. Li, X. Sun, T. Gong, J. Liu, J. Zuo, and Z. R. Zhang, Inhalable microparticles as carriers for pulmonary delivery of thymopentin-loaded solid lipid nanoparticles. *Pharm. Res.* 27, 1977 (**2010**).

8. Y. T. Yang, C. T. Chen, J. C. Yang, and T. Tsai, Spray-dried microparticles containing polymeric micelles encapsulating hematoporphyrin. *AAPS Journal* 12, 138 (**2010**).

9. R. J. Stenekes, A. E. Loebis, C. M. Fernandes, D. J. Crommelin, and W. E. Hennink, Degradable dextran microspheres for the controlled release of liposomes. *Int. J. Pharm.* 214, 17 (**2001**).

10. N. O. Dhoot and M. A. Wheatley, Microencapsulated liposomes in controlled drug delivery: strategies to modulate drug release and eliminate the burst effect. *J. Pharm. Sci.* 92, 679 (**2003**).

11. V. DiTizio, C. Karlgard, L. Lilge, A. E. Khoury, M. W. Mittelman, and F. DiCosmo, Localized drug delivery using crosslinked gelatin gels containing liposomes: factors influencing liposome stability and drug release. *J. Biomed. Mater. Res.* 51, 96 (**2000**).

12. I. Takagi, H. Shimizu, and T. Yotsuyanagi, Application of alginate gel as a vehicle for liposomes. I. Factors affecting the loading of drug-containing liposomes and drug release. *Chem. Pharm. Bull.* 44, 1941 (**1996**).

13. S. A. Svarovsky, M. J. Gonzalez-Moa, M. D. Robida, A. Y. Borovkov, and K. Sykes, Self-Assembled Micronanoplexes for Improved Biolistic Delivery of Nucleic Acids. *Mol. Pharm.* 6, 1927 (**2009**).

14. M. K. Lai, C. Y. Chang, Y. W. Lien, and R. C. Tsiang, Application of gold nanoparticles to microencapsulation of thioridazine. *J. Control Release* 111, 352 (**2006**).

15. S. Simovic, P. Heard, H. Hui, Y. Song, F. Peddie, A. K. Davey, A. Lewis, T. Rades, and C. A. Prestidge, Dry hybrid lipid-silica microcapsules engineered from submicron lipid droplets and nanoparticles as a novel delivery system for poorly soluble drugs. *Mol. Pharm.* 6, 861 (**2009**).

16. K. Hadinoto, P. Phanapavudhikul, Z. Kewu, and R. B. Tan, Dry powder aerosol delivery of large hollow nanoparticulate aggregates as prospective carriers of nanoparticulate drugs: effects of phospholipids. *Int. J. Pharm.* 333, 187 (**2007**).

17. K. Hadinoto, P. Phanapavudhikul, Z. Kewu, and R. B. Tan, Novel Formulation of Large Hollow Nanoparticles Aggregates as Potential Carriers in Inhaled Delivery of Nanoparticulate Drugs. *Ind. Eng. Chem. Res.* 45, 3697 (**2006**).

18. M. M. Arnold, E. M. Gorman, L. J. Schieber, E. J. Munson, and C. Berkland, NanoCipro encapsulation in monodisperse large porous PLGA microparticles. *J. Control Release* 121, 100 (**2007**).

19. C. Klingler, B. W. Muller, and H. Steckel, Insulin-micro- and nanoparticles for pulmonary delivery. *Int. J. Pharm.* 377, 173 (**2009**).

20. A. Z. Chen, Y. Li, F. T. Chau, T. Y. Lau, J. Y. Hu, Z. Zhao, and D. K. Mok, Microencapsulation of puerarin nanoparticles by poly(l-lactide) in a supercritical CO(2) process. *Acta Biomater.* 5, 2913 (**2009**).

21. F. Q. Li, Y. B. Fei, X. Chen, X. J. Qin, J. Y. Liu, Q. G. Zhu, and J. H. Hu, Anchoring of ulex europaeus agglutinin to chitosan nanoparticles-in-microparticles and their in vitro binding activity to bovine submaxillary gland mucin. *Chem. Pharm. Bull.* 57, 1045 (**2009**).

22. L. J. Peek, L. Roberts, and C. Berkland, Poly(D,L-lactide-co-glycolide) Nanoparticle Agglomerates as Carriers in Dry Powder Aerosol Formulation of Proteins. *Langmuir* 24, 9775 (**2008**).

23. D. T. O'Hagan, Microparticles and polymers for the mucosal delivery of vaccines. *Adv. Drug Deliv. Rev.* 34, 305 (**1998**).

24. S. S. Guterres, H. Fessi, G. Barratt, F. Puisieux, and J. P. Devissaguet, Poly (D,L-lactide) nanocapsules containing nonsteroidal anti-inflammatory drugs: gastrointestinal tolerance following intravenous and oral administration. *Pharm. Res.* 12, 1 (**1995**).

25. J. Price (ed.), Handbook of Pharmaceutical Excipients, The Pharmaceutical Press, London (**2003**).

26. M. D. Bhavsar and M. M. Amiji, Gastrointestinal distribution and in vivo gene transfection studies with nanoparticles-in-microsphere oral system (NiMOS). *J. Control Release* 119, 339 (**2007**).

27. M. D. Bhavsar, S. B. Tiwari, and M. M. Amiji, Formulation optimization for the nanoparticles-in-microsphere hybrid oral delivery system using factorial design. *J. Control Release* 110, 422 (**2006**).

28. M. D. Bhavsar and M. M. Amiji, Development of novel biodegradable polymeric nanoparticles-in-microsphere formulation for local plasmid DNA delivery in the gastrointestinal tract. *AAPS Pharm. Sci. Tech.* 9, 288 (**2008**).

29. C. Kriegel and M. Amiji, Oral TNF-α gene silencing using a polymeric microsphere-based delivery system for the treatment of inflammatory bowel disease. *J. Control Release* 150, 77 (**2011**).

30. M. D. Bhavsar and M. M. Amiji, Oral IL-10 gene delivery in a microsphere-based formulation for local transfection and therapeutic efficacy in inflammatory bowel disease. *Gene Ther.* 15, 1200 (**2008**).

31. T. M. Allen and A. Chonn, Large unilamellar liposomes with low uptake into the reticuloendothelial system. *FEBS Lett.* 223, 42 (**1987**).

32. A. Joshi, R. Keerthiprasad, R. D. Jayant, and R. Srivastava, Nano-in-micro alginate based hybrid particles. *Carbohydr. Polym.* 81, 790 (**2010**).

33. Y. Yeo and K. Park, Control of encapsulation efficiency and initial burst in polymeric microparticle systems. *Arch. Pharmacol. Res.* 27, 1 (**2004**).

34. A. Sheikh Hassan, A. Sapin, A. Lamprecht, E. Emond, F. El Ghazouani, and P. Maincent, Composite microparticles with *in vivo* reduction of the burst release effect. *Eur. J. Pharm. Biopharm.* 73, 337 (**2009**).

35. T. Freytag, A. Dashevsky, L. Tillman, G. E. Hardee, and R. Bodmeier, Improvement of the encapsulation efficiency of oligonucleotide-containing biodegradable microspheres. *J. Control Release* 69, 197 (**2000**).

36. A. S. Hasan, M. Socha, A. Lamprecht, F. E. Ghazouani, A. Sapin, M. Hoffman, P. Maincent, and N. Ubrich, Effect of the microencapsulation of nanoparticles on the reduction of burst release. *Int. J. Pharm.* 344, 53 (**2007**).

37. X. Huang and C. Brazel, On the importance and mechanisms of burst release in matrix-controlled drug delivery systems. *J. Control. Rel.* 73, 121 (**2001**).

38. J. Wang, B. A. Wang, and S. P. Schwendeman, Characterization of the initial burst release of a model peptide from poly(D,L-lactide-co-glycolide) microspheres. *J. Control Release* 82, 289 (**2002**).

39. O. L. Johnson and M. A. Tracy, Peptide and protein drug delivery, edited by E. Mathiowitz, John Wiley and Sons, USA (**1999**), pp. 816–832.

40. Y.-Y Yang, T.-S. Chung, and N. P. Ng, Morphology, drug distribution, and in vitro release profiles of biodegradable polymeric microspheres containing protein fabricated by double-emulsion solvent extraction/evaporation method. *Biomaterials* 22, 231 (**2001**).

41. G. Jian, B. C. Thanoo, and P. P. DeLuca, Effect of osmotic pressure in the solvent extraction phase on BSA release profile from PLGA microspheres. *Pharm. Dev. Technol.* 7, 391 (**2002**).

42. R. A. Jain, The manufacturing techniques of various drug loaded biodegradable poly(lactide-co-glycolide) (PLGA) devices. *Biomaterials.* 21, 2475 (**2000**).

43. C. Wang, W. Ye, Y. Zheng, X. Liu, and Z. Tong, Fabrication of drug-loaded biodegradable microcapsules for controlled release by combination of solvent evaporation and layer-by-layer self-assembly. *Int. J. Pharm.* 338, 165 (**2007**).

44. C. Berkland, K. Kim, and D. W. Pack, PLG microsphere size controls drug release rate through several competing factors. *Pharm Res.* 20, 1055 (**2003**).

45. B. Guiziou, D. J. Armstrong, P. N. Elliott, J. L. Ford, and C. Rostron, Investigation of in-vitro release characteristics of NSAID-loaded polylactic acid microspheres. *J. Microencapsul.* 13, 701 (**1996**).

46. A. Fernandez-Carballido, R. Herrero-Vanrell, I. T. Molina-Martinez, and P. Pastoriza, Biodegradable ibuprofen-loaded PLGA microspheres for intraarticular administration. Effect of Labrafil addition on release *in vitro. Int. J. Pharm.* 279, 33 (**2004**).

47. C. J. Thompson, D. Hansford, S. Higgins, C. Rostron, G. A. Hutcheon, and D. L. Munday, Evaluation of ibuprofen-loaded microspheres prepared from novel copolyesters. *Int. J. Pharm.* 329, 53 (**2007**).

48. I. M. El-Sherbiny and H. D. Smyth, Controlled release pulmonary administration of curcumin using swellable biocompatible microparticles. *Mol. Pharm.* 9, 269 (**2012**).

49. M. Hombreiro-Pérez, J. Siepmann, C. Zinutti, A. Lamprecht, N. Ubrich, M. Hoffman, R. Bodmeier and P. Maincent, Non-degradable microparticles containing a hydrophilic and/or a lipophilic drug: preparation, characterization and drug release modeling. *J. Control Rel.* 88, 413 (**2003**).

50. M. Jelvehgari, J. Barar, H. Valizadeh, and N. Heidari, Preparation and evaluation of poly (ε-caprolactone) nanoparticles-inmicroparticles by W/O/W emulsion method. *Iran J. Basic Med. Sci.* 13, 85 (**2010**).

51. W. D. Rhine, D. S. Hsieh, and R. Langer, Polymers for sustained macromolecule release: Procedures to fabricate reproducible delivery systems and control release kinetics. *J. Pharm. Sci.* 69, 265 (**1980**).

52. Y. Han, H. Tian, P. He, X. Chen, and X. Jing, Insulin nanoparticle preparation and encapsulation into poly(lactic-co-glycolic acid) microspheres by using an anhydrous system. *Int. J. Pharm.* 378, 159 (**2009**).

53. W. Al-Azzam, E. A. Pastrana, and K. Griebenow, Co-lyophilization of bovine serum albumin (bsa) with poly(ethylene glycol) improves efficiency of bsa encapsulation and stability in polyester microspheres by a solid-in-oil-in-oil technique. *Biotechnol. Lett.* 24, 1367 (**2002**).

54. W. T. Leach, D. T. Simpson, T. N. Val, E. C. Anuta, Z. Yu, R. O. Williams, 3rd, and K. P. Johnston, Uniform encapsulation of stable protein nanoparticles produced by spray freezing for the reduction of burst release. *J. Pharm. Sci.* 94, 56 (**2005**).

55. H. R. Costantino, L. Firouzabadian, K. Hogeland, C. C. Wu, C. Beganski, K. G. Carrasquillo, M. Cordova, K. Griebenow, S. E. Zale, and M. A. Tracy, Protein spray-freeze drying. Effect of atomization conditions on particle size and stability. *Pharm. Res.* 17, 1374 (**2000**).

56. S. Sant, V. Nadeau, and P. Hildgen, Effect of porosity on the release kinetics of propafenone-loaded PEG-g-PLA nanoparticles. *J. Control Release* 107, 203 (**2005**).

34

*J. Biomater. Tissue Eng. 3, 22–38, **2013***

REVIEW

57. A. Grenha, B. Seixo, and C. Remuñán-López, Microencapsulated chitosan nanoparticles for lung protein delivery. *Eur. J. Pharm. Sci.* 25, 427 (**2005**).

58. K. E. Lee, S. H. Cho, H. B. Lee, S. Y. Jeong, and S. H. Yuk, Microencapsulation of lipid nanoparticles containing lipophilic drug. *J. Microencapsul.* 20, 489 (**2003**).

59. H. Maeda, T. Nakagawa, N. Adachi, Y. Sakai, T. Yamamoto, and A. Matsuoka, Design of long-acting formulation of protein drugs with a double-layer structure and its application to rhG-CSF. *J. Control Release* 91, 281 (**2003**).

60. A. J. Thote, K. Ono, and R. B. Gupta (eds.), *AIChE Annual Meeting, Conference Proceedings*, Cincinnati, OH (**2005**), p. 8566.

61. S. Hua, H. Yang, and A. Wang, A pH-sensitive nanocomposite microsphere based on chitosan and montmorillonite with in vitro reduction of the burst release effect. *Drug. Dev. Ind. Pharm.* 36, 1106 (**2010**).

62. Y. Kakizawa, R. Nishio, T. Hirano, Y. Koshi, M. Nukiwa, M. Koiwa, J. Michizoe, and N. Ida, Controlled release of protein drugs from newly developed amphiphilic polymer-based microparticles composed of nanoparticles. *J. Control Release* 142, 8 (**2010**).

63. A. J. Thote and R. B. Gupta, Formation of nanoparticles of a hydrophilic drug using supercritical carbon dioxide and microencapsulation for sustained release. *Nanomedicine* 1, 85 (**2005**).

64. T. Ren, W. Yuan, H. Zhao, and T. Jin, Sustained-release polylactide-co-glycolide microspheres loaded with pre-formulated protein polysaccharide nanoparticles. *Micro and Nano Letters* 6, 70 (**2011**).

65. M. Jelvehgari, J. Barar, H. Valizadeh, B. D. Loveymi, and M. Ziapour, Controlled- and modulated-release drug-delivery systems. *Transaction on Nanotechnology* 17, 79 (**2010**).

66. Y. W. Chien, Encyclopedia of Pharmaceutical Technology, edited by J. Swarbrick and J. C. Boylan, Marcel Dekker, New York (**1990**), pp. 281–313.

67. S. Acharya and S. K. Sahoo, PLGA nanoparticles containing various anticancer agents and tumour delivery by EPR effect. *Adv. Drug. Deliv. Rev.* 63, 170 (**2011**).

68. J. S. Golub, Y. T. Kim, C. L. Duvall, R. V. Bellamkonda, D. Gupta, A. S. Lin, D. Weiss, W. R. Taylor, and R. E. Guldberg, Sustained VEGF delivery via PLGA nanoparticles promotes vascular growth. *Am. J. Physiol. Heart. Circ. Physiol.* 298, 1959 (**2010**).

69. D. Klose, F. Siepmann, K. Elkharraz, and J. Siepmann, PLGA-based drug delivery systems: importance of the type of drug and device geometry. *Int. J. Pharm.* 354, 95 (**2008**).

70. R. Bodmeier, K. H. Oh, and H. Chen, The effect of the addition of low molecular weight poly(dl-lactide) on drug release from biodegradable poly(dl-lactide) drug delivery systems. *Int. J. Pharm.* 51, 1 (**1989**).

71. J. K. Li, N. Wang, and X. S. Wu, A novel biodegradable system based on gelatin nanoparticles and poly(lactic-co-glycolic acid) microspheres for protein and peptide drug delivery. *J. Pharm. Sci.* 86, 891 (**1997**).

72. J. C. Imperiale, D. A. Chiappetta, and A. Sosnik, Nuevos nanosistemas de liberación de drogas mucoadhesivos para la liberación sostenida de inhibidores de proteasa en el tratamiento de HIV, *Proceedings of the XVIII Argentine Congress of Bioengineering*, Mar del Plata, Argentina (**2011**).

73. Z. Li, P. Chen, X. Xu, X. Ye, and J. Wang, Preparation of chitosan-sodium alginate microcapsules containing ZnS nanoparticles and its effect on the drug release. *Mat. Sci. Eng. C* 29, 2250 (**2009**).

74. H. Lis and N. Sharon, Lectins as molecules and as tools. *Annu. Rev. Biochem.* 55, 35 (**1986**).

75. C. M. Lehr, J. A. Bouwstra, W. Kok, A. B. Noach, A. G. de Boer, and H. E. Junginger, Bioadhesion by means of specific binding of tomato lectin. *Pharm. Res.* 9, 547 (**1992**).

76. G. Ponchel and J. Irache, Specific and non-specific bioadhesive particulate systems for oral delivery to the gastrointestinal tract. *Adv. Drug Deliv. Rev.* 34, 191 (**1998**).

77. C. M. Lehr, Lectin-mediated drug delivery: the second generation of bioadhesives. *J. Control Release* 65, 19 (**2000**).

78. A. Sosnik, D. A. Chiappetta, and A. M. Carcaboso, Drug delivery systems in HIV pharmacotherapy: what has been done and the challenges standing ahead. *J. Control Release* 138, 2 (**2009**).

79. A. Sosnik, A. M. Carcaboso, R. J. Glisoni, M. A. Moretton, and D. A. Chiappetta, New old challenges in tuberculosis: potentially effective nanotechnologies in drug delivery. *Adv. Drug. Del. Rev.* 62, 547 (**2010**).

80. A. Sosnik and M. Amiji, Nanotechnology solutions for infectious diseases in developing nations. Preface. *Adv. Drug Del. Rev.* 62, 375 (**2010**).

81. A. Sosnik, Nanotechnology contributions to the pharmacotherapy of pediatric HIV: A dual scientific and ethical challenge and a still pending agenda. *Nanomedicine-UK* 5, 833 (**2010**).

82. A. Sosnik, K. P. Seremeta, J. C. Imperiale, and D. A. Chiappetta, Novel formulation and drug delivery strategies for the treatment of pediatric poverty-related diseases. *Expert Op. Drug Deliv.* 9, 303 (**2012**).

83. A. Lamprecht, H. Yamamoto, H. Takeuchi, and Y. Kawashima, A pH-sensitive microsphere system for the colon delivery of tacrolimus containing nanoparticles. *J. Control Release* 104, 337 (**2005**).

84. A. Kikuchi and T. Okano, Pulsatile drug release control using hydrogels. *Adv. Drug Deliv. Rev.* 54, 53 (**2002**).

85. S. Wee and W. R. Gombotz, Protein release from alginate matrices. *Adv. Drug Deliv. Rev.* 31, 267 (**1998**).

86. J. H. Eldridge, C. J. Hammond, J. A. Meulbroek, J. K. Staas, R. M. Gilley, and T. R. Tice, Controlled vaccine release in the gut-associated lynphoid tissue. I. Orally administered biodegradable microspheres target the Peyer's patches *J. Control Release* 11, 205 (**1990**).

87. R. Martien, B. Loretz, and A. B. Schnurch, Oral gene delivery: Design of polymeric carrier systems shielding toward intestinal enzymatic attack. *Biopolymers* 83, 327 (**2006**).

88. T. Mizoe, T. Ozeki, and H. Okada, Preparation of drug nanoparticle-containing microparticles using a 4-fluid nozzle spray drier for oral, pulmonary, and injection dosage forms. *J. Control Release* 122, 10 (**2007**).

89. M. Tobio, J. Nolley, Y. Y. Guo, J. McIver, and M. J. Alonso, A novel system based on a poloxamer/PLGA blend as a tetanus toxoid delivery vehicle. *Pharm. Res.* 16, 682 (**1999**).

90. T. J. Carstensen, Modern Pharmaceutics, edited by G. S. Banker and C. T. Rhodes, Academic Press, New York (**1973**), Vol. 2, pp. 1–89.

91. J. L. Cleland, A. Daugherty, and R. Mrsny, Emerging protein delivery methods. *Curr. Opin. Biotechnol.* 12, 212 (**2001**).

92. R. Jalil and J. R. Nixon, Microencapsulation using poly (L-lactic acid) II: Preparative variables affecting microcapsule properties. *J. Microencapsul.* 7, 25 (**1990**).

93. Y. Wen, M. R. Gallego, L. F. Nielsen, L. Jorgensen, H. Everland, E. H. Møller, and H. M. Nielsen, Biodegradable nanocomposite microparticles as drug delivering injectable cell scaffolds. *J. Control Release* 156, 11 (**2011**).

94. H. J. Chung, I. K. Kim, T. G. Kim, and T. G. Park, Highly open porous biodegradable microcarriers: *In vitro* cultivation of chondrocytes for injectable delivery. *Tissue Eng. A* 14, 607 (**2008**).

95. Q. Hou, P. A. De Bank, and K. M. Shakesheff, Injectable scaffolds for tissue regeneration. *J. Mater. Chem.* 14, 1915 (**2004**).

96. J. S. Patton and R. M. Platz, Routes of delivery: Case studies: Pulmonary delivery of peptides and proteins for systemic action. *Adv. Drug Deliv. Rev.* 8, 179 (**1992**).

97. R. U. Agu, M. I. Ugwoke, M. Armand, R. Kinget, and N. Verbeke, The lung as a route for systemic delivery of therapeutic proteins and peptides. *Respir. Res.* 2, 198 (**2001**).

REVIEW

98. H. M. Courrier, N. Butz, and T. F. Vandamme, Pulmonary drug delivery systems: recent developments and prospects. *Critical Reviews in Therapeutic Drug Carrier Systems* 19, 425 (**2002**).
99. M. Jalalipour, K. Gilani, H. Tajerzadeh, A. R. Najafabadi, and M. Barghi, Characterization and aerodynamic evaluation of spray dried recombinant human growth hormone using protein stabilizing agents. *Int. J. Pharm.* 352, 209 (**2008**).
100. R. U. Agu, M. I. Ugwoke, M. Armand, R. Kinget, and N. Verbeke, The lung as a route for systemic delivery of therapeutic proteins and peptides. *Respiratory Research* 2, 198 (**2001**).
101. D. A. Edwards, A. Ben-Jebria, and R. J. Langer, Recent advances in pulmonary drug delivery using large, porous inhaled particles. *J. Appl. Physiol.* 85, 379 (**1998**).
102. D. A. LaVan, T. McGuire, and R. Langer, Small-scale systems for in vivo drug delivery. *Nat. Biotechnol.* 21, 1184 (**2003**).
103. R. H. Hastings, H. G. Folkesson, and M. A. Matthay, Mechanisms of alveolar protein clearance in the intact lung. *Am. J. Physiol. Lung. Cell Mol. Physiol.* 286, 679 (**2004**).
104. M. Duszyk, CFTR and lysozyme secretion in human airway epithelial cells. *Eur. J. Physiol.* 443, S45 (**2001**).
105. R. Fernández-Urrusuno, D. Romani, P. Calvo, J. L. Vila-Jato, and M. J. Alonso, Development of a freeze-dried formulation of insulin-loaded chitosan nanoparticles intended for nasal administration. *STP Pharm. Sci.* 9, 429 (**1999**).
106. A. E. John, N. W. Lukacs, A. A. Berlin, A. Palecanda, R. F. Bargatze, L. M. Stoolman, and J. O. Nagy, Discovery of a potent nanoparticle P-selectin antagonist with anti-inflammatory effects in allergic airway disease. *J. FASEB* 17, 2296 (**2003**).
107. M. Kumar, X. Kong, A. K. Behera, G. R. Hellermann, R. F. Lockey, and S. S. Mohapatra, Chitosan IFN-gamma-pDNA Nanoparticle (CIN) Therapy for Allergic Asthma. *Genet. Vaccines Ther.* 1, 3 (**2003**).
108. T. Mizoe, T. Ozeki, and H. Okada, Application of a four-fluid nozzle spray drier to prepare inhalable rifampicin-containing mannitol microparticles. *AAPS Pharm. Sci. Tech.* Published online 18 June, 9, 755 (**2008**).
109. J. Wendorf, M. Singh, J. Chesko, J. Kazzaz, E. Soewanan, M. Ugozzoli, and D. O'Hagan, A practical approach to the use of nanoparticles for vaccine delivery. *J. Pharm. Sci.* 95, 2738 (**2006**).
110. S. Schurch, P. Gehr, V. I. Hof, M. Geiser, and F. Green, Surfactant displaces particles toward the epithelium in airways and alveoli. *Resp. Physiol.* 80, 17 (**1990**).
111. K. Makino, N. Yamamoto, K. Higuchi, N. Harada, H. Ohshima, and H. Terada, Phagocytic uptake of polystyrene microspheres by alveolar macrophages: effects of the size and surface properties of the microspheres. *Colloid Surf. B* 27, 33 (**2003**).
112. C. J. Musante, J. D. Schroeter, J. A. Rosati, T. M. Crowder, A. J. Hickey, and T. B. Martonen, Factors affecting the deposition of inhaled porous drug particles. *J. Pharm. Sci.* 91, 1590 (**2002**).
113. J. N. Pritchard, The influence of lung deposition on clinical response. *J. Aerosol. Med.* 14, S19 (**2001**).
114. B. J. Lipworth, Targets for inhaled treatment. *Respir. Med.* 94, S13 (**2000**).
115. J. Heyder, J. Gebhart, G. Rudolf, C. F. Schiller, and W. Stahlhofen, Deposition of particles in the human respiratory tract in the size range 0.005–15 μm. *J. Aerosol. Sci.* 17, 811 (**1986**).
116. W. H. Finlay, K. W. Stapleton, and P. Zuberbuhler, Fine particle fraction as a measure of mass depositing in the lung during inhalation of nearly isotonic nebulized aerosols. *J. Aerosol. Sci.* 28, 1301 (**1997**).
117. W. H. Finlay and M. G. Gehmlich, Inertial sizing of aerosol inhaled from two dry powder inhalers with realistic breath patterns versus constant flow rates. *Int. J. Pharm.* 210, 83 (**2000**).
118. A. Clark, Formulation of proteins and peptides for inhalation. *Drug Deliv. Syst. Sci.* 2, 73 (**2002**).
119. S. Bozdag, K. Dillen, J. Vandervoort, and A. Ludwig, The effect of freeze-drying with different cryoprotectants and gamma-irradiation sterilization on the characteristics of ciprofloxacin HCl-loaded poly(D,L-lactide-glycolide) nanoparticles. *J. Pharm. Pharmacol.* 57, 699 (**2005**).
120. D. Quintanar-Guerrero, A. Ganem-Quintanar, E. Allemann, H. Fessi, and E. Doelker, Influence of the stabilizer coating layer on the purification and freeze-drying of poly(D,L-lactic acid) nanoparticles prepared by an emulsion-diffusion technique. *J. Microencapsul.* 15, 107 (**1998**).
121. L. A. Dailey, T. Schmehl, T. Gessler, M. Wittmar, F. Grimminger, W. Seeger, and T. Kissel, Nebulization of biodegradable nanoparticles: Impact of nebulizer technology and nanoparticle characteristics on aerosol features. *J. Control Release* 86, 131 (**2003**).
122. I. Gonda, Pharmaceutical Inhalation Aerosol Technology, Second edn., edited by A. J. Hickey, Targeting by Deposition, Informa Healthcare, USA (**2003**).
123. C. Bosquillon, C. Lombry, V. Préat, and R. Vanbever, Influence of formulation excipients and physical characteristics of inhalation dry powders on their aerosolization performance. *J. Control Release* 70, 329 (**2001**).
124. G. Oberdörster, E. Oberdörster, and J. Oberdörster, Nanotoxicology: An emerging discipline evolving from studies of ultrafine particles. *Environ. Health Perspect.* 113, 823 (**2005**).
125. N. Y. Chew and H. K. Chan, Use of solid corrugated particles to enhance powder aerosol performance. *Pharm. Res.* 18, 1570 (**2001**).
126. H. Chrystyn, Is total particle dose more important than particle distribution? *Resp. Med.* 91, 17 (**1997**).
127. J. O. Sham, Y. Zhang, W. H. Finlay, W. H. Roa, and R. Löbenberg, Formulation and characterization of spray-dried powders containing nanoparticles for aerosol delivery to the lung. *Int. J. Pharm.* 269, 457 (**2004**).
128. K. Ohashi, T. Kabasawa, T. Ozeki, and H. Okada, One-step preparation of rifampicin/poly(lactic-co-glycolic acid) nanoparticle-containing mannitol microspheres using a four-fluid nozzle spray drier for inhalation therapy of tuberculosis. *J. Control Release* 135, 19 (**2009**).
129. S. Al-Qadi, A. Grenha, and C. Remuñán-López, Microspheres loaded with polysaccharide nanoparticles for pulmonary delivery: Preparation, structure, and surface analysis. *Carbohydr. Polym.* 86, 25 (**2011**).
130. A. Grenha, C. I. Grainger, L. A. Dailey, B. Seijo, G. P. Martin, C. B. Remuñán-López, and B. Forbes Chitosan nanoparticles are compatible with respiratory epithelial cells *in vitro*. *Eur. J. Pharm. Sci.* 31, 73 (**2007**).
131. G. Pilcer, F. Vanderbist, and K. Amighi, Preparation and characterization of spray-dried tobramycin powders containing nanoparticles for pulmonary delivery. *Int. J. Pharm.* 365, 162 (**2009**).
132. A. Grenha, C. Remuñán-López, E. L. S. Carvalho, and B. Seijo, Microspheres containing lipid/chitosan nanoparticles complexes for pulmonary delivery of therapeutic proteins. *Eur. J. Pharm. Biopharm.* 69, 83 (**2008**).
133. N. Mohajel, A. R. Najafabadi, K. Azadmanesh, A. Vatanara, E. Moazeni, A. Rahimi, and K. Gilani, Optimization of a spray drying process to prepare dry powder microparticles containing plasmid nanocomplex. *Int. J. Pharm.* 423, 577 (**2012**).
134. F. Ahsan, I. P. Rivas, M. A. Khan, and A. I. Suarez-Torres, Targeting to macrophages: role of physicochemical properties of particulate carriers–liposomes and microspheres–on the phagocytosis by macrophages. *J. Control Release* 79, 29 (**2002**).
135. J. B. Lyczak, C. L. Cannon, and G. B. Pier, Lung infections associated with cystic fibrosis. *Clin. Microbiol. Rev.* 15, 194 (**2002**).
136. D. L. French, D. A. Edwards, and R. W. Niven, The influence of formulation on emission, deaggregation and deposition of dry powders for inhalation. *J. Aerosol. Sci.* 27, 769 (**1996**).
137. N. Tsapis, D. Bennett, B. Jackson, D. A. Weitz, and D. A. Edwards, Trojan particles: large porous carriers of nanoparticles for drug delivery. *Proc. Natl. Acad. Sci. U.S.A.* 99, 12001 (**2002**).

138. S. M. McAllister, H. O. Alpar, Z. Teitelbaum, and D. B. Bennett, Do interactions with phospholipids contribute to the prolonged retention of polypeptides within the lung? *Adv. Drug Deliv. Rev.* 19, 89 (**1996**).

139. J. Wan, J. B. Gordon, K. Muirhead, M. W. Hickey, and M. Coventry, Incorporation of nisin in micro-particles of calcium alginate. *Lett. Appl. Microbiol.* 24, 153 (**1997**).

140. Y. Y. Yang, T. S. Chung, and N. P. Ng, Morphology, drug distribution, and in vitro release profiles of biodegradable polymeric microspheres containing protein fabricated by double-emulsion solvent extraction/evaporation method. *Biomaterials* 22, 231 (**2001**).

141. A. H. Kibbe (ed.), Handbook of Pharmaceutical Excipients, American Pharmaceutical Association, Washington and Pharmaceutical Press, London (**2000**).

142. A. Wade and P. J. Weller (eds.), Handbook of Pharmaceutical Excipients, Second edn., The Pharmaceutical Press, Washington DC (**1994**), pp. 186–190.

143. M. G. Moldenhauer and J. G. Nairn, Formulation parameters affecting the preparation and properties of microencapsulated ion-exchange resins containing theophylline. *J. Pharm. Sci.* 8, 659 (**1990**).

144. W. Hennink, O. Franssen, W. van Dijk-Wolthuis, and H. Talsma, Dextran hydrogels for the controlled release of proteins. *J. Control Rel.* 48, 107 (**1997**).

145. K. Janes, P. Calvo, and M. Alonso, Polysaccharide colloidal particles as delivery systems for macromolecules. *Adv. Drug Deliv. Rev.* 47, 83 (**2001**).

146. C. Freitas and R. H. Müller, Spray-drying of solid lipid nanoparticles (SLN TM). *Eur. J. Pharm. Biopharm.* 46, 145 (**1998**).

147. P. O. Souilliac, C. R. Middaugh, and J. H. Rytting, Investigation of protein/carbohydrate interactions in the dried state. 2. Diffuse reflectance FTIR studies. *Int. J. Pharm.* 235, 207 (**2002**).

148. A. Grenha, B. Seijo, C. Serra, and C. Remuñán-López, Chitosan nanoparticle-loaded mannitol microspheres: structure and surface characterization. *Biomacromolecules.* 8, 2072 (**2007**).

149. N. V. Majeti and R. Kumar, A review of chitin and chitosan applications. *React. Funct. Polym.* 46, 1 (**2000**).

150. S. Cao, B. Liu, X. Deng, and S. Li, Core/shell particles containing 3-(methacryloxypropyl)-trimethoxysilane in the shell: synthesis, characterization, and applicati. *Macromol. Biosci.* 5, 669 (**2005**).

151. S. Koennings, A. Berie, J. Tessmar, T. Blunk, and A. Goepferich, Influence of wettability and surface activity on release behavior of hydrophilic substances from lipid matrices. *J. Control Release* 119, 173 (**2007**).

152. S. Hirano, H. Seino, Y. Akiyama, and I. Nonaka, Biocompatibility of chitosan by oral and intravenous administrations. *Polym. Mater. Sci. Eng.* 59, 897 (**1988**).

153. M. Issa, M. Koping-Hoggard, and P. Artursson, Chitosan and the mucosal delivery of biotechnology drugs. *Drug Discov. Today: Technologies* 2, 1 (**2005**).

154. F. Andrade, F. Goycoolea, D. A. Chiappetta, J. das Neves, A. Sosnik, and B. Sarmento, Chitosan-grafted copolymers and chitosan-ligand conjugates as matrices for pulmonary drug delivery. *Int. J. Carbohyd. Chem.* Article ID 865704 (**2011**).

155. C. M. Lehr, J. A. Bouwstra, E. H. Schacht, and H. E. Junginger, *In vitro* evaluation of mucoadhesive properties of chitosan and some other natural polymer. *Int. J. Pharm.* 78, 43 (**1992**).

156. S. A. Agnihotri, N. N. Mallikarjuna, and T. M. Aminabhavi, Recent advances on chitosan-based micro- and nanoparticles in drug delivery. *Journal of Control Release* 100, 5 (**2004**).

157. J. H. Park, S. Kwon, M. Lee, H. Chung, J. H. Kim, Y. S. Kim, R. W. Park, I. S. Kim, S. B. Seo, I. C. Kwon, and S. Y. Jeong, Self-assembled nanoparticles based on glycol chitosan bearing hydrophobic moieties as carriers for doxorubicin: in vivo biodistribution and anti-tumor activity. *Biomaterials* 27, 119 (**2006**).

158. P. Artursson, T. Lindmark, S. S. Davisa, and L. Illum, Effect of chitosan on the permeability of monolayers of intestinal epithelial cells (Caco-2). *Pharm. Res.* 11, 1358 (**1994**).

159. A. De Campos, A. Sánchez, and M. J. Alonso, Chitosan nanoparticles: a new vehicle for the improvement of the delivery of drugs to the ocular surface. Application to cyclosporin A. *Int. J. Pharm.* 224, 159 (**2001**).

160. G. Borchard, H. L. Lueszen, A. G. De Boer, J. C. Verhoef, C. M. Lehr, and H. E. Junginger, The potential of mucoadhesive polymers in enhancing intestinal peptide drug absorption. III: Effects of chitosan-glutamate and carbomer on epithelial tight junctions *in vitro*. *J. Control Release* 39, 131 (**1996**).

161. A. Portero, C. Remuñán-López, and H. M. Nielsen, The potential of chitosan in enhancing peptide and protein absorption across the TR146 cell culture model-an in vitro model of the buccal epithelium. *Pharm. Res.* 19, 169 (**2002**).

162. A. Bernkop-Schnürch, C. E. Kast, and D. Guggi, Permeation enhancing polymers in oral delivery of hydrophilic macromolecules: Thiomer/GSH systems. *J. Control Release* 93, 95 (**2003**).

163. R. A. Muzzarelli, Human enzymatic activities related to the therapeutic administration of chitin derivatives. *Cell. Mol. Life Sci.* 53, 131 (**1997**).

164. Z. Leonenko, M. Rodenstein, J. Dohner, L. M. Eng, and M. Amrein, Electrical surface potential of pulmonary surfactant. *Langmuir* 22, 10135 (**2006**).

165. T. S. Wiedmann, R. Bhatia, and L. W. Wattenberg, Drug solubilization in lung surfactant. *J. Control Release* 65, 43 (**2000**).

166. C. Evora, I. Soriano, R. A. Rogers, K. M. Shakesheff, J. Hanes, and R. Langer, Relating the phagocytosis of microparticles by alveolar macrophages to surface chemistry: the effect of 1,2-dipalmitoylphosphatidylcholine. *J. Control Release* 51, 143 (**1998**).

167. B. G. Jones, P. A. Dickinson, M. Gumbleton, and I. W. Kellaway, Lung surfactant phospholipids inhibit the uptake of respirable microspheres by the alveolar macrophage NR8383. *J. Pharm. Pharmacol.* 54, 1065 (**2002**).

168. D. A. Edwards, J. Hanes, G. Caponetti, J. Hrkach, A. Ben-Jebria, M. Eskew, J. Mintzes, D. Deaver, N. Lotan, and R. Langer, Large porous particles for pulmonary drug delivery. *Science* 276, 1868 (**1997**).

169. H. Steckel and H. Brandes, A novel spray-drying technique to produce low density particles for pulmonary delivery. *Int. J. Pharm.* 278, 187 (**2004**).

170. H. J. Chung, I. K. Kim, T. G. Kim, and T. G. Park, Highly Open Porous Biodegradable Microcarriers: In vitro Cultivation of Chondrocytes for Injectable Delivery. *Tissue Eng.* 14, 607 (**2008**).

171. S. Suarez, P. O'Hara, M. Kazantseva, C. E. Newcomer, R. Hopfer, D. N. McMurray, and A. J. Hickey, Respirable PLGA microspheres containing rifampicin for the treatment of tuberculosis: Screening in an infectious disease model. *Pharm. Res.* 18, 1315 (**2001**).

172. L. A. Dailey, N. Jekel, L. Fink, T. Gessler, T. Schmehl, M. Wittmar, T. Kissel, and W. Seeger, Investigation of the proinflammatory potential of biodegradable nanoparticle drug delivery systems in the lung. *Toxicol. Appl. Pharmacol.* 215, 100 (**2006**).

173. V. R. Sinha, K. Bansal, R. Kaushik, R. Kumria, and A. Trehan, Poly-epsilon-caprolactone microspheres and nanospheres: An overview. *Int. J. Pharm.* 278, 1 (**2004**).

174. F. Wu and T. Jin, Polymer-based sustained-release dosage forms for protein drugs, challenges, and recent advances. *AAPS Pharm. Sci. Tech.* 9, 1218 (**2009**).

175. T. H. Lee, J. J. Wang, and C. H. Wang, Controlled release of Etanidazole from double-walled biodegradable microspheres. *J. Control Release* 83, 437 (**2002**).

176. Y. Yeo, N. Baek, and K. Park, Microencapsulation methods for delivery of protein drugs. *Biotechnol. Bioproc. Eng.* 6, 213 (**2001**).

177. V. Sluzky, J. A. Tamada, A. M. Klibanov, and R. Langer, Kinetics of insulin aggregation in aqueous solutions upon agitation in the

REVIEW

presence of hydrophobic surfaces. *Proc. Natl. Acad. Sci.* 88, 9377 (**1991**).

178. E. R. Johnson, L. A. Lanaski, V. Gupta, M. J. Griffin, H. T. Gaud, T. Needham, and H. Zia, *Pharm. Res.* 7, S-181 (**1990**).

179. E. Kai and T. Ochiya, A method for oral DNA delivery with N-acetylated chitosan. *Pharm. Res.* 21, 838 (**2004**).

180. E. Walter, M. A. Croyle, B. L. Davidson, B. J. Roessler, J. M. Hilfinger, and G. L. Amidon, Adenovirus mediated gene transfer to intestinal epithelial cells as a potential approach for oral delivery of peptides and proteins. *J. Control Release* 46, 75 (**1997**).

181. D. J. Glover, H. J. Lipps, and D. A. Jans, Towards safe, non-viral therapeutic gene expression in humans. *Nat. Rev. Genet.* 6, 299 (**2005**).

182. C. W. Pouton and L. W. Seymour, Key issues in non-viral gene delivery. *Adv. Drug Deliv. Rev.* 34, 3 (**1998**).

183. J. M. Dang and K. W. Leong, Natural polymers for gene delivery and tissue engineering. *Adv. Drug Deliv. Rev.* 58, 487 (**2006**).

184. D. R. Sorensen, M. Leirdal, and M. Sioud, Gene silencing by systemic delivery of synthetic siRNAs in adult mice. *J. Mol. Biol.* 327, 761 (**2003**).

185. Y. Zhang, P. Cristofaro, R. Silbermann, O. Pusch, D. Boden, T. Konkin, V. Hovanesian, P. R. Monfils, M. Resnick, S. F. Moss, and B. Ramratnam, Engineering mucosal RNA interference *in vivo*. *Mol. Ther.* 14, 336 (**2006**).

186. S. Lecollinet, F. Gavard, M. J. Havenga, O. B. Spiller, A. Lemckert, J. Goudsmit, M. Eloit, and J. Richardson, Improved gene delivery to intestinal mucosa by adenoviral vectors bearing subgroup B and d fibers. *J. Virol* 80, 2747 (**2006**).

187. G. Romano, C. Pacilio, and A. Giordano, Gene transfer technology in therapy: current applications and future goals. *Stem Cells* 17, 191 (**1999**).

188. G. Han, C. T. Martin, and V. M. Rotello, Stability of gold nanoparticle-bound DNA toward biological, physical, and chemical agents. *Chem. Biol. Drug Des.* 67, 78 (**2005**).

REVIEW

Development of Electrospun Nanofibers for Biomedical Applications: State of the Art in Latin America

Pablo C. Caracciolo, Pablo R. Cortez Tornello, Florencia Montini Ballarin,
and Gustavo A. Abraham*

*Instituto de Investigaciones en Ciencia y Tecnología de Materiales, INTEMA (UNMdP-CONICET),
Av. Juan B. Justo 4302, B7608FDQ Mar del Plata, Argentina*

Electrospinning is a powerful processing technique with huge potential in many attractive and cutting-edge research fields. This technique allows the production of non-woven micro/nanofibrous materials, including polymers, ceramics and metals, with a wide range of morphologies and functionalities. The highly porous electrospun scaffolds are ideal for biomedical applications, in particular for tissue engineering and drug delivery of biologically active compounds. In this review, we summarize the works on electrospun micro/nanofibers for biomedical applications carried out by research groups from Latin American countries. Studies are mainly focused on nanofibrous polymeric systems for drug delivery of therepeutic and bioactive agents, tissue engineering scaffolds and sensors, as well as other biomedical applications.

Keywords: Nanofibers, Electrospinning, Tissue Engineering, Drug Delivery Systems, Biomedical Applications.

CONTENTS

1. INTRODUCTION

Nanostructured systems are promising for many different and novel applications. Current nanotechnological advances provide opportunities to characterize, manipulate and organize matter at the sub-micron and nanometer scale. Biomaterials with nano-scale organizations have been used as controlled drug delivery systems and artificial scaffolds for tissue engineering.[1,2] However, the development of nano-scale drug and biomacromolecule delivery systems with optimal bioavailability, effective targeting and no cytotoxicity is still a big challenge. On the other hand, the tradicional tissue engineering strategy uses bioresorbable porous scaffolds with appropriate requirements to regenerate functional tissues. Recent efforts are addressed to the control over cell behavior and tissue formation. The native extracellular matrix is mimicked by nano-scale topography.[3,4] The controlled release of bioactive agents is also a focus of attention, since it will enhance the performance of tissue engineered matrices.

The broad interest in nanomaterials is leading to the creation of a huge variety of nanostructured systems, including nanoparticles, nanocapsules, nanogels, nanofibers, nanotubes, and dendrimers, just to mention a few.[1,5–8] Electrospun nanofibers have served as a highly versatile platform for a broad range of applications in widely different areas such as catalysis, nanofluidics, sensors, medicine, energy, environmental engineering, biotechnology, defense and security, and healthcare.[9–12]

The development of biomimetic highly-porous scaffolds is essential for successful tissue engineering.[13] Polymeric nanofiber-based scaffolds provide a structural support for the cells to accommodate and nutrient transportation. Also, guide cell growth in the three-dimensional space into a specific tissue.[14] In this way, biomimetic electrospun

---

*Author to whom correspondence should be addressed.

matrices facilitate cell attachment, support cell growth, and regulate cell differentiation.[15–17]

Processing techniques to produce polymeric nanofibers include phase separation, self-assembly, and electrospinning.[18, 19] Phase separation does not requiere specialized equipment, and constructs can be prepared in molds with specific geometry. On the other hand, this method requires several steps to produce nanofibers of a limited number of polymers, and it is difficult to scale-up to a commercial stage. Self-assembly can be used for nanofiber fabrication,

Pablo C. Caracciolo obtained his Ph.D. in Materials Science from the School of Engineering, National University of Mar del Plata, Argentina. His doctoral research consisted of bioresorbable polyurethane matrices for tissue engineering applications. Currently, he is working at the Research Institute for Materials Science and Technology (INTEMA) as assistant researcher for the National Research Council (CONICET). His research interests include non viral gene delivery, biocompatible drug delivery systems, and electrospun nanofibrous materials.

Pablo R. Cortez Tornello received his B.S. degree in Bioengineering from the School of Engineering, National University of San Juan, Argentina. Currently, he is the recipient of a doctoral research fellowship (funded by CONICET) in Materials Science at the National University of Mar del Plata, Argentina. His main interests are drug delivery systems and polymeric porous structures for tissue engineering applications.
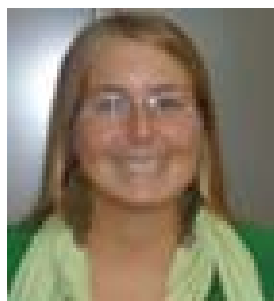
Florencia Montini Ballarin received her B.S. degree in Materials Engineering from the School of Engineering, National University of Mar del Plata, Argentina. Currently, she is the recipient of a doctoral research fellowship (funded by CONICET) in Materials Science at the same University. Her interests are focused on developing synthetic and semi-synthetic small diameter vascular grafts and aligned nanofibrous systems for tissue engineering applications.

Gustavo A. Abraham obtained his Ph.D. in Materials Science from the School of Engineering, National University of Mar del Plata, Argentina, and is working at the Research Institute for Materials Science and Technology (INTEMA) as independent researcher for the National Research Council (CONICET). He is Associate Professor of Chemistry and Biomaterials at the School of Engineering of the National University of Mar del Plata, Argentina. His research interests include polymeric biomaterials, scaffolding, tissue engineering, and biomimetic nanomaterials. He has authored more than 45 peer-reviewed research papers, 13 book chapters, and over 110 conference proceedings. His research supports are from the Argentinean National Agency of Scientific and Technological Promotion, the National Research Council, the Ibero-American Programme For Science, Technology and Development (CYTED), and the National University of Mar del Plata. He is an active member of the European Society for Biomaterials, Latin American Society for Biomaterials, Artificial Organs and Tissue Engineering, Argentinean Nanomedicine Association, and Argentinean Materials Association. He serves on the editorial board of the Journal of Biomaterials and Tissue Engineering as Regional Editor for South America. Dr. Abraham has been recognized with the Bernardo Houssay Award from the Ministry of Science, Technology and Productive Innovation of Argentina, in 2012.

but relies on intermolecular forces to assemble small molecules, peptides, proteins and nucleic acids into fibers. This process is limited to a few polymers and only creates short fibers of several micrometers. Electrospinning is currently the most promising technique to produce continuous nanofibers. In this process, solid fibers are produced from a polymeric fluid stream (solution or melt), forming highly porous non-woven micro/nanofibrous membranes with excellent pore interconnection. Advantages of electrospinning include a relatively inexpensive setup, and the possibility to create different fiber architectures for use in many areas of application.

In this review, we summarize the works reported on electrospun nanofibers for biomedical applications carried out by research groups from Latin American countries. These studies are mainly focused on nanofibrous polymeric systems for the delivery of therapeutic and bioactive agents, tissue engineering scaffolds and regenerative medicine, sensors and other applications to a lesser extent. First, a short historical introduction and process description are presented. Second, the advances in each one of the above mentioned areas are described and commented. Finally, in the concluding remarks section, a vision of the future research on this topic is presented.

2. THE ELECTROSPINNING TECHNIQUE

2.1. Brief Historical Introduction

Electrospinning (also known as electrostatic spinning) is an electrohydrodynamic process discovered by Lord Rayleigh as part of his investigations in electrospraying in the late 1800s. The first patents for electrospinning were granted in 1902 to Cooley and Morton, but major commercialization did not occur until the advances made by A. Formhals (patents for the fabrication of textile yarns in 1934–1944) and C. L. Norton (patents in the area of electrospinning from melts in 1936). The main theoretical basis for electrospinning was made by Sir Geoffrey Taylor (in 1964–1969) when he developed mathematical models for the shape of the cone formed by the fluid droplet at the tip of the polymer reservoir under the effect of an electric field (known as the Taylor cone).[2, 20]

After Taylor's work on the jet-forming process, attention focused on the understanding of the relationships between processing parameters and structural properties. Since the 1990s, when the rising interest in nanotechnology reawakened the interest in many technological areas, electrospinning has gained more attention. The great interest on the electrospinning process was quickly reflected by the large number of articles and patents published in the literature.[21–23] In recent years, the availability of commercial nanofiber electrospinning units has prompted further research in nanoscience and nanotechnology.

2.2. The Process

Nano/microfibers are produced when a polymer solution (or polymer melt) is subjected to a high-voltage electrostatic field operated between a metallic nozzle and a grounded collector as counter electrode. The transition from a charged droplet emerging from a die to a solid fiber is controlled by a set of complex physical instabilities.[24] A number of excellent reviews that describe and analyze the process can be found in the literature.[2, 10, 20, 23, 25, 26]

Electrospinning is a unique and versatile process to produce polymeric fibers in the diameter range of few nanometers to several micrometers (usually between 3 nm–5 μm).[15] Electrospun meshes form three-dimensional scaffolds with high porosity, interconnected pore structure, and high surface area-to-volume ratio.

The fibers produced from melt polymers are thicker (due to the higher viscosity and the lack of solvent evaporation), but the process has significant advantages in that no volatile solvent is required and much higher volumes of material can be produced. Advantages are clear, and progresses in the technology behind the process are being made to scale this processing technique in order to get equipments and products commercially available.

Although the major attraction of electrospinning is its simplicity, the process is governed by a number of parameters that greatly affect fiber formation and structure. The main parameters are polymer structure and molecular weight, polymer-solution properties (concentration, solvent, viscosity, conductivity and surface tension), processing parameters, such as applied electrical potential, polymer solution flow rate, distance between spinneret and collector (working distance), position, geometry and static or rotatory nature of the grounded or charged targets, and ambient parameters (temperature, humidity, and air velocity). Therefore, this process is not as simple and easy as it appears. In order to produce defect-free nanofibers with controlled fiber diameter distribution and orientation, these parameters must be precisely controlled. Detailed explanations of each parameter and its influence on the electrospinning process can be found in the literature.[2, 15]

In tissue engineering applications, the small fiber size intrinsic to electrospinning process can hinder efficient cellular infiltration.[27] In recent years, the preparation of electrospun scaffolds with controllable macroscopic porosity by several techniques, such as the combination of electrospinning with salt leaching[27–30] and salt leaching/gas foaming,[31] the use of auxiliary electrodes and chemical blowing agents,[32] cryogenic electrospinning,[33] and the use of tailored collectors,[34] have been reported. Nanofibers can be functionalized through encapsulation, grafting, coating or blending of biologically active compounds such as proteins, enzymes, and growth factors. Moreover, nanofibers can be assembled into a variety of arrays or architectures by manipulating their alignment, stacking, or folding.[17, 24, 35]

The production of individual fibers, random non-wovens, or orientationally highly ordered non-wovens can be achieved by an appropriate selection of electrode arrays or collector configurations.[14] The orientation of nanofibers is interesting for many tissue engineering applications where a distinct growth direction for the cells is required.[36–38] The basic setup has also been extended towards coaxial electrospinning of core–shell micro- and nanofibers, increasing the possibilities and potential areas of application.[39]

Although electrospinning is predominantly applied to polymer based materials including natural polymers, synthetic polymers, and composites,[10, 40] recently, its use has been extended towards the production of metal, ceramic and glass nanofibers exploiting precursor routes.[41]

3. ELECTROSPUN NANOFIBERS IN DRUG DELIVERY SYSTEMS

The controlled release of drugs and active principles is an efficient process to balance the delivery kinetics, minimizing the toxicity and side effects. To achieve a controlled and sustained release system, the active substance is included into a device that ensures a predictable release rate *in vivo*, being administered topically, by an injected or non-injected route.

Electrospun nanofibers exhibit highly attractive functional characteristics as potential drug delivery carriers. Their porous structure with interconnected pores, high specific surface area, and short diffusion passage length increase the dissolution rate of a particulate drug and help in mass transfer and efficient drug release.[2, 20, 42, 43] Moreover, depending on nanofiber morphology, porosity and composition, the release kinetics from a pharmaceutical dosage form can be designed as rapid, immediate, delayed or modified dissolution. The preparation of electrospun drug-loaded membranes offers other advantages, such as the ease of drug loading in simultaneous with fiber formation.

The bioavailability of poorly water-soluble drugs with pharmacological activity for the treatment of several diseases is a well known problem in the pharmaceutical industry. Besides, up to 40% of the active principles discovered in the last years are poorly soluble or lipophilic compounds, which lead to limited oral bioavailability, unpredictable absorption and lack of dose proportionality. Several strategies are available to solve these limitations, such as the use of solid dispersions, emulsions, liposomes, nanoparticles, and cyclodextrins, among others. In addition, the use of polymer-based electrospun micro/nanofibers containing dispersed drugs has also been reported for potential use in oral and topical drug delivery.[44]

The development of topical devices containing poorly water-soluble drugs for the treatment of skin diseases must achieve several requirements. The devices must contain solubilized drugs in a non-ionized state to accomplish therapeutical concentrations and to be optimally bioavailable

to the skin. These systems can be developed by several strategies, including solution/dispersion technologies.[45, 46] Although these techniques are at an early stage respect to pharmaceutical applications, they are suggested to be of high value in topical drug administration and wound healing.[44, 47] Moreover, new drugs developed for efficient treatment of infections are unable to distinguish between the membranes of the fungi and mammalian cells, resulting in undesirable side effects when administered orally for the treatment of epithelial fungal diseases.[48]

To reduce undesired side effects at the systemic level, our group developed polymer systems with dispersed antifungal agents for topical applications.[49] Microfibrous poly(lactide-co-glycolide) (PLGA 50:50) meshes containing Ketoconazole or Chalcone 1, both poorly water-soluble drugs, were prepared by electrospinning. Ketoconazole is a commercial drug with antifungal properties, whereas Chalcone 1 (2,4-dihydroxy-3-metoxichalcone) is a natural active principle with proven antifungal properties,[50] extracted from natural species *Zuccagnia punctata Cav.* (Fabaceae).[51] The fiber diameters resulted higher for drug-loaded meshes (Fig. 1). The absence of characteristic melting peaks of Ketoconazole and Chalcone 1 in the polymeric matrices suggests complete dissolution of the active principles. The hydrophilic and amorphous nature of PLGA, added to the observed plastification effects due
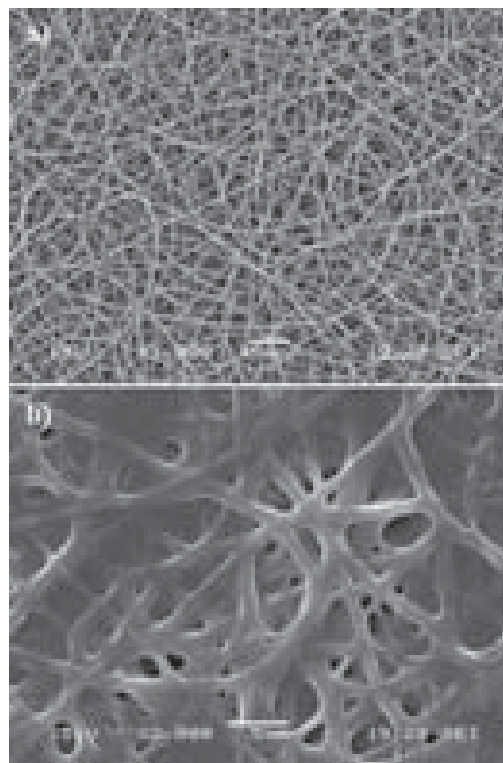
Fig. 1. SEM micrographs of electrospun meshes: (a) PLGA (×1000), (b) PLGA/Chalcone 1 (×3000). (Manuscript in preparation.)

to drug loading, should lead to drug release by hydrolytic degradation mechanism. The loaded amounts of the active principles resulted suitable for the treatment of fungal diseases by topical application, being potentially applicable for short-time exposures. Further studies to assess the release behavior of these matrices are being performed.

We have also developed microfibrous systems for antimycotic drug delivery applications. A poorly water-soluble antimycotic and bioactive agent, embelin, was dispersed in a biodegradable and biocompatible polymer matrix of poly(ε-caprolactone) (PCL).[52] Due to its hydrophobic character and semicrystalline structure, PCL exhibits a degradation time around two years under physiological conditions. PCL is degraded by hydrolysis, being the speed of this process dependent on the shape and size of the device, the dispersed bioactive agent, and the physiological characteristics of the biological environment. Embelin (2,5-dihydroxy-3-undecil-1,4-benzoquinone) is an active principle obtained from *Oxalis erythrorhiza* Gillies ex Hooker et Arnott (Oxalidaceae) collected in San Juan, Argentina.[53–55] This compound shows a diversity of relevant biological activities, such as *in vitro* cytotoxicity against B16 and XC tumor cell lines, anti-fertility effects, anticonvulsant, antidiabetic and antimicrobial activities. To our knowledge, this is the first work incorporating embelin into polymeric matrices without using diluents. The amount of drug in meshes preparation was selected to ensure the minimum inhibitory concentration of embelin (MIC index, 100 μg ml^{-1}) for both bactericidal and trypanocidal activities.[55, 56] Microfibrous embelin-loaded PCL meshes exhibited a significative decrease in drug crystallinity, indicating its good solubilization in the polymeric matrices. The polymer carrier stabilized the amorphous drug dispersion/solution, suppressing or retarding the tendency for the drug to recrystallize for a period long enough to make the system pharmaceutically useful.[57] Although the *in situ* bioavailability of a drug-loaded mesh strongly depends on its size and geometrical parameters, the morphological analyses commonly found in the literature do not take into account the real morphology of the matrices, which is considered in this work. Drug-loaded fibrous membranes showed higher bioavailability of the bioactive agent due to an increase of 86% in the area-to-volume ratio, providing an effective area per unit mass 5.8-fold higher than that found for the corresponding film. Embelin showed an initial burst release, probably the drug dispersed on the surface of the membrane (Fig. 2), followed by a slow release, suggesting a mechanism involving the diffusion of the active agent molecules through the PCL matrix to the aqueous solution. The better capacity of the membranes to expose amorphous embelin make them potential drug-loaded systems with improved efficiency, being the *in vivo* antifungal activity against dermatophytes *(Trichophyton mentagrophytes)* currently under investigation.

Recently, hyperbranched polyglycerol (HPGL) gels gained attention as biomaterials due to their topology,
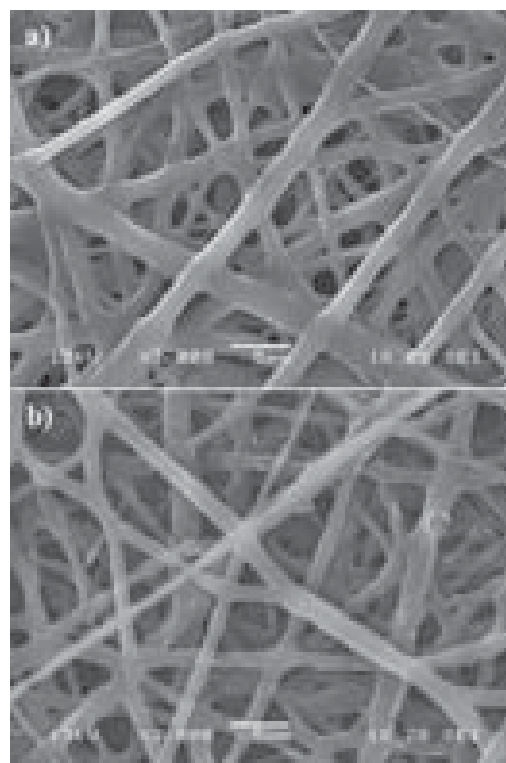
Fig. 2. SEM micrographs of electrospun meshes (×3000), (a) PCL and (b) PCL/Embelin (surface exposed to air). Adapted with permission from [52], P. R. C. Tornello et al., Dispersion and release of embelina from electrospun, biodegradable, polymeric membranes. *Polym. J.* (**2012**), doi:10.1038/pj.2012.80. © 2012, Nature Publishing Group.

which can lead to molecular capsules and compartments for guest bioactive molecules.[58] Thus, therapeutic agents can be loaded into this polymer to be topically absorbed, providing the desirable therapeutic effects within wound sites. Moreover, HPGL hydrogels can potentially increase both cell attachment and cell growth, due to their swelling ability, non-toxicity and biocompatible properties, acting as possible wound-healing accelerators. Motivated by the development of bioactive wound dressings, Vargas et al. worked on the preparation of electrospun HPGL hydrogel nanofibers containing *Calendula officinalis* (CO), and tested the anti-inflammatory activity for wound-healing applications.[59] A rapid release of CO from the electrospun HPGL nanofibers at physiological temperature was exhibited as result of the high swelling ability of the carrier,[60] as well as the high porosity and surface area of the electrospun HPGL–CO membranes, and probably their erosion within the medium. The CO release process, dependent on the CO content in the HPGL nanofibers, is diffusion-controlled, and the release kinetic agrees with the reservoir-type drug release system. Electrospun HPGL matrix was tough and hard, whereas electrospun HPGL–CO membranes resulted more soft and flexible, presenting higher elongation at break and lower tensile strength values with

REVIEW

increasing concentrations of the bioactive agent, possibly due to its plasticization effects. The electrospun HPGL–CO demonstrated a significantly higher work of adhesion relative to HPGL on biological tissue. The increase in flexibility of the HPGL–CO membranes could have improved the contact between the membrane and the biological tissue, hence promoting the penetration of the hydrated nanofibers into the tissue to form a strong bonding, leading to an increase in the adhesion strength.[61] The loaded electrospun HPGL–CO nanofibers displayed a low inflammatory reaction and fast reepithelialization after implantation in rats. These results of *in vivo* experiments suggest that HPGL–CO membranes might be interesting bioactive wound dressing materials for clinical applications.

Castillo-Ortega et al. also reported the preparation of a fibrous membrane containing a poorly water-soluble drug, obtained by coaxial electrospinning. The fibers were composed of poly(vinyl pyrrolidone) (PVP) as core polymer and cellulose acetate (CA) as shell material.[62] CA nanofibers were used for controlled drug release and tissue engineering applications, while PVP was widely explored for microencapsulation, controlled drug release, and articular cartilage replacement. The CA/PVP/CA membrane was not loaded during the electrospinning process, being the drug incorporated by immersion into an amoxicillin salt solution. The release behavior of amoxicillin resulted dependent on the pH of the medium. The amount of drug released at pH 7.2 was approximately three times higher than that observed at pH 3.0 for any given time. This pH-dependent behavior suggests a higher interaction by hydrogen-bonding at pH 3.0, between the protonated carboxylic groups in amoxicillin and the carbonyl groups present in CA and PVP, resulting a lower drug release. Even more, the equilibrium release of amoxicillin from the fibrous membrane was reached after 2 weeks approximately, regardless of the pH employed. Based on these results, the fibrous CA/PVP/CA membranes would have potential applications in oral administration as well as in controlled-release transdermal patches.

Besides drugs with limited solubility in aqueous media, proteins also have particular delivery requirements. There are many proteins of nutritional and therapeutic relevance, but due to their structural instability once they are extracted from their natural source, new and effective protein delivery systems are needed. Enzymes are proteins responsible in catalysing most of the chemical reactions taking place in the body, that, when affected by several pathologies, can lose its capacity to produce certain enzymes or the enzymes produced lack of catalytic activity. Hence, there is a need for proper and effective enzyme sustained release systems. Electrospun nanofibers are interesting alternatives, due to the generation of nanofibers in one step. Thereby, the exposure of proteins to harsh organic solvents and elevated temperatures can be avoided, reducing the risk of denaturalization. Several substances of biological interest, like plasmids, nerve growth factors and bovine serum albumin,[63–65] and enzymes, such as β-galactosidase, lysozyme and luciferase,[65–68] have been encapsulated and released from nanofibers. Moreno et al. successfully encapsulated the enzyme lactate dehydrogenase (LDH) in poly(vinyl alcohol) (PVA) nanofibers, using coaxial electrospinning.[69] This setup was chosen due to the poor miscibility of the enzyme in the PVA solution. The systems employing the enzyme as core solution displayed entangled fibers with bead defects, while the shell-enzyme membranes showed the presence of numerous agglomerates (Fig. 3). In all cases, the enzyme conserved its catalytic function after processing into nanofibers. The core-enzyme membranes displayed a burst release within the first two days, followed by a sustained release for about three weeks. The hydrophilic nature of PVA produces an immediate swelling of the shell layers, probably generating that both enzyme molecules immobilized in the interior of the nanofibers and the ones present in their surface are liberated to the medium. On the other hand, the shell-enzyme systems displayed a burst release during the first five days, due to the desorption of the enzyme molecules adsorbed at the surface of the nanofibers. After a 10-day release, a strong decrease in enzyme activity was observed. Also, the core-enzyme systems were soaked in methanol to generate a physical crosslinking by hydrogen-bonding among PVA chains, increasing its crystallinity and avoiding the loosening of the fibrous morphology. In this case, there is a steady increment in enzyme release until the fourth week. The crosslinking process increases the water resistant quality of the PVA nanofibers. These crosslinked-polymer membranes work in similar way to reservoir-type release devices, acting as diffusive barriers that regulate the rate of release of the enzyme molecules. This is an interesting high molecular-weight model for protein sustained release systems, and a potential enzyme controlled delivery system in the clinical treatment for the LDH deficiency disease.

The topical administration of nitric oxide (NO) has been presented as a potential treatment for diabetic foot ulcers (DFU) as well as for ulcers generated by the cutaneous leishmaniasis (CL) disease. It is estimated that 1.5 million people suffer from CL annually and more than 350 million are at risk of infection. In Latin America 62,000 new cases are reported every year, being endemic in 18 countries.[70] Ulcers have been treated with meglumine antimoniate (Glucantime) for more than 60 years, showing a cure rate greater than 85%.[71] However, this drug has been associated to several side effects (cardiac abnormalities, increased hepatic aminotransferase, pancreatitis). Additionally, the adherence to the treatment is affected by its duration (several weeks). Thus, new safe therapeutic options are needed. In several *in vitro* and *in vivo* studies, it has been demonstrated that NO plays a key role in the elimination of Leishmania intracellular amastigotes. On the other
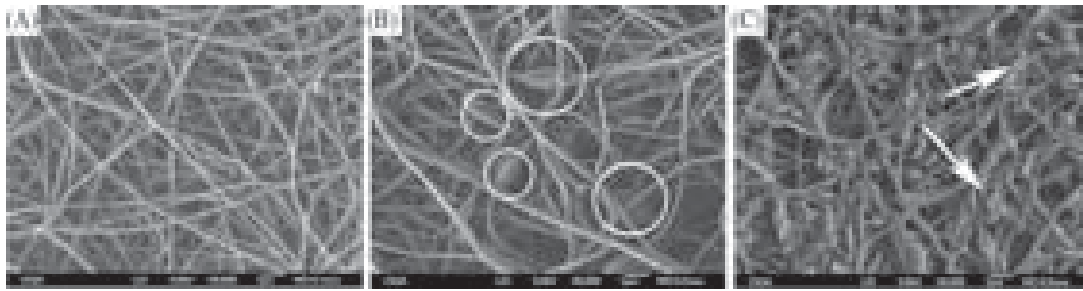
Fig. 3. SEM micrographs of PVA nanofibers (A) without enzyme, (B) employing the enzyme-solution as core-solution, and (C) employing the enzyme-solution as shell-solution. Adapted with permission from [69], I. Moreno, et al., Control release of lactate dehydrogenase encapsulated in poly(vinyl alcohol) nanofibers via electrospinning. *Eur. Polym. J.* 47, 1264 (**2011**). © 2011, Elsevier.

hand, diabetes mellitus constitutes one of the most important public health problems due to its high prevalence and enormous social and economic consequences. It is believed that there are more than 135 million diabetics worldwide, and this number is expected to increase to 300 million in the next 25 years.[72] DFU, one of the chronic consequences of diabetes mellitus, constitute the most important cause of non-traumatic amputation of inferior limbs. It has been described that the alteration of the immune and wound healing responses in diabetic patients is characterized, among others, by a minor production of NO.[73]

The topical treatments employing NO against CL ulcers in humans showed encouraging results and minimal side effects, but the main problem was the unsustained NO release, requiring multiple applications and hindering the adherence of the patients.[74, 75] To overcome this problem, Smith et al. developed a nanofiber NO releasing patch (NOP).[76] This device is a four-layer polymeric transdermal patch (Fig. 4), in which the principal components are stabilized and encapsulated in nanofibers which guarantee a constant NO release upon its hydration. The NO is generated by acidifying nitrite with ascorbic acid. Both components are encapsulated in polyurethane electrospun nanofibers to avoid an instant blast of NO, ensuring a maintained release of 3.5 μmol/cm^2 during 12 h or more depending upon the dosage.

With respect to CL disease, a clinical trial was conducted to determine the effectiveness of NOP respect to Glucantime, with less adverse events and lower cost. The cure rates after a 3-month treatment were 94.8% for the group that received Glucantime compared to 37.1% in the NOP group.[77] Despite the lower efficacy of the patch versus Glucantime, a significantly lower frequency of adverse events and a reduced variation in serum markers were observed in patients treated with the patch. These facts, added to the facility of topic administration justify the development of new systems for the treatment of CL. Thus, studies are currently in place to increase the amount of NO released to the infected area and to mimic the response of innate immune cells to pathogen infection. In addition, as topically administered NO is a potential treatment for chronic ulcers, a clinical trial has been proposed to evaluate the effectiveness and safety of this novel NO release wound dressing for the treatment of DFU.[78]
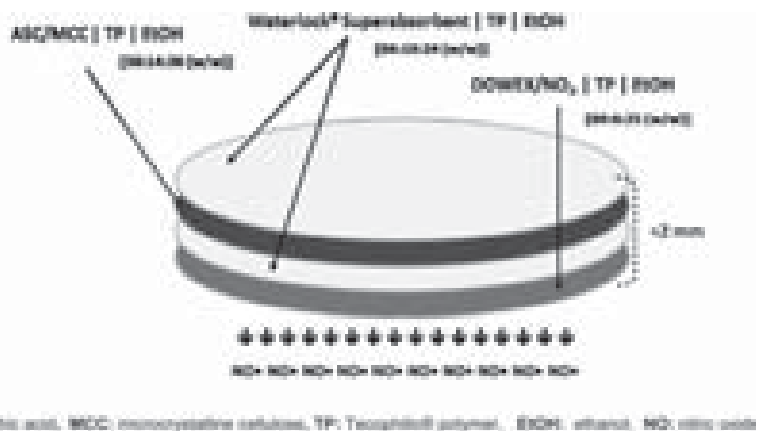
Fig. 4. Electrospun nitric oxide releasing patch (NOP). Cited with permission from [76], D. J. Smith, et al., Topical nitric oxide donor devices, [WO/2006/058318], Ref Type: Patent (**2006**). © 2006, The American Society of Tropical Medicine and Hygiene.

4. ELECTROSPUN SCAFFOLDS FOR TISSUE ENGINEERING

Millions of surgical procedures, requiring the use of tissue or organ substitutes to repair or replace those damaged or severely affected by a disease, are performed every year. The growth in life expectancy has also become an important factor of this enlarged demand. Although being the traditional approaches, biological implants present several disadvantages. Among others, xenograft implants generate thrombosis and calcification events; allograft transplantation is limited by the number of available donors; and autograft transplantation has restricted applications, generating pain and discomfort. Therefore, efforts in terms of healing and reconstruction of human tissue are being carried in the medical, biological, chemical and engineering fields. Tissue engineering has emerged in the last decades as an alternative multidisciplinary approach to circumvent these limitations.

Tissue engineering has recently been defined as 'the creation (or formation) of new tissue for the therapeutic reconstruction of the human body, by the deliberate and controlled stimulation of selected target cells through a systematic combination of molecular and mechanical signals.'[79] Although there is no mention of a biomaterial in this definition, in the classical tissue engineering approximation[80] a scaffold biomaterial is usually employed to support cell growth and provide shape to the developing tissue engineered construct, as well as to facilitate the delivery of those molecular and mechanical signals. Current challenges lie in the election/design of natural, synthetic or composite biocompatible and bioresorbable materials to produce scaffolds mimicking the biological functions of natural extracellular matrix (ECM).[81, 82] The ECM is a three-dimensional network in which collagen embedded in proteoglycans organizes in nanometer scale multifibrils.[83] The structure and morphology of the ECM also greatly contribute to the properties and functions of each organ. Hence, the development of nanostructured porous scaffolds with interconnected pores, wide pore size distributions, large surface areas and adequate mechanical properties also constitutes a dare. Together with the election of appropriate materials, these parameters affect not only cell survival, signalling, adhesion, proliferation, and reorganization, but also their gene expression and the preservation, or not, of their phenotype,[84] or their differentiation for the case of stem cells. Moreover, the ideal scaffold should also present seeded cells uniformly distributed throughout the entire matrix. Therefore, another challenge to be overcome by tissue engineering is the maintenance of cell viability after implantation. A functional vasculature is fundamental for the delivery of nutrients and removal of metabolites from the cells, otherwise cell survival is not possible. The support of this vasculature is mainly dependent on the surface and pore size characteristics of the scaffold, which control the adhesion and organization of the vascular endothelial cells into blood vessels.[85]

Up to date, a wide variety of materials and processing methods have been proposed for the design of scaffolds to regenerate human tissues. Bone, cartilage, skin, cardiovascular and neural tissues, spinal cord, blood vessels, tendons, ligaments, and organ tissue regeneration show promise for a large portion of individuals with special needs. Electrospinning recently emerged as a promising technology for the generation of non-woven nanofiber-based scaffolds, which not only mimic the nanoscale fibrous structure of natural ECM but also its spatial organization on the mesoscopic scale (control over fiber orientation and spatial placement). Matrices with appropriate fiber diameters, topology, texture, pore size, chemical compatibility and mechanical properties adequate for specific target tissues can be obtained.[86] In this way, electrospun matrices facilitate cell attachment, support cell growth, and regulate cell differentiation,[15–17, 87] providing an easy passage for nutrient intake and metabolic waste exchange,[88] which make them potentially applicable as wound dressing, vascular grafts, and tissue engineering scaffolds.[23, 89–91]

4.1. Soft Tissue Engineering Applications

Electrospinning has been used for the fabrication of nanofibrous scaffolds from numerous bioresorbable synthetic and natural polymers, blends, and composites.[23] Classical synthetic polyesters can provide the necessary strength for structural stability, and their electrospun scaffolds have been explored for the regeneration of bone tissue,[92, 93] musculoskeletal tissue,[94] myocardial tissue grafts,[95, 96] and blood vessel substitutes.[97, 98] However, they are relatively stiff, non-elastic materials and not ideally suited for engineering of soft flexible tissues such as cardiovascular, urological, or gastrointestinal tissues.

The development of soft-tissue engineering needs bioresorbable materials exhibiting elastomeric properties. Elastomeric polyurethane scaffolds can withstand the action of stress and load and undergo an elastic recovery with little or no hysteresis. In recent years, biocompatible and biodegradable segmented polyurethanes (SPU) have been investigated for applications in the tissue engineering field, such as cardiovascular tissue engineering,[99–101] musculoskeletal applications (anterior cruciate ligament,[102] knee joint meniscus,[103] smooth muscle cell constructs for contractile muscle[104, 105]) and nerve regeneration.[106] Their highly variable chemistry allows the preparation of biocompatible materials with controlled physico-chemical, mechanical, and biodegradation properties that can be achieved through the appropriate selection of monomers and the manipulation of hard and soft content. Biodegradation into non-toxic components can be promoted by the use of aliphatic diisocyanates. Bioresorbable polyester soft segments are commonly used to provide hydrolytically

labile soft segments,[107] whereas chain extenders containing easily hydrolyzable linkages increase the SPU degradation rate.[108]

Surprisingly, SPU and poly(urethane urea)s (SPUU) have been infrequently used for the fabrication of electrospun scaffolds. So far, only limited studies on nanofibrous polyurethanes have been reported as tissue engineering scaffolds.[109, 110] Prado et al. attempted to produce polyurethane fibers in the nanoscale for potential applications in tissue engineering.[111] Different solvent mixtures and a rotating collector were employed, but beaded nanofibers were obtained at best. The presence of interchain hydrogen bonding is significant enough to affect the viscosity, increasing the cohesiveness of the solution, and hindering or impeding the electrospinning process.[112] Among polyurethanes, SPUU exhibit three-dimentional networks of hydrogen-bonding due to the inter-urea hydrogen bonding.[113]

Our group reported the preparation, characterization and properties of novel electrospun elastomeric polyurethane scaffolds, employing bioresorbable SPU and SPUU, based on PCL, hexamethylene diisocyanate, and novel chain extenders containing urea groups or an aromatic amino acid derivative with ester groups.[114] These polymers were chosen because of their unique composition and mechanical properties,[115] as well as their promising *in vitro* biological properties.[116, 117] The optimization of the electrospinning parameters to obtain defect-free SPU and SPUU fibers with controlled diameters was difficult to achieve, due to the strong hydrogen-bonding interactions present in the polymeric structures. Common highly polar organic solvents, such as dimethylformamide (DMF) and dimethylacetamide (DMAc), solubilize SPU allowing the preparation of cast films, but usually fail when employed to electrospin their solutions, generating electrosprayed or bead-on-string systems. Figure 5 shows a bead-free fibrous

structure for the SPU containing an aromatic chain extender, obtained from a high-enough concentrated solution to cause chain entanglements with a low-enough viscosity to allow motion induced by the electric field. However, the processing of the SPUU in the same solvent mixture was not possible, obtaining at best beaded fibers. The highly hydrogen-bonded structure inhibits the formation of fibers using such solvents.

1,1,1,3,3,3-hexafluoro-2-propanol (HFP) has been reported to be a good solvent for electrospinning highly hydrogen-bonded macromolecules, such as proteins,[118, 119] polyamides,[120] SPU, and SPUU.[121] For this reason, its solutions were employed to process our SPU and SPUU. An effect of the concentration in the morphology was clearly observed. Diluted solutions of the SPUU led to electrospraying instead of electrospinning, due to the lack of sufficient polymer-chain entanglements. As the concentration increased, the solution became viscoelastic, taking a longer time to break up into drops, and obtaining a 'bead-on-string' morphology (Fig. 6(a)). With a further increase in concentration, the critical concentration was reached, and the polymer was able to form a network of entanglements, making the solution electrospinnable into uniform fibers (Fig. 6(b)).

Fig. 5. SEM micrograph of electrospun SPU matrix obtained from DMF/THF (50/50) solution 30 wt%. Adapted with permission from [114], P. C. Caracciolo et al., Electrospinning of novel biodegradable poly(ester urethane)s and poly(ester urethane urea)s for soft tissue engineering applications. *J. Mater. Sci.—Mater. Med.* 20, 2129 (**2009**). © 2009, Springer.
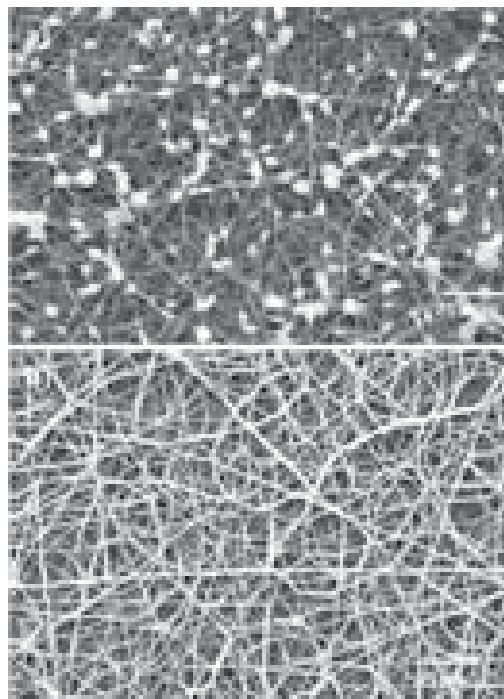
Fig. 6. SEM micrographs of electrospun SPUU matrices obtained from HFP solutions at different concentrations (a) 15 wt%; (b) 20 wt%. Adapted with permission from [114], P. C. Caracciolo et al., Electrospinning of novel biodegradable poly(ester urethane)s and poly(ester urethane urea)s for soft tissue-engineering applications. *J. Mater. Sci.—Mater. Med.* 20, 2129 (**2009**). © 2009, Springer.

The degradation properties of the SPU and SPUU electrospun membranes and films were also studied. The fibrous scaffolds exhibited lower mass-loss values and higher hydrolytic stability than the corresponding films after short-time assays, but they also experienced higher mass-loss under accelerated conditions.[122] These results suggest that the degradation rate is not constant, but depends on the chemical structure of the chain extenders, as well as the crystallinity and morphology of the materials.

In particular, SPUU matrices present low-enough hysteresis and elastic modulus to be a candidate for the design of cardiac patches along with the seeding of cardiomyocytes, to restore the functionality of infarcted tissue regions. To improve its performance for use in cardiac and vascular tissue regeneration, SPUU/polydioxanone (PDO) blends were processed into tubular electrospun scaffolds.[123] In order for vascular grafts to succeed, they need to match the biomechanical properties of the natural blood vessels. PDO is a semicrystalline, flexible and biodegradable polymer whose mechanical strength is capable of withstanding pulsatile blood flow. It also presents shape memory, preventing kink formation in vascular structures. The scaffolds showed randomly oriented bead-free fiber meshes with relatively narrow distribution of fiber diameters, comparable to the typical diameters of collagen fibers found in natural arteries (50 nm to 500 nm). The blend-fibers resulted rougher than pure SPUU fibers, which could be attributed to a higher crystallinity for the former. The porosity of the blend was also higher, which favors cell attachment and proliferation. The addition of PDO led to tubular scaffolds with improved mechanical properties respect to the corresponding plain SPUU scaffold, being both comparable to those of elastomeric polymers reported for cardiac tissue engineering.[124]

Our group also reported preliminary results for the development of poly(L-lactic acid) (PLLA) tubular electrospun scaffolds for potential applications as small-diameter vascular grafts in cardiovascular tissue engineering.[125] The matrices presented bead-free nanofibrous morphologies (Fig. 7), with narrow and unimodal diameter distributions independently of the rotation rate. The fiber orientation seemed to be in between a range of values (90–100°), however, the standard deviation resulted high, indicating that no preferential orientation was obtained. In spite of this, orientation of the nanofibers could be achieved for the 4 mm inner diameter graft with a non conductive mandril and electric field modifications. The thermal analysis did not show an influence in the rotation speed neither in the collector used. A decrease in the crystallinity was observed in contrast with the raw polyester. Shorter times for crystallization and spatial restrictions during the electrospinning process are expected to reduce chain mobility and thus, lower crystallization values are obtained. The more amorphous polymer should favor a faster hydrolytic degradation. Further studies regarding the incorporation of
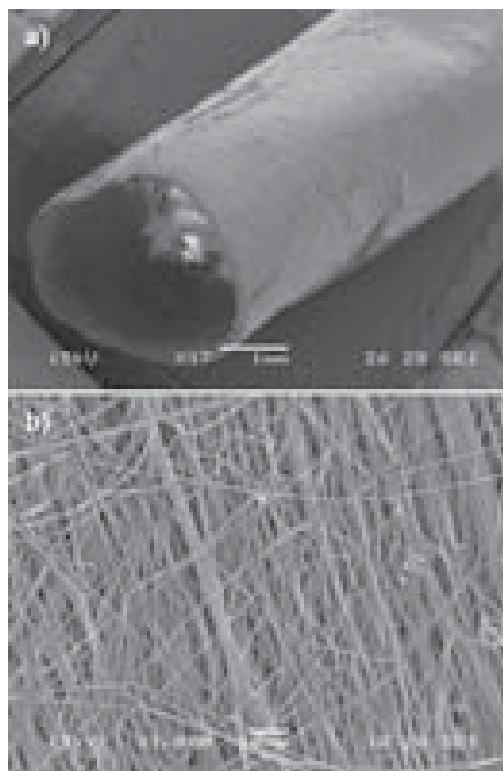
Fig. 7. SEM micrograph of a PLLA nanofibrous vascular graft: (a) tubular structure of 4 mm inner diameter, (b) fiber morphology at the inner surface (manuscript in preparation).

a bioresorbable polyurethane into the scaffold to mimic the properties of natural collagen/elastin ECM are being carried out.

Electrospun PDLLA scaffolds were also extensively reported in the literature. Branciforti et al. studied the influence of the solvent type, solution concentration and processing conditions on the morphology and properties of electrospun PDLLA matrices.[126] Regardless of the solvent mixture employed, all the scaffolds presented low crystallinity values, containing very small and imperfect crystals.

Motivated by the development of cardiac-tissue engineered scaffolds to restore cardiac function after myocardial infarction, Fernandes et al. prepared electrically active electrospun nanofibers based on hyperbranched poly(L-lysine) dendrimer (HPLys) containing polyaniline (PANI).[127] Because of its similarity to biological tissues, elasticity and biocompatible properties, hydrogels have been frequently used in combination with conductive polymers to obtain nanofibers for cardiac tissue engineering by electrospinning. The use of PANI, with tunable electroactive properties, is based on the evidence that cell functions could be modulated through electrical stimulation. Moreover, the biocompatibility of PANI can be improved by the incorporation of adhesive peptides, such

as HPLys.[128] HPLys hydrogels may act as surgical adhesives, via their swelling ability, promoting cardiomyocyte infiltration through their mesh structure. The HPLys-PANI nanofibers displayed a high swelling behavior, which decreases with higher PANI content, due to the formation of a rigid network with higher density of physical crosslinks. The matrices did not induce toxic effects on Chinese hamster ovary cells. Moreover, they promoted proliferation and differentiation of cardiomyocytes cells when exposed to electrical stimulation, increasing viability with the applied voltage. Both electroactivity and biocompatibility of the electrospun HPLys-PANI nanofibers suggest their use for the culture of cardiac cells as well as biocompatible electroactive scaffolds in cardiac tissue engineering, although cardiomyocyte viability assays during scaffold degradation should be performed.

In other work, de Morais et al. obtained electrospun scaffolds incorporating Spirulina (*Arthrospira* LEB 18),[129] a microalgae that exhibits highly favorable biological functions for tissue engineering. Clinical studies suggest that Spirulina contains polysaccharides with antiinflammatory effects and fatty acids with antibacterial and antifungal properties.[130] To obtain well-defined nanofiber matrices incorporating Spirulina, poly(ethylene oxide) (PEO) was used as a well known electrospinnable polymer. Electrospinning was facilitated by the increment in biomass composition, possibly due to the presence of salts in the cultivation medium which increased the conductivity of the solutions. However, the resulting fiber diameter and morphology seemed to be insensitive to conductivity variations. PEO bead-free nanofibrous matrices containing biomass contents up to 67 wt% were produced for subsequent studies in tissue engineering applications. These matrices are suggested as candidates for extracellular scaffolds for stem cell culture and future treatment of spinal cord injury.

Several electrospun matrices have been evaluated with different cell types for potential applications in tissue engineering. This approximation has limitations such as cell mobility after seeding and small pore dimensions to allow cell infiltration. Therefore, Zanatta et al. studied the incorporation of cells into PVA porous scaffolds during the electrospinning process, employing mesenchymal stem cells (MSCs) and mononuclear cells (MNCs).[131] Cell viability after electrospinning was assessed in order to study cell damage due to fiber formation. A reduction of MNCs viability from 80% in the PVA solution control group to 8.4% in the resulting nanofibers was observed, whereas MSCs showed a reduction from 64% to 19.6%. The viability decreased significantly after electrospinning, but the MSCs displayed a higher resistance to the process. The loss of cell viability was attributed to the limited access to nutrients due to the high viscosity of the solution, as well as the electric and mechanical stress during the process.[132] Studies by confocal laser scanning microscopy suggested that

cells were not encapsulated in the fibers, probably because of their small diameter. The cells were disposed among the fibers, providing a three-dimensional distribution along the scaffolds (Fig. 8). These results suggest that the incorporation of cells during the electrospinning process is viable, and it can be improved by the adjustment of the solution viscosity.

In other approach, Ramos et al. developed PCL electrospun matrices composed of random fibers with a wide range of diameter sizes (500 nm–5 μm).[133] The large spacing between the fibers resulted in a high porosity, which favors cellular penetration. In this way, the porosity generated proved to be a positive factor for the MSCs penetration, enabling the development of a cell support scaffold suitable for cartilage reconstruction.

Furlan et al. investigated the formation of oriented fibers containing PEO and pectin.[134] These morphologies were achieved by using a non-conventional electrospinning configuration, introducing two parallel electrodes instead of a plate. Pectin was incorporated into fibers as a bioactive, biodegradable and biocompatible heteropolysaccharide, having previously been employed for applications that include controlled drug release and implantable cell carriers. PEO was employed to favor the formation of fibers containing pectin, because of its biocompatibility and good electrospinnability. The incorporation of pectin led to a higher variation of fiber diameters, as well as larger sizes, probably due to cluster formation. The resulting flexible matrices presented a decrease in PEO chain alignment, as determined by FTIR. Nanofibers were also collected forming a perpendicular configuration by rotating the substrate 90°. The deposition of transversal fibers can be adopted to obtain scaffolds with defined shapes for application in tissue engineering.

4.2. Hard Tissue Engineering Applications

Around 200 million people are affected every year by musculoskeletal problems caused by accidents or diseases. The slow process of bone regeneration, added to the need for better filler materials in the reconstruction of large orthopaedic defects, as well as orthopaedic implants more suitable to their biological environment, are the main clinical reasons to develop bone tissue-engineering alternatives.[135] The use of scaffolds together with growth factors plays an important role in bone regeneration. The ideal matrix for such applications should be biodegradable, biocompatible, osteoconductive or osteoinductive, cheap, and with high surface area to volume ratio. A way to obtain a tridimensional scaffold mimicking bone-like properties is by coping its scale and composition.

Human bone is mainly a hydroxyapatite (HA) and type I collagen based composite. HA is the best bioactive calcium phosphate, being used in bone-tissue repairing applications due to its biocompatibility and osteoconductivity.
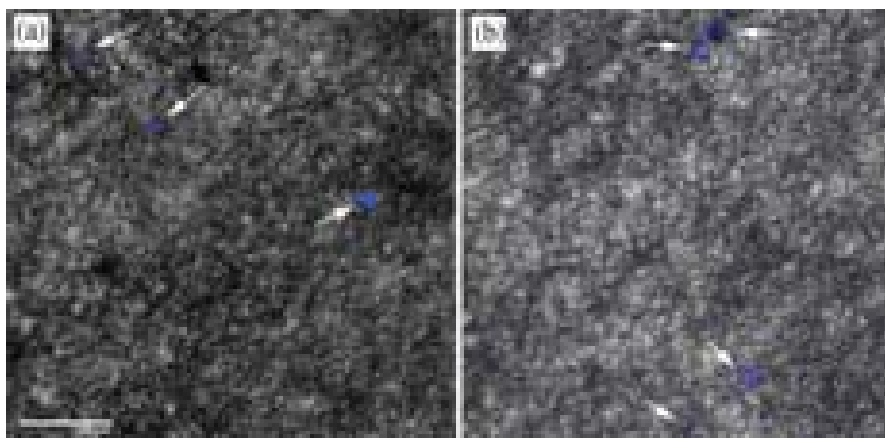
Fig. 8. Images of confocal laser scanning microscopy showing cells among the fibers: (a) Mononuclear cells, (b) mesenchymal stem cells. Arrows indicate cell nuclei. Nuclei stained with DAPI solution. Cited with permission from [131], G. Zanatta et al., Viability of mesenchymal stem cells during electrospinning. *Braz. J. Med. Biol. Res.* 45, 125 (**2012**). © 2012, Brazilian Journal of Medical and Biological Research.

The most important biomedical applications of HA are bone graft substitution in dental and orthopaedic applications and coating of biomedical implants. In recent years, many methods and techniques have been developed and applied to design advanced materials for bone replacement. The incorporation of nanoparticles can lead to scaffolds with improved *in vivo* and *in vitro* mechanical, chemical and biological properties. Thus, polymeric electrospun matrices incorporating HA nanoparticles could achieve the desired bone properties. The adhesion, proliferation and differentiation of osteoblast cells will depend on the structure and composition of the fibers, added to surface and mechanical properties, among others. Moreover, the attachment and migration of these anchorage-dependent cells inside the scaffold are expected to be favored by the high surface area and porosity of the electrospun fibers.

Recently, Rodriguez et al. prepared electrospun fibrous PLLA membranes containing dispersed HA nanoparticles (2–9 wt%).[136] Smooth bead-free fibers were obtained for all cases. The incorporation of HA was evidenced by the shift of the infrared carbonyl band of PLLA due to the interaction by hydrogen-bonding with the hydroxyl groups in HA. Furthermore, the membranes displayed a decrease in glass transition of PLLA, probably due to the enhanced mobility of the polymer chains because of the presence of HA. The mean diameter of the fibers increased considerably with the increment in HA content, generating an increment in pore diameter which could favor cell infiltration (Fig. 9). These scaffolds are promising for bone tissue engineering applications, and studies regarding cell adhesion and proliferation should be performed.

Vázquez-Hernández et al. reported the preliminary results on the preparation of three-dimensional HA/chitosan composite electrospun scaffolds.[137] Uniform fibers could not be obtained probably due to the high HA:chitosan ratios employed. Although none of the samples displayed a

Ca/P ratio according to the obtained for HA or native bone, the minerals were identified by X-ray diffraction as HA and monobasic calcium phosphate, which are constituents of human bones. Further studies improving the processing conditions could lead to better results for this system.

Electrospun scaffolds composed of hyperbranched polyglycerol (HPGL) nanofibers containing HA nanoparticles were recently reported.[138] HPGL hydrogels can potentially act as orthopaedic adhesives via their swelling ability, and also encourage osteoblast infiltration and bone formation through their mesh structure. Matrices with different HA content (0.5–5 wt%) consisting of uniform fibers, resulted elastic and flexible. The increasing content of HA reduced the swelling ability of the HPGL fibers, indicating the formation of higher physical intermolecular crosslinking. The *in vitro* evaluation of the scaffolds afforded no cytotoxicity, showing high cell viability. To evaluate the potential use of the HPGL-HA matrices as scaffolds for bone regeneration, the materials were cultured with human sarcoma osteogenic cells (SaOS$_2$), monitoring the alkaline phosphatase (ALP) activity as an indicator of the cellular activity on the scaffold. The ALP activity values resulted high, appearing to promote both a better proliferation and differentiation of SaSO$_2$ than the corresponding film scaffolds. HPLG-HA matrices could be suitable for bone tissue engineering, although studies regarding their physicochemical and mechanical properties are needed to support these results.

In another work, Pantojas et al. prepared three-dimensional electrospun membranes composed of a PLLA/poly(ethylene glycol) (PEG) blend.[139] Although PLLA is one of the most widely used polymers for biomedical applications, it is a stiff and hydrophobic material. Nevertheless, the addition of a small fraction of low molecular weight PEG improved the hydrophilicity of the blend. Meshes presented slightly lower pore sizes than the ones
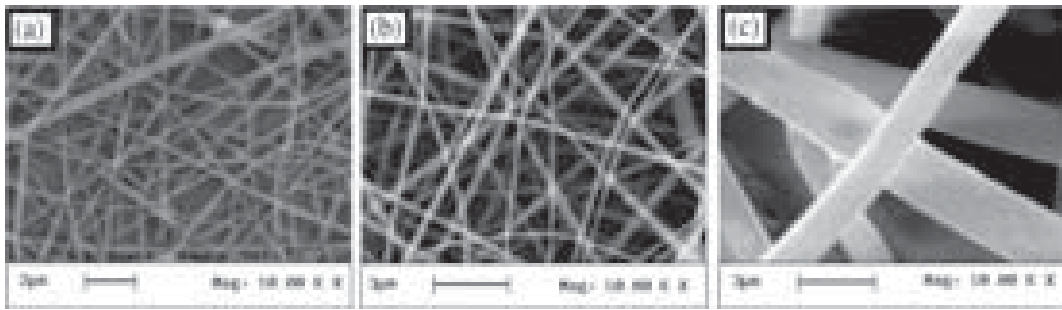
Fig. 9. Nanocomposite matrices containing HA/PLLA: (a) 1.96 wt%, (b) 4.76 wt%, and (c) 9 wt%. Cited with permission from [136], G. N. P. Rodriguez et al., Electrospun Scaffolds composed of poly(L-lactic acid) and hydroxyapatite. *Key Eng. Mater.* 493—494, 872 (**2012**). © 2012, Trans Tech Publications.

necessary to assess cell infiltration (25 to 100 μm). Fibers with porous surfaces were obtained when electrospinning 9% wt solutions. This morphology could be attributed to a rapid phase separation during electrospinning, where the solvent-rich regions apparently generate porous surfaces after evaporation. Surface pores can modify the wetting properties, increase surface area, influence the kinetics of biodegradation of the scaffold, and improve cell adhesion, acting as anchoring points for cells. Cell adhesion and proliferation studies should be performed to assess the effect of this surface modification.

The use of polymeric matrices loaded with silica, alumina or carbon nanotubes (CNT) is another approach to obtain composite materials for bone tissue engineering.[140, 141] These fillers have led to composite systems with significantly improved mechanical properties. Particularly, CNT rank among the highest modulus and strongest fibers known, and their structure allows surface functionalization for matrix-compatibility improvement or the introduction of new functional properties. The group of Volpato et al. reported the preparation of electrospun scaffolds composed of aligned fibers of polyamide 6 (PA 6) and carboxyl-functionalized multi-walled carbon nanotubes (MWCNT) for biomedical applications.[142] Since CNT biocompatibility is still under investigation with controversial results, a non-resorbable polymer was employed to avoid a potentially harmful CNT release.[143–145] The increased electrical conductivity of PA 6/MWCNT solutions respect to PA 6 solutions caused higher stretching and thus smaller fiber diameters, but also affected negatively the fiber alignment. The composite membranes contained the dispersed fillers aligned within the nanofiber axes, which allowed specific morphological and mechanical properties of the networks. The presence and alignment of the MWCNT, added to solvent evaporation and fiber stretching, led to the formation of superficial roughness and defects that could improve cell adhesion.

As expected by fiber alignment, anisotropic mechanical properties were found for the matrices. Only few works have reported a study of the mechanical behavior of CNT-reinforced electrospun membranes,[146, 147] finding an enhancement in the mechanical properties by the addition of CNT. However, the stiffness, ultimate tensile stress and strain decreased for these MWCNT-based networks. This decrease was attributed to the different net architecture, which displayed lower fiber alignment, and higher void and defect content. Consequently, these matrices could potentially be use for applications where low mechani-
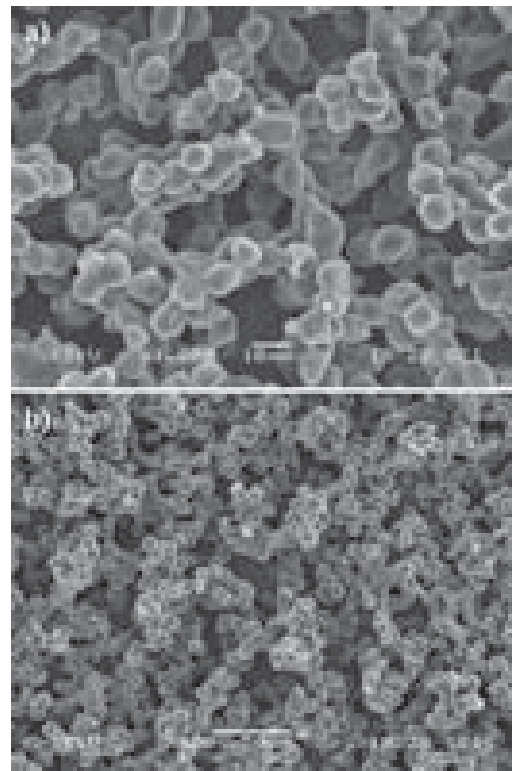
Fig. 10. SEM micrographs showing the surface morphology of PCL/PDIPF glass substrates covered with multilayers of microparticles formed by electrospraying at (a) 1000× and (b) 400× magnification. Adapted with permission from [151], J. M. Fernandez et al., Osteoblast behavior on novel porous polymeric scaffolds. *J. Biomater. Tissue Eng.* 1, 1 (**2011**). © 2011, American Scientific Publishers.

REVIEW

cal support is required, such as vertebra and spongy bone scaffolds.

In order to assess the effect of CNT-filled scaffolds on cell response, membranes were cultivated with MG63 cell line of osteoblasts. Cell activation and proliferation were enhanced by the surface modification caused by the addition of MWCNT. A significant increase in the ALP activity on the composite network was also observed, which means that cells are able to differentiate and produce an extracellular matrix. It is suggested that the surface roughness of the composite fibers governed the observed cell response due to protein interaction with the nanoscale patterning.[148, 149] Although longer term biological tests need to be performed regarding the CNT biological behaviour, these networks have encouraging profiles for use in biomedical applications.

Electrospraying of polymer solutions also enables the possibility of producing porous scaffolds to meet current challenges in tissue engineering applications, drug delivery systems and surface modification of medical implants. Although the process is affected by several variables, as for electrospinning, the breaking of the jet into droplets is a consequence of a lower concentration of the polymer solution.[43, 150] Our group has made a contribution in this field, preparing highly porous three-dimensional scaffolds obtained by electrosprayed microparticle deposition (Fig. 10).[151] In a previous work, films prepared from poly(ε-caprolactone)/poly(diisopropyl fumarate) proved to support adhesion, proliferation and differentiation of UMR106 and MC3T3E1 osteoblast-like cell lines without evidence of cytotoxicity.[152] Fernandez et al. employed this blend to obtain random polymer-microparticle matrices as better osteophilic environments for the growth and differentiation of osteoblasts. *In vitro* biological studies were carried out by culturing UMR106 and MC3T3E1 on the matrices. Electrosprayed scaffolds presented higher cell adhesion and proliferation, as well as higher ALP activity and type-I collagen production[153] than flat films of the same blend. The electrosprayed morphology improved cell incorporation into the scaffold (Fig. 11), being this fact crucial because cell infiltration is difficult to achieve in other porous membranes.[154] Despite the general finding that hydrophobic materials do not support adhesion and spreading of cells,[155] the rougher and more hydrophobic surfaces of the matrices enhanced osteoblast response as has also been reported in literature less frequently,[156] being this a controversial discussion.

5. SENSORS BASED ON NANOFIBROUS STRUCTURES

Typical polymeric sensors exist in the form of thin films for sensing a wide variety of substances in gas and fluid states. They have been extensively used for environment protection, industrial-process control, safety, security, defense and medical diagnosis applications. Common

requirements for a good sensor are small dimensions, low fabrication cost, fast response, easy operability, high sensitivity, selectivity and reliability.[157] To achieve a higher sensitivity and a faster response, an increase in specific surface area of the sensor is needed. Therefore, the use of electrospun nanofiber-based sensing materials is promising to obtain high-performing gas and fluid sensors. The development of sensors based on nanofibrous structures is the less explored area by Latin American research groups.

Several methods have been employed to obtain nanofibers with a sensing capacity, such as the use of a sensing polymer, the incorporation of sensing molecules during the electrospinning process, or after fiber formation via the coating/grafting technique. Humidity sensors based on polymeric layers enjoy a fast response time for
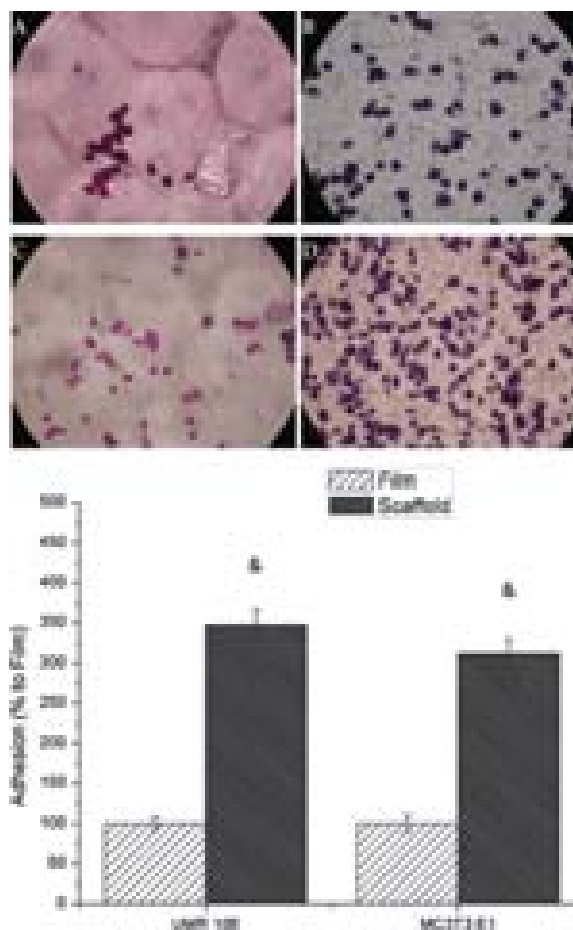
Fig. 11. Adhesion of UMR106 (A), (B) and MC3T3E1 (C), (D) osteoblasts plateled over the solvent-cast films (A), (C) and the electrosprayed scaffold (B), (D). Cells were incubated for 1 h and stained with Giemsa. The cells in ten fields per samples were counted and expressed as percentage of the cells in the cast film. Cited with permission from [151], J. M. Fernandez et al., Osteoblast behavior on novel porous polymeric scaffolds. *J. Biomater. Tissue Eng.* 1, 1 (**2011**). © 2011, American Scientific Publishers.

increasing humidity changes. However, the recovery time when the humidity decreases is longer than the response time, reducing drastically the overall dynamic performance. Poly(vynilidene fluoride) (PVdF) presents excellent resistance to heat, aging and abrasion, non toxicity, and unique electrical properties. It is generally used in structural health, monitoring systems as pressure and volume displacement sensors. Its exceptional chemical stability and mechanical flexibility at physiological temperature ($T_g \approx -35$ °C), makes it easy to conform to complex surfaces. Moreover, its biocompatibility makes PVdF a desirable candidate for biological environments.[158] Besides its sensing capability, PVdF is also applied in actuation mechanisms, which can be thermally, optically or electrically stimulated.

The group of Corres et al. developed a new optical fiber humidity sensor composed of a Multimode–Hollowcore–Multimode (MHM) structure coated with an electrospun nanoweb.[159] The MHM structure consists of one short silica hollow-core fiber segment spliced between two standard multimode fibers, where a PVdF nanoweb is deposited. The piezoelectric nature of PVdF has been employed for the development of gas and humidity film sensors. The low humidity permeability and the high humidity sensitivity of PVdF thin films are improved when employing an electrospun membrane with high surface to volume ratio and highly porous structure, generating a sensor that combines high sensitivity and reproducibility with a faster response to relative humidity changes. When exposed to human breathing, a repetitive response in the range from 50 to 70% of relative humidity with a rise time of 100 ms was found. This response is fast enough for the sensor to be used in medical applications, which require high dynamic performances, especially in the ranges in which human breathing has to be monitored. This sensor has a reduction in the response time (from 300 ms to 100 ms) compared to others based on ESA polymeric nano-film (PDDA/Poly-R478), and a comparable performance respect to superhydrophobic devices.[160]

González-Morán et al. also electrospun PVdF in order to develop a temperature sensor for biomedical applications.[161] This sensor was obtained by positioning the membrane on a couple of plates with cooper rings to ensure an electrical contact. The heat-sensing abilily is due to detection of changes on the membrane dielectric constant, which are then converted to frequency changes. These signals are transmitted to a receiver by means of frequency modulation, and make a telemetry temperature-sensor system. This sensor has several advantages for biomedical applications, as it is non invasive due to its pyroelectrical detection, there are no chemical reactions with the body or possible current discharges because it is completely isolated, and it does not require external electrical supply due its pyroelectricity. This cheap sensor displays a linear response in the range of 25–80 °C. It can be obtained in any

shape and size, being appropriate for monitoring different regions of adult human beings (37 °C), neonatals (36.5 °C to 37.5 °C) and biological environments.

6. OTHER BIOMEDICAL APPLICATIONS

6.1. Conducting Nanofibers

The development of ultrathin fibers from electroactive polymers has recently received much attention due to their useful properties with several potential applications such as electronic devices, optics and biomedical materials, protective clothing, filtration media, charge storage devices, sensors and actuators. In this context, PANI has been one of the most investigated conducting polymers due to its simple and relatively easy doping/dedoping chemistry, high environmental stability, and low cost of synthesis.[162] Multi-component polymer fibers have also been obtained by electrospinning. The blending of PLLA and its copolymers with other polymers has generated great interest and is considered one of the most innovative materials developed. Recently, PLLA/PANI blends have been used to prepare conducting nanofibers as promising materials for sensors and other electroactive applications.

Picciani et al. studied the structure and properties of electrospun conductive micro/nanofibers of PLLA/PANI blends and cast films with the same composition.[163] The electrical resistivity values for electrospun fibers were found to be about two orders of magnitude higher than those for the corresponding cast films. In addition, electrospun fibers presented a mechanical behavior more appropriate for their use in the preparation of electronic devices. The stress–strain behavior showed that PLLA/PANI electrospun matrices are stiffer than those without PANI. The group of Picciani et al. also electrospun PLLA/PANI blends doped with *p*-toluene sulfonic acid (TSA),[164] obtaining ultrafine fibers with diameters in the order of 100–200 nm and a significant reduction of bead formation. The fibers resulted homogeneous, indicating a good interaction between the components of the blend. The electrical conductivity of the electrospun matrices was lower than that for blend films produced by casting, probably because of the lower degree of crystallinity of PANI dispersions and the high porosity of the non-woven matrices. The presence of PANI in the blends significantly decreased bead formation because of changes in the dielectric constant, which was associated with an increase in the solution viscosity and charge density. The crystallinity of these fibers was lower than that for the corresponding blends prepared by film casting, and this could be attributed to the rapid evaporation of the solvent during the electrospinning process, which resulted in an amorphous structure.[165]

The influence of the electrospinning parameters on polyurethane and conductive composite nanofibers was studied by Ballarin.[166] Single wall carbon nanotubes (SWCNT) and PANI nanoparticles were used to prepare

REVIEW
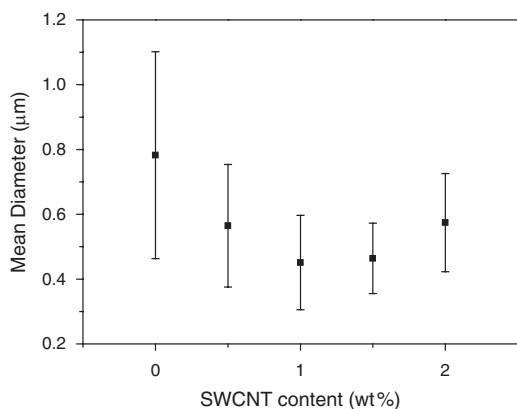
Fig. 12. Mean diameter as a funcion of SWCNT content in electrospun polyurethane nanocomposites. Cited with permission from [166], F. M. Ballarin, Engineering final project: Nanofibras Poliuretánicas y Compuestas de Interés Biomédico, Universidad Nacional de Mar del Plata, Argentina (**2009**). © 2009, Universidad Nacional de Mar del Plata, Argentina.

polyurethane nanocomposites. A biostable poly(ether urethane) was employed in this case, since the biocompatibility of the fillers is still under discussion. The effect of the solution intrinsic properties and processing parameters in fiber diameters were studied. As in the work of Picciani et al.[164] fiber diameters were reduced by the increase in the conductive nanoparticle concentration. Figure 12 shows the variation of mean diameters as a funcion of SWCNT content in polyurethane nanocomposites. A minimun in diameter was observed at 1 wt% nanotube concentration.[166] Conductivity values were in agreement with the change in fiber diameters, being these materials interesting candidates for biomedical applications.[167]

6.2. Nanofibers with Antimicrobial Properties

Martínez-Camacho et al. reported the preparation and properties of chitosan nanofibers, as well as the theoretical basis for understanding how the antimicrobial activity of chitosan could occur in the form of polymer nanofibers.[168] In most cases, the proposed mechanism is related either to the presence of positively charged amino groups at the surface of the nanofibers,[169] or is associated to the release of small chitosan oligomers that could penetrate bacterial cells and interact with DNA. Chitosan–PVA nanofibers showed a high antimicrobial activity against *Escherichia coli* and *Staphilococcus aureus* for large diameters, possibly due to a more effective contact surface area and, consequently, to a greater presence of amino groups to carry out the inhibition of microbial growth.[170] In other approach, Hidalgo et al. prepared electrospun PLLA scaffolds coated with chitosan by impregnation of the mats with chitosan solutions.[171]

Antimicrobial materials can be chemically engineered by adding functional antimicrobial agents onto their surface or within the matrix to either eliminate or inhibit the growth of microorganisms. Silver (Ag) is a powerful antimicrobial agent that inactivates several microorganisms, such as *Escherichia coli*, *Staphylococcus aureus*, *Klebsiella pneumoniae* and *Pseudomonas aeruginosa*. There are few works employing Ag as antimicrobial agent in PVA fibers prepared by electrospinning. In these works, either heat treatments, UV radiation or chemical reduction were employed to obtain Ag nanoparticles. However, it was demonstrated that it is possible to obtain PVA nanofibers containing Ag nanoparticles by electrospinning aqueous PVA solutions with $AgNO_3$ in a nitric acid medium (pH = 2–4), without any further processing.[172] Despite the fact that most of the produced nanoparticles should be occluded into the fibers, the composite matrices showed good values of antibacterial activities against *Staphylococcus aureus* (87.8%) and *Escherichia coli* (85.0%).

Novel hybrid fibrous membranes were developed by electrospinning blend solutions of poly(3-hydroxybutyrate-co-hydroxyvalerate) (PHBV) and chitosan.[173] The effect of solvent, employing different proportions of trifluoroacetic acid and HFP, PHBV/chitosan ratio, and chitosan molecular weight on solution spinnability, fiber morphology and size, and *in vitro* degradation were investigated. Continuous nanofiber structures were obtained. In general, mean fiber diameter increased as chitosan content and molecular weight increased, and decreased with the decrease of HFP content in the solvent. *In vitro* dissolution tests revealed that the hybrid fibers show much higher degradation rates than the neat PHBV.

6.3. Morphology and Adhesion Measurements

The fiber diameter, orientation and membrane porosity strongly influence cellular response, drug release, mechanical and adhesion properties. For this reason it is important to evaluate and quantify the morphology of the electrospun membranes in an automatic manner.

Gonzalez et al. developed an image processing technique to characterize grey level SEM micrographs.[174] The granulometric size function (SGF) was used to develop algorithms that allow the characterization of shape, size, stocking density and orientation of the electrospun fibers present in SEM images. Different morphologies were obtained by varying the electrospinning setup, the intrinsic properties of the polymer solution and processing parameters. 164 sample images belonging to 42 electrospun scaffolds of PLLA and PCL were processed. Different structural elements were used to scan the images and study diverse aspects of the membrane morphology. The occupancy rate, orientation and diameter of the nanofibers were properly estimated by the proposed algorithm. One of the main advantages of this algorithm is that it is not necessary to binarize images. Besides, the SGF also provides features on nanofiber statistics.

Topology of electrospun scaffolds is other important feature to analyze in electrospun membranes. Nanofibers

present a biomimetic fibrillar structure. It was probed that the hierarchical fibrillar structures of natural creatures produce dry adhesion by van der Waals (vdW) forces.[175, 176] For this reason, it is of interest to measure the adhesion properties of electrospun fibers. Our group studied the adhesion between PCL nanofibrous membranes by *T*-peel test for the first time.[177] The influence of fiber orientation on the adhesion properties was studied. Aligned fibers presented higher adhesion strength (758.7 ± 211.7 kPa) than the randomly oriented non-wovens (613.1 ± 79.9 kPa). These energy values probed that the surface asperities present in electrospun membranes contribute to enhanced adhesion. Even more, a well-aligned structure enhanced adhesion by introducing more contact points and a band-like morphology.[178] Adhesion strength changed marginally with peeling rates and conditioning pressures on the membranes. The morphology of the electrospun membranes after performing the peel test was studied. Neither plastic deformation nor interlocking was observed, demonstrating that the adhesion between the nanofibers was a result of interactions in the nanometer range. Finally, a single contact adhesion energy value (83.1 ± 32.5 mJ $\cdot$ m^2) was calculated by Johnson Kendall and Roberts (JKR) contact mechanics. This value was consistent with vdW adhesion forces, suggesting that vdW was the primary adhesion mechanism. Overall, this work demonstrated the increase in vdW adhesion of electrospun membranes by a change in fiber orientation.

7. CONCLUDING REMARKS

Nanofibrous scaffolds manufactured by electrospinning offer many advantages for the design of highly porous biomaterials useful in tissue engineering applications and drug delivery systems, among other emerging fields. In the last few years, this technique has become widely accepted in academia and industry. Despite this, research on electrospinning for biomedical applications is still at an early stage of development in Latin America, as demonstrated by the number of published works. Brazil, Argentina and Mexico are currently the leading Latin American countries in this field, followed by Colombia and Puerto Rico. Most of these research teams work in collaboration with groups having large expertise in the field. Main efforts are addressed to the development of novel electrospun biomaterials, drug-loaded systems, electrospun nanocomposites, characterization tools, biomedical textiles with functional properties and novel applications of nanofibrous non-woven mats.

References and Notes

1. M. Goldberg, R. Langer, and X. Jia, Nanostructured materials for applications in drug delivery and tissue engineering. *J. Biomater. Sci., Polym. Ed.* 18, 241 (**2007**).
2. T. J. Sill and H. A. von Recum, Electrospinning: Applications in drug delivery and tissue engineering. *Biomaterials* 29, 1989 (**2008**).
3. S. Sell, C. Barnes, M. Smith, M. McClure, P. Madurantakam, J. Grant, M. McManus, and G. Bowlin, Extracellular matrix regenerated: Tissue engineering via electrospun biomimetic nanofibers. *Polym. Int.* 56, 1349 (**2007**).
4. J. Venugopal, S. Low, A. T. Choon, and S. Ramakrishna, Interaction of cells and nanofiber scaffolds in tissue engineering. *J. Biomed. Mater. Res. Part B Appl. Biomater.* 84B, 34 (**2008**).
5. J. M. Oliveira, A. J. Salgado, N. Sousa, J. F. Mano, and R. L. Reis, Dendrimers and derivatives as a potential therapeutic tool in regenerative medicine strategies—A review. *Prog. Polym. Sci.* 35, 1163 (**2010**).
6. A. Kumari, S. K. Yadav, and S. C. Yadav, Biodegradable polymeric nanoparticles based drug delivery systems. *Colloids Surf., B: Biointerfaces* 75, 1 (**2010**).
7. R. Duncan, Polymer therapeutics as nanomedicines: New perspectives. *Curr. Opin. Biotechnol.* 22, 1 (**2011**).
8. G. A. Silva, P. Ducheyne, and R. L. Reis, Materials in particulate form for tissue engineering, basic concepts. *J. Tissue Eng. Regen. Med.* 1, 4 (**2007**).
9. S. Ramakrishna, K. Fujihara, W.-E. Teo, T. Yong, Z. Ma, and R. Ramaseshan, Electrospun nanofibers: Solving global issues. *Mater. Today* 9, 40 (**2006**).
10. Z.-M. Huang, Y.-Z. Zhang, M. Kotaki, and S. Ramakrishna, A review on polymer nanofibers by electrospinning and their applications in nanocomposites. *Compos. Sci. Technol.* 63, 2223 (**2003**).
11. R. Dersch, M. Steinhart, U. Boudriot, A. Greiner, and J. H. Wendorff, Nanoprocessing of polymers: Applications in medicine, sensors, catalysis, photonics. *Polym. Adv. Technol.* 16, 276 (**2005**).
12. J. Fang, H.-T. Niu, T. Lin, and X. G. Wang, Applications of electrospun nanofibers. *Chin. Sci. Bull.* 53, 2265 (**2008**).
13. S. Liao, S. Ramakrishna, and M. Ramalingam, Development of nanofiber biomaterials and stem cells in tissue engineering. *J. Biomater. Tissue Eng.* 1, 111 (**2011**).
14. J. Xie, X. Li, and Y. Xia, Putting electrospun nanofibers to work for biomedical research. *Macromol. Rapid Commun.* 29, 1775 (**2008**).
15. Q. P. Pham, U. Sharma, and A. G. Mikos, Electrospinning of polymeric nanofibers for tissue engineering applications: A review. *Tissue Eng.* 12, 1197 (**2006**).
16. R. Murugan and S. Ramakrishna, Nano-featured scaffolds for tissue engineering: A review of spinning methodologies. *Tissue Eng.* 12, 435 (**2006**).
17. S. Liao, B. Li, Z. Ma, H. Wei, C. Chan, and S. Ramakrishna, Biomimetic electrospun nanofibers for tissue regeneration. *Biomed. Mater.* 1, R45 (**2006**).
18. R. L. Dahlin, F. K. Kasper, and A. G. Mikos, Polymeric nanofibers in tissue engineering. *Tissue Eng. Part B: Reviews* 17, 349 (**2011**).
19. Z. Ma, M. Kotaki, R. Inai, and S. Ramakrishna, Potential of nanofiber matrix as tissue-engineering scaffolds. *Tissue Eng.* 11, 101 (**2005**).
20. N. Bhardwaj and S. C. Kundu, Electrospinning: A fascinating fiber fabrication technique. *Biotechnol. Adv.* 28, 325 (**2010**).
21. S. G. Kumbar, S. P. Nukavarapu, R. James, M. V. Hogan, and C. T. Laurencin, Recent patents on electrospun biomedical nanostructures: An overview. *Rec. Pat. Biomed. Eng.* 1, 68 (**2008**).
22. Y. Zhang, C. T. Lim, S. Ramakrishna, and Z.-M. Huang, Recent development of polymer nanofibers for biomedical and biotechnological applications. *J. Mater. Sci.—Mater. Med.* 16, 933 (**2005**).

REVIEW

23. A. Greiner and J. H. Wendorff, Electrospinning: A fascinating method for the preparation of ultrathin fibers. *Angew. Chem. Int. Ed.* 46, 5670 (**2007**).

24. A. Greiner and J. H. Wendorff, Functional self-assembled nanofibers by electrospinning. *Adv. Polym. Sci.* 219, 107 (**2008**).

25. D. Li and Y. Xia, Electrospinning of nanofibers: Reinventing the wheel? *Adv. Mater.* 16, 1151 (**2004**).

26. W. E. Teo and S. Ramakrishna, A review on electrospinning design and nanofibre assemblies. *Nanotechnology* 17, R89 (**2006**).

27. J. Nam, Y. Huang, S. Agarwal, and J. Lannutti, Improved cellular infiltration in electrospun fiber via engineered porosity. *Tissue Eng.* 13, 2249 (**2007**).

28. Y. Wang, B. Wang, G. Wang, T. Yin, and Q. Yu, A novel method for preparing electrospun fibers with nano-/micro-scale porous structures. *Polym. Bull.* 63, 259 (**2009**).

29. B. Wulkersdorfer, K. K. Kao, V. G. Agopian, A. Ahn, J. C. Dunn, B. M. Wu, and M. Stelznez, Bimodal porous scaffolds by sequential electrospinning of poly(glycolic acid) with sucrose particles. *Int. J. Polym. Sci.* 2010, 1 (**2010**).

30. L. D. Wright, T. Andric, and J. W. Freeman, Utilizing NaCl to increase the porosity of electrospun materials. *Mat. Sci. Eng. C* 31, 30 (**2011**).

31. Y. H. Lee, J. H. Lee, I.-G. An, C. Kim, D. S. Lee, Y. K. Lee, and J.-D. Nam, Electrospun dual-porosity structure and biodegradation morphology of montmorillonite reinforced PLLA nanocomposite scaffolds. *Biomaterials* 26, 3165 (**2005**).

32. G. H. Kim and W. D. Kim, Highly porous 3D nanofiber scaffold using an electrospinning technique. *J. Biomed. Mat. Res. Part B Appl. Biomater.* 81B, 104 (**2007**).

33. M. F. Leong, M. Z. Rasheed, T. C. Lim, and K. S. Chian, *In vitro* cell infiltration and *in vivo* cell infiltration and vascularization in a fibrous, highly porous poly(D,L-lactide) scaffold fabricated by cryogenic electrospinning technique. *J. Biomed. Mat. Res. Part A* 91A, 231 (**2009**).

34. C. Vaquette and J. J. Cooper-White, Increasing electrospun scaffold pore size with tailored collectors for improved cell penetration. *Acta Biomater.* 7, 2544 (**2011**).

35. R. Tzezana, E. Zussman, and S. Levenberg, A layered ultra-porous scaffold for tissue engineering, created via a hydrospinning method. *Tissue Eng. Part C* 14, 281 (**2008**).

36. D. Li, Y. Wang, and Y. Xia, Electrospinning nanofibers as uniaxially aligned arrays and layer-by-layer stacked films. *Adv. Mater.* 16, 361 (**2004**).

37. H. Lu, Z. Feng, Z. Gu, and C. Liu, Growth of outgrowth endothelial cells on aligned PLLA nanofibrous scaffolds. *J. Mater. Sci.—Mater. Med.* 20, 1937 (**2009**).

38. L.-S. Wan and Z.-K. Xu, Polymer surfaces structured with random or aligned electrospun nanofibers to promote the adhesion of blood platelets. *J. Biomed. Mat. Res. Part A* 89A, 168 (**2009**).

39. A. L. Yarin, Coaxial electrospinning and emulsion electrospinning of core–shell fibers. *Polym. Adv. Technol.* 22, 310 (**2011**).

40. J. D. Schiffman and C. L. Schauer, A review: Electrospinning of biopolymer nanofibers and their applications. *Polym. Rev.* 48, 317 (**2008**).

41. M. J. Laudenslager and W. M. Sigmund, Developments in electrohydrodynamic forming: Fabricating nanomaterials from charged liquids via electrospinning and electrospraying. *Am. Ceram. Soc. Bull.* 90, 22 (**2011**).

42. E.-R. Kenawy, F. I. Abdel-Hay, M. H. El-Newehy, and G. E. Wnek, Processing of polymer nanofibers through electrospinning as drug delivery systems. *Mat. Chem. Phys.* 113, 296 (**2009**).

43. S. Chakraborty, I.-C. Liao, A. Adler, and K. W. Leong, Electrohydrodynamics: A facile technique to fabricate drug delivery systems. *Adv. Drug Del. Rev.* 61, 1043 (**2009**).

44. M. E. Brewster, G. Verreck, I. Chun, J. Rosenblatt, J. Mensch, A. Van Dijck, M. Noppe, A. Ariën, M. Bruining, and J. Peeters, The use of polymer-based electrospun nanofibers containing amorphous drug dispersions for the delivery of poorly water-soluble pharmaceuticals. *Pharmazie* 59, 387 (**2004**).

45. C. Leuner and J. Dressman, Improving drug solubility for oral delivery using solid dispersions. *Eur. J. Pharm. Biopharm.* 50, 47 (**2000**).

46. A. T. M. Serajuddin, Solid dispersion of poorly water-soluble drugs: Early promises, subsequent problems, and recent breakthroughs. *J. Pharm. Sci.* 88, 1058 (**1999**).

47. G. Verreck, I. Chun, J. Peeters, J. Rosenblatt, and M. E. Brewster, Preparation and characterization of nanofibers containing amorphous drug dispersions generated by electrostatic spinning. *Pharm. Res.* 20, 810 (**2003**).

48. M. A. Allevato, R. Negroni, and R. Galimberti, Antifúngicos, Ayer, hoy y mañana. *Act. Terap. Dermatol.* 30, 8 (**2007**).

49. P. R. C. Tornello, G. E. Feresin, A. Tapia, G. A. Abraham, and T. R. Cuadrado, Dispositivos poliméricos microfibrosos bioabsorbibles con agentes antifúngicos dispersos. *Biocell* 36, A43 (**2012**).

50. L. Svetaz, M. B. Agüero, S. Alvarez, L. Luna, G. Feresin, A. Tapia, and S. Zacchino, Antifungal activity of *Zuccagnia punctata* Cav.: Evidence for the mechanism of action. *Planta Med.* 73, 1074 (**2007**).

51. M. A. Agüero, M. Gonzalez, B. Lima, L. Svetaz, M. Sánchez, S. Zacchino, G. E. Feresin, G. Schmeda-Hirschmann, J. Palermo, D. Wunderlin, and A. Tapia, Argentinian propolis from *Zuccagnia punctata* Cav. (Caesalpinieae) exudates: Phytochemical characterization and antifungal activity. *J. Agric. Food Chem.* 58, 194 (**2010**).

52. P. R. C. Tornello, G. E. Feresin, A. Tapia, I. G. Veiga, A. M. Moraes, G. A. Abraham, and T. R. Cuadrado, Dispersion and release of embelin from electrospun, biodegradable, polymeric membranes. *Polym. J.* (**2012**), in press, doi:10.1038/pj.2012.80.

53. K. Haq, M. Ali, and A. W. Siddiqui, New compounds from the seeds of *Embelia ribes* Burm. *Pharmazie* 60, 69 (**2005**).

54. M. Chitra, E. Sukumar, V. Suja, and C. S. S. Devi, Antitumor, anti-inflammatory and analgesic property of embelin, a plant product. *Chemotherapy* 40, 109 (**1994**).

55. G. E. Feresin, A. Tapia, M. Sortino, S. Zacchino, A. R. de Arias, A. Inchausti, G. Yaluff, J. Rodriguez, C. Theoduloz, and G. Schmeda-Hirschmann, Bioactive alkyl phenols and embelin from *Oxalis erythrorhiza. J. Ethnopharmacol.* 88, 241 (**2003**).

56. N. Radhakrishnan, A. Gnanamani, and A. B. Mandal, A potential antibacterial agent embelin, a natural benzoquinone extracted from *Embelia ribes. Biol. Med.* 3, 1 (**2011**).

57. P. Douglas, G. Andrews, D. Jones, and G. Walker, Analysis of *in vitro* drug dissolution from PCL melt extrusion. *Chem. Eng. J.* 164, 359 (**2010**).

58. H. Frey and R. Haag, Dendritic polyglycerol: A new versatile biocompatible material. *Mol. Biotechnol.* 90, 257 (**2002**).

59. E. A. T. Vargas, N. C. do Vale Baracho, J. de Brito, and A. A. A. de Queiroz, Hyperbranched polyglycerol electrospun nanofibers for wound dressing applications. *Acta Biomater.* 6, 1069 (**2010**).

60. M. Grassi and G. Grassi, Mathematical modelling and controlled drug delivery: Matrix systems. *Curr. Drug Deliv.* 2, 97 (**2005**).

61. N. A. Peppas and P. A. Buri, Surface, interfacial and molecular aspects of polymer bioadhesion on soft tissues. *J. Controlled Reeased* 2, 257 (**1985**).

62. M. M. Castillo-Ortega, A. Nájera-Luna, D. E. Rodríguez-Félix, J. C. Encinas, F. Rodríguez-Félix, J. Romero, and P. J. Herrera-Franco, Preparation, characterization and release of amoxicillin from cellulose acetate and poly(vinyl pyrrolidone) coaxial electrospun fibrous membranes. *Mater. Sci. Eng. C* 31, 1772 (**2011**).

63. H. Nie and C.-H. Wang, Fabrication and characterization of PLGA/Hap composite scaffolds for delivery of BMP-2 plasmid DNA. *J. Controlled Released* 120, 111 (**2007**).

64. C. M. Valmikinathan, S. Defroda, and X. Yu, Polycaprolactone and bovine serum albumin based nanofibers for controlled release of nerve growth factor. *Biomacromolecules* 10, 1084 (**2009**).

REVIEW

65. J. Zeng, A. Aigner, F. Czubayko, T. Kissel, J. H. Wendorff, and A. Greiner, Poly(vinyl alcohol) nanofibers by electrospinning as a protein delivery system and the retardation of enzyme release by additional polymer coatings. *Biomacromolecules* 6, 1484 (**2005**).

66. Y. Dror, J. Kuhn, R. Avrahami, and E. Zussman, Encapsulation of enzymes in biodegradable tubular structures. *Macromolecules* 41, 4187 (**2008**).

67. Y. Yang, X. Li, M. Qi, S. Zhou, and J. Weng, Release pattern and structural integrity of lysozyme encapsulated in core–sheath structured poly(DL-lactide) ultrafine fibers prepared by emulsion electrospinning. *Eur. J. Pharm. Biopharm.* 69, 106 (**2008**).

68. H. Jiang, Y. Hu, Y. Li, P. Zhao, K. Zhu, and W. Chen, A facile technique to prepare biodegradable coaxial electrospun nanofibers for controlled release of bioactive agents. *J. Contr. Rel.* 108, 237 (**2005**).

69. I. Moreno, V. González-González, and J. Romero-García, Control release of lactate dehydrogenase encapsulated in poly(vinyl alcohol) nanofibers via electrospinning. *Eur. Polym. J.* 47, 1264 (**2011**).

70. Panamerican Health Organization, Leishmaniasis: 2007 update, Available at: www.paho.org/English/AD/DPC/CD/leish-2007.htm. (**2009**).

71. E. P. Hendrickx, S. P. Agudelo, D. L. Munoz, J. A. Puerta, and I. D. V. Bernal, Lack of efficacy of mefloquine in the treatment of new world cutaneous leishmaniasis in Colombia. *Am. J. Trop. Med. Hyg.* 59, 889 (**1998**).

72. H. King, R. E. Aubert, and W. H. Herman, Global burden of diabetes, 1995–2025: Prevalence, numerical estimates, and projections. *Diabetes Care* 21, 1414 (**1998**).

73. H. M. Calvet and T. T. Yoshikawa, Infections in diabetes. *Infect. Dis. Clin. North. Am.* 15, 407 (**2001**).

74. R. N. Davidson, V. Yardley, S. L. Croft, P. Konecny, and N. Benjamin, A topical nitric oxide-generating therapy for cutaneous leishmaniasis. *Trans. R. Soc. Trop. Med. Hyg.* 94, 319 (**2000**).

75. P. Lopez-Jaramillo, C. Ruano, J. Rivera, E. Teran, R. Salazar-Irigoyen, J. V. Esplugues, and S. Moncada, Treatment of cutaneous leishmaniasis with nitric-oxide donor. *The Lancet* 351, 1176 (**1998**).

76. D. J. Smith, M. Lopez, and P. Lopez-Jaramillo, Topical nitric oxide donor devices, [WO/2006/058318], Ref Type: Patent (**2006**).

77. P. López-Jaramillo, M. Y. Rincón, R. G. García, S. Y. Silva, E. Smith, P. Kampeerapappun, C. García, D. J. Smith, M. López, and I. D. Vélez, A controlled, randomized-blinded clinical trial to assess the efficacy of a nitric oxide releasing patch in the treatment of cutaneous leishmaniasis by Leishmania (V.) panamensis. *Am. J. Trop. Med. Hyg.* 83, 97 (**2010**).

78. S. Y. Silva, L. C. Rueda, G. A. Márquez, M. López, D. J. Smith, C. A. Calderón, J. C. Castillo, J. Matute, C. F. Rueda-Clausen, A. Orduz, F. A. Silva, P. Kampeerapappun, M. Bhide, and P. López-Jaramillo, Double blind, randomized, placebo controlled clinical trial for the treatment of diabetic foot ulcers, using a nitric oxide releasing patch: Pathon. *Trials* 8, 26 (**2007**).

79. D. F. Williams, On the nature of biomaterials. *Biomaterials* 30, 5897 (**2009**).

80. D. F. Williams, To engineer is to create: The link between engineering and regeneration. *Trends Biotechnol.* 24, 4 (**2006**).

81. P. X. Ma, Biomimetic materials for tissue engineering. *Adv. Drug Del. Rev.* 60, 184 (**2008**).

82. B. P. Chan and K. W. Leong, Scaffolding in tissue engineering: General approaches and tissue-specific considerations. *Eur. Spine J.* 17, S467 (**2008**).

83. W. Tan, R. Krishnaraj, and T. A. Desai, Evaluation of nanostructured composite collagen-chitosan matrices for tissue engineering. *Tissue Eng.* 7, 203 (**2001**).

84. K. F. Leong, C. M. Cheah, and C. K. Chua, Solid freeform fabrication of three-dimensional scaffolds for engineering replacement tissues and organs. *Biomaterials* 24, 2363 (**2003**).

85. J. V. Araujo, A. Martins, I. B. Leonor, E. D. Pinho, R. L. Reis, and N. M. Neves, Surface controlled biomimetic coating of polycaprolactone nanofiber meshes to be used as bone extracellular matrix analogues. *J. Biomater. Sci. Polym. Ed.* 19, 1261 (**2008**).

86. M. M. Hohman, M. Shin, G. Rutledge, and M. P. Brenner, Electrospinning and electrically forced jets, I. Stability theory. *Phys. Fluids* 13, 2201 (**2001**).

87. V. Thomas, D. R. Dean, and Y. K. Vohra, Nanostructured biomaterials for regenerative medicine. *Curr. Nanosci.* 2, 155 (**2006**).

88. T. Subbiah, G. S. Bhat, R. W. Tock, S. Parameswaran, and S. S. Ramkumar, Electrospinning of nanofibers. *J. Appl. Polym. Sci.* 96, 557 (**2005**).

89. J. Lannutti, D. Reneker, T. Ma, D. Tomasko, and D. Farson, Electrospinning for tissue engineering scaffolds. *Mater. Sci. Eng. C* 27, 504 (**2007**).

90. J. Venugopal, Y. Z. Zhang, and S. Ramakrishna, Electrospun nanofibres: Biomedical applications. *J. Nanoeng. Nanosyst.* 218, 35 (**2005**).

91. V. Thomas, X. Zhang, S. A. Catledge, and Y. K. Vohra, Functionally graded electrospun scaffolds with tunable mechanical properties for vascular tissue regeneration. *Biomed. Mater.* 2, 224 (**2007**).

92. H. Yoshimoto, Y. M. Shin, H. Terai, and J. P. Vacanti, A biodegradable nanofiber scaffold by electrospinning and its potential for bone tissue engineering. *Biomaterials* 24, 2077 (**2003**).

93. M. Shin, H. Yoshimoto, and J. P. Vacanti, *In vivo* bone tissue engineering using mesenchymal stem cells on a novel electrospun nanofibrous scaffold. *Tissue Eng.* 10, 33 (**2004**).

94. C. M. Agrawal and R. B. Ray, Biodegradable polymeric scaffolds for musculoskeletal tissue engineering. *J. Biomed. Mater. Res.* 55, 141 (**2001**).

95. Q.-Z. Chen, A. Bismarck, U. Hansen, S. Junaid, M. Q. Tran, S. E. Harding, N. N. Ali, and A. R. Boccaccini, Characterisation of a soft elastomer poly(glycerol sebacate) designed to match the mechanical properties of myocardial tissue. *Biomaterials* 29, 47 (**2008**).

96. M. Shin, O. Ishii, T. Sueda, and J. P. Vacanti, Contractile cardiac grafts using a novel nanofibrous mesh. *Biomaterials* 25, 3717 (**2004**).

97. X. M. Mo, C. Y. Xu, M. Kotaki, and S. Ramakrishna, Electrospun P(LLA-CL) nanofiber: A biomimetic extracellular matrix for smooth muscle cell and endothelial cell proliferation. *Biomaterials* 25, 1883 (**2004**).

98. C. Y. Xu, R. Inai, M. Kotaki, and S. Ramakrishna, Aligned biodegradable nanofibrous structure: A potential scaffold for blood vessel engineering. *Biomaterials* 25, 877 (**2004**).

99. C. Alperin, P. W. Zandstra, and K. A. Woodhouse, Polyurethane films seeded with embryonic stem cell-derived cardiomyocytes for use in cardiac tissue engineering applications. *Biomaterials* 26, 7377 (**2005**).

100. K. L. Fujimoto, J. Guan, H. Oshima, T. Sakai, and W. R. Wagner, *In vivo* evaluation of a porous, elastic, biodegradable patch for reconstructive cardiac procedures. *Ann. Thorac. Surg.* 83, 648 (**2007**).

101. J. Guan, K. L. Fujimoto, M. S. Sacks, and W. R. Wagner, Preparation and characterization of highly porous, biodegradable polyurethane scaffolds for soft tissue applications. *Biomaterials* 26, 3961 (**2005**).

102. K. Gisselfält, B. Edberg, and P. Flodin, Synthesis and properties of degradable poly(urethane urea)s to be used for ligament reconstructions. *Biomacromolecules* 3, 951 (**2002**).

103. R. G. J. C. Heijkants, R. V. van Calck, T. G. van Tienen, J. H. de Groot, P. Buma, A. J. Pennings, R. P. H. Veth, and A. J. Schouten, Uncatalyzed synthesis, thermal and mechanical properties of polyurethanes based on poly(ε-caprolactone) and 1,4-butane diisocyanate with uniform hard segment. *Biomaterials* 26, 4219 (**2005**).

REVIEW

104. J. J. Stankus, J. Guan, K. Fujimoto, and W. R. Wagner, Microintegrating smooth muscle cells into a biodegradable, elastomeric fiber matrix. *Biomaterials* 27, 735 (**2006**).

105. S. A. Riboldi, N. Sadr, L. Pigini, P. Neuenschwander, M. Simonet, P. Mognol, M. Sampaolesi, G. Cossu, and S. Mantero, Skeletal myogenesis on highly orientated microfibrous polyesterurethane scaffolds. *J. Biomed. Mater. Res. Part A* 84A, 1094 (**2008**).

106. M. Borkenhagen, R. C. Stoll, P. Neuenschwander, U. W. Suter, and P. Aebischer, *In vivo* performance of a new biodegradable polyester urethane system used as a nerve guidance channel. *Biomaterials* 19, 2155 (**1998**).

107. J. Guan, M. S. Sacks, E. J. Beckman, and W. R. Wagner, Synthesis, characterization, and cytocompatibility of elastomeric, biodegradable poly(ester-urethane)ureas based on poly(caprolactone) and putrescine. *J. Biomed. Mater. Res. Part A* 61, 493 (**2002**).

108. T. Moore, Design and synthesis of biodegradable thermoplastic polyurethanes for tissue engineering, Ph.D. Thesis, Swinburne University of Technology, Australia (**2005**).

109. S. A. Riboldi, M. Sampaolesi, P. Neuenschwander, G. Cossu, and S. Mantero, Electrospun degradable polyesterurethane membranes: Potential scaffolds for skeletal muscle tissue engineering. *Biomaterials* 26, 4606 (**2005**).

110. S. Kidoaki, I. K. Kwon, and T. Matsuda, Structural features and mechanical properties of *in situ*-bonded meshes of segmented polyurethane electrospun from mixed solvents. *J. Biomed. Mater. Res. Part B Appl. Biomater.* 76B, 219 (**2006**).

111. M. A. Prado, F. J. de Siqueira, N. A. de Carvalho, V. D. Jahno, S. Einloft, R. Ligabue, J. Dullius, A. K. Alves, and C. P. Bergmann (eds.), Nanofibras de poliuretano bioabsorvível para a aplicação na engenharia de tecidos, *Proceedings of the 6th Latin American Congress of Artificial Organs and Biomaterials, COLAOB*, Gramado, Brazil, August (**2010**).

112. S. L. Shenoy, W. Douglas Bates, H. L. Frisch, and G. E. Wnek, Role of chain entanglements on fiber formation during electrospinning of polymer solutions: Good solvent, non-specific polymer-polymer interaction limit. *Polymer* 46, 3372 (**2005**).

113. V. Thomas and M. Jayabalan, Studies on the effect of virtual crosslinking on the hydrolytic stability of novel aliphatic polyurethane ureas for blood contact applications. *J. Biomed. Mater. Res. Part A* 56A, 144 (**2001**).

114. P. C. Caracciolo, V. Thomas, Y. K. Vohra, F. Buffa, and G. A. Abraham, Electrospinning of novel biodegradable poly(ester urethane)s and poly(ester urethane urea)s for soft tissue-engineering applications. *J. Mater. Sci.—Mater. Med.* 20, 2129 (**2009**).

115. P. C. Caracciolo, F. Buffa, and G. A. Abraham, Effect of the hard segment chemistry and structure on the thermal and mechanical properties of novel biomedical segmented poly(esterurethanes). *J. Mater. Sci.—Mater. Med.* 20, 145 (**2009**).

116. P. C. Caracciolo, A. A. A. de Queiroz, O. Z. Higa, F. Buffa, and G. A. Abraham, Segmented poly(esterurethane urea)s from novel urea–diol chain extenders: Synthesis, characterization and *in vitro* biological properties. *Acta Biomater.* 4, 976 (**2008**).

117. P. C. Caracciolo, Matrices Poliuretánicas Biorreabsorbibles para Aplicaciones en Ingeniería de Tejidos, Ph.D. Thesis, Universidad Nacional de Mar del Plata, Argentina (**2010**).

118. J. A. Matthews, G. E. Wnek, D. G. Simpson, and G. L. Bowlin, Electrospinning of collagen nanofibers. *Biomacromolecules* 3, 232 (**2002**).

119. M. Li, M. J. Mondrinos, M. R. Gandhi, F. K. Ko, A. S. Weiss, and P. I. Lelkes, electrospun protein fibers as matrices for tissue engineering. *Biomaterials* 26, 5999 (**2005**).

120. M. V. Jose, B. W. Steinert, V. Thomas, D. R. Dean, M. A. Abdalla, G. Price, and G. M. Janowski, Morphology and mechanical properties of Nylon 6/MWNT nanofibers. *Polymer* 48, 1096 (**2007**).

121. J. J. Stankus, J. Guan, and W. R. Wagner, Fabrication of biodegradable elastomeric scaffolds with sub-micron morphologies. *J. Biomed. Mater. Res. Part A* 70A, 603 (**2004**).

122. P. C. Caracciolo, F. Buffa, V. Thomas, Y. K. Vohra, and G. A. Abraham, Biodegradable polyurethanes: Comparative study of electrospun scaffolds and films. *J. Appl. Polym. Sci.* 121, 3292 (**2011**).

123. I. Stanishevskaya, V. Thomas, P. C. Caracciolo, G. A. Abraham, and Y. K. Vohra, Electrospun fibrous scaffolds from novel poly(ester urethane urea) and poly(dioxanone) for vascular tissue regeneration, *Proceedings of the European Polymer Congress (EPF)*, Granada, Spain, June–July (**2011**).

124. C.-H. Chen, H.-J. Wei, W.-W. Lin, I. Chiu, S.-M. Hwang, C.-C. Wang, W.-Y. Lee, Y. Chang, and H.-W. Sung, Porous tissue grafts sandwiched with multilayered mesenchymal stromal cell sheets induce tissue regeneration for cardiac repair. *Cardiovasc. Res.* 80, 88 (**2008**).

125. F. M. Ballarin, P. M. Frontini, and G. A. Abraham, Study of the nanofibrous morphology of small-diameter vascular grafts. *Biocell* 36, A7 (**2012**).

126. M. C. Branciforti, T. A. Custodio, L. M. Guerrini, L. Avérous, and R. E. S. Bretas, Characterization of nano-structured poly(D,L-lactic acid) nonwoven mats obtained from different solutions by electrospinning. *J. Macromol. Sci. Part B Phys.* 48, 1222 (**2009**).

127. E. G. R. Fernandes, V. Zucolotto, and A. A. De Queiroz, Electrospinning of hyperbranched poly-L-lysine/polyaniline nanofibers for application in cardiac tissue engineering. *J. Macromol. Sci. Part A Pure Appl. Chem.* 47, 1203 (**2010**).

128. G. Vlasov, Synthesis and utilization of hyperbranched poly(amino acids) as carriers of biologically active substances: Problems and solutions, Silicon Versus Carbon: Fundamental Nanoprocesses, Nanobiotechnology and Risks Assessment, edited by Y. Magarshak, S. Kozyrev, and A. K. Vaseashta, Springer, Netherlands (**2009**), pp. 319–340.

129. M. G. de Morais, C. Stillings, R. Dersch, M. Rudisile, P. Pranke, J. A. V. Costa, and J. Wendorff, Preparation of nanofibers containing the microalga Spirulina (Arthrospira). *Bioresour. Technol.* 101, 2872 (**2010**).

130. M. A. Borowitzka, Microalgae as source of pharmaceuticals and other biologically active compounds. *J. Appl. Physiol.* 7, 3 (**1995**).

131. G. Zanatta, D. Steffens, D. I. Braghirolli, R. A. Fernandes, C. A. Netto, and P. Pranke, Viability of mesenchymal stem cells during electrospinning. *Braz. J. Med. Biol. Res.* 45, 125 (**2012**).

132. J. A. van Aalst, C. R. Reed, L. Han, T. Andrady, M. Hromadka, S. Bernacki, K. Kolappa, J. B. Collins, and E. G. Loboa, Cellular incorporation into electrospun nanofibers: Retained viability, proliferation, and function in fibroblasts. *Ann. Plast. Surg.* 60, 577 (**2008**).

133. S. L. F. Ramos, P. B. Rego, G. B. C. Cardoso, S. T. O. Saad, C. A. C. Zavaglia, and M. A. d'Ávila (eds.), Redes de policaprolactona (PCL) obtidas por electrospinning: Principais propriedades e aplicações como biomaterial. *Proceedings of the 6th Latin American Congress of Artificial Organs and Biomaterials, COLAOB*, Gramado, Brazil, August (**2010**).

134. R. Furlan, J. A. M. Rosado, G. G. Rodriguez, E. R. Fachini, A. N. R. da Silva, and M. L. P. da Silva, Formation and characterization of oriented micro- and nanofibers containing poly(ethylene oxide) and pectin. *J. Electrochem. Soc.* 159, K66 (**2012**).

135. K. J. L. Burg, S. Porter, and J. F. Kellam, Biomaterial developments for bone tissue engineering. *Biomaterials* 21, 2347 (**2000**).

136. G. N. P. Rodriguez, L. R. Rodrigues, C. G. B. T. Dias, M. A. d'Ávila, and C. A. C. Zavaglia, Electrospun Scaffolds composed of poly(L-lactic acid) and hydroxyapatite. *Key Eng. Mater.* 493–494, 872 (**2012**).

137. F. Vázquez-Hernández, S. A. Lopez-Haro, M. A. M. Lira, M. L. Albor-Aguilera, V. Altuzar, and C. Mendoza-Barrera, Synthesis of HAp/chitosan composites via electrospinning: Preliminary results, *Proceedings of the 5th International Conference on Electrical Engineering, Computing Science and Automatic Control (CCE)*, Mexico City, Mexico, November (**2008**).

REVIEW

138. A. A. A. de Queiroz, J. C. Bressiani, A. H. Bressiani, O. Z. Higa, and G. A. Abraham, A novel bone scaffold based on hyperbranched polyglycerol fibers filled with hydroxyapatite nanoparticles: *In vitro* cell response. *Key Eng. Mater.* 396–398, 633 (**2009**).

139. V. M. Pantojas, E. Velez, D. Hernández, and W. Otaño, Initial study on fibers and coatings for the fabrication of bioscaffolds. *P. R. Health Sci. J.* 28, 258 (**2009**).

140. M. Kobayashi, T. Kikutani, T. Kukobo, and T. Nakamura, Direct bone formation on alumina bead composite. *J. Biomed. Mater. Res. Part A* 37, 554 (**1997**).

141. B. S. Harrison and A. Atala, Carbon nanotube applications for tissue engineering. *Biomaterials* 28, 344 (**2007**).

142. F. Z. Volpato, S. Lopes Fernandes Ramos, A. Motta, and C. Migliaresi, Physical and *in vitro* biological evaluation of a PA 6/MWCNT electrospun composite for biomedical applications. *J. Bioact. Compat. Polym.* 26, 35 (**2011**).

143. D. B. Warheit, B. R. Laurence, K. L. Reed, D. H. Roach, G. A. M. Reynolds, and T. R. Webb, Comparative pulmonary toxicity assessment of single-wall carbon nanotubes in rats. *Toxicol. Sci.* 77, 117 (**2004**).

144. P. Cherukuri, S. M. Bachilo, S. H. Litovsky, and R. B. Weisman, Near-infrared fluorescence microscopy of single-walled carbon nanotubes in phagocytic cells. *J. Am. Chem. Soc.* 126, 15638 (**2004**).

145. H.-X. Ren, X. Chen, J.-H. Liu, N. Gu, and X.-J. Huang, Toxicity of single-walled carbon nanotube: How we were wrong? *Mater. Today* 13, 6 (**2010**).

146. H. Zhang and Z. Chen, Fabrication and characterization of electrospun PLGA/MWNTs/hydroxyapatite biocomposite scaffolds for bone tissue engineering. *J. Bioact. Compat. Polym.* 25, 241 (**2010**).

147. R. Sen, B. Zhao, D. Perea, M. E. Itkis, H. Hu, J. Love, E. Bekyarova, and R. C. Haddon, Preparation of single-walled carbon nanotube reinforced polystyrene and polyurethane nanofibers and membranes by electrospinning. *Nano Lett.* 4, 459 (**2004**).

148. D. Khang, J. Lu, C. Yao, K. M. Haberstroh, and T. J. Webster, The role of nanometer and submicron surface features on vascular and bone cell adhesion on titanium. *Biomaterials* 29, 970 (**2008**).

149. S. Patel, K. Kurpinski, R. Quigley, H. Gao, B. S. Hsiao, M.-M. Poo, and L. Song, Bioactive nanofibers: Synergistic effects of nanotopography and chemical signaling on cell guidance. *Nano Lett.* 7, 2122 (**2007**).

150. N. Arya, S. Chakraborty, N. Dube, and D. S. Katti, Electrospraying: A facile technique for synthesis of chitosan-based micro/nanospheres for drug delivery applications. *J. Biomed. Mater. Res. Part B* 88B, 17 (**2009**).

151. J. M. Fernandez, M. S. Cortizo, A. M. Cortizo, and G. A. Abraham, Osteoblast behavior on novel porous polymeric scaffolds. *J. Biomater. Tissue Eng.* 1, 1 (**2011**).

152. M. S. Cortizo, M. S. Molinuevo, and A. M. Cortizo, Biocompatibility and biodegradation of polyesters and polyfumarates based-scaffold for bone tissue engineering. *J. Tissue Eng. Regen. Med.* 2, 33 (**2008**).

153. J. M. Fernández, G. A. Abraham, S. M. Cortizo, and A. M. Cortizo (eds.), Propiedades biológicas de matrices porosas y no porosas de PCL/PFIP, *Proceedings of the 6th Latin American Congress of Artificial Organs and Biomaterials, COLAOB*, Gramado, Brazil, August (**2010**).

154. V. Beachley and X. Wen, Polymer nanofibrous structures: Fabrication, biofunctionalization, and cell interactions. *Progr. Polym. Sci.* 35, 868 (**2010**).

155. K. Webb, V. Hlady, and P. A. Tresco, Relative importance of surface wettability and charged functional groups on NIH 3T3 fibroblast attachment, spreading, and cytoskeletal organization. *J. Biomed. Mater. Res. Part A* 41, 422 (**1998**).

156. Z. M. Liu, Q. Gu, Z. K. Xu, and T. Groth, Synergistic effect of polyelectrolyte multilayers and osteogenic growth medium

on differentiation of human mesenchymal stem cells. *Macromol. Biosci.* 10, 1043 (**2010**).

157. U. E. Spichiger-Keller, Chemical Sensors and Biosensors for Medical and Biological Applications, edited by W. Göpel, J. Hesse, J. N. Zemel, and H. Baltes, Wiley-VCH, Weinheim (**1998**), pp. 376–382.

158. J. Ryu, J. Park, B. Kim, and O. J. Park, Design and fabrication of a largely deformable sensorized polymer actuator. *Biosens. Bioelectron.* 21, 822 (**2005**).

159. J. M. Corres, Y. R. García, F. J. Arregui, and I. R. Matías, Optical fiber humidity sensors using PVdF electrospun nanowebs. *IEEE Sensors J.* 11, 2383 (**2011**).

160. A. Urrutia, P. J. Rivero, J. Goicoechea, F. J. Arregui, and I. R. Matías (eds.), Humidity sensor based on a long-period fiber grating coated with a hydrophobic thin film, *Proceedings of the European Workshop on Optical Fibre Sensors* (*EWOFS*), Porto, Portugal, September (**2010**).

161. C. O. González-Morán, C. J. Rodríguez-Montoya, and E. Suaste-Gómez (eds.), Preparation of membranes of poly(vynilidene fluoride) as temperatura sensors via electrospinning for biomedical applications, *Proceedings of the 7th International Conference on Electrical Engineering, Computing Science and Automatic Control* (*CCE*), Mexico City, Mexico, September (**2010**).

162. G. G. Wallace, G. M. Spinks, L. A. P. Kane-Maguire, and P. R. Teasdale, Conductive Electroactive Polymers: Intelligent Materials Systems, 2nd edn., CRC Press, Boca Raton (**2003**).

163. P. H. S. Picciani, E. S. Medeiros, Z. Pan, D. F. Wood, W. J. Orts, L. H. C. Mattoso, and B. G. Soares, Structural, electrical, mechanical, and thermal properties of electrospun poly(lactic acid)/polyaniline blend fibers. *Macromol. Mater. Eng.* 295, 618 (**2010**).

164. P. H. S. Picciani, B. G. Soares, E. S. Medeiros, F. G. de Souza, D. F. Wood, W. J. Orts, and L. H. C. Mattoso, Electrospinning of polyaniline/poly(lactic acid) ultrathin fibers: Process and statistical modeling using a non-gaussian approach. *Macromol. Theory Simul.* 18, 528 (**2009**).

165. P. H. S. Picciani, E. S. Medeiros, Z. Pan, W. J. Orts, L. H. C. Mattoso, and B. G. Soares, Development of conducting polyaniline/poly(lactic acid) nanofibers by electrospinning. *J. Appl. Polym. Sci.* 112, 744 (**2009**).

166. F. M. Ballarin, Engineering final project: Nanofibras Poliuretánicas y Compuestas de Interés Biomédico, Universidad Nacional de Mar del Plata, Argentina (**2009**).

167. M. Li, Y. Guo, Y. Wei, A. G. MacDiarmid, and P. I. Lelkes, Electrospinning polyaniline-contained gelatin nanofibers for tissue engineering applications. *Biomaterials* 27, 2705 (**2006**).

168. A. P. Martínez-Camacho, M. O. Cortez-Rocha, M. M. Castillo-Ortega, A. Burgos-Hernández, J. M. Ezquerra-Brauer, and M. Plascencia-Jatomea, Antimicrobial activity of chitosan nanofibers obtained by electrospinning. *Polym. Int.* 60, 1663 (**2011**).

169. S. Torres-Giner, M. J. Ocio, and J. M. Lagaron, Development of active antimicrobial fiber-based chitosan polysaccharide nanostructures using electrospinning. *Eng Life Sci.* 8, 303 (**2008**).

170. B. Son, B. Y. Yeom, S. H. Song, C. S. Lee, and T. S. Hwang, Antibacterial electrospun chitosan/poly(vinyl alcohol) nanofibers containing silver nitrate and titanium dioxide. *J. Appl. Polym. Sci.* 111, 2892 (**2009**).

171. I. A. Hidalgo, J. Ramírez, M. A. Sabino, A. Müller, Obtención de estructuras tipo andamio de poli(ácido) láctico para bioingeniería mediante electrospinning. *Rev. Latin Am. Metal. Mat.* S3, 28 (**2011**).

172. R. G. F. Costa, C. Ribeiro, and L. H. C. Mattoso, Preparation and characterization of PVA-Ag nanocomposite fibers with antibacterial activities. *Sci. Adv. Mater.* 2, 157 (**2010**).

173. B. Veleirinho, R. M. Ribeiro-do-Valle, and J. A. Lopes-da-Silva, Processing conditions and characterization of novel electrospun

poly(3-hydroxybutyrate-co-hydroxyvalerate)/chitosan blend fibers. *Mater. Lett.* 65, 2216 (**2011**).

174. M. A. Gonzalez, F. Montini Ballarin, M. Brun, G. A. Abraham, and V. L. Ballarin, Morphological quantification of polymer nanofibers in tissue engineering images. *L. A. A. R.* 42, 89 (**2012**).

175. K. Autumn, M. Sitti, Y. A. Liang, A. M. Peattie, W. R. Hansen, S. Sponberg, T. W. Kenny, R. Fearing, J. N. Israelachvili, and R. J. Full, Evidence for vdW adhesion in gecko setae. *Proc. Natl. Acad. Sci.* 99, 12252 (**2002**).

176. K. Autumn, Y. A. Liang, S. T. Hsieh, W. Zesch, W.-P. Chan, T. W. Kenny, R. Fearing, and R. J. Full, Adhesive force of a single gecko foot-hair. *Nature* 405, 681 (**2000**).

177. F. M. Ballarin, T. A. Blackledge, N. L. C. Davis, P. M. Frontini, G. A. Abraham, and S.-C. Wong, Effect of topology on the adhesive forces between electrospun polymer fibers studied using a *T*-peel test. *Polym. Eng. Sci.* Submitted.

178. C. Greiner, Size and shape effects in bioinspired fibrillar adhesives, University of Stuttgart, Germany (**2007**).

REVIEW

REVIEW

Vitamin C Based Nanostructures: Potential Utility in Ocular and Transdermal Therapy

Santiago D. Palma*, Gabriela V. Ullio Gamboa, and Daniel A. Allemandi

Departamento de Farmacia, Facultad de Ciencias Químicas, Universidad Nacional de Córdoba, UNITEFA-CONICET, Córdoba X5000HUA, Argentina

Alkyl vitamin C derivatives (ASCn) combine in their structure a lipophilic and a hydrophilic moiety and exhibit properties of typical surfactant molecules. Self-assembly properties of ASCn depend on the length of *n*-alkyl fatty chain. ASCn start to aggregate at temperatures (CMT, Krafft point) at which the solubility reaches the critical micellar concentration (CMC). Above this temperature, ASCn can aggregate in micelles or gel phase, depending of alkyl side chain. Upon cooling, for less soluble derivatives (ASC12, ASC14 and ASC16) liquid–crystal structures named coagels are obtained. They are able to solubilize insoluble and unstable drugs, protect them from any possible aggressive environment and promote their permeation through skin and mucosa. These systems possess very interesting properties making ASCn coagels promising pharmaceutical platforms for drug delivery. Results from investigations about all these properties will be described and analyzed in the present review with particular emphasis on the use of these systems for drug administration through ocular and transdermal routes.

Keywords: Ascorbic Acid, Nanostructures, Coagels, Drug Delivery.

CONTENTS

1. INTRODUCTION

The use of active surface compounds (surfactants) in pharmaceutical technology has been widely explored. They are commonly utilized as emulgent, solubilizing agent, suspension stabilizers, wetting agent, etc. In these cases, they are incorporated in the formulation in relative low concentrations where surfactant molecules remain disaggregated in a subcolloidal estate at the interface. However, depending on chemical structure, concentration and temperature, surfactants are able to form supramolecular aggregates with very particular properties when the concentration is raised.[1]

Solubility as well as molecular size defines the self assembly characteristics of the surfactants. It is well known that surfactants at determined concentrations (minimal aggregation concentration) begin to form aggregates as consequence of the increment of interactions between molecules. As concentration is raised, the interactions between adjacent structures are increased leading to the coalescence of the system in larger structures usually denominated liquid crystals. The formation of such structures can be evidenced through noticeable changes in viscosity, conductivity, birefringence and X-ray diffraction patterns. The different liquid crystal systems formed from surfactant-solvent interactions are defined as lyotropic liquid crystals (LLC).[2]

Polar lipids have been widely investigated as lyotropic liquid crystal precursors. Among the most studied compounds are fatty acid esthers such as monoglycerides and glycerates.[3, 4] In recent years, LLC systems have received considerable attention because of their high potential as drug vehicles. Among these systems, reversed cubic, hexagonal and lamellar mesophases are the most important and they have been extensively investigated for their ability to sustain the release of a wide range of bioactives, from low molecular weight drugs to proteins, peptides and nucleic acids.[5] Besides, these systems have shown promissory pharmaceutical performance for drug administration through different routes.[6–9]

*Author to whom correspondence should be addressed.

From several years ago we have been studying a group of polar lipids consisting of alkyl vitamin C derivatives (ASCn).[10–14] Their amphiphilic nature allows these compounds to form aggregates, mainly lamellar mesophases. By mean of these studies we were able to evaluate the potential utility of this new liquid crystal system, which has evidenced very interesting properties as pharmaceutical carrier. In this review, we focus on the description of the general properties of these systems and the results concerning their potential use for drug administration through ophthalmic and dermal routes.

2. CHARACTERISTICS OF ASCn

2.1. Physicochemical Properties

Ascorbic acid (AA) is one of the most powerful natural antioxidants but due to its poor solubility in hydrophobic media, its usefulness is limited to aqueous environments.

Ascorbyl-6-O-alkanoates (ASCn) retain the same radical-scavenging properties of ascorbic acid and their
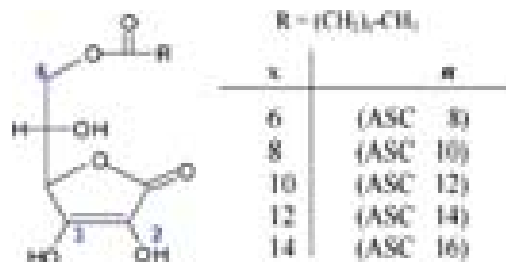
Fig. 1. Schematic chemical compositions of 6-O-alkyl ascorbic acid derivatives. Reproduced with permission from [24], S. Palma, et al., *Il Farmaco.* 58, 1271 (**2003**). © 2003, Elsevier.

antioxidant efficiency is comparable to other natural reducing agents, such as carotenes, polyphenols, and tocopherols.[15] ASCn are obtained through the estherification of hydroxyl group in position 6 of AA with fatty acids of variable length chain (Fig. 1).

The ASCn-water systems give liquid crystals on heating, which, on cooling, become gels with lamellar structure that exhibit sharp X-ray diffraction patterns and optical

Santiago D. Palma (38 years old), who trained in pharmacy, teaches Pharmaceutical Technology and Community Pharmacy at the Faculty of Chemical Sciences, National University of Córdoba, Argentina. Since 2005, Professor Palma is Scientist Researcher of National Scientific and Technical Research Council (CONICET). His research activity has resulted in the publication of over 35 original refereed scientific articles and more than 95 contributions at conferences. Currently, his interest is directed towards the conception of new pharmaceutical platforms for drug delivery.
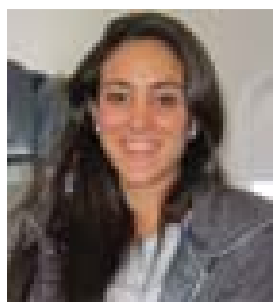
Gabriela V. Ullio Gamboa (26 years old) graduated as a pharmacist in 2009 and is currently studying for a Ph.D. at Chemistry School (National University of Cordoba-Argentina). She has fellowships for research activities from the Scientist Researcher of National Scientific and the Technical Research Council (CONICET). Her teaching activities involve lecturing, as well as practical classes, on the subject of Pharmacotechnia II at Pharmacy school. She is a member of a research team, directed by Professor Daniel Allemandi, which aims to develop new pharmaceutical platforms for drug delivery. Her subjects of research are nanotechonology and nanomedicines, covering both the development of encapsulation methods for active ingredients and drug targeting.

Daniel A. Allemandi (50 years old) graduated as a pharmacist in 1985 and Ph.D. in Pharmacy in 1993, at the National University of Cordoba-Argentina. He is Full Professor and researcher of the National Research Council (CONICET). His teaching activities at graduate and postgraduate level involve lecturing in topics related to Pharmaceutics and Biopharmaceutics. He is director of a team whose subjects of research are novel modified drug delivery systems with emphasis in nanoparticles and localized drug release. His work is supported by several grants provided by national scientific agencies. He is author and co-author or numerous papers and scientific articles concerning his expertise area.

birefringence (see next section). The semisolid consistency of such gels is an interesting property in order to formulate pharmaceutical dosage forms able to solubilize and stabilize different drugs for dermatological use. Therefore, these amphiphiles combine the powerful antioxidant properties of ascorbic acid with the capability of producing supramolecular aggregates.

The synthesis of ASCn was reported elsewhere.[16] The variation in side chain length has a direct influence on their physico-chemical properties, for example the melting point increases with the side chain length.[10] The pKa values for OH(3) and OH(2) are 4.2 and 11.6, respectively. Therefore, ascorbyl-6-O-alkanoates behave as anionic surfactants in pure water.[17]

Their amphiphilic nature allows these vitamin C derivatives to form aggregates (coagel) that provide an ideal environment for the solubilization of hydrophobic and sensitive drugs that might be otherwise easily degraded and oxidized when exposed to light, heat, dissolved oxygen, and other radical-producing species.

2.2. Phase Behavior and Aggregation Properties

At room temperature the water solubility of alkanoyl-6-o-ascorbic acids (ASCn) is poor, except for the short chained ASC8.[18–20] Their solubility increases with temperature, so that depending on the side chain length, the surfactants form clear micellar dispersions above a critical micellar concentration (CMC) and at temperatures higher than their critical micellar temperature (CMT).[21] On cooling, a solution of ascorbyl alkanoate produces an opaque curd.[22] Such a phase is typically termed semicrystalline mesophase, poorly hydrated crystal, or more usually *coagel*.

These supramolecular assemblies, in which the surfactant molecules are arranged in closely packed lamellar structures, undergo either a coagel-to-micelle or a coagel-to-gel phase transition depending on the aliphatic side chain length, as depicted in Figures 2 and 3.

The water in the system is in three different states[24] (Fig. 4). The first hydration layer is composed of about 11 water molecules per surfactant molecule which are strongly attached to the oxygen and the hydrogens of the –OH groups of the polar headgroups by hydrogen bonds and are not detectable by DSC, included in a 3 Å thick layer. The second hydration layer is formed by about 50–60 water molecules per surfactant one, which are associated with that of the first hydration layer and are then affected enough by the presence of the polar headgroups to have a different melting peak from that of bulk water. The second hydration layer is extended up to 9 Å from the polar group. Water not included in these two categories behaves as bulk water.

2.3. Rheology of Nanostructured Aggregates

The semisolid system formed from ASCn self-assembly shows very particular rheological behavior.[24] ASC8,
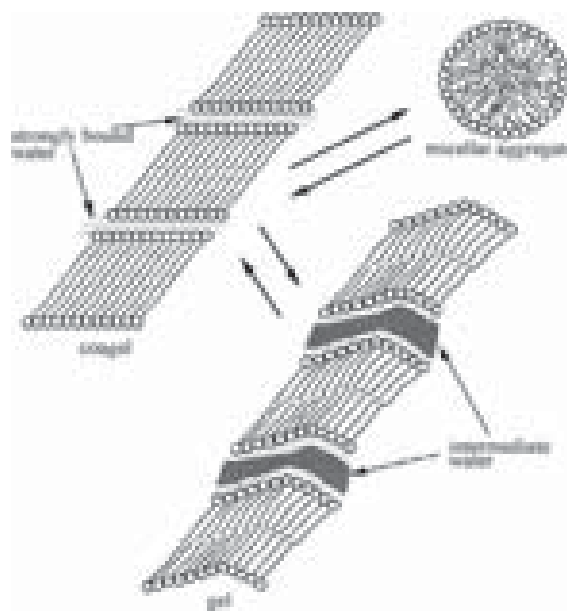
Fig. 2. Schematic picture of a coagel in equilibrium with a micelle or with a gel phase. Reproduced with permission from [10], S. Palma, et al., *Langmuir* 18, 9219 (**2002**). © 2002, Americman Chemical Society.

ASC12, ASC14, and ASC16 coagels show a complex rheology, with the appearance of spur rheograms, while coagels of ASC10 and ASC11 exhibit pseudoplastic flow. ASC11 also shows thixotropy (Fig. 5).

Coagels of ASC12, ASC14 and ASC16 form a 'house of cards' structure, where swelling and strengthening of the semisolid network occurs, due to the presence of water pools between the amphiphilic bilayers. On the other hand, for ASC10 and ASC11 coagels, this kind of arrangement apparently is not permitted and flexible bimolecular sheets arrange parallel to each other.

When a spur value is reached, ASC12, ASC14 and ASC16 coagels acquire pseudoplastic flow. In this way, according to the handling of the semisolids, the rheological properties of the system can change.

3. OCULAR DRUG DELIVERY SYSTEMS

Topical application on the eye's surface is the common method of drug administration to treat ocular diseases. However, a pharmaceutical carrier used for this objective has to be formulated according to the disease nature, as different pathologies may affect the external (conjunctivitis, blefaritis, dry eye syndrome, etc.) or internal (uveitis, endophthalmitis, glaucoma, etc.) segments of the eye.

It has been reported that the intraocular bioavailability is very low ($< 5\%$) after topical application, mainly due to the particular characteristics of the corneal epithelium. Since precorneal area receives most of the administered drug, it is expectable that high systemic absorption through
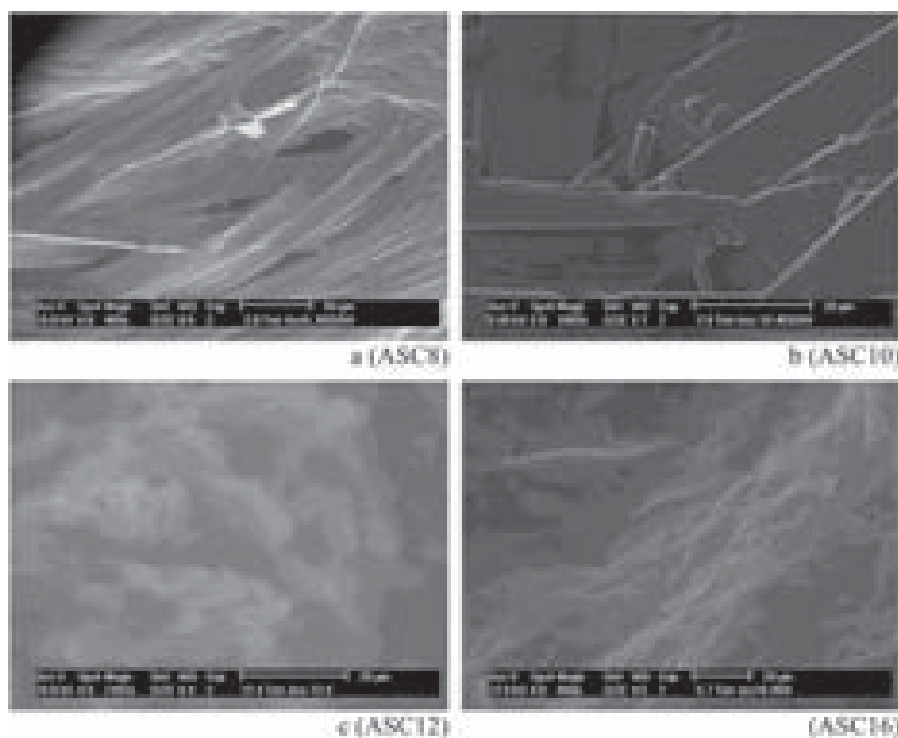
Fig. 3. ESEM pictures of ASCn. (a) ASC8, 400×, RH 60%, 3.9 Torr. (b) ASC10, 1663×, RH 45%, 2.9 Torr. (c) ASC12, RH 70%, 12.4 Torr. (d) ASC16, 800×, RH 85%, 5.7 Torr. Reproduced with permission from [10], S. Palma, et al., *Langmuir* 18, 9219 (**2002**). © 2002, Amerrican Chemical Society.

conjunctiva and nasolacrimal duct may occur.[25] The cornea is practically impermeable and, therefore, behaves as a very efficient barrier against chemical compounds.

In response, different strategies have been developed to improve drug permeation through this membrane. Among these, the use of absorption enhancers is perhaps one of the most effective.[26]

Regarding usual ocular pathologies, glaucoma involves progressive optic nerve damage associated with the loss of visual function and is frequently related to elevated intraocular pressure (IOP).[27]

Such pathology is usually treated with the administration of different classes of topical medications such as prostaglandin analogs (latanoprost, travoprost, and bimatoprost), selective β-adrenergic agonists (apraclonidine, brimonidine, and clonidine) and carbonic anhydrase inhibitors (CAIs; brinzolamide).

Nowadays, acetazolamide (AZM), a CAI, can be orally used for the reduction of IOP in patients suffering from glaucoma, in the preoperative management of closed-angle glaucoma, or as an adjuvant therapy in the treatment of open-angle glaucoma.[28]

However, in order to obtain the desired lowering in IOP, large oral doses of AZM have to be administered, and can lead to a wide range of side effects that usually appear due

to the extensive distribution of carbonic anhydrase in the body's organs.

These deleterious systemic side effects of AZM could be avoided if AZM is topically administered to the eyes. Nevertheless, the poor aqueous solubility (0.7 mg/mL) and low corneal permeability (4.1×10^{-6} g·cm/s) limit the ocular bioavailability of AZM.[29]

In a recent work[30] we reported the results concerning the potential utility of ASCn coagels for AZM ophthalmic administration. These systems were evaluated in terms of their *in vitro* permeability (isolated cornea), pharmacological effectiveness (IOP reduction in normotensive rabbits) and potential irritant effects.

Besides low permeability, the poor solubility of AZM in water is also a limiting factor for drug absorption. Regarding this, the lamellar structure of coagels may increase the amount of solubilized drug in the system. The highest AZM solubility ($> 0.5\%$ W/V) was observed for 2% ASC12 coagels, and in comparison to ringer's solutions, the apparent solubility of AZM was increased 4-fold.

Based on these results, for permeation studies, we used 2% ASC12 coagel containing AZM at 2 different concentrations (0.1% and 0.4%) aiming to evaluate the influence of drug concentration on the therapeutical response. Then, bearing in mind the pharmaceutical requirements
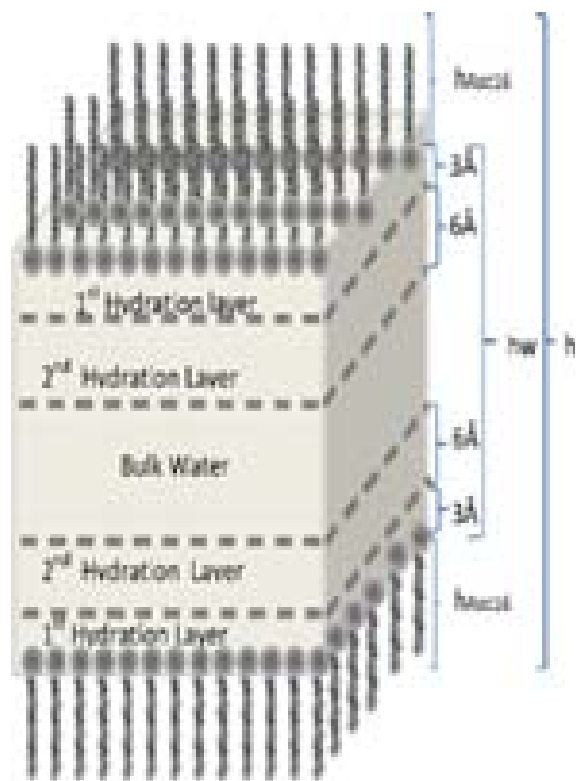
Fig. 4. Structural model of the hydrated aggregates (crystals and lamellar mesophases). Source: reproduced with permission from [23], L. Benedini, et al., *Colloids Surf., A: Physicochemical and Engineering Aspect.* 375, 178 (**2011**). © 2011, Elsevier.

for ophthalmic formulations such as tonicity and pH, the coagels were formulated using glucose isotonic solutions as vehicle.

The formulations obtained were slightly hypo-osmotic, although in compliance studies on animals, we detected neither discomfort nor histological evidence of mucosa damage. The low pH observed may be aggressive for ocular mucosa. However, the normal pH value of lacrimal fluid was rapidly restored (about 30 s) after administration of AZM coagel in rabbits, without any detectable side effects (unpublished data).

3.1. *In Vitro* Drug Release

This assay was performed in order to evaluate the effect of coagels on AZM release. Taking into account that a drug permeable membrane was used, the observed release kinetic should only be attributed to the influence of coagels on drug diffusion.

ASC12 coagels containing AZM showed to be able to modulate drug release (Fig. 6). In both cases (0.1% and 0.4%), a near-zero-order release was observed. As expected, the drug release was higher for AZM 0.4%.

3.2. Evaluation of AZM Transcorneal Permeation

The corneal epithelium is less permeable compared with other epithelial tissues (intestinal, nasal, bronchial, and tracheal), although it is more permeable than the stratum corneum.[31] The results concerning AZM permeation through the cornea are presented in Figure 7. In these assays, we also evaluated the permeation of AZM suspended in ringer's solution (AZM-R) and the marketed brinzolamide drug product AZOPT®. This marketed formulation containing 1% w/w of brinzolamide, according to the information provided by the producer (Alcon Laboratories), was used as a reference. Although this latest is a newer and lesser potent drug compared to AZM, nowadays is the selected drug for first instance treatment of glaucoma.

AZM-loaded coagels were able to promote AZM permeation, which was higher compared to ringer solution. This increase in permeation was proportional to AZM concentration according to the measured AZM steady-state flux (J) and apparent permeation coefficient (P_{app}) ($J = 1.43$ mg/min and $P_{app} = 3.04$ cm $\cdot$ s^{-1}).[31]

In this way, for AZM 0.1% the transcorneal permeation was thrice higher than AZM-R for the same drug concentration. This increase was even higher in the case of AZM 0.4% coagels, mainly due to the higher amount of AZM available for absorption. In the case of AZM-R, drug permeation was very low as consequence of the physicochemical properties of AZM. Similar results were observed with brizolamide (AZOPT®), although this drug is quite different to AZM. Therefore, based on these results, preliminary *in vitro* permeation studies have demonstrated that coagels could be an advantageous drug delivery system for the ocular administration of AZM.

3.3. *In Vivo* IOP Measurements

In order to evaluate the possible correlation of coagels behavior observed *in vitro* with the *in vivo* effect, the variation of IOP in rabbits after formulation administration was measured.

In Figure 8, we show the results concerning IOP diminution after the administration of the formulations under investigation. In the case of coagels containing AZM, the hipotensor effect (HE) was proportional to AZM concentration, whereas for AZM-R, this correlation was practically negligible. It was possible to appreciate the maximum difference in HE (24.84%–2.02%) 2 h post-administration for AZM 0.4% coagels in comparison to AZM-R. This implies that the effect of a higher concentration alone does not seem to be sufficient to explain this observation, as AZM-R is a solution where AZM is immediately available for absorption. Nevertheless, the corneal permeation and HE were both lower.

With regard to HE of AZOPT, this was similar to that observed for AZM 0.4% coagel during the first 2 h post-administration. However, this effect rapidly diminished for
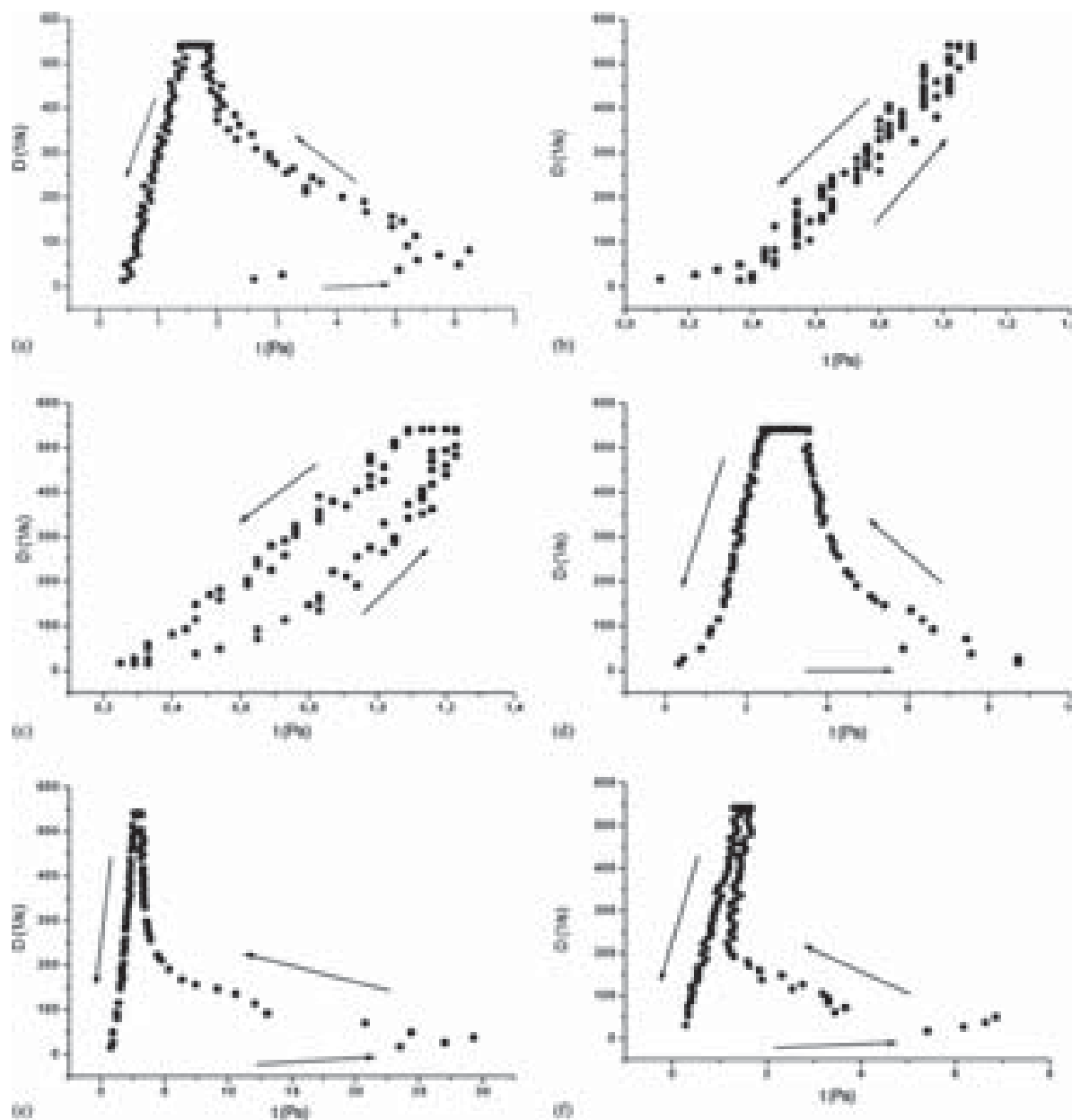
Fig. 5. Rheograms for ASCn coagels: (a) ASC8; (b) ASC10; (c) ASC11; (d) ASC12; (e) ASC14; and (f) ASC16. Reproduced with permission from [24], S. Palma, et al., *Il Farmaco.* 58, 1271 (**2003**). © 2003, Elsevier.

AZOPT after 2 h, whereas for AZM 0.4% coagel the HE reached a maximum at 2 h and remained at similar values during 3 h.

The behavior of AZM 0.1% coagel was quite different compared with earlier formulations. Its maximum HE was lower and was reached 3 h postadministration. After 4 h, the HE value was similar to the values observed for COA-AZM 0.4% and AZOPT at the same time. Evidently, according to Figure 8, lower AZM concentrations did not

facilitate rapid drug absorption due to the low concentration gradient that impelled the diffusion process. In this context, it is important to analyze the results taking into account the relative drug concentration in each formulation.

The AZM permeation from AZM 0.4% coagel and brinzolamide were initially similar. Although the AZM concentration from AZM 0.4% coagel was 2.5-fold lower than brinzolamide concentration (AZOPT), the former was able to permeate the drug more efficiently. Besides,
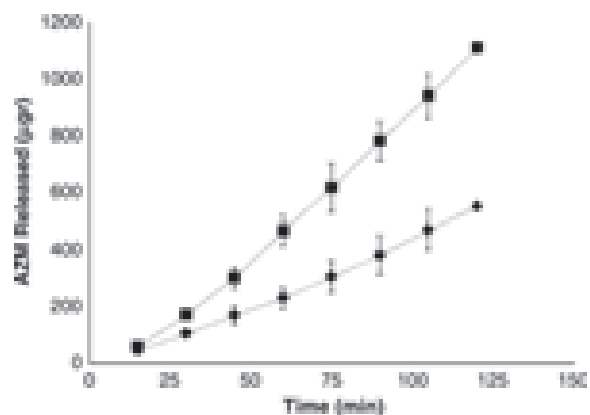
Fig. 6. *In vitro* release profile of acetazolamide (AZM) from ASC12 coagels. ■ AZM 0.4%; ♦ AZM 0.1%. Reproduced with permission from [30], L. I. Tártara, et al., *Journal of Ocular Pharmacology and Therapeutics* 28, 102 (**2012**). © 2012, Mary Ann Liebert, Inc.

Fig. 7. *Ex vivo* permeation profile through isolated rabbit cornea. Comparison between formulations of ASC12 coagels containing AZM and AZOPT commercial formulation. ■ AZM 0.4%; ♦ AZM 0.1%; • AZM-R; ▲ AZOPT®. Reproduced with permission from [30], L. I. Tártara, et al., *Journal of Ocular Pharmacology and Therapeutics* 28, 102 (**2012**). © 2012, Mary Ann Liebert, Inc.

4. TRANSDERMAL DRUG DELIVERY SYSTEMS

Several factors may influence the skin permeation, and consequently, the improvement in the therapeutic efficacy of topically delivered drugs. Among these, the release of drug from the formulation, drug penetration into the stratum corneum and drug diffusion into the deeper skin layers may be included.

The permeation of ASCn as well as its effect on "*in vitro*" and "*in vivo*" drug diffusion through rat and mice skin was evaluated.[12] ASCn permeation through rat skin epidermis was very fast and quantitatively significant. ASC12 appears to be the compound that possesses the highest capacity to enhance the penetration of the drug as well as for self-penetration through the epidermis.

The ability of these compounds to permeate the rat skin is related to their chemical composition, since the flux of ASCn decreases as alkyl chain length increases. Furthermore, a burst effect was observed with ASC12. Also, the permeation of anthralin from ASCn coagels applied on rat skin was very increased compared to other pharmaceutical systems such as liposomal and niosomal carriers,[32] being ASC12 the most effective enhancer.

In line with this, a subsequent study was conducted with the goal of characterizing the transdermal permeation of ibuprofen (IBU).[34, 35] In the case of ASC12 and ASC16 coagels, IBU release was sustained as indicated by the diffusion coefficient (*n*). IBU release from ASC16 was slightly lower than that of ASC12. This difference could be attributed to the higher viscosity of the former.[25]

Regarding IBU permeation through hairless mouse skin, we observed a noticeable increment in permeation in the case of ASCn coagels, especially for ASC12. The permeation of IBU from Arfen® (marketed formulation containing IBU 0.1%) was lower than ASC12 and ASC16. Considering lag time, Arfen® needed 4.5 h to saturate the skin, while ASC16 and ASC12 could cross the skin in 45 min and 60 min, respectively. We have previously corroborated the enhancing activity of ASC12 without noticeable injurious effects on the skin.[32] The influence of a co-solvent (PEG 400) was also evaluated.

ASC12 and ASC16 coagels increased IBU transdermal permeation about 21 and 12-fold compared to Arfen® ($p < 0.05$), respectively; demonstrating the ability of coagels to improve IBU skin permeation (Fig. 9). The addition of PEG to ASCn coagels produced a remarkable increase in IBU permeation compared to ASCn coagels.[34] This observation can be explained by the known enhancer properties of PEG. This polymer shows biocompatibility more suitable to the cutaneous administration with respect to short-chain alkanols also used as enhancers.

According to the attained results, both the *in vitro* test to characterize the drug partition from the vehicles and the *ex vivo* drug rat skin diffusion test to analyze the complexes interactions that occur between skin and excipients

brinzolamide is known to be intrinsically more permeable than AZM, implying that the promoter effect of coagels is really remarkable.

In order to evaluate the potential irritant effects of the formulations, we performed a histological examination by light microscopy of the treated corneas.[31] In all cases, the intensity of irritation was time dependent.

The sodium dodecyl sulphate solution (SDS 2%) used as positive control produced a serious injury after 30 min post-administration. Although this irritation gradually decreased, at 180 min, it was still considerable. On the other hand, as expected, the irritant effect of AZM-R was practically negligible along the time of examination (180 min). Finally, in the case of AZM 0.1% and AZM 0.4% coagels, a mild-to-moderate effect was observed.

Fig. 8. *In vivo* profile variation of intraocular pressure in rabbits. Comparison between formulations of coagels containing acetazolamide and marketed formulation. ● AZM-R; ♦ COA-AZM 0.1%; ■ COA-AZM 0.4%; ▲ AZOPT[®]. Reproduced with permission from [30], L. I. Tártara, et al., *Journal of Ocular Pharmacology and Therapeutics* 28, 102 (**2012**). © 2012, Mary Ann Liebert, Inc.

proved the efficacy of this new series of derivatives of 6-Oascorbic acid alkanoate.

The studied ASC16 and ASC12 coagels, defined as stable supramolecular assemblies in water or in water/PEG mixtures, allowed the solubilization of IBU (0.85%) and controlled the drug release rate. Our results demonstrated that ASC16 and ASC12 coagels and in particular those vehicles containing PEG, producing a higher amount of permeated drug through the skin compared to commercial Arfen®, are a promising tool as carriers for cutaneous IBU delivery.
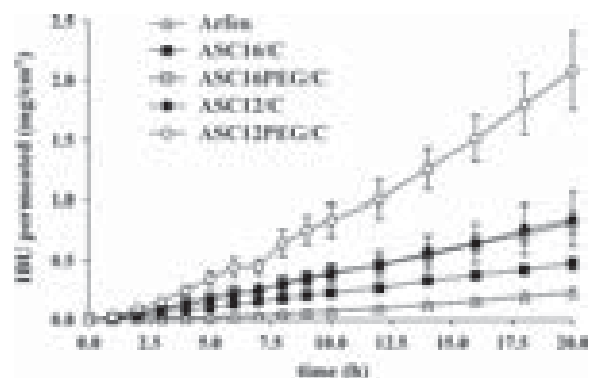
Fig. 9. Permeation profile through rat skin of IBU from ACS12PEG/C (s), ACS12/C (d), CS16PEG/C (h), ACS16/C (j) coagels and reference commercial formulation (4) (mean SE, $n = 6$). Reproduced with permission from [34], V. Saino et al., *European Journal of Pharmaceutics and Biopharmaceutics* 76, 443 (**2010**). © 2010, Elsevier.

5. SUMMARY AND PERSPECTIVE

The nanostructured systems derived from the self-assembly properties of ASCn showed appropriated characteristics as pharmaceutical platform for drug delivery, especially through administration routes where permeation enhancement is necessary. In this way, coagels of ASC16 and ASC12 were able to increase drug permeation in formulation intended for ocular and transdermal administration.

According to our studies carried out so far, ocular hypotensive drugs such as AZM were more effective when vehiculized in ASC12 coagels comparatively to other pharmaceutical systems or marketed formulations. Similar conclusions were obtained in the case of NASDs such as ibuprofen incorporated in ASC12 coagels and administrated topically on to the skin. Besides, other properties such as drug release modulation, antioxidant activity and adequate rheology make this kind of systems very promissory as pharmaceutical dosage form.

Based on these observations, very interesting perspectives are derived for the potential utility of ASCn coagels, since there is a wide range of relevant pharmaceutical drugs whose therapeutic effectiveness is dependent on its penetration capacity across mucoses.

68

J. Biomater. Tissue Eng. 3, 61–69, 2013

References and Notes

1. D. Myers, Surfactant Science and Technology, Second edn., VCH, New York (**1994**).

2. J. Clint (ed.), Surfactant Aggregation, Blackie, London (**1992**).

3. F. Caboi, G. S. Amico, P. Pitzalis, M. Monduzzi, T. Nylander, and K. Larsson, Addition of hydrophilic and lipophilic compounds of biological relevance to the monoolein:water system. I. Phase behavior. *Chem. Phys. Lipids* 109, 47 (**2001**).

4. J. C. Shah, Y. Sadhale, and D. M. Chilukuri, Cubic phase gels as drug delivery systems. *Advanced Drug Delivery Reviews* 47, 229 (**2001**).

5. C. Guo, J. Wang, F. Cao, R. J. Lee, and G. Zhai, Lyotropic liquid crystal systems in drug delivery. *Drug Discovery Today* 15, 1032 (**2010**).

6. L. Gan, S. Han, J. Shen, J. Zhu, C. Zhu, X. Zhang, and Y. Gan, Self-assembled liquid crystalline nanoparticles as a novel ophthalmic delivery system for dexamethasone: Improving preocular retention and ocular bioavailability. *Int. J. Pharm.* 396, 179 (**2010**).

7. J. Lee and I. W. Kellaway, *In vitro* peptide release from liquid crystalline buccal delivery systems. *Int. J. Pharm.* 195, 29 (**2000**).

8. L. S. Nielsen, L. Schubert, and J. Hansen, Bioadhesive drug delivery systems - I. Characterisation of mucoadhesive properties of systems based on glyceryl mono-oleate and glyceryl monolinoleate. *European Journal of Pharmaceutical Sciences* 6, 231 (**1998**).

9. C. C. Muller-Goymann, Physicochemical characterisation of colloidal drug delivery systems such as reverse micelles, vesicles, liquid crystals and nanoparticles for topical administration. *European Journal of Pharmaceutics and Biopharmaceutics* 58, 343 (**2004**).

10. S. Palma, R. Manzo, D. Allemandi, L. Fratoni, and P. Lo Nostro, Coagels from ascorbic acid derivatives. *Langmuir* 18, 9219 (**2002**).

11. M. Ambrosi, P. Lo Nostro, L. Fratoni, L. Dei, B. W. Ninham, S. Palma, R. H. Manzo, D. Allemandi, and P. Baglioni, Water of hydration in coagels. *Phys. Chem. Chem. Phys.* 6, 1401 (**2004**).

12. S. D. Palma, B. Maletto, P. Lo Nostro, R. H. Manzo, M. C. Pistoresi-Palencia, and D. A. Allemandi, Potential use of ascorbic acid–based surfactants as skin penetration enhancers. *Drug Dev. Ind. Pharm.* 32, 1 (**2006**).

13. M. Rasia, M. I. Spengler, S. Palma, R. Manzo, P. Lo Nostro, and D. Allemandi, Effect of ascorbic acid based amphiphiles on human erythrocytes membrane. *Clinical Hemorheology and Microcirculation.* 36, 133 (**2007**).

14. H. S. Nalwa (ed.), Handbook of Nanostructured Biomaterials and Their Applications in Nanobiotechnology, American Scientific Publishers, Los Angeles (**2005**), Vols. 1–2.

15. P. K. Martindale, The Complete Drug Reference, 34th edn., The Pharmaceutical Press, London (**2005**).

16. G. Capuzzi, G. Kulkarni, J. Fernandez, J. Vincieri, and P. Lo Nostro, Mixtures of ascorbyl-stearate and vitamin D3: A monolayer study at the gas/water interface. *J. Colloid Interface Sci.* 186, 271 (**1997**).

17. P. Lo Nostro, G. Capuzzi, and N. Mulinacci, Self-assembly and antioxidant properties of octanoyl-6-O-ascorbic acid. *Langmuir.* 4, 1744 (**2000**).

18. G. Capuzzi, P. Lo Nostro, K. Kulkarni, and J. E. Fernandez, Mixtures of stearoyl-6-O-ascorbic acid and α-tocopherol: A monolayer study at the gas/water interface. *Langmuir.* 12, 3957 (**1996**).

19. G. Capuzzi, P. Lo Nostro, K. Kulkarni, J. E. Fernandez, and F. F. Vincieri, Interactions of 6-O-stearoylascorbic acid and vitamin K1 in mixed langmuir films at the gas/water interface. *Langmuir* 12, 5413 (**1996**).

20. G. Capuzzi, K. Kulkarni, J. E. Fernandez, and F. F. Vincieri, P. Lo Nostro, Mixtures of ascorbyl-stearate and vitamin D3: A monolayer study at the gas/water interface. *J. Colloid Interface Sci.* 186, 271 (**1997**).

21. U. Kohler, P. W. Yang, S. Weng, and H. H. C. Mantsch, Structure and polymorphic phase behavior of ascorbyl palmitate in water. *J. Spectrosc.* 33, 122 (**1988**).

22. H.Sapper, D.G.Cameron and H.H.C. Mantsch.The thermotropic behavior of ascorbyl palmitate: An infrared spectroscopy study. *J. Chem.* 59, 2543 (**1981**).

23. L. Benedini, E. P. Schulz, P. V. Messina, S. D. Palma, D. A. Allemandi, and P. C. Schulz, *Colloids and Surfaces A: Physicochemical and Engineering Aspects* 375, 178 (**2011**).

24. S. Palma, A. Jiménez-Kairuz, L. Fratoni, P. Lo Nostro, R. Manzo and D. Allemandi. 6-O-alkyl Ascorbic Acid Derivatives as drug carriers: Structure and rheology of coagels. *Il Farmaco.* 58, 1271 (**2003**).

25. A. Urtti, Challenges and obstacles of ocular pharmacokinetics and drug delivery. *Adv. Drug Deliv. Rev.* 58, 1131 (**2006**).

26. D. Shulin, *PSSP* 1, 328 (**1998**).

27. J. G. Flanagan, Glaucoma update: Epidemiology and new approaches to medical management. *Ophthal. Physiol. Opt.* 18, 126 (**1998**).

28. I. P. Kaur, R. Smith, D. Aggarwal, and M. Kapil, Acetazolamide: Future perspective in topical glaucoma therapeutics. *Int. J. Pharm.* 248, 1 (**2002**).

29. M. W. Duffel, Y. S. Segarra, T. M. Ing, J. A. Dixson, C. F. Barfknecht, and R. D. Schoenwald, The carbonic anhydrases—Page 179. *J. Med. Chem.* 29, 1488 (**1986**).

30. L. I. Tártara, D. A. Quinteros, V. Saino, D. A. Allemandi, and S. D. Palma, Improvement of acetazolamide ocular permeation using ascorbyl laurate nanostructures as drug delivery system. *Journal of Ocular Pharmacology and Therapeutics* 28, 102 (**2012**).

31. Y. Rojanasakul, L. Y. Wang, M. Bhat, D. D. Glover, C. J. Malanga, and J. K. H. Ma, The transport Barrier of Epithelia: A comparative study on membrane permeability and charge selectivity in the rabbit. *Pharm. Res.* 9, 1029 (**1992**).

32. R. Agarwal, O. Katare, and S. Vyas, Preparation and *in vitro* evaluation of liposomal/niosomal delivery systems for antipsoriatic drug dithranol. *Int. J. Pharm.* 228, 43 (**2001**).

33. V. Saino, S. Palma, P. Chetoni and D. Allemandi, Effect of different coagels of 6-O-Ascorbic Acid alkanoates on permeation of Ibuprofen through hairless mouse skin. *Lat. Am. J. Pharm.* 28, 3438 (**2009**).

34. V. Saino, D. Monti, S. Burgalassi, S. Tampucci, S. Palma, D. Allemandi, and P. Chetoni, Optimization of skin permeation and distribution of ibuprofen by using nanostructures (coagels) based on alkyl vitamin C derivatives. *European Journal of Pharmaceutics and Biopharmaceutics* 76, 443 (**2010**).

REVIEW

REVIEW

The Intervention of Nanotechnology Against Epithelial Fungal Diseases

Leticia H. Higa, Priscila Schilrreff, Ana Paula Perez,
Maria José Morilla, and Eder L. Romero*

*Programa de Nanomedicinas, Universidad Nacional de Quilmes, Roque Saenz Pena 352,
Bernal, B1876 BXD, Buenos Aires, Argentina*

Fungal infections can attack epithelial tissues and, according to the immunological state of the patient, some of them invade deeper organs, becoming seriously life compromising. Besides, bloodstream and local infections associated with intravascular devices constitute a significant problem associated with increased mortality. Topical therapy is desirable since, in addition to targeting the site of infection, it reduces the risk of systemic side effects and increases patient compliance. In this review we describe the pros and cons of using nano-objects that being toxic in nature could be used to cover surfaces of medical devices, or can act as carriers for targeted delivery of antifungals to skin. Non-toxic nano-objects were also included because they improve the ocular delivery of antifungals, classically suffering from ineffective topical administration, difficult access for systemic medication or local invasive administration. The new preclinical developments of nanoparticulate agents against cutaneous and ocular mycosis are grouped in three main sections: (1) *In vitro* antifungal activity of metallic nanoparticles, (2) *In vitro* and *in vivo* antifungal activity of non metallic nanoparticles (3) Ocular delivery of non metallic nanoparticles.

Keywords: Nano-Objects, Metallic Nanoparticles, Epithelia, Fungi.

CONTENTS

*Author to whom correspondence should be addressed.

1. INTRODUCTION

Fungal infections can attack epithelial tissues and, according to the immunological state of the patient, some of them invade deeper organs, becoming seriously life compromising. In particular, the invasive fungal infections (IFIs)[1] are difficult to diagnose, prevent and treat. During the last two decades their incidence, prevalence and mortality increased dramatically worldwide.[2, 3] IFI mainly affects patients from developed countries with large population of hospitalized patients suffering serious underlying diseases,[4, 5] inmunodepressed due to chemotherapy, bone marrow, stem cells or other organ transplantation,[6–9] or submitted to intensive treatment including broad-spectrum antibiotic therapy.[8, 10] Additionally, host immunity can be impaired during infancy, in old age, by pregnancy, by disease, e.g., diabetes mellitus, or through the administration of antibiotics and glucocorticoids.[11] The most common fungal pathogens causing IFI are the species of *Candida* and *Aspergillus.*[12, 13] *Candida spp.* represent one of the most common pathogens often causing hospital-acquired sepsis with an associated mortality rate of up to 40%.[14] Due in part to effective control of *C. albicans* with azole prophylaxis, particularly with fluconazole (FLZ), the

Leticia H. Higa was born in Buenos Aires, Argentina, in 1975. She graduated in Biotechnology at Universidad Nacional de Quilmes (2003) and is a Ph.D. student at the same institution in the field of nanomedicine. Her research interests are focused on nano-vaccines (ultradeformable archaeosomes) for topical administration and solid lipid nanoparticles for drug delivery.

Priscila Schilrreff was educated at Quilmes National University (UNQ), Argentina where she obtained her degree in Biotechnology (2007). She is currently developing her doctoral research in Basic and Applied Science, at the Nanomedicine Research Program (NRP) at UNQ, Buenos Aires, Argentina. Her research work is focused on the design of Core–shell tecto-dendrimers and their interaction on melanoma cells.

Ana Paula Perez was born in Buenos Aires, Argentina, in 1983. She graduated in Biotechnology at Universidad Nacional de Quilmes (2005) and received her Ph.D. degree from the same university (2011) on the field of nanomedicine. Currently she has postdoctoral position at the Programa de Nanomedicinas, Universidad Nacional de Quilmes. Her research interests are focused on non metallic or hybrid nanoparticles designed for topical administration for drug delivery.

Maria José Morilla is Adjunct Professor of chemistry at Universidad Nacional de Quilmes and Adjunct Researcher of the National Science Research Council (CONICET). She received a Biotechnology degree of the Universidad Nacional de Quilmes in 1999 and a Ph.D. in Natural and Exact Science in 2003. Her Ph.D. research focused on the design of anti-chagasic liposomes. She is member of the Nanomedicine Research Program where she supervises projects on development of dendrimers and megamers for oral and mucose nano-delivery systems.

Eder L. Romero is Biochemist from University of La Plata, Argentina and received a Ph.D. in Exact Sciences (1996). Following a post-doctoral research in Groningen University, The Netherlands (1997–1998), she returned to Argentina being currently an Independent Researcher at the National Council of Scientific and Technological Research (CONICET) (2010) and Associate Professor of Chemistry (tenure position 2008), at the Department of Science and Technology, National University of Quilmes, Buenos Aires, Argentina. From 2007 she is leading the Nanomedicine Research Program (NRP). The NRP is aimed to develop and follow the intracellular traffic of nanomedicines to be applied for topical/mucosal routes against infectious and inflammatory diseases and also in developing vaccination strategies employing biodegradable nano vesicles, to be applied by parenteral/topical/mucosal routes.

REVIEW

aetiology of IFI has shown a shift from *C. albicans* to *Aspergillus* and other moulds.[15, 16] Latin American countries suffer from a significant burden of IFI, which need to be addressed in terms of public health policies.[17]

Skin mycosis on the other hand, are divided according to the level of tissue involvement into: superficial (which include diseases that generally do not provoke a significant histopathological inflammatory response in the host); cutaneous (which induce pathological changes in the host, although the fungus is confined to the *stratum corneum*, include: dermatophytosis, candidiasis and other non-dermatophyte infections) and deep or subcutaneous, which involve the dermis and subcutaneous tissues e.g., *sporotrichosis, coccidoiodomycosis, actinomycosis.*

Superficial mycosis does not usually threaten life but can be disfiguring and their unsightly appearance cause social stigmatization. The incidence of superficial mycoses is increasing and according to a recent report more than 25% of the world's population is affected;[18, 19] disease progression is more rapid and its severity increased in patients with compromised immune function.[20] In low- and middle-income countries, skin diseases are dominated by bacterial and fungal infections that may be modified by HIV induced immunosuppression.[21, 22]

Cutaneous candidiasis most often reoccurs and is rarely cured; hence patients receive therapy over a long time. Cutaneous candidiasis is an opportunistic infection that arises, in most cases, from endogenous, saprophytic candidal blastospores that selectively colonize oral, gastrointestinal, vaginal, and cutaneous epithelium. Additionally, in people with weakened immune systems, *Candida spp.* invades deeper tissues as well as the blood, causing life-threatening systemic candidiasis. Topical therapy is desirable since, in addition to targeting the site of infection, it reduces the risk of systemic side effects.

Besides, bloodstream and local infections associated with intravascular devices are a significant problem associated with increased mortality, length of hospitalization and healthcare costs. *Candida spp.*, together with coagulase-negative staphylococci, *Staphylococcus aureus*, *Enterococcus spp.* and Gram-negative bacilli are the main pathogens associated with catheter-related infections. These organisms usually enter the bloodstream from the skin insertion site or the catheter hub, whereas haematogenous seeding and contamination of the infused fluid are rare. Accordingly, the primary strategies used to prevent catheter-related infections focus on reduction of colonization at the insertion site and hubs, thus preventing microbial spread to the catheter tip lying in the bloodstream. Given the importance of cutaneous microorganisms in the pathogenesis of intravascular device-related infections, measures to reduce colonization at the insertion site are of the highest priority. Reducing skin and catheter colonization has long been associated with a reduced incidence of local and systemic infections. However, currently used topical antiseptics suffer from a short duration of killing activity.

Topical antibiotics may offer a longer period of protection but they are associated with an increased frequency of fungal infections or the emergence of bacterial resistance.[23, 24]

The first line treatments against epithelial and subcutaneous fungal infections are the polyene amphotericin B (AmB) and azole antifungals such as clotrimazole (CLZ), econazole nitrate (ECZ) and FLZ.[25] However, AmB is water-insoluble macrolide, consisting of seven double bonds along the hydrophobic moieties of the ring, multiple hydroxyl groups along the hydrophilic moieties and a mycosamine residue. Azole antifungals on the other hand, are highly lipophilic (although there are exceptions (e.g., FLZ) and they can readily partition into the lipid-rich intracellular space in the stratum corneum. In these cases, the challenge is to develop a simple stable formulation that facilitates drug delivery to the epidermis and dermis.[26] Undesirable systemic absorption is reported for AmB and FLZ. The existent topical formulations (e.g., Fungizone cream, lotion, gels, ointments) generally produce local reactions (including irritation, burning sensation, erythema, stinging, pruritic rash, and tenderness) in patients treated topically and therefore failed to achieve mycological eradication.[27] Other problems associated with creams include failed stability test, either chemical instability or physical separation of emulsion caused by the salting out effect of the imidazole salt when used at a concentration of about 1% or more. The toxic effects of conventional medication combined with the growing yeast resistance to antifungal therapy[28, 29] generate a pressing need for the search of new antimicrobial agents from natural and inorganic sources.[30–34]

1.1. The Intervention of Nanotechnology Against Epithelial Fungal Diseases

Prophylaxis and antifungal therapy require of new strategies capable of eliminating extracellular eukaryotic microorganism, that both colonize living beings and inert surfaces as biofilms. From the point of view of the classical medicinal chemistry, the filogenetic similitude between fungi and host demands the careful search for leading compounds acting on selected therapeutic targets. Apart from this, the search for antifungals could be enriched by new alternative approaches. For instance, the growing resistance against conventional chemotherapy has led to the use of agents that because of their non specific damage make difficult the assembling of survival mechanisms. Another way of improving therapeutic strategies is to control the delivery of classical drugs to accurately selected tissues or places within these tissues. It is here where Nanotechnology, being a source of structures with new quantum, mechanical, thermal and superficial properties, alone or in combination with classical drugs, can offer new therapeutic/prophylactic options. Nanotechnology encompasses a broad conjunct of techniques aimed to engineer, characterize and make use of structures of 1 (nanoplates),

2 (nanotubes) or 3 dimensions (nanoparticles) in the nanoscale, known as nano-objects. The upper limit of the nanoscale was fixed at 100 nm,[35] but in the nanopharmaceutical field the nano-scale is accepted to rise up to 200–300 nm. Biosynthesized molecules (such as hormones, proteins, nucleic acids) and drugs, whose activity depends on a primary structure and not on new phenomena derived from its size in the nano-scale, do not fit into the definition of nano-object.[36] Also the lower limit of the nanoscale was fixed in 1 nm in order to exclude atoms.[36] Beyond these constraints, there is no restriction in the chemical nature of nano-objects.

In this review we have focused on describing the nature and action mode of nano-objects that can be toxic in nature or that act as carriers for targeted delivery of classical antifungals. The covered targets will be the skin and the ocular epithelia, a place of difficult access for systemic medication or that requires local invasive administration and in general is ineffective. In this context, developing new antifungal agents, especially against the opportunistic *Candida,* a cutaneous mycosis that can become invasive and that can both infect skin epithelium and eye tissue, is of particular interest. The new preclinical developments of nano-objects against cutaneous and ocular mycosis are grouped in three main sections:

(1) *In vitro* antifungal activity of metallic nanoparticles,
(2) *In vitro* and *in vivo* antifungal activity of non metallic nanoparticles
(3) Ocular delivery of non metallic nanoparticles.

2. *IN VITRO* ANTIFUNGAL ACTIVITY OF METALLIC NANOPARTICLES

2.1. Silver Nanoparticles

The use of silver compounds as antimicrobials is well known from ancient times. Currently, silver compounds are used against bacterial infections in wounds.[37, 38] and in preventing bacterial colonization of prostheses and catheters.[39, 40] In this context, developing and characterizing different types of silver nanoparticles has became a task of paramount importance because of the singular responses induced in prokaryote and eukaryote cells as compared to silver cations (Ag^+).

Silver nanoparticles (AgNp) has emerged as a promising new type of antimicrobial agent. The action mechanism of AgNp is non specific and presumably broadly similar to that of Ag^+.[41] The weak acid Ag^+ has a great tendency to react with sulfur- or phosphorus-containing weak bases, such as R-S-R, R-SH, RS- or PR3. AgNp in biological media may act as a constant source of Ag^+ on particles' slow oxidation. Ag^+ released from the AgNp even at very low concentrations can bind to and thereby damage cells at multiple sites (Fig. 1). It has been observed that 10–20 nm AgNp are taken up by living cells.[42, 43] Sulfur-containing proteins in the membrane or inside the cells
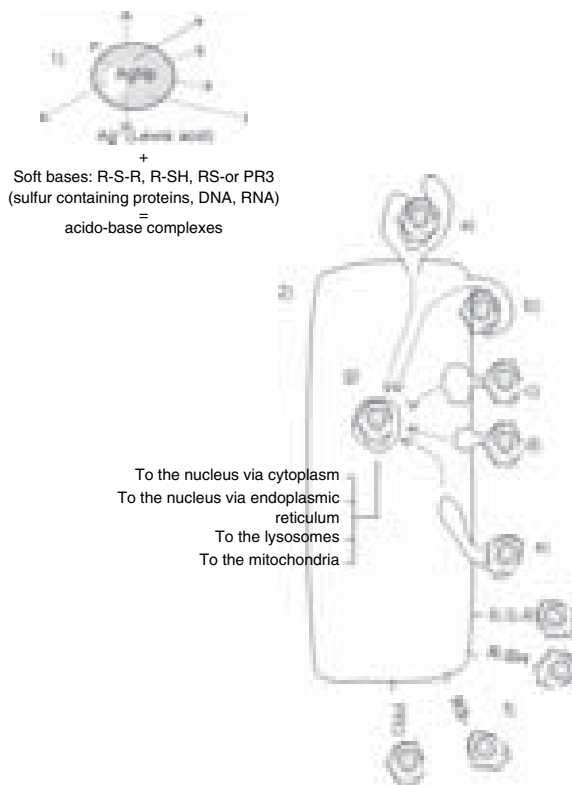
Fig. 1. (1) NpAg as a source of soluble Ag^+; (2) Interaction of AgNp with cells: (a)–(e): Internalization: according to the size, shape and surface characteristics of AgNp and on the cell type, different endocytic mechanisms will be involved in the uptake of AgNp: (a) phagocytosis, (b) macropynocytosis, (c) clathrin mediated endocytosis, (d) caveolin mediated endocytosis, (e) non clathrin, non caveolin mediated mechanisms; (g) endocytosed AgNp are not free but trapped within different types of cytoplasmic vesicles from where will be finally released to different targets; (f) in the absence of internalization AgNp can interact with weak basis at the cell surface.

and phosphorus—containing elements like DNA are likely to be the preferential sites for Ag^+ binding. The inhibition of respiratory enzyme(s), facilitate the generation of reactive oxygen species (ROS) and consequently damage the cell.

The bactericidal effect against both gram-positive and gram-negative bacteria including multiresistant strains of AgNp as well as silver nanocomposites or AgNp based materials has been intensively studied.[42, 44–48] Whereas most antibiotics only attack one specific structure of the microbial cell, Ag^+ interferes with the bacterial replication process and kills bacteria by binding to proteins of the cell wall, to thiol groups present in enzymes as well as to DNA and RNA.[49–52] AgNp were reported to kill bacteria at concentrations in the order of units of $\mu g/ml$.[45, 53] which do not produce acute toxic effects on human cells.[54, 55] In addition, AgNp have not been shown to cause bacterial resistance, currently complicating antibiotic therapy of bacterial infections.

The study of antifungal action of AgNp started by 2008, to find out that AgNp also affect yeast cells by attaching to the sulfur containing proteins of cell membranes, thus disrupting membrane potential. After exposure to AgNp, important changes in the membranes of *C. albicans* are observed, such as the formation of "pits" on the membrane surfaces that lead to pores and subsequent cell death.[56] Recently it was found that AgNp induce increased ROS and hydroxyl radical production in *C. albicans*, together with mitochondrial dysfunction and apoptotic features.[57] The activity of 3 nm diameter AgNp was comparable to that of AmB (IC80 1–5 μg/ml) and superior to that of FLZ (IC80 10–30 μg/ml) on ATCC strains of *Trichophyton mentagrophytes* and *Candida spp.* (Table I).[56, 58] AgNp was also found to exert activity on the mycelia. The antifungal activity of AgNp was also proved in biostabilization of footwear materials.[59] In this application, AgNp at 1% solution inhibited the growth of the majority of yeast-like fungal and mold strains. AgNp at 100 ppm totally inhibited bacterial growth, but its activity against molds and dermatophytes was observed to be lower, being reported that molds and bacteria were resistant to 50 ppm of AgNp.

Considering spherical particles of uniform size, a reduction in size from ~ 10 μm to 10 nm will increase the contact surface area by 10^9. This explains why the activity of AgNp is inversely related to its size: a large contact surface is expected to enhance the extent of microbicidal activity. On the other hand, recent reports emphasized that shape dependent interactions of AgNp played a crucial role in their microbicidal properties.[47] Spherical AgNp (generally with a cubo-octahedral or multiple-twinned decahedral or quasi-spherical morphology) predominantly have (100) facets along with small percentage of (111) facets, while in case of the rod-like AgNp (e.g., pentagonal rods), side surfaces are bound by (100) and the ends by (111) facets. It has been demonstrated that the reactivity of silver is favored by high-atom-density facets such as truncated triangular nanoplate in comparison to other particles that contain fewer than (111) facets, like spherical or rod-shaped particles.[42]

Interestingly, the bactericidal activity of AgNp is higher than its fungistatic (minimum inhibitory concentrations, MIC) and fungicidal (minimum fungicidal concentration, MFC) activities. The MIC and MFC of 25 nm mean size AgNp either plain or stabilized by sodium dodecyl sulfate (SDS), sodium polyoxyethylene sorbitan monooleate (Tween 80), Brij (35; 58, 97 and 98) surfactants, or the polymers polyvinylpyrrolidone (PVP; average molecular weights (MW) of 10,000; 40,000 and 360,000) and polyethylene glycol (PEG; MW of 1500; 4,000; 10,000 and 35,000) against *C. albicans* was recently determined.[60] At first sight the results were far from being promising. The MIC of plain AgNp against *C albicans II* showed no significant differences with the MIC of Ag^+ (Table I). It was observed that surfactant and polymer stabilization of AgNp (used at concentrations between 0.5

and 5×10^4% w/w) decreased the MIC. And even though the fungicidal activity (measured by development of MIC in time as well as by MFC) of Ag^+ against *C albicans* was higher (MFC of 135 μg/ml) than that of plain AgNp (MFC of 27 μg/ml), the MFC of SDS stabilized AgNp was 338 μg/ml. Remarkably, the main differences between Ag^+ and AgNp were found in their cytotoxicity against fibroblast BJ cells, that resulted in an absolute lethal concentration (LC100) value of 1 μg/ml for Ag^+ but ascended to 30 μg/ml for plain or PEG/PVP stabilized AgNp. The high cytotoxicity of surfactants solutions alone impaired further cytotoxicity test of surfactant stabilized AgNp. Both fungi and host cells are eukaryotes and this would explain the close values of MFC and LC100 of AgNp. The low concentrations of AgNp (below than 10 μg/ml) needed to exert bactericidal activity on the other hand, would obey to the fact that yeast cell type can resist higher concentrations of silver thanks to their improved cell organization and structure, and more efficient detoxification system than evolutionarily older prokaryotic types of bacteria. Overall, these studies showed that AgNp, in spite of their close MFC and LC100 values (27 vs. 30 μg/ml), are still safer antifungal than Ag^+. This is underscored by the far higher MFC than LC100 value (13.5 vs. 1 μg/ml) of Ag^+

Recently, 32.5 nm average size spherical AgNp obtained by extracellular biosynthesis by the fungus *Alternaria alternate,* were tested in combination with FLZ against *C. albicans,* among other skin fungi (Table I).[61] Topical treatment of severe life threatening skin fungal infections with FLZ is an efficient therapy and occupies a prominent position among the alternatives of treatment.[62] However, topical delivery of FLZ results in systemic absorption, skin irritation and therefore failing to achieve mycological eradication.[63] These problems affect patient compliance and compromise the efficacy of the therapy. Nonetheless AgNp significantly increases the antifungal activity of FLZ (measured as diameter of inhibition zone and increased fold area). The combination between FLZ and AgNp showed the maximum inhibition against *C. albicans*, followed by *Phoma glomerata* and *Trichoderma spp.,* whereas no significant enhancement of activity was found against *Pleospora herbarum* and *F. semitectum*.

In another approach, 7–20 nm AgNp synthesized by a proprietary biostabilization process, were found to exhibit good antifungal activity (Table I).[64] Interestingly, AgNp exhibited good anti-inflammatory properties as indicated by concentration-dependent inhibition of marker enzymes (matrix metalloproteinase 2 and 9). The post agent effect (a parameter measuring the length of time for which bacterial growth remains suppressed following brief exposure to the antimicrobial agent) varied with the type of organism (e.g., 10.5 h for *P. aeruginosa*, 1.3 h for *Staphylococcus spp*. and 1.6 h for *C. albicans*) indicating that dose regimen of the AgNp formulation should ensure sustained release of the antifungal. To meet this requirement, a gel formulation containing AgNp was prepared. As part of toxicity

74

J. Biomater. Tissue Eng. 3, 70–88, **2013**

Table I. Metallic nanoparticles used as *in vitro* antifungal agents.

Nanoparticle type	Fungus	Nanoparticles features and antifungal activity	Reference
AgNp	*C. albicans*	Formation of "pits" on the membrane surfaces	[56]
	C. albicans	Increased ROS and hydroxyl radical production	[57]
	Clinical isolates and ATCC strains of *Trichophyton mentagrophytes* and *Candida spp.*	3 nm AgNp; IC80 1–4 μg/ml	[56, 58]
	C. albicans II	Ag^+; MIC 0.21–1.69 μg/ml; MFC 13.5 μg/ml; LD 100 on fibroblast BJ cells 1 μg/ml	[60]
		Plain 25 nm AgNp; MIC 0.21–1.69 μg/ml; MFC 27 μg/ml; LD 100 30 μg/ml	
		25 nm SDS-AgNp; MIC 0.052 μg/ml; MFC 3.38 μg/ml	
	C. albicans	20–60 nm AgNp significantly increases the antifungal activity of FLZ	[61]
	C. albicans	7–20 nm AgNp MIC 25 μg/ml	[64]
		50% inhibition at 75 μg/ml with antifungal index 55.5% against *A. niger*	
		IC50 on Hep G2 cell line 251 μg/ml	
	C. albicans	500 nm × 50 × 50 nm square bases *salep* capped Ag nano-wedges MIC 5 μg/ml, MFC300 μg/ml	[65]
	C. albicans and C. glabrata adhered cells and biofilms	5 nm AgNp stabilized with ammonia MIC 0.4 and 3.3 μg/ml	[66]
	C. albicans, C. glabrata and *M. sympodialis*	1560 nm AgNp loaded within an inorganic matrix showed complete or nearly complete growth inhibition	[74]
	Aspergillus glaucus	14 nm $Ag@Fe_3O_4$; MIC 2 mg/ml	[76]
	Candida spp.	$Ag@Fe_3O_4$ with $\sim$70 nm Fe_3O_4 magnetic cores covered by a shell of $\sim$5 nm AgNp	[77]
		γ-Fe_2O_3@Ag with 20–40 nm AgNp cores covered by a shell of $\sim$5 nm γ-Fe_2O_3	
		Both nanocomposites MIC 1.9–31.3 μg/ml	
		26 nm AgNp; MIC 0.2 μg/ml	
ZnONp	*Fusarium spp.*	2–28 nm ZnONp less active than $CuSO_4 \cdot 5H_2O$	[98]
TiO_2Np	*C. albicans* biofilms	TiO_2Np were deposited on 50–100 nm diameter ZnO nanowires.	[101]
		Viability of cells significantly decreased nearly 4.3 times after 5 h exposure visible light	
	C. albicans biofilms	Branched carbon nanotube arrays covered with TiO_2Np	[102]
		Highly photocatalytic antifungal activity	
	Aspergillus niger, C. albicans, C. neoformans	250–300 nm TiO_2AgNp combined nanoparticles; MIC 3–25 μg/ml; LD50 on THP-1 monocytes 55.9 μg/ml	
		AgNp; MIC 20–25 nm; LD50 10 μg/ml	

studies, localization of AgNp in Hep G2 cell line, cell viability, biochemical effects and apoptotic/necrotic potential were assessed. It was found that AgNp localized in the mitochondria and had an IC50 value of 250 μg/ml. Even though they elicit an oxidative stress, cellular antioxidant systems (reduced glutathione content, superoxide dismutase, catalase) get triggered and prevent oxidative damage. Further, AgNp induce apoptosis at concentrations up to 250 μg/ml, which could favor scarless wound healing. Acute dermal toxicity studies on gel containing AgNp in Sprague-Dawley rats, showed complete safety for topical application. These results suggest that AgNp could provide a safer alternative to conventional antimicrobial agents in the form of a topical antimicrobial formulation.

On the other hand, highly sized *salep* capped Ag nano-wedges, were prepared by photochemical facile green synthesis. *Salep* (a palmate-tuber, multi-component polysaccharide with a high content in glucomannan possessing natural, neutral and watersoluble fibers) caused creation of flower-like self-assembled structures of the Ag nano-wedges. The MIC value of *salep*-Ag nano-wedges against *C. albicans* was similar to that of AmB (2.5–5 μg/ml). The MFC however, resulted to be excessively high (Table I).[65] These results, indicating poor fungicidal efficiency, could be owed to the large size of the poniards. Nonetheless, in order to assess the poniards safety, their cytotoxicity against host cells remains to be tested.

Recently the effect of 5 nm diameter AgNp stabilized with ammonia against *C. albicans* and *C. glabrata* adhered cells and biofilms, was tested. AgNp were applied to adhered cells (2 h) or biofilms (48 h) (Table I). It was

also determined that AgNp were more effective in reducing biofilm biomass when applied to adhered cells (2 h) than to pre-formed biofilms (48 h), with the exception of *C. glabrata* ATCC, which in both cases showed a reduction of ∼90%. AgNp were highly effective on adhered *C. glabrata* and respective biofilms. On *C. albicans* the effect was not so evident but there was also a reduction in the number of viable biofilm cells. These results suggest that AgNp could be an effective alternative to conventional antifungal agents for future therapies in Candida-associated denture stomatitis.[66]

A well known problem of silver is that it is toxic to human at high concentration.[47] The topical application of Ag compounds that can be significantly percutaneously absorbed can cause argyrosis and argyria, leading to a local or systemic tissue deposition of Ag in skin, nerve tissues and inner organs—particularly liver, spleen and kidney—with the attendant risk of organ dysfunction.[67–71] Therefore, maximum contamination levels for silver in drinking water (100 ppb).[72] and the occupational exposure limit to the various forms of silver (0.01 mg/m^3)[73] have been established in order to avoid the accumulation of silver in the human body. In this context, recently highly sized (1560 nm mean diameter) AgNp were loaded within an inorganic matrix, to impair its systemic absorption after topical application in mice. The silver contents of AgNp and silver sulphadiazine used as control at concentrations of 1% were calculated to be 880 ppm (880 μg/g) and 3020 ppm (3020 μg/g), respectively. Strikingly, AgNp at a 0.1% concentration exhibited comparable antibacterial and antifungal potencies as silver sulphadiazine at 0.1%, although its absorption was considerable lower. AgNp at 0.1% proved to be a potent antifungal agent, exhibiting complete or nearly complete growth inhibition of the dermatophytes *M. canis* and *T. rubrum*. Moreover, AgNp at ultra low doses of 0.001% was effective against *C. albicans C. glabrata* and *M. sympodialis*, yeast species often found in atopic dermatitis patients. Despite its 3.4-times lower silver content, the AgNp preparation exhibits an antimicrobial activity against the bacteria yeasts and dermatophytes tested, comparable to that of silver sulfadiazine at concentrations of 0.1%.[74]

2.2. Strategies Used to Impair Uncontrolled Dispersion of AgNp in the Environment: Magnetic AgNp

Extensive use and increasing demand for AgNp will lead to their accumulation in the environment, especially in landfills and water effluents. Non-targeted effects of AgNp on the population of microbes that play beneficial roles in the environment could have negative consequences.[75] Magnetic nanoparticles of iron oxides (Fe_3O_4 and/or γ-Fe_2O_3-maghemite-) represent one family of the most suitable candidates for the preparation of magnetic nanocomposites owing to their convenient magnetic application (e.g., superparamagnetism), biochemical properties (e.g., non-toxicity, biocompatibility, biodegradability) and low price.

An example of nanoparticles designed to prevent their uncontrolled release into the environment are the spherical 14 nm average size core–shell nanoparticles made of Fe_3O_4 (magnetite) core coated with AgNp (Ag@Fe_3O_4) at Ag and Fe concentration of 702 and 215.6 mg/l, respectively. The diamagnetic Ag shell prevents the agglomeration of the Fe_3O_4 during the formation of core–shell nanoparticles. The resulting core–shell nanoparticles were superparamagnetic in nature, although a 71% decrease in the magnetization of Ag@Fe_3O_4 with respect to Fe_3O_4 was observed. The Ag@ Fe_3O_4 can be recovered using a steel wool filter and recycled from the site of action by means of an external magnetic field, being detected by their absorption at 399 nm (the Surface Plasmon Resonance band of Ag@Fe_3O_4). However, although the recycling efficiency is > 80% over four cycles, the MIC values of Ag@Fe_3O_4 and AgNp against *Aspergillus glaucus* isolates were high (Table I). *A. glaucus* is the potential cause of fatal brain infections and hypersensitivity pneumonitis in immunocompromised patients and leads to death despite aggressive multidrug antifungal therapy. The elevated MIC values of this approach make mandatory the further investigation of the biocompatibility for the host, once the route of administration is decided.[76]

In a similar fashion, the antifungal activity of two types of nanocomposites including molecules of polyacrylate serving as a spacer among iron oxide and AgNp was recently tested.[77] In one hand, Ag@Fe_3O_4 nanoparticles made of Fe_3O_4 magnetic cores (∼70 nm) covered by a shell of AgNp (∼5 nm, 5.8% weight content) were prepared. On the other hand, γ-Fe_2O_3@Ag nanoparticles with a higher content (10.5%) of larger (20–40 nm) AgNp cores, covered by a shell of (∼5 nm) γ-Fe_2O_3 were also prepared. Both nanocomposites possess eminent magnetic properties (e.g., high value of magnetization achievable at relatively low applied fields, superparamagnetic and soft magnetic behavior at room temperature from the viewpoint of superconducting quantum interference device measurements, suppression of inter-particle magnetic interactions due to the molecules of polyacrylate) since they were very easily controlled by a low external magnetic field in the order of 1 Tesla. Both nanocomposites exhibited very significant antifungal activities against four *Candida* species (Table I) although these values were higher than the corresponding to 26 nm AgNp. Moreover, acute nanocomposite cytotoxicity against mice embryonal fibroblasts was observed at concentrations higher than 430 μg/ml (Ag@Fe_3O_4) and 292 μg/ml (γ-Fe_2O_3@Ag). Considering the non-cytotoxic nature of the polyacrylate linker, both kinds of Ag nanocomposites are well applicable for a targeted magnetic delivery of AgNp in medicinal and disinfection applications.

2.3. Nanoparticles of Semi-Conducting Oxides

Currently inorganic metal oxides (TiO_2, MgO, CaO and ZnO) have attracted interest as antimicrobial agents because of their safety and stability. Compared to organic materials, inorganic materials such as ZnO possess superior durability, greater selectivity and heat resistance.[78, 79]

In particular TiO_2 and ZnO semiconductors have been extensively studied as antimicrobial agents due to their photocatalytic activity under UV light.[80, 81] Photocatalysis is a light induced catalytic process whereby photogenerated electron–hole pairs ($e^- h^+$) in a semiconductor undergo redox reactions with molecules adsorbed onto the surface, thereby breaking them into smaller fragments. The electronic structure of semiconductors such as TiO_2, ZnO, Fe_2O_3, CdS and ZnS is characterized by a filled valence band and an empty conduction band and can act as sensitizers for light-induced redox processes. When a photon with energy of $h\nu$ matches or exceeds the bandgap energy of the semiconductor, an electron (e_{cb-}) is promoted from the valence band into the conduction band, leaving a hole (h_{vb+}) behind. The ($e^- h^+$) migrate to the nanoparticle surface and can recombine and dissipate the input energy as heat, get trapped in metastable surface states or react with electron donors and electron acceptors adsorbed on the semiconductor surface. In the absence of suitable ($e^- h^+$) scavengers, the stored energy is dissipated within a few nanoseconds by recombination. If a suitable scavenger or surface defect state is available to trap the electron or hole, recombination is prevented and subsequent redox reactions may occur. The h_{vb+} are powerful oxidants while the e_{cb-} are good reductants.[82] In general terms, the photocatalytic activity in aqueous oxygenated media produces ROS such as radical hydroxyle ($OH^•$) and H_2O_2 (Fig. 2). Surface area and surface defects play an important role in the photocatalytic activity of metal oxide nanostructures, as the molecules need to be adsorbed on to the photocatalytic surface for the redox reactions to occur. The higher the effective surface area, the higher will be the adsorption of molecules leading to better photocatalytic activity. One dimensional nanostructures, such as nanowires and nanorods, offer higher surface to volume ratio compared to nanoparticulate coatings on a flat plate.[83]

2.3.1. Zinc Oxide Nanoparticles

Zinc is a mineral element essential to human health and ZnO is a form in the daily supplement for zinc. The antibacterial and antifungal activity of bulk ZnO powders has been demonstrated already.[84, 85] ZnO is an *n*-type semiconductor with wide direct band gap (3.37 eV) and high exciton energy (60 meV) at room temperature which allows it to act as an efficient semiconducting and piezoelectric material. As its size is decreased, the band gap of ZnO (ZnONp) increases, as well as its surface area. ZnO is a polar crystal of positive zeta potential at the surface, Zn^{2+} lies within
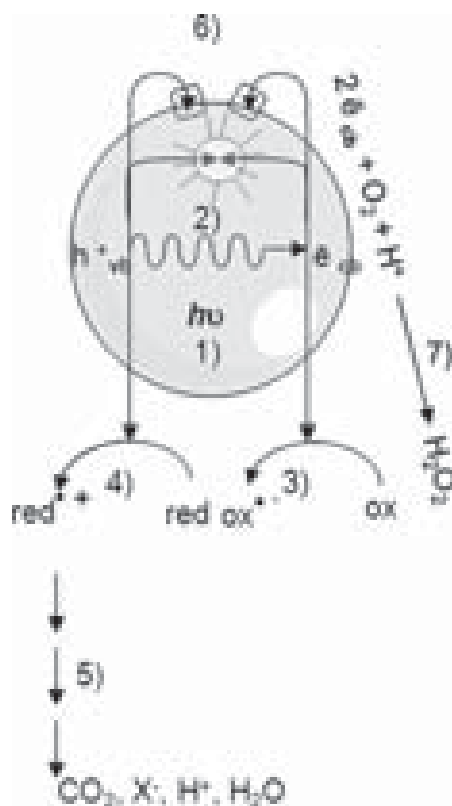
Fig. 2. Primary steps in the photoelectrochemical mechanism of photoactivated semiconductors (ZnO, TiO_2): (1) formation of charge carriers: conduction band electron (e_{cb}^-) and valence-band hole (h_{vb}^+) by a photon $h\nu$; (2) charge carrier recombination to liberate heat; (3) initiation of an oxidative pathway by a h_{vb}^+; (4) initiation of a reductive pathway by a e_{cb}^-; (5) further thermal (e.g., hydrolysis or reaction with active oxygen species) and photocatalytic reactions to yield mineralization products; (6) trapping of a e_{cb}^- in a dangling surficial bond to yield a trapped conduction-band electron e_{tr}^- or trapping of a h_{vb}^+ at a surficial group. Red is an electron donor (reductant) and Ox is an electron acceptor (oxidant). Dangling bond is a chemical bond associated with an atom in the surface layer of a solid that does not join the atom with a second atom but extends in the direction of the solid's exterior; (7) an example of oxigen reactive species generation (H_2O_2) in aerated solutions occurring via the reduction of adsorbed oxygen by e_{cb}^-.

a tetrahedral group of four oxygen ions. Zinc and oxygen atoms are arranged alternatively along the *c*-axis and the top surfaces are Zn terminated while the bottom surfaces are oxygen terminated. The high surface reactivity of ZnONp owes to a large number of native defect sites arising from oxygen nonstoichiometry. Because of this ZnONp exhibits comparatively higher reaction and mineralization rates and can generate hydroxyl ions more efficiently than TiO_2.[86]

After contact with ZnONp disruption of cell membrane activity has been observed and disorganization of the triple membrane was formerly reported in the Gram-negative *E. coli*.[87] The resulting increase of membrane permeability leads to accumulation of ZnONp in the bacterial membrane

followed by their cellular internalization, as also reported against *Pseudomona aeruginosa*.[88] The microbicidal activity of ZnONp is owed to the generation of ROS such as OH[•], H_2O_2, and O_2^{2-}, which is directly proportional to the exposed surface area.[89] ZnONp with defects can be activated by both UV and visible light. In the ZnONp surface the holes split H_2O molecules into OH and H^+. Dissolved oxygen molecules are transformed to superoxide radical anions ($^•O_2^-$), which in turn react with H^+ to generate ($HO_2^•$) radicals, which upon subsequent collision with electrons produce hydrogen peroxide anions (HO_2^-). They then react with hydrogen ions to produce molecules of H_2O_2. Since, the hydroxyl radicals and superoxides are negatively charged particles, they cannot penetrate into the cell membrane and remain in direct contact with the outer surface of the bacteria; however, H_2O_2 can penetrate into the cell and kill bacteria.

Similar to AgNp, an inverse relationship between bactericidal activity and size of ZnONp was shown. At a fixed concentration (1 mM), the bactericidal activity of 12 nm ZnONp is higher than that of 45 nm and 2 μm ZnONp. These differences are explained from the fact that a single isolated colony of 2 μm diameter bacteria can accommodate larger number of 12 nm than 45 nm and 2 μm ZnONp. ZnONp presumably remain tightly adsorbed on the surface of the leftover/dead bacteria, but continue to release peroxides into the medium. Besides, since size and specific surface area are inversely related: bulk ZnO exposes 5.11 m^2/g, but 47 nm ZnONp ascends to 68 m^2/g and 12 nm ZnONp to 115 m^2/g. Therefore, the smaller is the nanoparticle, the higher its production of ROS on the surface and its antibacterial activity. The abrasive surface texture of ZnONp is another possible explanation of its antibacterial effect. ZnONp have been found to be abrasive due to surface defects, revealed by a broad visible emission band in the region of 450–550 nm in a photoluminescence spectrum of ZnONp. The abrasiveness of ZnONp compared with bulk ZnO is caused by the uneven surface texture due to rough edges and corners. Opposite to the deleterious action of ZnONp, trace concentrations of Zn^{+2} ions are a supplement promoting the metabolic action of bacteria.[90] On the other hand, the release of soluble Zn^{+2} from the ZnONp are responsible for toxicity in lung cell lines,[91] while under realistic environmental conditions, similar results on algae have been reported.[92] Overall, ZnONp proved to be toxic against prokaryotic organisms at the concentrations of units of mM Zn. Nonetheless, ZnONp had minimal effects on eukaryote human T-lymphocytes cell viability at concentrations toxic to bacteria.[93]

The advantages of using ZnONp as antifungal agent have recently started to raise attention. For instance in agriculture the use of ZnONp does not affect the soil fertility in comparison to traditional antifungals.[94] Similar to what occurs with bacteria, the cytotoxic effect of ZnONp against fungi is mediated by bilayer rupture

resulting in the drainage of the cytoplasmic contents.[95–97] Recently antifungal activity of 2–28 nm ZnONp (hexagonal wurtzite) stabilized with surfactants isolated from *Acacia concinna* seeds, was determined.[98] It was observed that the size of the ZnONp drastically decreases from 28 nm to 2.5–5 nm with the surfactant stabilization. Surprisingly, this reduction in size is accompanied by a reduced activity of ZnONp against *Fusarium spp.*, when compared to that of standard antifungal 0.1 M $CuSO_4 \cdot 5H_2O$. Recently, anti *Candida* activity of glass supported ZnO nanrods were shown.[99]

2.3.2. Titanium Oxide Nanoparticles

The optical absorption in the ultraviolet region (peaking around 220 nm and covering only $\sim 5\%$ of the solar spectrum) and low photoefficiency of TiO_2Np are factors that deter its wide scale use for photocatalytic activities under sunlight. In spite of sharing similar band gap with ZnONp (3.2 eV), TiO_2Np can only be exited under UV light irradiation and its photocatalytic activity under solar and visible light is not efficient. TiO_2 exists in three main crystallographic structures e.g., anatase, rutile and brookite. It is also well-known that it is more difficult to obtain TiO_2Np with good crystallinity and high surface area from rutile than anatase. The photoexcited TiO_2 catalyst produces ($e^- h^+$) that migrate to the TiO_2 surface; ($\mathbf{h}_{vb}^+$) can react with adsorbed H_2O or OH^- at the catalyst/water interface to produce the highly reactive OH[•] and the ($\mathbf{e}_{cb}^-$) can react with oxygen vacancies to form radical superoxide (O_2^{-1}); finally, the various generated ROS can oxidize organic compounds or cells adsorbed on the TiO_2 surface, resulting in the death of the microorganisms.[100] In an approach aimed to enhance the visible light photocatalytic activity of TiO_2Np and improve its antifungal activity, anatase and rutile crystal TiO_2Np were deposited on 50–100 nm diameter ZnO nanowires. The resulting TiO_2Np/ZnO nanocomposite exhibited a low band gap and high visible light activity against *C. albicans* biofilms. The antifungal activity of the ZnO nanowires was higher than the TiO_2Np in dark. Also, the antifungal activity of the ZnO nanowires in dark was decreased by the TiO_2Np coating. But, viability of cells significantly decreased nearly 4.3 times due to photocatalytic activity of TiO_2Np/ZnO nanocomposite under after 5 h exposure visible light. The alloy structure at the interface of the TiO_2Np/ZnO is said to decrease the band gap that can be exited under visible light. Again, the excitation of the nanocomposite using the light exposure leads to generate ($e^- h^+$) and the ($\mathbf{h}_{vb+}$) lead to generate OH on the surface of the microorganism.[101]

Similarly, branched carbon nanotube (CNT) arrays covered with TiO_2Np presented antifungal effect on *C. albicans* biofilms under visible light. The $TiO_2Np/$ branched CNTs showed a highly improved photocatalytic antifungal activity in comparison with the $TiO_2Np/$non branched CNTs and TiO_2Np film. The excellent visible

78

J. Biomater. Tissue Eng. 3, 70–88, **2013**

light-induced photocatalytic antifungal activity of the TiO$_2$Np/branched CNTs was attributed to the generation of $(e^- h^+)$ by visible light excitation with a low recombination rate, in addition to the high surface area provided for the interaction between cells and nanostructures.[102]

As an example of an non photocatalytic use of TiO$_2$, recently 250–300 nm TiO$_2$AgNp combined nanoparticles (prepared by reaction between anatase TiO$_2$Np with Ag at 50:1 molar ratio) showed significant antifungal activity (Table I), although the activity resulted comparable to that of 20–25 nm AgNp used as control. The LD50 on THP-1 monocytes of the TiO$_2$AgNp was higher than that of AgNp. In spite of their higher size, TiO$_2$AgNp increased by nearly tenfolds the therapeutic index when used as antifungal agents as compared to AgNp.[103]

3. *IN VITRO* AND *IN VIVO* ANTIFUNGAL ACTIVITY OF NON METALLIC NANOPARTICLES

The following is a survey on preliminary improvements in delivery of conventional antifungals loaded in different types of nanovesicles (liposomes, niosomes, ethosomes and ultradeformable liposomes), solid lipid nanoparticles (SLN), nanostructured lipid carriers (NLC), polymeric micelles and microemulsions. The modified delivery after topical application led to better antifungal properties.

3.1. Nanovesicles

The skin delivery of AmB loaded in liposomes, ethosomes and ultradeformable liposomes was tested in a recent comparative assay (Table II).[104] The vesicles were further incorporated into Carbopol 934 hydrogel (1% w/w). Overall, 50–75% of AmB was released from gels after 24 h. *In vitro* assay on the AmB permeation across hairless rat skin showed that transdermal flux was maximal for ultradeformable liposomes and minimal for conventional liposomes. There were no differences between the transdermal flux of AmB in the dispersion of vesicles or within the gel. Skin retention of AmB was maximal for ultradeformable liposomes (81 μg) as compared to ethosomes (64 μg) and liposomes (45 μg). Confocal laser scanning microscopy study using rhodamine 123-loaded vesicles confirmed the penetration profile of the vesicles *in vivo*. Skin irritation test revealed negligible irritation scores for all the vesicular formulations. *In vitro* antifungal activity against fungal strain *Trychophytone rubrum* showed that AmB loaded in ultradeformable liposomes induced the largest zone of inhibition area.

The skin delivery of FLZ loaded in liposomes and niosomes incorporated into Carbopol gel (1% w/w) was tested for sustained release after localized application (Table II).[62] *In vitro* and *in vivo* skin penetration experiments showed a higher accumulation of FLZ when FLZ was loaded in liposomes. The *in vivo* localization studies in viable skin showed that liposomal gel produce 14.2- and 3.3-fold higher drug accumulation compared with plain gel and niosomal gel, respectively. Antifungal activity carried out on experimentally induced cutaneous candidiasis in immunosuppressed albino rats showed maximum therapeutic efficacy of liposomal gel, as the lowest number of colony forming units/ml was recorded following liposomal FLZ application.

The skin delivery of ECZ loaded in ethosomes incorporated into carbopol gel (1% w/w) with 2% w/w propylene glycol and 2% w/w *N*-methyl-2-pyrolidone as permeation enhancers was recently tested for therapeutic efficacy and storage stability (Table II).[105] Drug flux and permeation through albino rats skin were significantly higher in ethosomal formulation (0.46 μg/cm^2/hr and 91%, respectively) than for liposomes (soy lecithin), hydroethanolic gel and liposomal gel; this could indicate that ethanol enhances drug permeation across rat skin. The stability measurements of ethosomes revealed very low aggregation and insignificant growth in vesicular size for 180 days. The antifungal activity evaluated by cup plate method with strains of *C. albicans* showed that ethosomal formulation induced the largest zone of inhibition.

3.2. Polymeric Micelles

The skin delivery of azoles (CLZ, logP o/w 5.9, aqueous solubility 0.03 g/l; ECZ logP o/w 5.2, aqueous solubility 0.8 g/l; and FLZ logP o/w 0.4, aqueous solubility 0.001 g/l) loaded in polymeric micelles was recently determined (Table II).[106] Micelles differed in core hydrofobicity, from the more hydrofobic core mono-hexyl-substituted, followed by di-hexyl-substituted to the less hydrofobic core-polylactide. In spite of the expected ability of micelles to incorporate significant amounts of hydrophobic drugs in their core, CLZ showed poor incorporation efficiency (11–36%) in all the micellar systems. FLZ and ECZ on the other hand, were successfully encapsulated at 250 and 268 mg/g of drug contents and 83 to 98% incorporation efficiencies. Further assays were carried out with ECZ loaded in MPEG-dihexlPLA micelles. *In vitro* skin retention studies in porcine and human skin showed that ECZ deposition following 6 h application was ∼13-fold and 7.5-fold higher respectively, than that from ECZ commercial cream (Pevaryl® cream, 1% w/w ECZ). The amounts of ECZ deposited were 11 and 1.5 μg/cm^2, for porcine and human skin respectively. Confocal laser scanning microscopy studies using similarly-sized fluorescein loaded micelles showed that micells penetrate the skin mainly thought the follicular pathway.

3.3. Dendrimers

The effects of generation number and surface groups of poly(amidoamine) (PAMAM) dendrimers on aqueous

Table II. Non-metallic nanoparticles as antifungal agents.

Nanoparticle type	Fungus	Drug	Nanoparticles features	Reference
Nanovesicles	*Trychophytone rubrum*	AmB	1. Conventional liposomes:soybean phosphatidylcholine (soyPC)/cholesterol 7:3 molar ratio; 580 nm; 63% entrapment efficiency 2. Ethosomes:soyPC/ethanol 300:2 w/w; 220 nm; 84 entrapment efficiency 3. Ultradeformable liposomes:soyPC/sodium deoxycholate 85:15 w/w; 420 nm; 71% entrapment efficiency	[104]
	Experimentally induced cutaneous candidiasis	FLZ	350 nm liposomes and niosomes	[62]
	C. albicans	ECZ	Ethosomes:soy lecithin 3% w/w, ethanol 30% v/v; 200 nm; -75 mV Z potential; 80% entrapment efficiency	[105]
Polymeric micelles	Not tested	CLZ, FLZ and ECZ	30 to 40 nm micelles of amphiphilic methoxy-poly(ethylene glycol)-hexyl substituted polylactide (MPEG-hexPLA) block copolymers	[106]
Dendrimers	*C. parapsilosis* ATCC 22019 and susceptible and drug resistant clinical strains of *C. albicans*, *C. glabrata*, *C. krusei*, *C. dubliniensis* and *C. tropicalis*	CLZ	Poly(amidoamine) (PAMAM) dendrimers generation 2 (G2) and generation 3 (G3) with amine (PAMAM-NH$_2$) or hydroxyl surface groups (PAMAM-OH)	[107]
Lipid nanoparticles	Experimentally induced cutaneous candidiasis	FLZ	1. SLN:glyceryl behenate as core and 2:1 ratio of egg PC and pluronic F-68 as emulsifiers; 180 nm; 25 mV Z potential; 75% entrapment efficiency 2. NLC:glyceryl behenate and oleic acid as core and egg PC and pluronic F-68 as emulsifiers; 130 nm; -29 mV Z potential; 81% entrapment efficiency	[108]
Microemulsions	*C. albicans and* skin fungal infections (tinea corporis, tinea circinata and tinea pedis).	CLZ	1. Lemon oil/Tween 80/*n*-butanol/water 2. Isopropyl myristate/Tween 80/*n*-butanol/water	[109]

solubility and antifungal activity of CLZ was determined in 2009 (Table II).[107] It was found that PAMAM-NH$_2$ dendrimers improved CLZ solubility in a higher extent than the other polymers. PAMAM-NH$_2$ G3 and G2 exhibited the highest solubilising potential for CLZ (around 6.7-fold, from 0.38 to 2.55 μg/ml). Antifungal activity was evaluated using broth microdilution method. MIC and MFC values significantly indicate that PAMAM-NH$_2$ dendrimers increased the antifungal activity of CLZ against all the *Candida* cultures. CLZ in solution of PAMAM-NH$_2$ G2 was 4-32-fold more potent than pure CLZ, at a dendrimer concentration of 10 mg/ml, that the authors postulate as non-toxic.

3.4. Lipid Nanoparticles

Recently, SLN and NLC were developed with the aim of improving the skin delivery of FLZ (Table II).[108] *In vitro* skin-permeation and retention studies in hairless rat skin

showed that the amount of permeated drug was higher for plain drug solution (41 μg/cm^2). The SLN and NLC based formulations decreased the amount of permeated FLZ to 14 and 12 μg/cm^2, respectively. Besides, NLC and SLN based formulations induced 2.12-fold and 1.73-fold higher amounts of FLZ accumulation in the skin respectively, as compared to the plain solution. The lipid nanoparticles induced a maximal accumulation of FLZ within the *stratum corneum*, with 16% and 14% drug retention from NLC and SLN respectively, as compared to 10% from plain solution. After topical application of the lipid nanoparticles to hairless rats, NLC and SLN induced 1.7-fold and 1.5-fold higher retention of FLZ within the *stratum corneum* as compared to plain solution. On the other hand, the amount of drug recovered from viable skin followed the same order as recorded in *stratum corneum*; but its accumulation was significantly low. Antifungal activity of FLZ loaded in SLN and NLC was carried out on experimentally induced cutaneous candidiasis on

80

*J. Biomater. Tissue Eng. 3, 70–88, **2013***

REVIEW

immunosuppressed Sprague-Dawley rats infected with *C. albicans*. The topical treatments were applied once daily for 3 consecutive days 24 h after the infection was induced. The animals treated with both FLZ loaded in NLC and SLN demonstrated a low fungal burden in skin, with a colony count significantly less abundant than those treated with plain solution.

3.5. Microemulsions

Microemulsions have recently been used to improve the clinical outcome of topical CLZ (Table II).[109] 60% of the CLZ loaded in lemon oil and isopropyl myristate based microemulsion was released within 8 h. The *in vitro* permeation studies on mice skin of the CLZ loaded microemulsion (formulated as liquid or incorporated into 1% carbopol gel), showed significantly higher skin retention of CLZ over the marketed CLZ cream. Moreover, the gel provided two- to three-fold increased skin retention compared to their corresponding liquid microemulsion. The isopropyl myristate based microemulsion was more stable than those based on lemon oil. *In vitro* antifungal activity of CLZ loaded in microemulsion as liquid and gel against *C. albicans* showed that the mean diameter of the inhibition zone for microemulsion was significant higher than that of CLZ cream. Moreover, clinical evaluation proved that 1- and 2-weeks after treatment, 1% CLZ microemulsion gel showed a significant reduction in the scores of symptoms of the evaluated skin fungal infections. The overall evaluation of the clinical efficacy of microemulsion gel was good to excellent in 92.31% of the patients. Moreover, the preparation was well tolerated by all patients with no discontinuation of treatment due to any side effects.

4. OCULAR DELIVERY OF NON METALLIC NANOPARTICLES

Ocular fungal infections may involve the cornea (keratitis), the interior of the eye (endophthalmitis), the retina (retinitis) or the orbit and may occur following trauma (including surgery) or upon systemic disseminated infection. Fungal infections of the retina are among the most devastating ocular infections.[110] Fungal infections with *Candida*, *Fusarium*, *Curvularia* and *Aspergillus* can lead to serious ulceration of the cornea and must be treated rapidly. The most common among these infections is candidal chorioretinitis, usually caused by *C. albicans*.[111] Aspergillus species is the second most common fungal group that infects the choroid and the retina.[112]

In general, common routes of administration for the anterior-segment of the eye (cornea, conjunctiva, sclera, anterior uvea) are topical instillation and subconjunctival injection, whereas for the posterior-segment (retina, vitreous, choroid) common routes include systemic dosing, periocular and intravitreal (IVT) injections, and topical dosing.[113]

Upon systemic administration, the tight junctions of blood-ocular barrier in the retinal capillary and the iris/ciliary endothelial cells, keep most drugs out of the eye.[114] On the other hand, IVT administration is able to maximize the intraocular level of drug in the vitreous and the retina while avoiding toxicities associated with systemic treatment.[115] However, to reach and to maintain effective therapy, repeated injections are necessary. Frequent administration of drugs via this route can lead to endophthalmitis, damage to lens, retinal detachment and hemorrhage. Moreover, high acute intraocular drug concentrations may induce severe local toxicity and increase intraocular pressure.

Topical route is the preferred route of drug administration, primarily for reasons of better patient compliance and cost affordability. However, topical drug delivery to the eye is often impaired by removal mechanisms (blinking, tears, and nasolacrymal drainage) and by the relatively impermeable corneal barriers. The three membranes of the cornea (epithelium, inner stroma and endothelium) act as lipophilic selective barrier for small molecules, preventing the paracellular diffusion of macromolecules and maintaining normal corneal hydration.[116, 117] Usually, less than 5% of topically administered drug penetrates the cornea and reaches intraocular tissues.[118] The conjunctiva and sclera are more permeable than the cornea for drugs topically applied into the eye, but the circulation removes the drugs before it can be absorbed by inner ocular tissues. Both trans-conjunctival penetration and trans-nasal absorption after drainage are generally undesirable, not only because of the loss of active ingredient but also because of possible severe systemic side effects.

Topical AmB (0.1–0.3%) is the standard treatment for ocular infections due to *Candida* and related fungi while other polyene macrolide natamycin (5%) is the usual treatment of filamentous fungi such as *Fusarium*.[119] The current formulation of AmB eye drops (Fungizone®) contains deoxycholate, necessary to solubilize the poorly water soluble AmB,[120] which renders their instillation painful and leads to poor compliance and aggravation of symptoms, especially when direct IVT injection of AmB deoxycholate is used to treat fungal endophtalmitis. Although doses of 5 to 10 μg of IVT AmB are recommended and generally well tolerated, doses as low as 1.0 μg have caused marked retinal damage.[121]

In this context, nanoparticles could advantage the conventional ocular dosage forms, by offering increased residence time of drugs on the corneal surface, reduction in the amount of dose, reduction in systemic toxicity of drug, increased drug concentrations in the infected tissue and suitability for poorly water-soluble drugs.[122, 123] Other potential advantages are the possibility of self-administration by patients as eyedrops; no impairment of sight because of small dimensions of the delivery systems; protection against metabolic enzymes (such as peptidases and nucleases); possible uptake by corneal cells;

Table III. Non-metallic nanoparticles in ocular delivery.

Nanoparticle type	Fungus	Drug	Nanoparticles features	Reference
Nanovesicles	Not tested	AmB	Liposomes:egg PC/cholesterol/tocopherol succinate at 3:5:1 molar ratio	[124, 125]
	Experimentally induced *C. albicans* endophthalmitis	AmB	Liposomes:PC/phosphatidylglycerol/cholesterol at 4:1:3 molar ratio	[126]
	Not tested	AmB	1. AmB lipid complex:dimyristoyl phosphatidylcholine and dimyristoyl phosphatidyl-glycerol in a molar ratio of 3:10:7; micron sized ribbon-like structure 1–6 μm 2. AmBisome:unilamellar liposomes:hydrogenated soy PC/cholesterol/disteroylphosphatidylglycerol and AmB in a molar ratio of 2:1:0.8:0.4; < 100 nm	[129]
	Not tested	AmB	Extemporaneous lipid emulsion of AmB, prepared by mixing concentrated alkaline solution of AmB with Intralipid $\sim$ 20% followed by neutralization and buffered	[120]
	Not tested	KTZ	1. Ultradeformable niosomes:span 60/tween 80; 80:20 w/w; 120 nm 2. non-ultradeformable niosomes:span 60/cholesterol; 80:20; w/w	[133]
Polymeric nanoparticles	*Fusarium solani*	AmB	Eudragit, 130 to 300 nm; +19 to +42 mV zeta potential	[143, 144]
	C. albicans	ECZ	Chitosan nanoparticles:sulfobutylether-β-cyclodextrin (SBE-β-CD) cross linker; 185 nm, +25 mV Z potential; 45% entrapment efficiency; 50% of drug release over 8 h	[148]

and possible reduction of the number of instillation or injection.

4.1. Nanovesicles

Liposomal AmB were formerly employed for IVT administration. The toxicity upon IVT administration of liposome-intercalated AmB was compared to AmB deoxycholate in rabbits[124] and rhesus monkeys (Table III).[125] It was found that liposomes markedly reduce the ocular toxicity of AmB in terms of vitreal band formation, focal retinal damage and retinal atrophy or necrosis. Liposomes also reduce the toxicity of AmB by at least four fold compared to AmB deoxycholate and as much as 30 μg of AmB may be tolerated by the IVT route in rhesus monkey.

In a further study, a rabbit model was used to compare the safety and efficacy of liposomal AmB with that of AmB deoxycholate up to 40 μg in experimentally induced *C. albicans* endophthalmitis (Table III).[126] Similar to the earlier study, it was concluded that reduced toxicity occurred at higher doses of liposomal AmB than AmB deoxycholate. However, higher doses of the lipid formulation were associated with decreased efficacy.

The first comparative toxicity study of three commercial AmB formulations (AmB deoxycholate, AmB lipid complex[127] and AmBisome,[128] Table III) on IVT administration on rabbits was carried out in 2003.[129] Although cataract formation was observed in the majority of the animals (75%), this was a result of the injection technique. From 10 μg for ABCL and 30 μg for AmB deoxycholate the appearance of vitreal opacities or bands was observed,

but were absent in AmBisome-treated eyes. All the IVT administrations caused however, vitreal inflammation and retinal necrosis or atrophy. Retinal ganglion cell loss was found to be similar among the various treatment groups (81%–97%). In general, cell loss was mild to moderate with severity increasing with increasing doses. In this work however, the antifungal efficacy of the formulations was not assessed.

The first topical application of AmB formulations was reported by 1996. The tolerability of 400 nm extemporaneous lipid emulsion of AmB (Table III).[120] The results showed that the tolerance to AmB deoxycholate decreased with the number of instillations. On the contrary, AmB emulsion showed a very good tolerance, even after the fifth instillation on rabbits. The intraocular penetration of the AmB in the emulsion was not improved in comparison with AmB deoxycholate. The average concentration for the AmB deoxycholate group was indeed higher than the emulsion group, not significant in the aqueous humour (0.49 μg/ml vs. 0.3 μg/ml, respectively) and slightly significant in the cornea (500 μg/ml vs. 275 μg/ml, respectively). The presence of sodium deoxycholate might explain this difference. This substance, which is an absorption promoter, caused lesions in the cornea whose seriousness could increase with the number of instillations, thus facilitating the passage of the AmB into the ocular tissues. The AmB concentration both in the aqueous humour and in the cornea resulted in average higher than the MIC of fungi (around 0.2 μg/ml); while the plasmatic concentrations remained lower than 20 ng/ml.

REVIEW

Simultaneously, the ocular bioavailability of AmBisome was equal or better than that of AmB deoxycholate in the cornea of rabbits, but caused lower ocular toxicity.[130] After the first 15 min, the corneal AmB levels were significantly higher for animals receiving AmB deoxycholate than those treated with AmBisome. Later, AmB corneal drug levels showed no differences and remained stable following the. Drug levels in the aqueous humor did not differ between the two AmB preparations and remained below therapeutically effective concentrations.

A problem associated with the commercial formulation of AmBisome is its low shelf life once reconstituted. According to the manufacturer's instructions, AmBisome can only be kept refrigerated for 1 week after reconstitution. A longer shelf-life at ambient temperature would be preferable for a preparation made in a hospital pharmacy and delivered to patients. In this context, a study in 2007,[131] showed that the hydrodynamic diameter remained constant at 108 ± 30 nm with a polydispersity index lower than 0.15, after 6 months at room temperature or at $+2$–8 °C. AmB content was maintained between 94 and 107%. AmB and soy PC proportions remained constant, indicating that the liposomes remained intact and retained the drug. These results show the feasibility of an ophthalmic preparation based on liposomal AmB developed in hospital pharmacies

Elastic (ultradeformable) liposomes were used to increase the ocular bioavailability of the poorly water soluble antiviral ganciclovir after topical application.[132] Ganciclovir elastic liposomes (PC/cholesterol/sodium deoxycholate, 2:1.7:1 w/w, 200 nm), showed a 3.9-fold higher *ex vivo* transcorneal permeability than ganciclovir solution and 1.7-fold higher ocular bioavailability in rabbits than that of ganciclovir solution with similar precorneal clearance. The results were attributed to the small particle size (200 nm) and the elasticity of liposomes. The authors proposed that ultradeformable liposomes can enter the corneal structure which is similar to the *stratum corneum*.

A similar approach was employed to increase the corneal permeability of the highly lipophilic ketoconazole (KTZ), which posses a short ocular half life (19 min in aqueous humour and 43 min in cornea) by loading KTZ in ultradeformable niosomes.[133] Even though KTZ lipophilicity may help in its permeation, its large molecular weight (531.44 Da) impedes its transport across biological membranes. Further, while its high lipid solubility can ensure its passage across corneal epithelium, its further passage through the hydrophilic corneal stroma is hampered.[134] Moreover, the limiting water solubility (0.04 mg/ml) makes difficult to present KTZ in a solubilised form on the corneal surface, being a prerequisite for an ocular formulation. Ultradeformable niosomes (spanlastics) were tested for *ex vivo* corneal permeability, *in vivo* safety and *in vivo* ocular distribution. It was found that the corneal permeation of KTZ loaded in ultradeformable and

non-ultradeformable niosomes were increased above that of KTZ suspension. The flux and total amount of permeated KTZ from ultradeformable niosomes was significantly higher than that from niosomes and KTZ aqueous suspension (2.6 μg/min/cm^2; 1153 μg) > (2.0 μg/min/cm^2; 860 μg) > (1.5 μg/min/cm^2; 625 μg) respectively. The amount of KTZ permeated was highest for ultradeformable niosomes (23.1%) and lowest for suspension (12.5%). The non-irritant/corrosive nature of KTZ encapsulated in ultradeformable niosomes when applied to dermal tissues and upon acute or chronic use to ocular tissues was confirmed. Both empty and KTZ loaded ultradeformable niosomes did not show any significant toxic effect on cell proliferation of normal human gingival fibroblast cell line and were non-genotoxic. The *in vivo* studies of local biodistribution were encouraging. Fluorescent vesicles were found within the aqueous humor and vitreous 4 h post instillation in rabbit eyes of 6-carboxyfluorescein loaded in ultradeformable niosomes, but not after instillation of carboxyfluorescein solution. Moreover, after repeated instillations of 6-carboxyfluorescein loaded in ultradeformable niosomes, fluorescence was found in both the aqueous and vitreous samples from 2 h onwards. Cryo-sections of rabbit eye, 2 h post single drop instillation, showed fluorescence and fluorescent vesicles in different eye tissues including the retinal layer. These results confirm that spanlastics can be used to deliver drugs to the posterior segment of the eye, although the mechanism is unknown.

An interesting study has recently showed that liposomes can target the retina when administered topically as eye drops.[135] It was shown that liposomes (distearoyl-phosphatidylcholine-DSPC, 105 nm, −66 mV Z potential) are able to deliver hydrophobic molecules into the retina. The fluorescence emission of the hydrophobic dye coumarin-6, was found in the posterior segment of the eye after submicron-sized liposomes containing coumarin-6 were topically administered as eye drops. The magnitude of fluorescence in the retina was closely related to the particle size (MLV vs. LUV-6000 nm vs. 105 nm) and rigidity of the liposomes (EggPC vs. DSPC). Submicron-sized liposomes with rigid structures could be potential carriers for targeting the posterior segment of the eye. Absorption of liposomes after topical administration to the surface of the eye seemed to occur mainly via three routes: the systemic, corneal and non-corneal pathways.[136] Epifluorescence microscopy of the entire eye revealed that the delivery route of liposomes to the posterior segment of the eye may not occur via corneal penetration or systemic delivery caused by nasolachrymal drainage.

4.2. Polymeric Nanoparticles

Polymers used to make nanospheres or nanocapsules aimed to ocular delivery must be biodegradable and transparent. In general, the active molecules are confined to polymeric matrices by relatively strong noncovalent

REVIEW

interactions such as ionic, hydrogen bonding, hydrophobic or dipole. Upon administration onto the eye, the particles are maintained at the delivery site and the drug is released from their matrix through diffusion, chemical reaction, polymer degradation or ion exchange mechanisms. Without bioadhesion, nanoparticles are eliminated from the pre-corneal site almost as quickly as aqueous solutions, so cationic polymers are used to make nanoparticles, in order to maximized interaction with negatively charged cornea. These nanoparticles would act as depots and it is speculated that would not be absorbed as occurs with liposomes.

Polyalkylcyanoacrylate (PACA) nanospheres and nanocapsules have been shown to improve and prolong the corneal penetration of anti-inflammatory hydrophilic and lipophilic drugs (triamcinolone[137] and dexamethasone[138]). Despite these positive results, the potential of PACA nanoparticles is limited because they cause disruption of the corneal epithelium cell membrane.[139]

Eudragit is cationic a copolymer of poly (ethylacrylate, methyl-methacrylate, and chloro trimethyl-ammonioethyl methacrylate) containing 8.8–12% for Eudragit RL and 4.5–7.0% for Eudragit RS of quaternary ammonium groups. Eudragit is insoluble at physiologic pH values and capable of limited swelling, thus representing a good material for the dispersion of drugs. Upon topical administration of Eudragit RL and RS nanoparticles in rabbits eyes, sustained release and increased absorption of the incorporated nonsteroidal anti-inflammatory drugs (ibuprofen and flurbiprofen) were observed.[140] Furthermore, no signs of inflammation or discomfort were detected in the rabbits' eyes, suggesting a local tolerance of these nanoparticles.[141, 142] The higher content of quaternary ammonium groups of Eudragit RL 100 increases its water permeability and provides a faster drug release than Eudragit RS 100.

AmB was loaded in nanoparticles (Np) made of Eudragit RL 100[143] and Eudragit RS 100,[144] prepared by a solvent displacement process avoiding the use of toxic chlorinated organic solvents (Table III). PVA, a highly aqueous soluble surfactant, was needed for physical stability of the Np suspension and also for maintaining desired viscosity. The size of the Np remained within 130 to 300 nm with positive zeta potential even after 6 months. *In vitro* release studies in simulated tear fluid (pH 7.4) revealed that nearly 60% AmB was fastly released from the two types of Np within 30 minutes. The antimicrobial activity against *Fusarium solani* by paper disk diffusion method showed that the antifungal activity of AmB loaded in the two types of Np was equal to or slightly lower than that of free-AmB solution. *In vivo* eye irritation study by a modified Draize test showed that, following topical instillation of nanoparticles to a rabbit's eye there was no irritation. The ocular penetration of AmB loaded Eudragit Np was not assayed, so the advantages of these formulations over other AmB formulations can not be addressed. Moreover as Nps were administered only

once in the irritation study, toxicity of these Np can not be discarded.

Other cationic mucoadhesive and biodegradable polymer that has demonstrated excellent ocular compatibility[145, 146] and prolonged contact time with rabbit's ocular surface is chitosan.[147] Chitosan nanoparticles can be spontaneously formed through ionic gelation using negatively charged compounds such as the precipitating agent sodium tripolyphosphate. Chitosan nanoparticles were prepared using sulfobutylether-β-cyclodextrin (SBE-β-CD) containing ECZ as polyanionic crosslinker and their potential as ocular drug delivery systems was studied (Table III).[148] The unique properties of SBE-β-CD (being polyanionic and a solubilizing agent) makes it a versatile substance, which can form nanoparticles with chitosan by ionic gelation and in addition solubilize poorly water soluble drugs. To test their use as ocular drug delivery, sterile 6 mm diameter filter paper discs were placed under the eyelid of albino rabbit for 1 min at specific time intervals following a single instillation of the investigated formulae in the conjunctival sac of the right eyes of rabbits. The discs were then placed in *C. albicans* inoculated tubes and the growth inhibition of yeast was evaluated by measuring the cultures' optical density at 600 nm. Results showed that the ECZ loaded chitosan/SBE-β-CD nanoparticles provided to the eye surface greater antifungal effect than that of ECZ solution. The differences in ECZ effect between the nanoparticles and the solution were significantly higher at all times assayed with the exception of time 1 h. The ECZ antifungal effect associated with the application of nanoparticles increased gradually with time showing a maximum at 4 h post-administration and decreased gradually afterwards. Since the controls with chitosan and CD alone are lacking, it is not possible to owe the obtained effect to the combination of both.

5. CONCLUSIONS

The idea of testing most of the above described nano-objects as antifungal agents has emerged nearly five years ago. The inherent structural complexity of each nano-object makes necessary the inclusion of substantial quantitative data, since structure of nanoparticles and biological activity (or function) is highly related. Even though the toxic effects of nano-objects deserve to be carefully highlighted, it is of equal importance to avoid toxicological issues that could spoil the development of potentially benefit nanotechnologies for human health. A key to solve this challenge is to increase our knowledge on the interactions between nano-objects and biological systems. This is required to build regulatory guidelines for the use of nanomaterials in consumer products and in health, as repeatedly stressed for instance by the *Scientific Committee on Emerging and Newly Identified Health Risks* (SCENIHR, European Commission). Vesicles reviewed here for ocular delivery have shown their relative safety when administered by

84

*J. Biomater. Tissue Eng. 3, 70–88, **2013***

parenteral routes and already entered the clinics against other pathologies nearly twenty years ago. However, especially for metallic nanoparticles, only *in vitro* tests of their antifungal activity have been reported. Thus, there is still an important lack of critical information on pre-clinical efficacy and safety in animal models of fungal infection. Data on biocompatibility in human beings is even more scarce, a fact that envisions a difficult pathway to the translation. Besides, validated methods for large scale production are still absent. Although results on antifungal metallic nanoparticles looks promising, there remain the challenges of demonstrating that (a) the same mechanisms mediating oxidative stress and responsible for fungi elimination are innocuous for human beings, and (b) the absence of eco-toxicity. Nonetheless, different to other therapeutic strategies employing nanoparticles, the applications reviewed here, are or should be intended for the topical route. This is advantageous in terms of avoiding the expectance of acute infusion related toxicity (such as the complement activation related pseudo allergy). Given the nature of the oxidative damage, determining the toxicity after repeated doses, in longitudinal studies, will be required. Because of this, the development of antifungal metallic nano-objects with high therapeutic indices will be of critical importance.

References and Notes

1. M. R. McGinnis, Dermatophytosis, Tropical Infectious Diseases: Principles, Pathogens, and Practice, edited by R. L. Guerrant, D. H. Walker, and P. F. Weller, Churchill Livingstone, New York (**1999**), pp. 609–615.
2. M. Ellis, Invasive fungal infections: Evolving challenges for diagnosis and therapeutics. *Mol. Immunol.* 38, 947 (**2002**).
3. M. M. McNeil, S. L. Nash, R. A. Hajjeh, M. A. Phelan, L. A. Conn, B. D. Plikaytis, and D. W. Warnock, Trends in mortality due to invasive mycotic diseases in the United States. *Clin. Infect. Dis.* 33, 641 (**2001**).
4. M. C. Arendrup, K. Fuursted, B. Gahrn-Hansen, I. M. Jensen, J. D. Knudsen, B. Lundgren, H. C. Schonheyder, and M. Tvede, Seminational surveillance of fungemia in Denmark: notably high rates of fungemia and numbers of isolates with reduced azole susceptibility. *J. Clin. Microbiol.* 43, 4434 (**2005**).
5. D. A. Enoch, H. A. Ludlam, and N. M. Brown, Invasive fungal infections: A review of epidemiology and management options. *J. Med. Microbiol.* 55, 809 (**2006**).
6. T. F. Patterson, W. R. Kirkpatrick, M. White, J. W. Hiemenz, J. R. Wingard, B. Dupont, M. G. Rinaldi, D. A. Stevens, and J. R. Graybill, Invasive aspergillosis, disease spectrum, treatment practices, and outcomes, I3 aspergillus study group. *Medicine* (Baltimore) 79, 250 (**2000**).
7. S. J. Lin, J. Schranz, and S. M. Teutsch, Aspergillosis case-fatality rate: Systematic review of the literature. *Clin. Infect. Dis.* 32, 358 (**2001**).
8. P. G. Pappas, J. H. Rex, J. Lee, R. J. Hamill, R. A. Larsen, W. Powderly, C. A. Kauffman, N. Hyslop, J. E. Mangino, S. Chapman, H. W. Horowitz, J. E. Edwards, W. E. Dismukes, and N. M. S. Group, A prospective observational study of candidemia: Epidemiology, therapy, and influences on mortality in hospitalized adult and pediatric patients. *Clin. Infect. Dis.* 37, 634 (**2003**).
9. K. A. Marr, R. A. Carter, F. Crippa, A. Wald, and L. Corey, Epidemiology and outcome of mould infections in hematopoietic stem cell transplant recipients. *Clin. Infect. Dis.* 34, 909 (**2002**).
10. G. S. Martin, D. M. Mannino, S. Eaton, and M. Moss, The epidemiology of sepsis in the United States from 1979 through 2000. *N. Engl. J. Med.* 348, 1546 (**2003**).
11. J. D. Davis, Superficial fungal infections of the skin: Tinea corporis, tinea pedis, and Candida intertrigo. *Prim. Care Update Ob. Gyns.* 2, 157 (**1995**).
12. M. A. Pfaller and D. J. Diekema, Epidemiology of invasive candidiasis: A persistent public health problem. *Clin. Microbiol. Rev.* 20, 133 (**2007**).
13. B. H. Segal and T. J. Walsh, Current approaches to diagnosis and treatment of invasive aspergillosis. *Am. J. Respir Crit. Care Med.* 173, 707 (**2006**).
14. T. F. Patterson, Treatment and prevention of fungal infections, Focus on Candidemia, Applied Clinical Education, New York (**2007**), pp. VII–VIII.
15. A. H. Groll, P. M. Shah, C. Mentzel, M. Schneider, G. Just-Nuebling, and K. Huebner, Trends in the postmortem epidemiology of invasive fungal infections at a university hospital. *J. Infect.* 33, 23 (**1996**).
16. K. A. Marr, K. Seidel, T. C. White, and R. A. Bowden, Candidemia in allogeneic blood and marrow transplant recipients: Evolution of risk factors after the adoption of prophylactic fluconazole. *J. Infect. Dis.* 181, 309 (**2000**).
17. G. San-Blas and E. Burger, Experimental medical mycological research in Latin America—A 2000–2009 overview. *Rev. Iberoam. Micol.* 28, 1 (**2011**).
18. M. Ameen, Epidemiology of superficial fungal infections. *Clin. Dermatol.* 28, 197 (**2010**).
19. R. Hay, Superficial fungal infections. *Medicine* 37, 610 (**2009**).
20. E. S. M. Ramos, C. M. Lima, R. C. Schechtman, B. M. Trope, and S. Carneiro, Superficial mycoses in immunodepressed patients (AIDS). *Clin. Dermatol.* 28, 217 (**2010**).
21. N. B., The skin, Principles of Medicine in Africa, edited by E. Parry, R. Godfrey, D. Mabey, and G. Hill, Cambridge University Press, Cambridge, UK (**2004**), pp. 1264–1301.
22. B. Naafs and V. Padovese, Rural dermatology in the tropics. *Clin. Dermatol.* 27, 252 (**2009**).
23. L. Oliveira, J. Graham, C. Lok, S. MacFarlane, and D. Zimmerman, Risk factors for yeast superinfection in the treatment of suspected exit site infections: A case-control study. *J. Vasc. Access.* 9, 35 (**2008**).
24. M. Perez-Fontan, M. Rosales, A. Rodriguez-Carmona, T. G. Falcon, and F. Valdes, Mupirocin resistance after long-term use for Staphylococcus aureus colonization in patients undergoing chronic peritoneal dialysis. *Am. J. Kidney Dis.* 39, 337 (**2002**).
25. H. Hof, Developments in the epidemiolgy of invasive fungal infections—Implications for the empiric and targeted antifungal therapy. *Mycoses* 51, 1 (**2008**).
26. A. Naik, Y. N. Kalia, and R. H. Guy, Transdermal drug delivery: Overcoming the skin's barrier function. *Pharm. Sci. Technolo. Today* 3, 318 (**2000**).
27. S. Bidkar, D. Jain, A. Padsalg, K. Patel, and V. Mokale, Formulation development and evaluation of fluconazole gel in various polymer bases. *As. J. Pharm.* 1, 63 (**2007**).
28. T. C. White, S. Holleman, F. Dy, L. F. Mirels, and D. A. Stevens, Resistance mechanisms in clinical isolates of Candida albicans. *Antimicrob Agents Chemother* 46, 1704 (**2002**).
29. S. Perea, J. L. Lopez-Ribot, W. R. Kirkpatrick, R. K. McAtee, R. A. Santillan, M. Martinez, D. Calabrese, D. Sangland, and T. F. Patterson, Prevalence of molecular mechanisms of resistance to azole antifungal agents in Candida albicans strains displaying high-level fluconazole resistance isolated from human immunodeficiency virus-infected patients. *Antimicrob Agents Chemother* 45, 2676 (**2001**).
30. G. D. Wright, Resisting resistance: New chemical strategies for battling superbugs. *Chem. Biol.* 7, R127 (**2000**).

J. Biomater. Tissue Eng. 3, 70–88, 2013

85

31. G. D. Wright, Bacterial resistance to antibiotics: Enzymatic degradation and modification. *Adv. Drug Deliv. Rev.* 57, 1451 (**2005**).

32. T. N. Kim, Q. L. Feng, J. O. Kim, J. Wu, H. Wang, G. C. Chen, and F. Z. Cui, Antimicrobial effects of metal ions (Ag^+, Cu^{2+}, Zn^{2+}) in hydroxyapatite. *J. Mater. Sci. Mater. Med.* 9, 129 (**1998**).

33. K. H. Cho, J. E. Park, T. Osaka, and S. G. Park, The study of antimicrobial activity and preservative effects of nanosilver ingredient. *Electrochim. Acta* 51, 956 (**2005**).

34. A. Espinel-Ingroff, Novel antifungal agents, targets or therapeutic strategies for the treatment of invasive fungal diseases: A review of the literature (2005–2009). *Rev. Iberoam. Micol.* 26, 15 (**2009**).

35. National Nanotechnology Initiative (U.S.) and United States, National Nanotechnology Coordination Office, National Nanotechnology Initiative, National Nanotechnology Coordination Office, Washington, D.C.

36. B.S. Institution, *Terminology for Nanomaterials* (**2007**).

37. B. S. Atiyeh, M. Costagliola, S. N. Hayek, and S. A. Dibo, Effect of silver on burn wound infection control and healing: Review of the literature. *Burns* 33, 139 (**2007**).

38. U. Jappe, D. Heuck, B. Strommenger, C. Wendt, G. Werner, D. Altmann, and W. Witte, Staphylococcus aureus in dermatology outpatients with special emphasis on community-associated methicillin-resistant strains. *J. Invest. Dermatol.* 128, 2655 (**2008**).

39. J. Hardes, H. Ahrens, C. Gebert, A. Streitbuerger, H. Buerger, M. Erren, A. Gunsel, C. Wedemeyer, G. Saxler, W. Winkelmann, and G. Gosheger, Lack of toxicological side-effects in silver-coated megaprostheses in humans. *Biomaterials* 28, 2869 (**2007**).

40. M. E. Rupp, T. Fitzgerald, N. Marion, V. Helget, S. Puumala, J. R. Anderson, and P. D. Fey, Effect of silver-coated urinary catheters: efficacy, cost-effectiveness, and antimicrobial resistance. *Am. J. Infect. Control* 32, 445 (**2004**).

41. G. K. Vertelov, Y. A. Krutyakov, O. V. Efremenkova, A. Y. Olenin, and G. V. Lisichkin, A versatile synthesis of highly bactericidal Myramistin (R) stabilized silver nanoparticles. *Nanotechnology* 19, 355707 (**2008**).

42. J. R. Morones, J. L. Elechiguerra, A. Camacho, K. Holt, J. B. Kouri, J. T. Ramirez, and M. J. Yacaman, The bactericidal effect of silver nanoparticles. *Nanotechnology* 16, 2346 (**2005**).

43. M. Raffi, F. Hussain, T. M. Bhatti, J. I. Akhter, A. Hameed, and M. M. Hasan, Antibacterial characterization of silver nanoparticles against *E. Coli* ATCC-15224. *J. Mater. Sci. Technol.* 24, 192 (**2008**).

44. E. Falletta, M. Bonini, E. Fratini, A. Lo Nostro, G. Pesavento, A. Becheri, P. Lo Nostro, P. Canton, and P. Baglioni, Clusters of poly(acrylates) and silver nanoparticles: Structure and applications for antimicrobial fabrics. *J. Phys. Chem. C.* 112, 11758 (**2008**).

45. S. Shrivastava, T. Bera, A. Roy, G. Singh, P. Ramachandrarao, and D. Dash, Characterization of enhanced antibacterial effects of novel silver nanoparticles. *Nanotechnology* 18, 9 (**2007**).

46. W. C. Chiang, C. Schroll, L. R. Hilbert, P. Moller, and T. Tolker-Nielsen, Silver-palladium surfaces inhibit biofilm formation. *Appl. Environ. Microbiol.* 75, 1674 (**2009**).

47. S. Pal, Y. K. Tak, and J. M. Song, Does the antibacterial activity of silver nanoparticles dependonthe shape of the nanoparticle? A study of the gram-negative bacterium *Escherichia coli. Appl. Environ. Microbiol.* 73, 1712 (**2007**).

48. N. Silvestry-Rodriguez, K. R. Bright, D. C. Slack, D. R. Uhlmann, and C. P. Gerba, Silver as a residual disinfectant to prevent biofilm formation in water distribution systems. *Appl. Environ. Microbiol.* 74, 1639 (**2008**).

49. A. B. Lansdown, Silver I: Its antibacterial properties and mechanism of action. *J. Wound Care* 11, 125 (**2002**).

50. R. White and K. Cutting, Exploring the effects of silver in wound management—What is optimal. *Wounds* 18, 307 (**2006**).

51. I. Sondi and B. Salopek-Sondi, Silver nanoparticles as antimicrobial agent: A case study on *E. coli* as a model for Gram-negative bacteria. *J. Colloid Interface Sci.* 275, 177 (**2004**).

52. J. Zheng, X. Wu, M. Wang, D. Ran, W. Xu, and J. Yang, Study on the interaction between silver nanoparticles and nucleic acids in the presence of cetyltrimethylammonium bromide and its analytical application. *Talanta* 74, 526 (**2008**).

53. A. Panacek, L. Kvítek, R. Prucek, M. Kolar, R. Vecerova, N. Pizúrova, V. K. Sharma, T. Nevecna, and R. Zboril, Silver colloid nanoparticles: Synthesis, characterization, and their antibacterial activity. *J. Phys. Chem. B* 110, 16248 (**2006**).

54. P. V. Asha Rani, G. L. K. Mun, M. P. Hande, and S. Valiyaveettil, Cytotoxicity and genotoxicity of silver nanoparticles in human cells. *ACS Nano* 3, 279 (**2009**).

55. C. Carlson, S. M. Hussain, A. M. Schrand, L. K. Braydich-Stolle, K. L. Hess, R. L. Jones, and J. J. Schlager, Unique cellular interaction of silver nanoparticles: Size-dependent generation of reactive oxygen species. *J. Phys. Chem. B* 112, 13608 (**2008**).

56. K. J. Kim, W. S. Sung, B. K. Suh, S. K. Moon, J. S. Choi, J. G. Kim, and D. G. Lee, Antifungal activity and mode of action of silver nano-particles on Candida albicans. *Biometals* 22, 235 (**2009**).

57. I.-S. Hwang, J. Lee, J. H. Hwang, K.-J. Kim, and D. G. Lee, Silver nanoparticles induce apoptotic cell death in through the increase of hydroxyl radicals. *FEBS Journal* 279, 1327 (**2012**).

58. K. J. Kim, W. S. Sung, S. K. Moon, J. S. Choi, J. G. Kim, and D. G. Lee, Antifungal effect of silver nanoparticles on dermatophytes. *J. Microbiol. Biotechnol.* 18, 1482 (**2008**).

59. M. Falkiewicz-Dulik and A. B. Macura, Nanosilver as substance biostabilising footwear materials in the foot mycosis prophylaxis. *Mikologia Lekarska* 15, 145 (**2008**).

60. A. Panacek, M. Kolar, R. Vecerova, R. Prucek, J. Soukupova, V. Krystof, P. Hamal, R. Zboril, and L. Kvitek, Antifungal activity of silver nanoparticles against Candida spp. *Biomaterials* 30, 6333 (**2009**).

61. M. Gajbhiye, J. Kesharwani, A. Ingle, A. Gade, and M. Rai, Fungus-mediated synthesis of silver nanoparticles and their activity against pathogenic fungi in combination with fluconazole. *Nanomedicine* 5, 382 (**2009**).

62. M. Gupta, A. K. Goyal, S. R. Paliwal, R. Paliwal, N. Mishra, B. Vaidya, D. Dube, S. K. Jain, and S. P. Vyas, Development and characterization of effective topical liposomal system for localized treatment of cutaneous candidiasis. *J. Liposome Res.* 20, 341 (**2010**).

63. S. Bidkar, D. Jain, A. Padsalg, K. Patel, and V. Mokale, Formulation development and evaluation of fluconazole gel in various polymer bases. *As. J. Pharm.* 1, 63 (**2007**).

64. J. Jain, S. Arora, J.M. Rajwade, P. Omray, S. Khandelwal, and K. M. Paknikar, Silver nanoparticles in therapeutics: Development of an antimicrobial gel formulation for topical use. *Mol. Pharm.* 6, 1388 (**2009**).

65. A. Pourjavadi and R. Soleyman, Novel silver nano-wedges as real poniards for killing of microorganisms. *Mater. Res. Bull.* 46, 1860 (**2011**).

66. D. R. Monteiro, L. F. Gorup, S. Silva, M. Negri, E. R. de Camargo, R. Oliveira, D.B. Barbosa, and M. Henriques, Silver colloidal nanoparticles: Antifungal effect against adhered cells and biofilms of Candida albicans and Candida glabrata biofouling. *The Journal of Bioadhesion and Biofilm Research* 27 (**2011**).

67. A. T. Wan, R. A. Conyers, C. J. Coombs, and J. P. Masterton, Determination of silver in blood, urine, and tissues of volunteers and burn patients. *Clin. Chem.* 37, 1683 (**1991**).

68. S. Maitre, K. Jaber, J. L. Perrot, C. Guy, and F. Cambazard, Increased serum and urinary levels of silver during treatment with topical silver sulfadiazine. *Ann. Dermatol. Venereol.* 129, 217 (**2002**).

69. A. B. Lansdown and A. Williams, How safe is silver in wound care? *J. Wound Care* 13, 131 (**2004**).

70. C. J. Coombs, A. T. Wan, J. P. Masterton, R. A. Conyers, J. Pedersen, and Y. T. Chia, Do burn patients have a silver lining? *Burns* 18, 179 (**1992**).

86

*J. Biomater. Tissue Eng. 3, 70–88, **2013***

REVIEW

71. C. Flohr, J. Heague, I. Leach, and J. English, Topical silver sulfadiazine-induced systemic argyria in a patient with severe generalized dystrophic epidermolysis bullosa. *Br. J. Dermatol.* 159, 740 (**2008**).

72. D. Kello, WHO drinking water quality guidelines for selected herbicides. *Food Addit. Contam.* 6, S79 (**1989**).

73. P. L. Drake and K. J. Hazelwood, Exposure-related health effects of silver and silver compounds: A review. *Ann Occup Hyg* 49, 575 (**2005**).

74. O. Brandt, M. Mildner, A. E. Egger, M. Groessl, U. Rix, M. Posch, B. K. Keppler, C. Strupp, B. Mueller, and G. Stingl, Nanoscalic silver possesses broad-spectrum antimicrobial activities and exhibits fewer toxicological side effects than silver sulfadiazine. *Nanomedicine* (**2011**).

75. M. J. Eckelman and T. E. Graedel, Silver emissions and their environmental impacts: A multilevel assessment. *Environ. Sci. Technol.* 41, 6283 (**2007**).

76. B. Chudasama, A. K. Vala, N. Andhariya, R. V. Upadhyay, and R. V. Mehta, Antifungal activity of multifunctional Fe_3O_4—Ag nanocolloids. *J. Magnetism Magnetic Mat.* 323, 1233 (**2011**).

77. R. Prucek, J. Tucek, M. Kilianova, A. Panacek, L. Kvitek, J. Filip, M. Kolar, K. Tomankova, and R. Zboril, The targeted antibacterial and antifungal properties of magnetic nanocomposite of iron oxide and silver nanoparticles. *Biomaterials* 32, 4704 (**2011**).

78. N. Padmavathy and R. Vijayaraghavan, Enhanced bioactivity of ZnO nanoparticles—An antimicrobial study. *Sci. Technol. Adv. Mater.* 9, 1 (**2008**).

79. G. Applerot, A. Lipovsky, R. Dror, N. Perkas, Y. Nitzan, R. Lubart, and A. Gedanken, Enhanced antibacterial activity of nanocrystalline ZnO due to increased ROS-mediated cell injury. *Adv. Funct. Mater.* 19, 842 (**2009**).

80. A. Fortuny, C. Bengoa, J. Font, and A. Fabregat, Bimetallic catalysts for continuous catalytic wet air oxidation of phenol. *J. Hazard Mater.* 64, 181 (**1999**).

81. S. Rana, J. Rawat, M. M. Sorensson, and R. D. Misra, Antimicrobial function of Nd^{3+}-doped anatase titania-coated nickel ferrite composite nanoparticles: A biomaterial system. *Acta Biomater.* 2, 421 (**2006**).

82. M. R. Hoffmann, S. T. Martin, W. Choi, and D. W. Bahnemannt, Environmental applications of semiconductor photocatalysis. *Chem. Rev.* 95, 69 (**1995**).

83. S. Baruah, M. A. Mahmood, M. T. Myint, T. Bora, and J. Dutta, Enhanced visible light photocatalysis through fast crystallization of zinc oxide nanorods. *Beilstein J. Nanotechnol.* 1, 14 (**2010**).

84. J. Sawai and T. Yoshikawa, Quantitative evaluation of antifungal activity of metallic oxide powders (MgO, CaO and ZnO) by an indirect conductimetric assay. *J. Appl. Microbiol.* 96, 803 (**2004**).

85. O. Yamamoto, T. Hamada, N. Tokui, and Y. Sasaguri, Comparison of three *in vitro* assay systems used for assessing cytotoxic effect of heavy metals on cultured human keratinocytes. *J UOEH* 23, 35 (**2001**).

86. K. J. Klabunde, J. Stark, O. Koper, C. Mohs, D. G. Park, S. Decker, Y. Jiang, I. Lagadic, and D. Zhang, Nanocrystals as stoichiometricreagents with uniquesurfacechemistry. *J. Phys. Ch.* 100, 12142 (**1996**).

87. R. Brayner, R. Ferrari-Iliou, N. Brivois, S. Djediat, M. F. Benedetti, and F. Fievet, Toxicological impact studies based on Escherichia coli bacteria in ultrafine ZnO nanoparticles colloidal medium. *Nano Lett.* 6, 866 (**2006**).

88. K. Feris, C. Otto, J. Tinker, D. Wingett, A. Punnoose, A. Thurber, M. Kongara, M. Sabetian, B. Quinn, C. Hanna, and D. Pink, Electrostatic interactions affect nanoparticle-mediated toxicity to gram-negative bacterium Pseudomonas aeruginosa PAO1. *Langmuir* 26, 4429 (**2010**).

89. A. E. Nel, L. Madler, D. Velegol, T. Xia, E. M. Hoek, P. Somasundaran, F. Klaessig, V. Castranova, and M. Thompson, Understanding biophysicochemical interactions at the nano-bio interface. *Nat. Mater.* 8, 543 (**2009**).

90. N. Padmavathy and R. Vijayaraghavan, Enhanced bioactivity of ZnO nanoparticles—An antimicrobial study. *Sci. Technol. Adv. Mater.* 9 (**2008**).

91. T. J. Brunner, P. Wick, P. Manser, P. Spohn, R. N. Grass, L. K. Limbach, A. Bruinink, and W. J. Stark, *In vitro* cytotoxicity of oxide nanoparticles: Comparison to asbestos, silica, and the effect of particle solubility. *Environ. Sci. Technol.* 40, 4374 (**2006**).

92. N. M. Franklin, N. J. Rogers, S. C. Apte, G. E. Batley, G. E. Gadd, and P. S. Casey, Comparative toxicity of nanoparticulate ZnO, bulk ZnO, and $ZnCl_2$ to a freshwater microalga (Pseudokirchneriella subcapitata): The importance of particle solubility. *Environ. Sci. Technol.* 41, 8484 (**2007**).

93. K. M. Reddy, K. Feris, J. Bell, D. G. Wingett, C. Hanley, and A. Punnoose, Selective toxicity of zinc oxide nanoparticles to prokaryotic and eukaryotic systems. *Appl. Phys. Lett.* 90, 2139021 (**2007**).

94. L. He, Y. Liu, A. Mustapha, and M. Lin, Antifungal activity of zinc oxide nanoparticles against Botrytis cinerea and Penicillium expansum. *Microbiol. Res.* 166, 207 (**2011**).

95. Q. Wan, T. H. Wang, and J. C. Zhao, Enhanced photocatalytic activity of ZnO nanotetrapods. *Appl. Phys. Lett.* 87, 83105 (**2005**).

96. N. Jones, B. Ray, K. T. Ranjit, and A. C. Manna, Antibacterial activity of ZnO nanoparticle suspensions on a broad spectrum of microorganisms. *FEMS Microbiol. Lett.* 279, 71 (**2008**).

97. A. L. Neal, What can be inferred from bacterium-nanoparticle interactions about the potential consequences of environmental exposure to nanoparticles? *Ecotoxicology* 17, 362 (**2008**).

98. D. Sharma, J. Rajput, B. S. Kaith, M. Kaur, and S. Sharma, Synthesis of ZnO nanoparticles and study of their antibacterial and antifungal properties. *Thin Solid Films* 519, 1224 (**2010**).

99. M. Eskandari, N. Haghighi, V. Ahmadi, F. Haghighi, and S. R. Mohammadi, Growth and investigation of antifungal properties of ZnO nanorod arrays on the glass. *Physica B, Condensed Matter* 406, 112 (**2011**).

100. G. Fu, P. S. Vary, and C. T. Lin, Anatase TiO_2 nanocomposites for antimicrobial coatings. *J. Phys. Chem. B* 109, 8889 (**2005**).

101. N. Haghighia, Y. Abdia, and F. Haghighib, Light-induced antifungal activity of TiO_2 nanoparticles/ZnO nanowires. *Appl. Surf. Sci.* 257, 10096 (**2011**).

102. S. Darbari, Y. Abdi, F. Haghighi, S. Mohajerzadeh, and N. Haghighi, Investigating the antifungal activity of TiO_2 nanoparticles deposited on branched carbon nanotube arrays. *J. Phys. D: Appl. Phys.* 44, 245401 (**2011**).

103. F. Martinez-Gutierrez, P. L. Olive, A. Banuelos, E. Orrantia, N. Nino, E. M. Sanchez, F. Ruiz, H. Bach, and Y. Av-Gay, Synthesis, characterization, and evaluation of antimicrobial and cytotoxic effect of silver and titanium nanoparticles. *Nanomedicine* 6, 681 (**2010**).

104. M. Devi, M. S. Kumar, and N. Mahadevan, Amphotericin-B loaded vesicular systems for the treatment of topical fungal infection. *Int. J. Rec. Adv. Pharm. Res.* 4, 37 (**2011**).

105. P. Verma and K. Pathak, Nanosized ethanolic vesicles loaded with econazole nitrate for the treatment of deep fungal infections through topical gel formulation. *Nanomedicine* 8, 489 (**2012**).

106. Y. G. Bachhav, K. Mondon, Y. N. Kalia, R. Gurny, and M. Möller, Novel micelle formulations to increase cutaneous bioavailability of azole antifungals. *J. Control Rel.* 153, 126 (**2011**).

107. K. Winnicka, K. Sosnowska, P. Wieczorek, P. T. Sacha, and E. Tryniszewska, Poly(amidoamine) dendrimers increase antifungal activity of clotrimazole. *Biol. Pharm. Bull.* 34, 1129 (**2011**).

108. M. Gupta and S. P. Vyas, Development, characterization and *in vivo* assessment of effective lipidic nanoparticles for dermal delivery of fluconazole against cutaneous candidiasis. *Chem. Phys. Lipids* (**2012**).

109. F. M. Hashem, D. S. Shaker, M. K. Ghorab, M. Nasr, and A. Ismail, Formulation, characterization, and clinical evaluation of microemulsion containing clotrimazole for topical delivery. *AAPS Pharm. Sci. Tech.* 12, 879 (**2011**).

110. T. H. Pettit, J. E. Edwards, and E. P. Purdy, Endogenous fungal endophthalmitis, Ocular Infection and Immunity, edited by J. S. Pepose, G. N. Holland, and K. R. Wilhelmus, St. Louis, Mosby, MO (**1996**), pp. 1262–1285.

111. Y. Ahuja, S. M. Couch, R. R. Razonable, and S. J. Bakri, Infectious retinitis: A review. *Retin. Physician* (**2008**).

112. J. R. Iv, S. A. McNeil, T. M. Johnson, S. F. Bradley, P. H. Kazanjian, and C. A. Kauffman, Endogenous Aspergillus endophthalmitis: Report of 3 cases and review of the literature. *Medicine (Baltimore)* 81, 311 (**2002**).

113. H. Z. Bu, H. J. Gukasyan, L. Goulet, X. J. Lou, C. Xiang, and T. Koudriakova, Ocular disposition, pharmacokinetics, efficacy and safety of nanoparticle-formulated ophthalmic drugs. *Curr. Drug Metab.* 8, 91 (**2007**).

114. A. Urtti, Challenges and obstacles of ocular pharmacokinetics and drug delivery. *Adv. Drug Deliv. Rev.* 58, 1131 (**2006**).

115. G. A. Peyman, E. M. Lad, and D. M. Moshfeghi, Intravitreal injection of therapeutic agents. *Retina* 29, 875 (**2009**).

116. I. P. Kaur, A. Garg, A. K. Singla, and D. Aggarwal, Vesicular systems in ocular drug delivery: An overview. *Int. J. Pharm.* 269, 1 (**2004**).

117. C. L. Bourlais, L. Acar, H. Zia, P. A. Sado, T. Needham, and R. Leverge, Ophthalmic drug delivery systems—Recent advances. *Prog. Retin Eye Res.* 17, 33 (**1998**).

118. J. C. Lang, Ocular drug delivery conventional ocular formulations. *Adv. Drug Deliv. Rev.* 16, 39 (**1995**).

119. P. A. Thomas, Fungal infections of the cornea. *Eye (Lond.)* 17, 852 (**2003**).

120. T. Cohen, H. Sauvageon-Martre, D. Brossard, F. D'Hermies, C. Bardin, F. Chast, and J. C. Chaumeil, Amphotericin B eye drops as a lipidic emulsion. *Int. J. Pharm.* 137, 249 (**1996**).

121. E. N. Souri and W. R. Green, Intravitreal amphotericin B toxicity. *Am. J. Ophthalmol.* 78, 77 (**1974**).

122. R. Gaudana, J. Jwala, S. H. Boddu, and A. K. Mitra, Recent perspectives in ocular drug delivery. *Pharm. Res.* 26, 1197 (**2009**).

123. E. M. D. Amo and A. Urtti, Current and future ophthalmic drug delivery systems, a shift to the posterior segment. *Drug Discov. Today* 13, 135 (**2008**).

124. C. Tremblay, M. Barza, F. Szoka, M. Lahav, and J. Baum, Reduced toxicity of liposome-associated amphotericin B injected intravitreally in rabbits. *Invest. Ophthalmol. Vis. Sci.* 26, 711 (**1985**).

125. M. Barza, J. Baum, C. Tremblay, F. Szoka, and D. J. D'Amico, Ocular toxicity of intravitreally injected liposomal amphotericin B in rhesus monkeys. *Am. J. Ophthalmol.* 100, 259 (**1985**).

126. K. R. Liu, G. A. Peyman, and B. Khoobehi, Efficacy of liposome-bound amphotericin B for the treatment of experimental fungal endophthalmitis in rabbits. *Invest. Ophthalmol. Vis. Sci.* 30, 1527 (**1989**).

127. A. S. Janoff, L. T. Boni, M. C. Popescu, S. R. Minchey, P. R. Cullis, T. D. Madden, T. Taraschi, S. M. Gruner, E. Shyamsunder, M. W. Tate, et al., Unusual lipid structures selectively reduce the toxicity of amphotericin B. *Proc. Natl. Acad. Sci. USA* 85, 6122 (**1988**).

128. J. Adler-Moore and R. T. Proffitt, AmBisome: Liposomal formulation, structure, mechanism of action and pre-clinical experience. *J. Antimicrob Chemother* 49, 21 (**2002**).

129. J. P. Cannon, R. Fiscella, S. Pattharachayakul, K. W. Garey, F. De Alba, S. Piscitelli, D. P. Edward, and L. H. Danziger, Comparative toxicity and concentrations of intravitreal amphotericin B formulations in a rabbit model. *Invest. Ophthalmol. Vis. Sci.* 44, 2112 (**2003**).

130. U. Pleyer, J. Grammer, J. H. Pleyer, P. Kosmidis, D. Friess, K. H. Schmidt, and H. J. Thiel, Amphotericin B bioavailibility in the cornea. Studies with local administration of liposome incorporated amphotericin B. *Ophthalmology* 92, 469 (**1995**).

131. K. Morand, A. C. Bartoletti, A. Bochot, G. Barratt, M. L. Brandely, and F. Chast, Liposomal amphotericin B eye drops to treat fungal keratitis: Physico-chemical and formulation stability. *Int. J. Pharm.* 344, 150 (**2007**).

132. Y. Shen and J. Tu, Preparation and ocular pharmacokinetics of ganciclovir liposomes. *AAPS J.* 9, E371 (**2007**).

133. S. Kakkar and I. P. Kaur, Spanlastics—A novel nanovesicular carrier system for ocular delivery. *Int. J. Pharm.* 413, 202 (**2011**).

134. J. Barar, A. R. Javadzadeh, and Y. Omidi, Ocular novel drug delivery: Impacts of membranes and barriers. *Expert Opin. Drug Deliv.* 5, 567 (**2008**).

135. K. Hironaka, Y. Inokuchi, Y. Tozuka, M. Shimazawa, H. Hara, and H. Takeuchi, Design and evaluation of a liposomal delivery system targeting the posterior segment of the eye. *J. Control Release* 136, 247 (**2009**).

136. P. M. Hughes, O. Olejnik, J. E. Chang-Lin, and C. G. Wilson, Topical and systemic drug delivery to the posterior segments. *Adv. Drug Deliv. Rev.* 57, 2010 (**2005**).

137. J. Valero, M. A. Egea, M. Espina, F. Gamisans, and M. L. Garcia, Effect of polymerization coadjuvants on nancapsule elaboration and triamcinolone entrapment. *Drug Dev. Ind. Pharm.* 22, 167 (**1996**).

138. C. Gomez-Gaete, N. Tsapis, M. Besnard, A. Bochot, and E. Fattal, Encapsulation of dexamethasone into biodegradable polymeric nanoparticles. *Int. J. Pharm.* 331, 153 (**2007**).

139. A. Zimmer, J. Kreuter, and J. Robinson, Studies on the transport pathway of PBCA Nps in ocular tissues. *J Microencapsul* 84, 497 (**1991**).

140. R. Pignatello, C. Bucolo, and G. Puglisi, Ocular tolerability of Eudragit RS100 and RL100 nanosuspensions as carriers for ophthalmic controlled drug delivery. *J. Pharm. Sci.* 91, 2636 (**2002**).

141. R. Pignatello, C. Bucolo, P. Ferrara, A. Maltese, A. Puleo, and G. Puglisi, Eudragit RS100 nanosuspensions for the ophthalmic controlled delivery of ibuprofen. *Eur. J. Pharm. Sci.* 16, 53 (**2002**).

142. R. Pignatello, C. Bucolo, G. Spedalieri, A. Maltese, and G. Puglisi, Flurbiprofen-loaded acrylate polymer nanosuspensions for ophthalmic application. *Biomaterials* 23, 3247 (**2002**).

143. S. Das, P. K. Suresh, and R. Desmukh, Design of Eudragit RL 100 nanoparticles by nanoprecipitation method for ocular drug delivery. *Nanomedicine* 6, 318 (**2010**).

144. S. Das and P. K. Suresh, Nanosuspension: a new vehicle for the improvement of the delivery of drugs to the ocular surface, application to amphotericin B. *Nanomedicine* 7, 242 (**2011**).

145. A. Enriquez de Salamanca, Y. Diebold, M. Calonge, C. Garcia-Vazquez, S. Callejo, A. Vila, and M. J. Alonso, Chitosan nanoparticles as a potential drug delivery system for the ocular surface: Toxicity, uptake mechanism and *in vivo* tolerance. *Invest. Ophthalmol. Vis. Sci.* 47, 1416 (**2006**).

146. M. J. Alonso and A. Sanchez, The potential of chitosan in ocular drug delivery. *J. Pharm. Pharmacol.* 55, 1451 (**2003**).

147. O. Felt, P. Furrer, J. M. Mayer, B. Plazonnet, P. Buri, and R. Gurny, Topical use of chitosan in ophthalmology: Tolerance assessment and evaluation of precorneal retention. *Int. J. Pharm.* 180, 185 (**1999**).

148. A. A. Mahmoud, G. S. El-Feky, R. Kamel, and G. E. Awad, Chitosan/sulfobutylether-beta-cyclodextrin nanoparticles as a potential approach for ocular drug delivery. *Int. J. Pharm.* 413, 229 (**2011**).

REVIEW

88

*J. Biomater. Tissue Eng. 3, 70–88, **2013***

Advances in the Use of Supercritical Fluids for the Production of Poly(α-hydroxyester) Particles Incorporating Bioactive Agents

Priscila S. C. Sacchetin[1], Paulo T. V. Rosa[2], and Ângela M. Moraes[1, *]

[1]*School of Chemical Engineering, University of Campinas, Campinas, 13083-852, Brazil*
[2]*Institute of Chemistry, University of Campinas, Campinas, 13083-970, Brazil*

Encapsulation of active agents in particulate systems has several advantages over other types of therapeutic formulations, since these systems allow the controlled release of the agent as well as preventing from being degraded prematurely in the body. Nano and microparticles are particularly attractive for this purpose, being capable of releasing active agents through different delivery routes, such as intravenous, subcutaneous, pulmonary, and oral ones. Supercritical fluid technology has proved to be a viable alternative for their preparation, being able to efficiently promote the nucleation and growth of particles from polymers and lipids, among other materials, designed specifically for pharmaceutical applications. Different approaches can be used for the production of particles via supercritical fluid technology, depending on the choice of vehicle material and also on the physico-chemical characteristics of the active agent. The supercritical fluid can be used as a solvent, as an anti-solvent or as a solute, efficiently resulting in particles with high active agent load, narrow size distribution and through processes involving low amounts of organic solvents. This technology is gaining strength in the pharmaceutical area and recent advances will be discussed in this work, focusing more particularly on particles constituted of biocompatible poly(α-hydroxyesters).

Keywords: Supercritical Fluids, Nanoparticles, Microparticles, Polymers, Liposomes, Active Agents.

REVIEW

CONTENTS

1. GENERAL OVERVIEW

The development of drugs and other bioactive agents such as nutraceuticals in the form of micro and nanoscale devices have been growing enormously lately. Drug delivery systems consisting of hydrogel and polymeric nano and microparticles, ceramic and magnetic nanoparticles, as well as of liposomes, solid lipid particles, cyclodextrins, fullerenes, polymeric micelles, dendrimers and hyper-branched polymers produced by different methods may be useful in a wide range of applications, including therapeutics, diagnostics, imaging, and cosmetics, as recently discussed by many authors.[1–13]

Given that, in addition to chemically synthesized drugs, more complex molecules such as peptides, proteins and nucleic acids may be efficiently incorporated and transported in micro and nanoparticulate systems, the use of these devices as carriers of immunizing agents is also quite attractive.[2, 4, 6, 7, 14–16]

While the dimensions of microparticles may be in the range from 1 to 1000 μm, the size range of nanomaterials comprises limits from 0.2 nm (more commonly 1 nm) to 100 nm in at least one dimension.[17, 18] However, not only materials with an external dimension in the nanoscale may be defined as nanomaterials, but also those having an internal structure or a surface structure in the nanoscale.[17] In this sense, the term nanomaterial is appropriate to

---

*Author to whom correspondence should be addressed.

describe a solid or porous material whose structure fits the descriptions above regarding their dimensions, being applicable to films, fibers, tubes, powders, particles, spheres, capsules and nanostructures such as fullerenes, dendrimers and quantum dots.[18]

Based on the market performance in the last 10 years, the impact of nanomaterials in many industrial fields and technologies will surely grow in the near future. The worldwide production of nanomaterials was estimated to be more than 230,000 tons in 2011, experiencing a tenfold increase from 2002.[19] It is predicted,[19] in a conservative way, that the production of nanomaterials in 2016 will reach 350,000 tons, with higher market demands in healthcare, electronics, energy, chemicals, coatings and catalysts. It is supposed that the market for products involving nanotechnology as a key element in their production could reach the astounding figure of three trillion dollars by 2020, with penetration in the pharmaceutical industrial sector estimated around 50%.[20]

In the specific case of the development of micro and nanoparticles aiming at applications in the area of controlled release of active agents, benefits related to size control of free drugs comprise improved stability and better control on their solubilization rates, and consequently, on their bioavailability. The use of polymeric dispersants in different drug nanosuspensions, as an example, can provide sufficient redispersibility after drug processing by vacuum, convection and freeze drying.[21] For drugs incorporated in micro and nanostructures as composites formed with polymers or other types of compounds, the advantages, in addition to those pointed out for unincorporated drugs, include masking unpleasant taste and changing both drug pharmacokinetics and biodistribution. Increases of clearance time and reduction of adverse effects along with protection from harsh environmental conditions such as those found, for instance, in the stomach or intestines[16, 22–24] are further potential advantages of drug incorporation in particulate drug release systems.

Nanoparticles may have significantly different properties and behavior from those of their isolated atoms or of those of microparticles or their bulk counterparts. The changes in properties may be attributed to the quantum
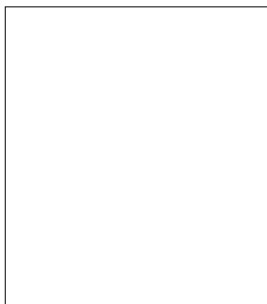
Priscila S. C. Sacchetin
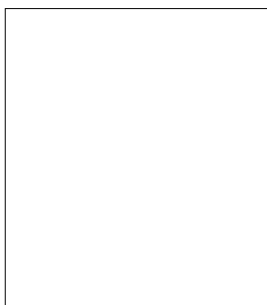
Paulo T. V. Rosa

Ângela M. Moraes

REVIEW
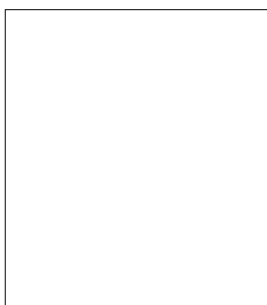
effects associated to materials of very small sizes and to the large surface area to volume ratio.[25] The increase in surface area can alter, for instance, the reactivity of the material, while quantum effects at the nanoscale may affect the magnetic, thermal, optical and electrical behavior of the material, as well as their biological properties. Added to that, functionalization of particle surfaces may broaden even more their characteristics and application scope.

Nanoparticles, though, are not as stable as microparticles mostly due to their higher specific surface energy and Gibbs free energy, requiring, as a consequence, extra energy to reach proper particle size reduction in comparison to systems in which microparticles are formed. The methodologies to obtain nanoparticles are based on two essentially different approaches, as pointed by Lee et al.[26] In the first approach, based on thermodynamic principles, stabilizers or media with suitable compositions are used. Examples of processes that exploit this strategy are emulsion-based methods in which surfactants or polymers are employed and also spraying processes using supercritical fluids. In the second approach, which is based on kinetic aspects, the extra energy input is provided through jets or electrospraying and medium to high shear extrusion processes. Another way to classify the nanoparticles production techniques is to use the recently defined terms top-down and bottom-up strategies. In the first case, procedures such as etching, milling, crushing, grinding and attrition of larger material are involved while, in the second, the processes involve assembling smaller subunits to obtain the product with the desired nanoscale properties.[27] In any case, increased efficiency is attained if both strategies are combined.

These and other different methodologies used to produce polymeric micro and nanoparticles have been presented and discussed in detail in the literature, as in the recent work of Lima et al.[1] Emulsion formation, phase separation, spray drying, ionic gelation, polyelectrolyte complexation and precipitation in the presence of supercritical fluids are amongst the most commonly employed. Alternative approaches include the use of comminution processes, such as micronization and nanoparticle production of poorly water-soluble drugs through wet milling in the presence of polymers as stabilizers,[28] lithography[29,30] and microfluidic devices.[9,31–33]

A variety of materials can be used for the production of nanoparticles, such as chemically synthesized polymers, polysaccharides, proteins, metals, metal oxides, oxide and non-oxide ceramics, silicates and lipids, among others. Synthetic polymers frequently used in the formulation of micro and nanoparticle-based drug delivery systems often belong to the classes of poly(amides), poly(aminoacids), poly(esters), poly(orthoesters), poly(urethanes) or poly(acrylamides).[1] From these, poly(esters), isolated or combined with other compounds, are by far the most used[34] and, among these, the most important are the degradable aliphatic homopolymers poly(glycolic acid) (PGA),

poly(lactic acid) (PLA) and poly(caprolactone) (PCL), together with the heteropolymer poly(lactide-co-glycolide) (PLGA) as recently reviewed by Lima et al.[1]

For the production of particles specifically from poly(α-hydroxyesters), the development of technologies based on the use of supercritical fluids has played an important role in the last 25 years. Processes involving the use of carbon dioxide are particularly frequent due to many attractive characteristics of this compound, such as low cost, high availability, recyclability, non-toxicity, chemical stability, non-flammability and mild critical point conditions (pressure of 7.4 MPa bar and temperature of 31.33 °C). These properties allow the substitution of many problematic volatile organic solvents in drug processing by the more environmentally safe CO_2 and, for these reasons, until 2008, more than 98% of the applications of supercritical fluid technology for the preparation and control of the specific physical form of pharmaceutical substances were developed using carbon dioxide, according to Pasquali et al.[35]

A good number of recent comprehensive publications on traditional methods of obtaining micro and nanoparticles for pharmaceutical and medical use is registered in the literature, as well as some specifically focusing on supercritical fluid technologies.[11,35–46] Therefore, the authors selected to address in this paper strategies for obtaining micro and nanoparticles for application in health care specifically from poly(α-hydroxyesters) through supercritical technologies using CO_2. The different methodologies that have been developed lately and their phenomenological bases, as well as their main advantages and limitations, will be discussed in the following sections.

2. SUPERCRITICAL TECHNOLOGY METHODOLOGIES FOR THE PRODUCTION OF POLY(α-HYDROXYESTER) NANOPARTICLES

Depending on the temperature and pressure to which a substance is subjected it can be found as a gas, a liquid and a solid. If a mixture of a liquid and a gas of some substance is confined in a recipient of constant volume and if this mixture is heated, the pressure of the system will increase and the differences of the physical-chemistry properties of the phases will decrease. This effect continues until a point where there are no differences between the properties of the phases and thus the system becomes uniform. This point is known as critical point and the fluids that are subjected to temperatures and pressures above of this point are known as supercritical fluids. Since there is no distinction between the liquid phase and the gas phase in this region, there is no surface tension in a supercritical fluid. The transport parameters of these fluids (low viscosity and high diffusion coefficients) and the high solvent power (due to the high density as a result of the high

REVIEW

pressure), gives high mass transfer rates in processes that involve this type of fluids.

There are many methods using supercritical fluids reported in the literature to produce micro and nanoparticles from both inorganic and organic materials. The methods are classified depending on the role that the supercritical fluid plays in the particle formation processes. The supercritical fluids can be used either as an anti-solvent, as a solvent or as a solute, and since there are several reviews of these methods available in the literature, only the approaches effectively used for the production of particles from poly(α-hydroxyesters) will be discussed herein. Those processes are schematically represented in Figure 1.

2.1. Gas Anti-Solvent (GAS)

The GAS is a batchwise method used to produce particles from compounds with low solubility in supercritical fluids. In order to do that, the compound should be dissolved in an organic solvent that has high solubility in the supercritical fluid. The introduction of the supercritical fluid in a chamber containing the organic solution of the desired compound will result in the expansion of the

solution, with a consequent reduction in the solubility of the compound and its precipitation in the form of particles after a certain amount of supercritical fluid is incorporated in the solution. The formed particles can be recovered by filtering the suspension and the remaining organic solvent can by removed by rinsing the settled particles with the supercritical fluid.

In the GAS method the supercritical fluid is used as an antisolvent. Factors such as the temperature of the precipitation chamber, pressurization rate, the type of the organic solvent used, the solution concentration and also the type of supercritical fluid used can have some effect on the precipitated particle size. In spite of the simplicity of this method, it has low particle productivity associated with the batch operation and a low supercritical fluid fraction observed in the precipitation vessel, resulting in low particle yields.

Two examples listed in the literature of the use of the GAS process to produce poly(α-hydroxyester) microparticles are the works of Roy et al.[47] and Kang et al.[48] In the first, the production of microcapsules of theophylline coated with PLA using carbon dioxide or trifluoromethane as the supercritical fluid was described.[47] The use of
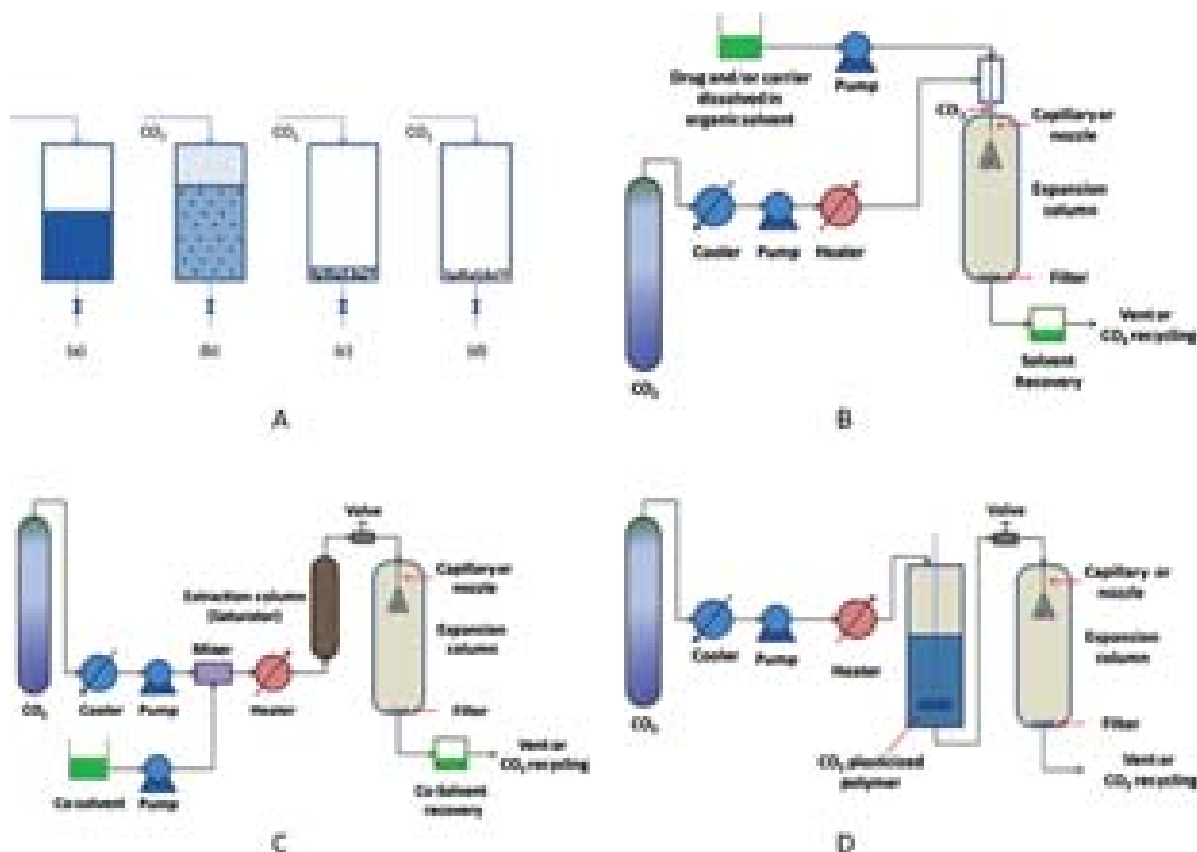

Fig. 1. Schematic representation of the: (A) GAS method, showing the steps (a) adittion of organic solution; (b) expansion of organic solution; (c) filtration of precipitates; (d) removal of remaining organic solvent; (B) SAS method; (C) RESS method; (D) PGSS method.

supercritical CO_2 as an anti-solvent resulted in higher process yields and lower mean particle size in the production of pure theophylline particles, but only trifluoromethane was able to produce microparticles with mean sizes from 100 to 140 μm. Kang et al.[48] produced microparticles containing both bovine serum albumin (BSA) and PLLA, using supercritical CO_2 as antisolvent. The particles produced seemed aggregated, having a mean particle size, as determined by microscopy, of around 2.5 μm.

2.2. Supercritical Anti-Solvent (SAS)

The SAS method is semi-continuous, being an extension of the GAS technique, and is the preferentially used strategy to produce poly(α-hydroxyester) particles. In this case, an organic solvent solution of the compound that will form the particles is continuously injected into a chamber filled with the supercritical fluid. The injection is carried out through a capillary tube, resulting in a solution jet at the entrance of the precipitation vessel. Depending on the viscosity and density of both the solution and the supercritical fluid, the velocity of the jet, and on the diameter and length of the capillary tube, this jet can break up into four distinct forms,[49] namely the Rayleigh, first wind-induced, second-wind induced and atomization regimes. In the Rayleigh regime, droplets larger than the internal capillary diameter are formed. In the first wind-induced regime, jet break-up occurs distant from the capillary exit, resulting in droplets with sizes comparable to the diameter of the capillary. In the second wind-induced regime, on the other hand, small droplets are produced closer to the capillary exit, while in the atomization regime, the droplets are formed just after the exit of the capillary tube, being much smaller than the capillary diameter. The first two regimes can be observed at relatively low velocities and the last two, at high velocities.

In order to understand the particle formation in this process, jet disruption should be investigated together with some other phenomena, such as mass transfer and phase equilibria, as well as the nucleation and crystal growth mechanism and kinetic behavior.[50–61]

The increase of the organic solution flow rate keeping the supercritical fluid flow rate either constant at a high value or increasing proportionally with the solution flow rate will result in a better atomization of the solution into the precipitation chamber, with a consequent decrease of the mean diameter of the particles.[58, 59, 62] Otherwise, if the solution flow rate is increased, keeping the supercritical fluid flow rate at a low value, the fraction of organic solvent in the precipitation chamber will increase and aggregation of the formed particles might be observed.[61, 63] Recently, Reverchon and De Marco[64] have shown the effect of the phase inside the precipitation chamber on the size of the formed particles. Nanoparticles can be obtained if the chamber is maintained in conditions above the organic solvent and

antisolvent mixture critical point. On the other hand, if a liquid phase or a two phase condition (gas and liquid) is maintained in the precipitation vessel, a mixture of nano and micro particles is obtained. Finally, if a gaseous mixture is observed in the chamber, it can result in expanded microparticle formation (particles with a void core). These different phases can be attained by the proper selection of pressure, temperature and both supercritical fluid and organic solution flow rates.

When the pressure in the precipitation vessel is increased, the solubility of the organic solvent in the supercritical fluid increases, while its diffusion coefficient decreases and the medium viscosity increases. So, the overall effect of increasing the pressure in the chamber depends on the balance of these factors or on the phase of the mixture inside the precipitation chamber. Some authors[41, 54, 62, 65, 66] observed that an increase in the chamber pressure results in particle diameter decrease, while others[59, 61] observed the opposite.

The organic solution concentration also has some effect on the mean diameter of particles produced by SAS. Higher supersaturation levels can be obtained at low contact times between the solution and the supercritical fluid for high solution concentrations, but nanoparticles are observed to be formed using low organic solution concentrations.[53] This fact can be related to the higher condensation rates observed for higher solution concentrations[54, 61, 66] and an increase in the size of particles obtained by SAS is observed by increasing the organic solution concentration. Rossmann et al.[65] observed that the increase of the solution concentration had a distinct effect on the particle size, depending on the material that was being processed, increasing it for yttrium acetate and decreasing it for paracetamol. One reason for this difference can be the solvent used to produce the particles. For the first system, DMSO was used and, in the second, ethanol was the selected organic solvent.

Temperature can have an opposite effect on the particle size if compared with pressure. In general, increasing the system temperature leads to increases in particle diameter due to lower efficiency of solvent removal.[54, 65]

A decrease in the capillary inner diameter generally results in a decrease in particle diameter, mainly due to the increase in the jet velocity at the entrance of the precipitation chamber and also to the decrease in jet width.[59]

Small variations of the SAS method can receive different denominations. In the precipitation with compressed antisolvent (PCA) technique, the antisolvent is used in subcritical instead of supercritical condition. In the aerosol solvent extraction system (ASES) process, the solution is injected into the precipitation chamber using a nozzle and not through a capillary. At high solvent flow rates there is no difference between the performance of the ASES and SAS processes. In the Solution Enhanced Dispersion of Supercritical Fluids (SEDS) method, the solution enters in contact with the supercritical fluid inside a specially designed

coaxial nozzle. This mixture can improve the atomization characteristics of the system and produce smaller particles.

Another specific case of the SAS process is the production of particles from the injection of a microemulsion inside the precipitation chamber. This method is known as Supercritical Fluid Extraction of Emulsion (SFEE), and was used by different groups to produce magnetic nanoparticles,[67] nanoparticles for gene delivery,[68] and nanoparticles for lysozyme[69] or ketoprofen[70] delivery using PLGA as polymer and PVA as surfactant.

2.3. Rapid Expansion of Supercritical Solution (RESS)

RESS was the first supercritical technology used to produce micro and nano particles.[71] In this method, it is necessary to solubilize the target solid compound in a supercritical fluid in an extraction vessel and to perform a controlled depressurization of the solution in a precipitation chamber. This methodology has limited application for the production of particles from poly(α-hydroxyesters) polymers due to their low solubility in the normally used supercritical fluids.

In order to increase the poly(α-hydroxyester) polymer solubility in the supercritical fluid, organic solvents such as dichloromethane, ethanol and tetrahydrofuran can be used.[72–76]

The size of the particles formed through the RESS processes will depend on the pre-expansion pressure, solution flow rate and temperature, dissolution time, nozzle inside diameter and polymer molar mass polydispersity. The main parameter for RESS is the pre-expansion pressure, since the supersaturation in the precipitation chamber will occur due to the difference in solubility of the compound at high pressure in the extraction column and at low pressure of the precipitation vessel. Thus, high pre-expansion pressure can result in particles with small diameters. Since the expansion process is fast, high supersaturation levels are observed and small particles can be obtained.

When the depressurization is carried out in a vessel filled with a liquid solvent, this method is denominated as RESOLV (rapid expansion of a supercritical solution into a liquid solvent). For poly(α-hydroxyester) polymers, aqueous solutions containing stabilizing agents such as NaCl, polymers or surfactants can be used as a particle receptor solvent. These stabilizer agents may reduce the aggregation tendency of the particles, resulting in products with low sizes. With this technique, nanoparticles of PLA can be successfully produced.[77, 78]

2.4. Particles from Gas Saturated Solutions (PGSS)

In PGSS, the supercritical fluid is solubilized in the polymer (the opposite occurs in the RESS process). Since the supercritical fluid is absorbed by the polymer, it will act

as a plasticizer and the mixture will behave as a polymer melt. The mixture then flows through a capillary tube and is expanded in a precipitation chamber, where the particles are formed.

The main advantage of this method is the absence of organic solvent to produce the particles, and other advantages are the use of mild to moderate pressures, suitability for highly viscous substances, and adequacy to large scale process.[36] However, since the polymer/supercritical fluid solution has a relatively high viscosity and also high polymer concentration, the particles formed by this method are larger than those obtained using the other supercritical methodologies mentioned, but with narrower size distribution.[36]

The operational parameters that have influence on the particle diameter are the pre-expansion pressure and temperature, the polymer to supercritical fluid mass ratio in the pre-expansion chamber and the nozzle inner diameter.

In the next section some more specific details of the use of poly(α-hydroxyester) polymers to obtain particles using supercritical technologies will be presented.

3. CHARACTERISTICS OF THE MAIN POLY(α-HYDROXYESTERS) USED IN THE PRODUCTION OF MICRO AND NANOPARTICLES

Particulate systems containing active agents can be obtained from different types of biodegradable poly(α-hydroxyesters). Many advantages arise from the use of such synthetic polymers, such as their homogeneity in molar mass, their biodegradability, bioresorbability, and biocompatibility, and the prospects of introducing reactive groups in their structure or obtaining polymer blends, which makes possible better tuning of many of their properties.[1, 79] Emphasis will be given herein to three types of polymers, namely PLA, PLGA and PCL, frequently used for the production of particles for drug delivery applications through supercritical fluid-based technologies.

A set of relevant studies performed with these polymers is summarized in Table I. The production of particles of pure polymer, of polymer mixtures and also of particles incorporating a variety of active agents is described. It can be observed that the supercritical technology is very versatile and is capable of producing particles with a vast variety of sizes. In spite of that, the majority of the poly(α-hydroxyester) particles formed using supercritical technologies have size ranges rather in the micrometer scale than in the nanometer range, as shown at Figure 2. The SAS method is the most used approach, and the organic solvent most frequently used to solubilize the polymers or to increase polyester solubility in the supercritical fluid is dichloromethane, DCM. Particles of the nanoscale size range can be obtained using RESS, RESOLV and

Table I. Characteristics of microparticulate systems produced by supercritical fluid technology incorporating active agents or not.

Matrix composition	Production method	Solvent	Operational conditions	Active agent	Loading efficiency	Diameter	Reference
PLA	PCA	DCM	Pressure: 10.1 MPa, Temperature: 36 °C Mass flow rate of the CO$_2$: 10–15 mL/min	NP	NP	0.4–1.6 μm	Sarkari et al.[80]
	SAS	DCM	Pressure: 8–10 MPa, Temperature: 308 k Mass flow rate of the CO$_2$: 40 g/h	Diuron	NP	1–5 μm	Taki et al.[81]
	SAS	DCM	Pressure: 8–17 MPa, Temperature: 304–333 K Mass flow rate of the CO$_2$: 11–14 g/min	NP	NP	4–14 μm	Rantakyla et al.[82]
	ASES	DCM, methanol	Pressure: 7.6 MPa, Temperature: 298 K Mass flow rate of the CO$_2$: 1–2 mL/min	Parahydroxy-benzoic acid and lysozyme	5.7–9.2%[a]	1.2–2 μm	Tu et al.[83]
	SAS	DCM	Pressure: 10–14.5 MPa, Temperature: 308 K Mass flow rate of the CO$_2$: 40 g/h	Herbicide	NA	1–5 μm	Boutin et al.[84]
	PCA	DCM	Pressure: 6–12 MPa, Temperature: 293–308 K Mass flow rate of the CO$_2$: 180 g/min	NP	NP	0.1–50 μm	Diego et al.[85]
	RESS	ethanol	Pressure: 10–20 MPa Temperature: 313 K Mass flow rate of the CO$_2$: NA	NP	NP	2–5 μm	Matsuyama et al.[76]
	SAS	DCM	Pressure: 8.38–9.43 MPa Temperature: 313–323 K Mass flow rate of the CO$_2$: NA,	NP	NP	0.2–5.5 μm	Obrzut et al.[86]
	SAS	DCM	Pressure: 6.5–16 MPa, Temperature: 309–333 K Mass flow rate of the CO$_2$: 67 mL/min	Theophylline	NA	5–95 μm	Roy et al.[47]
	RESS	Tetrahydrofuran	Pressure: 34.6 MPa, Temperature: 305–366 K Mass flow rate of the CO$_2$: NA	NP	NP	30–100 nm	Sane and Thies[75]
	SAS	DCM	Pressure: 6.5 9 MPa, Temperature: 308–318 K Mass flow rate of the CO$_2$: 2.1–4.8 kg/h	Lutein	NP	1–5 μm	Miguel et al.[62]
	SAS	DCM	Pressure: 13.8, 17.2 and 20.7 MPa, Temperature: 306, 313 and 323 K Mass flow rate of the CO$_2$:1.5 g/min	Rifampicin	33.4–91.73%[a]	5 μm	Patomchaiviwat et al.[87]
	SEDS	DCM	Pressure: 12 MPa, Temperature: 306 K Mass flow rate of the CO$_2$: 16 NL/h	Fe$_3$O$_4$	NA	803 nm	Chen et al.[88]
	SEDS	DCM/ethanol	Pressure: 12 MPa, Temperature: 306 K Mass flow rate of the CO$_2$: 25 NL/h	Puerarin	NP	675 nm	Chen et al.[89]
	RESOLV	NP	Pressure: 34 MPa, Temperature: 373 K Mass flow rate of the CO$_2$: NA	Retinyl palmitate	0.9–6.2 wt%[b]	30–160 nm	Sane and Limtrakul[77]

J. Biomater. Tissue Eng. 3, 89–107, **2013**

95

REVIEW

Table I.   Continued.

Matrix composition	Production method	Solvent	Operational conditions	Active agent	Loading efficiency	Diameter	Reference
	SEDS	DCM	Pressure: 10.13 MPa, Temperature: 273 K Mass flow rate of the CO_2: 45 mL/min	Carotene	NA	30 μm	He et al.[90]
	RESS	DCM/methanol	Pressure: 38 MPa, Temperature: 333 K Mass flow rate of the CO_2: NA	NP	NP	270–730 nm	Ul-haq et al.[73]
	PGSS	NP	Pressure: 7.5 MPa, Temperature: 305 K Mass flow rate of the CO_2: NA	Tetanus toxoid	78.1%[NA]	22.8 μm	Baxendale et al.[91]
	SEDS	DCM/ethanol	Pressure: 12 MPa, Temperature: 306 K Mass flow rate of the CO_2: 300 mL/min	Morphine	4.73%[b]	2.45μm	Zhang et al.[92]
PLGA	SAS	Acetone	Pressure: 8.96 and 11.03 MPa, Temperature: 306, 311 and 315 K Mass flow rate of the CO_2: 0.8, 1.8 and 2.8 mL/min	NP	NP	4.6–24.8 μm	Wang et al.[93]
	SAS	DCM	Pressure: 8.96 MPa, Temperature: 306 K Mass flow rate of the CO_2: 1.5 L/min	Hydrocortisone	5.4–25.2%[NA]	30 μm	Wang et al.[94]
	RESS	Ethanol	Pressure: 25 MPa, Temperature: 313 and 423 k Mass flow rate of the CO_2: NA	SiO_2 and TiO_2	NP	10 to 100 nm	Kongsombut et al.[74]
	NP	Ethyl acetate	Pressure: 8 MPa, Temperature: 318 K Mass flow rate of the CO_2: 0.4 mL/h	pDNA	2–20%[c]	149–322 nm	Mayo et al.[68]
	SFEE	Ethyl acetate	Pressure: 8 MPa, Temperature: 311 K Mass flow rate of the CO_2: 0.3 kg/h	NP	NP	1–3.5 μm	Porta et al.[95]
PCL	PGSS	NP	Pressure: 6–11 and 15 MPa, Temperature: 323 and 343 K Mass flow rate of the CO_2: NA	β-carotene	340 ppm[d]	270–650 μm	Paz et al.[96]
	SAS	DCM	Pressure: 30 MPa, Temperature: 313 K Mass flow rate of the CO_2: 20 g/min	Rosmarinus officinalis	62.2–82.8%[a]	255–618 nm	Yesil-Celiktas and Cetin-Uyanikgil[97]
PLA/PLGA	SEDS	DCM	Pressure: 12 MPa, Temperature: 306 K Mass flow rate of the CO_2: 18 L/h	Indomethacin	2.8%[b]	1.7–2.4 μm	Kang et al.[98]
	SEDS	DCM	Pressure: 12 MPa, Temperature: 306 K Mass flow rate of the CO_2: 300 mL/min	Paclitaxel	14.71–16.33%[a]	1.4–8.6 μm	Kang et al.[99]
	PGSS	NP	Pressure: 7.6 MPa, Temperature: 305 K Mass flow rate of the CO_2: NA	hGH	5.5–6.4%[a]	56 to 104 μm	Jordan et al.[100]

REVIEW

Table I. Continued.

Matrix composition	Production method	Solvent	Operational conditions	Active agent	Loading efficiency	Diameter	Reference
PLA and PHB	ASES	DCM	Pressure: 15 MPa, Temperature: 309 K Mass flow rate of the CO_2: 5 mL/min	NP	NP	3.6–162 μm	Breitenbach et al.[101]
PLA/PEG	GAS	DCM	Pressure: 10–15 MPa, Temperature: 278–303 K Mass flow rate of the CO_2: 900–1800 NL/h	Insulin	84.6%[a]	360–720 nm	Caliceti et al.[102]
PLA and PMMA	RESOLV	Ethanol	Pressure: 20 MPa Temperature: 353 K Mass flow rate of the CO_2: NA	NP	NP	100 nm	Meziani et al.[78]
PMMA/PCL	NP	DCM	Pressure: 11 MPa, Temperature: 315 K Mass flow rate of the CO_2: 6.6–102 mL/min	Cholesterol	30%[NA]	0.25–15 μm	Vega-González et al.[103]
PMMA/PCL	SAS	DCM	Pressure: 11 MPa, Temperature: 313 K Mass flow rate of the CO_2: 100 mL/min	NP	NP	> 1–3 μm	Vega-González et al.[104]
PLGA, PLA, and PCL	SEDS	DCM, acetone, ethyl acetate, hexane and isopropanol	Pressure: 13 and 16 MPa, Temperature: 308 or 313 K Mass flow rate of the CO_2: 21 mL/min	Hydrocortisone	22%[e]	5.6–83 μm	Ghaderi et al.[105]
PLA/PEG/PLA	SEDS	DCM	Pressure: 12 MPa, Temperature: 306 K Mass flow rate of the CO_2: NA	Paclitaxel	5.1–7.1%[f]	712–4800 nm	Ouyang et al.[106]
PLA/PEG/PLA	RESS	DCM	Pressure: 12 MPa, Temperature: 306 K Mass flow rate of the CO_2: NA	NP	NP	2.2 μm	Chen et al.[72]
PLGA/Chitosan/mPEG	PGSS	NP	Pressure: 7.5 MPa, Temperature: 305 K Mass flow rate of the CO_2: NA	NP	NP	45.3–97.1 μm	Casettari et al.[107]

Notes: PLA: Poly lactic acid; PLGA: Poly (lactic-co-glycolic acid); PCL: Polycaprolactone; PHB: poly(b-hydroxy-butyric acid); PEG: Poly(ethylene glycol); PMMA: polymethylmethacrylate; mPEG: methoxy polyethylene glycol; SAS: supercritical antisolvent process; ASES: aerosol solvent extraction system process; PCA: Precipitation using a compressed antisolvent; RESS: Rapid expansion of supercritical solutions; SEDS: solution-enhanced dispersion by supercritical fluids; RESOLV: rapid expansion of supercritical solutions into liquid solvents; PGSS: particle from gas-saturated-solutions; SFEE: supercritical emulsion extraction; NP: not performed; NA: not available; DCM: dichloromethane; NL/h: standard liters per hour. Definition of active agent loading efficiencies: (a) % drug loading efficiency = (measured drug loading/theoretical drug loading) $\times$ 100%; (b) % drug loading efficiency (wt) = (mass of drug encapsulated/total mass of particles) $\times$ 100; (c) % drug loading efficiency = amount of drug removed from the supernatant − total amount of drug initially sprayed in the emulsion formulation; (d) Particles dissolved in DCM and analysed by UV/VIS spectrophotometer; (e) % drug loading efficiency = (entrapped drug per batch of microparticles/initially added drug per batch of microparticles) $\times$ 100; (f) % drug loading efficiency = (weight of drug encapsulated in the microspheres/weight of drug-loaded microspheress) $\times$ 100.

SFEE techniques when proper operating conditions are selected. Larger particles can be manufactured using the PGSS method. Active agent loading efficiencies varying from 2 to 92% are described, depending on both the supercritical technology and the operational conditions utilized.

3.1. Poly(lactic Acid)

The first polymers obtained from lactic acid were produced in 1932, being further developed by the Dupont and Ethicon companies. The development of these materials was restricted to the medical field for a long time due to

REVIEW
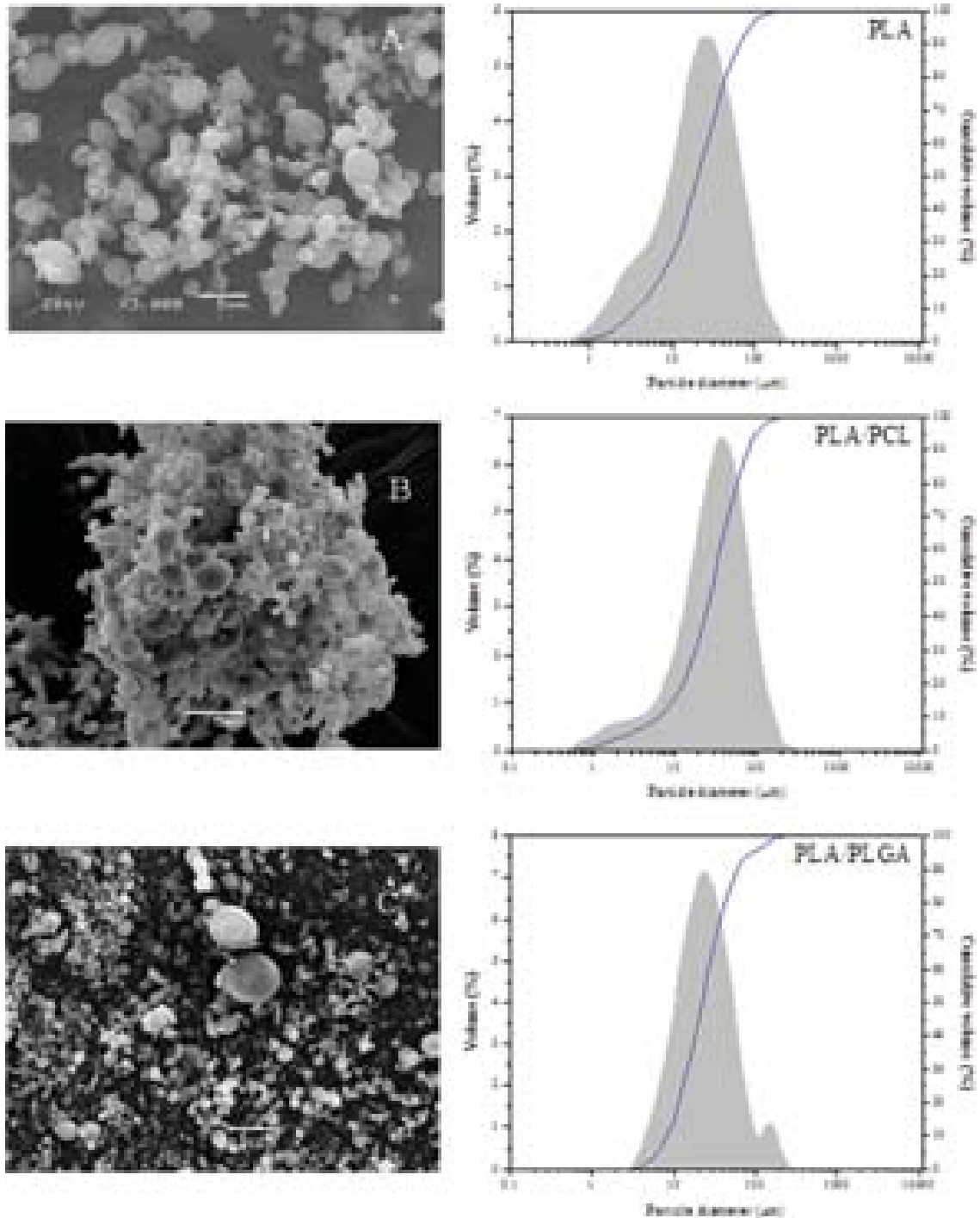
Fig. 2. Scanning electronic microscopy images of typical particles obtained by SAS with: (A) PLA; (B) PLA/PCL; (C) PLA/PLGA, and their respective size distribution analyzed by laser diffraction technique.

prohibitive production costs, and only at the end of the 80's were products applicable to other fields obtained.[108]

Among the absorbable polymers, poly(lactic acid) has been considered as one of the most promising compounds

for the fabrication of biomaterials. Its raw material, lactic acid (or lactide), can be obtained by fermentation of renewable and degradable resources such as corn and rice. PLA may then be chemically synthesized by the

condensation polymerization of the isomers L- and D-lactide (or lactic acid) or by the ring-opening polymerization of lactide.[109] Also according to Pan and Inoue,[109] polymerization of the optically pure monomers leads to the formation of poly(L-lactide), PLLA or poly(D-lactide), PDLA, while the polymerization of the racemic lactide mixture results in the formation of amorphous poly(D,L-lactide) PDLLA. The chirality of the lactic acid units allows the production of polymers with distinguishable degradation rates having different physical and mechanical properties just by adjusting the polymeric material manufacturing conditions.[110] Both PLLA and PDLA are stereoregular semicrystalline polymers, with a melting temperature (T_m) between 173–178 °C, a glass transition temperature (T_g) of approximately 60 °C[109] and crystallinity varying from 37 to 72%.[110] PDLLA, on the other hand, is amorphous, especially due to the random distribution of L and D-lactic acid units,[110] which provides a faster degradation rate in comparison to the stereoregular counterparts. For this reason, when fast active agent release is desired, it is the preferential candidate for developing drug delivery vehicles.[109]

A wide variety of physical properties of PLA-based materials may be handled for stereoregularity by changing the proportion of D and L-lactic acid units in the polymer chain. PLA stereocomplexation has been used to improve the structure, thermal stability, degradation and mechanical properties of PLA materials.[111]

Some of the most relevant physicochemical characteristics of PLA have been discussed by Södergard and Stolt.[112] The solubility of PLA-based polymers is highly dependent on their molar mass, degree of crystallinity and other co-monomer units present in the polymer chain. Enantiomerically pure PLA is more easily solubilized in chrorinated and fluorinated organic solvents, dioxane, dioxolane, furane, and insoluble in water, alcohols and unsubstituted hydrocarbons.

Regarding miscibility with other macromolecules, PLA may form heterogeneous and homogeneous blends with other polymers, a very important feature, since it allows changing characteristics such as the degradation rate, permeability and drug release profiles, in addition to thermal and mechanical properties.[112] These blends may be tuned to produce soft and elastic materials as well as very hard materials with high mechanical strength. In cases where high mechanical resistance is desired, the semicrystalline PLA is preferable to the mainly amorphous PLA. The polymer molar mass, as well as its degree of crystallinity also play important roles in defining the mechanical properties of the material. The tensile strength of PLLA increases by a factor of two when the average molar mass is increased from 50 to 100 KDa.[113]

PLA thermal stability is, in general, quite limited, especially at high temperatures. Gupta and Deshmukh[114] suggest that the thermal degradation kinetics of PLA may

be considered of first order, involving primarily thermohydrolysis and thermoxidative and transesterification reactions. The temperature is also responsible for controlling the hydrolysis process, since at higher temperatures the rate of hydrolysis is increased, also resulting in greater flexibility of the polymer chains, particularly when the process occurs at temperatures above the glass transition temperature.[115] The hydrolysis of the polymer chains, which leads to molecular fragmentation, is affected by several factors, such as the PLA chemical structure, average molar mass and molar mass distribution, purity, morphology, sample shape, size and the conditions employed during the hydrolysis process.[116]

In aqueous solutions, PLA hydrolysis occurs in two stages,[110] beginning with water diffusion into the amorphous regions, which are then degraded. Afterwards, the crystalline domains are attacked, from the edge toward the center. For this reason, PDLLA copolymers are generally less resistant to hydrolytic degradation than PLLA/PDLA blends, since the faster hydrolysis rate for the copolymer is explained by the lower degree of crystallinity and stereocomplexation.[117]

In the stage of hydrolytic degradation of the crystalline regions, the increase in the rate of weight loss results in complete absorption of the polymer[118] as a consequence of the autocatalytic effect activated by the increase in the amount of carboxyl groups.

Due to the characteristics described above, PLA has received great attention in the development of micro- and nanoparticles for the controlled release of drugs. Its use is primarily centered in the intravenous administration route, since this material has high stability and can act as an efficient drug depot for slow release for long periods.

Several processes of production of PLA-based devices using spraying in supercritical fluids have been proposed and investigated in detail.[47, 62, 72–73, 75–78, 81, 82, 84, 86–89, 98, 99, 106, 119]

Rantakyla et al.[82] have tested the formation of particles from PLLA solutions in dichloromethane, observing that the smallest particles (4 μm) were obtained at 304 K and 8.0 MPa by using CO_2 as supercritical fluid in the SAS process. Increasing the temperature from 308 to 323 K and the pressure from 10 to 14 MPa resulted in larger particles, and massive particle agglomeration was noticed at 333 K and 17 MPa. The temperature, pressure, CO_2 velocity and density, nozzle diameter, interfacial tension between liquid and CO_2, and Reynolds and Weber numbers had a small effect on droplet formation. As the droplet and particle formation regime did not explain the observed changes of particle sizes, it was suggested that the size of the initial droplets formed at the nozzle did not affect the final particle size.

A high-resolution imaging system was used by Obrzut et al.[86] to study the influence of the nozzle outlet distance on PLA particle formation from methylene chloride solutions by SAS. The camera and lens were positioned at

a selected axial distance from the nozzle and the particle mean size was evaluated at a fixed density of 0.33 ± 0.02 g/cm^3 at different pressure and temperature combinations and also using a fixed temperature (323 K) with selected pressure and density combinations. Two distinct regimes of jet break up were observed, depending on the process conditions. As the break up length decreased, a transition in the jet break up regime from atomization to a gas-like plume was noted. A reduction in the jet break up length occurred both due to increases in pressure and temperature at fixed density experiments and at higher pressures and densities used in fixed temperatures experiments. PLA particle size distributions are very similar at all conditions, except at the lowest CO_2 density (84 bar and 0.24 g/cm^3), the only condition predicted to be subcritical at equilibrium. The larger particles obtained at this condition were a result of the effect of the thermophysical properties on the spray characteristics, mass transfer, and nucleation.

SAS processes have been used not only to study the particle process formation itself but also to incorporate several drugs in PLA-based systems. Taki et al.[81] have evaluated a co-precipitation approach using a supercritical antisolvent technique for the development of a controlled delivery system for the herbicide diuron in amorphous PLLA microparticles. The initial concentrations of diuron and PLLA in dichloromethane, equal to, respectively, 3 and 0.1% in weight, had an influence upon morphology and shape of the spherical particles formed. The increase of solution viscosity due to higher polymer concentrations lead to a stabilizing effect on the jet, yielding bigger droplets. High polymer concentrations may reduce the atomization forces so that they are not sufficient to break the jet into droplets, thus allowing faster precipitation rather than droplet formation. The authors also noted that the PLA particle growth rates were 10000 times higher than the growth rates of diuron particles in aqueous solution despite the very short precipitation time during the SAS process. Boutin et al.[84] also studied the precipitation of diuron, but using PLLA as a coating matrix. Different organic solvents were tested (dichoromethane and tetrahydrofuran) and the experiments performed showed that increasing the pressure from 10 to 14.5 MPa at 308 K results in an increase in the CO_2 density, which in turn induces a better dispersion of the organic solution in CO_2 and, hence, a decrease in droplet size. As a consequence, super-saturation within the liquid phase is reached more rapidly, thus preventing diuron crystal growth and resulting in the formation of particles composed of herbicide embedded in the polymer matrix at high concentrations. Changes in the capillary diameter also have shown effects on particle size and morphology, since the mean diameter of the particles and the particle size distribution increases with the capillary diameter. However, convergent effects on droplet size will depend on both the capillary diameter and the liquid velocity, since the formation of bigger

droplets is a result of a smaller specific surface area and of a slower mass transfer through the interface.[84]

A SAS process was also used to produce theophylline particles as pure crystals or as a solid formulation in a composite with PLA.[47] In this case, CO_2 and trifluoromethane were used as antisolvents on the process and both led to theophylline precipitation, with hexagonal and triangular shapes, respectively. For those cases in which PLA was used as a coating for theophylline, the predominat macroscopic aspect was powder, independent of the antisolvent used. Despite the differences in shape, the dissolution kinetics of theophylline were similar for both cases. The drug was completely dissolved in less than one hour, also independent of the antisolvent used. When PLA was used to coat theophylline using CO_2 as antisolvent, it was noted that the polymer did not interfere with the precipitation behavior of the drug, allowing sustained drug release (for over 14 hours). Similar results were obtained when the antisolvent employed was CHF_3, suggesting that the drug release was controlled by diffusion.

Miguel et al.[62] used ethyl acetate as solvent in a process used for precipitation of lutein and co-precipitation of lutein/PLA. The authors observed the occurrence of changes in lutein particle morphology from agglomerated microparticles to polygonal crystals when the CO_2/solution flow ratio was increased or the initial concentration of the lutein solution was decreased. The co-precipitation of lutein with PLA resulted in reduction of the particle size with changes in the polymer/drug ratio from 34.3 to 68.6 wt%, leading to particles with mean sizes from 1 to 5 μm. The production by SAS of L-PLA particles having similar mean diameters (around 5 μm) and loaded with rifampicin was also reported by Patomchaiviwat et al.[87] Althought the loading efficiency of the antibiotic was not high, the microparticles could be successfully used for dry powder inhalation applications due their suitable size. Decreasing the polymer content and also the operating temperature made the particles more irregular and agglomerated, since smaller particle sizes smaller seems to be associated with increasing the polymer/solute concentration ratio.

The SEDS process may be also used to produce PLA particles, as shown by Chen et al.[88] Fe_3O_4-PLLA magnetic particles were successfully prepared, using indomethacin as a drug model in this study. The particles produced had a mean size of 803 nm, with a core–shell structure. The addition of the drug increased the mean size to 901 nm. The particles proved to be biocompatible and not cytotoxic, thus allowing for biomedical applications. In another study, Chen et al.[89] reported the production of micronized particles of puerarin (an isoflavonoid) as well as of PLA particles containing this drug. The micronized puerarin nanoparticles were suspended in a highly saturated PLLA-DCM solution by ultrasonic dispersion and then were incorporated in the polymer by the SAS method.

100

J. Biomater. Tissue Eng. 3, 89–107, 2013

The use of ethanol as an organic non-solvent for puerarin micronization allowed obtaining a homogeneous solution with a higher saturation ratio and a lower concentration. This approach led to the formation of particles with a narrow size distribution, with a mean size of 188 nm. In this case, supercritical CO_2 was used both as an anti-solvent, due to its chemical properties, and as a spray enhancer, due to its mechanical effects. Particles of PLA containing puerarin were much bigger in diameter (675 nm).

Similarly, Zhang et al.[92] proposed a modification of the SEDS process to produce PLLA particles containing morphine, consisting of the use of an organic solution (ethanol), which was miscible with water and soluble in supercritical CO_2. The use of this modification lead to the formation of hydrogen bonds and/or similar interactions between the solvents, promoting the mutual miscibility between the water and the supercritical CO_2. Particles with mean diameter of 2.45 μm were then obtained, with a morphine loading of approximately 4.73%. This study suggests that the modified SEDS method may be used to obtain particles incorporating water-soluble drugs for sustained release applications.

Particles containing drugs formed from blends of PLA and other polymers were also studied using the SEDS process. Chemically bonded triblock copolymers with various PEG contents and PLA homopolymer were used to incorporate paclitaxel in PLA and PLA-PEG-PLA particles.[98] The addition of PEG allowed producing particles with high hydrophilicity and the content of this particular polymer in the range from 5 to 50% (w/w) affected the shape of particles, which exhibited sphere-like shapes and smooth surfaces. PLA-PEG-PLA microparticles exhibit morphology similar to that of PLA microparticles when the PEG content is relatively low, while larger particle sizes, irregular shapes and more intense aggregation are observed when the PEG content exceeds 15% in weight. According to the authors, CO_2 acted as a plasticizer in the process, inhibiting the particle formation process at higher PEG contents. The sizes of the drug-loaded particles obtained (712 to 2670 nm) were comparable to those of placebo PLA microparticles with the same PEG content (from 825 to 2670 nm). The drug load (5.1 to 7.1%) and encapsulation efficiency (25.5 to 35.5%) of the microparticles produced decreased with the increase of PEG content in the copolymer matrix. This approach can then be used to produce particles containing drugs for applications in which prolonged circulation times in the bloodstream are required.

PLA particles have been produced by modification of the traditional RESS by expanding the supercritical solution into a liquid instead of into a gas phase, a method known as RESOLV.[78] In the presence of a water-soluble polymer or surfactant, aqueous suspensions of well-dispersed polymeric particles could remain stable for an extended period of time to potentially allow further processing. The use

of three stabilizing agents in the RESS process was studied by Sane and Limtrakul[77] to form PLLA nanoparticles loaded with retinyl palmitate (RP), a light-sensitive compound associated with adverse effects at high doses. PLA was used to coat the active agent and the particles produced had an average size range of 40–110 nm. As a result of polymer and retinyl palmitate insolubility in water, it is usual to observe a severe agglomeration tendency of PLLA/RP particles in pure water owing to their hydrophobic nature. In this paper, the use of the nonionic, polymeric surfactants Pluronic F127 and Pluronic F68, and also of the anionic surfactant sodium dodecyl sulfate (SDS) to stabilize the PLLA/RP particle dispersion was tested to overcome the agglomeration tendency. Pluronic F127 was considered the most effective stabilizer for dispersing the PLLA/retinyl palmitate particles, while Pluronic F68 and SDS were less effective.

Finally, it is also possible to produce PLA particles at room temperature through the solvent-free method PGSS. Through this specific process, supercritical carbon dioxide dissolves into the polymer, lowering the glass transition temperature and plasticizing it. Single shot vaccines of tetanus toxoid (TT) can be manufactured using this technique.[91] *In vivo* tests have shown that the formulations employed were similar to multiple injections of a commercially available alum-adsorbed tetanus toxoid. This study shows the potential of this technique to reduce the need for booster doses in a vaccine administration regimen.

3.2. Poly(lactide-co-glycolide)

Another compound which has been extensively studied is poly(lactide-co-glycolide), PLGA, a copolymer formed from one or more than three different monomers of hydroxyacids, D-lactic, L-lactic and/or glycolic acids.[120] PLGA is one of the most popular synthetic polymers used for the development of controlled release devices for humans due to its biodegradability and biocompatibility.[121] According to Panyam and Labhasetwar,[122] PLGA undergoes hydrolysis upon implantation into the body, forming biologically compatible and metabolizable moieties that are eventually removed from the body through the citric acid cycle. PLGA has an amorphous structure, because the constituents poly(acid lactic) and poly(glycolic acid) are not naturally able to pack tightly into one another.[110] As reported by Mungargi et al.[123] the most widely used PLGA composition (which presents the highest biodegradation rate) has a 50:50 ratio of lactic and glycolic acid, degrading in about 50–60 days, but other combinations of monomer ratios have also been used, such as 65:35, 75:25 and 85:15, which have progressively longer *in vivo* life times.

According to Kumari et al.[124] PLGA has been used to obtain medicines, vaccines and nanoparticles for gene delivery systems and for the presentation of antigens and

growth factors. Studies performed by Eldridged et al.[125] have demonstrated that PLGA particles smaller than 10 μm may be efficiently phagocytosized by macrophages and that larger particles tend to rupture before they are phagocytosized, whicht may reduce the absorption efficiency of the entrapped active agent.

There are several factors that can influence the release profile of active agents incorporated into PLGA-based particles. As described by Kumari et al.[124] particle mean diameter, size distribution, surface morphology, surface chemistry, surface charge, surface adhesion, surface erosion, internal porosity, drug encapsulation efficiency, drug stability, drug diffusivity, drug release kinetics and hemodynamics must be considered. Furthermore, changes in PLGA molar mass and copolymer composition can result in different drug release behaviors. Increases in molar mass and in lactic acid content tend to reduce the drug release rate, while zero order release kinetics is obtained if PLGA with low molar mass is used. For high molar mass PLGA and different copolymer compositions, drug release behavior usually depends on the square root of time.[124]

PLGA has been used in the development of systems for the controlled release of proteins despite the negative effect of the acid-catalyzed nature of the polymer degradation on protein stability.[123] According to the same authors,[123] PLGA hydrolysis leads to the accumulation of acidic monomers, resulting in a reduction of pH of microenvironment and denaturation of the encapsulated proteins. Thus, several process modifications during particle production have been tested to overcome problems associated with protein degradation, such as coating the active agent with other materials prior to the incorporation in the particles[126–129] and adding stabilizers such as trehalose and albumin[130] or by complexing proteins with zinc and/or addition of antacid excipients.[131]

Coating and encapsulation of fine particles with PLGA using supercritical antisolvent processes were investigated by Wang et al.[93] A suspension of silica particles in an acetone–PLGA solution was used to evaluate the effects of process parameters. The coated particles seemed to be severely agglomerated as the polymer weight fraction was increased from 12.5 to 25.0%, reaching a mean size of 10 μm. High pressure also plays a critical role in the agglomeration of the particles, since increasing the pressure led to an increase at the average size of the agglomerates to 24.8 μm, probably due to the reduction of the glass transition temperature of the polymer. The amount of CO_2 absorbed by the polymer matrix changed the degree of plasticization of PLGA, favoring the redistribution of the coating on the surface of the particles. The operating temperature, on the other hand, appeared to have little effect on agglomeration, since at temperatures below the glass transition temperature such an effect was not observed. However, at temperatures above T_g, strong particle agglomeration was noticed, probably because of the

sintering effect on the particles. The use of surfactants to suppress agglomeration was not effective.

PLGA particle production as a strategy to coat hydrocortisone particles through the use of a supercritical antisolvent process is also described in the literature.[94] When the polymer to drug ratio was increased from 1:4 to 1:2, PLGA was more effectively deposited on the surface of the drug particles. At a 1:1 polymer to drug ratio, an improvement in drug encapsulation efficiency was observed, however the polymer was not evenly distributed on the surface of the particles, mostly due to the irregularity of the hydrocortisone particles themselves. Similar methods can be used for encapsulating proteins and other types of active agents, since this approach does not require dissolving the host particles (drugs) in organic solvents before the polymer coating process. There is a clear advantage to this approach, because the use of non toxic organic solvents is indeed a recurring issue in particle formation processes. As shown by Mayo et al.[68] 85:15 PLGA nanoparticles incorporating high amounts of the non-viral plasmidial DNA pEGFP and pFlt23 K (up to around 20% in weight), with incorporation efficiencies close to 100%, may be successfully obtained using ethyl acetate instead of DCM, resulting in particles containing low residual organic solvent levels (below 50 ppm). These results are quite relevant, showing that the supercritical fluid technology is a feasible alternative to obtain particles narrow in size and loaded with plasmids, with potential application in gene therapy.

PLA/PLGA-based particles may also be efficiently produced, as shown by Kang et al.[98, 99] and Jordan et al.[100] PLA/PLGA particles loaded with indomethacin were prepared by Kang et al.[98] through the SEDS method using DCM as solvent. The particles obtained showed a mean diameter of 2.35 μm, while placebo PLLA/PLGA microparticles were even smaller, presenting a mean size of 1.65 μm. Jordan et al.[100] on the other hand, attained much larger PLGA/PLA particles (around 93 μm) through the use of the PGSS strategy. The main advantage of this approach over the SEDS method is that it does not require the use of organic solvents. In addition, the PGSS method usually results in high drug encapsulation, allowing the production of particles incorporating molecules presenting no structural changes resulting from the processing at high loading efficiencies (near to 20–30%, depending on the type of active compound used).[132] This approach was used to circumvent the difficulty of forming fine particles from amorphous PLGA only, as both polymers have different nucleation rates in the supercritical process. This strategy is commonly used not only to solve the fine particle formation problem but also to modulate the degradation rates of PLLA/PLGA blends due to the different degradation rates of PLLA and PLGA.[100]

It is possible to use other approaches to improve the delivery of drugs incorporated in PLGA nano or microparticle systems, such as coating them with polymers such as

the mucoadhesive polycation chitosan, which is capable of providing longer residence times in mucosal tissue applications and rapid absorption of the drug.[107] The combination of PLGA/chitosan system with methoxy polyethylene glycol has been studied as well, showing improvement in the morphology and the processability of the particles themselves.[107]

3.3. Polycaprolactone

Polycaprolactone (PCL) is another polymeric material which has significant use in the biomaterials field. This compound is a linear[133] poly(α-hydroxyester) formed of repeating units of hexanoate,[134] with hydrophobic characteristics. Its repeating unit consists of a relatively polar ester group and five non-polar methylene groups.[135] It is a semicrystalline polymer,[133] presenting crystallinity between 45–69%[110] and low melting temperature (60 °C). Its physical, mechanical and also thermal properties are dependent on its molar mass and on its degree of crystallinity.[134]

The main attributes that make this polymer so suitable for the production of controlled drug delivery devices are its high permeability to many drugs and its non-toxic character.[136] In addition, its biodegradability can be easily improved to suitable periods by combination with other synthetic polymers.[137] *In vivo*, its degradation time is on the order of three years,[138] and its relatively easy degradation when exposed to physiological conditions is attributed to the presence of unstable ester groups in its structure.[135]

According to Sinha et al.[136] PCL was first identified in 1973, and its properties of biodegradability were then characterized. Initially, it was suggested that the degradation of PCL showed a two-stage pattern.[139] In the first stage, a decrease in the polymer molar mass without mass loss and/or deformation is observed, while in the second stage, the polymer molar mass would be reduced to 5000 Da. The same authors observed that at 40 °C the degradation rate was identical to polymer *in vitro* hydrolysis, obeying first-order kinetics. More recently it was proposed that in the first stage of the PCL degradation process, the amorphous phase of the polymer was degraded, leading to an increase in polymer crystallinity, while its molar mass remained constant.[136] In the second stage, cleavage of the ester bridges occurs, resulting in polymer mass loss[134] due to chain scission. This allows the production of smaller polymer fragments that diffuse out of the matrix, thus increasing the probability of phagocytosis. Cleavage of the terminal chains under high temperature is commonly observed, while random cleavage occurs at low temperatures.[140] Finally, the product of degradation of PCL, 6-hydroxycaproic acid, is absorbed or removed under physiological conditions[141] through the tricarboxylic acid cycle.[137]

The increased use of PCL in the production of controlled delivery devices is attributed to its ability to form

drug carriers that allow high drug permeation, to the fact that no acidification of the microenvironment during degradation is observed, and to its ability to easily form blends.[136]

Thus, blending PCL with other polymers may improve and/or maintain its mechanical properties, diminish blend toxicity, provide a partial biodegradable character and control the release of bioactive molecules.[142]

Vega-González et al.[103] evaluated the use of a PMMA/PCLA-based blend for loading cholesterol. However, cholesterol incorporation was not successful, mainly due its solubility in CO_2 and in a CO_2/DCM mixture. Decreasing the contact time and CO_2 density in order to reduce cholesterol loss during the process of encapsulation would be attractive alternatives to improve process efficiency. Pigments such as β-carotene, active against oxidation and degradation processes,[96] were also loaded in PCL particles (with a size range of 270–650 μm) by the PGSS process. In this study, it was observed that decreasing of PCL molar mass led to a decrease in mean particle diameter. Larger particles were obtained if both the system pressure and temperature were increased.

In some cases, the use of supercritical fluid technology results in higher efficiency of drug incorporation when compared to other methods. High encapsulation efficiency of rosemary extract in PCL particles (82.8%) was attained when a supercritical antisolvent process was employed, as described by Yesil-Celiktas and Cetin-Uyanikgil.[97] The traditional technology of solvent evaporation gave lower values (62.2%), and the increase in encapsulation efficiency was attributed to the presence of CO_2, that dilutes the polymer/drug mixture, thus decreasing the equilibrium concentration and mole fraction of the solute. In this situation, the chemical potential is reduced, thereby enhancing encapsulation efficiency. It was observed that the mean particle size decreased from 696 to 254 nm with the increase in pressure from 20 to 30 MPa. Furthermore, the particles obtained through the supercritical fluid method exhibited better sphere structures and smoother surfaces than the particles produced by the solvent evaporation method. In addition to lower mean particle size, more appropriate particle size distribution and higher encapsulation efficiency were achieved for the particles prepared through the supercritical fluid approach. However, the active compound diffusion rate and the release profiles in aqueous medium from both types of particles were very similar.

4. FINAL REMARKS

The encapsulation or co-precipitation of bioactive agents with polymers aiming at the production of devices for controlled release or to protect them from the environment is receiving special attention in recent years. Among the available polymers used for that purpose stand the poly(α-hydroxyesters) PLA, PLGA and PCL and amongst the

REVIEW

methodologies to effectively produce these devices, special interest has been given lately to supercritical fluid-based technologies. Their significance is mainly related to the versatility of these methods, which allow manufacturing particles with sizes from nano to micrometers. Independent of the advantages of the use of supercritical fluid technologies, such as safety regarding solvent choice, many parameters should be optimized to obtain particles with a particular set of characteristics, and most of the time this is not a trivial task. The understanding of the effects of the operational conditions on the size of the particles produced is of paramount importance to develop a specific and reproducible method. Specific issues such as the removal of organic chloride solvents that are usually employed in these methods without extracting the active compound, the scale up of the process, the control of particle morphology and size and improvement in the loading efficiency should still be further addressed to transform these methods into standard industrial choices.

References and Notes

1. A. C. Lima, P. Sher, and J. F. Mano, Production methodologies of polymeric and hydrogel particles for drug delivery applications. *Expert Opin. Drug Deliv.* 9, 231 (**2012**).
2. S. Parveen, R. Misra, and S. K. Sahoo, Nanoparticles: A boon to drug delivery, therapeutics, diagnostics and imaging. *Nanomedicine: Nanotechnol. Biol. Med.* 8, 147 (**2012**).
3. M. E. Helgeson, S. C. Chapin, and P. S. Doyle, Hydrogel microparticles from lithographic processes: Novel materials for fundamental and applied colloid science. *Curr. Opin. Colloid Interface Sci.* 16, 106 (**2011**).
4. Y. Krishnamachari, S. M. Geary, C. D. Lemke, and A. K. Salem, Nanoparticle delivery systems in cancer vaccines. *Pharm. Res.* 28, 215 (**2011**).
5. M. B. Oliveira and J. F. Mano, Polymer-based microparticles in tissue engineering and regenerative medicine. *Biotechnol. Prog.* 27, 897 (**2011**).
6. H. Peniche and C. Peniche, Chitosan nanoparticles: A contribution to nanomedicines. *Polym. Int.* 60, 883 (**2011**).
7. K. C. Petkar, S. S. Chavhan, S. Agatonovik-Kustrin, and K. K. Sawant, Nanostructured materials in drug and gene delivery: A review of the state of the art. *Crit. Rev. Ther. Drug Carrier Syst.* 28, 101 (**2011**).
8. J. P. Rao and K. E. Geckeler, Polymer nanoparticles: Preparation techniques and size-control parameters. *Prog. Polym Sci.* 36, 887 (**2011**).
9. V. T. Tran, J. P. Benoit, and M. C. Venier-Julienne, Why and how to prepare biodegradable, monodispersed, polymeric microparticles in the field of pharmacy? *Int. J. Pharm.* 407, 1 (**2011**).
10. S. Vrignaud, J. P. Benoit, and P. Saulnier, Strategies for the nanoencapsulation of hydrophilic molecules in polymer-based nanoparticles. *Biomaterials* 32, 8593 (**2011**).
11. J. Zhong and L. C. Dai, Liposomal preparation by supercritical fluids technology. *Afr. J. Biotechnol.* 10, 16406 (**2011**).
12. M. Irfan and M. Seiler, Encapsulation using hyperbranched polymers: From research and technologies to emerging applications. *Ind. Eng. Chem. Res.* 49, 1169 (**2010**).
13. N. V. N. Jyothi, P. M. Prasanna, S. R. Sakarkar, K. S. Prabha, P. S. Ramaiah, and G. Y. Srawan, Microencapsulation techniques, factors influencing encapsulation efficiency. *J. Microencapsulation* 27, 187 (**2010**).
14. K. Blecher, A. Nasir, and A. Friedman, The growing role of nanotechnology in combating infectious disease. *Virulence* 2, 395 (**2011**).
15. A. Mahapatro and D. K. Singh, Biodegradable nanoparticles are excellent vehicle for site directed *in-vivo* delivery of drugs and vaccines. *J. Nanobiotechnol.* 9, 1 (**2011**).
16. L. Plapied, N. Duhem, A. Rieux, and V. Préat, Fate of polymeric nanocarriers for oral drug delivery. *Curr. Opin. Colloid Interface Sci.* 16, 228 (**2011**).
17. G. Lövestam, H. Rauscher, G. Roebben, B. S. Klüttgen, N. Gibson, J. P. Putaud, and H. Stamm, Considerations on a definition of nanomaterial for regulatory purposes, Publications Office of the European Union, Luxembourg (**2010**), p. 36.
18. K. Byrappa, S. Ohara, and T. Adschiri, Nanoparticles synthesis using supercritical fluid technology—towards biomedical applications. *Adv. Drug Delivery Rev.* 60, 299 (**2008**).
19. Future Markets Inc., The Global Market for Nanomaterials 2002—2016, Production Volumes, Revenues and End User Market Demand, available at www.futuremarketsinc.com. (**2012**), p. 342.
20. M. C. Roco, The long view of nanotechnology development: The national nanotechnology initiative at 10 years. *J. Nanopart. Res.* 13, 427 (**2011**).
21. S. Kim and J. Lee, Effective polymeric dispersants for vacuum, convection and freeze drying of drug nanosuspensions. *Int. J. Pharm.* 397, 218 (**2010**).
22. P. S. C. Sacchetin, A. M. Moraes, C. A. G. Leal, and H. C. P. Figueiredo, Production by emulsion method of alginate microparticles containing inactivated Flavobacterium columnare for oral fish vaccination. *Quim. Nova* 33, 263 (**2010**).
23. A. P. Rodrigues, D. Hirsch, H. C. P. Figueiredo, P. V. Logatto, and A. M. Moraes, Production and characterisation of alginate microparticles incorporating *Aeromonas hydrophila* designed for fish oral vaccination. *Process Biochem.* 41, 638 (**2006**).
24. T. Jung, W. Kamm, A. Breitenbach, E. Kaiserling, J. X. Xiao, and T. Kissel, Biodegradable nanoparticles for oral delivery of peptides: Is there a role for polymers to affect mucosal uptake? *Eur. J. Pharm. Biopharm.* 50, 147 (**2000**).
25. D. Williams, The relationship between biomaterials and nanotechnology. *Biomaterials* 29, 1737 (**2008**).
26. J. Lee, J. Y. Choi, and C. H. Park, Characteristics of polymers enabling nano-comminution of water-insoluble drugs. *Int. J. Pharm.* 355, 328 (**2008**).
27. H. K. Chan and P. C. L. Kwok, Production methods for nanodrug particles using the bottom-up approach. *Adv. Drug Delivery Rev.* 63, 406 (**2011**).
28. A. Bhakay, M. Merwade, E. Bilgili, and R. N. Dave, Novel aspects of wet milling for the production of microsuspensions and nanosuspensions of poorly water-soluble drugs. *Drug Dev. Ind. Pharm.* 37, 963 (**2011**).
29. Z. Shaoli and Z. Wei, Topical review: Design, fabrication, and applications of hybrid nanostructured array. *J. Nanomaterials* 2012, 1 (**2012**).
30. J. Pan, S. Y. Chan, W. G. Lee, and L. F. Kang, Microfabricated particulate drug-delivery systems. *Biotechnol. J.* 6, 1477 (**2011**).
31. P. W. Chen, R. M. Erb, and A. R. Studart, Designer polymer-based microcapsules made using microfluidics. *Langmuir* 28, 144 (**2012**).
32. J. T. Wang, J. Wang, and J. J. Han, Fabrication of advanced particles and particle-based materials assisted by droplet-based microfluidics. *Small* 7, 1728 (**2011**).
33. D. Dendukuri and P. S. Doyle, The synthesis and assembly of polymeric microparticles using microfluidics. *Adv. Mater.* 21, 4071 (**2009**).
34. N. Mishra, A. K. Goyal, K. Khatri, B. Vaidya, R. Paliwal, S. Rai, A. Mehta, S. Tiwari, S. Vyas, and S. P. Vyas, Biodegradable polymer-based particulate carrier(s) for the delivery of proteins and peptides. *Anti-Inflammatory Anti-Allergy Agents Med. Chem.* 7, 240 (**2008**).

35. I. Pasquali, R. Bettini, and F. Giordano, Supercritical fluid technologies: An innovative approach for manipulating the solid-state of pharmaceuticals. *Adv. Drug Delivery Rev.* 60, 399 (**2008**).

36. O. Yesil-Celiktas and D. Senyay, The Breadth and Intensity of Supercritical Particle Formation Research with an Emphasis on Publication and Patent Disclosures. *Ind. Eng. Chem. Res.* 49, 7017 (**2010**).

37. M. J. Cocero, A. Martín, F. Mattea, and S. Varona, Encapsulation and o-precipitation processes with supercritical fluids: Fundamentals and applications. *J. Supercrit. Fluids* 47, 546 (**2009**).

38. K. Mishima, Biodegradable particle formation for drug and gene delivery using supercritical fluid and dense gas. *Adv. Drug Delivery Rev.* 60, 411 (**2008**).

39. K. Moribe, Y. Tozuka, and K. Yamamoto, Supercritical carbon dioxide processing of active pharmaceutical ingredients for polymorphic control and for complex formation. *Adv. Drug Delivery Rev.* 60, 328 (**2008**).

40. I. Pasquali and R. Bettini, Are pharmaceutics really going supercritical? *Int. J. Pharm.* 364, 176 (**2008**).

41. E. Reverchon, R. Adami, G. Caputo, and I. De Marco, Spherical microparticles production by supercritical antisolvent precipitation: Interpretation of results. *J. Supercrit. Fluids* 47, 70 (**2008**).

42. T. Yasuji, H. Takeuchi, and Y. Kawashima, Particle design of poorly water-soluble drug substances using supercritical fluid technologies. *Adv. Drug Delivery Rev.* 60, 388 (**2008**).

43. M. Bahrami and S. Ranjbarian, Production of micro- and nano-composite particles by supercritical carbon dioxide. *J. Supercrit. Fluids* 40, 263 (**2007**).

44. C. Aymonier, A. Loppinet-Serani, H. Reverón, Y. Garrabos, and F. Cansell, Review of supercritical fluids in inorganic materials science. *J. Supercrit. Fluids* 38, 242 (**2006**).

45. E. Reverchon and R. Adami, Nanomaterials and supercritical fluids. *J. Supercrit. Fluids* 37, 1 (**2006**).

46. S. D. Yeo and E. Kiran, Formation of polymer particles with supercritical fluids: A review. *J. Supercrit. Fluids* 34, 287 (**2005**).

47. C. Roy, A. Vega-Gonzalez, and P. Subra-Paternault, Theophylline formulation by supercritical antisolvents. *Int. J. Pharm.* 343, 79 (**2007**).

48. Y. Kang, C. Yang, P. Ouyang, G. Yin, Z. Huang, Y. Yao, and X. Liao, The preparation of BSA-PLLA microparticles in a batch supercritical anti-solvent process. *Carbohydr. Polym.* 77, 244 (**2009**).

49. S. P. Lin and R. D. Reitz, Drop and spray formation from a liquid jet. *Annu. Rev. Fluid Mech.* 30, 85 (**1998**).

50. A. Erriguible, S. Vincent, and P. Subra-Paternault, Numerical investigations of liquid jet breakup in pressurized carbon dioxide: Conditions of two-phase flow in supercritical antisolvent process. *J. Supercrit. Fluids* 63, 16 (**2012**).

51. F. Marra, I. De Marco, and E. Reverchon, Numerical analysis of the characteristic times controlling supercritical antisolvent micronization. *Chem. Eng. Sci.* 71, 39 (**2012**).

52. A. Braeuer, R. Adami, S. Dowy, M. Rossmann, and A. Leipertz, Observation of liquid solution volume expansion during particle precipitation in the supercritical CO_2 antisolvent process. *J. Supercrit. Fluids* 56, 121 (**2011**).

53. A. Braeuer, S. Dowy, E. Torino, M. Rossmann, S. K. Luther, E. Schluecker, A. Leipertz, and E. Reverchon, Analysis of the supercritical antisolvent mechanisms governing particles precipitation and morphology by in situ laser scattering techniques. *Chem. Eng. J.* 173, 258 (**2011**).

54. I. De Marco and E. Reverchon, Influence of pressure, temperature and concentration on the mechanisms of particle precipitation in supercritical antisolvent micronization. *J. Supercrit. Fluids* 58, 295 (**2011**).

55. J. Baldyga, R. Czarnocki, B. Y. Shekunov, and K. B. Smith, Particle formation in supercritical fluids—Scale-up problem. *Chem. Eng. Res. Des.* 88, 331 (**2010**).

56. E. Reverchon, S. Torino, A. Dowy, A. Braeuer, and A. Leipertz, Interactions of phase equilibria, jet fluid dynamics and mass transfer during supercritical antisolvent micronization. *Chem. Eng. J.* 156, 446 (**2010**).

57. T. Petit-Gas, O. Boutin, I. Raspo, and E. Badens, Role of hydrodynamics in supercritical antisolvent processes. *J. Supercrit. Fluids* 51, 248 (**2009**).

58. A. Bouchard, N. Jovanovic, A. H. de Boer, A. Martín, W. Jiskoot, D. J. A. Crommelin, G. W. Hofland, and G. J. Witkamp, Effect of the spraying conditions and nozzle design on the shape and size distribution of particles obtained with supercritical fluid drying. *Eur. J. Pharm. Biopharm.* 70, 389 (**2008**).

59. A. Gokhale, B. Khusid, R. N. Dave, and R. Pfeffer, Effect of solvent strength and operating pressure on the formation of submicrometer polymer particles in supercritical microjets. *J. Supercrit. Fluids* 43, 341 (**2007**).

60. E. Badens, O. Boutin, and G. Charbit, Laminar jet dispersion and jet atomization in pressurized carbon dioxide. *J. Supercrit. Fluids* 36, 81 (**2005**).

61. A. Martin and M. J. Cocero, Numerical modeling of jet hydrodynamics, mass transfer, and crystallization kinetics in the supercritical antisolvent (SAS) process. *J. Supercrit. Fluids* 32, 203 (**2004**).

62. F. Miguel, A. Martín, F. Mattea, and M. J. Cocero, Precipitation of lutein and co-precipitation of lutein and poly-lactic acid with the supercritical anti-solvent process. *Chem. Eng. Proc.* 47, 1594 (**2008**).

63. E. Carretier, E. Badens, P. Guichardon, O. Boutin, and G. Charbit, New insight into micromixing in supercritical CO_2 using a chemical method. *Ind. Eng. Chem. Res.* 42, 332 (**2003**).

64. E. Reverchon and I. De Marco, Mechanisms controlling supercritical antisolvent precipitate morphology. *Chem. Eng. J.* 169, 358 (**2011**).

65. M. Rossmann, A. Braeuer, S. Dowy, T. G. Gallinger, A. Leipertz, and E. Schluecker, Solute solubility as criterion for the appearance of amorphous particle precipitation or crystallization in the supercritical antisolvent (SAS) process. *J. Supercrit. Fluids* 66, 350 (**2012**).

66. E. Reverchon, I. De Marco, and E. Torino, Nanoparticles production by supercritical antisolvent precipitation: A general interpretation. *J. Supercrit. Fluids* 43, 126 (**2007**).

67. M. Furlan, J. Kluge, M. Mazzotti, and M. Lattuada, Preparation of biocompatible magnetite–PLGA composite nanoparticles using supercritical fluid extraction of emulsions. *J. Supercrit. Fluids* 54, 348 (**2010**).

68. A. S. Mayo, B. K. Ambati, and U. B. Kompella, Gene delivery nanoparticles fabricated by supercritical fluid extraction of emulsions. *Int. J. Pharm.* 387, 278 (**2010**).

69. J. Kluge, F. Fusaro, N. Casas, M. Mazzotti, and G. Muhrer, Production of PLGA micro- and nanocomposites by supercritical fluid extraction of emulsions: I. Encapsulation of lysozyme. *J. Supercrit. Fluids* 50, 327 (**2009**).

70. J. Kluge, F. Fusaro, N. Casas, M. Mazzotti, and G. Muhrer, Production of PLGA micro- and nanocomposites by supercritical fluid extraction of emulsions: II. Encapsulation of ketoprofen. *J. Supercrit. Fluids* 50, 336 (**2009**).

71. M. A. McHugh and V. J. Krukonis, Supercritical Fluid Extraction: Principles and Practice, 2nd edn., Butterworth-Heinemann, Boston (**1994**).

72. A. Chen, Z. Zhao, S. Wang, Y. Li, C. Zhao, and Y. Liu, A continuous RESS process to prepare PLA–PEG–PLA microparticles. *J. Supercrit. Fluids* 59, 92 (**2011**).

73. M. I. Ul-Haq, A. Acosta-Ramírez, P. Mehrkhodavandi, and R. Signorell, Influence of polydispersity of poly(lactic acid) on particle formation by rapid expansion of supercritical CO_2 solutions. *J. Supercrit. Fluids* 51, 376 (**2010**).

REVIEW

74. B. Kongsombut, A. Tsutsumi, N. Suankaew, and T. Charinpanitkul, Encapsulation of SiO_2 and TiO_2 fine powders with poly(DL-lactic-co-glycolic acid) by rapid expansion of supercritical CO_2 incorporated with ethanol cosolvent. *Ind. Eng. Chem. Res.* 48, 11230 (**2009**).

75. A. Sane and M. C. Thies, Effect of material properties and processing conditions on RESS of poly(L-lactide). *J. Supercrit. Fluids* 40, 134 (**2007**).

76. K. Matsuyama, Z. Donghuib, T. Urabea, and K. Mishima, Formation of l-poly(lactic acid) microspheres by rapid expansion of CO_2 saturated polymer suspensions. *J. Supercrit. Fluids* 33, 275 (**2005**).

77. A. Sane and J. Limtrakul, Formation of retinyl palmitate-loaded poly(L-lactide) nanoparticles using rapid expansion of supercritical solutions into liquid solvents (RESOLV). *J. Supercrit. Fluids* 51, 230 (**2009**).

78. M. J. Meziani, P. Pathak, T. Desai, and Y. Sun, Supercritical fluid processing of nanoscale particles from biodegradable and biocompatible polymers. *Ind. Eng. Chem. Res.* 45, 3420 (**2006**).

79. H. Tian, Z. Tang, X. Zhuang, X. Chen, and X. Jing, Biodegradable synthetic polymers: Preparation, functionalization and biomedical application. *Prog. Polym. Sci.* 37, 237 (**2012**).

80. M. Sarkari, I. Darrat, and B. L. Kutson, Generation of microparticles using CO_2 and CO_2-philic antisolvents. *AIChE J.* 46, 1850 (**2000**).

81. S. Taki, E. Badens, and G. Charbit, Controlled release system formed by supercritical anti-solvent coprecipitation of a herbicide and a biodegradable polymer. *J. Supercrit. Fluids* 21, 61 (**2001**).

82. M. Rantakyla, M. Jantti, O. Aaltonen, and M. Hurme, The effect of initial drop size on particle size in the supercritical antisolvent precipitation (SAS) technique. *J. Supercrit. Fluids* 24, 251 (**2002**).

83. L. S. Tu, F. Dehghcini, and N. R. Foster, Micronisation and microencapsulation of pharmaceuticals using a carbon dioxide antisolvent. *Powder Technol.* 126, 134 (**2002**).

84. O. Boutin, E. Badens, E. Carretier, and G. Charbit, Co-precipitation of a herbicide and biodegradable materials by the supercritical antisolvent technique. *J. Supercrit. Fluids* 31, 89 (**2004**).

85. Y. P. Diego, H. C. Pellikaan, F. E. Wubbolts, G. J. Witkamp, and P. J. Jansens, Operating regimes and mechanism of particle formation during the precipitation of polymers using the PCA process. *J. Supercrit. Fluids* 35, 147 (**2005**).

86. D. L. Obrzut, P. W. Bell, C. B. Roberts, and S. R. Duke, Effect of process conditions on the spray characteristics of a PLA + methylene chloride solution in the supercritical antisolvent precipitation process. *J. Supercrit. Fluids* 42, 299 (**2007**).

87. V. Patomchaiviwat, O. Paeratakul, and P. Kulvanich, Formation of inhalable rifampicin-poly(L-lactide) microparticles by supercritical anti-solvent process. *AAPS Pharm. Sci. Tech.* 9, 1119 (**2008**).

88. A. Z. Chen, Y. Q. Kang, X. M. Pu, G. F. Yin, Y. Li, and J. Y. Hu, Development of Fe3O4-poly(L-lactide) magnetic microparticles in supercritical CO_2. *J. Colloid Interface Sci.* 330, 317 (**2009**).

89. A.-Z. Chen, Y. Li, F.-T. Chau, T.-Y. Lau, J.-Y. Hu, Z. Zhao, and D. K.-W. Mok, Microencapsulation of puerarin nanoparticles by poly(L-lactide) in a supercritical CO_2 process. *Acta Biomater.* 5, 2913 (**2009**).

90. W. He, Z. Jiang, Q. Suo, and G. Li, Mechanism of dispersing an active component into a polymeric carrier by the SEDS-PA process. *J. Mater. Sci.* 45, 467 (**2010**).

91. A. J. Baxendale, P. Van Hooffa, L. G. Durrant, I. Spendloveb, S. M. Howdle, H. M. Woods, M. J. Whitaker, O. R. Davies, A. Naylor, A. L. Lewis, and L. Illum, Single shot tetanus vaccine manufactured by a supercritical fluid encapsulation technology. *Int. J. Pharm.* 413, 147 (**2011**).

92. Y. Zhang, X. Liao, G. Yin, P. Yuan, Z. Huang, J. Gu, Y. Yao, and X. Chen, Preparation of water soluble drugs-loaded microparticles using modified solution enhanced dispersion by supercritical CO_2. *Powder Technol.* 221, 343 (**2012**).

93. Y. Wang, R. Pfeffer, R. Dave, and R. Enick, Polymer encapsulation of fine particles by a supercritical antisolvent process. *Am. Inst. Chem. Eng.* 51, 440 (**2005**).

94. Y. Wang, Y. Wang, J. Yang, R. Pfeffer, R. Dave, and B. Michniak, The application of supercritical solvent process for sustained drug delivery. *Powder Technol.* 164, 94 (**2006**).

95. G. D. Porta, N. Falco, and E. Reverchon, Continuous supercritical emulsions extraction: A new technology for biopolymer microparticles production. *Biotechnol. Bioeng.* 108, 676 (**2011**).

96. E. Paz, A. Martín, C. M. M. Duarte, and M. J. Cocero, Formulation of β-carotene with poly-(ε-caprolactones) by PGSS process. *Powder Technol.* 217, 77 (**2012**).

97. O. Yesil-Celiktas and E. O. Cetin-Uyanikgil, *In vitro* release kinetics of polycaprolactone encapsulated plant extract fabricated by supercritical antisolvent process and solvent evaporation method. *J. Supercrit. Fluids* 62, 219 (**2012**).

98. Y. Kang, J. Wua, G. Yin, Z. Huang, Y. Yao, X. Liao, A. Chen, X. Pu, and L. Liao, Preparation, characterization and *in vitro* cytotoxicity of indomethacin-loaded PLLA/PLGA microparticles using supercritical CO_2 technique. *Eur. J. Pharm. Biopharm.* 70, 85 (**2008**).

99. Y. Kang, G. Yin, P. Ouyang, Z. Huang, Y. Yao, X. Liao, A. Chen, and X. Pu, Preparation of PLLA/PLGA microparticles using solution enhanced dispersion by supercritical fluids (SEDS). *J. Colloid Interface Sci.* 322, 87 (**2008**).

100. F. Jordan, A. Naylor, C. A. Kelly, S. M. Howdle, A. Lewis, and L. Illum, Sustained release hGH microsphere formulation produced by a novel supercritical fluid technology: *In vivo* studies. *J. Controlled Release* 141, 153 (**2010**).

101. A. Breitenbach, D. Mohre, and T. Kissel, Biodegradable semicrystalline comb polyesters influence the microsphere production by means of a supercritical fluid extraction technique (ASES). *J. Controlled Released* 63, 53 (**2000**).

102. P. Caliceti, S. Salmaso, N. Elvassore, and A. Bertucco, Effective protein release from PEG/PLA nano-particles produced by compressed gas anti-solvent precipitation techniques. *J. Controlled Released* 94, 195 (**2004**).

103. A. Vega-Gonzalez, C. Domingo, C. Elvira, and P. Subra, Precipitation of PMMA/PCL blends using supercritical carbon dioxide. *J. Appl. Polym. Sci.* 91, 2422 (**2004**).

104. A. Vega-González, P. Subra-Paternault, A. M. López-Periago, C. A. García-González, and C. Domingo, Supercritical CO_2 antisolvent precipitation of polymer networks of l-PLA, PMMA and PMMA/PCL blends for biomedical applications. *Eur. Polym. J.* 44, 1081 (**2008**).

105. R. Ghaderi, P. Artursson, and J. Carlfors, A new method for preparing biodegradable microparticles and entrapment of hydrocortisone in DL-PLG microparticles using supercritical fluids. *Eur. J. Pharm. Sci.* 10, 1 (**2000**).

106. P. Ouyang, Y. Kang, G. Yin, Z. Huang, Y. Yao, and X. Liao, Fabrication of hydrophilic paclitaxel-loaded PLA-PEG-PLA microparticles via SEDS process. *Front. Mater. Sci. China* 3, 15 (**2009**).

107. L. Casettari, E. Castagnino, S. Stolnik, A. Lewis, S. M. Howdle, and L. Illum, Surface characterisation of bioadhesive PLGA/chitosan microparticles produced by supercritical fluid technology. *Pharm. Res.* 28, 1668 (**2011**).

108. R. A. Gross and B. Kalra, Biodegradable polymers for the environment. *Science* 297, 803 (**2002**).

109. P. Pan and Y. Inoue, Polymorphism and isomorphism in biodegradable polyesters. *Prog. Polym. Sci.* 34, 605 (**2009**).

110. Y. Dong, S. Liao, M. Ngiam, C. K. Chan, and S. Ramakrishna, Degradation behaviors of electrospun resorbable polyester nanofibers. *Tissue Eng. Part B* 15, 333 (**2009**).

111. H. Tsuji, Poly(lactide) stereocomplexes: Formation, structure, properties, degradation, and applications. *Macromol. Biosci.* 5, 569 (**2005**).

106

*J. Biomater. Tissue Eng. 3, 89–107, **2013***

112. A. Södergård and M. Stolt, Properties of lactic acid based polymers and their correlation with composition. *Prog. Polym. Sci.* 27, 1123 (**2002**).

113. I. Engelberg and J. Kohn, Physico-mechanical properties of degradable polymers used in medical applications: A comparative study. *Biomaterials* 12, 292 (**1991**).

114. M. C. Gupta and V. G. Deshmukh, Thermal oxidative degradation of poly-lactic acid Part I: Activation energy of thermal degradation in air. *Colloid Polym. Sci.* 260, 308 (**1982**).

115. D. K. Gilding and A. M. Reed, Biodegradable polymers for use in surgery-polyglycolic/poly(actic acid) homo- and copolymers: 1. *Polymer* 20, 1459 (**1979**).

116. M. Vert, S. Li, and H. Garreau, More about the degradation of LA/GA-derived matrices in aqueous media. *J. Controlled Release* 16, 15 (**1991**).

117. S. R. Andersson, M. Hakkarainen, S. Inkinen, A. Sodergård, and A. C. Albertsson, Polylactide stereocomplexation leads to higher hydrolytic stability but more acidic hydrolysis product pattern. *Biomacromolecules* 11, 1067 (**2010**).

118. S. M. Li, H. Garreau, and M. Vert, *In vivo* degradation of massive poly(a-hydroxy acids): Validation of *in vitro* findings. *J. Mater. Sci.: Mater. Med.* 1, 123 (**1990**).

119. K. Matsuyama and K. Mishima, Formation of TiO$_2$–polymer composite microparticles by rapid expansion of CO$_2$ saturated polymer suspensions with high shear mixing. *J. Supercrit. Fluids* 40, 117 (**2007**).

120. W. Jiang, R. K. Gupta, M. C. Deshpande, and S. P. Schwendeman, Biodegradable poly(lactic-co-glycolic acid) microparticulates for injectable controlled antigen delivery. *Adv. Drug Delivery Rev.* 57, 391 (**2005**).

121. M. Vajdy and D. T. O'Hagan, Microparticles for intranasal immunization. *Adv. Drug Delivery Rev.* 51, 127 (**2001**).

122. J. Panyam and V. Labhasetwar, Biodegradable nanoparticles for drug and gene delivery to cells and tissue. *Adv. Drug Delivery Rev.* 55, 329 (**2003**).

123. R. C. Mundargi, V. R. Babu, V. Rangaswamy, P. Patel, and T. M. Aminabhavi, Nano/micro technologies for delivering macromolecular therapeutics using poly(D,L-lactide-co-glycolide) and its derivatives. *J. Control. Release* 125, 193 (**2008**).

124. A. Kumari, S. K. Yadav, and S. C. Yadav, Biodegradable polymeric nanoparticles based drug delivery systems, *Colloids Surf., B* 75, 1 (**2010**).

125. J. H. Eldridge, J. K. Staas, J. A. Meulbroek, J. R. Mcghee, T. R. Tice, and R. M. Gilley, Biodegradable microspheres as a vaccine delivery system. *Mol. Immunol.* 28, 287 (**1991**).

126. C. H. Zheng, J. Q. Gao, Y. P. Zhang, and W. Q. Liang, A protein delivery system: Biodegradable alginate-chitosan-poly(lactic-co-glycolic acid) composite microspheres. *Biochem. Biophys. Res. Commun.* 323, 1321 (**2004**).

127. L. S. Liu, Y. J. Won, P. H. Cooke, D. R. Coffin, M. L. Fishman, K. B. Hicks, and P. X. Ma, Preparation of poly(lactic acid) and pectin composite films intended for applications in antimicrobial packaging. *Biomaterials* 25, 3201 (**2004**).

128. C. Martínez-Sancho, R. Herrero-Vanrell, and S. Negro, Optimisation of aciclovir poly(D,L-lactide-co-glycolide) microspheres for intravitreal administration using a factorial design study. *Int. J. Pharm.* 273, 45 (**2004**).

129. S. D. Patil, F. Papadimitrakopoulos, and D. J. Burgess, Dexamethasone-loaded poly(lactic-co-glycolic) acid microspheres/poly(vinyl alcohol) hydrogel composite coatings for inflammation control. *Diabetes Technol. Ther.* 6, 887 (**2004**).

130. P. Johansen, Y. Men, R. Audran, G. Corradin, H. P. Merkle, and B. Gander, Improving stability and release kinetics of microencapsulated tetanus toxoid by co-encapsulation of additives. *Pharm. Res.* 15, 1103 (**1998**).

131. H. L. Jiang, J. F. Jin, Y. Q. Hu, and K. J. Zhu, Improvement of protein loading and modulation of protein release from poly(lactide-co-glycolide) microspheres by complexation of proteins with polyanions. *J. Microencapsul.* 21, 615 (**2004**).

132. O. R. Davies, A. L. Lewis, M. J. Whitaker, H. Tai, K. M. Shakesheff, and S. M. Howdle, Applications of supercritical CO$_2$ in the fabrication of polymer systems for drug delivery and tissue engineering. *Adv. Drug Delivery Rev.* 60, 373 (**2008**).

133. G. Gorrasi, L. Vertuccio, L. Annunziata, C. Pellecchia, and D. Pappalardo, Correlations between microstructural characterization and thermal properties of well defined poly(e-caprolactone) samples by ring opening polymerization with neutral and cationic bis(2,4,6-triisopropylphenyl)tin(IV) compounds. *React. Funct. Polym.* 70, 151 (**2010**).

134. M. Labet and W. Thielemans, Synthesis of polycaprolactone: A review. *Chem. Soc. Rev.* 38, 3484 (**2009**).

135. X. Wei, C. Gong, M. Gou, S. Fu, Q. Guo, S. Shi, F. Luo, G. Guo, L. Qiu, and Z. Qian, Biodegradable poly(epsilon-caprolactone)-poly(ethylene glycol) copolymers as drug delivery system. *Int. J. Pharm.* 381, 1 (**2009**).

136. V. R. Sinha, K. Bansal, R. Kaushik, R. Kumria, and A. Trehan, Poly-epsilon-caprolactone microspheres and nanospheres: An overview. *Int. J. Pharm.* 278, 1 (**2004**).

137. Y. Wan, B. Xiao, S. Dalai, X. Cao, and Q. Wu, Development of polycaprolactone/chitosan blend porous scaffolds. *J. Mater. Sci.: Mater. Med.* 20, 719 (**2009**).

138. H. Sun, L. Mei, C. Song, X. Cui, and P. Wang, The *in vivo* degradation, absorption and excretion of PCL-based implant. *Biomaterials* 27, 1735 (**2006**).

139. C. G. Pitt, A. Schinder, and A. Capronor, A biodegradable delivery system for levonorgestrel, Long-Acting Contraceptive Systems, edited by G. L. Zatachini, Harper and Row, Philadelphia (**1984**), pp. 63—84.

140. P. Joshi and G. Madras, Degradation of Poly(caprolactone) in supercritical fluids. *Polym. Degrad. Stab.* 93, 1901 (**2008**).

141. F. Lince, D. L. Marchisio, and A. A. Barresi, Strategies to control the particle size distribution of poly-caprolactone nanoparticles for pharmaceutical application. *J. Colloid Interface Sci.* 322, 505 (**2008**).

142. C. Elvira, A. Fanovich, M. Fernandez, J. Fraile, J. San Roman, and C. Domingo, Evaluation of drug delivery characteristics of microspheres of PMMA-PCL-cholesterol obtained by supercritical-CO$_2$ impregnation and by dissolution-evaporation techniques. *J. Controlled Release* 99, 231 (**2004**).

REVIEW

Controlling the Interaction Between Cells and Silica Nanoparticles

Andrea Mathilde Mebert, Daniela Edhit Camporotondi, María Lucia Foglia,
Gisela Solange Alvarez, Pablo Luis Santo Orihuela, Luis Eduardo Diaz,
and Martín Federico Desimone*

*Facultad de Farmacia y Bioquímica, Universidad de Buenos Aires, Junín 956 Piso 3°,
(1113) Ciudad Autónoma de Buenos Aires, Argentina*

In recent years, the application of silica nanoparticles in the biomedical field experienced a great development, showing a sharp increase in the number of published articles and patents. The driving forces for these and future developments are the possibility to design nanoparticles with homogeneous size and structure and amenable to specific grafting. In this way, it is possible to control the interaction of nanoparticles with cells. Moreover, it is possible to tune the characteristics of the nanoparticles to meet the requirements of each specific cell and desired application. Herein, we present different strategies developed to optimize the size, morphology, surface topography, elemental ratio, hydrophobic/hydrophilic balance, and erosion rate, which contribute to understand the nature of this inherently complicated cell-nanoparticles interactions mechanism, which will determine the resulting function performance.

Keywords: Cells, Nanoparticles, Silica, Toxicity.

REVIEW

CONTENTS

1. INTRODUCTION

The sol–gel process has several well-known advantages such as a choice of high purity precursors (monomers or condensed species), homogeneity of the obtained material with different shapes (i.e., gels, films, particles)[1,2] and especially the possibility of making hybrids and composite materials with new chemical and mechanical properties, conductivity and permeability.[3–5] Moreover, slight changes

in experimental parameters such as pH, additives, and concentration can lead to substantial modification of the resulting material.[6,7] In recent years, biomedical applications of sol–gel technology have received extensive coverage.[8–13] Particularly, the application of silica nanoparticles in the biomedical field experienced a great development, showing a sharp increase in the number of published articles and patents.[14,15] The driving forces for these and future developments are the possibility to design nanoparticles with homogeneous size, structure and amenable to specific grafting, which provides structural support and delivery systems for therapeutic purposes.[16–18]

The effect of various silica formulations such as plain, mesoporous and hollow silica nanoparticles are being currently investigated. Nowadays, different silica nanoparticles can be obtained through well known procedures.[19–25] The most popular is undoubtedly the Stöber method.[22] This method allows the synthesis of monodisperse, spherical silica nanoparticles that range from 5 to 2000 nm, through an ammonia-catalyzed reaction of tetraethylorthosilicate (TEOS) with water in low-molecular-weight alcohols.[26] Another method used to obtain solid silica particles involves the preparation of water-in-oil microemulsions, where the droplets of the water polar phase dispersed in a continuous oil phase are used as nanoreactors for the synthesis of silica nanoparticles.[24,27] Secondly, hollow silica

Andrea Mathilde Mebert was born in Erlangen, Germany, in 1983. As a child she moved to Buenos Aires, Argentina, where she graduated in Pharmacy from the University of Buenos Aires (2010). She currently holds a doctoral fellowship granted by Agencia Nacional de Promoción Científica y Tecnológica and she is working on her Ph.D. She also holds a first level laboratory instructor at the Department of Analytical and Physical Chemistry of the Faculty of Pharmacy and Biochemistry, University of Buenos Aires. Her researches are oriented to biomaterials including nanomaterials.

Daniela Edhit Camporotondi was born in Buenos Aires, Argentina, in 1986. This year, she graduated in Pharmacy at University of Buenos Aires. Since 2009, she has been working as a second level laboratory instructor at the Department of Analytical and Physical Chemistry of the Faculty of Pharmacy and Biochemistry, and she has been taking part of the biocompatible nanomaterials research project as well.

María Lucia Foglia was born in Buenos Aires in 1984. She graduated in Pharmacy from the University of Buenos Aires in 2008 and is working on her Ph.D. since 2009 in the same institution. She currently holds a doctoral fellowship granted by the National Research Council (CONICET) and a teaching assistant position in Instrumental Analysis at the Faculty of Pharmacy and Biochemistry, which belongs to the University of Buenos Aires. Her research interests include the obtention of biomaterials by the sol–gel route and the possibility to incorporate nanoparticles for drug delivery.

Gisela Solange Alvarez was born in Buenos Aires in 1980. She graduated in Biochemistry (2005) and Pharmacy (2008) at Universidad de Buenos Aires and received her Ph.D. degree in the Biotechnology field from the same institution (2010). She currently holds a full teaching assistant position in Instrumental Analysis of the Faculty of Pharmacy and Biochemistry at Universidad de Buenos Aires. Her research interests are focused on biomaterials and nanocarriers for drug delivery and at the moment she is holding a posdoctoral fellowship granted by the National Research Council (CONICET).
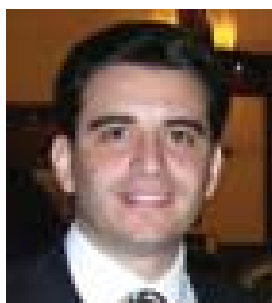
Pablo Luis Santo Orihuela was born in Buenos Aires in 1974. He graduated in Biochemistry (2001) at Universidad de Buenos Aires and received his Ph.D. degree in Toxicology from the same institution (2008). He received his M.Sc. in Pest Control and its Environmental Impact from Universidad de General San Martín, Buenos Aires. He currently holds a teaching assistant position in Instrumental Analysis of the Faculty of Pharmacy and Biochemistry at Universidad de Buenos Aires. His research interests are focused on insecticides, nanocarriers, biochemical and molecular bases of insecticides resistance of vector human disease insects.

REVIEW

Luis Eduardo Diaz is full professor of Instrumental Analytical Chemistry and Head of the Department of Analytical, Inorganic, and Physicochemical Chemistry of the Faculty of Pharmacy and Biochemistry at the University of Buenos Aires (Argentina). Today he currently leads a research group working on: (a) biomaterials, especially in bioceramics, drug delivery systems and smart targeted nanosystems for drug delivery, and (b) hybrid bioremediation systems.

Martún Federico Desimone was born in 1974 in Buenos Aires, Argentina. He graduated from Pharmacy and Biochemistry at University of Buenos Aires and received his Ph.D. degree from the same University. After a postdoctoral period in the University of the Basque Country, Spain, with Professor Dr. J. L. Pedraz, he joined in 2008, the Thibaud Coradin's group in the Laboratoire Chimie de la Matiére Condensée de Paris. Actually, he holds an Adjunct Professor position in the Faculty of Pharmacy and Biochemistry at the University of Buenos Aires. He is a CONICET researcher and the director of the biocompatible nanomaterials project.

REVIEW

nanoparticles (HSNP) are gaining great attention. They consist of hollow spherical particles with typical sizes below 200 nm and a shell of silica. Such structure provides some advantages over solid (plain) ones because of its low density and large surface area (Scheme 1).[20, 21, 28]

In addition, their size will also determine the mechanism and rate of nanoparticles cell uptake and their ability to permeate through tissues. Moreover, particle shape (i.e.,: spherical, tubes) and surface properties (i.e.,: positively or negatively charge) have a great impact on different aspects of cellular functions including cell proliferation, apoptosis, cytoskeleton formation, adhesion and migration. Thus, although silica is generally accepted as having low toxicity, the biocompatibility of silica nanoparticles (SiNPs) as a "new" kind of material should be revisited.[29] In this way, it is possible to control the interaction of nanoparticles with cells. This interaction is sometimes mediated by the type and concentration of the protein layer adsorbed to the nanoparticles that interact with integrins present in the cell membrane. Thus, a careful consideration must be given to control the interaction of nanoparticles with macromolecules and cells present in biological systems. Such interactions play a key role in the stability, aggregation and dissolution of silica nanoparticles and in the uptake by phagocyte mononuclear cells or even other cells types. In addition, the transendothelial permeability in various normal or damaged tissues, the uptake by cells and particle clearance should be taken into account.

Therefore, it is possible to tune the characteristics of the nanoparticles to meet the requirements of each specific cell and desired application.[30] Especially, silica nanoparticles have gained ground in the pharmaceutical field and have been widely studied in the context of drug delivery and drug targeting.[31–36] Indeed, a huge amount of cosmetic products and pharmaceutical formulations contain nanoparticles. In this sense, it was suggested that an ideal drug delivery system should be inert, biocompatible, mechanically strong, comfortable for the patient, capable of achieving high drug loading, safe from accidental release, simple to administer and remove, and easy to fabricate and sterilize.[37, 38] Silica nanoparticles meets nearly all the requirements, thus it is not surprising the great attention that they are receiving from researchers and industries.[39, 40]
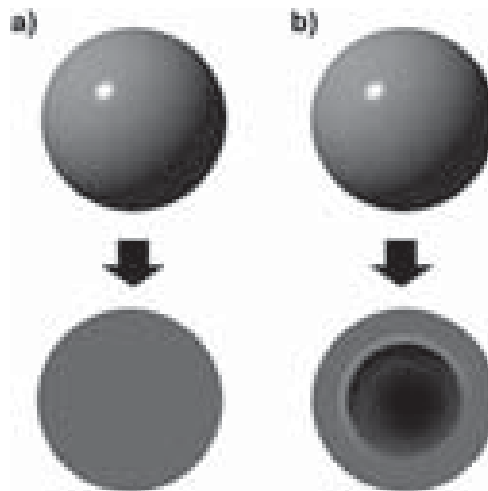
Scheme 1. Schematic representation of: (a) plain nanoparticles and (b) hollow nanoparticles.

110

J. Biomater. Tissue Eng. 3, 108–121, 2013

The great advances in the application of silica nanoparticles also require a careful characterization of the biocompatibility, immune response and toxicological effects that they may cause. The study of the immune response against nanoparticles is actually being studied[41] for multiple reasons such as the elucidation of new targets for drug delivery systems,[42–44] as vaccination adjuvants[45, 46] or for toxicological studies.[47–50] It is worth to mention that nanoparticles interact with the immune system in different ways, having the possibility to trigger both the innate and adaptive immune response. Both innate and adaptive immune responses work in a coordinated manner to mount an effective immune response in the body that prevents or protects against foreign material, mostly microorganisms, but also dust and particles, entering and/or affecting the organism.[41] Furthermore, cell cultures can be used in toxicity screening both through estimation of the basal functions of the cell (i.e., those processes common to all types of cells) or through testing on specialized cell functions. Several parameters are used to assess the effect of nanoparticles over cell functions. These parameters include vital staining, proliferation test, cytosolic enzyme release, and cytokine production, among others. Special attention should be given if nanoparticles are intended to treat or prevent infections. In this case, it is highly desirable that the formulation possess a strong activity against microorganisms without affecting host cells.

In the case of cell interaction with nanoparticles, some works have been published which try to elucidate the mechanism either for cell toxicity or for cell growth stimulation in other cases. Herein, we present different strategies developed to optimize the size, morphology, surface topography, elemental ratio, hydrophobic/hydrophilic balance, and erosion rate, which contribute to understand the nature of this inherently complicated cell-nanoparticles interactions mechanism, which will determine the resulting function performance.

2. *IN VITRO* ASSAYS

Biocompatibility is always a matter of study in medical research. In this sense, the effect on human health of a therapeutic, occupational or accidental exposure to nanoparticles should be thoroughly investigated. Consequently, many studies have been performed in this field but still very little is known about the human body's response to nanoparticles.

Research has shown that the response depends not only on nanoparticle composition, but also on many factors like size, shape, mass and the method of synthesis involved, which can influence cell toxicity.[51] Even though there are works whose results seem to contradict those obtained by other researchers, there are some generalizations which are worthwhile of considering when working with nanoparticles.

2.1. Effect of Concentration and Size of SiNPs

From the analysis of the literature available, it has been found that cellular response to SiNPs is concentration dependent,[52–54] even though increasing SiNPs concentration will also increase the effect produced and eventually the probability of cell toxicity.[55]

On the other hand, the size of the nanoparticles is related to the surface which will ultimately be in contact with the cells. In this sense, it would be expected that a higher interaction will be established with smaller sized particles. This higher interaction can be favorable or unfavorable, depending on the characteristics of the material employed. Furthermore, smaller sized nanoparticles are more rapidly taken up by cells, thus speeding the reaction to them. It was reported that as a consequence of the treatment of Langerhans cells with silica particles, with diameters of 70, 300, and 1000 nm, cellular uptake and cytotoxicity increased with the decrease in particle size.[56]

Indeed, when considering size alone, it has been extensively reported that cytotoxicity increases when nanoparticle size is reduced.[50, 57] However, this was observed when cells were exposed to silica nanoparticles ranging from 50 to 500 nm and not in those with less than 50 nm.[52, 58] Because agglomeration of nanoparticles can take place quite easily, another approach points out the fact that when surface area is taken into account it can be generally accepted that the larger the surface area, the higher the toxicity.[59]

Morishige et al. found that unmodified amorphous microsized silica particles (i.e.,: 1000 nm) induced higher levels of IL-1b production in THP-1 human macrophage like cells whereas smaller particles (30 to 300 nm) did not induce such a significant production.[60] In a related work, Waters et al. suggested that the response of macrophages to SiNPs depends on the nominal surface area basis rather than on particle mass or number. They arrived to this conclusion using unopsonized amorphous silica nanoparticles ranging from 7 to 500 nm diameter and measured the stimulation of inflammatory protein secretion and the induced macrophage cytotoxicity.[59] Oberdörster et al. also reported that particles with greater specific surface areas per mass are more biologically active.[61] Same results were found in mouse keratinocytes (HEL-30) exposed for 24 h to 30, 48, 118, and 535 nm SiNPs. Indeed, silica nanoparticles exhibiting the highest specific surface area showed more toxic effects.[54] When working with endothelial cells (EAHY926 cell line), surface area also seems to be an important parameter in cytotoxicity, as it was seen with the smallest SiNPs (14–16 nm diameter), which led to a 50% reduction of viability when used at a lower concentration than 19, 60, 104, and 335 nm monodisperse amorphous spherical silica particles.[62]

2.2. Effect of Crystalline Form and Porosity

Silica can be divided into crystalline or amorphous (noncrystalline), all having the same basic molecular formula

(almost 100% SiO_2).[63] Because inhalation of crystalline silica dust is well known to cause silicosis, it is commonly accepted that this form of silica is more toxic. However, in a recent publication, Constantini et al. compared the uptake and toxicity of amorphous silica to crystalline silica in various cell types, such as mouse alveolar macrophage (MH-S) cells, mouse lung epithelial type II, mouse skin melanoma, monkey kidney fibroblast, human adenocarcinoma cells and cervical epithelial cells among others. They found out that, whereas all cells are able to take up silica nanoparticles, only macrophages showed extreme sensitivity, and in this case crystalline silica and amorphous silica killed the cells with equal strength.[64]

Other works dealing with mesoporous silica nanoparticles try to explain the effect of the porosity on the final response.[65–67] Lee et al. compared the effect *in vitro* and *in vivo* of mesoporous silica nanoparticles (MSNs) with non-porous colloidal silica of the same size and shape. Results showed that MSNs induced less activation of MAPKs, NF-kB and caspase-3 leading to a lower cytotoxicity and inflammatory response when compared to non-porous silica nanoparticles. Moreover, the results of the hazard test for identification of contact hypersensitivity performed *in vivo* were congruent with those obtained *in vitro*.[65]

2.3. Effect of Surface Modification

It seems that covering the anionic surface of silica nanoparticles, often with cationic compounds, results in reduced toxicity when compared to particles without any modification. Tao et al. reported different mesoporosity-dependent and functional group-dependent cytotoxicity and endocytosis of various silica nanomaterials on suspended and adherent cells. They confirmed that the functionalization of mesoporous nanomaterials, namely by amination with positively charged quaternary amines, is able to prevent cellular injury as the rate of cell internalization is significantly diminished.[68] In relation to nanoparticle modification, Chen et al. synthesized silicon nanoparticles chemically modified with sodium chloride or sodium iodide (diameters of 10–100 nm) as novel non-viral vectors for DNA transfer into cells. Results showed a better efficiency of DNA transfection with the advantage of protection of DNA against degradation. Microscopy assays showed no cytotoxicity during adhesion and entry of the nanoparticles into HT1080 cells. *In vivo* experiments with mice revealed accumulation of nanoparticles within the cells of the brain, liver, spleen, lung, kidney, intestine and prostate without pathological cell changes or mortality.[69] There are more works suggesting the potential of modified silica nanoparticles as gene carriers with very low or no cell toxicity observed. As an example, the ability of cationic SiNPs to transfect galactosidase expression plasmid DNA pCMVβ reporter gene was successful in Cos-1 cells *in vitro*[70, 71] and in the mouse lung *in vivo*.[71] Furthermore, SiNPs with surface cationic amino groups were efficiently taken up *in vitro* and succeeded to deliver DNA to the nucleus.[72] In addition, Bharali et al. found promising the use of amino-functionalized silica organically modified nanoparticles for future direction and effective therapeutic manipulation of neural stem/progenitor cells and *in vivo* targeted brain therapy.[73] Mumin et al. demonstrated that phosphonate functionalization of mesoporous SiNPs with a resulting foam structure (i.e.,: 65 nm) leads to increased levels of interaction or internalization by dendritic cells.[74]

Surface modification can drastically change cellular response to nanoparticles. For example Gyenge et al. tried core–shell silica nanoparticles with hydroxyl-, aminopropyl- or PEGylated surface modifications (200–300 nm) encapsulating a fluorescent dye to evaluate their uptake in the human head and neck squamous cell carcinoma cell line UMB-SCC 745 and found that the uptake of PEGylated SiNPs was minimal even after 24 h in contrast to hydroxyl- and aminopropyl-modified SiNPs.[75]

In relation to the mechanism involved in the protection given by modification with cationic compounds, which will be further discussed, Dutta et al. proposed that serum proteins which commonly adsorb on the surface of amorphous silica nanoparticles could influence the biological fate of SiNPs and in fact they observed that surfactant coated nanoparticles, which prevented proteins from binding to their surface, inhibited cytotoxicity.[76] Considering the amount of surface modification possibilities this is probably an interesting point for optimization in the design of SiNPs for different proposes.

2.4. Cell Type

Another interesting fact is that not all the cells show the same response to silica nanoparticles, which can be related to different interaction mechanisms or to different degrees of interaction. As an example, 3T3 fibroblasts, bronchiolar epithelial cells (hT) and RAW 264.7 macrophages were used to test viability when exposed to 30 nm silica or titanium nanoparticles in different concentrations and three different diameters of multi-wall carbon nanotubes. As expected, it was found that size and composition do affect cellular response but this is cell type dependant in such a way that it is recommended to focus nanoparticle engineering on the potential cell type which may be finally exposed to them. Likewise, Malugin et al. tried modified (–COOH and –NH_2) and unmodified silica nanoparticles from 50–500 nm in human prostate carcinoma DU145, colon carcinoma HCT116 and murine macrophages RAW 264.7 cells. They found that phagocytic cells are more susceptible to amorphous silica nanoparticles than epithelial cells.[52]

2.5. Cellular Uptake

In order to design drug loaded nanoparticles as well as to diminish the toxicity of the before mentioned SiNPs,

it is necessary to know more about the different ways the particles obtained will enter the target cell.[77] There are essentially four mechanisms of endocytosis by means of which nanoparticles enter the cells: clathrin-mediated endocytosis, caveolae-mediated endocytosis, phagocytosis and macropinocytosis, though a discussion has grown around this classification and it may need to be updated. Nanoparticles taken up by endocytosis are firstly enclosed within early endosomes, phagosomes and macropinosomes respectively. These vesicles will later become multivesicular bodies, also known as late endosomes, and eventually fuse with lysosomes.[78] In general terms, larger particles are taken up by phagocytosis while smaller ones by endocytosis (Scheme 2). Strictly speaking, phagocytosis is a process occurring only in highly specialized cells, e.g., macrophages, although other cells may use phagocytic-like mechanisms too.[79] In this sense, Zhang et al. identified an optimal NP radius at which the cellular uptake reaches a maximum and they showed that the cellular uptake of NPs is regulated by membrane tension, which can be elaborately controlled by particle size. The optimal NP radius reported for endocytosis was on the order of 25–30 nm.[80] Similarly, SiNPs uptake by HeLa cells is size-dependent and the maximum uptake by cells occurs at a nanoparticle size of 50 nm. These findings suggested that MSNs 50 nm
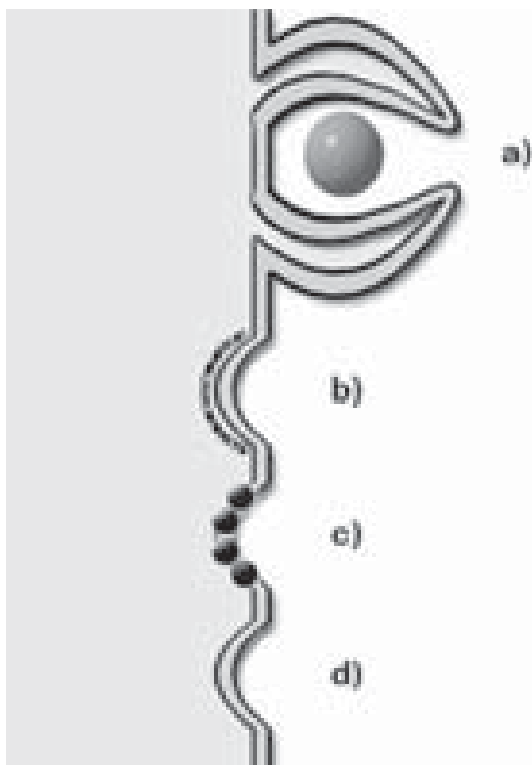
in diameter may be the most suitable candidate to serve as a carrier for further studies in biological applications.[81]

Not only size but also concentration probably influences one of the various uptake mechanisms that have been described as potential cell capture pathways for nanoparticles. In this sense, an interesting observation was made by Choi et al. who described that when working with low SiNPs concentrations, namely 7.28×10^{-4} μg/ml, silica was dispersed throughout the cytoplasm whereas at higher concentrations they appeared to be engulfed in phagocitic vacuoles, and therefore suggested that concentration may affect silica nanoparticles uptake.[82]

When it comes to size, it has been suggested that modified (–COOH, –NH$_2$, –SO$_3$H, –CHO) and unmodified 1000 nm silica particles are taken by THP-1 cells with similar frequencies by actin-dependent phagocytosis.[52, 83] On the other hand, other groups working with silica nanoparticles ranging from 50 to 500 nm claimed that within this range they do not enter the cells through the phagocytic pathway but through a different mechanism, presumingly endocytosis.[52] Moreover, recently Quignard et al. demonstrated that positive charged SiNPs (i.e.,: 200 and 40 nm) are easily uptaken by human dermal fibroblast, through a macropinocytosis, without impacting on cell viability. On the other hand, the small SiNPs (i.e.,: 10 nm positively and negatively charged) show high and fast cytotoxicity compared to the largest ones at a similar dose, but only the negatively-charged colloids induced genotoxicity effects.[84] One interesting point that deserves more attention is that SiNPs are prone to dissolve in culture media. The dissolution process was also confirmed by several works that monitors the cell culture medium where it was demonstrated that it contains both colloidal and soluble silica species.[84–87] Apparently, as it was shown by Xing et al. not only size and concentration affect cellular uptake of SiNPs. Their experimental results demonstrated that uptake of silica-coated nanoparticles by HeLa cells was higher at 37 °C than at 4 °C and concluded it was time and energy dependent process.[88] Analysis of the intracellular localization of silica nanoparticles revealed that SiNPs penetrated into the nucleus, whereas SiNPs modified with amine or carboxyl groups showed no nuclear localization. These results suggest that intracellular localization is a critical factor underlying the cytotoxicity of these silica nanoparticles.[89]

2.6. Cell Damage Mechanism

Different cells have different metabolisms and thus it would be expected that the extent of cell interaction and toxicity will vary when considering different cells being exposed to the same silica nanoparticles. Concerning the mechanism of cell toxicity, several studies propose that nanomaterials cause lysosomal membrane destabilization induced by reactive oxygen species (ROS) generation, which would ultimately lead to apoptosis.[31, 58, 90–94]

Scheme 2. Mechanisms of endocytosis by means of which nanoparticles enter the cells: (a) phagocytosis (b) endocytosis clathrin dependent (c) endocytosis caveolin dependent (d) endocitosis non-clathrin non-caveolin dependent.

Indeed, human embryonic kidney (HEK293) cells[95] and human bronchoalveolar carcinoma-derived cells,[96] for example, showed dose dependent cytotoxicity associated with increased oxidative stress when exposed to SiNPs. In the case of liver cells, Ye et al. reported that exposure to SiNPs of the normal human hepatic cell line (L-02) caused cytotoxicity in size, dose and time dependent manners, with 21 nm SiNPs inducing oxidative stress, apoptosis and increased p53 and Bax expression.[97] On the other hand, Lu et al. tested the biological response of normal human L-02 hepatocytes and HepG2 hepatoma cells to SiNPs and stated that the first ones showed only slight toxicity when compared to the antiproliferation activity seen in the second ones.[98]

The mechanisms of toxicity in human HepG2 hepatoma cells by 7 to 50 nm or 14 nm silica nanoparticles were studied by Lu et al.[98] and Ahmad et al.[99] respectively. Both found that in these cells nanoparticles produce toxicity in a dose dependent manner. The expressions p53 and caspase-3 (proapoptotic) were up-regulated, whereas the expression of bcl-2 (antiapoptotic member of the Bcl-2 family) was down-regulated. Lu et al. found decreased the expression of procaspase-9 and no significant change in expression of Bax (propapoptotic member of the Bcl-2 family), whereas Ahamed et al. found that the proapoptotic gene bax was up-regulated in HepG2 cells treated with silica nanoparticles. Both found an increase in ROS and decrease in glutathione (GSH) (antioxidant) levels. This suggests that in these cells nanoparticles induced apoptosis mediated through ROS via p53, bax/bcl-2 and caspase pathways.[99]

When considering macrophage cells, Morishige et al. suggested that ROS production induced by phagocytosis of unmodified 1000 nm silica particles triggered endosomal rupture followed by the activation of the pro-inflammatory complex NLRP3 inflammasome (NLR family, pyrin domain containing 3) and subsequent interleukin-1b (IL-1b) production.[60] In addition, SiNPs induced an elevated level of reactive oxygen species (ROS), leading to DNA damage.[100] When surface modification with several functional groups ($-COOH$, $-NH_2$, $-SO_3H$, $-CHO$) was performed, it dramatically suppressed IL-1b production by reducing ROS production in THP-1 human macrophage-like cells. The inflammatory effect *in vivo* in intraperitoneally injected (1 mg) mice showed the same results when compared to IL-1b production *in vitro*.[52, 83] Furthermore, unmodified silica nanoparticles from 50 to 500 nm induced a more severe plasma membrane damage in RAW264.7 macrophages than surface functionalized ($-COOH$ and $-NH_2$).[52] In relation to the immune system, Lucarelli et al. suggested the possibility of inadequate defense against certain infections after exposure to SiNPs (15 nm) due to the inhibition of the expression of toll-like receptor (TLR) and proinflammatory cytokine production in macrophages.[101] Meanwhile, Winter et al. reported that SiNPs (14 nm) activate murine bone marrow-derived dendritic cells and activate inflammasome.[102] In another work,

in which human umbilical vein endothelial cells (HUVECs) were exposed to silicon dioxide nanoparticles with diameters of 304 nm and 310 nm, results showed that NP induced exocytosis of Weibel-Palade bodies, associated with the release of von Willebrand factor and necrotic cell death.[83]

However, in some cells, ROS production does not seem to be associated to citotoxicity of silica nanoparticles. In relation to this, Yu et al. did not found significant differences between HEL-30 controls and those treated with different sizes (30, 48, 118, and 535 nm) and different concentrations of amorphous SiNPs and suggested that either direct physical disruption of membranes or another unknown mechanism could be involved in the observed size-dependent toxicity.[54] Moreover, Tao et al. studied the effect of two types of mesoporous silica nanoparticles on mitochondrial oxygen consumption and found out that in their presence glucose supported respiration was delayed without contribution of reactive oxygen species, because cellular GSH remained unchanged.[103]

Finally, Sohaebuddin et al. concluded that, depending on the exposed cell type, the same material can cause different intracellular responses and potential mechanisms of toxicity, as it was shown that nanomaterial-associated lysosomal membrane destabilization is responsible for the nanomaterial-induced toxicity in 3T3 fibroblasts, but not in hT bronchiolar epithelial cells and RAW macrophages and suggest that cytotoxicity of SiNPs in these cell lines may be associated with mitochondrial membrane potential reduction.[51]

Interactions between particles with mitochondria could also generate additional oxidant species. Indeed, increased oxygen consumption was observed in lung tissue cubes of animals exposed to particles.[104] This observation is also supported by an increased NADPH oxidase activity. It is worth to mention that this enzyme play a role as potent superoxide anion producer enzyme which is expressed both in phagocytic and nonphagocytic cells.[105] Moreover, increased mitochondrial oxygen consumption, NO production and phospholipid oxidation in lung homogenates exposed to particles was also observed.

3. *IN VIVO* ASSAYS

Although there are lots of scientific works concerning the potential toxicity of silica nanoparticles over different types of cell culture, little information is provided about the toxicity on living organisms. Furthermore, these *in vivo* results are often contradictory and the question about the possibility to safely administrate silica nanoparticles to living organisms remains open. In this section the results reported on biocompatibility, biodistribution and clearance of silica nanoparticles will be discuss.

3.1. Toxicity of SiNPs

Some authors found low toxicity of silica nanoparticles after their injection in animals. It has been reported

114

*J. Biomater. Tissue Eng. 3, 108–121, **2013***

the synthesis of ultrafine organically modified silica (ORMOSIL) nanoparticles with diameters of 20 nm, conjugated with a near-infrared fluorophore for optical bioimaging. ORMOSIL NPs mainly accumulated in the liver and spleen and did not show any toxicity, adverse effect or any other abnormalities in the tissues of injected animals after 15 days studies.[106] In another experiment, the results of single and repeated dose toxicity of mesoporous hollow silica nanoparticles (MHSiNPs) demonstrated low toxicity of these new nanostructures *in vivo* when repeated and single dose toxicity were evaluated for 110 nm (MHSiNPs) after their delivery through the blood stream of mice. The LD50 of MHSNs was greater than 1000 mg/kg, while in repeated administration; 80 mg/kg continuous injection for 14 days did not produce animal death. No toxicity was found in liver, spleen, lung and kidney in MHSiNPs-injected mice at 40 and 160 mg/kg single dose and there were no abnormalities in the spleen, kidney and lung in MHSiNPs-injected mice at 500 and 1280 mg/kg. However, lymphocytic infiltration, microgranulation and degenerative necrosis of hepatocytes were observed in the liver at 500 and 1280 mg/kg single administration. In this study, MHSNs were found to be distributed in the liver and spleen after 24 h intravenous injection. Macrophage resident in liver and spleen was the target cell of MHSiNPs.[107] This is in concordance with other results where liver damage caused by mesoporous hollow silica nanoparticles was also demonstrated after continuous intraperitoneal injection into mice twice a week for 6 weeks. The administration of MHSiNPs at 50 mg/kg increased liver injury markers in serum, such as alanine aminotransferase (ALT), inflammatory cytokines interleukin-1 beta (IL-1b) and tumor necrosis factor-alpha (TNF-α). Histological analysis revealed lymphocytic infiltration and silicotic nodular like lesions in liver where activated kupffer cells played a key role similar to alveolar macrophage in the process of silicosis.[108, 109] Moreover, it was observed that 30 mg of intraperitoneally administered silica particles invariably resulted in death or distress of mice; in contrast it was found that even 100 mg of poly(lactic-co-glycolic) (PLGA) acid microspheres cause no detectable toxicity in mice of the same strain and mass indicating that silica tested would appear 100 times more lethal than PLGA particles.[66]

Apparently, there is a relationship between toxicity and sizes, shapes, surface area or chemical modification on the surface of silica nanoparticles which also condition the grade of dispersion of the particles. An experiment was performed where different sizes (50, 100 and 200 nm) of silica particles were used to evaluate their level of toxicity. The 200 nm particles were taken up faster and more intensively than the other sizes by macrophages of the spleen and liver and disappeared thereafter. In the liver, there was a significant increase in the incidence and severity of inflammation for 100 and 200 nm silica nanoparticles treatment groups at 12 h. The 50 nm particles induced only a slight inflammatory response at the same time.[110] However, all particle sizes remained aggregate in the spleen through macrophage trapping after 4 weeks. The aggregation state of nanoparticles is an important factor for distribution and excretion in the body. A previous study showed quantum dots that remained nano-sized *in vivo* are excreted via the kidney, and quantum dots that aggregated into larger particles remained in liver tissue until 5 days after a single intravenous injection.[111] There are several reports in the literature which indicate that larger particles tend to accumulate more into the liver as compared to the smaller ones.[112, 113]

Other studies have shown that exposures to nanoscale particles produce greater inflammatory and cytotoxic effects when compared to exposures to larger sized particles at equivalent mass concentration. As a particle decreases in size, the surface area increases and a greater proportion of atoms/molecules are found at the surface compared to those inside. Thus, nanoparticles have a much larger surface area per unit mass compared with larger particles. The increase in the surface-to-volume ratio results in the increase of the particle surface energy which may render them more biologically reactive.[114] Therefore it is considered that nanoparticles can be more reactive with biological components and have adverse effects due to large surface area and much particle number. Lu et al. found in their study that all sizes (30, 70 and 300 nm) of silica nanoparticles tested caused injury in the liver and caused lung inflammation without affecting the spleen, heart and kidneys. Furthermore, they proved that particles of 30 nm were the most toxic among the three sizes as determined via biochemical assays and histopathological examinations at 10 mg/kg. However, the other SiNPs sizes could also induce liver injury when the dose was increased. It was reported that, surface area had a greater effect than particle number on the toxicity of silica nanoparticles in the liver.[115] The DNA damage caused by amorphous SiNPs of 15 and 55 nm in liver, lung and blood cells and micronuclei in circulating reticulocytes were measured after three consecutive intravenous injections to rats at 48, 24 and 4 h before sacrifice. Silica particles caused a small but reproducible increase in DNA damage and micronucleated reticulocytes when tested at their maximum tolerated dose (MTD) but no genotoxic effects were observed at lower doses. These effects were probably caused through inflammatory cell-derived oxidants such as inflammatory markers, TNF-α and IL-6, found in rats' plasma. The same experiment was performed using gold nanoparticles and no genotoxic effects were observed.[116]

The toxicity of silica nanoparticles includes many aspects which were evaluated by other authors as well. For example, it has been shown that silica and titanium dioxide nanoparticles with diameters of 70 nm and 35 nm, respectively, can cause pregnancy complications when injected intravenously into pregnant mice. These nanoparticles were found in the placenta, fetal liver and fetal brain, and mice treated with these nanoparticles had smaller uteri and smaller fetuses than untreated controls. However,

it was also found that larger (300 and 1000 nm) silica particles did not induce these complications.[117] In addition, it was reported that systemically administered SiNPs can penetrate the blood-testis barrier and were detected within sertoli cells and spermatocytes, including in the nuclei of spermatocytes.[118, 119]

When SiNPs are not administered to the blood stream but subcutaneously, their toxic effect is also of great importance, particularly for local drug applications. The cytotoxicity and biocompatibility of mesoporous silicates in particle sizes 150, 800 and 4000 nm injected subcutaneously in rats were analyzed. At early time points the authors found large deposits of the material subcutaneously but very small amounts or no particles were observed after 2–3 months and there was an inflammatory reaction at the beginning which decreased substantially with time. There was no significant injury to surrounding tissues like muscle, nerve or blood vessels.[66] Bionanocomposites based on the association between biological polymers and inorganic colloids are an emerging class of materials.[120] Nanocomposite silica-collagen materials derived from concentrated collagen hydrogels and silica nanoparticles were evaluated *in vivo* to establish their potentialities for biological dressings. It was determined through the experiments that silicification significantly improved the mechanical and thermal stability of the collagen network and that nanocomposites favor the metabolic activity of immobilized human dermal fibroblasts while decreasing the hydrogel contraction. When studying *in vivo* implantation of bulk hydrogels in subcutaneous sites of rats after 1 week, it was noticed that these materials were colonized and vascularized without inducing strong inflammatory response.[121]

3.2. Degradation and Excretion

Several reviews suggest that silica nanoparticles are degradable over time in the body. Liu et al. found that about 50% of MHSiNPs was removed from the body over 4 weeks after injection. The particles would be excreted from the body with a clearance time of over 4 weeks and this long circulation time of MHSiNPs provides the possibility of using them as drug carriers for controlled release applications *in vivo*.[107] Excretion to urine and feces showed different patterns depending on particles size. At 12 h, 50 nm SiNPs reached the highest concentration in urine while 100 nm particles had a peak concentration at 24 h and neither three sized silica NPs (50, 100 and 200 nm) were detected in urine 1 week after intravenous injection. Silica nanoparticles eliminated slower via feces than in urine. The 50 nm silica nanoparticles excreted faster than the other two particle sizes and 200 nm silica particles were excreted from urine and feces at lower concentrations than the other two. This fact could be useful as nanoparticles for therapy need to have a long retention time for targeting and therapy. However, a long retention time could also caused *in vivo* toxic effects.[110]

Not only the size and surface area are important to evaluate the toxicity, distribution and excretion of SiNPs but also their surface chemical characteristics. In this sense, highly positive charge, mesoporous silica nanoparticles (MSNs) administered *in vivo* revealed markedly different uptake and elimination behaviors in comparison to less charged moieties. The first ones were quickly excreted from the liver into the gastrointestinal tract, while less charged moieties remained sequestered within the liver. Taken together these findings, the authors suggest that charge-dependent adsorption of serum proteins greatly facilitates the hepatobiliary excretion of silica nanoparticles, and that nanoparticle residence time *in vivo* can be regulated by manipulation of surface charge.[122] Moreover, the biodistribution and urinary excretion of different surface-modified silica nanoparticles (SiNPs) in mice were investigated using an *in vivo* optical imaging system. Three types of surface-modified SiNPs, including OH-SiNPs, COOH-SiNPs, and PEG-SiNPs with a size of 45 nm were prepared. Intravenous injection of these SiNPs followed by fluorescence tracing *in vivo* indicated that OH-SiNPs, COOH-SiNPs, and PEG-SiNPs were all cleared from the systemic blood circulation, but that both the clearance time and subsequent biological organ deposition were dependent on the surface chemical modification. The PEG-SiNPs exhibited relatively longer blood circulation times and lower uptake by the reticuloendothelial system organs than OH-SiNPs and COOH-SiNPs and all three types of SiNPs were partly excreted through the renal excretion route.[123]

One of the main problems in silica nanoparticle administration is their accumulation and rapid clearance by the reticuloendothelial system, which results in short circulation times. This short half-life decreases the exposure of nanoparticles to the blood–brain barrier (BBB) and consequently dissuades the interaction of NPs with the brain vascular endothelial cells and reduces their opportunity to cross the BBB. PEGylation of nanoparticles has then become the most widely used approach to increase the circulation lifetime of nanoparticles. Neutral charge and hydrophilicity are desired surface characteristic of the nanoparticles in order to avoid the rapid uptake by monocytes and consequently by organ-resident phagocytic cells (i.e., Kupffer cells in the liver). Most of the strategies to reach those requirements use hydrophilic polymers (i.e., polyethylene glycol) that, in addition, show steric effects which help to stabilize the nanoparticles preventing agglomeration.[124, 125]

A study was performed where fluorescein-doped magnetic silica nanoparticles (FMSiNPs) and PEGylated PAMAM conjugated fluorescein-doped magnetic silica nanoparticles (PEGylated PFMSNs) were used to demonstrate that PEGylated PFMSNs could penetrate the BBB through transcytosis of vascular endothelial cells, diffusing into cerebral parenchyma and distributing in the neurons. In contrast, non-PEGylated FMSiNPs were not found to cross the BBB. Moreover, the PEGylated PFMSNs may

not induce cumulative intoxication to the brain.[126] It was reported that nanosized silica-overcoated magnetic particles containing Rhodamine B isothiocyanate can also penetrate the blood–brain barrier without any apparent toxicity.[127]

4. CONCLUSION

Silica nanoparticles seem to have low toxicity and to be biocompatible when administered locally but they appear to be quite toxic systemically, leading to lymphocytic infiltration, microgranulation and degenerative necrosis in liver tissue.

Regarding the size, larger silica nanoparticles appear to be taken up faster and more intensively by macrophages than smaller ones, causing liver inflammation. On the other hand, as far as it is possible to assume, the smaller the particle, the greater surface/volume ratio, resulting in surface energy raise and consequently, more biologically reactivity. Additionally, increasing the dose could also induce liver damage, independently of the SiNPs size. Instead, when SiNPs are subcutaneously administered, the inflammatory reaction only appears at the beginning, and then decreases leaving no damage in surrounding tissues.

It was also found that size was related to nanoparticles excretion. Smaller SiNPs are excreted faster than larger one, providing the possibility of getting a long retention time for controlled drug delivery. Modifying the chemical surface could manage the chance to regulate the excretion too. Hepatobiliary excretion is enhanced by giving the nanoparticle's surface a highly positive charge. Alternatively, PEGylation allows obtaining longer blood circulation times, lower uptake by the reticuloendothelial system organs, and also penetration of the blood–brain barrier.

Regarding the possibilities given by surface modification and the results obtained by the different authors, it can be concluded that the properties of SiNPs can be mastered to meet the desired therapeutic requirements. In this sense, when anticancer properties are expected, then naked SiNPs can be useful and higher uptakes rates would cause selective toxicity in the chosen target. On the other side, when a therapeutic action or enhancement is needed, then modifying the surface of the nanoparticles could help reach the final objective.

References and Notes

1. C. Brinker and G. Scherer, Sol–Gel Science, Academic Press, San Diego, USA (**1990**).
2. R. K. Iler, The Chemistry of Silica, J Wiley, New York, USA (**1979**).
3. N. Baccile, F. Babonneau, B. Thomas, and T. Coradin, Introducing ecodesign in silica sol–gel materials. *J. Mater. Chem.* 19, 8537 (**2009**).
4. C. Sanchez, B. Julián, P. Belleville, and M. Popall, Applications of hybrid organic-inorganic nanocomposites. *J. Mater. Chem.* 15, 3559 (**2005**).
5. C. Sanchez, L. Rozes, F. Ribot, C. Laberty-Robert, D. Grosso, C. Sassoye, C. Boissiere, and L. Nicole, "Chimie douce": A land of opportunities for the designed construction of functional inorganic and hybrid organic-inorganic nanomaterials. *Comptes. Rendus. Chimie.* 13, 3 (**2010**).
6. G. J. D. A. A. Soler-Illia, C. Sanchez, B. Lebeau, and J. Patarin, Chemical strategies to design textured materials: From microporous and mesoporous oxides to nanonetworks and hierarchical structures. *Chem. Rev.* 102, 4093 (**2002**).
7. E. Ruiz-Hitzky, P. Aranda, M. Darder, and M. Ogawa, Hybrid and biohybrid silicate based materials: Molecular versus block-assembling bottom-up processes. *Chem. Soc. Rev.* 40, 801 (**2011**).
8. D. Avnir, O. Lev, and J. Livage, Recent bio-applications of sol–gel materials. *J. Mater. Chem.* 16, 1013 (**2006**).
9. T. Coradin, M. Boissiere, and J. Livage, Sol–gel chemistry in medicinal science. *Current Med. Chem.* 13, 99 (**2006**).
10. T. Coradin and J. Livage, Aqueous silicates in biological sol–gel applications: New perspectives for old precursors. *Accounts Chem. Res.* 40, 819 (**2007**).
11. V. Kandimalla, V. S. Tripathi, and H. Ju, Immobilization of biomolecules in sol–gels: Biological and analytical applications. *Critical Rev. Anal. Chem.* 36, 73 (**2006**).
12. S. Y. Gadre and P. I. Gouma, Biodoped ceramics: Synthesis, properties, and applications. *J. Amer. Ceramic Soc.* 89, 2987 (**2006**).
13. M. F. Desimone, G. S. Alvarez, M. L. Foglia, and L. E. Diaz, Development of sol–gel hybrid materials for whole cell immobilization. *Recent Pat. Biotechnol.* 3, 55 (**2009**).
14. M. L. Foglia, G. S. Alvarez, P. N. Catalano, A. M. Mebert, L. E. Diaz, T. Coradin, and M. F. Desimone, Recent patents on the synthesis and application of silica nanoparticles for drug delivery. *Recent Pat. Biotechnol.* 5, 54 (**2011**).
15. Q. He and J. Shi, Mesoporous silica nanoparticle based nano drug delivery systems: Synthesis, controlled drug release and delivery, pharmacokinetics and biocompatibility. *J. Mater. Chem.* 21, 5845 (**2011**).
16. J. Wu, J. Silvent, T. Coradin, and C. Aime, Biochemical investigation of the formation of three-dimensional networks from DNA-grafted large silica particles. *Langmuir* 28, 2156 (**2012**).
17. Y. L. Choi, J. H. Lee, J. Jaworski, and J. H. Jung, Mesoporous silica nanoparticles functionalized with a thymidine derivative for controlled release. *J. Mater. Chem.* 22, 9455 (**2012**).
18. K. C. W. Wu and Y. Yamauchi, Controlling physical features of mesoporous silica nanoparticles (MSNs) for emerging applications. *J. Mater. Chem.* 22, 1251 (**2012**).
19. C. Barbé, J. Bartlett, L. Kong, K. Finnie, H. Q. Lin, M. Larkin, S. Calleja, A. Bush, and G. Calleja, Silica particles: A novel drug-delivery system. *Adv. Mater.* 16, 1959 (**2004**).
20. J.-F. Chen, H.-M. Ding, J.-X. Wang, and L. Shao, Preparation and characterization of porous hollow silica nanoparticles for drug delivery application. *Biomaterials* 25, 723 (**2004**).

REVIEW

21. Z. Z. Li, L. X. Wen, L. Shao, and J. F. Chen, Fabrication of porous hollow silica nanoparticles and their applications in drug release control. *J. Control Release* 98, 245 (**2004**).

22. W. Stöber, A. Fink, and E. Bohn, Controlled growth of monodisperse silica spheres in the micron size range. *J. Colloids Interf. Sci.* 26, 62 (**1968**).

23. K. S. Finnie, J. R. Bartlett, C. J. A. Barbé, and L. Kong, Formation of Silica Nanoparticles in Microemulsions. *Langmuir* 23, 3017 (**2007**).

24. L. M. Gan, K. Zhang, and C. H. Chew, Preparation of silica nanoparticles from sodium orthosilicate in inverse microemulsions. *Colloids Surf. A* 110, 199 (**1996**).

25. G. H. Bogush, M. A. Tracy, and C. F. Zukoski Iv, Preparation of monodisperse silica particles: Control of size and mass fraction. *J. Non-Crystalline Solids* 104, 95 (**1988**).

26. K. Nozawa, H. Gailhanou, L. Raison, P. Panizza, H. Ushiki, E. Sellier, J. P. Delville, and M. H. Delville, Smart control of monodisperse stober silica particles: Effect of reactant addition rate on growth process. *Langmuir* 21, 1516 (**2004**).

27. R. P. Bagwe, C. Yang, L. R. Hilliard, and W. Tan, Optimization of dye-doped silica nanoparticles prepared using a reverse microemulsion method. *Langmuir* 20, 8336 (**2004**).

28. F. Caruso, R. A. Caruso, and H. Möhwald, Nanoengineering of inorganic and hybrid hollow spheres by colloidal templating. *Science* 282, 1111 (**1998**).

29. F. Tang, L. Li, and D. Chen, Mesoporous silica nanoparticles: Synthesis, biocompatibility and drug delivery. *Adv. Mater.* 24, 1504 (**2012**).

30. J. M. Rosenholm, C. Sahlgren, and M. Linden, Towards multifunctional, targeted drug delivery systems using mesoporous silica nanoparticles—Opportunities & challenges. *Nanoscale* 2, 1870 (**2010**).

31. Y. Liu, C. Lou, H. Yang, M. Shi, and H. Miyoshi, Silica nanoparticles as promising drug/gene delivery carriers and fluorescent nanoprobes: Recent advances. *Current Cancer Drug Targets* 11, 156 (**2010**).

32. S. C. McBain, H. H. P. Yiu, and J. Dobson, Magnetic nanoparticles for gene and drug delivery. *Int. J. Nanomed.* 3, 169 (**2008**).

33. C. P. Tsai, C. Y. Chen, Y. Hung, F. H. Chang, and C. Y. Mou, Monoclonal antibody-functionalized mesoporous silica nanoparticles (MSN) for selective targeting breast cancer cells. *J. Mater. Chem.* 19, 5737 (**2009**).

34. K. Unger, H. Rupprecht, B. Valentin, and W. Kircher, The use of porous and surface modified silicas as drug delivery and stabilizing agents. *Drug Develop. Ind. Pharm.* 9, 69 (**2008**).

35. L. Pasqua, F. Testa, R. Aiello, S. Cundari, and J. B. Nagy, Preparation of bifunctional hybrid mesoporous silica potentially useful for drug targeting. *Microporous Mesoporous Mater.* 103, 166 (**2007**).

36. J. M. Rosenholm, A. Meinander, E. Peuhu, R. Niemi, J. E. Eriksson, C. Sahlgren, and M. Linden, Targeting of Porous Hybrid Silica Nanoparticles to Cancer Cells. *ACS Nano* 3, 197 (**2008**).

37. D. T. Birnbaum and L. Brannon-Peppas, Polymers in controlled release. *Polymer News* 27, 13 (**2002**).

38. L. Branno-Peppas and L. Brannon-Peppas (ed.), Polymers in Controlled Release, John Wiley & Sons, New York, (**2002**).

39. M. Vallet-Regí, E. Ruiz-Hernández, B. González, and A. Baeza, Design of Smart Nanomaterials for Drug and Gene Delivery. *J. Biomater. Tissue Eng.* 1, 6 (**2011**).

40. S.-H. Wu, Y. Hung, and C.-Y. Mou, Mesoporous silica nanoparticles as nanocarriers. *Chem. Comm.* 47, 9972 (**2011**).

41. S. Hussain, J. A. J. Vanoirbeek, and P. H. M. Hoet, Interactions of nanomaterials with the immune system. *Nanomed. Nanobiotechnol.* 4, 169 (**2012**).

42. M. Gary-Bobo, O. Hocine, D. Brevet, M. Maynadier, L. Raehm, S. Richeter, V. Charasson, B. Loock, A. Morère, P. Maillard, M. Garcia, and J.-O. Durand, Cancer therapy improvement with mesoporous silica nanoparticles combining targeting, drug delivery and PDT. *Int. J. Pharm.* 423, 509 (**2011**).

43. E. Verraedt, M. Pendela, E. Adams, J. Hoogmartens, and J. A. Martens, Controlled release of chlorhexidine from amorphous microporous silica. *J. Control Release* 142, 47 (**2010**).

44. P. Demuth, M. Hurley, C. Wu, S. Galanie, M. R. Zachariah, and P. Deshong, Mesoscale porous silica as drug delivery vehicles: Synthesis, characterization, and pH-sensitive release profiles. *Microporous Mesoporous Mater.* 141, 128 (**2011**).

45. L. V. Carvalho, R. D. C. Ruiz, K. Scaramuzzi, E. B. Marengo, J. R. Matos, D. V. Tambourgi, M. C. A. Fantini, and O. A. Anna, Immunological parameters related to the adjuvant effect of the ordered mesoporous silica SBA-15. *Vaccine* 28, 7829 (**2010**).

46. L. P. Mercuri, L. V. Carvalho, F. A. Lima, C. Quayle, M. C. A. Fantini, G. S. Tanaka, W. H. Cabrera, M. F. D. Furtado, D. V. Tambourgi, J. D. R. Matos, M. Jaroniec, and O. A. Sant'Anna, Ordered mesoporous silica SBA-15: A new effective adjuvant to induce antibody response. *Small* 2, 254 (**2006**).

47. P. Berntsen, C. Y. Park, B. Rothen-Rutishauser, A. Tsuda, T. M. Sager, R. M. Molina, T. C. Donaghey, A. M. Alencar, D. I. Kasahara, T. Ericsson, E. J. Millet, J. Swenson, D. J. Tschumperlin, J. P. Butler, J. D. Brain, J. J. Fredberg, P. Gehr, and E. H. Zhou, Biomechanical effects of environmental and engineered particles on human airway smooth muscle cells. *J. Royal Soc. Inter.* 7, S331 (**2010**).

48. K. Wittmaack, In search of the most relevant parameter for quantifying lung inflammatory response to nanoparticle exposure: Particle number, surface area, or what? *Environ. Health Persp.* 115, 187 (**2007**).

49. B. Fadeel and A. E. Garcia-Bennett, Better safe than sorry: Understanding the toxicological properties of inorganic nanoparticles manufactured for biomedical applications. *Adv. Drug. Deliv. Rev.* 62, 362 (**2009**).

50. A. Nel, T. Xia, L. Mädler, and N. Li, Toxic potential of materials at the nanolevel. *Science* 311, 622 (**2006**).

51. S. K. Sohaebuddin, P. T. Thevenot, D. Baker, J. W. Eaton, and L. Tang, Nanomaterial cytotoxicity is composition, size, and cell type dependent. *Particle Fibre Toxicol.* 7, 22 (**2010**).

52. A. Malugin, H. Herd, and H. Ghandehari, Differential toxicity of amorphous silica nanoparticles toward phagocytic and epithelial cells. *J. Nanopart. Res.* 13, 5381 (**2011**).

53. M. V. D. Z. Park, I. Lynch, S. Ramírez-García, K. A. Dawson, L. De La Fonteyne, E. Gremmer, W. Slob, J. J. Briedé, A. Elsaesser, C. V. Howard, H. Van Loveren, and W. H. De Jong, In vitro evaluation of cytotoxic and inflammatory properties of silica nanoparticles of different sizes in murine RAW 264.7 macrophages. *J. Nanopart. Res.* 13, 6775 (**2011**).

54. K. Yu, C. Grabinski, A. Schrand, R. Murdock, W. Wang, B. Gu, J. Schlager, and S. Hussain, Toxicity of amorphous silica nanoparticles in mouse keratinocytes. *J. Nanopart. Res.* 11, 15 (**2009**).

55. A. Kunzmann, B. Andersson, C. Vogt, N. Feliu, F. Ye, S. Gabrielsson, M. S. Toprak, T. Buerki-Thurnherr, S. Laurent, M. Vahter, H. Krug, M. Muhammed, A. Scheynius, and B. Fadeel, Efficient internalization of silica-coated iron oxide nanoparticles of different sizes by primary human macrophages and dendritic cells. *Toxicol. Appl. Pharmacol.* 253, 81 (**2011**).

56. H. Nabeshi, T. Yoshikawa, K. Matsuyama, Y. Nakazato, A. Arimori, M. Isobe, S. Tochigi, S. Kondoh, T. Hirai, T. Akase, T. Yamashita, K. Yamashita, K. Yoshida, K. Nagano, Y. Abe, Y. Yoshioka, H. Kamada, T. Imazawa, N. Itoh, S. I. Tsunoda, and Y. Tsutsumi, Size-dependent cytotoxic effects of amorphous silica nanoparticles on Langerhans cells. *Pharmazie* 65, 199 (**2010**).

57. T. Hirai, T. Yoshikawa, H. Nabeshi, T. Yoshida, S. Tochigi, M. Uji, K. Ichihashi, T. Akase, T. Yamashita, K. Yamashita, K. Nagano, Y. Abe, H. Kamada, S. Tsunoda, Y. Yoshioka, N. Itoh, and Y. Tsutsumi, Size-dependent immune-modulating effect of amorphous nanosilica particles. *Pharmazie* 66, 727 (**2011**).

118

*J. Biomater. Tissue Eng. 3, 108–121, **2013***

REVIEW

58. E. J. Park, J. Yi, K. H. Chung, D. Y. Ryu, J. Choi, and K. Park, Oxidative stress and apoptosis induced by titanium dioxide nanoparticles in cultured BEAS-2B cells. *Toxicol. Lett.* 180, 222 (**2008**).

59. K. M. Waters, L. M. Masiello, R. C. Zangar, B. J. Tarasevich, N. J. Karin, R. D. Quesenberry, S. Bandyopadhyay, J. G. Teeguarden, J. G. Pounds, and B. D. Thrall, Macrophage responses to silica nanoparticles are highly conserved across particle sizes. *Toxicol. Sci.* 107, 553 (**2009**).

60. T. Morishige, Y. Yoshioka, H. Inakura, A. Tanabe, X. Yao, S. Narimatsu, Y. Monobe, T. Imazawa, S. I. Tsunoda, Y. Tsutsumi, Y. Mukai, N. Okada, and S. Nakagawa, The effect of surface modification of amorphous silica particles on NLRP3 inflammasome mediated IL-1Î² production, ROS production and endosomal rupture. *Biomaterials* 31, 6833 (**2010**).

61. G. Oberdörster, E. Oberdörster, and J. Oberdöster, Nanotoxicology: An emerging discipline evolving from studies of ultrafine particles. *Environ. Health Persp.* 113, 823 (**2005**).

62. D. Napierska, L. C. J. Thomassen, V. Rabolli, D. Lison, L. Gonzalez, M. Kirsch-Volders, J. A. Martens, and P. H. Hoet, Size-dependent cytotoxicity of monodisperse silica nanoparticles in human endothelial cells. *Small* 5, 846 (**2009**).

63. J. H. E. Arts, H. Muijser, E. Duistermaat, K. Junker, and C. F. Kuper, Five-day inhalation toxicity study of three types of synthetic amorphous silicas in Wistar rats and post-exposure evaluations for up to 3 months. *Food Chem. Toxicol.* 45, 1856 (**2007**).

64. L. M. Costantini, R. M. Gilberti, and D. A. Knecht, The phagocytosis and toxicity of amorphous silica. *PLoS ONE* 6, e14647 (**2011**).

65. S. Lee, H. S. Yun, and S. H. Kim, The comparative effects of mesoporous silica nanoparticles and colloidal silica on inflammation and apoptosis. *Biomaterials* 32, 9434 (**2011**).

66. S. P. Hudson, R. F. Padera, R. Langer, and D. S. Kohane, The biocompatibility of mesoporous silicates. *Biomaterials* 29, 4045 (**2008**).

67. Y.-S. Lin and C. L. Haynes, Impacts of mesoporous silica nanoparticle size, pore ordering, and pore integrity on hemolytic activity. *J. Amer. Chem. Soc.* 132, 4834 (**2010**).

68. Z. Tao, B. B. Toms, J. Goodisman, and T. Asefa, Mesoporosity and functional group dependent endocytosis and cytotoxicity of silica nanomaterials. *Chem. Res. Toxicol.* 22, 1869 (**2009**).

69. Y. Chen, Z. Xue, D. Zheng, K. Xia, Y. Zhao, T. Liu, Z. Long, and J. Xia, Sodium chloride modified silica nanoparticles as a non-viral vector with a high efficiency of DNA transfer into cells. *Current Gene Therapy* 3, 273 (**2003**).

70. C. Kneuer, M. Sameti, U. Bakowsky, T. Schiestel, H. Schirra, H. Schmidt, and C. M. Lehr, A nonviral DNA delivery system based on surface modified silica-nanoparticles can efficiently transfect cells *in vitro*. *Bioconj. Chem.* 11, 926 (**2000**).

71. M. N. V. Ravi Kumar, M. Sameti, S. S. Mohapatra, X. Kong, R. F. Lockey, U. Bakowsky, G. Lindenblatt, H. Schmidt, and C. M. Lehr, Cationic silica nanoparticles as gene carriers: Synthesis, characterization and transfection efficiency *in vitro* and *In vivo*. *J. Nanosci. Nanotechnol.* 4, 876 (**2004**).

72. I. Roy, T. Y. Ohulchanskyy, D. J. Bharali, H. E. Pudavar, R. A. Mistretta, N. Kaur, and P. N. Prasad, Optical tracking of organically modified silica nanoparticles as DNA carriers: A nonviral, nanomedicine approach for gene delivery. *PNAS* 102, 279 (**2005**).

73. D. J. Bharali, I. Klejbor, E. K. Stachowiak, P. Dutta, I. Roy, N. Kaur, E. J. Bergey, P. N. Prasad, and M. K. Stachowiak, Organically modified silica nanoparticles: A nonviral vector for *in vivo* gene delivery and expression in the brain. *PNAS* 102, 11539 (**2005**).

74. A. M. Mumin, J. W. Barrett, G. A. Dekaban, and J. Zhang, Dendritic cell internalization of foam-structured fluorescent mesoporous silica nanoparticles. *J. Colloids Interf. Sci.* 353, 156 (**2011**).

75. E. B. Gyenge, A. Darphin, A. Wirth, U. Pieles, H. Walt, M. Bredell, and C. Maake, Uptake and fate of surface modified silica nanoparticles in head and neck squamous cell carcinoma. *J. Nanobiotechnol.* 9, 32 (**2011**).

76. D. Dutta, S. K. Sundaram, J. G. Teeguarden, B. J. Riley, L. S. Fifield, J. M. Jacobs, S. R. Addleman, G. A. Kaysen, B. M. Moudgil, and T. J. Weber, Adsorbed proteins influence the biological activity and molecular targeting of nanomaterials. *Toxicol. Sci.* 100, 303 (**2007**).

77. M. Massignani, C. LoPresti, A. Blanazs, J. Madsen, S. P. Armes, A. L. Lewis, and G. Battaglia, Controlling Cellular Uptake by Surface Chemistry, Size, and Surface Topology at the Nanoscale. *Small* 5, 2424 (**2009**).

78. T.-G. Iversen, T. Skotland, and K. Sandvig, Endocytosis and intracellular transport of nanoparticles: Present knowledge and need for future studies. *Nano Today* 6, 176 (**2011**).

79. N. Daum, C. Tscheka, A. Neumeyer, and M. Schneider, Novel approaches for drug delivery systems in nanomedicine: effects of particle design and shape. *Nanomed. Nanobiotechnol.* 4, 52 (**2012**).

80. S. Zhang, J. Li, G. Lykotrafitis, G. Bao, and S. Suresh, Size-Dependent Endocytosis of Nanoparticles. *Adv. Mater.* 21, 419 (**2009**).

81. F. Lu, S.-H. Wu, Y. Hung, and C.-Y. Mou, Size Effect on Cell Uptake in Well-Suspended, Uniform Mesoporous Silica Nanoparticles. *Small* 5, 1408 (**2009**).

82. J. Choi, Q. Zheng, H. E. Katz, and T. R. Guilarte, Silica-based nanoparticle uptake and cellular response by primary microglia. *Environ. Health Persp.* 118, 589 (**2010**).

83. A. T. Bauer, E. A. Strozyk, C. Gorzelanny, C. Westerhausen, A. Desch, M. F. Schneider, and S. W. Schneider, Cytotoxicity of silica nanoparticles through exocytosis of von Willebrand factor and necrotic cell death in primary human endothelial cells. *Biomaterials* 32, 8385 (**2011**).

84. S. Quignard, G. Mosser, M. Boissière, and T. Coradin, Long-term fate of silica nanoparticles interacting with human dermal fibroblasts. *Biomaterials* 33, 4431 (**2012**).

85. M. F. Desimone, C. Hélary, G. Mosser, M. M. Giraud-Guille, J. Livage, and T. Coradin, Fibroblast encapsulation in hybrid silica-collagen hydrogels. *J. Mater. Chem.* 20, 666 (**2010**).

86. M. F. Desimone, C. Hélary, I. B. Rietveld, I. Bataille, G. Mosser, M. M. Giraud-Guille, J. Livage, and T. Coradin, Silica-collagen bionanocomposites as three-dimensional scaffolds for fibroblast immobilization. *Acta Biomater.* 6, 3998 (**2010**).

87. S. Quignard, G. J. Copello, C. Aimé, I. Bataille, C. Helary, M. F. Desimone, and T. Coradin, Influence of silicification on the structural and biological properties of buffer-mediated collagen hydrogels. *Adv. Eng. Mater.* 14, B51 (**2012**).

88. X. Xing, X. He, J. Peng, K. Wang, and W. Tan, Uptake of silica-coated nanoparticles by HeLa cells. *J. Nanosci. Nanotechnol.* 5, 1688 (**2005**).

89. H. Nabeshi, T. Yoshikawa, A. Arimori, T. Yoshida, S. Tochigi, T. Hirai, T. Akase, K. Nagano, Y. Abe, H. Kamada, S. Tsunoda, N. Itoh, Y. Yoshioka, and Y. Tsutsumi, Effect of surface properties of silica nanoparticles on their cytotoxicity and cellular distribution in murine macrophages. *Nanoscale Res. Lett.* 6, X1 (**2011**).

90. T. C. Long, J. Tajuba, P. Sama, N. Saleh, C. Swartz, J. Parker, S. Hester, G. V. Lowry, and B. Veronesi, Nanosize titanium dioxide stimulates reactive oxygen species in brain microglia and damages neurons *in vitro*. *Environ. Health Persp.* 115, 1631 (**2007**).

91. J. K. Su, M. K. Byeong, J. L. Young, and W. C. Hai, Titanium dioxide nanoparticles trigger p53-mediated damage response in peripheral blood lymphocytes. *Environ. Mol. Mutag.* 49, 399 (**2008**).

92. M. Thibodeau, C. Giardina, and A. K. Hubbard, Silica-induced caspase activation in mouse alveolar macrophages is dependent upon

mitochondrial integrity and aspartic proteolysis. *Toxicol. Sci.* 76, 91 (**2003**).

93. R. Meneghini, Iron Homeostasis, Oxidative Stress, and DNA Damage. *Free Rad. Biol. Med.* 23, 783 (**1997**).

94. M. S. Cooke, M. D. Evans, M. Dizdaroglu, and J. Lunec, Oxidative DNA damage: mechanisms, mutation, and disease. *FASEB J.* 17, 1195 (**2003**).

95. F. Wang, F. Gao, M. Lan, H. Yuan, Y. Huang, and J. Liu, Oxidative stress contributes to silica nanoparticle-induced cytotoxicity in human embryonic kidney cells. *Toxicol. In Vitro* 23, 808 (**2009**).

96. W. Lin, Y. W. Huang, X. D. Zhou, and Y. Ma, *In vitro* toxicity of silica nanoparticles in human lung cancer cells. *Toxicol. Appl. Pharmacol.* 217, 252 (**2006**).

97. Y. Ye, J. Liu, J. Xu, L. Sun, M. Chen, and M. Lan, Nano-SiO$_2$ induces apoptosis via activation of p53 and Bax mediated by oxidative stress in human hepatic cell line. *Toxicol, In Vitro* 24, 751 (**2010**).

98. Q. J. X. Lu, H. Zhou, Q. Gan, W. Tang, J. Lu, Y. Yuan, and C. Liu, *In vitro* cytotoxicity and induction of apoptosis by silica nanoparticles in human HepG2 hepatoma cells. *Int. J. Nanomed.* 6, 1889 (**2011**).

99. J. Ahmad, M. Ahamed, M. J. Akhtar, S. A. Alrokayan, M. A. Siddiqui, J. Musarrat, and A. A. Al-Khedhairy, Apoptosis induction by silica nanoparticles mediated through reactive oxygen species in human liver cell line HepG2. *Toxicol. Appl. Pharmacol.* 259, 160 (**2012**).

100. H. Nabeshi, T. Yoshikawa, K. Matsuyama, Y. Nakazato, S. Tochigi, S. Kondoh, T. Hirai, T. Akase, K. Nagano, Y. Abe, Y. Yoshioka, H. Kamada, N. Itoh, S. I. Tsunoda, and Y. Tsutsumi, Amorphous nanosilica induce endocytosis-dependent ROS generation and DNA damage in human keratinocytes. *Particle Fibre Toxicol.* 8, 1 (**2011**).

101. M. Lucarelli, A. M. Gatti, G. Savarino, P. Quattroni, L. Martinelli, E. Monari, and D. Boraschi, Innate defence functions of macrophages can be biased by nano-sized ceramic and metallic particles. *European Cytokine Network* 15, 339 (**2004**).

102. M. Winter, H. D. Beer, V. Hornung, U. Kärmer, R. P. F. Schins, and I. Förster, Activation of the inflammasome by amorphous silica and TiO2 nanoparticles in murine dendritic cells. *Nanotoxicol.* 5, 326 (**2011**).

103. Z. Tao, M. P. Morrow, T. Asefa, K. K. Sharma, C. Duncan, A. Anan, H. S. Penefsky, J. Goodisman, and A. K. Souid, Mesoporous silica nanoparticles inhibit cellular respiration. *Nano Lett.* 8, 1517 (**2008**).

104. N. D. Magnani, T. Marchini, D. R. Tasat, S. Alvarez, and P. A. Evelson, Lung oxidative metabolism after exposure to ambient particles. *Biochem. Biophys. Res. Commun.* 412, 667 (**2011**).

105. N. Louhelainen, M. Myllärniemi, I. Rahman, and V. L. Kinnula, Airway biomarkers of the oxidant burden in asthma and chronic obstructive pulmonary disease: Current and future perspectives. *International Journal of COPD* 3, 585 (**2008**).

106. R. Kumar, I. Roy, T. Y. Ohulchanskyy, L. A. Vathy, E. J. Bergey, M. Sajjad, and P. N. Prasad, *In vivo* biodistribution and clearance studies using multimodal organically modified silica nanoparticles. *ACS Nano* 4, 699 (**2010**).

107. T. Liu, L. Li, X. Teng, X. Huang, H. Liu, D. Chen, J. Ren, J. He, and F. Tang, Single and repeated dose toxicity of mesoporous hollow silica nanoparticles in intravenously exposed mice. *Biomaterials* 32, 1657 (**2011**).

108. T. Liu, L. Li, C. Fu, H. Liu, D. Chen, and F. Tang, Pathological mechanisms of liver injury caused by continuous intraperitoneal injection of silica nanoparticles. *Biomaterials* 33, 2399 (**2012**).

109. G. Xie, J. Sun, G. Zhong, L. Shi, and D. Zhang, Biodistribution and toxicity of intravenously administered silica nanoparticles in mice. *Arch. Toxicol.* 84, 183 (**2010**).

110. M. Cho, W.-S. Cho, M. Choi, S. J. Kim, B. S. Han, S. H. Kim, H. O. Kim, Y. Y. Sheen, and J. Jeong, The impact of size on tissue distribution and elimination by single intravenous injection of silica nanoparticles. *Toxicol. Lett.* 189, 177 (**2009**).

111. Z. Chen, H. Chen, H. Meng, G. Xing, X. Gao, B. Sun, X. Shi, H. Yuan, C. Zhang, R. Liu, F. Zhao, Y. Zhao, and X. Fang, Biodistribution and metabolic paths of silica coated CdSeS quantum dots. *Toxicol. Appl. Pharmacol.* 230, 364 (**2008**).

112. S. Nagayama, K. Ogawara, Y. Fukuoka, K. Higaki, and T. Kimura, Time-Dependent Changes in Opsonin Amount Associated on Nanoparticles Alter Their Hepatic Uptake Characteristics. *Int. J. Pharm.* 342, 215 (**2007**).

113. Q. He, Z. Zhang, F. Gao, Y. Li, and J. Shi, *In vivo* Biodistribution and Urinary Excretion of Mesoporous Silica Nanoparticles: Effects of Particle Size and PEGylation. *Small* 7, 271 (**2011**).

114. G. Oberdörster, A. Maynard, K. Donaldson, V. Castranova, J. Fitzpatrick, K. Ausman, J. Carter, B. Karn, W. Kreyling, D. Lai, S. Olin, N. Monteiro-Riviere, D. Warheit, and H. Yang, Principles for characterizing the potential human health effects from exposure to nanomaterials: elements of a screening strategy. *Particle Fibre Toxicol.* 2, 8 (**2005**).

115. X. Lu, Y. Tian, Q. Zhao, T. Jin, S. Xiao, and X. Fan, Integrated metabonomics analysis of the size-response relationship of silica nanoparticles-induced toxicity in mice. *Nanotechnol.* 22, 055101 (**2011**).

116. T. R. Downs, M. E. Crosby, T. Hu, S. Kumar, A. Sullivan, K. Sarlo, B. Reeder, M. Lynch, M. Wagner, T. Mills, and S. Pfuhler, Silica nanoparticles administered at the maximum tolerated dose induce genotoxic effects through an inflammatory reaction while gold nanoparticles do not. *Mutation Research/Genetic Toxicol. Environmental Mutagenesis* 745, 38 (**2012**).

117. K. Yamashita, Y. Yoshioka, K. Higashisaka, K. Mimura, Y. Morishita, M. Nozaki, T. Yoshida, T. Ogura, H. Nabeshi, K. Nagano, Y. Abe, H. Kamada, Y. Monobe, T. Imazawa, H. Aoshima, K. Shishido, Y. Kawai, T. Mayumi, S. I. Tsunoda, N. Itoh, T. Yoshikawa, I. Yanagihara, S. Saito, and Y. Tsutsumi, Silica and titanium dioxide nanoparticles cause pregnancy complications in mice. *Nature Nanotechnol.* 6, 321 (**2011**).

118. Y. Morishita, Y. Yoshioka, H. Satoh, N. Nojiri, K. Nagano, Y. Abe, H. Kamada, S. I. Tsunoda, H. Nabeshi, T. Yoshikawa, and Y. Tsutsumi, Distribution and histologic effects of intravenously administered amorphous nanosilica particles in the testes of mice. *Biochem. Biophys. Res. Comm.* 420, 297 (**2012**).

119. Z. Lan and W. X. Yang, Nanoparticles and spermatogenesis: How do nanoparticles affect spermatogenesis and penetrate the blood-testis barrier. *Nanomed.* 7, 579 (**2012**).

120. C. Aimé and T. Coradin, Nanocomposites from biopolymer hydrogels: Blueprints for white biotechnology and green materials chemistry. *J. Polymer Sci. Part B: Polymer Phys.* 50, 669 (**2012**).

121. M. F. Desimone, C. Hélary, S. Quignard, I. B. Rietveld, I. Bataille, G. J. Copello, G. Mosser, M.-M. Giraud-Guille, J. Livage, A. Meddahi-Pellé, and T. Coradin, *In vitro* studies and preliminary *in vivo* evaluation of silicified concentrated collagen hydrogels. *ACS Appl. Mater. Interf.* 3, 3831 (**2011**).

122. J. S. Souris, C. H. Lee, S. H. Cheng, C. T. Chen, C. S. Yang, J. A. A. Ho, C. Y. Mou, and L. W. Lo, Surface charge-mediated rapid hepatobiliary excretion of mesoporous silica nanoparticles. *Biomaterials* 31, 5564 (**2010**).

123. X. He, H. Nie, K. Wang, W. Tan, X. Wu, and P. Zhang, *In vivo* study of biodistribution and urinary excretion of surface-modified silica nanoparticles. *Anal. Chem.* 80, 9597 (**2008**).

124. C. Yagüe, M. Moros, V. Grazu, M. Arruebo, and J. Santamaría, Synthesis and stealthing study of bare and PEGylated silica micro- and nanoparticles as potential drug-delivery vectors. *Chem. Eng. J.* 137, 45 (**2008**).

REVIEW

125. Q. He, J. Zhang, J. Shi, Z. Zhu, L. Zhang, W. Bu, L. Guo, and Y. Chen, The effect of PEGylation of mesoporous silica nanoparticles on nonspecific binding of serum proteins and cellular responses. *Biomaterials* 31, 1085 (**2009**).

126. S. Ku, F. Yan, Y. Wang, Y. Sun, N. Yang, and L. Ye, The blood-brain barrier penetration and distribution of PEGylated fluorescein-doped magnetic silica nanoparticles in rat brain. *Biochem. Biophys. Res. Comm.* 394, 871 (**2010**).

127. J. S. Kim, T.-J. Yoon, K. N. Yu, B. G. Kim, S. J. Park, H. W. Kim, K. H. Lee, S. B. Park, J.-K. Lee, and M. H. Cho, Toxicity and tissue distribution of magnetic nanoparticles in mice. *Toxicol. Sci.* 89, 338 (**2006**).

REVIEW

Vitamin E TPGS Used as Emulsifier in the Preparation of Nanoparticulate Systems

Ezequiel Bernabeu[1] and Diego A. Chiappetta[1, 2, *]

[1]*Faculty of Pharmacy and Biochemistry, Department of Pharmaceutical Technology,*
University of Buenos Aires, Buenos Aires CP1113, Argentina
[2]*National Science Research Council (CONICET), Faculty of Pharmacy and Biochemistry,*
Department of Pharmaceutical Technology, University of Buenos Aires,
Buenos Aires CP1113, Argentina

In recent years, nanoparticulate systems have matured from simple devices to multifunctional and more complex systems. They are biodegradable, stable in blood, non-toxic, and non immunogenic construct, capable of delivering drugs in a specific site, thereby improving efficacy. Their capabilities as drug delivery system and the interaction with the biological cells in the target tissue are dependent on their physicochemical properties such as particles size, size distribution, surface charge and morphology. Polymeric nanoparticles are usually produced by two classical methods: nanoprecipitation and emulsion-solvent evaporation technique. In such process, a number of preparation parameters can affect the nature of the nanoparticles as: drug, polymer concentration, temperature, solvent volume, aqueous:organic phase ratio, type and concentration of emulsifier and so forth. One of the most important formulation parameters involves the emulsifier, which is necessary as surfactant stabilizer in the process to form nanoparticles. D-α-tocopheryl polyethylene glycol (PEG) 1000 succinate (TPGS) is a water soluble derivate of natural source vitamin E. It is amphipathic and hydrophilic, exhibiting the characteristics of a typical surface-active agent. This review summarizes recently available information regarding the emulsifying effects of TPGS on the preparation, characterization, *in vitro* release and *in vivo* performance of the nanoparticulate systems, and the advantages of TPGS-drug conjugates.

Keywords: Biodegradable Polymeric Nanoparticles, TPGS-Copolymers, TPGS-Drug Conjugates, Vitamin E TPGS.

CONTENTS

---

*Author to whom correspondence should be addressed.

1. INTRODUCTION

Nanomedicine is defined as a nanotechnology medical application which exploits and assimilates recent scientific advances to prevent, diagnose, treat and cure human disease.[1] The continued progress in this field allows us to focus on new drug delivery systems and molecules development to improve illness treatment. The ideal goal for diseases treatment is a high efficient and safety drug transport to the right place at appropiated concentrations for an adequate period of time. Nanoparticulate systems can increase the efficacy and safety of drugs by improving solubility, protecting against metabolism, controlling release and drug targeting.[2] The mingy concentrations of drugs reaching the target tissues and the limited retention time at the cellular level are one of the main factors contributing to treatment failure. These "nano" drug delivery systems seek to concentrate the drug in the site of interest, reducing the relative concentration of the drug in the

rest of body to improve the medical treatments. Today, commercially available nanotechnology products are an effective alternative drug delivery platform used for the treatment of complex disease.[3] Generally, these products are designed to overcome the problems of drug poor solubility and bioavailability. Nowadays, almost 60% of drugs coming from synthesis are aqueous poorly soluble which led to low oral bioavailability.[4] For example, a water insoluble chemotherapy drug such as paclitaxel (PTX) has been reformulated into albumin nanoparticles (Abraxane®) with a mean particle size of 130 nm.[5] This nanoparticulate system allowed the administration of higher doses of PTX with shorter infusion duration than Taxol® (PTX-solution). For example, the infusion duration is 3 h for Taxol® and only 30 min for Abraxane®. Another encouraging issue was the possibility of overcome solvent-related problems of PTX.[3]

In recent years, nanoparticles (NPs) have matured from simple devices to more complex systems. NPs are defined as solid systems that usually share, as a common feature, a size range from a few nanometers (nm) to several hundred nm.[6] Nanoparticulate systems materials must be biocompatible and biodegradable for their use in the clinic. These biomaterials should be reduce, metabolize and eliminate by the body's natural pathways.[7] The choice of biomaterials with different physicochemical properties (molecular weight, hydrophilic–lipophilic balance and crystallinity) allows the modulation of drug delivery rates. Depending on the method of preparation, it is possible to generate nanocapsules or nanospheres.[8–11] The nanocapsules are vesicular systems in which the drug is adsorbed on the surface of the particle or placed in liquid interior surrounded by the polymeric layer. In contrast, the nanospheres are constituted by a spherical matrix, where the drug can be entrapped within the particle or adsorbed on the surface.[12] A very important point in the nanoparticulate systems is the particle surface. Once in the bloodstream, charged NPs without surface modification can be rapidly opsonized and massively cleared by the fixed macrophages. As a general rule, hydrophobic particles can be opsonized more quickly that hydrophilic particles due the enhanced adsorbability of blood serum proteins on these surfaces.[13] Surface modification of NPs with hydrophilic polymers and/or non-ionic surfactants is the most common way to slow, or even avoid, protein opsonization and to improve the surface properties of the system. These hydrophilic polymers or non-ionic surfactants are adsorbed or grafted in the surface of NPs in order to block electrostatic and hydrophobic interactions that promote opsonization process. This phenomena is denominated PEGylation.[13–14] The polymers and non-ionic surfactants more used in the NPs surface modification include polysaccharides, polyacrylamide, poly(vinyl alcohol), poly(N-vinyl-2-pyrrolidone), polyethylene glycol (PEG), and PEG-containing copolymers such as poloxamers, poloxamines, polysorbates, and PEG copolymers.[13] Recently, other polymers such as polyoxazolines, poly(amino acids), polybetaines and polyglycerols have been applied as surface coating agents.[15] One surfactant used recently for surface coating is the
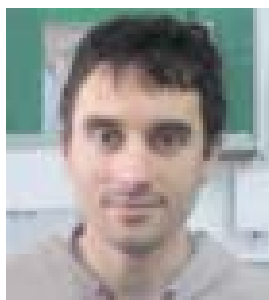
Ezequiel Bernabeu was born in Buenos Aires, Argentine, in 1978. He graduated in Pharmacy at Universidad de Buenos Aires in 2007. In the same year, he received a fellowship in pharmacokinetic and pharmaceutical technology from the Pharmacy Service of Paediatric Hospital J.P. Garrahan, Argentine. In 2010, he moved to the Department of Pharmaceutical Technology from the same University and obtained a doctoral fellowship from the National Agency for Promotion of Science and Technology, Argentine. He currently is doing his Ph.D under the guidance of Prof. Dr. D.A. Chiappetta. He has about three publications and six presentations in scientific meetings. His research interests are focused on biopolymers, modification of polycaprolactone, and their applications as nanosystems for drug delivery.

Diego A. Chiappetta was born in Buenos Aires, Argentine, in 1975. He graduated in Pharmacy at Universidad de Buenos Aires (2001) and received his Ph.D. degree from the same university (2006) on the area of Pharmaceutical Technology. In 2007–2008, he obtained a postdoctoral fellowship from the National Science Research Council (CONICET) at the Department of Pharmaceutical Technology of the Faculty of Pharmacy and Biochemistry. At present, Dr. Diego Chiappetta holds a position of Adjunct Professor in the Department of Pharmaceutical Technology where too is Assistant Investigator of CONICET. His research interests are focused on drug delivery "nano" systems, including polymeric micelles and polymeric nanoparticles for drug delivery. He is a founding member of the Argentine Association of Nanomedicine (NANOMED-AR). He has published 46 research articles, 1 book chapter and holds 2 patent applications. He is reviewer of international journals in the field of Pharmaceutical Sciences. He has undertaken projects funded by University of Buenos Aires and by Ministry of Science and Technology of Argentine. He was awarded with diverse national and international scientific prizes and distinctions.

REVIEW

D-α-tocopheryl polyethylene glycol 1000 succinate (vitamin E TPGS or TPGS).[16–18] TPGS is a water-soluble derivative of natural source vitamin E and PEG. This molecule results from the esterification of vitamin E succinate with PEG. It contains a lipophilic and a hydrophilic portion (Scheme 1), making it similar to a conventional surface-active agent.[19] Another very important feature is that TPGS can be intact absorbed in the gastrointestinal tracts, and inhibits efflux pumps such as *P*-glycoprotein (*P*-gp). Therefore cytotoxicity of anticancer agents with low oral bioavailability can be enhanced.[16] Also, several authors have also demonstrated the effects of TPGS as an effective oral absorption enhancer for improving bioavailability of several poor absorbed drugs.[20–23]

This review summarizes recently available information regarding the emulsifying effects of TPGS on preparation, characterization, *in vitro* release and *in vivo* performance of nanoparticulate systems, and the advantages of TPGS-drug conjugates.

2. APPLICATIONS AND ADVANTAGES OF TPGS IN NANOPARTICLES FOR DRUG DELIVERY

TPGS is a water-soluble form of the natural Vitamin E (α-tocopherol) which has been approved by the Food and Drug Administration (FDA) as a safe pharmaceutical excipient in drug formulation.[24] TPGS contains 260 mg/g of vitamin E (387 IU/g) and a molecular weight of ~ 1513 Da. It is a waxy solid which is water miscible in all parts and it presents a HLB value of about 13.2. Also, TPGS is soluble in common excipients used in both preclinical and commercial formulations such as ethanol and PEG400.[25] TPGS melting point is range between 37 and 41 °C.[26] It has been administered satisfactorily for vitamin E deficiency treatment in patients with cystic fibrosis, Crohn's disease, congenital hepatic cholestasis, short bowel and also in premature infants with low birth weight.[27–31] Due to its physicochemical properties it has been used as an oral absorption enhancer to improved oral bioavailability of poorly absorbed drugs such as amprenavir, cyclosporine A and vitamin D.[32–34] In some cases, the bioavailability
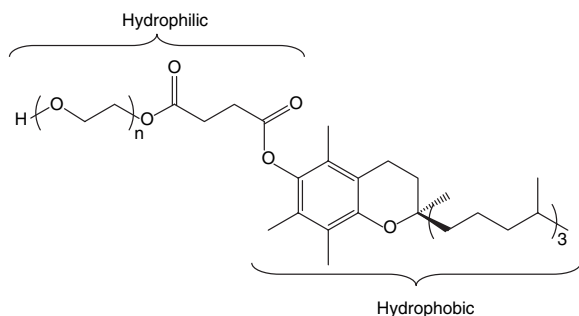
improvement could be observed at levels below the TPGS CMC value (0.02% w/v at 37 °C).[35–37] Nevertheless, these improvement could be also attributed to the enhanced on drug solubility due to micellar solubilization and/or TPGS capacity to inhibit *P*-gp.[38] Lately, several authors have described that α-tocopheryl succinate (α-TOS) has antineoplastic activity *in vitro* on many cancer cells lines.[39] Also, Youk et al. reported that TPGS was more potent than α-TOS in carcinoma growth inhibition in human lung cells.[40] Additional experiments are still necessary to confirm the potential anticancer activity of TPGS.

In recent years, TPGS has been used as an emulsifier for provide stability in the preparation of NPs. Generally, TPGS can be used in a concentration range from 0.015 to 0.06% w/v.[41] Some researchers use concentrations of up to 1% w/v[42] and others up to 5% w/v for the preparation of different NPs.[43] As emulsifier, TPGS was 67 times more effective than polyvinyl alcohol (PVA) in poly-lactic-*co*-glycolic acid (PLGA) NPs preparation by o/w emulsion solvent evaporation method.[41] Further, TPGS could achieve good efficiency of encapsulation (EE) for hydrophobic drugs resulting, in some cases, as high as 100%.[44–45] Additionally, TPGS could be used as a matrix component to improve NPs pharmaceutical properties. To achieve this, an interesting alternative was the synthesis of polymers such as poly-lactic acid (PLA) or poly-ε-caprolactone (PCL) with TPGS to form different copolymers. PTX-loaded PLA-TPGS NPs presented a faster PXT release rate than PTX-loaded PLGA NPs due to the higher hydrophilic character imposed by TPGS.[46] At the cellular level, it has been reported that NPs fabricated with TPGS as emulsifier could have higher cellular uptake efficiency compared to PVA-coated NPs in Caco-2 cells.[47] In Human colon adenocarcinoma cells (HT-29 cells), cellular uptake increased as follows PVA-emulsified PLGA NPs (27%) < TPGS-emulsified PLGA NPs (40%) < PLA-TPGS NPs (53%).[46] These are encouraging results but other experiments should be performed using multiple cell types and *in vivo* models to identify the true benefit.

3. BIODEGRADABLE POLYMERS USED IN NANOPARTICULATES SYSTEMS USING TPGS AS EMULSIFIER/STABILIZER

Nanoparticulates systems can be prepared from preformed polymers or from a monomer during its polymerization by several methods.[48] The most commonly-applied strategy for polymeric NPs production relies on premade polymers.[49] Because of the non toxic properties and biocompatibility of the degradation products, it is better to use biodegradable polymers. These can be from a natural or a synthetic origin. Natural biodegradable polymers are based on its low cost, its biocompatibility and its solubility in aqueous medium. Despite these advantages, they have a limited use due to the variability in its composition and molecular weight between batches. On the other

Scheme 1. Chemical structure of TPGS.

hand, synthetic biodegradable polymers have a high reproducibility between batches. This allows controlling and predicting the degradation kinetics of these polymers.[50] The synthetic biodegradable polymers more studied and used for NPs preparation, using TPGS as surfactant, are PLA[51] and PLGA.[45, 47, 52–54] PLA and PLGA belong to polyesters aliphatic family which was initially developed by the pharmaceutical industry for use as degradable surgical sutures.[55] Other polyester commonly used is poly-ε-caprolactone (PCL) which is less expensive than PLA and PLGA.[56] This family has gained popularity, mainly because of their noteworthy properties in terms of biocompatibility, biodegradability, and by its approval for use in human by the FDA.[57] This is relevant for the pharmaceutical industry because, FDA-approved pharmaceutical excipients appear as a better alternative for the development of pharmaceutical products than other new copolymers under evaluation which need long and expensive biocompatibility assays.

Particularly, these NPs are usually produced by two classical methods: nanoprecipitation and emulsion-solvent evaporation technique. In both techniques, NPs are formed by the precipitation of polymer in a TPGS-containing aqueous phase followed by solvent evaporation. In the nanoprecipitation, the polymer and drug are dissolved in an organic solvent miscible with water (e.g., acetone) and then mixed into an aqueous phase with TPGS. After the addition of the organic phase, the diffusion of the solvent into the aqueous phase will cause the polymer to precipitate, and drug-loaded NPs, will be form. In the emulsion-solvent evaporation method, the polymer and drug are dissolved in a non water-miscible solvent (e.g., dichloromethane, ethyl acetate) and mixed into an aqueous phase with TPGS forming an oil-in-water emulsion. This dispersion is formed upon mixing by sonication or high speed homogenization of the two phases and particles form upon solvent evaporation. The emulsion-solvent evaporation method is used to encapsulate either hydrophobic or hydrophilic drugs.[41] If the drug is hydrophilic, the technique should be modified to form a water-in-oil-in-water (w/o/w) emulsion. TPGS plays a key role to improve the characteristics of the NPs (size, surface morphology, drug loading and drug release).[57–60]

3.1. PLA and PLGA NPs Emulsified/Stabilized with TPGS

Several approaches have been proposed for the preparation of PLA and PLGA NPs (Table I). PLGA NPs are frequently used for the encapsulation of various anticancer drugs such as PTX. It is an antineoplastic agent (mitotic inhibitor) with poor water solubility and effective for various cancer especially ovarian and breast cancer. The commercial formulation (Taxol®) is formulated with high Cremophor EL concentrations, which has been associated with severe side effects.[61] Mu et al. reported that

optimizing the formulation parameters, drug EE could be as high as 100% for PTX-loaded PLGA NPs with TPGS as emulsifier agent.[41] Also, under the same fabrication condition, the required amount of TPGS was 67 times lower than the required amount of PVA to achieve the same emulsifying effects. This point is very important because it would need only a small amount of surfactant to produce NPs. For example 1% w/v of PVA would be equivalent to 0.015% w/v of TPGS. Other study has demonstrated that, PLA and PLGA NPs prepared with a TPGS concentration between 0.02–0.03% w/v showed the best nanoparticle yield. Also different NPs formulations fabricated with two PLGA types (75:25 and 50:50) and 0.03% w/v of TPGS, as emulsifier, showed EE between 49 and 84%. These NPs presented a hydrodynamic diameter ranged between 370–655 nm. Under SEM and AFM observation, all particles had a fine spherical shape. As to the *in vitro* release assays, an initial release burst was prominent during the first day ($\geq 15\%$). Then, the release gradually decreases and remains constant even after 1 month.[41] Win and Feng evaluated this type of NPs on *in vitro* assays with HT-29 cells. PTX loaded-PLGA NPs showed higher toxicity than the commercial formulation.[52] *In vitro* cytotoxicity studies in C6 glioma cells revealed that PTX-loaded PLGA NPs ($IC_{50} = 9.6$ μg/ml) showed 3.40 times greater cytotoxicity than PTX solution ($IC_{50} = 32.7$ μg/ml) in 48 h culture at 37 °C. In addition, the mortality was almost despicable for the blank PLGA NPs.[62] More over, Feng's group evaluated PTX-loaded PLGA NPs for oral chemotherapy. These NPs presented spherical shape of 200–300 nm diameters with an EE of 80.9%. NPs *In vivo* evaluation achieved more than 10 times higher oral bioavailability than Taxol®, which result 9.74-fold higher therapeutic effect and 12.56-fold longer sustainable therapeutic time than Taxol®.[63] In case of I.V. route, NPs produced a significant increase in the half life of PTX in an *in vivo* s.c. C6 cells xenograft model. Moreover, a single administration of NPs achieved a sustained therapeutic effect for 7 days, while PTX solution effect remained only for 22.2 hours. In addition, these NPs administered via intratumoral were 1.5 times more effective than Taxol® to suppress tumor growth.[63] Also, PTX-loaded TPGS-emulsified PLGA NPs administered I.V. increased the AUC (area-under-the-curve) by a factor of 4.9 compared to Taxol®.[52]

Due to complications presented by the I.V. route, the oral route is a very good alternative for ambulatory cancer patient's therapy. For this reason, the deeply investigation of the oral administration of the traditionally I.V.-administered anticancer drugs represent a real challenge.[64] Caco-2 cell line (colon adenocarcinoma) can be used to *in vitro* simulate the gastrointestinal barrier and to evaluate cellular uptake of oral anticancer drugs. Win and Feng prepared PVA-emulsified and TPGS-emulsified coumarine-6-labelled PLGA NPs to evaluate uptake cellular. Images of confocal laser scanning microscopy (CLSM)

Table I. Examples of NPs prepared with biodegradable polymers using TPGS as emulsifier/stabilizer.

Polymer	Preparation method	Drug	Size (nm)	PDI	EE%	Comments	Ref.
PLGA (50:50)	Emulsion-solvent evaporation	PTX	~685	0.005	100	In comparison with PVA, the TPGS could significantly improve the encapsulation efficiency of the drug in the NPs.	[46]
PLGA (50:50); (75:25) and PLA	Emulsion-solvent evaporation	PTX	~515; ~272 and ~589 for each polymer	0.005; 0.245 and 0.326	~53; ~50 and ~43	NPs of nanometer size with narrow distribution can be obtained.	[41]
PLGA (50:50)	Emulsion-solvent evaporation	PTX	~236	0.012	~66	The AUC for 48 h for TPGS emulsified PLGA NPs of PTX were found 4.9 times larger than that for the Taxol®.	[52]
PLGA (50:50)	Emulsion-solvent evaporation	PTX	~288	0.028	~93	TPGS-emulsified NPs have great advantages versus PVA-emulsified NPs for local delivery of antiproliferative drugs.	[54]
PLGA (50:50)	Emulsion-solvent evaporation	Atorvastatin calcium	~140	0.150	~35	NPs presented better efficacy and safety parameters that marketed formulation.	[69]
PLGA	Emulsion-solvent evaporation	PTX	200–300	N.D.	~81	NPs achieved more than 10 times higher oral bioavailability than Taxol®, which resulted 9.74-fold higher therapeutic effect than Taxol®.	[63]
PLGA	Emulsion-solvent evaporation	Iron oxides	~280	0.120	N.D.	NPs were tested *in vivo* using xenograft mice. They are able to reach the tumor by EPR as shown by magnetic resonance imaging.	[123]
	Nanoprecipitation		~220	0.109	N.D.		
PLGA (50:50)	Emulsion-solvent evaporation	Meloxicam	1st population: 68–82; 2nd population: 367–475	0.449–0.651	50–58	NPs produced with TPGS showed bimodal size distribution. An increase in sonication time leads to an increase in the production of smaller particles with narrower size distribution.	[44]

Notes: *Abbreviations*: PLGA, poly-lactic-*co*-glycolic acid; PTX, paclitaxel; PVA, polyvinyl alcohol; TPGS, D-α-tocopheryl polyethylene glycol (PEG) 1000 succinate; AUC, area under curve; N.D., not data.

126

*J. Biomater. Tissue Eng. 3, 122–134, **2013***

REVIEW

clearly showed that the particles were internalized in the cells and that surface modification of PLGA NPs with vitamin E TPGS improved the cellular uptake (1.4 fold).[47] More recently, Zhao and Feng evaluated TPGS-emulsified PTX-PLGA NPs for oral chemotherapy. The NPs developed showed an oral bioavailability 10 times greater than Taxol® in rats.[63]

With other therapeutic purpose, PTX has been used in treatment of coronary in-stent restenosis with PTX-coated balloon catheters.[65] Considering this application, Feng et al. encapsulated PTX in PLGA NPs using PVA or TPGS as emulsifier agent. These NPs were tested for the treatment and prevention of restenosis in coronary artery smooth muscle cells (CASMCs) and in an animal model (rabbit). *In vitro* study showed that PVA and TPGS-emulsified NPs presented higher antiproliferative effects than Taxol® (3.66 and 5.15 times, respectively). Furthermore, TPGS-emulsified NPs ($IC_{50} = 160$ ng/ml) was 47% more effective than Taxol® ($IC_{50} = 748$ ng/ml) and 1.3% more effective than PVA-emulsified PLGA NPs ($IC_{50} = 204$ ng/ml). *In vivo* model of restenosis was used only to observe the uptake of fluorescent NPs.[54]

Not only PXT but also a variety of therapeutic agents with different aqueous solubility could be encapsulated in PLGA NPs using TPGS as emulsifier. For example, rifampicin and estradiol valerate were chosen as model of hydrophilic and hydrophobic drugs, respectively. TPGS was a good emulsifier in terms of loading efficiency with estradiol (insoluble) and not so good for rifampicin, a slightly water-soluble molecule.[53] Other drug with low solubility and membrane permeability is amphotericin B (AmB). It is an antifungal and antileishmanial drug with negligible absorption when it is orally administered. Therapy with conventional dosage form of AmB (Fungizone®) involves I.V. administration over long periods of times according to disease.[66] However, its therapeutic effect is limited due to several drug-related side effects as renal toxicity.[67] The existence of an effective and safe AmB oral formulation would have great impact in the clinical field. AmB-loaded PLGA NPs of ∼ 170 nm were prepared by nanoprecipitation method employing TPGS as stabilizer. These NPs were administered I.V. in rats to determine the potential nephrotoxicity. The animals treated with Fungizone® presented a significant increase in blood urea nitrogen and plasma creatinine levels compared to control; while AmB-loaded PLGA NPs showed lower levels demonstrating greater safety. Also, the relative bioavailability of AmB was ∼ 800% for the NPs ($AUC_{0-inf} = 7939$ ng · h/ml) as compared to Fungizone® ($AUC_{0-inf} = 1001$ ng · h/ml).[68] These NPs offer a valuable possibility of treating systemic fungal infection and leishmaniasis by oral route. Similarly, NPs prepared with PLGA and TPGS as emulsifier were used to encapsulate statins by emulsion evaporation method.[69] Statins are a class of drugs used to decrease blood cholesterol levels achieving important benefits for the large populations of individuals at high risk

for coronary disease.[70] Statins have rare but severe adverse effects, particularly muscle aches or muscle weakness with increase in creatine phosphokinasa (CPK). This muscle weakness is named "Myophaty." The myotoxicity of the statins varies as follows: atorvastatin > (pravastatin = simvastatin = lovastatin) > fluvastatin.[71] Meena et al. prepared atorvastatin-loaded PLGA NPs using TPGS as stabilizer demonstrating equal effectiveness in comparison to Lipicure® (commercial formulation), at a 66%-reduced dose in treating the hyperlipidemia. Also, NPs showed non negligible myotoxicity in comparison to the marketed formulation.[69] Once more, TPGS-emulsified NPs showed significant improvement compared with commercially available formulations.

3.2. Nanoparticles Prepared with TPGS-Copolymers

The synthesis of biodegradable copolymers based upon TPGS as a matrix component has great potential for the manufacture of polymeric NPs (Table II). Thus, we can prevent desorption of TPGS from the NPs surface.[60] Moreover, NPs surface modifications with TPGS also provide a platform for conjugation of ligands, and prevent the opsonization.[72–73] Recently, the properties combination of both, polymers and TPGS, have been explored in order to synthesized different copolymers such as PLA-TPGS,[74–75] PLGA-TPGS,[76–78] PCL-TPGS,[79] PCL-PLA-TPGS[80] and PCL-PGA-TPGS.[81] Some authors have used these copolymers for NPs preparation. For example NPs fabricated of PLA-TPGS copolymer were prepared by modified solvent extraction technique with and without TPGS as emulsifier. In both cases, PTX-loaded PLA-TPGS NPs of ∼ 300 nm showed higher EE and achieve a faster drug release than PLGA NPs.[82] Furthermore, the PLA-TPGS NPs showed higher cellular uptake compared to traditional PLGA NPs in HT-29 cells. The IC_{50} of PTX-loaded PLA-TPGS NPs was decreased 14 fold for HT-29 and 2 fold for Caco-2 cells after 48 hours incubation in comparison to PTX solution. I.V. administration of PTX-loaded PLA-TPGS NPs in rats revealed 1.6-fold larger AUC values and enhanced the plasma residence times of drugs compared to commercial formulation.[83]

NPs containing TPGS have been proposed to provide an innovate solution for oral chemotherapy. Feng et al. prepared PLA-TPGS NPs incorporating montmorillotine (PLA-TPGS/MMT NPs) a potent detoxifier for oral delivery of chemotherapeutic agent as docetaxel (DTX). The *in vitro* activity of DTX-loaded PLA-TPGS NPs could be enhanced by combining it with MMT. *In vitro* studies in MCF-7 cells, DTX formulated in PLA-TPGS ($IC_{50} = 5.11$ μg/ml) and PLA-TPGS/MTT ($IC_{50} = 3.68$ μg/ml) were ∼ 2 and ∼ 3-fold more effective than the Taxotere® (DTX solution) ($IC_{50} = 11.3$ μg/ml) after 24 h treatment, respectively. Moreover, *in vivo* experiments with

Table II. Examples of NPs prepared with TPGS-copolymers.

Copolymer	Preparation method	Drug	Size (nm)	PDI	EE%	Comments	Ref.
PLA-TPGS	Emulsion-solvent evaporation	PTX	∼300	>0.20	62–92	PLA-TPGS copolymer can greatly increase the drug encapsulation efficiency and achieve much faster drug release than the PLGA nanoparticles to meet the therapeutic needs.	[74]
PLA-TPGS	Emulsion-solvent evaporation	PTX	∼300	0.20–0.30	60–90	The novel PLA-TPGS NP formulation of paclitaxel also showed significant advantages in achieving larger cytotoxicity and smaller IC_{50} over the Taxol®.	[46]
PLA-TPGS	Doble emulsion-solvent evaporation	BSA	260–360	0.21–0.34	44–75	PLA-TPGS NPs have advantages over the PLGA NPs: smaller size, more uniform size distribution, higher EE, and desired release profile and more importantly, protect the activity of the formulated proteins.	[85]
PLA-TPGS:TPGS-COOH	Emulsion-solvent evaporation	PTX	310–330	0.14–0.32	∼51	PLA-TPGS copolymer is employed as matrix and the TPGS-COOH copolymer is used to facilitate folate decoration for targeting the cancer cells rich of the folate receptors on their surface. NPs have great advantages versus the pristine drug and the folate-decoration can significantly promote targeted delivery of the drug to the corresponding cancer cells.	[98]
PLA-TPGS	Emulsion-solvent evaporation	QDs	∼200	∼0.15	46	QDs were encapsulated in the interior of the polymeric matrix. These NPs can be used for molecular imaging for detection of diseases at their earliest stage.	[73]
PLA-TPGS:TPGS-COOH	Emulsion-solvent evaporation	QDs	∼280	0.16–0.20	∼45	QDs-loaded PLA-TPGS/TPGS-COOH NPs showed lower *in vitro* cytotoxicity compared to free QDs.	[72]
PLA-TPGS	Nanoprecipitation	DTX	228–245	∼0.27	∼60	IC_{50} data showed that the Tf adsorbed PLA-TPGS NPs of DTX could be 23.4%, 16.9% and 229% more efficient than the PLGA NPs, the PLA-TPGS NPs and Taxotere® after 24 h treatment, respectively	[94]
PLA-TPGS	Emulsion-solvent evaporation	DOX	∼130	0.06	98	PLA-TPGS NPs showed the inhibition of *P*-gp activity and improvement in intracellular accumulation and nuclear localization of DOX.	[121]
PLGA-TPGS	Emulsion-solvent evaporation	DTX	207–290	0.32–0.49	59–99	DTX-loaded PLGA-TPGS NPs could achieve much faster drug release in comparison with PLGA NPs. Also, PLGA-TPGS NPs were biocompatible, and DTX-loaded PLGA-TPGS NPs had significant cytotoxicity against Hela cells.	[77]
PCL-PLA-TPGS	Emulsion-solvent evaporation	DTX	∼200	>0.20	54	DTX-loaded PCL-PLA-TPGS NPs presented advantages over Taxotere® in terms of cytotoxicity against HeLa cells.	[80]
PLA-TPGS:TPGS-COOH	Nanoprecipitation	DTX	160–240	0.09–0.20	N.D.	Adjusting the PLA-TPGS:TPGS-COOH blend ratio could controlled the targeting effects in HER2 positive breast cancer cells.	[102]

Notes: *Abbreviations*: PLA, poly-lactic acid; TPGS, D-α-tocopheryl polyethylene glycol (PEG) 1000 succinate; PTX, paclitaxel; BSA, bovine serum albumin; PLGA, poly-lactic-*co*-glycolic acid; PVA, polyvinyl alcohol; QDs, Organic Quantum Dots; DTX, docetaxel; DOX, doxorubicin; PCL, poly-ε-caprolactone; N.D., not data.

128

J. Biomater. Tissue Eng. 3, 122–134, 2013

rats showed that the oral administration of NPs achieved ~ 20 times longer half life of DTX. Additionally, the oral bioavailability of DTX could be increased to 91.3% by the PLA-TPGS formulation compared to 3.6% for Taxotere®.[84] PLA-TPGS NPs also can be used for delivery and protection of peptides and protein. Lee et al. showed that modulating the ratio weight content of PLA:TPGS could affect the burst release characteristic from the albumin (BSA)-loading PLA-TPGS NPs. Unfortunately, the EE decreased from 75.6% to 44.3% when the TPGS's content in the copolymers was increased from 3.4% to 12%.[85] Another novel approach was the synthesis of PLGA-TPGS for the delivery of anticancer drugs. PLGA-TPGS NPs encapsulating DTX showed a significant anti-proliferative activity *in vitro* against HeLa cells. This activity is positively correlated to greater cellular uptake and little toxicity of the drug-free PLGA-TPGS NPs.[86] In other study, Ma et al. developed a formulation based on PCL-PLA-TPGS random copolymer for NPs formulation of DTX. The IC_{50} value for DTX incorporated into PCL-PLA-TPGS NPs toward HeLa cells was determined to be 4.6 μg/ml versus 28.1 μg/ml for Taxotere®, after 72 h. In addition, the cummulative drug release was 12.2% for PCL-PLA-TPGS NPs after 72 h.[87] An interesting strategy for increase retention time at the cell surface is modify the surface charge of NPs. Chen and co-workers prepared PLGA-TPGS NPs with a cationic surfactant didodecyldimethylammonium bromide (DMAB) to change the surface charge of NPs. Zeta potential values confirmed that surface modification with DMAB changed the PLGA-TPGS NPs from a negative to a positive surface charge. DMAB-modified PLGA-TPGS NPs (+32 mV) have significantly higher level of the cellular uptake than that of DMAB-modified PLGA NPs (−29 mV) and unmodified PLGA-TPGS NPs (−22 mV).[88] All studies demonstrate that TPGS-copolymers are very promising for the preparation of novel nanocarriers for drug delivery, but more assays are necessary to ensure biodegradability and biocompatibility.

4. TPGS IN NANOPARTICLES-BASED TARGETED DRUG DELIVERY

Generally, tumor cells express many molecules on their surface at levels higher than normal cells. For example, the transferrin receptor (TfR1) is ubiquitously expressed in normal human tissue but it is overexpressed on surface of many malignant cells. This high expression, its ability to internalize by endocytosis, and the necessity of iron for cancer cell proliferation make this receptor a widely accessible portal for entry of drugs into solid tumor.[6] Recent studies involve the coupling of transferrin (Tf), antibodies against TfR or peptides to the NPs surface.[89–91] Thus, Zheng and co-workers prepared hybrid NPs composed of PLGA, phosphatidylcholine (PC) and TPGS, with and without Tf, for targeted delivery of an aromatase inhibitor

(7α-APTDAD).[92] TPGS was used as stabilizer because hybrid NPs exhibit high drug loading but little stability in saline solutions. This inconvenient could be improved by adding TPGS[93] which provides steric stabilization of NPs due to the hydrophilic PEG chain. 7α-APTDAD is a potent irreversible aromatase inhibitor with activity in many cell lines including human mammary carcinoma MCF-7 cells and choriocarcinoma JAr cells.[94] None of the formulations studied showed significant cytotoxicity at 24 h against breast cancer cell line (SKBR-3 cells). Therefore, the drug and the NPs were essentially non-toxic to SKBR-3 cells. On the other hand, Tf-PLGA NPs were visualized into endosomal vesicles indicating receptor-mediated endocytosis by CLSM. Finally, aromatase inhibition by the drug-loaded Tf-NPs in SKBR-3 cells was more effective than that by the non-targeted NPs.[83] The presence of Tf improves the efficiency and specificity of drug delivery systems. In other study, DTX-loaded PLA-TPGS NPs were prepared by nanoprecipitation and Tf was adsorbed on NPs surface (DTX-PLA-TPGS/Tf). Different formulations were evaluated *in vitro* with C6 glioma cells. IC_{50} data showed that DTX-PLA-TPGS/Tf NPs could be 23.4%, 16.9% and 229% more efficient than DTX-PLGA NPs, DTX-PLA-TPGS NPs and Taxotere® after 24 h treatment, respectively. Also, the confocal images of C6 glioma cell line with 6-coumarin loaded NPs formulations showed that the intracellular uptake of PLA-TPGS/Tf NPs was significantly enhanced compared with PLA-TPGS NPs.[95]

The blood brain barrier (BBB) presents important obstacles in the treatment of brain tumors because it regulates the internal environment of the brain selecting the passage of desired molecules from the blood to the brain parenchyma. The presence of TfR in the luminal membrane of capillary endothelium of the BBB suggests that this mechanism could be exploited to solve the problems of brain drug administration.[96] For example, Gang and Feng investigated the biodistribution of 6-coumarin loaded NPs in rats. The concentration of 6-coumarin in the brain tissue from the PLA-TPGS/Tf was higher than the PLA-TPGS NPs. PLA-TPGS NPs presented lower concentration in the brain than PLA-TPGS/Tf, but higher than PLGA NPs; this is probably due to the TPGS inhibitory function in the *P*-gp efflux transporters present in the BBB.[86]

Other strategy for tumor targeting, involves folate-modified nanocarriers because folate receptor is frequently overexpressed in many malignant cells.[97] Zhang et al. synthesized TPGS-folate (TPGS-FOL) to decorate NPs prepared with doxorubicin (DOX) conjugated to PLGA-TPGS (DOX-PLGA-TPGS). TPGS-FOL was blended with DOX-PLGA-TPGS at various ratios to control the targeting process. In the cellular uptake assay, the NPs prepared with a ratio 1:1 TPGS-FOL:DOX-PLGA-TPGS showed an increase of 1.3 fold for MCF-7 and 1.2 fold for C6 glioma cells after 6 hours cell culture compared to NPs prepared without TPGS-FOL. The MCF-7 and C6 cell viability

REVIEW

was decreased from 50.8% and 49.6% for NPs without TPGS-FOL to 8.2% and 30.6% for TPGS-FOL:DOX-PLGA-TPGS (1:1) NPs, respectively, after incubation for 24 hours.[98] The NPs with TPGS-FOL presented better *in vitro* cytotoxicity probably due to targeting effects of FOL in the cancer cells with overexpression of the FOL receptors. Similarly, PTX-loaded FOL decorated NPs (FOL-PTX-NPs) were prepared with blends of two copolymers PLA-TPGS and TPGS-carboxylic acid terminated (TPGS-COOH), which facilitated the conjugation of ligands such as folate. *In vitro* studies with MCF-7 and C6 cells demonstrated that FOL-PTX-NPs were more effective in decrease the cell viability than non-targeted NPs and Taxol®.[99] More recently, TPGS-FOL and PTX conjugated to monomethoxy-poly-(ethylene glycol)-*b*-poly-(lactide) (mPEG-PLA-PTX) were used to prepare NPs with various molar ratios of both copolymers. *In vitro* assays demonstrated that the cytotoxicity of PTX-loaded NPs to C6 and Hella cells were improved by folate component.[100] A similar strategy was used to combine Herceptin® (a FDA approved monoclonal antibody named trastuzumab) to the surface of NPs composed of PLA-TPGS and TPGS-COOH for targeting delivery of DOX to breast cancer cells overexpressing the human epidermal growth factor receptor 2 (HER2 receptor).[101] Zhao and co-workers found than adjusting the PLA-TPGS:TPGS-COOH blend ratio could controlled the targeting effects in HER2 positive breast cancer cells of two ways: controlling the surface density of TPGS-COOH, and adjusting the feeding concentration of herceptin in the conjugation process. This fact had a direct impact on cellular uptake and cytotoxicity.[102] All these *in vitro* studies shows a high selectivity of the NPs decorated with ligands, however, *in vivo* experiments are needed to confirm a real effect at the site of action.

5. TPGS-DRUG CONJUGATES

Polymer-drug conjugates are platforms therapeutics for drug delivery composed of a polymer covalently bound to a drug trough a linker, generally biodegradable. Many polymer-drug conjugates are in different stages of clinical studies or have entered into routine clinical use in oncology.[103] DOX is an anthracycline antibiotic used in the treatment of a wide range of cancers, unfortunately its clinical application is limited because of severe side effects, including cardiotoxicity, myelosupresion, and neprotoxicity.[104] To minimize the adverse effects of DOX, it has been chemically conjugated to TPGS, changing significantly the intracellular and tissue biodistribution of pristine DOX.[105] This DOX-TPGS conjugated has shown higher cytotoxicity *in vitro* against MCF-7 and C6 cells at low drug concentration. The IC$_{50}$ of DOX-TPGS conjugated in comparison to free DOX was 84.1% more effective for MCF-7 and 42.2% more effective for C6

cells after 72 hours culture.[106] Also, DOX-TPGS conjugate has been chemically conjugated to folate-hydrazide (FOL-DOX-TPGS) in an effort to deliver DOX directly to cancer cell that overexpressing high levels of folate receptor. The IC$_{50}$ of FOL-DOX-TPGS, DOX-TPGS and free DOX were 0.59, 22.8 and 27.9 μM, respectively. Therefore, the IC$_{50}$ of FOL-DOX-TPGS in comparison to free DOX was reduced by 45 fold for MCF-7 cells.[97] The pharmacokinetics of DOX-TPGS and FOL-DOX-TPGS were evaluated in rats. The half life of DOX in plasma was 10.2, 10.5, and 2.69 hours by DOX-TPGS, FOL-DOX-TPGS and pristine DOX, respectively. Therefore, the conjugates delay the blood clearance and have similar biodistribution.[97–98] More importantly, both conjugates decreased the heart accumulation of DOX. The AUC was increased by more than ~ 15 times.[97] The previously results show that polymer-drug conjugates are a viable strategy for formulation of drug delivery systems. Importantly, the inhibitory effect of *P*-gp motivates the search of TPGS-drug conjugates to solve problems associated with drug's pharmacokinetic. However, these conjugates have the drug chemically conjugated to the polymer and therefore they are new chemical entities.

6. INHIBITION OF EFFLUX TRANSPORTER FOR TPGS

P-gp is a class of multi-drug resistance (MDR) protein that it is present on the cell membrane and cause the efflux of drugs reducing its efficacy. Naturally, these ATP dependent transporter proteins are expressed in a wide range of normal tissues to minimize the exposure to potentially toxic xenobiotics.[107] *P*-gp is extensively distributed and expressed normally in the intestinal epithelium, liver, kidney, placenta, adrenal gland and capillary endothelial cells comprising the BBB and blood-testis barrier.[108] Also, it is overexpressed in cancer cells and is responsible for one of the MDR mechanisms most extensively studied in this kind of cells. The MDR is a major clinical problem to the success of cancer therapy.[109] Approximately 50% of marketed drugs have lately been identified to be *P*-gp substrates, inhibitors or inducers.[110] *P*-gp inhibitors have been developed and co-administrated with chemotherapeutic agents (e.g., verapamil, cyclosporine A), however, the efficacy of these inhibitors was largely compromised by pharmacokinetic interactions and increased side effects.[111] Several excipients used in marketed formulations (e.g., PEG400, TPGS, polysorbate 80, Solutol HS 15, Labrasol, Cremophor EL and different poloxamers) are potential candidate to enhance drug absorption. They were identified as more or less potent *P*-gp inhibitors.[112–114] Wempe and co-workers investigated the potential of novel TPGS analogs using Caco2 permeability model.[115] *In vitro* results showed that TPGS concentration of 30 μM ($< 0.005\%$ w/v) reduced rhodamine 123

(*P*-gp substrate) efflux by 33% compared to cyclosporine (*P*-gp inhibitor) that show a complete efflux inhibition. *In vivo* studies confirmed TPGS ability to inhibit *P*-gp mediated efflux, resulting in significant improvement of PTX bioavailability in rats and increased oral talinolol and cyclosporine bioavailability in humans.[116–118] Most recent studies revealed that modulation of ATPase activity correlated with inhibitory potential for *P*-gp mediated efflux. Therefore, TPGS modulates *P*-gp efflux transport via *P*-gp-ATPase inhibition.[119–120] Furthermore, TPGS inhibitory potential may be increased or decreased by a modification of the PEG chain length. Collnot and co-workers synthesized TPGS analogues (TPGS 200-6000) finding that TPGS 1000 was the most potent inhibitor of rhodamine 123 transport in Caco-2 monolayers.[121] Li et al. prepared DOX-loaded PLA-TPGS NPs and founded that the activity of *P*-glycoprotein in drug-resistant breast cancer MCF-7/ADR cells was decreased after incubation with these NPs.[122] NPs prepared with TPGS could exhibit inhibitory effect on *P*-gp to enhance drugs bioavailability. Certainly, the potential function of TPGS as an inhibitor of efflux pump makes it a suitable choice for the NPs manufacture.

7. CONCLUSIONS

The present work has reviewed the use of TPGS as emulsifier in the preparation of NPs. TPGS has many advantages over conventional surfactants. This can increase the solubility, permeability and bioavailability of many drugs which are difficult to deliver orally. Also, TPGS can modulate *P*-gp efflux transport and improve the bioavailability of various drugs. In recent years, TPGS has been used as a very good emulsifier for produce NPs. As stated, TPGS is more effective as emulsifier than traditional PVA, present better performance in emulsification and drug encapsulation efficiency. Due to its structure, TPGS can be used in the replacement of PEG to coat the NPs surface and enhance cellular uptake, *in vitro* cancer cell cytotoxicity, and more desirable *in vivo* pharmacokinetics. The applications of TPGS in nanomedicine are numerous, therefore will be necessary more research about on the pharmacokinetics, biodistribution, and safety of these drug delivery systems. Finally, the largest number of publications is in cancer. This opens the possibility to work in other diseases exploiting this information.

References and Notes

1. I. Rubinstein and G. L. Weinberg, Nanomedicines for chronic non-infectious arthritis: The clinician's perspective. *Maturitas* 73, 68 (**2012**).
2. I. Szelenyi, Nanomedicine: Evolutionary and revolutionary developments in the treatment of certain inflammatory diseases. *Inflamm. Res.* 61, 1 (**2012**).
3. B. S. Zolnik and N. Sadrieh, Regulatory perspective on the importance of ADME assessment of nanoscale material containing drugs. *Adv. Drug Deliver. Rev.* 61, 422 (**2009**).
4. J.-U. A. H. Junghanns and R. H. Müller, Nanocrystal technology, drug delivery and clinical applications. *Int. J. Nanomedicine* 3, 295 (**2008**).
5. http://www.abraxane.com/docs/Abraxane_PrescribingInformation.pdf.
6. T. R. Daniels, E. Bernabeu, J. A. Rodríguez, S. Patel, M. Kozman, D. A. Chiappetta, E. Holler, J. Y. Ljubimova, G. Helguera, and M. L. Penichet, The transferrin receptor and the targeted delivery of therapeutic agents against cancer. *Biochimica. et Biophysica. Acta* 1820, 291 (**2012**).
7. R. A. Jain, The manufacturing techniques of various drug loaded biodegradable poly(lactide-co-glycolide) (PLGA) devices. *Biomaterials* 21, 2475 (**2000**).
8. K. S. Soppimath, T. M. Aminabhavi, A. R. Kulkarni, and W. E. Rudzinski, Biodegradable polymeric nanoparticles as drug delivery devices. *J. Control Release* 70, 1 (**2001**).
9. C. Vauthier and K. Bouchemal, Methods for the preparation and manufacture of polymeric nanoparticles. *Pharm. Res.* 26, 1025 (**2009**).
10. I. Brigger, C. Dubernet, and P. Couvreur, Nanoparticles in cancer therapy and diagnosis. *Adv. Drug Deliver. Rev.* 54, 631 (**2002**).
11. G. Modi, V. Pillay, and Y. E. Choonara, Advances in the treatment of neurodegenerative disorders employing nanotechnology. *Ann. N.Y. Acad. Sci.* 1184, 154 (**2010**).
12. C. P. Reis, R. J. Neufeld, A. J. Ribeiro, and F. Veiga, Nanoencapsulation I. Methods for preparation of drug-loaded polymeric nanoparticles. *Nanomedicine: NBM* 2, 8 (**2006**).
13. D. E. Owens III and N. A. Peppas, Opsonization, biodistribution, and pharmacokinetics of polymeric nanoparticles. *Int. J. Pharm.* 307, 93 (**2006**).
14. A. S. Hoffman, The origins and evolution of controlled drug delivery systems. *J. Control Release* 132, 153 (**2008**).
15. Z. Amoozgar and Y. Yeo, Recent advances in stealth coating of nanoparticle drug delivery systems. *WIREs Nanomed. Nanobiotechnol.* 4, 219 (**2012**).
16. L. Mu, P.-H. Seow, S.-N. Ang, and S.-S. Feng, Study on surfactant coating of polymeric nanoparticles for controlled delivery of anticancer drug. *Colloid. Polym. Sci.* 283, 58 (**2004**).
17. N. Jalali, F. Moztarzadeh, M. Mozafari, S. Asgari, M. Motevalian, and S. Naghavi Alhosseini, Surface modification of poly(lactide-co-glycolide) nanoparticles by D-*α*-tocopheryl polyethylene glycol 1000 succinate as potential carrier for the delivery of drugs to the brain. *Colloids Surf. A: Physicochem. Eng. Aspects* 392, 335 (**2011**).
18. M. S. Muthu, S. A. Kulkarni, A. Raju, and S.-S. Feng, Theranostic liposomes of TPGS coating for targeted co-delivery of docetaxel and quantum dots. *Biomaterials* 33, 3494 (**2012**).
19. M. A. Repka and J. W. McGinity, Influence of Vitamin E TPGS on the properties of hydrophilic films produced by hot-melt extrusion. *Int. J. Pharm.* 202, 63 (**2000**).
20. W. Chen, Y.-Q. Miao, D.-J. Fan, S.-S. Yang, X. Lin, L.-K. Meng, and X. Tang, Bioavailability study of berberine and the enhancing effects of TPGS on intestinal absorption in rats. *AAPS Pharm. Sci. Tech.* 12, 705 (**2011**).
21. D. R. Mudra and R. T. Borchardt, Absorption barriers in the rat intestinal mucosa. 3: Effects of polyethoxylated solubilizing agents

REVIEW

on drug permeation and metabolism. *J. Pharm. Sci.* 99, 1016 (**2010**).

22. Y. V. Rama Prasad, S. P. Puthli, S. Eaimtrakarn, M. Ishida, Y. Yoshikawa, N. Shibata, and K. Takada, Enhanced intestinal absorption of vancomycin with Labrasol and D-α-tocopheryl PEG 1000 succinate in rats. *Int. J. Pharm.* 250, 181 (**2003**).

23. H.-J. Cho, P. Balakrishnan, S.-J. Chung, C.-K. Shim, and D.-D. Kim, Evaluation of protein stability and *in vitro* permeation of lyophilized polysaccharides-based microparticles for intranasal protein delivery. *Int. J. Pharm.* 416, 77 (**2011**).

24. A. Yan, A. Von Dem Bussche, A. B. Kane, and R. H. Hurt, Tocopheryl polyethylene glycol succinate as a safe, antioxidant surfactant for processing carbon nanotubes and fullerenes. *Carbon* 45, 2463 (**2007**).

25. J. Li, B. Yang, J. Levons, S. Pinnamaneni, and K. Raghavan, Phase behavior of TPGS–PEG400/1450 systems and their application to liquid formulation: A formulation platform approach. *J. Pharm. Sci.* 100, 4907 (**2011**).

26. S. H. W. Wu and W. K. Hopkins, Characteristics of *d*-tocopheryl polyethylene glycol 1000 succinate for applications as an absorption enhancer in drug delivery system. *Pharm. Technol.* 23, 52 (**1999**).

27. E. Jacquemin, B. Hermeziu, Y. Kibleur, I. Friteau, D. Mathieu, F. L. Coz, D. Moyse, M. Gérardin, E. Jacqz-Aigrain, and A. Munck, Bioavailability of oral vitamin E formulations in adult volunteers and children with chronic cholestasis or cystic fibrosis. *J. Clin. Pharm. Therapeutics* 34, 515 (**2009**).

28. M. G. Traber, T. D. Schiano, A. C. Steephen, H. J. Kayden, and M. Shike, Efficacy of water soluble vitamin E in the treatment of vitamin E malabsorption in short-bowel syndrome. *Am. J. Clin. Nutr.* 59, 1270 (**1994**).

29. R. J. Sokol, N. Butler-Simon, C. Conner, J. E. Heubi, F. R. Sinatra, F. J. Suchy, M. B. Heyman, J. Perrault, R. J. Rothbaum, and J. Levy, Multicenter trial of d-alpha-tocopheryl polyethylene glycol 1000 succinate for treatment of vitamin E deficiency in children with chronic cholestasis. *Gastroenterology* 104, 1727 (**1993**).

30. K. Papas, J. Kalbfleisch, and R. Mohon, Bioavailability of a novel, water-soluble vitamin E formulation in malabsorbing patients. *Digestive Diseases and Sciences* 52, 347 (**2007**).

31. S. Gross and D. K. Melhorn, Vitamin E dependent anemia in the premature infant. III. Comparative hemoglobin, vitamin E, and erythrocyte phospholipid responses following absorption of either water soluble or fat soluble d alpha tocopheryl. *J. Pediatrics* 85, 753 (**1974**).

32. L. Yu, A. Bridgers, J. Polli, A. Vickers, S. Long, A. Roy, R. Winnike, and M. Coffin, Vitamin E-TPGS increases absorption flux of an HIV protease inhibitor by enhancing its solubility and permeability. *Pharm. Res.* 16, 1812 (**1999**).

33. T. Chang, L. Z. Benet, and M. F. Hebert, The effect of water-soluble vitamin E on cyclosporine pharmacokinetics in healthy volunteers. *Clin. Pharmacol. Therapeutics* 59, 297 (**1996**).

34. E. A. Argao, J. E. Heubi, B. W. Hollis, and R. C. Tsang, *d*-α-Tocopheryl polyethylene glycol-1000 succinate enhances the absorption of vitamin D in chronic cholestatic liver disease of infancy and childhood. *Pediatric Research* 31, 146 (**1992**).

35. R. C. Rowe, P. J. Sheskey, and M. E. Quinn (eds.), Handbook of Pharmaceutical Excipients, 6th edn., edited by Pharmaceutical Press and American Pharmacists Association (**2009**).

36. J. M. Dintaman and J. A. Silverman, Inhibition of *P*-glycoprotein by D-α-tocopheryl polyethylene glycol 1000 succinate (TPGS). *Pharm. Res.* 16, 1550 (**1999**).

37. L. M. Chan, S. Lowes, and B. H. Hirst, The ABCs of drug transport in intestine and liver: Efflux proteins limiting drug absorption and bioavailability. *Eur. J. Pharm. Sci.* 21, 25 (**2004**).

38. M. V. S. Varma and R. Panchagnula, Enhanced oral paclitaxel absorption with vitamin E-TPGS: Effect of solubility and permeability *in vitro*, *in situ* and *in vivo*. *Eur. J. Pharm. Sci.* 25, 445 (**2005**).

39. M. Birringer, J. H. EyTina, B. A. Salvatore, and J. Neuzil, Vitamin E analogues as inducers of apoptosis: Structure-function relation. *British J. Cancer* 88, 1948 (**2003**).

40. H.-J. Youk, E. Lee, M.-K. Choi, Y.-J. Lee, H. C. Jun, S.-H. Kim, C.-H. Lee, and S.-J. Lim, Enhanced anticancer efficacy of α-tocopheryl succinate by conjugation with polyethylene glycol. *J. Control Release* 107, 43 (**2005**).

41. L. Mu and S. S. Feng, A novel controlled release formulation for the anticancer drug paclitaxel (Taxol): PLGA nanoparticles containing vitamin E TPGS. *J. Control Release* 86, 33 (**2003**).

42. J. Shaikh, D. D. Ankola, V. Beniwal, D. Singh, and M. N. V. Ravi Kumar, Nanoparticle encapsulation improves oral bioavailability of curcumin by at least 9-fold when compared to curcumin administered with piperine as absorption enhancer. *Eur. J. Pharm. Sci.* 37, 223 (**2009**).

43. P. Parhi, C. Mohanty, and S. K. Sahoo, Enhanced cellular uptake and *in vivo* pharmacokinetics of rapamycin-loaded cubic phase nanoparticles for cancer therapy. *Acta Biomaterialia* 7, 3656 (**2011**).

44. C. Sengel, C. Hasçiçek, and N. Gönül, Design of vitamin E D-α-tocopheryl polyethylene glycol 1000 succinate-emulsified poly (D,L-Lactide-co-glycolide) nanoparticles: Influence of duration of ultrasonication energy. *J. Young Pharmacists* 3, 171 (**2011**).

45. L. Mu and S. S. Feng, Vitamin E TPGS used as emulsifier in the solvent evaporation/extraction technique for fabrication of polymeric nanospheres for controlled release of paclitaxel (Taxol®). *J. Control Release* 80, 129 (**2002**).

46. Z. P. Zhang and S. S. Feng, The drug encapsulation efficiency, *in vitro* drug release, cellular uptake and cytotoxicity of paclitaxel-loaded poly(lactide)-tocopheryl polyethylene glycol succinate nanoparticles. *Biomaterials* 27, 4025 (**2006**).

47. K. Y. Win and S. S. Feng, Effects of particle size and surface coating on cellular uptake of polymeric nanoparticles for oral delivery of anticancer drugs. *Biomaterials* 26, 2713 (**2005**).

48. C. Roney, P. Kulkarni, V. Arora, P. Antich, F. Bonte, A. Wu, N. N. Mallikarjuana, S. Manohar, H.-F. Liang, A. R. Kulkarni, H.-W. Sung, M. Sairam, and T. M. Aminabhavi, Targeted nanoparticles for drug delivery through the blood–brain barrier for Alzheimer's disease. *J. Control Release* 108, 193 (**2005**).

49. G. Gaucher, R. H. Marchessault, and J.-C. J. Leroux, Polyester-based micelles and nanoparticles for the parenteral delivery delivery of taxanes. *J. Control Release* 143, 2 (**2010**).

50. D. Chiappetta, M. J. Legaspi, V. Niselman, R. Pasquali, E. Gergic, A. C. R. Llimós, and C. Bregni, Biodegradable microspheres of poly(D, L-lactide) containing progesterone. *Ars Pharm.* 46, 383 (**2005**).

51. J. Xie and C.-H. Wang, Self-assembled biodegradable nanoparticles developed by direct dialysis for the delivery of paclitaxel. *Pharm. Res.* 22, 2079 (**2005**).

52. K. Y. Win and S.-S. Feng, *In vitro* and *in vivo* studies on vitamin E TPGS-emulsified poly(D, L-lactic-co-glycolic acid) nanoparticles for paclitaxel formulation. *Biomaterials* 27, 2285 (**2006**).

53. F. Esmaeili, F. Atyabi, and R. Dinarvand, Preparation of PLGA nanoparticles using TPGS in the spontaneous emulsification solvent diffusion method. *J. Experimental Nanoscience* 2, 183 (**2007**).

54. S.-S. Feng, W. Zeng, Y. T. Lim, L. Zhao, K. Y. Win, R. Oakley, S. H. Teoh, R. C. H. Lee, and S. Pan, Vitamin E TPGS-emulsified poly(lactic-co-glycolic acid) nanoparticles for cardiovascular restenosis treatment. *Nanomedicine* 2, 333 (**2007**).

55. J. C. Middleton and A. J. Tipton, Synthetic biodegradable polymers as orthopedic devices. *Biomaterials* 21, 2335 (**2000**).

56. A. M. Puga, A. Rey-Rico, B. Magariños, C. Alvarez-Lorenzo, and A. Concheiro, Hot melt poly-e-caprolactone/poloxamine

implantable matrices for sustained delivery of ciprofloxacin. *Acta Biomaterialia* 8, 1507 (**2012**).

57. U. Bilati, E. Allémann, and E. Doelker, Strategic approaches for overcoming peptide and protein instability within biodegradable nano- and microparticles. *Eur. J. Pharm. Biopharm.* 59, 375 (**2005**).

58. C. E. Mora-Huertas, H. Fessi, and A. Elasissari, Polymer-based nanocapsules for drug delivery. *Int. J. Pharm.* 385, 113 (**2010**).

59. J. Xie and C.-H. Wang, Self-assemble biodegradable nanoparticles developed by direct dialysis for the delivery of paclitaxel. *Pharm. Res.* 22, 2079 (**2005**).

60. L. Mu and S. S. Feng, PLGA/TPGS nanoparticles for controlled release of paclitaxel: Effects of the emulsifier and the drug loading ratio. *Pharm. Res.* 20, 1864 (**2003**).

61. A. K. Singla, A. Garg, and D. Aggarwal, Paclitaxel and its formulations. *Int. J. Pharm.* 235, 179 (**2002**).

62. S. S. Feng, L. Y. Zhao, Z. P. Zhang, G. Bhakta, Y. W. Khin, Y. C. Dong, and S. Chien, Chemotherapeutic engineering: Vitamin E TPGS-emulsified nanoparticles of biodegradable polymers realized sustainable paclitaxel chemotherapy for 168 h *in vivo. Chem. Eng. Sci.* 62, 6641 (**2007**).

63. L. Zhao and S. S. Feng, Enhanced oral bioavailability of paclitaxel formulated in vitamin E-TPGS emulsified nanoparticles of biodegradable polymers: *In vitro* and *in vivo* studies. *J. Pharm. Sci.* 99, 3552 (**2010**).

64. H. L. McLeod and W. E. Evans, Oral cancer chemotherapy: The promise and the pitfalls. *Clinical Cancer Res.* 5, 2699 (**1999**).

65. B. Scheller, C. Hehrlein, W. Bocksch, W. Rutsch, D. Haghi, U. Dietz, M. Böhm, and U. Speck, Treatment of coronary in-stent restenosis with a paclitaxel-coated balloon catheter. *N. Engl. J. Med.* 355, 2113 (**2006**).

66. http://www.cdc.gov/fungal/candidiasis/invasive/treatment.html [accessed March 2012].

67. C. Leon, R. Taylor, K. H. Bartlett, and K. M. Wasan, Effect of heat-treatment and the role of phospholipases on Fungizone®-induced cytotoxicity within human kidney proximal tubular (HK-2) cells and Aspergillus fumigatus. *Int. J. Pharm.* 298, 211 (**2005**).

68. J. L. Italia, M. M. Yahya, D. Singh, and M. N. V. R. Kumar, Biodegradable nanoparticles improve oral bioavailability of amphotericin b and show reduced nephrotoxicity compared to intravenous Fungizone®. *Pharm. Res.* 26, 1324 (**2009**).

69. A. K. Meena, D. Venkat Ratnam, G. Chandraiah, D. D. Ankola, P. R. Rao, and M. N. V. R. Kumar, Oral nanoparticulate atorvastatin calcium is more efficient and safe in comparison to lipicure® in treating hyperlipidemia. *Lipids* 43, 231 (**2008**).

70. C. Bolego, R. Baetta, S. Bellosta, A. Corsini, and R. Paoletti, Safety considerations for statins. *Current Opinion in Lipidology* 13, 637 (**2002**).

71. M. A. Silva, A. C. Swanson, P. J. Gandhi, and G. R. Tataronis, Statin-related adverse events: A meta-analysis. *Clin. Ther.* 28, 26 (**2006**).

72. J. Pan and S. S. Feng, Targeting and imaging cancer cells by Folate-decorated, quantum dots (QDs)-loaded nanoparticles of biodegradable polymers. *Biomaterials* 30, 1176 (**2009**).

73. J. Pan, Y. Wang, and S.-S. Feng, Formulation, characterization, and *in vitro* evaluation of quantum dots loaded in poly(Lactide)-vitamin E TPGS nanoparticles for cellular and molecular imaging. *Biotech. Bioengineering.* 101, 622 (**2008**).

74. Z. Zhang and S.-S. Feng, Nanoparticles of poly(lactide)/vitamin E TPGS copolymer for cancer chemotherapy: Synthesis, formulation, characterization and *in vitro* drug release. *Biomaterials* 27, 262 (**2006**).

75. Z. Zhang and S.-S. Feng, Self-assembled nanoparticles of poly(lactide)-vitamin E TPGS copolymers for oral chemotherapy. *Int. J. Pharm.* 324, 191 (**2006**).

76. Z. Zhang, S. H. Lee, and S. S. Feng, Folate-decorated poly(lactide-co-glycolide)-vitamin E TPGS nanoparticles for targeted drug delivery. *Biomaterials* 28, 1889 (**2007**).

77. Y. Ma, Y. Zheng, K. Liu, G. Tian, Y. Tian, L. Xu, F. Yan, L. Huang, and L. Mei, Nanoparticles of poly(Lactide-Co-Glycolide)-d-a-tocopheryl polyethylene glycol 1000 succinate random copolymer for cancer treatment. *Nanoscale Res. Lett.* 5, 1161 (**2010**).

78. H. Chen, Y. Zheng, G. Tian, Y. Tian, X. Zeng, G. Liu, K. Liu, L. Li, Z. Li, L. Mei, and L. Huang, Oral delivery of DMAB-modified docetaxel loaded PLGA-TPGS nanoparticles for cancer chemotherapy. *Nanoscale Res. Lett.* 6, 4 (**2011**).

79. F. Ren, Q. Jing, J. Cui, and Y. Shen, Synthesis and characterization of D-α-tocopheryl polyethylene glycol 1000 succinate-block-poly (ε-caprolactone) copolymer used as carriers for microparticles. *J. Dispersion Sci. Technol.* 30, 1129 (**2009**).

80. Y. Ma, L. Huang, C. Song, X. Zeng, G. Liu, and L. Mei, Nanoparticle formulation of poly(3-caprolactone-co-lactide)-D-a-tocopheryl polyethylene glycol 1000 succinate random copolymer for cervical cancer treatment. *Polymer* 51, 5952 (**2010**).

81. L. Huang, H. Chen, Y. Zheng, X. Song, R. Liu, K. Liu, X. Zeng, and L. Mei, Nanoformulation of D-α-tocopheryl polyethylene glycol 1000 succinate-b-poly(ε-caprolactone-ran-glycolide) diblock copolymer for breast cancer therapy. *Integr. Biol.* 3, 993 (**2011**).

82. Z. P. Zhang and S. S. Feng, Nanoparticles of poly(lactide)/vitamin E TPGS copolymer for cancer chemotherapy: Synthesis, formulation, characterization and *in vitro* drug release. *Biomaterials* 27, 262 (**2006**).

83. Z. Zhang, S. H. Lee, C. W. Gan, and S. S. Feng, *In vitro* and *in vivo* investigation on PLA-TPGS nanoparticles for controlled and sustained small molecule chemotherapy. *Pharm. Res.* 25, 1925 (**2008**).

84. S. S. Feng, L. Mei, P. Anitha, C. W. Gan, and W. Y. Zhou, Poly(lactide)-vitamin E derivative/montmorillonite nanoparticle formulations for the oral delivery of docetaxel. *Biomaterials* 30, 3297 (**2009**).

85. S. H. Lee, Z. Zhang, and S.-S. Feng, Nanoparticles of poly(lactide)—tocopheryl polyethylene glycol succinate (PLA-TPGS) copolymers for protein drug delivery. *Biomaterials.* 28, 2041 (**2007**).

86. Y. Ma, Y. Zheng, K. Liu, G. Tian, Y. Tian, L. Xu, F. Yan, L. Huang, and L. Mei, Nanoparticles of poly(lactide-co-glycolide)-d-a-tocopheryl polyethyleneglycol succinate random copolymer for cancer treatment. *Nanoscale Res. Lett.* 5, 1161 (**2010**).

87. Y. D. Ma, L. Q. Huang, C. X. Song, X. W. Zeng, G. Liu, and L. Mei, Nanoparticle formulation of poly(epsilon-caprolactone-co-lactide)-D-alpha-tocopheryl polyethyleneglycol 1000 succinate random copolymer for cervical cancer treatment. *Polymer* 51, 5952 (**2010**).

88. H. Chen, Y. Zheng, G. Tian, Y. Tian, X. Zeng, G. Liu, K. Liu, L. Li, Z. Li, L. Mei, and L. Huang, Oral delivery of DMAB-modified docetaxel-loaded PLGA-TPGS nanoparticles for cancer chemotherapy. *Nanoscale Res. Lett.* 6, 4 (**2011**).

89. Z. Pang, H. Gao, Y. Yu, J. Chen, L. Guo, J. Ren, Z. Wen, J. Su, and X. Jiang, Brain delivery and cellular internalization mechanisms for transferrin conjugated biodegradable polymersomes. *Int. J. Pharm.* 415, 284 (**2011**).

90. R. T. Carroll, D. Bhatia, W. Geldenhuys, R. Bhatia, N. Miladore, A. Bishayee, and V. Sutariya, Brain-targeted delivery of Tempol-loaded nanoparticles for neurological disorders. *J. Drug Targeting* 18, 665 (**2010**).

91. L. Han, R. Huang, S. Liu, S. Huang, and C. Jiang, Peptide-conjugated PAMAM for targeted doxorubicin delivery to transferrin receptor overexpressed tumors. *Mol. Pharm.* 7, 2156 (**2010**).

92. Y. Zheng, B. Yu, W. Weecharangsan, L. Piao, M. Darby, Y. Mao, R. Koynova, X. Yang, H. Li, S. Xu, L. J. Lee, Y. Sugimoto, R. W. Brueggemeier, and R. J. Lee, Transferrin-conjugated lipid-coated PLGA nanoparticles for targeted delivery of aromatase inhibitor 7α-APTADD to breast cancer cells. *Int. J. Pharm.* 390, 234 (**2010**).

REVIEW

93. W. S. Cheow and K. Hadinoto, Factors affecting drug encapsulation and stability of lipid-polymer hybrid nanoparticles. *Colloids Surf. B: Biointerfaces* 85, 214 (**2011**).

94. R. W. Brueggemeier and N. E. Katlic, Aromatase inhibition by an enzyme-activated irreversible inhibitor in human carcinoma cell cultures. *Cancer Res.* 50, 3652 (**1990**).

95. C. W. Gan and S. S. Feng, Transferrin-conjugated nanoparticles of Poly(lactide)-d-α-Tocopheryl polyethylene glycol succinate diblock copolymer for targeted drug delivery across the blood–brain barrier. *Biomaterials* 31, 7748 (**2010**).

96. J. Chang, Y. Jallouli, M. Kroubi, X.-B. Yuan, W. Feng, C.-S. Kang, P.-Y. Pu, and D. Betbeder, Characterization of endocytosis of transferrin-coated PLGA nanoparticles by the blood–brain barrier. *Int. J. Pharm.* 379, 285 (**2009**).

97. B. Mishra, B. B. Patel, and S. Tiwari, Colloidal nanocarriers: A review on formulation technology, types and applications toward targeted drug delivery. *Nanomedicine: NBM.* 6, 9 (**2010**).

98. Z. Zhang, S. H. Lee, and S. S. Feng, Folate-decorated poly(lactide-co-glycolide)-vitamin E TPGS nanoparticles for targeted drug delivery. *Biomaterials* 28, 1889 (**2007**).

99. J. Pan and S. S. Feng, Targeted delivery of paclitaxel using folate-decorated poly(lactide)-vitamin E TPGS nanoparticles. *Biomaterials* 29, 2663 (**2008**).

100. J. Wang, W. Liu, Q. Tu, J. Wang, N. Song, Y. Zhang, N. Nie, and J. Wang, Folate-decorated hybrid polymeric nanoparticles for chemically and physically combined paclitaxel loading and targeted delivery. *Biomacromolecules* 12, 228 (**2011**).

101. B. F. Sun and S. S. Feng, Trastuzumab-functionalized nanoparticles of biodegradable copolymers for targeted delivery of Docetaxel. *Nanomedicine (Lond.)* 4, 431 (**2009**).

102. J. Zhao, Y. Mi, Y. Liu, and S. S. Feng, Quantitative control of targeting effect of anticancer drugs formulated by ligand-conjugated nanoparticles of biodegradable copolymer blend. *Biomaterials* 33, 1948 (**2012**).

103. F. Greco and M. J. Vicent, Combination therapy: Opportunities and challenges for polymer-drug conjugates as anticancer nanomedicines. *Adv. Drug Delivery Rev.* 61, 1203 (**2009**).

104. M. C. Perry, Continuous Intravenous Infusion Chemotherapy, edited by J. W. Pine, The Chemotherapy Source Book, vol. 4th edn., Lippincott Williams and Wilkins, Philadelphia (**2008**).

105. N. Cao and S. S. Feng, Doxorubicin conjugated to d-α-tocopheryl polyethylene glycol 1000 succinate (TPGS): Conjugation chemistry, characterization, *in vitro* and *in vivo* evaluation. *Biomaterials* 29, 3856 (**2008**).

106. V. Anbharasi, N. Cao, and S. S. Feng, Doxorubicin conjugated to D-α-tocopheryl polyethylene glycol succinate and folic acid as a prodrug for targeted chemotherapy. *J. Biomed. Materials Res. A* 94, 730 (**2010**).

107. M. V. S. Varma, Y. Ashokraj, C. S. Dey, and R. Panchagnula, *P*-glycoprotein inhibitors and their screening: A perspective from bioavailability enhancement. *Pharmacol. Res.* 48, 347 (**2003**).

108. J. Sun, Z.-G. He, G. Cheng, S.-J. Wang, X.-H. Hao, and M.-J. Zou, Multidrug resistance *P*-glycoprotein: Crucial significance in drug disposition and interaction. *Med. Sci. Monit.* 10, RA5 (**2004**).

109. J. Hunter and B. H. Hirst, Intestinal secretion of drugs. The role of P-glycoprotein and related drug efflux systems in limiting oral drug absorption. *Adv. Drug Delivery Rev.* 25, 129 (**1997**).

110. J. P. Keogh and J. R. Kunta, Development, validation and utility of an *in vitro* technique for assessment of potential clinical drug–drug interactions involving *P*-glycoprotein. *Eur. J. Pharm. Sci.* 27, 543 (**2006**).

111. J. M. Koziara, T. R. Whisman, M. T. Tseng, and R. J. Mumper, *In-vitro* efficacy of novel paclitaxel nanoparticles in paclitaxel-resistant human colorectal tumors. *J. Control Release* 112, 312 (**2006**).

112. G. Cornaire, J. Woodley, P. Hermann, A. Cloarec, C. Arellano, and G. Houin, Impact of excipients on the absorption of *P*-glycoprotein substrates *in vitro* and *in vivo*. *Int. J. Pharm.* 278, 119 (**2004**).

113. B. D. Rege, J. P. Y. Kao, and J. E. Polli, Effects of nonionic surfactants on membrane transporters in Caco-2 cell monolayers. *Eur. J. Pharm. Sci.* 16, 237 (**2002**).

114. K. Bogman, F. Erne-Brand, J. Alsenz, and J. Drewe, The role of surfactants in the reversal of active transport mediated by multidrug resistance proteins. *J. Pharm. Sci.* 92, 1250 (**2003**).

115. M. F. Wempe, C. Wright, J. L. Little, J. W. Lightner, S. E. Large, G. B. Caflisch, C. M. Buchanan, P. J. Rice, V. J. Wacher, K. M. Ruble, and K. J. Edgar, Inhibiting efflux with novel non-ionic surfactants: Rational design based on vitamin E TPGS. *Int. J. Pharm.* 370, 93 (**2009**).

116. M. V. Varma and R. Panchagnula, Enhanced oral paclitaxel absorption with vitamin E-TPGS: Effect on solubility and permeability *in vitro*, *in situ* and *in vivo*. *Eur. J. Pharm. Sci.* 25, 445 (**2005**).

117. K. Bogman, Y. Zysset, L. Degen, G. Hopfgartner, H. Gutmann, J. Alsenz, and J. Drewe, *P*-glycoprotein and surfactants: Effect on intestinal talinolol absorption. *Clin. Pharmacol. Therapeutics* 77, 24 (**2005**).

118. T. Chang, L. Z. Benet, and M. F. Hebert, The effect of water-soluble vitamin E on cyclosporine pharmacokinetics in healthy volunteers. *Clin. Pharmacol. Therapeutics* 59, 297 (**1996**).

119. E. M. Collnot, C. Baldes, M. F. Wempe, R. Kappl, J. Hüttermann, J. A. Hyatt, K. J. Edgar, U. F. Schaefer, and C. M. Lehr, Mechanism of inhibition of P-glycoprotein mediated efflux by vitamin E TPGS: Influence on ATPase activity and membrane fluidity. *Mol. Pharm.* 4, 465 (**2007**).

120. E. M. Collnot, C. Baldes, U. F. Schaefer, K. J. Edgar, M. F. Wempe, and C. M. Lehr, Vitamin e TPGS *P*-glycoprotein inhibition mechanism: Influence on conformational flexibility, intracellular ATP levels, and role of time and site of access. *Mol. Pharm.* 7, 642 (**2010**).

121. E. M. Collnot, C. Baldes, M. F. Wempe, J. Hyatt, L. Navarro, K. J. Edgar, U. F. Schaefer, and C. M. Lehr, Influence of vitamin E TPGS poly(ethlyene glycol) chain length on apical efflux transporters in Caco-2 cell monolayers. *J. Control Release* 111, 35 (**2006**).

122. P.-Y. Li, P.-S. Lai, W.-C. Hung, and W.-J. Syu, Poly(L-lactide)-vitamin E TPGS nanoparticles enhanced the cytotoxicity of doxorubicin in drug-resistant MCF-7 breast cancer cells. *Biomacromolecules* 11, 2576 (**2010**).

123. C. Prashant, M. Dipak, Y. C. Xian, C. Kai-Hsiang, D. Jun, and F. S. Shen, Superparamagnetic iron oxides formulated in polylactide-co-glycolide/ D-alpha-tocopherol polyethylene glycol 1000 succinate (PLGA/TPGS) nanoparticles for high contrast MRI. *1st Middle East Conference on Biomedical Engineering*, Sharjah, United Arab Emirates (**2011**), MECBME art. no. 5752145, pp. 379.

REVIEW

Capping Gold Nanoparticles with Modified Chitosan Polymers for Biomedical Applications

Juan F. Mena[1], Andrónico Neira-Carrillo[2, *], M. Yazdani Pedram[3], and Marcelo J. Kogan[1, *]

[1]*Facultad de Ciencias Químicas y Farmacéuticas, Departamento de Química Farmacológica y Toxicológica, Universidad de Chile, Sergio Livingstone 1007, Independencia, Santiago, Chile*
[2]*Departamento Ciencias Biológicas Animales, Universidad de Chile, Avda. Santa Rosa 11735, La Pintana, Santiago, Chile*
[3]*Facultad de Ciencias Químicas y Farmacéuticas, Departamento de Química Orgánica y Fisicoquímica, Universidad de Chile, Sergio Livingstone 1007, Independencia, Santiago, Chile*

With the purpose of obtaining stable and non-toxic nanocomposites with potential biomedical applications we coated gold nanoparticles (AuNP) with chitosan (CHI) and CHI grafted with poly(*N*-isopropilacrylamide) (PNIPAAm) and poly(*N*,*N*-dimethylacrylamide) (PDMAAm). We used a grafting reaction carried out by free radical initiation mechanism using potassium persulfate. We characterized the grafted CHI by FT-IR and thermogravimetry, grafting parameters were also calculated. Gold nanoparticles (AuNP) were obtained by reduction of the auric salt with citrate. Nanocomposites were obtained by mixing dropwise polymer solution into a AuNP solution under intense stirring, with variable AuNP:copolymer ratios. These were characterized using UV-Visible spectrophotometry and transmission electronic microscopy (TEM). The effects on cell viability of neuroblastoma SHSY-5Y cells were evaluated performing the MTT assay. CHI and the grafted CHI with PNIPA did not show effects on cell viability while PDMA presented a certain degree of toxicity. Notably the nanocomposites did not show effects on cell viability. The new nanomaterials can be useful for new drug delivery systems.

Keywords: Gold Nanoparticles, Chitosan, Drug Delivery, Nanotoxicology.

RESEARCH ARTICLE

1. INTRODUCTION

Gold nanoparticles (AuNP), thanks to their size and properties are useful in a variety of biologic applications, such as: control drug release agents,[1] transfection enhancement vector,[1] DNA coupling agent,[2] computed tomography contrast agent,[3] among many others. One of the most important properties of AuNP is their capacities to absorb energy from an oscillate magnetic field source or a laser irradiation dissipating that energy locally and selectively destroying tumor cells or toxic aggregates.[4] This effect has been used as an effective agent for thermal therapy in cancer treatment.[5]

AuNP could be bind to molecules to address them to specific targets. We can accomplish this by coupling them with biocompatible molecules such as peptides, proteins, oligomers and biopolymers which provides stability and helps to direct the particles to a desire target. For the development of a new strategy for Alzheimer's disease treatment, in our group we bind AuNP to toxic aggregates

of β-amyloid involved in the mentioned pathology. The aggregates were irradiated with microwaves in the presence of the nanoparticles. The local heat delivered to by the metallic nanoparticles produced the destruction of the aggregates which could be useful for a kind of molecular surgery for therapeutically purposes.[4] On the other hand, we demonstrated that AuNP injected intraperitoneally in rats cross the blood brain barrier to reach the brain however in a very low proportions with respect to the injected doses. This could be explained due to the capping with plasma proteins (opsonins) that favor the interaction with the reticule endothelial system and retention in liver and spleen which contribute to diminish the bioavailability to the brain.[6, 7] To overcome this problem it is possible to create AuNP-biopolymer nanocomposites to enhance the biocompatibility of the AuNP. CHI is a natural biopolymer that have been widely studied in biomedical and possess physical and chemical properties such as high biodegradability, biocompatibility and low toxicity.[8] For instance, Trickler et al. encapsulated paclitaxel, an anticancer drug, on AuNP-CHI nanocomposites increasing the anti-tumor activity of the drug when compared to conventional

---

*Author to whom correspondence should be addressed.

Paclitaxel formulations.[9] There's also plenty of studies that use CHI as a nose-to-brain direct delivery of drugs that show enhance results compared to equivalent drug in oral administration.[10] Also, poly(*N*-isopropylacrylamide) and poly(*N,N*-dimethylacrylamide) are two polymers that have been used extensively in drug delivery studies.[11, 12] In this work, we synthesized and characterized CHI grafted with *N*-isopropylacrylamide (CHI-*g*-PNIPAAm) and chitosan grafted with *N,N*-dimethylacrylamide (CHI-*g*-PDMAAm) employing a free radical polymerization approach. We used these copolymers for capping of AuNP and studied their effects on cell viability in neuroblastoma SHSY-5Y by using the MTT assay. These new nanomaterials were also characterized by using UV-visible spectroscopy and TEM.

2. MATERIALS AND METHODS

High molecular weight CHI, purchased from Sigma-Aldrich, with the degree of deacetylation of 83% was used for the synthesis of copolymers. Potassium persulfate (KPS) from J. T. Baker was used as initiator for the copolymerization reactions. Both monomers, *N*-isopropylacrylamide of 97% purity and *N,N*-dimethylacrylamide of 99% purity were also purchased from Sigma-Aldrich. 2,2-Azobis(2-amidinopropane) from FLUKA was used as initiator for homopolymerization of *N*-isopropylacrylamide and potassium persulfate from J. T. Baker was used for homopolymerization of *N,N*-dimethylacrylamide. Tetrachloroauric monohydrate salt was acquired from Aldrich and sodium citrate dihydratate from Fluka as the reduction agent for the reaction. For the cell culture work the following materials were used: streptomycin-penicillin antibiotic, GIBCO; phosphate buffered saline (PBS), Sigma; Dulbecco's modified Eagle's medium (DMEM), Biological Industries; Fetal Bovine Serum (FBS), GIBCO; and sequencing grade modified trypsin, Biological Industries. Finally, dimethylthiazol-diphenyltetrazol bromide (MTT) from Invitrogen was used for cell viability tests. All organic solvents were of analytical grade.

3. COPOLYMERIZATION REACTION

An amount of 0.5 g purified CHI was introduced in a 100 mL polymerization tube. It was dissolved with 20 mL of 2% v/v acetic acid at room temperature. Then 0.108 g of KPS dissolved in 2% v/v acetic acid was added and the reaction volume was completed to 40 mL by adding the required volume of 2% v/v acetic acid solution. Then, 2.4 g of the desired monomer was added to the reaction mixture. The polymerization tube was sealed and immersed in a thermoregulated bath at 60 °C for 1 h. The resulting product was diluted with water and precipitated with acetone in order to remove unreacted monomer and undesired homopolymer. The graft copolymer was separated by centrifugation and was lyophilized during 24 h.

4. SYNTHESIS OF AuNP

The AuNP synthesis was carried out following the Turkevich method by reduction of $HAuCl_4$ via citrate solution that has been used in our previews work.[6] A fresh solution of $HAuCl_4$ 1 mM was prepared (100 mL) and set in reflux system under intense stirring for 30 min. A 10 mL solution of sodium citrate dihydrate 38.8 mM was heated at 50–60 °C and poured over the $HAuCl_4$ solution, after that the reflux was maintained for about 30 min. The resulting product is colloid solution of AuNP of 12 nm coated with citrate. The solution was filtered through a 0.45 μm cellulose acetate membrane Millipore syringe filters to remove any precipitate, the pH was adjusted to 8.0 using dilute NaOH solution, the final solution was stored at 4 °C. AuNP were characterized by UV-Visible spectrometry and observed by transmission electronic microscopy (TEM).

5. COATING OF AuNP WITH BIOPOLYMERS: OBTENTION OF NANOCOMPOSITES

A stock solution of AuNP 0.001% wt/v in citrate 1.2 mM was prepared, we also prepare a 0.2% wt/v solution of each copolymer in acetic acid 2% v/v subsequently diluted those with solutions of 0.1% wt/v or 0.05% wt/v or 0.01% wt/v or 0.005% wt/v. The copolymer solutions were sonicated for 1 hour, CHI and CHI-*g*-PDMAAm were filtered on a 0.2 μm cellulose acetate membrane filter while CHI-*g*-PNIPAAm was filtered on a 0.45 μm cellulose acetate membrane filter. In order to obtain the nanocomposites different ratios of AuNP/copolymer were used. To a 5 mL aliquot of AuNP 0.001% wt/v solution, under intense stirring, we added 5 mL of copolymers 0.1% wt/v solution (the same volume of the above mentioned solutions were added) drop wise, yielding a ratio solution of 1:100 AuNP:polymer. The resulting solution was then centrifuged at 8000 rpm for 15 min, and the residue was washed using milliQ water, after washed the residue four times was re-suspended by using a vortex in 5 mL of milli-Q water. The same procedure was applied for the three copolymers and their respective dissolutions.

6. CELL CULTURE

Cytotoxic effect was evaluated using a human neuroblastoma cell line SHSY-5Y. Cells were cultured every 4 days in an incubator at 37 °C and 5% CO_2 in a 250 mL filter cap flasks containing 10 mL of DMEM supplemented with 10% bovine fetal serum (BFS inactivated, Invitrogen) and 100 U/mL penicillin with 100 μg/mL streptomycin (Invitrogen). First neuroblastoma cells were washed thoroughly with PBS, and then incubated with 1 mL of Trypsine for 3 min to detach the cells. To quench the action of the trypsine, 2 mL of DMEM was added to the flask and centrifuged at 1000 rpm for 4 min. The resulting pellet was

re-suspended in 10 mL of DMEM, a 100 μL aliquot was release in a new flask to continue the culture line.

3500 cell per well were seeded in a 96 wells flat bottom plate and incubated for 24 h at 37 °C and 5% CO_2. Samples were exposed to ultraviolet light for sterilization purposes. After the 24 h, the culture medium cell was replaced with 80 μL of new medium. A 20 μl of sample solution was added to at least 5 wells per plate an incubated for 24 h. MTT cell viability assay was performed by removing the medium from each well and incubating the cells for 4 h at 37 °C with 100 μL of 1 mg/mL MTT solution in PBS. After that time, the excess of MTT was removed and the remaining formazan crystals at the bottom of the well were dissolved in isopropanol and quantified by measuring the absorbance at 490 nm with a 650 nm reference. The resulting absorbance was compared with the control as a percentage of cell viability.

7. CHARACTERIZATION OF POLYMERS, AuNP, AND NANOCOMPOSITES

For UV-spectroscopy characterization of AuNP and nanocomposites we used a Perkin-Elmer LAMBDA 25 UV/Vis spectrometer and analyze 2 mL of sample in a 1 cm length cuvette on a range of 300–900 nm. FT-IR analysis for characterization of the polymers was carried out using a BRUKER IR spectroscope model IFS-28. Thermogravimetric evaluation was performed using NETZSCH Thermal Analysis IRIS F-209 equipment. For TEM images of nanoparticles and nanocomposites, we used 200 mesh cooper grids dyed with uranyl acetate 2%, and visualization was accomplished with a JEOL equipment JEM-1010 model.

8. RESULTS AND DISCUSSION

Grafting parameters such as grafting percentage (%G) and grafting efficiency (%E) were calculated as shown in Eqs. (1) and (2), respectively.

$$\%G = \left(\frac{W_1 - W_0}{W_0} \right) \times 100 \quad (1)$$

$$\%E = \left(\frac{W_1 - W_0}{W_2} \right) \times 100 \quad (2)$$

Where W_0, W_1, W_2 are weight of the initial CHI, grafted CHI after washing and weight of initial monomer, respectively. For the CHI-g-PNIPAAm the final values for %G and %E were 58% and 24% respectively, while for CHI-g-PDMAAm were 167% and 70%, respectively. These values indicated that grafting was achieved under the conditions used in this work which is further demonstrated by FT-IR spectroscopy.

Evidence of grafting was obtained by comparing the FT-IR spectra of CHI and CHI-g-PNIPAAm shown in
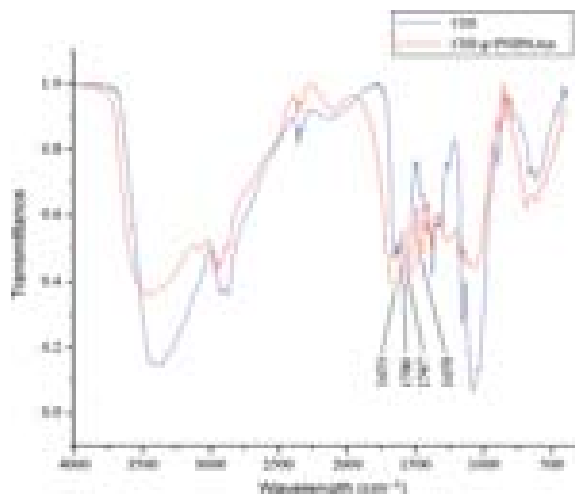

Fig. 1. FT-IR spectrum of CHI and CHI-g-PNIPAAm.

Figure 1. FT-IR of CHI presents two main characteristic absorption bands, one at 1653 cm^{-1} attributed to the mono-substituted amide bending bonds (C=O) and the other at 1586 cm^{-1} corresponding to the amine I (N—H) bending bonds. It is seen that the 1586 cm^{-1} band is shifted to 1547 cm^{-1} in the CHI-g-PNIPAAm spectrum, we also can notice clearly a peak at 1459 cm^{-1} due to the presence of the grafted PNIPAAm on the CHI backbone.

Evidence for the grafting of PDMAAm onto CHI was also obtained by comparing the FT-IR spectra of CHI and CHI-g-PDMAAm (Fig. 2). Both characteristic absorption bands of the CHI are shifted to 1636 cm^{-1} and 1499 cm^{-1}, respectively. Furthermore, two new bands appear at 1455 cm^{-1} and 1431 cm^{-1} corresponding to vibration bands of the methyl groups of the grafted PDMAAm chains.

TGA-DTG analysis was also conducted for the grafted chitosans. CHI and both homopolymers, PNIPAAm and
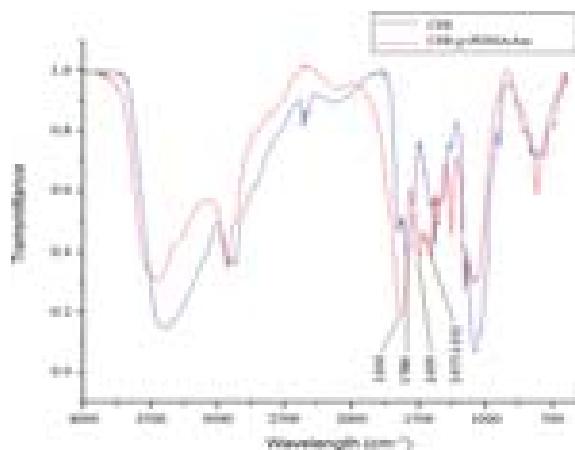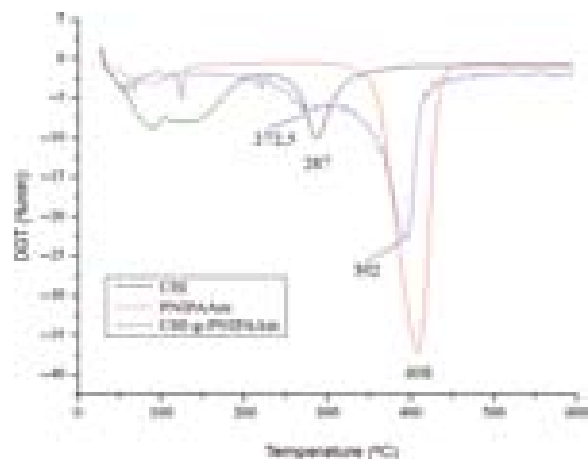

Fig. 2. FT-IR spectrum of CHI and CHI-g-PDMAAm

RESEARCH ARTICLE

Fig. 3. TGA-DWA analysis CHI-*g*-PNIPAAm, CHI and PNIPAAm homopolymer.

Fig. 5. TEM image and UV-Vis spectra of synthesized AuNP.

PDMAAm, present one unique degradation event as shown in Figures 3 and 4 respectively. Grafted CH presents two events, each corresponding to CHI and the respective homopolymer. The presence of these degradation events and the fact that they shift to different degradation temperatures demonstrate that grating was achieved.

AuNP of 12 nm were synthesized using the procedure describe before. Nanoparticles were characterized by TEM and UV-Vis (Fig. 5). UV-Visible spectra clearly presents a definite absorption peak at 520 nm (Fig. 5) which could be related with sizes of AuNP between 10 and 20 nm.[6] AuNP exhibits surface plasmon band at 520 nm due to collective oscillations of the electron at the surface of the nanoparticles that is correlated with the electromagnetic field of the incoming light, these results are in accordance with our previous work.[13] On the other hand the sizes of the nanoparticles were 13 ± 1.23 nm.

Fig. 4. TGA-DWA analysis CHI-*g*-PDMAAm, CHI, PDMAAm homopolymer.

Figure 6 shows UV-Visible spectra of nanocomposites using four different ratios of AuNP and CHI, CHI-*g*-PNIPAAm and CHI-*g*-PDMAAm named as IP and DM respectively. Surface of the AuNP possess a negative charge conferred by the citrate coverage.[14] On the other hand, CHI is positively charged under weak acidic conditions due to the protonation of the amine groups in the polymeric bone-chains.[15] In this conditions, electrostatic attractions occur between both species and CHI will be adsorbed onto the surface of the AuNP, as expected.[16] The AuNP absorption peak shows a bathochromic shift from 520 nm to 538–569 nm in all four ratios. The shift in the peaks is caused by the encapsulation of AuNP with polymer which changes the plasmon surface band of the original nanostructures; this can be noted as an increase in size which can be seen in the TEM images. Also the intensity of the absorbance peak decreases along with lower concentrations of CHI. This can be explained by the different grades of encapsulations of the AuNP, as the concentration of the polymer decreases the lower degree of capping of the nanoparticle lead to a more unstable structure that aggregate during centrifugation, this produce a lower concentration of the final product yielding a lower absorbance peak.

The capping of the AuNP with all the polymers was further confirmed by using TEM analysis. Figure 7 shows TEM images of the three nanocomposites in their 1:100 ratio AuNP/copolymer. As was mentioned before, a shift toward a higher wavelength in the UV-spectra denotes an increase in size of the AuNP due to coated copolymer. The presence of a coating could be visualized in the TEM image (Fig. 7), and enhanced in the inserts.

Cytotoxicity studies were conducted to the copolymers and the nanocomposites using the MTT cell viability assay. Neuroblastoma cell line SHSY-5Y was selected for the cell viability studies due to the possible application of the new nanomaterials in Alzheimer's disease.[4] In an MTT assay, the concentration of formazan generated once the
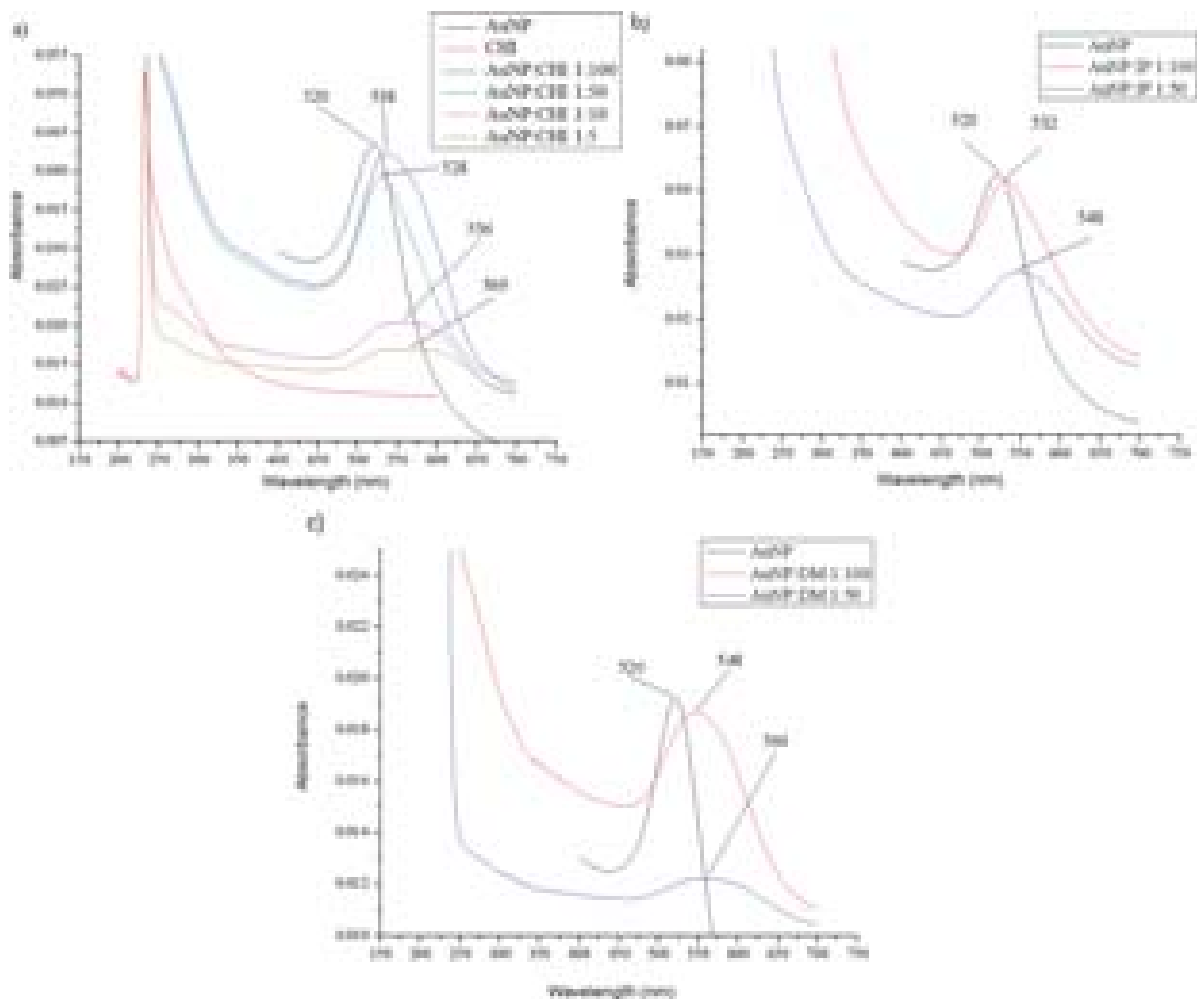
Fig. 6. UV spectra characterization of: (a) CHI capping the AuNP; (b) CHI-*g*-PNIPAAm capping the AuNP; and (c) CHI-*g*-PDMAAm capping the AuNP.

MTT reagent is reduced (thanks to the action of mito-chondrial enzymes in metabolically active cells) is directly proportional to the cell viability. The concentration of for-mazan was measured spectrophotometrically at 490 nm.

The results are shown in Figure 8. CHI and CHI-*g*-PNIPAAm did not showed effects on cell viability in none of their respective dilutions studied, in opposition, we can see a slight toxic effect using the four dissolutions of
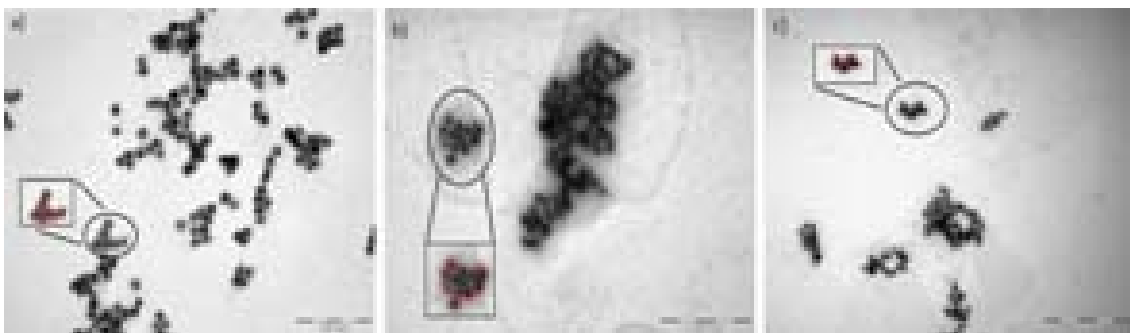
Fig. 7. TEM images of: (a) CHI capping the AuNP; (b) CHI-*g*-PNIPAAm capping the AuNP; and (c) CHI-*g*-PDMAAm capping the AuNP.
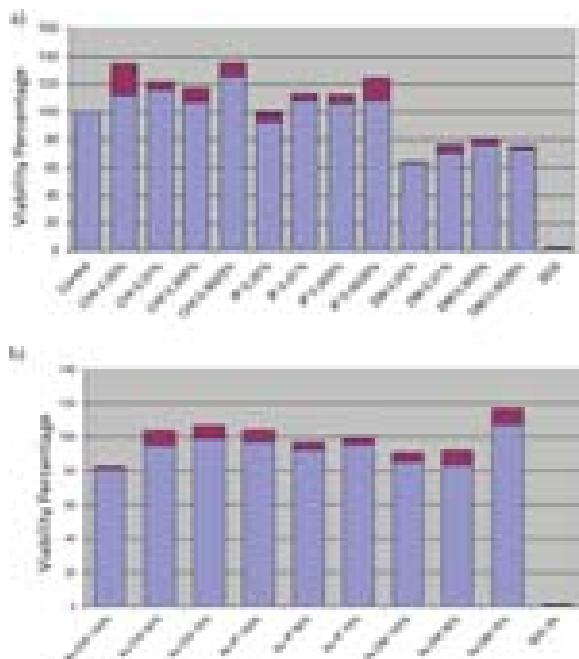
Fig. 8. MTT assay results for: (a) CHI, CHI-*g*-PNIPAAm and CHI-*g*-PDMAAm; and (b) Nanocomposites of AuNP capped with CHI, CHI-*g*-PNIPAAm and CHI-*g*-PDMAAm. Homopolymers and CHI dilutions were prepared using acetic acid 2%, while nanocomposites solutions were prepared using de nanocomposites described in the procedure as the starting 100% and subsequently diluted in MilliQ water. Only for ratios 1:100 of AuNP:Copolymers were studied. The experiments are in triplicate and repeated three independent times.

CHI-*g*-PDMAAm used in the test. Despite this fact, once AuNP are capped with the CHI-*g*-PDMAAm the toxic effect was reduced considerably while AuNP capped with CHI and CHI-*g*-PNIPAAm presents no effects on cell viability possibly due the neutralization of the positive charges that are present in CHI and grafted CHI.

9. CONCLUSION

The nanocomposites obtained in this work show low effects on cell viability being interesting candidates to be used for the improvement of the delivery of nanoparticles to the brain after intravenously or nasal administration for the treatment or diagnosis of Alzheimer's disease. Experiments in this area are currently in progress in our laboratory.

References and Notes

1. D. Li, G. Li, P. Li, L Zhang, Z. Liu, J. Wang, E. Wang, The enhancement of transfection efficiency of cationic liposomes by didodecyldimethylammonium bromide coated gold nanoparticles. *Biomaterials* 31, 1850 (**2010**).
2. K. Hamad-Schifferli, J. J. Schwartz, A. T. Santos, S. Zhang, and J. M. Jacobson, Remote electronic control of DNA hybridization through inductive coupling to an attached metal nanocrystal antenna. *Nature* 415, 152 (**2002**).
3. D. Kim, Y. Y. Jeong, and S. Jon, A drug-loaded aptamer-gold nanoparticle bioconjugate for combined CT imaging and therapy of prostate cancer. *ACS Nano* 4, 3689 (**2010**).
4. M. J. Kogan, N.G. Bastus, R. Amigo, D. Grillo-Bosch, E. Araya, A. Turiel, A. Labarta, E. Giralt, and V. F. Puntes, Nanoparticle-mediated local and remote manipulation of protein aggregation. *Nano Lett.* 6, 110 (**2006**).
5. E. C. Dreaden, M. A. Mackey, X. Huang, B. Kang, and M. A. El-Sayed, Beating cancer in multiple ways using nanogold. *Chem. Soc. Rev.* 40, 3391 (**2011**).
6. M. J. Kogan, I. Olmedo, L. Hosta, A. R. Guerrero, L. J. Cruz, and F. Albericio, Peptides and metallic nanoparticles for biomedical applications. *Nanomedicine* 2, 287 (**2007**).
7. S. Guerrero, E.Araya, J. L. Fiedler, J. I. Arias, C. Adura, F. Albericio, E. Giralt, J. L. Arias, M. S. Fernández, and M. J. Kogan, Improving the brain delivery of gold nanoparticles by conjugation with an amphipathic peptide. *Nanomedicine* (*Lond.*) 5, 897 (**2010**).
8. J. Zhang, W. Xia, L. Ping, C. Qinyuan, T. Talba, G. Wenxiu, and L. Bo, Chitosan Modification and Pharmaceutical/ Biomedical Applications. *Marine Drugs* 8, 1962 (**2010**).
9. W. J. Trickler, A. A. Nagvekar, and A. K. Dash, The *in vitro* Subcellular localization and *in vivo* efficacy of novel chitosan/gmo nanostructures containing paclitaxel. *Pharm. Res.* 26, 1963 (**2009**).
10. B. Luppi, F. Bigucci, T. Cerchiara, and V. Zecchi, Chitosan-based hydrogels for nasal drug delivery: From inserts to nanoparticles. *Expert Opinion on Drug Delivery* 7, 811 (**2010**).
11. M. Babič, D. Horák, P. Jendelová, K. Glogarová, V. Herynek, M. Trchová, K. Likavčanová, P. Lesný, E. Pollert, M. Hájek, and E. Syková, Poly(*N*,*N*-dimethylacrylamide)-coated maghemite nanoparticles for stem cell labeling. *Bioconjugate Chem.* 20, 283 (**2009**).
12. J. Qin, Y. S. Jo, J. E. Ihm, D. K. Kim, and M. Muhammed, Thermosensitive nanospheres with a gold layer revealed as low-cytotoxic drug vehicles. *Langmuir* 21, 9346 (**2005**).
13. I. Olmedo, E. Araya, F. Sanz, E. Medina, J. Arbiol, P. Toledo, A. Álvarez-Lueje, E. Giralt, and M. J. Kogan, How changes in the sequence of the peptide CLPFFD-NH$_2$ can modify the conjugation and stability of gold nanoparticles and their affinity for *β*-amyloid fibrils. *Bioconjugate Chem.* 19, 1154 (**2008**).
14. W. B. Tan and Y. Zhang, Surface modification of gold and quantum dot nanoparticles with chitosan for bioapplications. *Journal of Biomedical Materials Research Part A* 75A, 56 (**2005**).
15. H.-M. Kang, Y.-L. Cai, and P.-S. Liu, Synthesis, characterization and thermal sensitivity of chitosan-based graft copolymers. *Carbohydr. Res.* 341, 2851 (**2006**).
16. B. Wang, K. Chen, S. Jiang, F. Reincke, W. Tong, D. Wang, and C. Gao, Chitosan-mediated synthesis of gold nanoparticles on patterned poly(dimethylsiloxane) surfaces. *Biomacromolecules* 7, 1203 (**2006**).

140

*J. Biomater. Tissue Eng. 3, 135–140, **2013***

Molecular Dynamics Study on the Encapsulation of Prilocaine in Liposomes at Physiological pH

Giovanni Giupponi[1], María Florencia Martini[2], and Mónica Pickholz[2, *]

[1]*Departament de Fisica Fonamental, Universitat de Barcelona, Carrer Martii Franques, 08028 Barcelona, Spain*
[2]*Department of Pharmaceutical Technology, Universidad de Buenos Aires, Junin 954 RA-1053 Buenos Aires, Argentina and CONICET*

In this work, we investigated the concentration effects on the encapsulation of prilocaine (PLC), an aminoamide local anesthetic, into a small unilamellar liposome, at physiological pH. On the line of our previous work, we have carried out Molecular Dynamics (MD) simulations using a coarse grain (CG) model that allow us to reach the microsecond time scale. At physiological pH there is a partition between protonated and neutral PLCs. In order to estimate the protonated/neutral PLC ratio at physiological pH (7.4), we have used the Henderson-Hasselbach equation. We have studied three PLC:lipid molar concentrations, ranging between 10:10 to 1:4. We essentially found that all neutral PLC molecules rapidly diffuse into the hydrophobic region of the vesicle adopting an asymmetric bimodal distribution. Moreover, protonated PLC molecules partition between the external monolayer of the vesicle and the water phase, having a high rate of exchange between this two phases, with no access to the inner part of the liposome in a concentration dependent way. In this way, we found that the behavior of PLCs at physiological pH is a combination of high and low pH, especially at low concentration of local anesthetics.

Keywords: Coarse Grain, Local Anesthetics, Liposome, Molecular Dynamics, Prilocaine, Physiological pH.

1. INTRODUCTION

The development of safer and more effective local anesthetics (LA)—pain relief drugs—has come a long way since the earliest experiments with cocaine.[1] Nowadays, a growing number of new anesthetics are used in medicine and odontology. The structure and physicochemical features of each LA determine drug potency, onset of action of sensory block and toxicity.[2] However, the relatively short duration of analgesia—due to their transfer and redistribution from the site of injection—still restricts their clinical use for the treatment of chronic pain.[3] In the last decades the development of LA drug-delivery systems made possible to manipulate some biopharmaceutical and pharmacological properties of LA, improving their therapeutic effects (long duration of action associated to low systemic toxicity) and pointing them as promising alternatives to favor the clinical use of LA agents.[4, 5]

Liposomes-spherical vesicles consisting of one or more phospholipid bilayers—are currently used as effective drug carriers. For example, there are vesicle formulations for antitumor anthracyclines,[4] antifungal[5] and many

others.[6, 7] Liposomes are very versatile structures: their physicochemical properties can be modified by changing the types of lipids and their proportions in the liposomal formulation, the size of the vesicle, the charge of the surface (positive, negative, or neutral), the pH sensitivity, temperature sensitivity, etc.[9] In this way, liposomes can be carriers for hydrophilic or hydrophobic compounds. The size of the liposomal vesicles significantly influences drug distribution.[8, 9] The encapsulation of LAs into liposomes for drug-delivery purposes has been proposed for the first time by Gesztes et al.[10] Nowadays, diverse studies have been demonstrated the clinical effectiveness of liposomal formulations containing different anesthetics.[11, 12] The advantages of encapsulating LA in liposomes are the slow drug release, prolonged anesthetic effect and reduced toxicity towards the cardiovascular and central nervous systems.[4] Intensive research is focused on anesthetics trapped into liposomes, in order to enhance their activity and pharmacokinetic properties.[5]

It is important to remark that the pH of a parenteral infusion is found between 4 and 8.[13] The reason for that is related with the patient's acceptance: infused solutions of pH smaller than 3 cause pain and phlebitis, and pH greater

---

*Author to whom correspondence should be addressed.

than 8 cause inflammation and venous irritation. In particular, most of LAs are weak bases with pKA values between 7.5 and 8.8.[14] In this way, a partition between their charged and uncharged forms is found at physiologic pH. This partition could be quantified by the Henderson-Hasselbach equation,

$$pH = pK_a + \log \frac{[\text{neutral}]}{[\text{protonated}]} \quad (1)$$

The values between [..] represent the molar concentrations of neutral and protonated species, respectively.

The knowledge of the interaction of LA with lipids is essential in order to improve the use of liposomes as LAs drug carriers. Many techniques are used in order to elucidate these interactions.[15–17] In particular, fully atomistic molecular dynamics (MD) simulations are very powerful to study the interaction of anesthetics with model membranes, as shown for the number of articles in the literature.[15, 18–21]
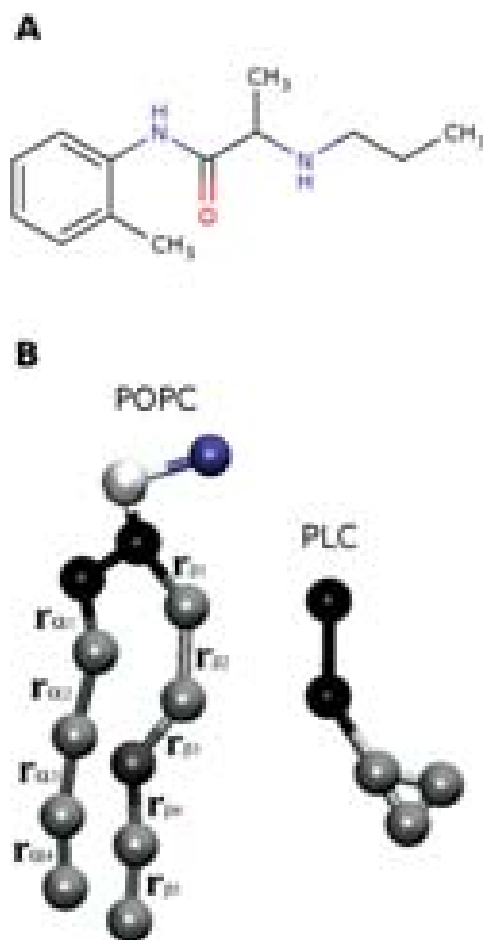
Fig. 1. (A) Chemical structure of protonated prilocaine (*p*PLC), (B) Coarse-grain representation of POPC phospholipid and PLC molecules. The ester (E) and the vectors of a consecutive sites of the lipid tails $\vec{r}\alpha i$ ($i = 1.4$) for the palmitoil chain, and $\vec{r}\beta j$ ($j = 1.5$) for the oleoyl chain are shown.

However, it is not possible to reach these detailed studies for big systems and long times. In this way, the use of simplified models could help us to reach important phenomena. Very recently, we have studied the encapsulation of LA prilocaine (PLC, see its chemical structure in Fig. 1(A)) into a liposome using a Coarse Grain (CG) model.[22] In this study we considered the PLCs at their neutral (high pH) and protonated (low pH) state. Regarding the importance of the formulations at physiological pH, here we extend our simulations in order to take this effect into account. At physiological pH there is a partition between neutral (*n*PLC) and protonated (*p*PLC) prilocaine molecules. The ratio of this partition was, *p*PLC/*n*PLC, was estimated as ∼ 1.6, taking into account the apparent pKa of PLC in membranes is 7.6[23] and a pH of 7.4 in Henderson-Hasselbach equation (Eq. (1)). We studied three concentrations of PLC that meet this ratio. It is important to keep in mind that the protonation/deprotonation of the PLCs is a dynamical process. However, as a first approximation we consider only a fixed number of neutral and protonated species in our simulations. In next section we describe the methodology used in this study, followed by the results and conclusions.

2. METHODOLOGY

In this work, we carried out molecular dynamics simulations using a coarse grain model within the MARTINI force field[?] that can be used to investigate macromolecular phenomena at the microsecond scale.[24–30] This method aims at a systematic and portable representation for water, phospholipids, and other small molecules in terms of a few building blocks, or coarse grained (CG) particles. These CG particles interact with potential parameters optimized for use in a broad range of biomolecular applications. Four heavy atoms to one CG particle mapping rule is generally followed, and hydrogen atoms are neglected because of their small size and mass. This model considers four main types of CG particles: polar (P), nonpolar (N), apolar (C), and charged (Q). In Figure 1, we show an scheme of the CG 1-palmitoyl-2-oleoyl-sn-glycero-3-phosphatidylcholine (POPC) lipid and the CG PLC molecule, used in his work. The prilocaine molecules have been parameterized in our previous work, within this scheme.[22] The structure of the neutral PLC (*n*PLC) is essentially the same of the protonated one (*p*PLC). However, the type of CG particles and charge are different, in order to consider the charge of the protonated molecule. Besides, a chloride counterion was added in order to form a salt with *p*PLC. The rest of the CG particles for lipids, water, and ions follow the standard force field. For a detailed description of force features and parameters, see Ref. [24]. We have used the P4 model of water, instead the new developed polarizable water[31] in order to be consistent with our previous work.

In this work we study the encapsulation of a mixture of neutral and protonated PLC—in order to emulate the partition of protonated and neutral species as fisiological pH—in a POPC lipid vesicle. We considered three different concentrations that respect the 1.6 ratio:

(a) 54 *p*PLC and 34 *n*PLC,
(b) 88 *p*PLC and 55 *n*PLC, and
(c) 141 *p*PLC and 88 *n*PLC.

The chosen concentrations were thought in order to compare with our previous work:[22] the
(a) condition represents the same lipid:PLC ratio (10:1) used in the simulations of the previous work, the
(b) condition has the same amount of *p*PLC, even though in the presence of the correspondent number of *n*PLC and
(c) condition has the same amount of *n*PLC, even though in the presence of the corresponding *p*PLC.[22]

The starting point for this simulation was a preassembled POPC vesicle, containing 877 lipids (254 and 623 for the internal and external monolayer, respectively), 81550 P4 water particles. The PLCs were initially (randomly) distributed in the water phase for the case (a) (lower concentration). Besides, chloride counterions were always added randomly in the water phase, in the same concentration than *p*PLC, in order to ensure electroneutrality

The following cases were built up by addition of the extra molecules into the external water phase, starting from the equilibrated previous case. We have equilibrated the systems for 250 ns within the NPT ensemble. After equilibration, we run the system in the NVT ensemble for 1 μs.

The simulations were carried out with the GROMACS 4.0 simulation package,[32] using a simulation timestep of 40 femtoseconds with a nonbonded and electrostatic cutoff of 12 Å. The reference temperature was set to 325 K using a Berendsen thermostat with a time constant of 1.0 ps. For NPT runs, Berendsen pressure coupling was used with a reference pressure of 1 bar, time constant 5.0 ps and a compressibility of 3×10^{-5} bar^{-1}. On a computational note, we report that a fully atomistic representation of the same systems would need around a million atoms to be run with a typical simulation timestep of 2 femtoseconds. As drug diffusion and adsorption phenomena involve characteristic scales of tens of nanometers and hundreds of nanoseconds, we conclude that extensive fully atomistic simulations reaching the microsecond of such phenomena are impractical even using big supercomputers, leaving coarse grained force fields the only feasible models.

3. RESULTS

In this work, we have studied the encapsulation of three different concentrations of prilocaines, with the same *p*PLC/*n*PLC ratio: going from $\sim$1:10 (case a) to 1:4 lipid:LA ratio (case c), into a POPC lipid vesicle. Here, we discuss the main results of our study.

It is important to highlight here that most of the studied *observable* properties are converged during the NPT equilibration period. In this way, properties shown here are averaged at the stationary state of the system.

In order to have a first glance to the encapsulation mechanism, we visually check the stability of the vesicle and the diffusion of the drug. In Figure 2, we show, as an example, three snapshots that corresponding to case (a). The *n*PLC and *p*PLC are represented in green and red, respectively, and water and couterions sites were removed for visualization purpose. In this figure, the snapshot (A) corresponds to the initial configuration: the PLCs were randomly distributed in the water phase. The other two snapshots were taken at the end of the NPT equilibration run $t = 0.25$ μs and at the end of the NVT run $t = 1.25$ μs. Snapshots B and C clearly show that most of the nPLCs quickly diffused into the vesicle during the equilibration period, and remained inside during the whole simulation time, while the *p*PLC partition into both phases. Similar results were found for cases (b) and (c) (snapshots not shown).

In order to check the overall organization of the systems under study and the stability of the vesicle we computed the radial electron density profile (REDP), by time averaging the net charge $Q(r)$ (the nuclear charge corresponding to all of the atoms represented by each CG site) contained in the volume between consecutive spheres, by

$$REDP(r) \propto \left\langle \frac{Q(r)}{4/3\pi((r+\delta)^3 - r^3)} \right\rangle \qquad (2)$$

In Figure 3 we show the REDP of the 3 different systems under study: (a) 54 *p*PLC–34 *n*PLC, (b) 88 *p*PLC–55 *n*PLC, and (c) 141 *p*PLC–88 *n*PLC calculated by averaging over the 1 μs NVT simulations run. In this figure, the REDP corresponding to the POPC and water components is shown in black and blue, respectively. Comparison of the overall organization of water and vesicle and their interfaces show no noticeable difference between the three cases. In these figures, the pPLCs (in red) and nPLCs (in green) densities have been magnified 5 times for visualization purposes. We can notice that *n*PLC molecules are essentially found inside the vesicle, following a bimodal distribution for the three cases (as found in previous work[22]). By the other hand, *p*PLC molecules partitioned between the water/lipid interface of the external monolayer and the water phase, with no access to the bilayer center. Looking to the different groups (ring and tail) of the *p*PLC molecules, we find a preferential orientation of the *p*PLC molecules (results not shown), with the ring pointing to the lipid tail region and the *p*PLC tail to the the polar head groups. This fact was better described in previous publication for the low pH case, and we will not enter deeper here. On the contrary, *n*PLC does not show a preferential orientation inside the lipid membrane.

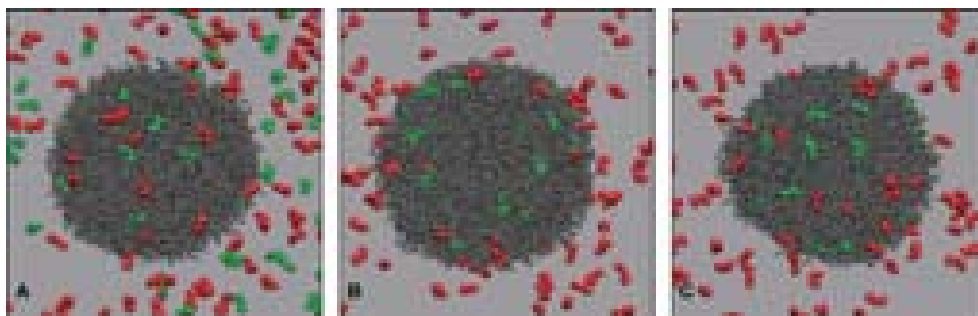Until now, we got the qualitative idea that nPLCs are essentially found inside the vesicle and *p*PLC partition

Fig. 2. Snapshots from the molecular dynamics simulations of PLC in POPC vesicles: *n*PLC in green and *p*PLC in red. The snapshots correspond to (A) the initial configuration, (B) after 250 ns of NPT run, and (C) after 1 μs of NVT run. Water and sites were removed for clarity.

between both phases. We calculate the number of PLC molecules absorbed by the vesicle as a function of time, using $\langle r \rangle = 75.0$ Å, as external vesicle radius, which is the averaged over the NVT simulation time radius. In Figures 4(A) and (B) we have separated the nPLCs and *p*PLC numbers, cases (a) in green, (b) in red and (c) in blue, respectively. We can see from Figure 4(A) that *n*PLC are essentially inside the vesicle independently on concentrations. By the other hand, in Figure 4(B) we can see

an increasing number of *p*PLC inside the vesicle with the increasing of concentration. In Table I we summarized the average numbers of *n*PLC, *p*PLC and the total number of PLC encapsulated into the vesicle.

We found a little decreases of this number (from 20.7 to 19.2), when compared with the system with the same amount of *p*PLC, but in absence of *n*PLC. In this way, the presence of *n*PLC slightly diminishes the possibility of *p*PLC to get inside the vesicle.
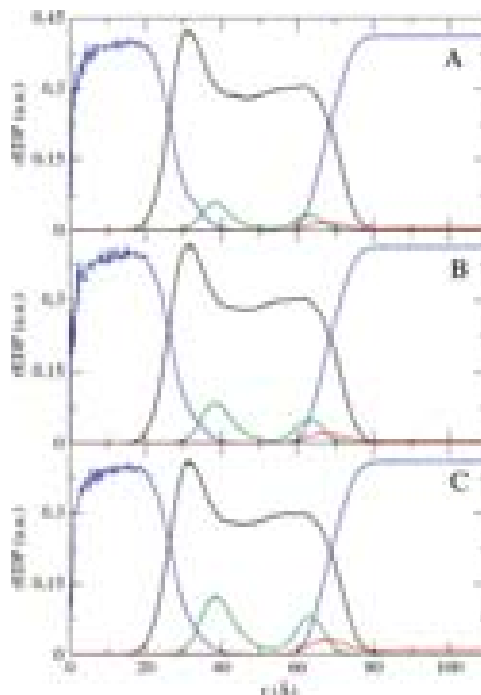

Fig. 3. Radial electron density profile (REDP) of the different components of the PLC/vesicle as a function of the r coordinate; $r = 0$ corresponds to the vesicle center. The colors are blue for water, black for POPC, green for neutral PLC, and red for protonated PLC. (A) 54 *p*PLC–34 *n*PLC, (B) 88 *p*PLC–55 *n*PLC, and (C) 141 *p*PLC–88 *n*PLC derived, from the 1 μs NVT simulations. The REDP of *n*PLC and *p*PLC were amplified 5 times for visualization purposes.
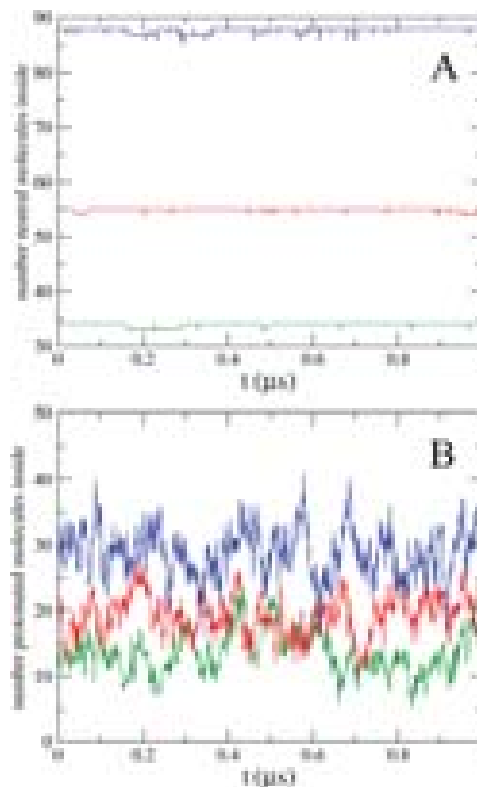

Fig. 4. Number of (A) *n*PLC and (B) *p*PLC molecules inside the vesicle as function of time for concentration *p*54*n*34 (green), *p*88*n*55 (red) and *p*141*n*88 (blue).

Table I. Number of neutral (N_{nPLC}), protonated prilocaine (N_{pPLC}) and total (N_{total}) molecules encapsulated into the vesicle.

Case	N_{nPLC}	N_{pPLC}	N_{total}
Case (a)	33.86(1)	13.6(1)	47.5
Case (b)	54.91(1)	19.2(1)	74.1
Case (c)	87.79(2)	28.9(1)	116.7

The distribution of PLCs inside the vesicle was shown in Figure 3. However, because of the spherical geometries of the system, density is difficult to visualize. In this way, we have calculated the average number of PLCs (center of mass) as function of the distance to the vesicle center. The protonated case is shown in Figure 5: (A) case (a), (B) case (b), (C) low pH case from Ref. [22] and (D) case (c). We can see from these figures that a main peak is found for the anesthetics inside the vesicle. The maxima are found essentially at a radius of ~ 69 Å. Its position does not change with concentration but the intensity does. We can see that these peaks extend more than the 75 Å.[22] This could be explained, by the interactions of the external pPLC close to the surface, that interact with the lipid polar head. In this way, an effective encapsulation is found, ranging at the radius of 80 Å. However, in average, the extra encapsulation is quite low (~ 1–2 pPLC molecules). It is important to remark here that exist a fast exchange of pPLC between the vesicle and the aqueous phase for all the studied concentrations.[22] Besides, as found in previous work, pPLCs cannot access to the inner monolayer by diffusion.

The numbers of nPLCs (center of mass) as function of the distance to the vesicle center are shown in Figure 6: (A) case (a), (B) case (b), (C) high pH case from Ref. [22] and D-case (c). As we mention earlier, we observe two well defined peaks that correspond to the partition of nPLC in each of the monolayers: the inner (D_1) and outer (D_2) peaks, that correspond to the nPLC partitioned into the
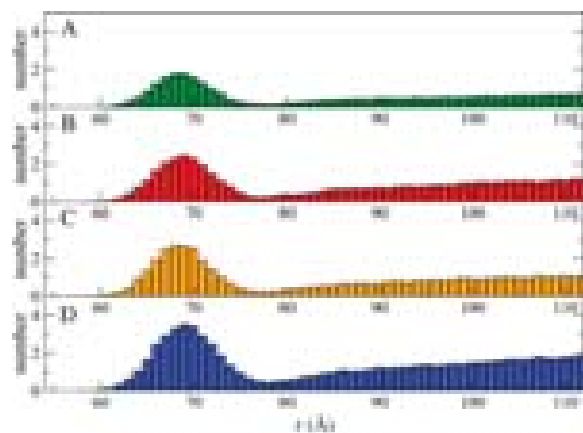
Fig. 5. Histogram of the number of protonated PLC as function of the radial distance for the different conditions: (A) case (a) in green, (B) case (b) in red, (C) 88 pPLC (Ref. [22]) (orange) and (D) case (c) in blue.
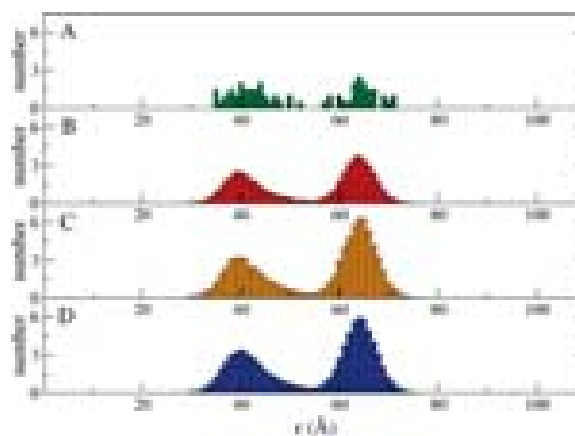
Fig. 6. Histogram of the number of neutral PLC as function of the radial distance for the different conditions: (A) case (a) in green, (B) case (b) (red), (C) 88 nPLC (from Ref. [22]) (orange), (D) case (c) in blue.

internal and external monolayer, respectively. We can see that both peaks increase with concentration, however the maxima remain at the same distance of the bilayer center (~ 39 Å, and ~ 65 Å, respectively). We have calculated the number of nPLC partitioned in each of the monolayers. Taken into account the asymmetry of the monolayers we use as a criteria the cut radius as the middle of the gap in Figure 5(A) (54 Å) and used this difference for all the cases. Because of the asymmetry of the monolayers, it is more adequate to compare the number nPLC per lipid ($nPLC_{lip}$), shown in Table II. It is important to keep in mind that from the experimental point of view, it was reported in the literature a very high lipid:neutral LA ratio (3:1 or higher).[15, 17] We can see from Table II that the number of $nPLC_{lip}$ increases with concentration. Furthermore, the $nPLC_{lip}$ is higher for the inner monolayer for all the concentrations. Besides, if we compare the case (c) in which the number of nPLC is 88 (and 141 pPLC) with our earlier paper (Ref. [22]) in which only 88 nPLC where present, also presented in Table II, we can see that an increase of the inner $nPLC_{lip}$ (from 0.137 to 0.146) with a concomitant decrease of the outer monolayer (from 0.084 to 0.081). However these little differences are not meaningful within the error bars. By the other hand,

Table II. Number of neutral per lipid, $nPLC_{lip}$, in internal and external monolayers and ratio between the number of nPLC corresponding to peaks D_1 (internal monolayer) and D_2 (external monolayer), for the 3 concentrations, the same information of the system at high pH was also included.

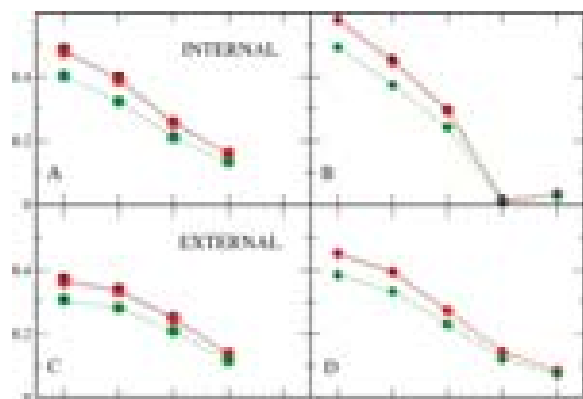| Case	Peak D_1:$nPLC_{lip}$	Peak D_2:$nPLC_{lip}$	D_1/D_2
Case (a)	0.070(2)	0.024(1)	1.2(1)
Case (b)	0.096(4)	0.049(2)	0.8(1)
Case (c)	0.146(6)	0.081(3)	0.7(1)
Ref. [22]	0.137(6)	0.084(3)	0.7(1)

145

Fig. 7. Generalized order parameter of the inner (A) and (B) and outer (C) and (D) shell of the vesicle. Left pannels (A) and (C) correspond to the saturated palmitoyl chain and right pannels (B) and (D) to the insaturated oleoyl chain for the different conditions: case (a) in green, case (b) in red and case (c) in blue.

looking at the *n*PLC center of mass trajectories, we can see crossing events of these molecules between monolayers for all the studied cases. These crossing events were already reported,[1, 15, 33] here we will not enter in more details.

The effects of the solutes on the conformation of the lipid chains can be studied by monitoring the average orientation of the covalent bonds of the effective sites located in the interior of the bilayer. In this way, we have, also, studied the order parameter of the lipid tails. In this case, because of spherical symmetry of the system, we have defined the angle θ between the vectors of consecutive sites of the lipid tails and the radial versor, $\hat{r}$ and $-\hat{r}$, for the outer and inner monolayer, respectively. We have named the vectors between the consecutive CG sites as $\vec{r}_\alpha i$ ($i = 1, 4$) for the palmitoil chain, and $\vec{r}_{\beta j}$ ($j = 1, 5$) for the oleoyl chain, as shown in Figure 1(B). We have calculated the average the order parameter through the averaging of the second Legendre polynomial over all lipids and time for each of the described vectors, as

$$S = \frac{1}{2} \langle 3\cos^2\theta - 1 \rangle \qquad (3)$$

In Figure 7, we show the generalized order parameter for saturated (left panels: (A) and (C)) and unsaturated (right panels: (B) and (D)) chains, for the inner (top panels) and the outer (bottom panels) shell of the liposome. As an overall view of this figure, we can notice (as expected) that the tails of the outer monolayer are more organized that inner one. The reason for that is related with the curvature and the limiting factor for the vesicle density. There is important to point out that the unsaturated tail is always more disorder that the saturated one due to the kinks of the trans-gauche conformation.[34] Respect to the concentration effects, we can see an overall organization of the lipid tails, from case (a) to case (b). However, essentially no changes of chain organization were observed between case (b) and (c).

4. CONCLUSIONS

In this work we have studied, by molecular dynamics simulations, the interaction of the local anesthetic prilocaine with small liposomes at physiological pH using a coarse grain model.[24] The use of a coarse grain model allowed us to reach relevant time and length scales of drug diffusion, otherwise impossible to observe using fully atomistic molecular dynamics. Very recently, we have studied the encapsulation process of neutral (high pH) and protonated (low pH) prilocaine in a POPC vesicle.[22] This work shed light in many aspects of the encapsulation. However, it is undoubtedly the necessity of the understanding this kind of system at physiological pH, since the pH of an infused solution should be in the range 4 to 8 to have a good patient acceptance. Moreover, the existence of the two species of PLC is needed in order to obtain the desire clinical effects: neutral molecules acts as a reservoir, while the protonated specie enhanced the exchange of the LA with the water phase. At physiological pH, there is a partition between neutral and protonated PLCs species. In this direction, and as a first step, we have worked with three concentration corresponding to pH 7.4.

The studied concentrations range between $\sim$1:10 to 1:4 were calculated through the Eq. (1). Nevertheless, the rigidity of the used model do not allow the protonation/deprotonation processes during the simulation run.

The behavior of PLCs at physiological pH was found essentially as a combination of high and low pH: we found that all neutral PLC molecules rapidly diffuse into the hydrophobic region of the vesicle adopting an asymmetric bimodal density distribution. With concentration, the peaks position remain the same, however increase in concentration per lipid, especially on the external monolayer. By the other hand, protonated PLC are found to partition between the external monolayer and the water phase. Most of protonated drug present a great exchange between the vesicle and water phase (attaching/detaching cycles). No major difference was found in the studied concentration range. At higher simulations we observed that the increase of neutral species slightly precludes the protonated species to enter. In this study we have compared the physiological pH conditions studies with the high and low pH published before.

As a final remark, we would like to mention that molecular dynamics simulations are a very powerful tool to investigate different aspects of the encapsulation/liberation processes regarding the development/understanding the drug delivery systems at the nanoscale.

References and Notes

1. J. Calatayud and A. González, History of the development and evolution of local anesthesia since the coca leaf. *Anesthesiology* 98, 1503 (**2003**).

2. C. Cereda, G. Brunetto, D. de Araujo, and E. de Paula, Liposomal formulations of prilocaine, lidocaine and mepivacaine prolong analgesic duration. *Canadian Journal of Anesthesia* 53, 1092 (**2006**).

3. E. de Paula, C. Cereda, G. Tofoli, M. Franz-Montan, L. Fraceto, and D. R. de Araujo, Drug delivery systems for local anesthetics. *Recent Patents on Drug Delivery and Formulation* 4, 23 (**2010**).

4. T. P. Herringson and J. G. Altin, Increasing the antitumor efficacy of doxorubicin-loaded liposomes with peptides anchored via a chelator lipid. *Journal of Drug Targeting* 19, 681 (**2011**).

5. S. M. Rudramurthy, M. Jatana, R. Singh, and A. Chakrabarti, *In vitro* antifungal activity of Indian liposomal amphotericin B against clinical isolates of emerging species of yeast and moulds, and its comparison with amphotericin B deoxycholate, voriconazole, itraconazole and fluconazole. *Mycoses* doi:10.1111/j.1439-0507.2012.02197.x. (**2012**), in press.

6. L. Lajavardi, S. Camelo, F. Agnely, W. Luo, B. Goldenberg, M.-C. Naud, F. Behar-Cohen, Y. de Kozak, and A. Bochot, New formulation of vasoactive intestinal peptide using liposomes in hyaluronic acid gel for uveitis. *J. Controlled Release* 139, 22 (**2009**).

7. Z. Drulis-Kawa and A. Dorotkiewicz-Jach, Liposomes as delivery systems for antibiotics. *Int. J. Pharm.* 387, 187 (**2010**).

8. G. Gregoriadis, Engineering liposomes for drug delivery: Progress and problems. *Trends in Biotechnology* 13, 527 (**1995**).

9. A. Sharma and U. Sharma, Liposomes in drug delivery: Progress and limitations. *Int. J. Pharm.* 154, 123 (**1997**).

10. A. Gesztes and M. Mezei, Topical anesthesia of the skin by liposome-encapsulated tetracaine. *Anesth. Analg.* 67, 1079 (**1988**).

11. J. G. Boogaerts, N. D. Lafont, A. G. Declerq, C. L. Hongwen, E. T. Gravet, J. A. Bianchi, and F. J. Legros, Epidural administration of liposome-associated bupivacaine for the management of postsurgical pain: A first study. *J. Clin. Anesth.* 6, 315 (**1994**).

12. G. J. Grant, Y. Barenholz, E. M. Bolotin, M. Bansinath, H. Turndor, B. Piskoun, and E. M. Davidson, A novel liposomal bupivacaine formulation to produce ultralong-acting analgesia. *Anesthesiol* 316, 133 (**2004**).

13. K. E. Bertch, Handbook on Injectable Drugs, 16th edn., Pharmaceutical Press, London (**2011**), Vol. 80, pp. 1008–9.

14. Y. Canos-Rius, N. Martan-Biosca, S. Sagrado, R. Villanueva-Camaatas, and M. Medina-Hernandez, Experimental and theoretical investigation of the micellar-assisted solubilization of ibuprofen in aqueous media. *European Journal of Medicinal Chemistry* 40, 215 (**2005**).

15. E. de Paula, S. Schreier, H. Jarrell, and L. Fraceto, Experimental and theoretical investigation of the micellar-assisted solubilization of ibuprofen in aqueous media. *Biophys. Chem.* 132, 47 (**2008**).

16. L. Cabeça, M. Pickholz, E. de Paula, and A. J. Marsaioli, Liposome-prilocaine interaction mapping evaluated through STD NMR and molecular dynamics simulations. *J. Phys. Chem. B* 113, 2365 (**2009**).

17. L. Fraceto, A. Spisni, S. Schreier, and E. de Paula, Differential effects of uncharged aminoamide local anesthetics on phospholipid bilayers, as monitored by 1H-NMR measurements. *Biophys. Chem.* 115, 11 (**2005**).

18. M. Pasenkiewicz-Gierula, T. Róg, J. Grochowski, P. Serda, R. Czarnecki, T. Librowski, and S. Lochy'nski, Effects of a carane derivative local anesthetic on a phospholipid bilayer studied by molecular dynamics simulation. *Biophys. J.* 85, 1248 (**2003**).

19. C.-J. Holgberg, A. Maliniak, and A. Lyubartsev, Preferential location of lidocaine and etidocaine in lecithin bilayers as determined by EPR, fluorescence and 2H NMR. *Biophys. Chem.* 125, 416 (**2007**).

20. M. Pickholz, L. Fraceto, and E. de Paula, Distribution of neutral prilocaine in a phospholipid bilayer: Insights from molecular dynamics simulations. *Int. J. Quantum Chem.* 108, 2386 (**2008**).

21. E. Prates, P. Souza, M. Pickholz, and M. Skaf, CHARMM-based parameterization of neutral articaines—A widely used local anesthetic. *Int. J. Quantum Chem.* 111, 1339 (**2011**).

22. M. Pickholz and G. Giupponi, Coarse grained simulations of local anesthetics encapsulated into a liposome, *J. Phys. Chem. B* 114, 7009 (**2010**).

23. S. Malheiros, L. Pinto, L. Gottardo, D. Yokaichiya, L. F. Fraceto, N. C. Meirelles, and E. de Paula, A new look at the hemolytic effect of local anesthetics, considering their real membrane/water partitioning at pH 7.4. *Biophys. Chem.* 110, 213 (**2004**).

24. S. Marrink, H. Risselada, S. Yefimov, D. Tieleman, and A. de Vries, The MARTINI force field: Coarse grained model for biomolecular simulations. *J. Phys. Chem. B* 111, 7812 (**2007**).

25. S. Marrink and A. Mark, The mechanism of vesicle fusion as revealed by molecular dynamics simulations. of small phospholipid vesicles. *JACS* 125, 15233 (**2003**).

26. S. Marrink and A. Mark, The mechanism of vesicle fusion as revealed by molecular dynamics simulations. *JACS* 125, 11144 (**2003**).

27. P. Kasson and V. Pande, Control of membrane fusion mechanism by lipid composition: Predictions from ensemble molecular dynamics. *PLoS Computational Biology* 3, 2228 (**2007**).

28. S. Yefimov, E. Van Der Giessen, P. Onck, and S. Marrink, Mechanosensitive membrane channels in action. *Biophys. J.* 94, 2994 (**2008**).

29. X. Periole, T. Huber, S.-J. Marrink, and T. Sakmar, G protein-coupled receptors self-assemble in dynamics simulations of model bilayers. *JACS* 129, 10126 (**2007**).

30. H. Risselada and S. Marrink, Curvature effects on lipid packing and dynamics in liposomes revealed by coarse grained molecular dynamics simulations. *Phys. Chem. Chem. Phys.* 11, 2056 (**2009**).

31. T. Ha-Duong, N. Basdevant, and D. Borgis, A polarizable water model for coarse-grained proteins simulations. *Chem. Phys. Lett.* 468, 79 (**2009**).

32. B. Hess, C. Kutzner, D. Van Der Spoel, and E. Lindahl, GROMACS 4: Algorithms for highly efficient, load-balanced, and scalable molecular simulation. *Journal of Chemical Theory and Computation* 4, 435 (**2008**).

33. C. Högberg and A. Lyubartsev, Effect of local anesthetic lidocaine on electrostatic properties of a lipid bilayer. *Biophysical. J.* 94, 525 (**2008**).

34. C. Ho, S. J. Slater, and C. D. Stubbs, Hydration and order in lipid bilayers. *Biochemistry* 34, 6188 (**1995**).

RESEARCH ARTICLE

Photodynamic Therapy Mediated by Liposomal Chloroaluminum-Phthalocyanine Induces Necrosis in Oral Cancer Cells

João Paulo Figueiró Longo[1], Larissa Naves Duarte de Melo[1], Maitê Cevallos Mijan[1],
Caroline Rodrigues Alves Valois[1], Graziella Anselmo Joanitti[1], Andreza Ribeiro Simioni[2],
Antonio Cláudio Tedesco[2], and Ricardo Bentes de Azevedo[1], *

[1] *Department of Genetics and Morphology, Institute of Biology, University of Brasília, Brasília, 70910-900, Brazil*
[2] *Department of Chemical and Philosophy, University of São Paulo-USP, Ribeirão Preto, 14040-901, Brazil*

Photodynamic Therapy is an alternative therapeutic modality applied on treatment of malignant neoplasms in different anatomical sites, such as oral cavity. It requires the action of three components simultaneously: (i) photosensitizers, (ii) light and (iii) molecular oxygen. The interaction between these components promotes tumor destruction by two main mechanisms: direct cell harm, such as apoptosis and/or necrosis, and indirect effects like vasculature shutdown and induction of immune response against tumor tissue. In this context, this study aimed to evaluate the effectiveness of Photodynamic Therapy mediated by liposomal chloroaluminum-phthalocyanine in different oral cancer cell lines (OSCC and HSG), and in OSCC-induced tumors in nude mice. The results showed that PDT induces a significant cellular death *in vitro*, and the *in vivo* results resulted in the induction tumor death mainly by necrosis, with the disruption of tumor blood vessels. We concluded that PDT mediated by liposomal chloroaluminum-phthalocyanine is an effective protocol to induce destruction of oral cancer cell cultures—OSCC and HSG and the death was predominantly necrosis in both *in vitro* and *in vivo* experiments.

Keywords: Photodynamic Therapy, Phthalocyanines, Liposomes, Necrosis.

1. INTRODUCTION

The incidence of oral cancer has continued to increase in recent years.[1] The most common treatments are: surgical intervention, radiotherapy, chemotherapy, or a combination of all three methods.[2] However, these treatments have a number of side effects which usually result in deformities of the maxillo-mandibular complex, with both esthetic and functional damage.[3, 4]

In order to minimize these effects, new therapies, such as Photodynamic Therapy (PDT), have been proposed as alternative oral cancer treatments.[4] PDT requires the simultaneous action of three components: (i) photosensitizer drugs, (ii) light, and (iii) molecular oxygen. The light source activates the photosensitizers which subsequently react with oxygen and other biomolecules by the transference of electrons or hydrogen. These reactions lead to the generation of reactive oxygen species (ROS), such as free radicals (especially singlet and triplet oxygen species), that promote cellular destruction.[5]

The first photosensitizers applied in clinical PDT protocols were haematoporphyrin derivatives. However, their purified fractions have shown disadvantages such as poor penetration and high skin phototoxicity.[4] Second-generation photosensitizers have been developed which, together with other characteristics, improve phototoxicity and photophysical properties.[6] Phthalocyanines are among the latest second-generation photosensitizers and present a variety of metal ions in their chemical structure, such as aluminum(III) and zinc(II), that enhance phthalocyanine phototoxicity. In addition, phthalocyanines are chemically pure compounds which absorb light at longer wavelengths (absorption peak around 670 nm), which permits an increase in light penetration in biological tissues.[6, 7]

The development of a drug delivery system (DDS) carrying photosensitizers may increase the advantages of PDT, since these carriers are more absorbed by tumor tissue.[7, 8] Of the available DDS, liposomes provide a simple and

---

*Author to whom correspondence should be addressed.

biocompatible option that has been proposed to carry and deliver photosensitizers for PDT. Liposomes are preferentially absorbed by tumor sites and surrounding vessels, and thereby lead to a preferential tumor accumulation.[8, 9]

In this study, the efficacy of PDT mediated by a liposomal chloroaluminum-phthalocyanine (AlClPc) formulation for oral cancer application was evaluated using both *in vitro* and *in vivo* experiments. First, the viability and cellular death pathway were evaluated in oral cancer cell lines–oral squamous cancer cells (OSCC) and human salivary gland cancer cells (HSG). PDT mediated by liposomal AlClPc was subsequently evaluated in a nude mice tumor model induced with OSCC cells. As discussed later in this paper, these findings support the effectiveness of PDT mediated by liposomal AlClPc in the treatment of oral cancer and thus provide a scientific base for the inclusion of this drug in future clinical trial.

2. MATERIALS AND METHODS

2.1. PDT

Chloroaluminum-phthalocyanine (AlClPc) was provided by Aldrich Chemical Company. The small unilamellar liposomes used as the DDS were prepared according to the protocol previously described in the literature.[10] All the experiments were performed up to 10 days after the liposomal synthesis. A continuous diode laser (BWF light source-Tech in) was used to excite AlClPc at 670 nm. The PDT parameters are explained in the results section.

2.2. *In Vitro* Studies

2.2.1. Cell Culture

Cell lines derived from human oral squamous carcinoma (OSCC) and human salivary gland (HSG) tumors were maintained in 75 cm² culture dishes with Dulbecco's modified Eagle's medium (DMEM) medium supplemented with 10% of fetal bovine serum, 100 U/mL penicillin, and streptomycin (100 μg/mL). Cells were incubated at: 80% humidity, 5% of CO_2 and 37 °C.

2.2.2. Liposomal Interaction with OSCC Cells

The protocol consisted of the replacement of culture media by liposomal solution containing 5 μM of AlClPc. The cells, 12-well plates with 50% confluent OSCC cells, were exposed for different periods (5, 15, and 30 minutes) in

the dark. At each time period, the liposomal solution was removed, and a solution of DMSO was added to the culture well to produce a cell lysate and solubilize the AlClPc molecules. The specific fluorescence of AlClPc (Excitation: 350 nm/Emission: 670 nm) was then detected in the cell lysates. The fraction of liposomal interaction was calculated by dividing the cell lysate fluorescence values by the initial liposomal samples fluorescence and this result multiplied by 100.

2.2.3. Treatment

When confluence was reached, cells were tripsinized, centrifuged and replicated to culture plaques of 96, 24 or 12 wells, in cell densities of 10^4, 10^5, 5×10^5 cells/ml, respectively, according to the different assays. Cells were submitted to treatments following a twenty-four hour incubation period. The treatment started with the replacement of culture medium by the liposomal solution containing 5 μM of AlClPc. After 30 minutes of liposome exposure (time defined previously), the liposomal solution was replaced by a PBS sterile solution. After that, laser irradiation was uniformly applied in each individual culture well, in a final energy density of 7 J/cm². Previous experiments with different laser irradiation fluences (3.5; 7; 14; 28 J/cm²) in the PDT protocol promoted a significant cell death (up to 80%) with 7 J/cm² and this cell death did not improve with the increase of energy doses (Fig. 1).

After this procedure, cells were incubated at the same conditions as cell maintenance for 2 or 24 h. All the *in vitro* experiments were conducted in triplicate and repeated three times.

2.2.4. Cell Viability Analysis

Membrane integrity was evaluated using the Trypan Blue assay, at 2 h and 24 h timepoints after treatment. The metabolic capacity of the cells was evaluated using the 3-(4,5-Dimethylthiazol-2-yl)-2,5-diphenyl tetrazolium bromide (MTT) assay.

2.2.5. DNA Fragmentation

Cells were tripsinized, centrifuged and resuspended in 100 μL of DMEM. Two hundred μL of lyses buffer with Propidium Iodide (0.1% sodium citrate, 0.1% TritonX-100 and 20 μg/mL of PI) was added. The homogenate was protected from light for 30 minutes and then analyzed in a flow cytometer (FACS-Calibur, Becton Dickinson). Propidium Iodide stain DNA molecules allowing detection of fragmented DNA by flow cytometry analysis.[11]

2.2.6. Morphological Analysis

A cover glass was placed on the bottom before plating the cells. Two and 24 h after treatment, cells were fixed

Table I. Experimental groups and treatment regimen.

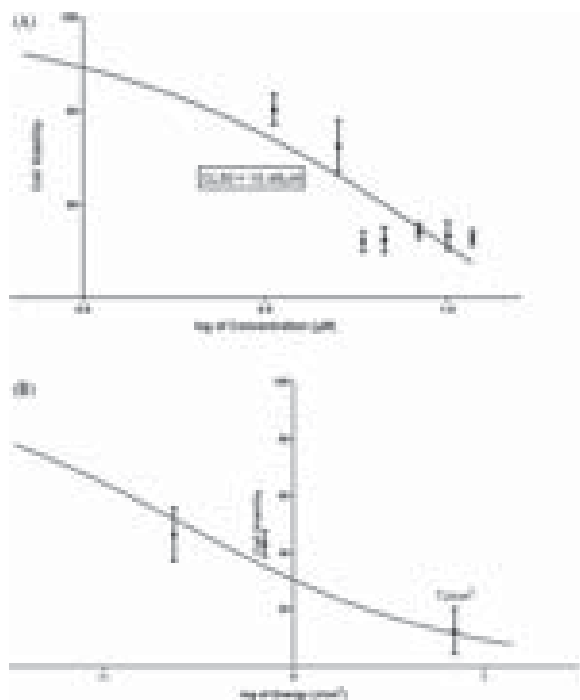| Group	Solution for 30 minutes incubation	Irradiation
Control (C)	PBS	None
Drug (D)	Liposomal AlClPc (5 μM)	None
Laser (L)	PBS	7 J/cm²
PDT (PDT)	Liposomal AlClPc (5 μM)	7 J/cm²

Fig. 1. Dark Toxicity of AlClPc liposomes (A) and laser energy dependence (B) influence in OSCC cell line viability. The 50% lethal concentration of the AlClPc-liposome was 10.48 μM.

with 2% paraformaldehyde, stained with crystal violet and dehydrated using alcohol and xylene baths. The cover glasses were added to slides and analyzed under an optical microscope (Axiophot Zeiss-Germany).

2.3. Animal Model

Nude Balb/c mice (CEMIB, Campinas, Brazil) were used in the experiments. In accordance with the Animal Research Ethics Committee of the University of Brasilia, the animals were maintained in plastic cages under controlled aseptic environment conditions with a 12 h light/dark cycle and free access to water and food. For the

animal model, OSCC cell suspensions (10^6 cells/100 μL PBS) were aseptically injected into the mouse subcutaneous dorsum. Three weeks after the injection of cells, the tumor reached 6–8 mm in diameter.

2.3.1. Experimental Groups

Tumor nude mice ($n = 8$) were randomly divided into two experimental groups: (1) PDT; (2) Tumor Control. PDT mice received an intraperitoneal injection of 500 μL of the 5 μM liposomal AlClPc solution 24 hours before laser irradiation with a fluence rate of 100 J/cm^2 and a total potency of 80 mW. The irradiation fields were standardized in 10 mm of circular diameter and the total time of irradiation was set as 16 minutes of irradiation.[12]

For laser irradiation, animals were anesthetized with xylazine (5 mg/kg)/ketamine (15 mg/kg) intraperitoneal injection. This protocol was repeated in interval of 7 days for three times (Fig. 2). Tumor control group mice received an intraperitoneal injection of 500 μL PBS and were anesthetized at the same time as PDT treated mice.

2.3.2. In Vivo PDT Evaluation

2.3.2.1. Clinical Analyses and Tumor Growth. Animals were monitored daily for weight, tumor volume and tumor aspect/coloration. The tumor volumes were estimated after calculating the tumor area by multiplication of the largest and the smallest diameter in millimeters.

2.3.2.2. Histopathological. After the treatment period (Fig. 2), OSCC subcutaneous tumors were completely excised and processed for histopathological analysis.

2.3.2.3. Density of Blood vessels in tumor tissues. A total of 5 histological sections, with 100 μm distance between sections, was analyzed per tumor sample. All histological sections were photographed and viable tumor area was quantified in Image ProPlus 5.1 software. Functional blood vessels were also quantified in an optical microscopy analyses, and proportional blood vessels/tumor area was obtained. The blood vessels were considered functional when the endothelial layer was intact and the
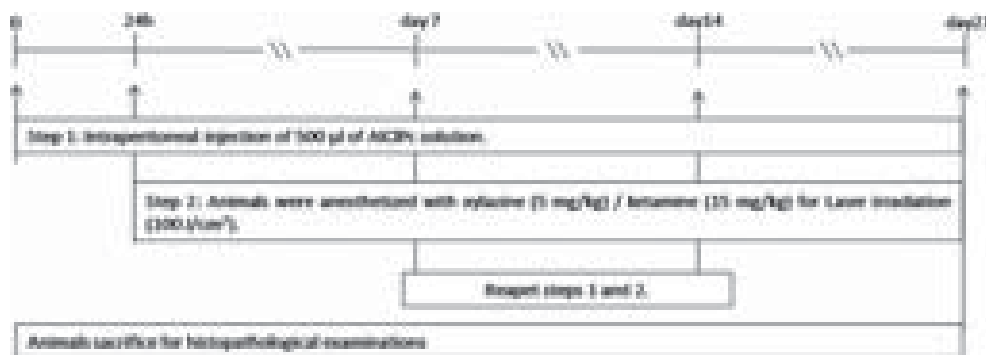

Fig. 2. Study design for photodynamic therapy in OSCC-induced subcutaneous tumors.

vascular bed was indentified without thrombus formation. A total of 4 tumors were analyzed in both the control and PDT-treated tumors.

2.4. Statistical Analysis

All of the *in vitro* experiments were performed in triplicate. Statistical analysis was performed using the R 2.4.1 ANOVA program parametric test and the Tukey test. The results were considered significant if $p < 0.05$.

3. RESULTS

The PDT protocols parameters (liposomal concentration and laser energy) applied in the subsequent experiments were based in a series of experiments conduced in the OSCC cell lines. Figure 1 presents the dark toxicity (Fig. 1(a)) and the laser energy dependence (Fig. 1(b)) of the PDT protocol. All subsequent experiments used the 5 μM liposomal concentration and 7 J/cm^2 laser energy for the PDT treatments. As described by Nunes et al. (2004),[10] liposomes with 5 μM of AlClPc may be the best concentration of this AlClPc-liposomal solution, because higher concentrations of AlClPc in liposomes induce the aggregation of these molecules and decreases the functionality of these systems for PDT purposes.

3.1. *In Vitro* Results

3.1.1. Cytoplasmic Membrane Integrity

As shown in Figure 3, all controls groups (*Control, Drug and Laser*) showed more than 89% of viability 3 hours and 24 hours after the experiments. In contrast, the level of cell viability of the PDT group was always lower than 18.64%. These results were similar for both OSCC and HSG cells.

3.1.2. AlClPc-Liposome Interaction with OSCC Cells

The AlClPc-liposome interaction with the OSCC cells was greater after 30 minutes of exposure (Fig. 4). This protocol was than used for the PDT experiments against the cancer cell lines.

3.1.3. Cell Metabolism

PDT induced cell death to approximately 94% for HSG and OSCC at both time points (Fig. 5). On the other hand, the C, D and L groups showed no significant changes with regards to the number of viable cells, which was approximately 97% (Fig. 5). This data was consistent with the Trypan blue assay results, showing that PDT treated cells promoted not only a reduction in cell proliferation, but also a decrease in cell metabolism thereby leading to massive destruction of tumor cells.
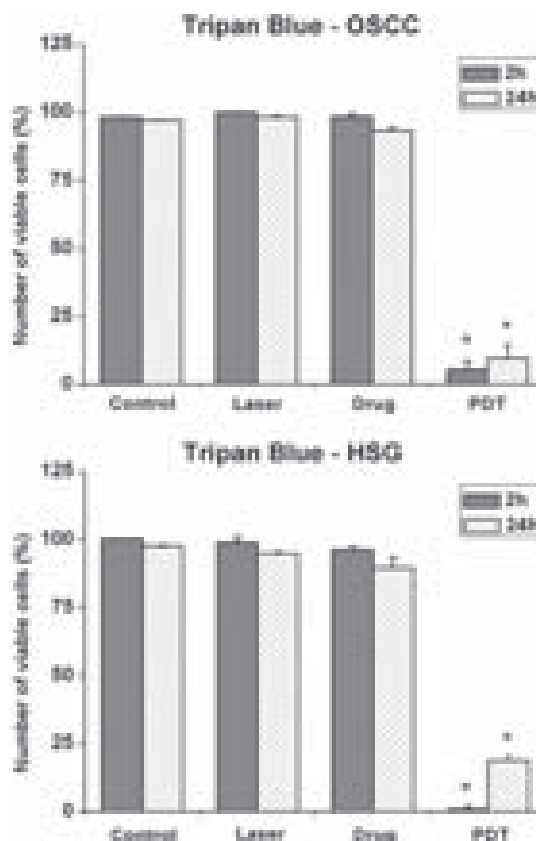

Fig. 3. Trypan blue assay of cell lines OSCC (A) and HSG (B). The graph shows cell viability 2 h and 24 h after the treatment. *Statistically significant differences compared to control groups at the same time.

3.1.4. DNA Fragmentation

The pattern provided by the *PDT* group 2 hours after the application of therapy was approximately 33% of the DNA fragmentation in both HSG and OSCC. Control groups
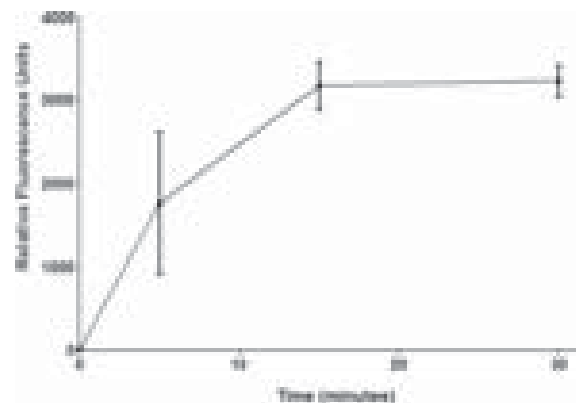

Fig. 4. AlClPc-liposome internalization by OSCC cell line. The fluorescent AlClPc detection was performed with the OSCC cell lysates after different time-point of liposome exposure. The results represent the average and standard deviation of a quadruplicate experiment.
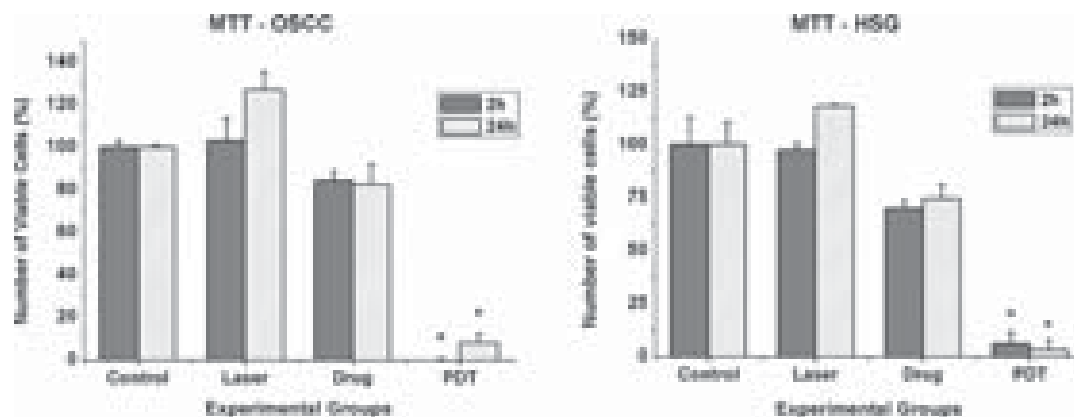
Fig. 5. MTT assay of cell lines OSCC (A) and HSG (B). The graph shows cell viability 2 h and 24 h after the treatment. *Statistically significant differences compared to control groups at the same time.

only had 10% of DNA fragmentation. 24 hours after treatment, the cell lines presented 58% and 96% of DNA fragmentation for OSCC and HSG, respectively. The *D* group showed higher fragmentation when compared to the *C* and *L* groups, but these results are not statistically significant (Fig. 6).

3.1.5. Morphological Analysis

Control group cells showed a star shape with clearly defined cytoplasm and a well-defined evident nucleolus. Photomicrography of the *PDT* group showed several morphological changes 2 hours and 24 hours after the therapy including: decreased cytoplasmic volume, cytoplasmic membrane disruption, loss of the star shape, loss of contact with neighbors, presence of vacuoles, and an increase in the nuclear-cytoplasmic ratio. In addition, following PDT, both cell lines presented picnotic nuclei, loss of nuclear membrane integrity and cytoplasmic membrane blebbing, which are morphological characteristics compatible with

cellular necrosis. After 24 hours of PDT treatment, the number of cells dramatically decreased in comparison to control groups (Fig. 7).

3.2. *In Vivo* Results

3.2.1. Clinical Analysis and Tumor Growth

Clinically, the treated tumor presented an inflammation pattern, characterized by edema and erythematosis (Fig. 8). No effects in overall health of mice were observed, as shown by the comparison between mice bodyweight of both control and PDT groups (mean of 2.3 ± 2.5 g). In additional, no skin phototoxicity was observed in all mice used in these experiments (Fig. 8).

In Figure 9 it is possible to compare control and PDT tumor volumes. The increase/decrease in volume was compared to the initial (100%) tumor volume on Day 1. Control and PDT treated tumors had similar volume patterns until the second week, with a significant decrease in
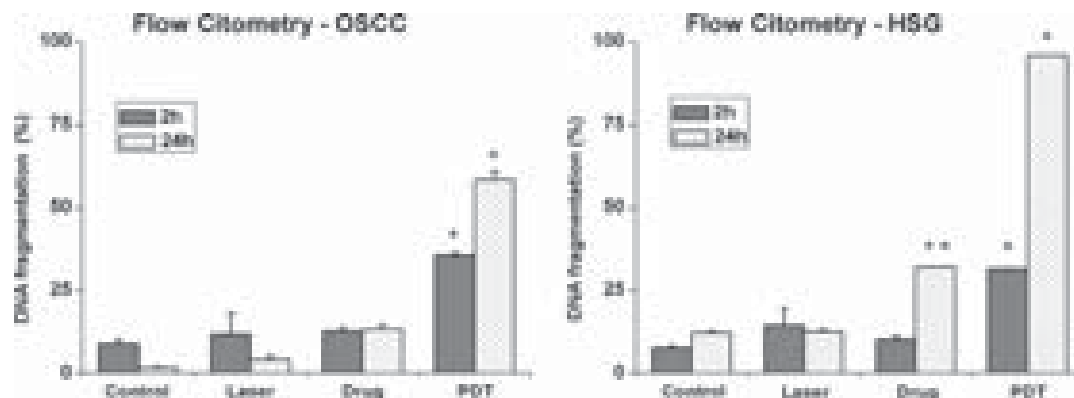

Fig. 6. Flow cytometry assay of cell lines OSCC (A) and HSG (B). The graph shows the percentage of DNA fragmentation 2 h and 24 h after the treatment. *Statistically significant differences compared to control groups at the same time. **Statistically significant ifferences compared to the same group at different time.
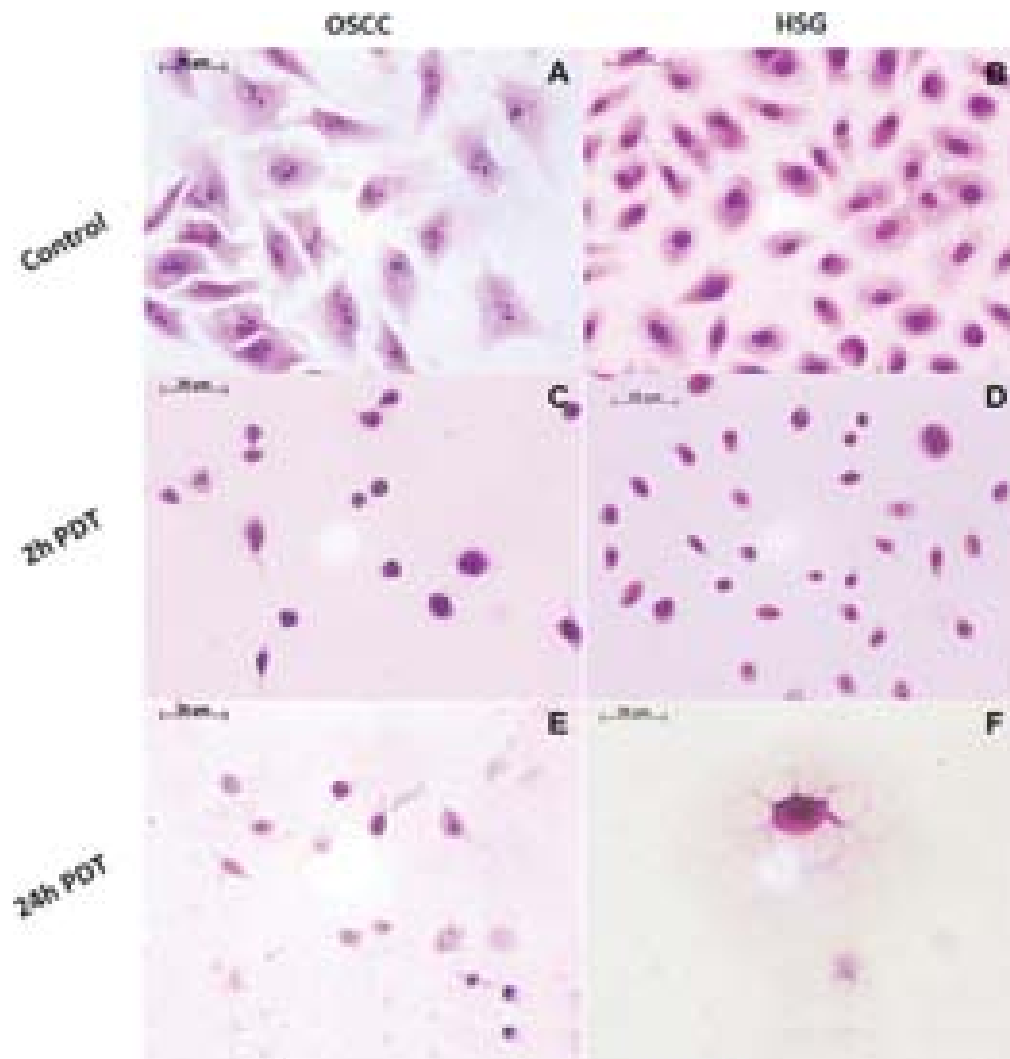
Fig. 7. Photomicrography of OSCC (column 1) and HSG (column 2) cells. Control OSCC (A) and HSG (B) cells. Two hours after PDT treatment: (C) (OSCC) and (D) (HSG) cells, with reduction in cellular volume, nucleus condensation and membrane blebbing—necrosis characterization. (E) (OSCC) and (F) (HSG) are at 24 h after PDT treatment, there is a reduction in cellular number and membrane vacuolization.

PDT tumor volume in the third week. The body weight of the animals did not change during the experimental period.

3.2.2. Histopathological Analysis

Histological examination showed *control* tumors with a necrotic core in tumor mass, characterized by the tissue eosinophilia, absence of nuclear structures and cytoplasmic limits among tumor cells. This is a pattern generally observed in solid tumors without a complex angiogenesis process, leading to death of central tumor cells by hypoxia and denutrition. Viable OSCC cells were only found in control tumors near vascular regions, especially near skin subcutaneous connective tissue (Fig. 8). Therefore, the comparative effectiveness evaluation of PDT treatment was performed in this layer.

The *PDT* tumors, in contrast to *control* tumors, showed tissue necrosis in the overall tumor mass, including areas next to the blood vessels. No necrotic signals were identified in skin overlying tumors. However, isolated viable OSCC-like cells were identified in necrotic mass on *PDT* treated tumors. It was also observed vasculature depletion with presence of thrombosis (Fig. 10).

Control tumors presented a blood vessel density of 7.7 blood vessels/mm^2. PDT-treated tumors did not present viable tumor tissues, so the blood vessel density was considered zero. Figures 10(a) and (b) shows the presence of functional blood vessels in viable tumor tissues from the control animals, as well as the necrotic tumor tissue, and
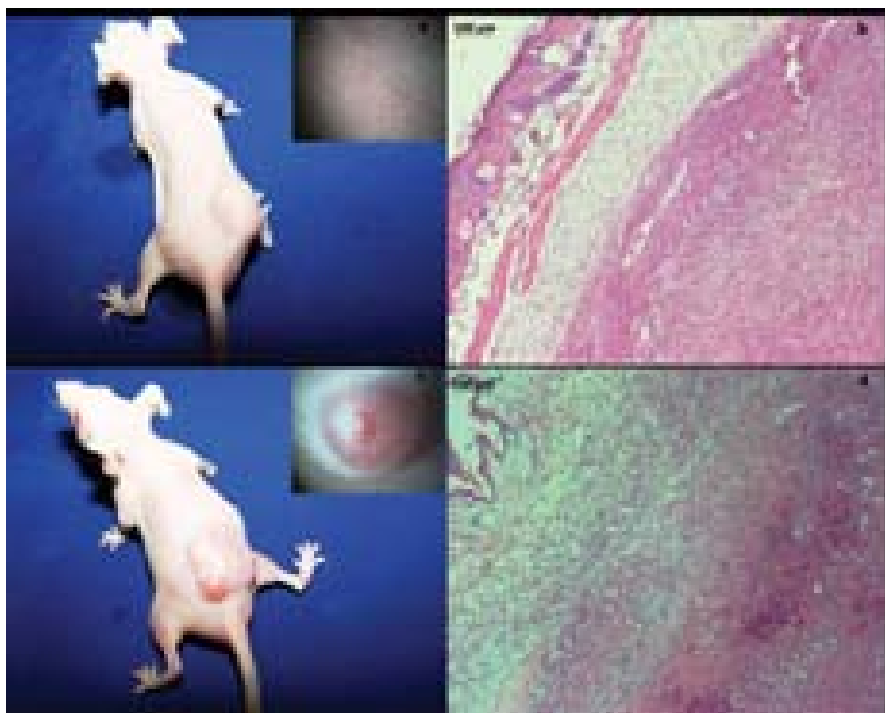
Fig. 8. Clinical aspect of control nude mice with detail normal aspect of skin overlying tumors (a), with histological viable OSCC tumor cells near skin subcutaneous conjunctive (b). PDT treated mice showed an increase in tumor vascular activity and inflammatory pattern in detail (c), histology showed tumor necrosis, identified by tissue eosinophilia, absence of nuclear structures and cytoplasmic limits among tumor cells, predominantly in tumor mass after PDT treatment (d).
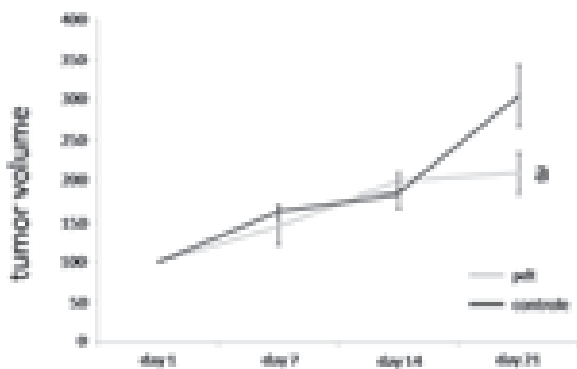

Fig. 9. Tumor growth during treatment. Tumor volume varied according to initial (100%) volume on day 1. a represents significant difference compared to control ($p < 0.05$).

the shutdown damaged blood vessels from the PDT-treated tumors (Figs. 10(c) and (d)).

4. DISCUSSION

Photodynamic Therapy is a clinically approved treatment of malignant and nonmalignant lesions.[13] In the present study, we showed the efficacy of PDT mediated by liposomal AlClPc *in vitro* by comparing two different oral cancer cell lines (OSCC and HSG), together with the response

of OSCC tumor induced, in a nude mice model, after PDT. Cell death after PDT was mainly induced by necrosis, which is consistent with the pattern obtained in other studies.[14]

Several studies showed that PDT effects are related with cell type dependence.[15] Our *in vitro* results showed a high citotoxicity induced by PDT mediated by liposomal AlClPc, with more than 90% of cell mortality for both tumor cell types, thereby showing that the effectiveness of PDT was not affected by the cell type evaluated. This observation led us to note that the final result of the treatment at least for these two oral cancer cell lines was mostly dependent on the photosensitizer and irradiation dosimetry.

Cytoplasmic membrane disruption, observed in Trypan Blue and morphological assays, together with the significant increase in DNA fragmentation in PDT-treated cells, suggests necrosis cell death pathway observed *in vitro*. This necrosis process could be the result of a high internalization of the liposomal photosensitizer in tumor cells, and also due to the high dose of energy applied. The 7 J/cm^2 dose was enough to promote cell damage at 2 h post-treatment. In agreement with the *in vitro* data, tissue necrosis was predominant in tumor area after PDT *in vivo*.

We used a systemic administration approach to treat OSCC tumors in the nude mice and to test the selectivity of the delivery of this liposomal preparation to the tumor
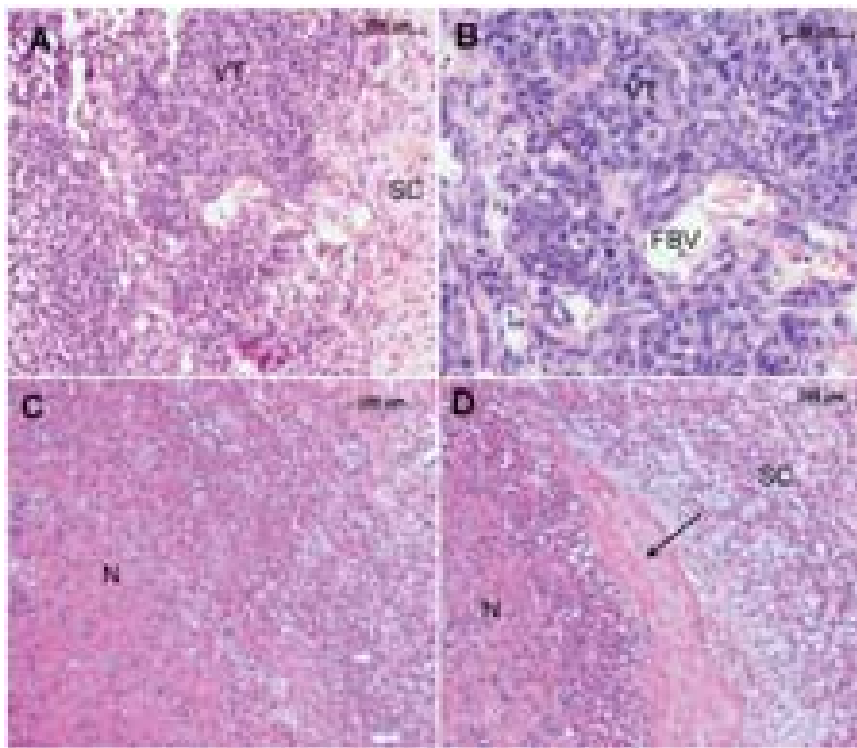
Fig. 10. The presence of blood vessels in OSCC control tumors in sections (A) and (B). In opposite, the PDT treated tumors presents the necrotic tumor tissue with shutdown damage blood vessels (arrow).

tissues. As observed in the clinical and the histopathological results, the overlying skin, including the subcutaneous tissues, of the treated animals were not affected. On the other hand, the OSCC tumor tissues were strongly affected, suggesting that the AlClPc-liposomes were preferentially delivered to the tumor sites instead of the normal tissues.

Photodynamic treatment induced necrosis produces a non-specific release of cellular and tissue immunogenic debris that leads to an intense immunological response against tumor tissues. According to Castano et al. (2006),[16] the release of different immunogenic debris from stressed malignant tissues may serve as links between photodynamic therapy and the subsequent immune response resulting in a complementary anticancer activity. Immunological activation in PDT-treated tumors may afford an advantage over conventional chemotherapy and radiotherapy that are both immunosuppressive and have a lot of side effects.[4, 17] In fact, the recruitment of inflammatory cells near to the treated tumor was observed in our *in vivo* model supporting this hypothesis.

In addition to direct tumor destruction, the necrosis detected in OSCC tumors after liposomal AlClPc photoactivation can also be related to vascular shutdown (Fig. 10). The vascular shutdown observed in our results may occur due to photosensitizer intravascular activation which promotes a series of tissue reactions as endothelial damage, vasoconstriction and platelet aggregation. These events contribute to thrombus formation and vascular damage leading to tumor infarction and neoplasm death.[18] The depletion of oxygen and nutrient supply in tumor areas are significant factors related to tumor necrosis.[19]

Selective accumulation of photosensitizers on tumors and rapid elimination from normal tissues are requirements for an ideal therapy. In the present study, PDT-treated tumors showed the preservation of overlying tumor skin, with OSCC tumor necrosis (Fig. 8). It indicates that liposomal AlClPc was preferentially delivered to tumor tissues. Preferential tumor drug accumulation could be explained by an increase in neoplastic vascular permeability to liposome vesicles. Whereas the majority of vessel tissues in the body have pores of approximately 6 nm in diameter, tumor vessels have vascular pores of approximately 300 nm, which allow liposome infiltration.[18, 19] Collectively, our results provide a positive perspective for the clinical use of liposomal AlClPc in the reduction of side effects when compared to other first generation photosensitizers that promote skin phototoxicity.[8, 18, 19]

5. CONCLUSION

In conclusion, Photodynamic Therapy mediated by liposomal chloroaluminumphthalocyanine has been shown to be a promising treatment for cancer of oral origin. This work

demonstrates its effectiveness both *in vitro* and *in vivo* using the HSG and OSCC cell lines, and a nude mice model, respectively. As for the death pathway, we can conclude that there is a predominance of necrosis, which does not exclude the possibility of a late process of apoptosis. These results provide a scientific basis for the use of this drug in other experiments, both *in vitro* and *in vivo,* such as in the future implementation of PDT mediated by liposomal AlClPc in clinical trials.

References and Notes

1. G. A. Colditz, T. A. Sellers, and E. Trapido, Epidemiology— identifying the causes and preventability of cancer? *Nature Reviews Cancer* 6, 75 (**2005**).

2. A. Sharwani, W. Jerjes, C. Hopper, M. P. Lewis, M. El-Maaytah, H. S. M. Khalil, A. J. MacRobert, and V. Salih, Photodynamic therapy down-regulates the invasion promoting factors in human oral cancer. *Archives of Oral Biology* 51, 1104 (**2006**).

3. L. Balducci and W. B. Ershler, Cancer and ageing: A nexus at several levels. *Nature Reviews Cancer* 5, 655 (**2005**).

4. O. Bettendorf, J. Piffko, and A. Bankfalvi, Prognostic and predictive factors in oral squamous cell cancer: Important tools for planning individual therapy? *Oral Oncology* 40, 110 (**2004**).

5. C. Hopper, C. Niziol, and M. Sidhu, The cost-effectiveness of Foscan mediated photodynamic therapy (Foscan-PDT) compared with extensive palliative surgery and palliative chemotherapy for patients with advanced head and neck cancer in the UK. *Oral Oncology* 40, 372 (**2004**).

6. M. Ochsner, Photophysical and photobiological processes in the photodynamic therapy of tumours. *Journal of Photochemistry and Photobiology B: Biology* 39, 1 (**1997**).

7. L. A. Muehlmann, G. A. Joanitti, J. R. Silva, J. P. F. Longo, and R. B. Azevedo, Liposomal photosensitizers: Potential platforms for anticancer photodynamic therapy. *Brazilian Journal of Medical and Biological Research* 44, 729 (**2011**).

8. R. D. Almeida, B. J. Manadas, A. P. Carvalho, and C. B. Duarte, Intracellular signaling mechanisms in photodynamic therapy. *Biochimica et Biophysica Acta (BBA).-Reviews on Cancer* 1704, 59 (**2004**).

9. R. R. Allison, G. H. Downie, R. Cuenca, X. H. Hu, C. J. H. Childs, and C. H. Sibata, Photosensitizers in clinical PDT. *Photodiagnosis and Photodynamic Therapy* 1, 27 (**2004**).

10. R. R. Allison, H. C. Mota, V. S. Bagnato, and C. H. Sibata, Bionanotechnology and photodynamic therapy—State of the art review. *Photodiagnosis and Photodynamic Therapy* 5, 19 (**2008**).

11. K. Ichikawa, T. Hikita, N. Maeda, S. Yonezawa, Y. Takeuchi, T. Asai, Y. Namba, and N. Oku, Antiangiogenic photodynamic therapy (PDT) by using long-circulating liposomes modified with peptide specific to angiogenic vessels. *Biochimica et Biophysica Acta (BBA)-Biomembranes* 1669, 69 (**2005**).

12. Y. Sadzuka, F. Iwasaki, I. Sugiyama, K. Horiuchi, T. Hirano, H. Ozawa, N. Kanayama, and N. Oku, Phototoxicity of coproporphyrin as a novel photodynamic therapy was enhanced by liposomalization. *Toxicology Letters* 182, 110 (**2008**).

13. S. M. T. Nunes, F. S. Sguilla, and A. C. Tedesco, Photophysical studies of zinc phthalocyanine and chloroaluminum phthalocyanine incorporated into liposomes in the presence of additives. *Brazilian Journal of Medical and Biological Research* 37, 273 (**2004**).

14. I. Nicoletti, G. Migliorati, M. C. Pagliacci, F. Grignani, and C. Riccardi, A rapid and simple method for measuring thymocyte apoptosis by propidium iodide staining and flow cytometry. *Journal of Immunological Methods* 139, 271 (**1991**).

15. J. P. F. Longo, S. P. Lozzi, A. R. Simioni, P. C. Morais, A. C. Tedesco, and R. B. Azevedo Photodynamic therapy with aluminum-chloro-phtalocyanine induces necrosis and vascular damage in mice tongue tumors. *Journal of Photochemistry and Photobiology B: Biology* 94, 143 (**2009**).

16. A. S. L. Derycke and P. A. M. de Witte, Liposomes for photodynamic therapy. *Advanced Drug Delivery Reviews* 56, 17 (**2004**).

17. M. A. Biel, Photodynamic therapy treatment of early oral and laryngeal cancers. *Photochemistry and Photobiology* 83, 1063 (**2007**).

18. I. Cecic and M. Korbelik, Mediators of peripheral blood neutrophilia induced by photodynamic therapy of solid tumors. *Cancer Letters* 183, 43 (**2002**).

19. H. Nakaseko, M. Kobayashi, Y. Akita, Y. Tamada, and Y. Matsumoto, Histological changes and involvement of apoptosis after photodynamic therapy for actinic keratoses. *British Journal of Dermatology* 148, 122 (**2003**).

20. D. Mitton and R. Ackroyd, History of photodynamic therapy in Great Britain. *Photodiagnosis and Photodynamic Therapy* 2, 239 (**2005**).

21. C. Fabris, G. Valduga, G. Miotto, L. Borsetto, G. Jori, S. Garbisa, and S. Reddi, Photosensitization with zinc(II) phthalocyanine as a switch in the decision between apoptosis and necrosis. *Cancer Research* 61, 7495 (**2001**).

22. E. C. C. Tapajós, J. P. Longo, A. R. Simioni, Z. G. M. Lacava, M. Santos, P. C. Morais, A. C. Tedesco, and R. B. Azevedo, *In vitro* photodynamic therapy on human oral keratinocytes using chloroaluminum-phthalocyanine. *Oral Oncology* 44, 1073 (**2008**).

23. S. L. Haywood-Small, D. I. Vernon, J. Griffiths, J. Schofield, and S. B. Brown, Phthalocyanine-mediated photodynamic therapy induces cell death and a G0/G1 cell cycle arrest in cervical cancer cells. *Biochemical and Biophysical Research Communications* 339, 569 (**2006**).

24. J. Mikeš, J. Kleban, V. Saková, V. Horváth, E. Jamborová, A. Vaculová, A. Kozubík, J. Hofmanová, and P. Fedoročko, Necrosis predominates in the cell death of human colon adenocarcinoma HT-29 cells treated under variable conditions of photodynamic therapy with hypericin. *Photochemical and Photobiological Sciences* 6, 758 (**2007**).

25. L. Wyld, M. W. R. Reed, and N. J. Brown, Differential cell death response to photodynamic therapy is dependent on dose and cell type. *British Journal of Cancer* 84, 1384 (**2001**).

26. W. H. Boehncke, A. Rück, J. Naumann, W. Sterry, and R. Kaufmann, Comparison of sensitivity towards photodynamic therapy of cutaneous resident and infiltrating cell types *in vitro*. *Lasers in Surgery and Medicine* 19, 451 (**1996**).

27. A. P. Castano, P. Mroz, and M. R. Hamblin, Photodynamic therapy and anti-tumour immunity. *Nature Reviews Cancer* 6, 535 (**2006**).

28. C. Hopper, A. Kübler, H. Lewis, I. B. Tan, and G. Putnam, *m*THPC-mediated photodynamic therapy for early oral squamous cell carcinoma. *International Journal of Cancer* 111, 138 (**2004**).

29. A. S. Sobolev, D. A. Jans, and A. A. Rosenkranz, Targeted intracellular delivery of photosensitizers. *Progress in Biophysics and Molecular Biology* 73, 51 (**2000**).

30. G. M. Tozer, C. Kanthou, and B. C. Baguley, Disrupting tumour blood vessels. *Nature Reviews Cancer* 5, 423 (**2005**).

RESEARCH ARTICLE

Nanomodification of Chitosan Microspheres with Dendron Molecules

Ana Agustina Aldana, Miriam C. Strumia, and Marisa Martinelli*

*Facultad de Ciencias Químicas, Departamento de Química Orgánica, IMBIV-CONICET,
Universidad Nacional de Córdoba, Haya de la Torre y Medina Allende,
(X5000HUA), Córdoba, Argentina*

The importance of dendritic structures in biology and medicine lies in their multivalency. Dendrons represent a structural component of the parent dendrimer; they have nano-dimensions and their immobilization on surfaces would lead to structural features within this dimensional range. Novel dendronized surface of chitosan microspheres was prepared by reaction between cross-linked biopolymer and Behera's or bis Behera's amine dendrons. According to FTIR analysis, it can be concluded that the dendronization took place; the shape and size were homogeneous and independent of the dendronization, according SEM images. Interactions between dendron-polymer network and hydrophilic/hydrophobic characteristics of the dendron modify the physical properties of the microspheres. The swelling studies of dendronized films at pH 1.2 and 7.4 evidenced the so-called "dendritic effect." In addition, the microspheres remained stable for an extended period. The highlights of the present research were to develop nanostructured dendronized surfaces on spheres of polymer supports that seem to be appropriate for biomedical applications. The work aimed at studying the effect of dendronization of the surface on the original properties of chitosan microspheres.

Keywords: Dendronized Polymer, Nanostructured Surface, Chitosan, Biomaterials.

RESEARCH ARTICLE

1. INTRODUCTION

Nanomaterials include different types of materials with dimensions under 100 nm or presenting structural features under this dimensional threshold. Moreover, nanomedicine is the application of nanotechnology in monitoring, diagnosing, preventing, repairing or curing diseases and damaged tissues in biological systems.

Several studies have generally led to the conclusion that the response of host organisms to the presence of nanomaterials is different and certainly superior when compared with conventional materials used so far.[1–2] For a bone graft to be successful, it seems that a biomaterial with superficial nano-features possessing a superior surface reactivity available for growth factors and other biospecies to be immobilized could represent notable advances.

Dendritic structures and their built-in nanoscopic and multifunctional features are receiving considerable scientific interest. Biomedically, dendritic polymers have been extensively studied for preparing drug/gene delivery systems, designing protein resistant surfaces, fabricating diagnostic agent and constructing biosensor devices. Generally,

the term dendritic polymer is used to denote the family of structurally branched molecules covering dendrons, dendronized polymers, perfect dendrimer and hyperbranched polymers.[3]

The main reason for the use of dendrimers/dendrons in biology and medicine is their multivalency, caused by the presence of a large number of surface end groups within the same molecule that can interact with biological receptors or with other chemical entities to a greater extent, generating hierarchical complexes with high binding affinities. These multivalent interactions are considerably stronger than the individual bonding of a corresponding number of monovalent ligands to a multivalent receptor; they are the most predominant phenomena in biological systems, particularly for recognition and attachment, signal transduction, and numerous cellular interactions.[4]

The multiple surface functional groups of dendritic molecules enable simultaneous incorporation of drugs and biological ligands for active targeting.[5] A number of targeting signals such as folic acid,[6] monoclonal antibodies,[7] saccharides[8] and peptides[9] have been successfully introduced into the periphery of dendrimers.

Dendritic scaffolds can easily mimic the so-called "ligand clustering" effect due to the vicinal presence of active

---

*Author to whom correspondence should be addressed.

157

functional groups within an adjustable distance. The immobilization of dendritic molecules on surfaces would lead to structural features within this dimensional range. Particularly, the combination of dendrons and polymers gives the dendronized polymers, macromolecules with dimensions on the nanometer scale and controlled hierarchical structure. They represent a merger of these two concepts and are a promising approach toward a novel generation of smart materials.[10]

In this context, the chemical approach of the present work aimed at developing nanostructured surfaces on natural polymer supports (microspheres of chitosan) that seem to be appropriate for biomedical applications such as, carrier and drug delivery. Thus, they were functionalized with dendritic molecules and the products were characterized showing their properties and potential applications as biomaterials.

Chitosan has shown interesting applications as biomaterial[11] due to its excellent biocompatibility, low toxicity, immunostimulatory activity, antibacterial and antifungal action, and anticoagulant properties. Furthermore, degradation products of chitosan have been shown to be non-toxic, non-immunogenic and non-carcinogenic. Hence, our goal is to obtain a new material by modification of chitosan using dendritic molecules of different generation or chemical structure.

The aim of this research is to find new properties in these products and maintain the well-known advantages of chitosan.

2. EXPERIMENTAL DETAILS

2.1. Materials

The following chemicals were purchased and used: epichlorohydrin, ECH (Riedel-de Häen); sodium carbonate (Cicarelli); Behera's amine (Frontier Scientific); thionyl chloride (Merck); 5-nitroisophtalic acid 99% (Anedra); palladium, 10 wt% on activated carbon, Pd/C (Aldrich); silica gel 60 (Merck); potassium bromide 99% FT-IR grade (Aldrich); chloroform-d 99.8% D (Aldrich); Chitosan, Ch (85% DA, LMW, Aldrich). Solvents were obtained from Sintorgan, purified by distillation, and dried.

2.2. Instrumental and Techniques

Fourier Transform Infrared (FT-IR) spectra were obtained on a Nicolet Avatar 360 FT-IR spectrometer on KBr discs. A Thermo Scientific Smart Diffuse Reflectance accessory was used to obtain Diffuse Reflectance Infrared (DRI) spectra. SiC discs were used to abrade the surface of different samples. All spectra were obtained with 32 scans at a 4.0 cm^{-1} resolution in a range between 4000 and 650 cm^{-1}.

Nuclear Magnetic Resonance (NMR) spectra were obtained in $CDCl_3$ using a Bruker 400 MHz NMR spectrometer. Scanning electron micrographs (SEM) of the

microspheres were obtained by means of a [Philips SEM 501B] at 12 kV at the Instituto Nacional de Tecnología Industrial (INTI), Córdoba, Argentina. SEM micrographics were obtained in order to analyze the microsphere morphology. Before scanning, the dried samples were gold-coated.

2.3. Methods

2.3.1. Preparation of Chitosan Microspheres

Chitosan microspheres were prepared by dissolution of polymer (1.000 g) in a 5% (V/V) acetic acid solution (35 mL). Chitosan solution was then added dropwise by a dropper into a precipitation bath containing 0.5 M NaOH solution (500 mL). This step neutralized the acetic acid within the chitosan gel, thus coagulating the gel to spherical uniform chitosan gel beads. A magnetic stirrer was used to stir the aqueous NaOH solution continuously at 200 rpm to prevent chitosan beads from sticking to one another or to the glassware surface. The wet chitosan beads were filtered and extensively rinsed with distilled water to remove NaOH. They were then air-dried to eliminate water. After that, the microspheres were modified with ECH according to the following procedure.

Ch-ECH microspheres: 0.500 g of chitosan microspheres were added to 0.1 M of ECH solution (30 mL) to obtain a 1:1 ratio with chitosan (mol ECH: mol CH_2OH). The mixture was heated to 45 °C for 2 h and stirred continuously using a magnetic stirrer at 200 rpm. Afterwards the beads were filtered, washed with distilled water to remove excess ECH, and air-dried. The oxirane groups were determined by the pyridinium chloride method.[12]

2.3.2. Synthesis of Bis Behera's Amine Dendron (BB)

5-Nitroisophthalic acid (diacid) was converted into diacid chloride with thionyl chloride. $SOCl_2$ (10 mL) was added to the diacid (0.4000 g, 16 mmol) in anhydrous THF (10 mL) under nitrogen atmosphere and allowed to react for 4 h under reflux. The diacid chloride (470 mg, 2.00 mmol) and triethylamine, TEA (0.5 mL), were dissolved in anhydrous THF (50 mL) and reacted with Behera's amine (1.6600 g, 4.00 mmol) for 24 h under stirring at room temperature. A white solid was obtained and purified by column chromatography (yield 80%).

Finally, dendritic molecule (0.8000 g, 0.80 mmol) dissolved in methanol (20 mL) was reduced at 40 psi H_2 room temperature with 100 mg of Pd/C 10%. Dendron BB was obtained with a 95% of yield (0.7418 g).[13]

Bis Behera's amine dendron (BB): FT-IR (cm^{-1}): the signals at 1667 and 1535 were assigned to band (C=O stretching vibrations) and band II (N–H bending vibrations) corresponding to the amide group, respectively. The carbonyl absorption band of ester appeared at 1736. ^{13}C NMR $(CDCl_3)$ (δ, ppm): 173.1 (C=O ester); 163.3 (C=O amide); 148.3 (CNO_2); 136.9 ($C_{3 \text{ and } 5}$ aromatic);

158

*J. Biomater. Tissue Eng. 3, 157–163, **2013***

116.0 (C_4 aromatic); 118.0 ($C_{2\ and\ 6}$ aromatic); 80.9 (OCCH$_3$); 58.4 (CONHC); 30.3 (CH$_2$CH$_2$CO); 29.9 (CH$_2$CH$_2$CO) and 27.9 (OCCH$_3$). ^{1}H NMR (CDCl$_3$) (δ, ppm): 7.25 (*s*, 2H, CH aromatic); 7.38 (*s*, 1H, CH aromatic); 2.25 (*m*, 12H, CCH$_2$CH$_2$CO); 2.08 (*m*, 12H, CCH$_2$CH$_2$CO) and 1.36 (*s*, 54H, OC(CH$_3$)$_3$).

2.3.3. Dendronization of Ch-ECH Microspheres

Ch-ECH microspheres were swollen in water (100 mg mL^{-1}) for 24 h. After that, Behera's amine (AB) and bis Behera's amine (BB) (4.50 mg and 10.7 mg, respectively), dissolved in 0.2 M Na$_2$CO$_3$ (0.08 mL), were added to the microspheres and stirred at 60 °C for 36 h.[14] The mol ratio used was 1:0.6 corresponding to the epoxy:dendron. Ch-ECH-AB and Ch-ECH-BB products were filtered and washed with water, 0.1 N acetic acid solution and water again. The products were dried. The amount of bonded dendrons was obtained through oxirane group determination by the pyridinium chloride method.[12]

2.3.4. Hydrolysis of t-Butyl Groups of Dendritic (AB and BB) Periphery

Hydrolysis of ester groups on the dendritic surface was carried out in 85% v/v formic acid at 60 °C during four days. After that, microspheres were washed and dried. The microspheres obtained were called Ch-ECH-ABh and Ch-ECH-BBh The degree of hydrolysis was determined by acid-base title.

2.3.5. Thermal Analysis

Differential scanning calorimetry (DSC) measurements were taken using a V5.4 A TA Instrument on samples with mass of about 2 mg, at a heating rate of 10 °C·min^{-1}, and testing temperature ranging from 50 to 400 °C. Thermogravimetric Analysis (TGA) measurements were conducted using a 2950 TGA HR V5.4 A TA Instrument, on samples with masses of about 5 mg at heating rates of 10 °C min^{-1}; the samples were tested in nitrogen from 40 to 400 °C.

2.3.6. Swelling Studies

The water sorption capacity of the chitosan microspheres was determined by swelling in buffer of pH 7.4 and 1.2 at room temperature. A known weight (200 mg) of each product was placed in the medium for 7 h, which is the appropriate dosage time. The swollen microspheres were collected at different times, superficially dried with tissue paper, and weighed immediately on an analytical balance. The percentage swelling (E_{sw}) in the medium was calculated using Eq. (1):

$$E_{sw}(\%) = \frac{W_e - W_o}{W_o} \cdot 100 \qquad (1)$$

where W_e denotes the weight of the chitosan microspheres at equilibrium swelling, and W_o is the initial weight of the chitosan microspheres. Each swelling experiment was repeated twice, and the average value was taken as the E_{sw} value.

3. RESULTS AND DISCUSSION

3.1. Synthesis

First, amine groups of microspheres of chitosan were activated through reaction with epyclorhydrine (ECH). This molecule is a spacer arm and a cross-linking agent to
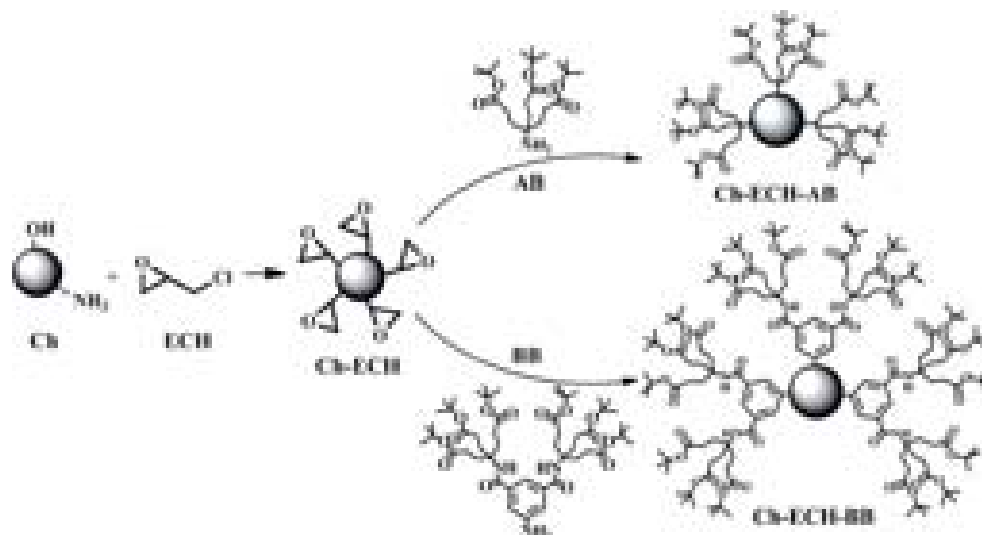

Fig. 1. Pathway used to reach the dendronized chitosan microspheres. (a) Activation of chitosan (Ch) with epyclorhydrine (ECH) to yield Ch-ECH; (b) coupling of Behera's amine (AB) and bis Behera's amine (BB) dendrons on Ch-ECH to yield Ch-ECH-AB and Ch-ECH-BB microspheres, respectively.

Table I. Coupling of Behera's amine (AB) and bis Behera's amine (BB) dendrons on Ch-ECH matrix and percentage of hydrolysis of functional periphery groups (ester to acid).

Matrix	Epoxy groups[a] mol/g matrix	Dendron mol/g matrix	% Hydrolysis of ester groups
Ch-ECH	1.80×10^{-4}	–	–
Ch-ECH-AB	7.20×10^{-5}	1.08×10^{-4}	–
Ch-ECH-ABh	7.20×10^{-5}	1.08×10^{-4}	45.7
Ch-ECH-BB	1.53×10^{-4}	2.70×10^{-5}	–
Ch-ECH-BBh	1.53×10^{-4}	2.70×10^{-5}	97.4

Note: [a]Epoxy groups on matrix that are free after dendronization.

facilitate the subsequent covalent bond of the dendrons and to improve the stability of the chitosan microspheres. Figure 1 shows a synthetic scheme.

For the dendronization of the surface of microspheres, the Behera's amine (AB) and bis Behera's amine (BB) dendrons were used, to yield Ch-ECH-AB and Ch-ECH-BB, respectively. The AB and BB dendrons were selected for their well-known property as nucleophiles for the opening of the epoxide groups and biocompatible properties.[15] Table I shows the percentage incorporation of the dendrons.

According to the results, the amount of AB dendron incorporated into the structures was higher than that of BB dendron, probably due to steric hindrance.

The ester groups on the periphery of the dendron were hydrolyzed to acid groups. This approach was carried out to have a surface with different hydrophilic/hydrophobic characteristics and affinity to different drug. Greater percentage of hydrolysis was obtained for the reaction of Ch-BB to yield Ch-BBh. These results show that by changing the dendron size and the degree of dendronization, the functional groups of the periphery are more accessible and reactive.

3.2. Characterization

3.2.1. Diffuse Reflectance Infrared (DRI)

Firstly, characterization of the unmodified and dendronized spheres was carried out by Diffuse Reflectance-IR. Infrared spectrum of Ch-ECH revealed a new signal at 3027 cm^{-1} corresponding to C–H stretching vibration of the epoxy group; the stretching vibration of C–O–C appears at 1033, 1249 and 827 cm^{-1}. The typical absorptions of chitosan were also present.

Dendronized products showed a typical band at 1729 cm^{-1} corresponding to C=O stretching of the ester dendron, confirming the presence of AB and BB. Other changes in the spectra were not observed for the dendronized sample due to the high intensity of the absorption bands of chitosan.

3.2.2. Scanning Electron Micrographs

It is interesting to note the shape and size of the particle on various biological aspects involved in drug delivery for the development of carriers for specific biomedical applications.[5] Thus, the dendronized chitosan microspheres were characterized by SEM. The mean diameter was in the range of 0.8–1.2 mm. The spheres were homogeneous with no variation in size after dendronization (Fig. 2).

3.2.3. Thermal Analysis

Figure 3 shows the TGA and DSC thermograms for the Ch, Ch-ECH and Ch–ECH–AB samples. The thermogravimetric profiles in Figure 3(a) reveal two stages of mass loss. The first degradation stage at around 100–150 °C, with a mass loss of 2–10%, elates mainly to the loss of
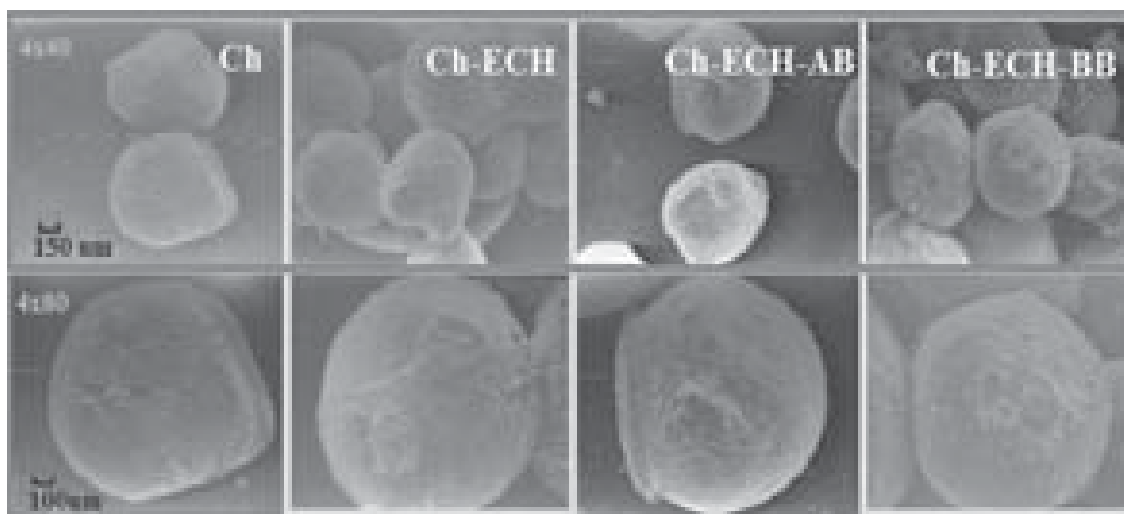
Fig. 2. Scanning electron micrograph (SEM) images of Ch-ECH and Ch-ECH-AB microspheres.

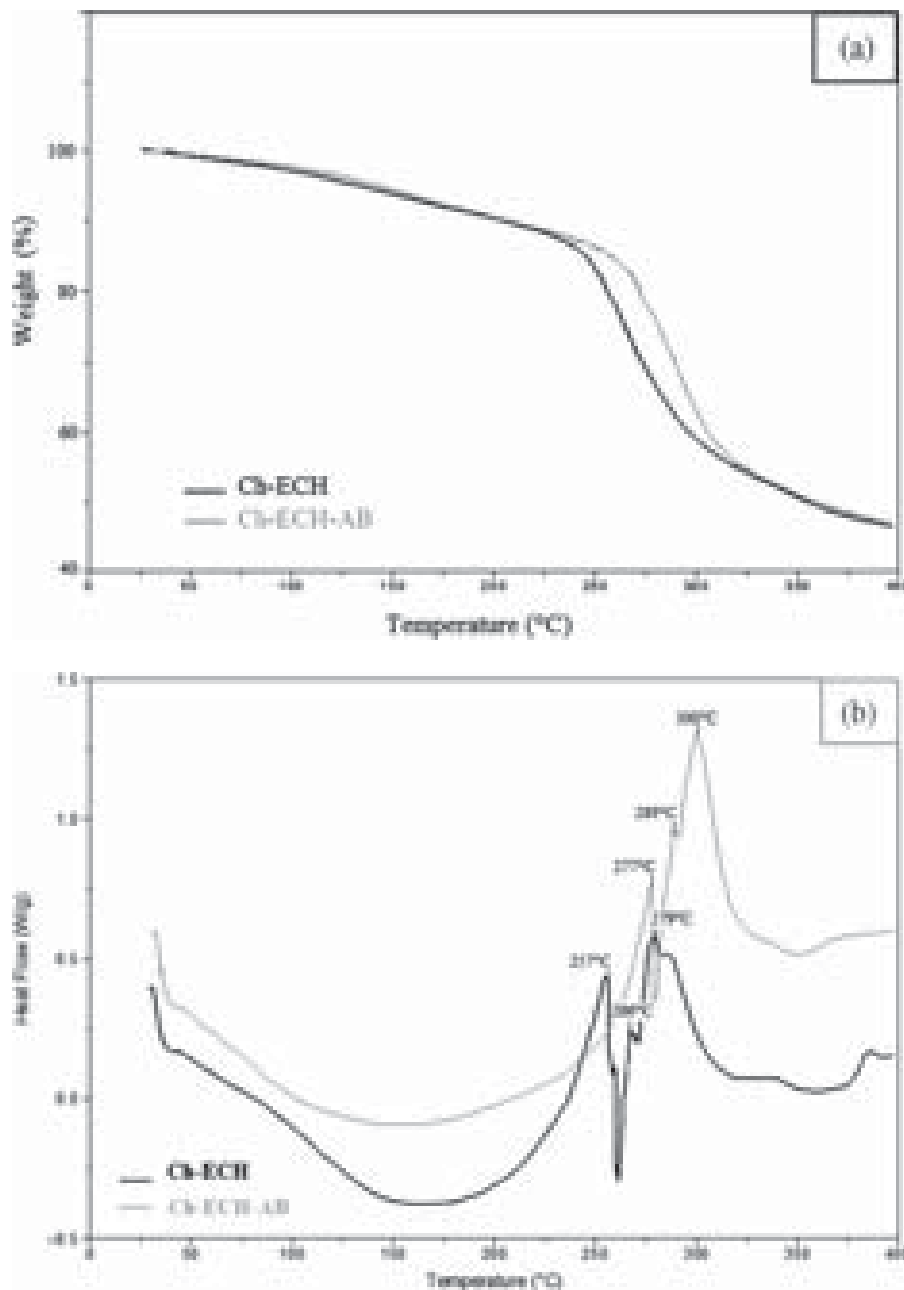**160**

*J. Biomater. Tissue Eng. 3, 157–163, **2013***

Fig. 3. Thermal analysis of Ch-ECH and Ch-ECH-AB: (a) Differential scanning calorimetry (DSC); (b) and Thermo-gravimetric Analysis (TGA).

water physically adsorbed on the surface of the materials. The Ch undergoes a mass loss of 50% at 298 °C. The second degradation stage of Ch-ECH and Ch-ECH-AB was observed at 264 °C and 296 °C, respectively, with a mass loss around 40%. These values represent the temperatures of maximum mass losses of the polymeric materials and were established from the first derivative thermogravimetric plots. The temperature of the second degradation stage of Ch-ECH-AB is higher than that of the Ch-ECH,

indicating that the new matrix is thermally more stable than the undendronized microspheres.

The DSC thermogram (Fig. 3(b)) for Ch-ECH shows three exothermic peaks at 256.6, 266.7 and 279.0 °C. In the DSC thermogram for Ch-ECH-AB, three exothermic peaks can be observed, at 277.4, 288.9 and 300.6 °C. These exothermic peaks can be attributed to the thermal degradation of the materials. A significant difference in the position of the exothermic peaks of Ch-ECH and Ch-ECH-AB

was observed, which indicates surface modification of the microspheres.[16]

The characterization results confirmed that the formation of the new material (Ch-ECH-AB) occurred successfully.

3.2.4. Swelling Studies

Szoka et al. have proposed that the entry and passage of polymeric drug carriers with approximately the same hydrodynamic volumes through pores are greatly influenced by particle shape and degree of flexibility conferred by various molecular architectures.[5] Thus, it is important to study the swelling behavior of the microspheres at different pH values (Fig. 4).

Generally, the swelling values of the dendronized products at pH 1.2 were the highest. When pH is lower than pKa of amine groups of chitosan (pKa $\approx$ 6.5), it was positively charged and the swelling was high owing to the repulsion between their chains.[17] At pH 1.2 dendronized products Ch-ECH-BB showed higher swelling than Ch-ECH-AB. Thus, an increase in the size of the dendron led to a marked increase in swelling owing to a disruption of the interactions between the chains. Moreover, the percentage dendronization is the lowest and the presence of protonated amine gropus greatly contributes to the repulsion between the chains. The higher hydrophilic character was evidenced in the swelling value of Ch-ECH-ABh with respect to Ch-ECH-AB. By contrast, for Ch-ECH-BBh the acid groups on the periphery are close enough to form hydrogen bonds themselves and these interactions hinder the entry of water into the network. Ch-ECH-BB presented a higher value than Ch-ECH-BBh.

At the highest pH examined (7.4), Ch-ECH-AB and Ch-ECH-BB showed no important difference in relation to non-dendronized microspheres.

For Ch-ECH-ABh and Ch-ECH-BBh microspheres, the swelling values increase at pH 7.4 with respect to non-hydrolyzed microspheres. It is probably due to acid groups on the periphery which are ionized at high pH and produce repulsive interactions. The difference in swelling values for the hydrolyzed microspheres compared with those non-hydrolyzed was higher between Ch-ECH-BBh and Ch-ECH-BB. This result agrees with the higher percentage of hydrolysis of Ch-ECH-BBh than with that of

Ch-ECH-ABh (Table I). Moreover, the swelling value of Ch-ECH-BBh decreased with respect to non-hydrolyzed *tert*-buthyl groups at pH 1.2 since it presents most of the amount of acid groups on periphery of dendron. Probably, the acid-acid group interaction is higher than the acid group-water interaction.

The swelling index depended on the pH due to the different balance between positive (NH_3^+) and negative (COO^-) charges. The degree of dendronizacion, size dendron and amount and type of functional group on the periphery of the dendron are the factors that control of the behavior of the matrices. These results showed the so-called "dendritic effect."

4. CONCLUSION

The well known advantages of chitosan and the multifunctionality of the dendronizacion in the chitosan microspheres obtained. The surface with multivalent properties allows a material to be potentially applicable to different therapies to be used as macrocarriers for the controlled drug release. The most relevant result involves having shown the so-called "dendritic effect." A hydrophilic/hydrophobic balance was found through the dendronizacion surface; the properties of the dendronized chitosan changes with the size of the dendron, the number and type of functional group in the periphery.

The highlight of this research is represented by innovative biomaterials whose biomimetism is ensured through a special surface chemistry and through a specific topography.

On the synthetic level, the different approaches for preparing nanostructures or nanomodifications with precise shape control have their own associated advantages and challenges. A sound understanding of the morphological dynamics will be especially useful in predicting and ensuring consistency in the drug delivery performance of materials consisting of biodegradable and/or stimuli-responsive functionalities *in vivo*.

In a future, we will carry out different studies about the potential applications of the microspheres obtained: as support for immobilized metal ion chromatography affinity (IMAC), and for purification of protein, or as drug delivery system by the incorporation of targeting signals such folic acid or to coordinate hydrophobic drugs.

Fig. 4. Swelling behavior of Ch-ECH, Ch-ECH-AB, Ch-ECH-ABh, Ch-ECH-BB and Ch-ECH-BBh microspheres at pH 1.2 (■) and 7.4 (▨).

References and Notes

1. L. Zhang and T. J. Webster, *Nanotoday* 4, 66 (**2009**).
2. I. C. Stancu, *React. Funct. Polymers* 70, 314 (**2010**).
3. M. A. Quadir and R. Haag, *J. Controlled Release* 161, 484 (**2012**).
4. T. L. Reiko, G. Hans-J, and C. L. Yuan, *Carbohydrate Res.* 254, 269 (**1994**).
5. S. Venkataraman, J. L. Hedrick, Z. Y. Ong, C. Yang, P. L. Rachel, P. T. Hammond, and Y. Y. Yang, *Adv. Drug. Delivery Rev.* 63, 1228 (**2011**).
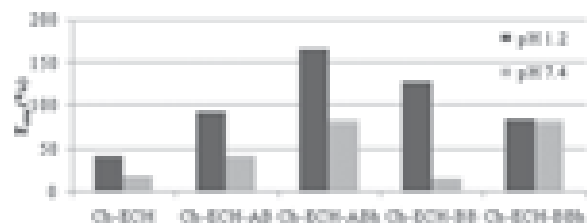
6. U. Gupta, S. K. D. Dwivedi, H. K. Bid, R. Konwar, and N. K. Jain, *Int. J. Pharm.* 393, 185 (**2010**).

7. A. K. Patri, A. Myc, J. Beals, T. P. Thomas, N. H. Bander, and J. R. Baker, *Bioconjug. Chem.* 15, 1174 (**2004**).

8. J. Huang, F. Gao, X. X. Tang, J. H. Yu, D. X. Wang, S. Y. Liu, and Y. P. Li, *Polym. Int.* 59, 1390 (**2010**).

9. J. M. Oliveira, A. J. Salgado, N. Sousa, J. F. Mano, and R. L. Reis, *Prog. Polym. Sci.* 35, 1163 (**2010**).

10. E. Östmark, J. Lindqvist, D. L. Nyström, and E. Malmström, *Biomacromolecules* 8, 3815 (**2007**).

11. H Sashiwa and S. Aiba, *Prog. Polym. Sci.* 29, 887 (**2004**).

12. H. Lee and K. Neville, Handbook of Epoxy Resins, Mc-Graw-Hill Inc., New York (**1967**), p. 17.

13. M. Martinelli, M. Calderón, C. Alvarez, I., and M. C. Strumia, *React. Funct. Polym.* 67, 1018 (**2007**).

14. A. A. Aldana, M. Martinelli, and M. Strumia, *Macromolecular Symposia* 298, 99 (**2010**).

15. A. A. Williams, E. W. Sugandhi1, R. V. Macri1, J. O. Falkinham, and R. D. Gandour, *J. Antimicrobial Chemotherapy* 59, 451 (**2006**).

16. R. Laus, *J. Hazard. Mater.* 183, 233 (**2010**).

17. C. K. S. Pillai, W. Paul, and C. P. Sharma, *Prog. Polym. Sci.* 34, 641 (**2009**).

RESEARCH ARTICLE

Novel Self-Assembled Nanoparticles of Testosterone-Modified Glycol Chitosan and Fructose Chitosan for Controlled Release

Javier Pérez Quiñones[1, *], Kurt V. Gothelf[2], Jørgen Kjems[2], Angeles Heras[3], Claudia Schmidt[4], and Carlos Peniche[5]

[1] Faculty of Chemistry, Center of Natural Products, University of Havana, Havana, Cuba; Zapata s/n entre G y Carlitos Aguirre, Plaza de la Revolución, 10400 La Habana, Cuba
[2] Interdisciplinary Nanoscience Center iNANO, Aarhus University, Aarhus, Denmark; C.F. Møllers Allé 3, 8000 Aarhus C., Denmark
[3] Instituto de Estudios Biofuncionales/Dpto Química Física II, Facultad de Farmacia, Universidad Complutense de Madrid, Madrid, Spain; Facultad de Farmacia, Ciudad Universitaria 28040 MADRID, Spain
[4] Department of Chemistry, University of Paderborn, Paderborn, Germany; Warburger Str. 100, D-33098 Paderborn, Germany
[5] Center of Biomaterials, University of Havana, Havana, Cuba; Ave. Universidad s/n entre G y Ronda, Vedado, 10400 La Habana, Cuba

Glycol chitosan (GC) and fructose chitosan (FC) were linked to testosterone hemisuccinate through water-soluble carbodiimide activation. The resulting conjugates formed self-assembled nanoparticles in aqueous solution with particle sizes of 245–332 nm as measured by dynamic light scattering and testosterone content of 3% and 8% (w/w) for GC and FC conjugates, respectively. The particles appeared as 45–90 nm almost spherical nanoparticles when studied by scanning and transmission electron microscopy upon drying. Particles were also characterized by differential scanning calorimetry and wide-angle X-ray diffraction. Drug linking to both types of chitosan derivatives was confirmed by FTIR spectroscopy and proton NMR. *In vitro* testosterone release studies performed in water at acid pH indicated that the drug release was dependent on the acidity of the solution, testosterone content and the chitosan matrix. Almost constant release rates were observed initially. These results indicate that the obtained nanoparticles could be good candidates for testosterone delivery to humans and animals.

Keywords: Controlled Release, Chitosan, Self-Aggregated Nanoparticles, Testosterone.

RESEARCH ARTICLE

1. INTRODUCTION

Testosterone is an important sexual steroid hormone from the androgen group, widely found in animal kingdom (mammals, birds and other vertebrates).[1,2] This anabolic steroid is the main male sex hormone with a key role in the development of male reproductive organs and the expression of secondary sexual characters in men (increase of muscle and bone mass, of body hair growth). The benefices for human health (i.e., prevention of osteoporosis and Alzheimer's dementia, regulation of platelet aggregation in humans, treatments of post-menopausal women and control of type 2 diabetes) are well documented.[3–5] The androgenic and anabolic effects of testosterone at different stages of human life are thoroughly studied.[6] Several testosterone derivatives have been used in anti-aging and replacement therapy for hypogonadism treatment.[7] However, the direct use of testosterone, its derivatives and other anabolic steroids comes with a high rate of side effects and health problems such as breast or gynecological cancers, sleep apnea, acceleration of prostate cancer growth and male infertility.[8–10] Hence, the controlled release of low testosterone doses in blood is receiving interest for its potential applications in medicine and pharmacy. In this context, preparation of self-assembled polymeric nanoparticles, based in natural biopolymers (i.e., chitosan and derivatives, cellulose, sodium alginate), as drug delivery systems is particularly promising.[11–13]

Chitosan (CS) is a natural polymer, consisting of β $(1 \rightarrow 4)$ linked glucosamine units, with some proportion of *N*-acetylglucosamine units. It is obtained by extensive deacetylation of chitin.[14,15] CS is a biomaterial with excellent properties and beneficial effects for animals and humans;[16–18] but its applicability in medicine and pharma-

---

*Author to whom correspondence should be addressed.

ceutical field is limited due to water solubility restricted to acid pH and the short time stability of self-aggregated CS conjugates in solution.[19, 20] Some chitosan derivatives overcome these limitations, still showing good biocompatibility (i.e., glycol chitosan (GC), fructose chitosan (FC), succinyl chitosan).[21–23] GC has been hydrophobically functionalized with 5β-cholanic and other moieties, forming self-aggregated nanoparticles in aqueous solution for controlled release of proteins and genes or imaging purposes.[20–21, 23–24] However, to our knowledge the preparation of covalently linked testosterone-GC and testosterone-FC conjugates for controlled release of testosterone has not been yet reported.

The preparation of testosterone-GC and -FC conjugates will potentially enable controlled delivery of testosterone, overcoming low aqueous solubility of this drug, and combining its effects on humans and animals with the biocompatibility and microbicidal properties of the chitosan matrix.[25–28]

This article reports on the covalent linking of testosterone hemisuccinate to GC and FC, forming self-aggregated nanoparticles in aqueous solution, to achieve their controlled release. The obtained nanoparticles were loaded with testosterone and testosterone hemisuccinate, in order to deliver higher steroid quantities.

2. MATERIALS AND METHODS

2.1. Materials

GC (acetylation degree, DA = 19.1% determined by ^{1}H-NMR, Mw = 4.1×10^5) and CS (acetylation degree, DA = 19.8% determined by ^{1}H-NMR, Mw = 4.3×10^5) were purchased from Sigma-Aldrich. 1-ethyl-3-(3′-dimethylamino)carbodiimide hydrochloride (EDC), *N*-hydroxisuccinimide, testosterone, fructose, solvents and reagents employed were purchased from Sigma-Aldrich and used without further purification.

The structures of testosterone hemisuccinate (MSTest), partially acetylated glycol chitosan (GC) and fructose chitosan (FC) are shown in Figure 1.

2.1.1. Synthesis of Testosterone Hemisuccinate

Testosterone hemisuccinate was synthesized by base-catalysed traditional esterification in pyridine of testosterone with succinic anhydride.[29, 30] To this end, 1 gram (c.a. 3.5 mmol) of testosterone was dissolved in 25 mL of pyridine, 3 grams (c.a. 30 mmol) of succinic anhydride were added and stirred. Then nitrogen flow was passed 5 min trough solution and the reaction was refluxed overnight in argon atmosphere. Reaction mixture was poured into a cold 0.1% (v/v) HCl aqueous solution. Ice was added to keep the mixture cold for 2 h. The resulting testosterone hemisuccinate was separated by filtration, washed with cold water and dried under vacuum at 60 °C.
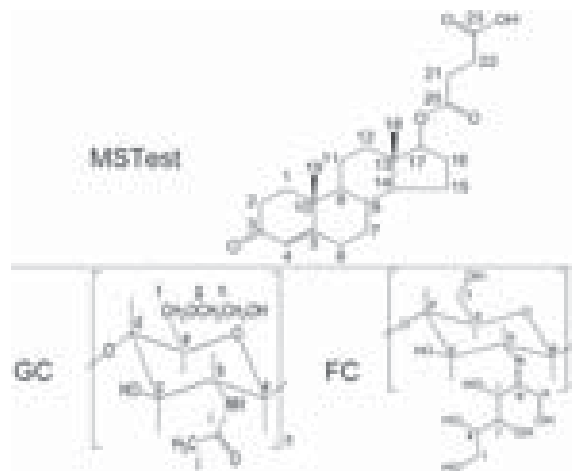

Fig. 1. Structures of testosterone hemisuccinate (MSTest), partially acetylated glycol chitosan (GC) and fructose chitosan (FC).

2.1.2. Synthesis of Fructose Chitosan

FC (substitution degree 5.6%-mol) was prepared by Maillard reaction of chitosan (1%, w/v) with fructose (1%, w/v) in 0.2 M aqueous acetic acid solution at 65 °C for 5 days.[22, 31] After reaction, the solution was neutralized with 2 M NaOH followed by centrifugation (8000 g, 10 min, 20 °C). The supernatant was dialyzed (MWCO: 12000–14000) against double-distilled water for 4 days. The dialyzed solution was freeze-dried affording a yellow, powder wool-like product.

2.1.3. Preparation of Testosterone-GC and Testosterone-FC Conjugates

One hundred and thirty milligrams (0.61 mmol) of GC, or 200 mg (c.a. 0.5 mmol) of FC were dissolved in 8 mL of double-distilled water and diluted with 24 mL of anhydrous ethanol. Then 38 mg (0.20 mmol) of EDC and 23 mg (0.20 mmol) of *N*-hydroxisuccinimide were added and stirred until solution clearance. Fifty-eight milligrams (0.15 mmol) of testosterone hemisuccinate were dissolved in 32 mL of ethanol/water solution (85:15, v/v) and slowly added with stirring to the GC or FC solution. The reaction mixture was stirred 72 hours at room temperature, dialyzed (MWCO: 6000–8000) against ethanol/water mixture (90:10, 66:33, 50:50 and 0:100, v/v), each one for 2 days with 16 exchanges. The dialyzed solution was freeze-dried affording a white, cotton wool-like product.

2.2. Characterization

The testosterone-modified GC and FC conjugates were characterized by FTIR spectroscopy using a Perkin-Elmer FTIR spectrophotometer with 32 scans and 4 cm^{-1} resolution. Samples were prepared by the KBr pellet method. Elemental analyses were performed on a Varian MicroCube

Analyzer with burning temperature of 1150 °C. The ¹H-NMR spectra were recorded with an OXFORD NMR AS400 (VARIAN) spectrometer operating at 400.46 MHz for ¹H at 25 °C with concentrations c.a. 25–8 mg mL⁻¹ in d2-water and d4-methanol/d2-water (66%, v/v) and analyzed with the VNMRJ software, version 2.2.[32] Wide-angle X-ray diffraction (WAXD) analysis of the powered samples was performed using a Rigaku SmartLab X-Ray diffractometer with Cu K$_\alpha$ radiation (40 kV, 30 mA, $\lambda = 0.15418$ nm), data collected at a scan rate of 5° min⁻¹ with a scan angle from 4 to 50°. Calorimetric curves were obtained with a Perkin-Elmer Differential Scanning Calorimeter Pyris 1 and analyzed with the Pyris 1 software (version 6.0.0.033). DSC studies were conducted using sample weights of approximately 5 mg, under nitrogen dynamic flow of 20.0 mL min⁻¹ and a heating-cooling rate of 10 °C min⁻¹.[32–34] Samples were deposited in aluminium capsules and hermetically sealed. Indium was used to calibrate the instrument. Enthalpy (ΔH in J/g dry weight) and peak temperature were computed automatically. Samples were heated and cooled from −30 to 300 °C. Dynamic light scattering (DLS) studies were performed using Zetasizer Nano (Malvern Instruments, UK) at 25 °C to obtain the particle size and zeta potential. The size and morphology of testosterone-modified GC and FC dried nanoparticles were studied by transmission electron microscopy (TEM) with a Philips CM20 operating at 200 kV and scanning electron microscopy (SEM) with a FEI Nova NanoSEM 600 electron microscope. The samples were stirred 48 hours in double-distilled water (c.a. 1 mg mL⁻¹) and a drop of it was deposited on carbon plates. The excess solution was removed with filter paper and air-dried. The SEM samples were coated with gold. The TEM samples were negative stained with a drop of uranyl acetate solution (1%-wt).

2.3. *In Vitro* Drug Release Studies

In vitro testosterone release from testosterone-modified GC and FC nanoparticles was studied by UV detection at 243 nm of the delivered testosterone at various pH. 10 mg of nanoparticles dissolved in buffer solutions (5 mL) at different pH were placed in dialysis bags (MWCO: 14000) and dialyzed against the release media at 37 °C with constant agitation at 100 rpm. The entire media was removed at determined time intervals, and replaced with the same volume of fresh media. The amount of testosterone released was determined by UV spectrophotometry and calculated from a previously obtained calibration curve. These studies were conducted in triplicate for each sample. The experiments were not performed under sink conditions because the low aqueous solubility of testosterone, its low content on samples and the small testosterone UV extinction coefficient made it necessary to evaporate as much release media as possible, in order to achieve a sufficiently high testosterone concentration in 3 mL of ethanol for UV determination.

3. RESULTS AND DISCUSSION

3.1. Preparation of Testosterone-Modified GC and FC Nanoparticles

Testosterone-modified GC and FC nanoparticles with steroid substitution of 1.5%-mol and 5.4%-mol (determined by elemental analysis), respectively, equivalent to 2.7 and 7.9-wt of testosterone were created which self-assembled into nanoparticles in water due to their hydrophilic/hydrophobic moieties. The particles structure is affected by the polarity of the media, as observed in proton NMR peak differences in d2-water compared to d4-methanol/d2-water (66%, v/v).

3.2. Proton NMR Results

The proton NMR spectra of GC-testosterone and FC-testosterone conjugates are shown in Figure 2. The placebo MSTest, CS, FC and GC are also shown for comparison.

The ¹H-NMR spectrum of testosterone hemisuccinate (MSTest) in d4-methanol (Fig. 2I(a)) showed the characteristic steroidal peaks at 0.89 ppm (s, 3H, CH_3, H_{18}), 1.20–1.24 ppm (s, 3H, CH_3, H_{19}), 2.57–2.59 ppm ($2s$, 4H, $2CH_2$, $H_{21} + H_{22}$ of succinyl moiety).

The ¹H-NMR spectrum of GC (Fig. 2I(b)) showed the characteristic signals of the saccharide protons at 2.09 ppm (s, CH_3 of $CH_3CO–$), 2.74 ppm (s, 2H, C_b sugar protons of N-unsubstituted glucosamine units), 3.2–4.0 ppm (C_c to C_h sugar protons) and 4.49 ppm (s, C_a anomeric sugar proton).[35, 36]

The proton NMR spectrum of GC-MSTest conjugate (Figs. 2I(c) and (d)), presented peaks at 0.90–0.95 ppm (CH_3, H_{18}), 1.29/1.33 ppm ($CH + CH_2 + CH_3$, $H_6 + H_7 + H_{11} + H_{12} + H_{15} + H_{19}$), 1.60–1.98 ppm ($CH + CH_2$, H_1 to H_5, H_{16}), 2.51–2.62 ppm (CH_2, $H_{21} + H_{22}$ of succinyl moiety), 4.21/4.23 ppm and 4.56/4.57 ppm (CH, C_a anomeric sugar proton of testosterone substituted and free GC respectively). Addition of d4-methanol to previously prepared d2-water solution of GC-MSTest, until a composition of d4-methanol/d2-water (66%, v/v), enhance the peak intensity in the proton NMR spectrum and produces a slight downfield shifting (Fig. 2I(d)), due to a better solubility and amphiphilic behaviour of testosterone hemisuccinate GC conjugate.

Proton NMR spectrum of CS (Fig. 2II(a)) showed characteristic peaks at 2.10 ppm (s, CH_3 of $CH_3CO–$), 3.19 ppm (s, 1H, H_b), 3.75 ppm (s, 1H, H_e), 3.80 ppm (s, 1H, H_{f*}) and 3.91 ppm (s, 3H, $H_c + H_d + H_f$) as reported for crab chitosans.[37, 38] The ¹H-NMR of FC (Fig. 2II(b)) was dominated by CS peaks; but it is observed a signal at 4.54 ppm (CH, C_a anomeric sugar proton of FC-substituted glucosamine units).
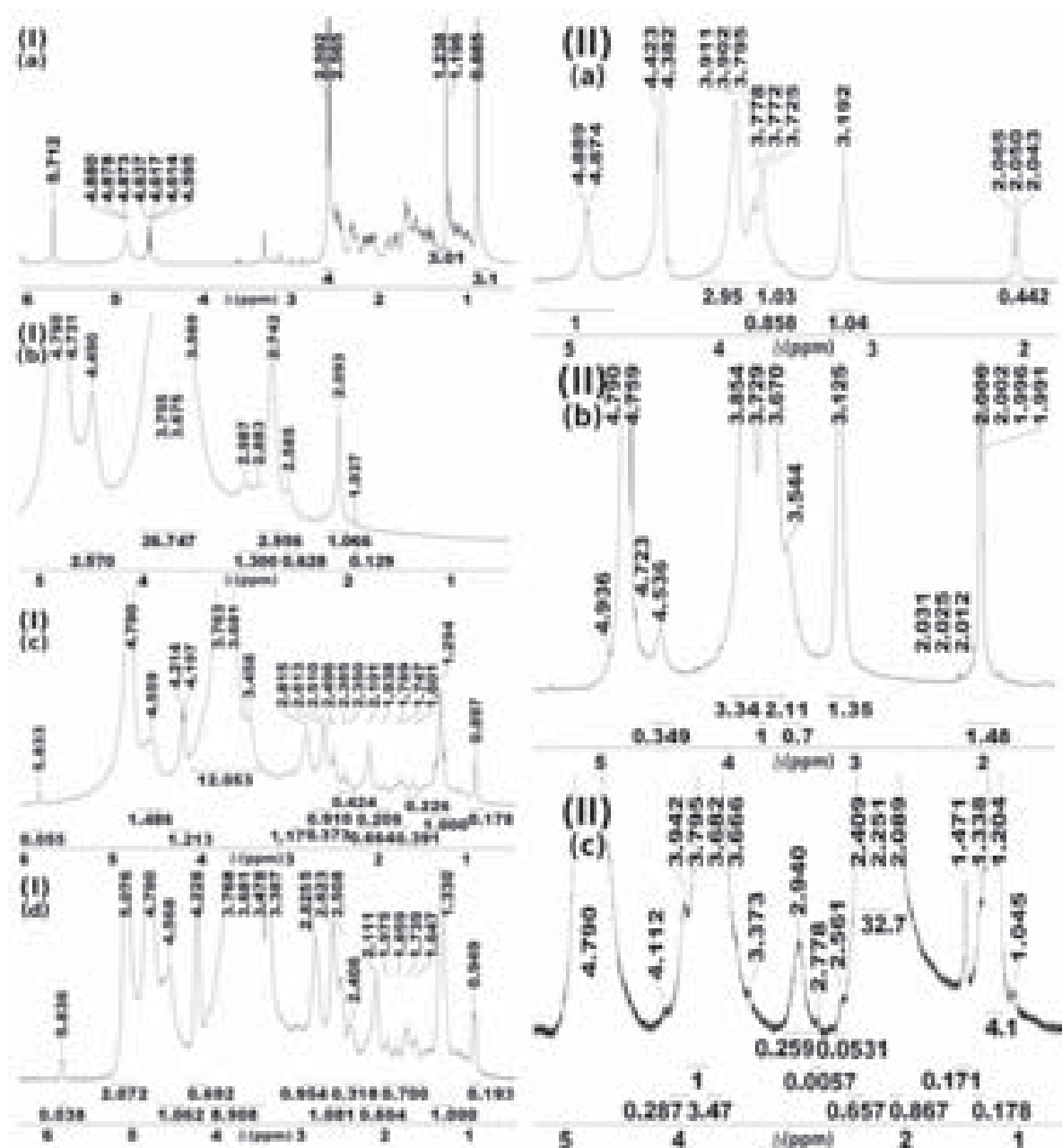
Fig. 2. Proton NMR spectra of (I): (a) MSTest at 25 mg mL^{-1} in CD$_3$OD at 25 °C, (b) GC, (c) GC-MSTest at 25 mg mL^{-1} in D$_2$O at 25 °C, (d) GC-MSTest at 8 mg mL^{-1} in CD$_3$OD/D$_2$O (2:1) at 25 °C; (II): (a) CS at 10 mg mL^{-1} in CD$_3$COOD/D$_2$O (1:3) at 25 °C, (b) FC and (c) FC-MSTest at 8 mg mL^{-1} in D$_2$O at 25 °C (see Fig. 1 for structures).

The proton NMR spectrum of FC-MSTest conjugate (Fig. 2II(c)) showed, in addition to CS peaks, signals at 1.05 ppm (CH$_3$, H$_{18}$), 1.20–1.34 ppm (CH + CH$_2$ + CH$_3$, H$_6$ + H$_7$ + H$_{11}$ + H$_{12}$ + H$_{15}$ + H$_{19}$), 1.47 ppm (CH + CH$_2$, H$_1$ + H$_{16}$), 2.56 ppm (CH$_2$, H$_{21}$ + H$_{22}$ of succinyl moiety), 2.94/3.19–3.13 ppm (CH, H$_b$ of testosterone-substituted and free glucosamine units respectively), 4.11/4.38–4.42/4.54 ppm (CH, C$_a$ anomeric sugar proton

of testosterone-substituted glucosamine, free glucosamine and FC-substituted glucosamine units respectively).

3.3. FTIR Spectroscopy

The FTIR spectra of GC-testosterone and FC-testosterone conjugates are shown in Figure 3. The spectra of GC, CS and FC are also included for comparison.
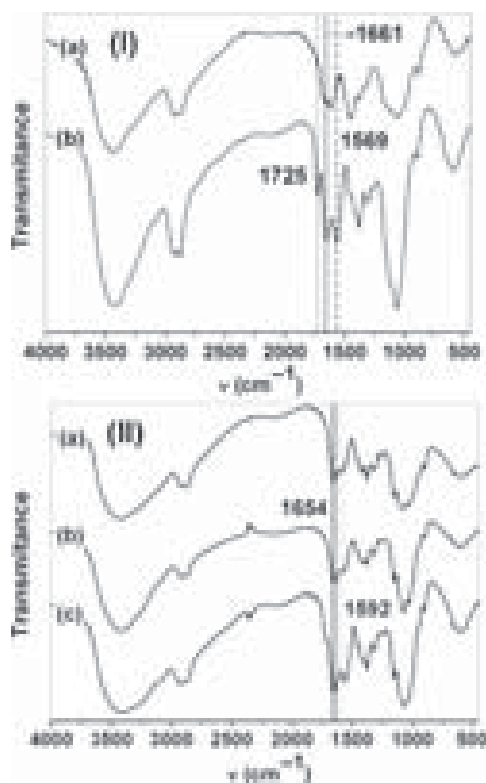
Fig. 3. Infrared spectra of (I): (a) GC and (b) GC-MSTest; (II): (a) CS, (b) FC and (c) FC-MSTest (see Fig. 1 for structures).

The IR spectrum of GC (Fig. 3(a)), presented absorption peaks at 3432 cm^{-1} (O–H stretching overlapped with N–H stretching), 2926 cm^{-1} and 2870 cm^{-1} (aliphatic C–H stretching band), 1650 cm^{-1} (Amide 1 band, C=O stretching of acetyl group), 1616 cm^{-1} (N–H bending) and 1450–1380 cm^{-1} (C–H bending). The absorption peaks at 1160 cm^{-1} (antisymmetric stretching of the C—O—C bridge), 1120 and 1066 cm^{-1} (skeletal vibrations involving the C—O stretching) related to its saccharide structure are observed.[32, 34]

The spectrum of GC-testosterone conjugate is dominated by the broad GC peaks; however the intense C=O peak of the ester linkage is present at 1725 cm^{-1} (Fig. 3(b)). The intense peak at 1569 cm^{-1} and the increase in the amide *I* band at 1661 cm^{-1} confirm the amide linkage between the GC and testosterone hemisuccinate.

The IR spectrum of chitosan (Fig. 3II(a)) presented characteristic absorption peaks at 2942–2784 cm^{-1} (aliphatic C–H stretching band), 1658 cm^{-1} (Amide 1) and 1597 cm^{-1} (–NH$_2$) bending and 1321 cm^{-1} (Amide III). Absorption peaks at 1154 cm^{-1} (antisymmetric stretching of the C—O—C bridge), 1082 and 1032 cm^{-1} (skeletal vibrations involving the C—O stretching) are due to its saccharide structure.[34] FC presents a quite similar spectrum, due to lack of additional functional groups to those of chitosan (Fig. 3II(b)).

Testosterone-modified FC conjugate presents, in addition to CS peaks, ketone C=O absorptions at 1716 cm^{-1} (ketone carbonyl, testosterone) and an intense peak at 1557 cm^{-1}; indicative of amide linkage between testosterone hemisuccinate and FC (Fig. 3II(c)).

3.4. X-Ray Diffraction Studies

The wide-angle X-ray diffraction patterns of testosterone hemisuccinate, GC, testosterone-modified GC, chitosan, FC and FC-testosterone conjugates are shown in Figure 4.

GC presents two intense peaks at 2θ 7.7° and 20.1°.

GC-MSTest showed a broad and intense peak at 20.4°. The absence of intense peaks at 7.7 and 20.1° attributed to GC indicates that GC is absent as crystalline phase. The characteristic peaks of pure testosterone hemisuccinate were also absent.

Chitosan showed two intense peaks at 10.5° and 19.8°. These peaks are attributed to the $(020)_h$ planes of the hydrated crystalline structure and reflections of the hydrated polymorph.[39]

FC presents two intense and broad peaks at 10.0° and 19.9°, and a shoulder at 21.9°.

Testosterone-modified FC yielded a quite broad and intense peak at 18.7–21.1°. The absence of peak at 10.0–10.5° and the broadening between 18.7–21.1° indicates that FC lacks as crystalline phase but with an increased contribution of amorphous phase.

3.5. Differential Scanning Calorimetry Studies

The DSC curves of GC placebo, testosterone-modified GC, CS placebo, FC and testosterone-modified FC, under nitrogen in the temperature range from −30 to 300 °C are shown in Figure 5.
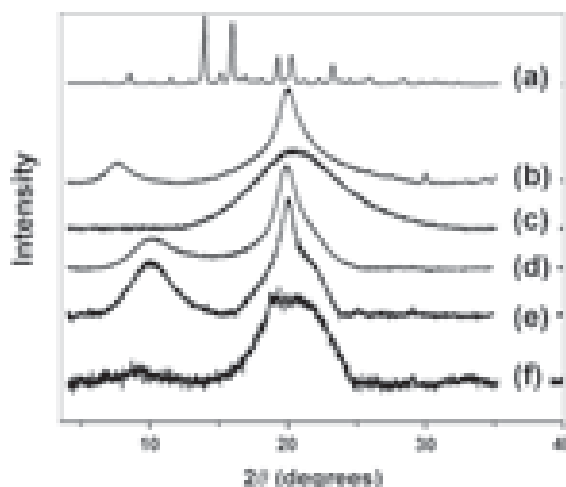

Fig. 4. Wide-angle X-ray diffraction patterns of: (a) MSTest, (b) GC, (c) GC-MSTest, (d) CS, (e) FC and (f) FC-MSTest (see Fig. 1 for structures).
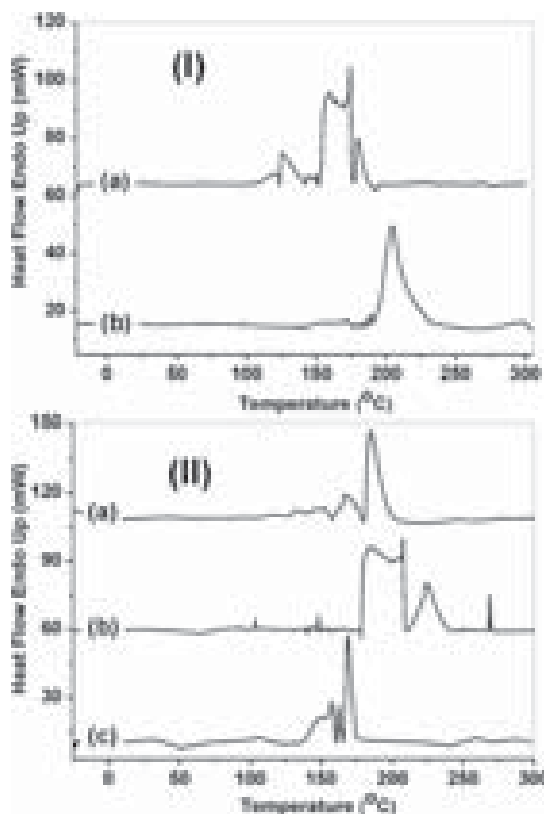
Fig. 5. DSC Curves of (I): (a) GC and (b) GC-MSTest; (II): (a) CS, (b) FC and (c) FC-MSTest (see Fig. 1 for structures).

GC is presented by three endothermic peaks at 123.6 °C, 175.1 °C and 180.9 °C (Fig. 5I(a)), with associated peak enthalpies (ΔH) of 81.9 J/g, 510.5 J/g and 72.1 J/g, respectively. These endothermic peaks must result from the melting of glycol chitosan crystals and dissociation of GC chains. Testosterone-modified GC (Fig. 5I(b)) showed an intense endothermic peak at 204.8 °C with corresponding ΔH of 863.3 J/g, associated with melting of GC with linked testosterone hemisuccinate, dissociation and decomposition of testosterone-modified GC chains.

The DSC of CS placebo (Fig. 5II(a)) showed two endothermic peaks at 170.4 and 187.0 °C, with an associated ΔH of 3.5 J/g and 120.6 J/g, respectively. The total ΔH of these effects is 124.1 J/g. These endothermic effects must result mainly from the melting and dissociation of chitosan crystals, as reported for crab CSs.[34]

The DSC curve of FC (Fig. 5II(b)) showed endothermic peaks at 207.5 °C, 224.3 °C and 269.0 °C, with associated ΔH of 3416.5 J/g, 906.7 J/g and 51.5 J/g, respectively. These endothermic effects must result from the melting of fructose chitosan crystals and dissociation of FC chains. Linked testosterone hemisuccinate-FC (Fig. 5II(c)) presents three intense endothermic peaks at 158.9 °C, 164.7 °C and 170.9 °C, with associated ΔH of 103.7 J/g, 15.1 J/g and 126.5 J/g, respectively. These peaks

may result from the melting of testosterone-modified FC as well as dissociation and decomposition of modified CS chains.

3.6. Dynamic Light Scattering Studies and Electron Microscopy

Dynamic light scattering studies conducted in triplicate revealed an average testosterone-GC and testosterone-FC particles diameters of 332 ± 4 nm and 245 ± 1 nm with polydispersity indexes of 0.57 ± 0.03 and 0.238 ± 0.007, and zeta potentials of 9.7 ± 0.6 mV and 11 ± 3 mV, respectively. These small nanoparticles were accompanied by c.a. 1–6%-mol aggregates of about 4.4–5.6 μm size.

Figure 6 shows the SEM and TEM images of testosterone-modified GC and FC nanoparticles. The SEM images showed almost spherically shaped nanoparticles smaller than 100–200 nm. Transmission electron microscopy images provided more information, showing spherically shaped nanoparticles with 70–85 nm (Fig. 6(c)) and 25–40 nm (Fig. 6(f)) mean diameters for GC-MSTest and FC-MSTest conjugates, respectively.

3.7. Release Studies at Different pH

The calculated testosterone released after 30 min at different pH are shown in Table II. The quantity released from testosterone-modified GC and FC conjugates increases as the solution acidity increases. These releases are pH-dependent and affected by the ester hydrolysis of the linkage between the testosterone and the succinyl group on GC-MSTest and FC-MSTest conjugates, respectively.

The release profiles of testosterone at 37 ± 2 °C in buffer solution (pH = 6.0), expressed as per cent cumulative release against time for testosterone-modified GC and FC are presented in Figure 7. These studies were performed

Table I. X-ray peaks of testosterone hemisuccinate, GC, GC-MSTest, chitosan, FC and FC-MSTest conjugates by WAXD (see Fig. 1 for structures).

Samples				$2\,\theta$ (degrees)					
MSTest	8.6*	11.5*	14.0	15.2*	16.0	16.9*	19.3	20.3	23.2
GC	7.7	20.1	30.0*	34.4*	35.1*	37.9*	39.8*	41.0*	41.3*
GC-MSTest	–	20.4	–	–	–	–	–	–	–
CS	10.5	19.8	–	–	–	–	–	–	–
FC	10.0	19.9	21.9	–	–	–	–	–	–
FC-MSTest	18.7	21.1	–	–	–	–	–	–	–

Note: *Stands for peaks of low intensity.

Table II. % Testosterone released (%-wt) at 37 ± 2 °C in buffer solutions after 30 min. (see Fig. 1 for structures).

Sample	% (pH 6)	% (pH 5)	% (pH 4)	% (pH 2)
GC-MSTest	10.1 ± 0.6	14.3 ± 0.4	20.4 ± 0.2	27.6 ± 0.7
FC-MSTest	–	5.2 ± 0.3	8.0 ± 0.5	16.8 ± 0.1

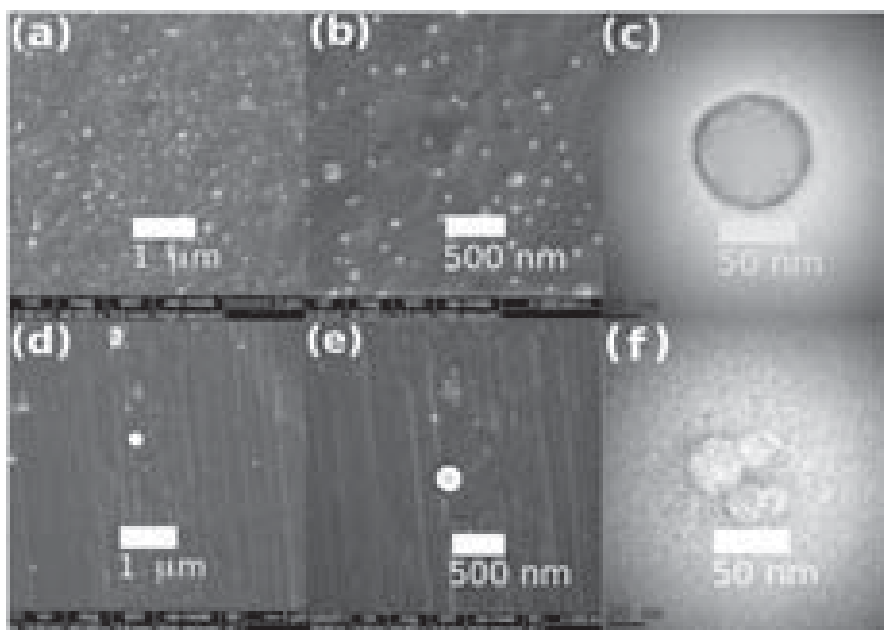**Fig. 6.** Scanning electron micrographs of GC-testosterone conjugate nanoparticles at: (a) 40000×, (b) 85000× magnifications and (c) transmission electron micrograph at 100000× magnifications; scanning electron micrographs of FC-testosterone conjugate nanoparticles at: (d) 40000×, (e) 85000× magnifications and (f) transmission electron micrograph at 100000× magnifications (see Fig. 1 for structures).

at pH 6 to simulate as much as possible physiological conditions (pH 7.4), but acidic conditions are needed to achieve the hydrolysis of the ester linkage and the testosterone release.

Testosterone was delivered with almost constant release (zero order kinetics) during the first 4 and 8 h from the testosterone-modified GC and FC conjugates, respectively. Releases were not quantitative in both cases, reaching c.a. 52% and 33% after 68 hours from GC and FC conjugates, respectively.

Testosterone release was slower from nanoparticles of modified FC than from those of modified GC, probably

due to the smaller hydrated size and more compact hydrophobic core of the latter.

4. CONCLUSIONS

GC and FC were successfully linked to testosterone hemisuccinate with a functionalization of up to 1.5 and 5.4%-mol respectively, as confirmed by elemental analysis and proton NMR. These conjugates were able to form self-assembled nanoparticles in aqueous solution, as result of partial hydrophobic modification of the chitosans with the testosterone moiety. The testosterone release percent in
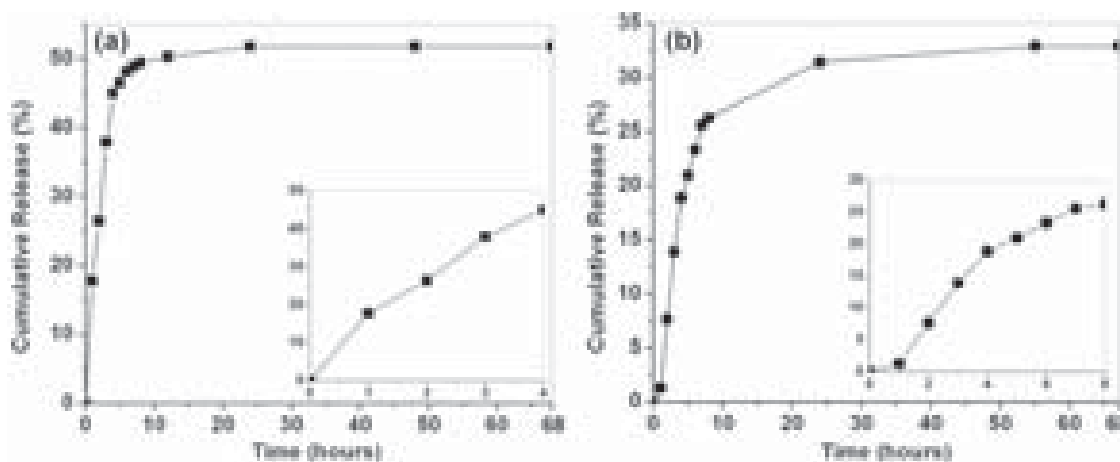

Fig. 7. *In vitro* release profile at 37 ± 2 °C of: (a) GC-MSTest and (b) FC-MSTest in buffer solution (pH = 6.0) (see Fig. 1 for structures).

water at different acid pH indicated a drug release dependence on the acidity of the solution. *In vitro* sustained release was observed up to 68 hours, reaching between 33–52%-wt of the testosterone linked to the functionalized chitosans. These results indicate that the obtained nanoparticles could be good candidates for testosterone delivery to animals and humans.

References and Notes

1. N. Arguedas, M. E. Clark, E. D. Ketterson, D. S. Monk, V. Nolan, P. G. Parker, S. A. Raouf, W. L. Reed, and E. Snajdr, Physiological effects on demography: A long-term experimental study of testosterone's effects on fitness. *American Nature* 167, 667 (**2006**).
2. R. M. Cox and H. B. John-Alder, Testosterone has opposite effects on male growth in lizards (Sceloporus spp.) with opposite patterns of sexual size dimorphism. *J. Experim. Biology* 208, 4679 (**2005**).
3. S. Alkaade, N. Bassil, and J. E. Morley, The benefits and risks of testosterone replacement therapy: A review. *Therapy Clinical Risk Management* 5, 427 (**2009**).
4. S. Bandelow, M. Combrinck, E. Hogervorst, and A. D. Smith, Low free testosterone is an independent risk factor for Alzheimer's disease. *Experimental Gerontology* 39, 1633 (**2004**).
5. C. Bouchard, G. D. Braunstein, S. R. Davis, M. Gass, A. L. Hirschberg, H. Koch, R. Kroll, M. Moreau, A. Moufarege, S. Pack, N. Panay, C. Rodenberg, and J. Studd, Testosterone for low libido in postmenopausal women not taking estrogen. *New England Journal Medicine* 359, 2005 (**2008**).
6. R. M. Francis and S. P. Tuck, Testosterone, bone and osteoporosis. *Frontier Hormone Research* 37, 123 (**2009**).
7. A. Aleman, J. L. Bosch, M. H. Emmelot-Vonk, D. E. Grobbee, T. M. Lock, H. R. Nakhai-Pour, Y. T. van der Schouw, and H. J. Verhaar, Effect of testosterone supplementation on functional mobility, cognition, and other parameters in older men: A randomized controlled trial. *Journal of the American Medical Association* 299, 39 (**2008**).
8. M. L. Andersen and S. Tufik, The effects of testosterone on sleep and sleep-disordered breathing in men: Its bidirectional interaction with erectile function. *Sleep Medical Reviews* 12, 365 (**2008**).
9. A. Morgentaler and C. Schulman, Testosterone and prostate safety. *Frontier Hormones Research* 37, 197 (**2009**).
10. W. H. Walker, Molecular mechanisms of testosterone action in spermatogenesis. *Steroids* 74, 602 (**2009**).
11. N. Beheshti, A.-L. Kjøniksen, K. D. Knudsen, B. Nyström, and K. Zhu, Rheological and structural aspects on association of hydrophobically modified polysaccharides. *Soft Matter.* 5, 1328 (**2009**).
12. M. Chen, R. Li, X. Li, L. Liu, Y. Liu, Y. Wang, W. Yang, Q. Zhang, and Z. Zhou, Preparation and characterization of self-assembled nanoparticles of 6-O-cholesterol-modified chitosan for drug delivery. *Carbohydrate Polymers* 84, 1244 (**2011**).
13. Y. Jing-Mou, Q. Li-Yan, J. Yi, and L. Yong-Jie, Polymeric nanoparticles of cholesterol-modified glycol chitosan for doxorubicin delivery: Preparation and *in-vitro* and *in-vivo* characterization. *Journal of Pharmacy and Pharmacology* 61, 713 (**2009**).
14. K. Fink, S. Höhne, F. Simon, and S. Spange, Hydrophobically functionalized chitosan particles. *Journal of Adhesion Science and Technology* 23, 297 (**2009**).
15. R. A. A. Muzzarelli, Chitin, Pergamon Press, Oxford (**1997**).
16. S. Bagheri-Khoulenjani, H. Mirzadeh, and S. M. Taghizadeh, An investigation on the short-term biodegradability of chitosan with various molecular weights and degrees of deacetylation. *Carbohydrate Polymers* 78, 773 (**2009**).
17. S. Dhaliwal, S. Jain, H. P. Singh, and A. K. Tiwary, Mucoadhesive microspheres for gastroretentive delivery of acyclovir: *In vitro* and *in vivo* evaluation. *The American Association of Pharmaceutical Scientists Journal* 10, 322 (**2008**).
18. D. Raafat and H.-G. Sahl, Chitosan and its antimicrobial potential—A critical literature survey. *Microbial Biotechnology* 2, 186 (**2009**).
19. V. G. Babak, T. A. Babushkina, T. P. Klimova, E. A. Stepnova, V. E. Tikhonov, and E. V. Vorontsov, New approach to the quaternization of chitosan and its amphiphilic derivatives. *European Polymer Journal* 43, 2414 (**2007**).
20. Y. Jing-Mou, Q. Li-Yan, J. Yi, and L. Yong-Jie, Self-aggregated nanoparticles of cholesterol-modified glycol chitosan conjugate: Preparation, characterization, and preliminary assessment as a new drug delivery carrier. *European Polymer Journal* 44, 555 (**2008**).
21. Y. W. Cho, H. Chung, S. Y. Jeong, K. Kim, J. H. Park, and Y. J. Son, Preparation and characterization of self-assembled nanoparticles based on glycol chitosan bearing adriamycin. *Colloid Polymer Science* 284, 763 (**2006**).
22. Y. C. Chung, C. F. Li, and C. F. Tsai, Preparation and characterization of water-soluble chitosan produced by Maillard reaction. *Fisheries Science* 72, 1096 (**2006**).
23. X. Chen, K. Choi, Y. Choi, S. Y. Jeong, J. F. Leary, D.-E. Lee, S. Lee, S. J. Lee, K. Kim, H. Koo, I. C. Kwon, S. Min, and K. Park, Tumor-homing photosensitizer-conjugated glycol chitosan nanoparticles for synchronous photodynamic imaging and therapy based on cellular on/off system. *Biomaterials* 32, 4021 (**2011**).
24. H. Chung, S. Y. Jeong, K. Kim, I. C. Kwon, S. Kwon, and J. H. Park, Physicochemical characterizations of self-assembled nanoparticles of glycol chitosan-deoxycholic acid conjugates. *Biomacromolecules* 6, 1154 (**2005**).
25. B. C. Amsden, D. K. Knight, and S. N. Shapka, Structure, depolymerization, and cytocompatibility evaluation of glycol chitosan. *Journal of Biomedical Materials Research Part A* 83A, 787 (**2007**).
26. X. G. Chen, M. Kong, C. G. Liu, C. S. Liu, X. H. Meng, and L. J. Yu, Antibacterial mechanism of chitosan microspheres in a solid dispersing system against *E. coli. Colloids Surf. B: Biointerfaces* 65, 197 (**2008**).
27. Y. Du, H. Li, Y. Liu, C. Qin, Q. Xiao, and J. Zhu, Water-solubility of chitosan and its antimicrobial activity. *Carbohydrate Polymers* 63, 367 (**2006**).
28. T. Kean and M. Thanou, Biodegradation, biodistribution and toxicity of chitosan. *Advanced Drug Delivery Reviews* 62, 3 (**2010**).
29. T. Abe, K. Hasunuma, and M. Kurokawa, Vitamin E orotate and a method of producing the same, US Patent 3944550 (**1976**).
30. A. Martínez-García and R. Martínez, Microwave assisted synthesis of diosgenin esters of maleic and itaconic acids. *Synthetic Communications* 38, 1917 (**2008**).
31. C.-C. Chen, Y.-C. Chung, and C.-L. Kuo, Preparation and important functional properties of water-soluble chitosan produced through Maillard reaction. *Bioresource Technology* 96, 1473 (**2005**).
32. C. P. Covas, J. P. Quiñones, C. Schmidt, and R. Szopko, Novel drug delivery systems: Chitosan conjugates covalently attached to steroids

with potential anticancer and agrochemical activity. *Carbohydrate Polymers* 84, 858 (**2011**).

33. E. R. Dockal, J. E. Santos, and J. P. Soares, Characterizacao de quitosanas comerciais de diferentes origens. *Polimeros: Ciencia e Tecnologia* 13, 242 (**2003**).

34. Y. Coll, H. Curiel, C. Peniche, and J. Pérez, Microspheres of chitosan for controlled delivery of brassinosteroids with biological activity as agrochemicals. *Carbohydrate Polymers* 80, 915 (**2010**).

35. A. I. Gray, L. Noble, L. Sadiq, and I. F. Uchegbu, A non-covalently cross-linked chitosan based hydrogel. *International Journal of Pharmaceutics* 192, 173 (**1999**).

36. A. I. Gray, A. Mahmoud, L. Sadiq, A. G. Schätzleinä, I. F. Uchegbu, R. D. Waigh, and W. Wang, Quaternary ammonium palmitoyl glycol chitosan—A new polysoap for drug delivery. *International Journal of Pharmaceutics* 224, 185 (**2001**).

37. M. Berrada, M. D. Buschmann, A. Gupta, M. Lavertu, A. Rodrigues, A. N. Serreqi, D. Wang, and Z. Xia, A validated 1H NMR method for the determination of the degree of deacetylation of chitosan. *Journal of Pharmaceutical and Biomedical Analysis* 32, 1149 (**2003**).

38. A. Hirai, A. Nakajima, and H. Odani, Determination of degree of deacetylation of chitosan by ^{1}H NMR spectroscopy. *Polym. Bull.* 26, 87 (**1991**).

39. L. David, A. Domard, J.-M. Lucas, A. Osorio-Madrazo, C. Peniche-Covas, and S. Trombotto, Kinetics study of the solid-state acid hydrolysis of chitosan: Evolution of the crystallinity and macromolecular structure. *Biomacromolecules* 11, 1376 (**2010**).

RESEARCH ARTICLE